

frontiers RESEARCH TOPICS



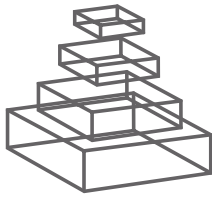
INTRACELLULAR BIOMINERALIZATION IN BACTERIA

Topic Editors

Wei Lin, Karim Benzerara, Damien Faivre and
Yongxin Pan



frontiers in
MICROBIOLOGY



FRONTIERS COPYRIGHT STATEMENT

© Copyright 2007-2014
Frontiers Media SA.
All rights reserved.

All content included on this site, such as text, graphics, logos, button icons, images, video/audio clips, downloads, data compilations and software, is the property of or is licensed to Frontiers Media SA ("Frontiers") or its licensees and/or subcontractors. The copyright in the text of individual articles is the property of their respective authors, subject to a license granted to Frontiers.

The compilation of articles constituting this e-book, wherever published, as well as the compilation of all other content on this site, is the exclusive property of Frontiers. For the conditions for downloading and copying of e-books from Frontiers' website, please see the Terms for Website Use. If purchasing Frontiers e-books from other websites or sources, the conditions of the website concerned apply.

Images and graphics not forming part of user-contributed materials may not be downloaded or copied without permission.

Individual articles may be downloaded and reproduced in accordance with the principles of the CC-BY licence subject to any copyright or other notices. They may not be re-sold as an e-book.

As author or other contributor you grant a CC-BY licence to others to reproduce your articles, including any graphics and third-party materials supplied by you, in accordance with the Conditions for Website Use and subject to any copyright notices which you include in connection with your articles and materials.

All copyright, and all rights therein, are protected by national and international copyright laws.

The above represents a summary only. For the full conditions see the Conditions for Authors and the Conditions for Website Use.

ISSN 1664-8714

ISBN 978-2-88919-272-4

DOI 10.3389/978-2-88919-272-4

ABOUT FRONTIERS

Frontiers is more than just an open-access publisher of scholarly articles: it is a pioneering approach to the world of academia, radically improving the way scholarly research is managed. The grand vision of Frontiers is a world where all people have an equal opportunity to seek, share and generate knowledge. Frontiers provides immediate and permanent online open access to all its publications, but this alone is not enough to realize our grand goals.

FRONTIERS JOURNAL SERIES

The Frontiers Journal Series is a multi-tier and interdisciplinary set of open-access, online journals, promising a paradigm shift from the current review, selection and dissemination processes in academic publishing.

All Frontiers journals are driven by researchers for researchers; therefore, they constitute a service to the scholarly community. At the same time, the Frontiers Journal Series operates on a revolutionary invention, the tiered publishing system, initially addressing specific communities of scholars, and gradually climbing up to broader public understanding, thus serving the interests of the lay society, too.

DEDICATION TO QUALITY

Each Frontiers article is a landmark of the highest quality, thanks to genuinely collaborative interactions between authors and review editors, who include some of the world's best academicians. Research must be certified by peers before entering a stream of knowledge that may eventually reach the public - and shape society; therefore, Frontiers only applies the most rigorous and unbiased reviews.

Frontiers revolutionizes research publishing by freely delivering the most outstanding research, evaluated with no bias from both the academic and social point of view.

By applying the most advanced information technologies, Frontiers is catapulting scholarly publishing into a new generation.

WHAT ARE FRONTIERS RESEARCH TOPICS?

Frontiers Research Topics are very popular trademarks of the Frontiers Journals Series: they are collections of at least ten articles, all centered on a particular subject. With their unique mix of varied contributions from Original Research to Review Articles, Frontiers Research Topics unify the most influential researchers, the latest key findings and historical advances in a hot research area!

Find out more on how to host your own Frontiers Research Topic or contribute to one as an author by contacting the Frontiers Editorial Office: researchtopics@frontiersin.org

INTRACELLULAR BIOMINERALIZATION IN BACTERIA

Topic Editors:

Wei Lin, Chinese Academy of Sciences, China

Karim Benzerara, Sorbonne Universités - UPMC Univ Paris 06, France

Damien Faivre, Max Planck Institute of Colloids and Interfaces, Germany

Yongxin Pan, Chinese Academy of Sciences, China



Scanning transmission electron microscopy (STEM) image of an uncultured magnetotactic bacterial strain MYR-1 belonging to the Nitrospirae phylum isolated from Lake Miyun near Beijing, China. Cells of MYR-1 are 6–10 μm in length and produce up to 1000 bullet-shaped magnetite magnetosomes arranged into 3–5 bundles of chains (green particles). Besides magnetosomes, MYR-1 cells commonly form numerous sulfur-rich globules (blue spherical particles), indicating its potential contributions to the biogeochemical cycles of both iron and sulfur in nature.

Photo by Dr. Jinhua Li from the Institute of Geology and Geophysics, Chinese Academy of Sciences.

formation in prokaryotic cells. The geological significance of intracellular biomineralization is important; spectacular examples are fossil magnetosomes that may significantly contribute

Bacteria can sequester metals and other ions intracellularly in various forms ranging from poorly ordered deposits to well-ordered mineral crystals. Magnetotactic bacteria provide one example of such intracellular deposits. They synthesize intracellular magnetic minerals of magnetite (Fe_3O_4) and/or greigite (Fe_3S_4) magnetosomes which are generally less than 150 nm and organized into one or multiple chain structures. The magnetosome chain(s) act like a compass needle to facilitate the navigation of magnetotactic bacteria by using the Earth's magnetic field. Due to their ubiquitous distribution in aquatic and sedimentary environments, magnetotactic bacteria play important roles in global iron cycling. Other intracellular mineral phases have been evidenced in bacteria such as As_2S_3 , CaCO_3 , CdS , $\text{Se}(0)$ or various metal phosphates which may play as well a significant role in the geochemical cycle of these elements. However, in contrast to magnetotactic bacteria, the biological and environmental function of these particles remains a matter of debate. In recent years, such intracellularly biomineralizing bacteria have become an attractive model system for investigating the molecular mechanisms of organelle-like structure

to the bulk magnetization of sediments and act as potential archives of paleoenvironmental changes. In addition, intracellular mineral deposits formed by bacteria have potentially versatile applications in biotechnological and biomedical fields.

After more than four decades of research, the knowledge on intracellularly biomimetic bacteria has greatly improved. The aim of this Research Topic is to highlight recent advances in our understanding of intracellular biomimetic mineralization by bacteria. Magnetotactic bacteria are a system of choice for that topic but other intracellularly biomimetic bacteria may bring a unique perspective on that process. Research papers, reviews, perspectives, and opinion papers on (i) the diversity and ecology of intracellularly biomimetic bacteria, (ii) the molecular mechanisms of intracellular biomimetic mineralization, (iii) the chemo- and magneto-taxis behaviors of magnetotactic bacteria, (iv) the involvement of intracellularly biomimetic bacteria in local or global biogeochemical cycling, (v) the paleoenvironmental reconstructions and paleomagnetic signals based on fossil magnetosomes, (vi) and the applications of intracellular minerals in biomaterial and biotechnology were welcomed.

Table of Contents

- 06 *Intracellular Biomineralization in Bacteria***
Wei Lin, Karim Benzerara, Damien Faivre and Yongxin Pan
- 08 *Phylogenetic Significance of Composition and Crystal Morphology of Magnetosome Minerals***
Mihály Pósfai, Christopher Lefèvre, Dennis Trubitsyn, Dennis A. Bazylinski and Richard Frankel
- 23 *Isolation, Cultivation and Genomic Analysis of Magnetosome Biomineratization Genes of a New Genus of South-Seeking Magnetotactic Cocci Within the Alphaproteobacteria***
Viviana Morillo, Fernanda Abreu, Ana C. Araujo, Luiz G. P. de Almeida, Alex Enrich-Prast, Marcos Farina, Ana T. R. de Vasconcelos, Dennis A. Bazylinski and Ulysses Lins
- 35 *Magnetotactic Bacteria From Pavilion Lake, British Columbia***
Zachery Oestreicher, Steven K. Lower, Eric Rees, Dennis A. Bazylinski and Brian H. Lower
- 41 *Swimming Motion of Rod-Shaped Magnetotactic Bacteria: The Effects of Shape and Growing Magnetic Moment***
Dali Kong, Wei Lin, Yongxin Pan and Keke Zhang
- 52 *The Magnetosome Model: Insights Into the Mechanisms of Bacterial Biomineratization***
Lilah Rahn-Lee and Arash Komeili
- 60 *Structure and Evolution of the Magnetochrome Domains: No Longer Alone***
Pascal Arnoux, Marina I. Siponen, Christopher T. Lefèvre, Nicolas Ginet and David Pignol
- 67 *Structure Prediction of Magnetosome-Associated Proteins***
Hila Nudelman and Raz Zarivach
- 84 *The Effect and Role of Environmental Conditions on Magnetosome Synthesis***
Cristina Moisescu, Ioan I. Ardelean and Liane G. Benning
- 96 *Changes of Cell Growth and Magnetosome Biomineratization in Magnetospirillum Magneticum AMB-1 After Ultraviolet-B Irradiation***
Yinzhou Wang, Wei Lin, Jinhua Li and Yongxin Pan
- 106 *Paleomagnetic and Paleoenvironmental Implications of Magnetofossil Occurrences in Late Miocene Marine Sediments From the Guadalquivir Basin, SW Spain***
Juan C. Larrasoña, Qingsong Liu, Pengxiang Hu, Andrew P. Roberts, Pilar Mata, Jorge Civis, Francisco J. Sierra and José N. Pérez-Asensio

121 *Surface Expression of Protein a on Magnetosomes and Capture of Pathogenic Bacteria by Magnetosome/Antibody Complexes*

Jun Xu, Junying Hu, Lingzi Liu, Li Li, Xu Wang, Huiyuan Zhang, Wei Jiang, Jiesheng Tian, Ying Li and Jilun Li

129 *A Key Time Point for Cell Growth and Magnetosome Synthesis of *Magnetospirillum Gryphiswaldense* Based on Real-Time Analysis of Physiological Factors*

Jing Yang, Shuqi Li, Xiuliang Huang, Tao Tang, Weizhong Jiang, Tongwei Zhang and Ying Li



Intracellular biomineralization in bacteria

Wei Lin^{1,2*}, Karim Benzerara^{3*}, Damien Faivre^{4*} and Yongxin Pan^{1,2*}

¹ Biogeomagnetism Group, Paleomagnetism and Geochronology Laboratory, Key Laboratory of Earth and Planetary Physics, Institute of Geology and Geophysics, Chinese Academy of Sciences, Beijing, China

² France-China Bio-Mineralization and Nano-Structures Laboratory, Chinese Academy of Sciences, Beijing, China

³ Institut de Minéralogie, de Physique des Matériaux et de Cosmochimie, Université Pierre et Marie Curie, Sorbonne Universités, CNRS UMR 7590, Muséum National d'Histoire Naturelle, IRD UMR 206, Paris, France

⁴ Department of Biomaterials, Max Planck Institute of Colloids and Interfaces, Potsdam, Germany

*Correspondence: weilin0408@gmail.com; karim.benzerara@impmc.jussieu.fr; damien.faivre@mpikg.mpg.de; yxpan@mail.igcas.ac.cn

Edited and reviewed by:

Jonathan P Zehr, University of California, Santa Cruz, USA

Keywords: microbial biomineralization, magnetotactic bacteria, magnetosome, magnetotaxis, iron cycling, biosignature, ancient environment

Microorganisms have populated the Earth for billions of years and their activities are important forces shaping our planetary environments through biogeochemical cycles. In particular, microbial biomineralization that selectively take up environmental elements and deposit minerals either intracellularly or extracellularly is of great interest, because these processes play vital roles in the global cycles of numerous elements, such as Fe, Mn, Ca, As, O, S, and P, etc. Biominerals, the products of biomineralization, not only serve as important biosignatures for the search of traces of past life and the reconstruction of ancient environments but also have many important commercial applications.

Recent advances in sequencing technologies, molecular analyses and approaches for assaying protein functions pave the way for rapid progress in microbial biomineralization research. The objective of this research topic is to highlight the latest advances in our understanding of intracellular biomineralization in bacteria, with a focus on the magnetotactic bacteria (MTB), a group of phylogenetically diverse microbes synthesizing magnetic minerals of magnetite (Fe_3O_4) and/or greigite (Fe_3S_4) magnetosomes in cells. Magnetosomes are generally less than 150 nm in length, covered by lipid bilayer membrane and organized into one or multiple chain structures that act like a compass needle to facilitate the navigation of MTB using the Earth's magnetic field. The uniform nano sizes, superior magnetic properties and perfect chain arrangement suggest a strict genetic control of magnetosome synthesis in MTB cells, which provides an attractive model system for investigating the mechanisms of bacterial intracellular biomineralization. This research topic provides a selection of interesting and challenging topics of research on the diversity, ecology, evolution, genomics, and biochemistry of MTB. The applications of magnetosomes in biotechnology and paleoenvironmental reconstruction are also covered here.

This research topic begins with a review on the relationship between all known magnetosome crystal habits and the phylogenetic affiliations of MTB (Pósfai et al., 2013), which serves as guide to better understand the evolutionary history of magnetosome formation and magnetotaxis in MTB. Following this review, Morillo et al. (2014) report the first cultivation and genomic characterization of a south-seeking *Alphaproteobacteria* magnetotactic coccus *Magnetofaba australis* strain IT-1 from the Southern Hemisphere. The findings of their study provide important

clues to the evolution of magnetotactic *Alphaproteobacteria*. Oestreicher et al. (2013) examine the morphological and phylogenetic diversity of MTB in a freshwater lake containing microbialites. Their results raise the interesting question of whether MTB magnetosomes could be preserved in microbialites and serve as robust biomarkers. Kong et al. (2014) investigate the swimming behavior of a rod-shaped magnetotactic *Nitrospirae*, with hundreds bullet-shaped magnetite magnetosomes per cell, under the influence of a magnetic field. The authors have developed the first mathematical model to describe both the magnetotactic motion and orientation of this rod-shaped bacterium.

Three articles deal with the mechanisms of magnetosome biomineralization. Rahn-Lee and Komeili (2013) summarize the recent advances in the molecular mechanisms of magnetosome synthesis and discuss their implications for understanding bacterial intracellular biomineralization in general. Arnoux et al. (2014) focus on those magnetosome-associated proteins containing a *c*-type cytochrome domain. The authors evaluate the evolution of these proteins, and a model is proposed, which offers a different perspective on the evolution of magnetosome formation. Through bioinformatics approaches, Nudelman and Zarivach (2014) perform 3D structural predictions of all known magnetosome-associated proteins in *Magnetospirillum gryphiswaldense* strain MSR-1. Their results propose a comprehensive review of the functional features of biomineralization proteins.

Three papers explore the effects of environmental factors on magnetosome formation and their implications for the ancient environment. Moisescu et al. (2014) review the recent advances in understanding the effects of chemical and physical factors on magnetosome synthesis. They also discuss the potential of magnetosomes as biomarkers for ancient life and the role of MTB in iron cycling. The study by Wang et al. (2013) focuses on the influence of ultraviolet-B radiation on *Magnetospirillum magneticum* strain AMB-1. The authors note that ultraviolet-B radiation could affect both cell growth and magnetite synthesis, and suggest that magnetosomes may have evolutionary benefits for the survival of MTB under extreme environments. A paleo- and rock-magnetic study of marine sediments from the Guadalquivir Basin, Spain by Larrasoña et al. (2014) reveals dominance of fossil magnetosome chains in sediments. Their results indicate that

fossil magnetosomes could provide important paleomagnetic and paleoenvironmental information.

Finally, the articles by Xu et al. (2014) and Yang et al. (2013) focus on the production and application of magnetosomes from *Magnetospirillum gryphiswaldense* strain MSR-1. Xu et al. (2014) report the expression of staphylococcal protein A on the surface of extracted magnetosomes. These functionalized magnetosomes are capable of efficiently detecting pathogenic *Vibrio parahaemolyticus*. Yang et al. (2013) perform experiments with a large-scale culture of *M. gryphiswaldense* and identify the key time point for cell growth as well as magnetosome formation. The high-yield production achieved in their study suggests great opportunities for further applications of magnetite magnetosomes in various commercial fields.

We are very grateful to all the authors for their contributions and to all of the reviewers involved in processing these papers. We hope that this research topic will provide an in-depth exploration of microbial biomineralization and stimulate new investigators and more questions within this fascinating field.

REFERENCES

- Arnoux, P., Siponen, M. I., Lefèvre, C. T., Ginet, N., and Pignol, D. (2014). Structure and evolution of the magnetochrome domains: no longer alone. *Front. Microbiol.* 5:117. doi: 10.3389/fmicb.2014.00117
- Kong, D., Lin, W., Pan, Y., and Zhang, K. (2014). Swimming motion of rod-shaped magnetotactic bacteria: the effects of shape and growing magnetic moment. *Front. Microbiol.* 5:8. doi: 10.3389/fmicb.2014.00008
- Larrasoña, J. C., Liu, Q., Hu, P., Roberts, A. P., Mata, P., Civis, J. et al. (2014). Paleomagnetic and paleoenvironmental implications of magnetofossil occurrences in late Miocene marine sediments from the Guadalquivir Basin, SW Spain. *Front. Microbiol.* 5:71. doi: 10.3389/fmicb.2014.00071
- Moisescu, C., Ardelean, I., and Benning, L. G. (2014). The effect and role of environmental conditions on magnetosome synthesis. *Front. Microbiol.* 5:49. doi: 10.3389/fmicb.2014.00049
- Morillo, V., Abreu, F., Araujo, A. C., Almeida, L. G. P. D., Prast, A. E., Farina, M., et al. (2014). Isolation, cultivation and genomic analysis of magnetosome biomineralization genes of a new genus of South-seeking magnetotactic cocci within the *Alphaproteobacteria*. *Front. Microbiol.* 5:72. doi: 10.3389/fmicb.2014.00072
- Nudelman, H., and Zarivach, R. (2014). Structure prediction of magnetosome-associated proteins. *Front. Microbiol.* 5:9. doi: 10.3389/fmicb.2014.00009
- Oestreicher, Z., Lower, S. K., Rees, E., Bazylinski, D. A., and Lower, B. H. (2013). Magnetotactic bacteria from Pavilion Lake, British Columbia. *Front. Microbiol.* 4:406. doi: 10.3389/fmicb.2013.00406
- Pósfai, M., Lefèvre, C., Trubitsyn, D., Bazylinski, D. A., and Frankel, R. (2013). Phylogenetic significance of composition and crystal morphology of magnetosome minerals. *Front. Microbiol.* 4:344. doi: 10.3389/fmicb.2013.00344
- Rahn-Lee, L., and Komeili, A. (2013). The magnetosome model: insights into the mechanisms of bacterial biomineralization. *Front. Microbiol.* 4:352. doi: 10.3389/fmicb.2013.00352
- Wang, Y., Lin, W., Li, J., and Pan, Y. (2013). Changes of cell growth and magnetosome biomineralization in *Magnetospirillum magneticum* AMB-1 after ultraviolet-B irradiation. *Front. Microbiol.* 4:397. doi: 10.3389/fmicb.2013.00397
- Xu, J., Hu, J., Liu, L., Li, L., Wang, X., Zhang, H., et al. (2014). Surface expression of protein A on magnetosomes and capture of pathogenic bacteria by magnetosome/antibody complexes. *Front. Microbiol.* 5:136. doi: 10.3389/fmicb.2014.00136
- Yang, J., Li, S., Huang, X., Tang, T., Jiang, W., Zhang, T., et al. (2013). A key time point for cell growth and magnetosome synthesis of *Magnetospirillum gryphiswaldense* based on real-time analysis of physiological factors. *Front. Microbiol.* 4:210. doi: 10.3389/fmicb.2013.00210

Conflict of Interest Statement: The authors declare that the research was conducted in the absence of any commercial or financial relationships that could be construed as a potential conflict of interest.

Received: 14 May 2014; accepted: 28 May 2014; published online: 12 June 2014.

Citation: Lin W, Benzerara K, Faivre D and Pan Y (2014) Intracellular biomineralization in bacteria. *Front. Microbiol.* 5:293. doi: 10.3389/fmicb.2014.00293

This article was submitted to Aquatic Microbiology, a section of the journal *Frontiers in Microbiology*.

Copyright © 2014 Lin, Benzerara, Faivre and Pan. This is an open-access article distributed under the terms of the Creative Commons Attribution License (CC BY). The use, distribution or reproduction in other forums is permitted, provided the original author(s) or licensor are credited and that the original publication in this journal is cited, in accordance with accepted academic practice. No use, distribution or reproduction is permitted which does not comply with these terms.



Phylogenetic significance of composition and crystal morphology of magnetosome minerals

Mihály Pósfai¹, Christopher T. Lefèvre², Denis Trubitsyn³, Dennis A. Bazylinski³ and Richard B. Frankel^{4*}

¹ Department of Earth and Environmental Sciences, University of Pannonia, Veszprém, Hungary

² Laboratoire de Bioénergétique Cellulaire, Biologie Végétale et Microbiologie Environnementales, CEA/CNRS/Aix-Marseille Université, Saint Paul lez Durance, France

³ School of Life Sciences, University of Nevada at Las Vegas, Las Vegas, NV, USA

⁴ Department of Physics, California Polytechnic State University, San Luis Obispo, CA, USA

Edited by:

Wei Lin, Chinese Academy of Sciences, China

Reviewed by:

Ulysses Lins, Universidade Federal do Rio de Janeiro, Brazil

Arash Komeili, University of California, Berkeley, USA

***Correspondence:**

Richard B. Frankel, Department of Physics, California Polytechnic State University, 1 Grand Avenue, San Luis Obispo, CA 93407, USA
e-mail: rfrankel@calpoly.edu

INTRODUCTION

All magnetotactic bacteria (MTB) contain magnetosomes comprising nano-scale, magnetite (Fe_3O_4) or greigite (Fe_3S_4) crystals enclosed in phospholipid bilayer membranes (Gorby et al., 1988; Bazylinski and Frankel, 2004). The magnetosomes constitute a permanent magnetic dipole moment in the cell, and are essential for magnetotaxis. The magnetosome membrane is derived by invagination of the cytoplasmic membrane (Komeili et al., 2004) and is the locus of biological control over the nucleation and growth of the mineral crystal. Most MTB species or strains exclusively produce either magnetite (Frankel et al., 1979) or greigite magnetosomes (Mann et al., 1990), although several MTB can produce magnetosomes of both kinds, depending on environmental conditions (Bazylinski et al., 1993; Kasama et al., 2006; Lins et al., 2007; Lefèvre et al., 2011c; Wang et al., 2013).

The crystal size, crystallographic orientation and arrangement of magnetosomes in MTB are all highly significant for the magnetic properties of the cell (Frankel and Blakemore, 1980; Mann et al., 1984a,b; Moskowitz et al., 1988; Bazylinski and Frankel, 2003). With a few exceptions, the lengths of individual magnetosome crystals range from about 35 to 120 nm (Devouard et al., 1998) (Table 1); this is within the permanent single-magnetic-domain (SD) size range for both minerals (Butler and Banerjee, 1975). In the majority of MTB, the magnetosomes are organized in one or more straight chains of various lengths, parallel to the axis of motility of the cell. In cells of some species, however, there are multiple individual chains or a chain with multiple strands (Vali and Kirschvink, 1991) or even dispersed aggregates or clusters of magnetosomes that occur in some magnetotactic cocci (Towe and Moench, 1981; Cox et al., 2002; Zhang et al., 2012).

Magnetotactic bacteria (MTB) biominerlize magnetosomes, nano-scale crystals of magnetite or greigite in membrane enclosures that comprise a permanent magnetic dipole in each cell. MTB control the mineral composition, habit, size, and crystallographic orientation of the magnetosomes, as well as their arrangement within the cell. Studies involving magnetosomes that contain mineral and biological phases require multidisciplinary efforts. Here we use crystallographic, genomic and phylogenetic perspectives to review the correlations between magnetosome mineral habits and the phylogenetic affiliations of MTB, and show that these correlations have important implications for the evolution of magnetosome synthesis, and thus magnetotaxis.

Keywords: magnetotactic bacteria, magnetite, greigite, magnetosomes, morphology, biominerlization, evolution

When magnetosomes are arranged in chains, magnetic interactions between them cause their magnetic moments to orient parallel to each other along the chain axis (Frankel and Blakemore, 1980; Frankel, 1984), resulting in a permanent, magnetic dipole. The permanent magnetism of magnetosome chains has been demonstrated by electron holography in the electron microscope (Dunin-Borkowski et al., 1998), by pulsed magnetic field remanence measurements on individual cells (Penninga et al., 1995; Hanzlik et al., 2002) and by magnetic imaging directly in living cells (Le Sage et al., 2013).

The magnetosome membrane originates from the cytoplasmic membrane and contains unique proteins that are not present in the cytoplasmic or outer membranes (Komeili, 2012). These proteins, specific to MTB, are designated with the prefix Mam or Mms, although some are not found in every species of MTB. The Mms proteins in particular are present only in certain phylogenetic groups of MTB. While not all Mam proteins are found in the magnetosome membrane, all Mms proteins are. The Mam and Mms proteins are thought to be responsible for biominerlization of the magnetosome crystal, the organization of the magnetosome chain, and the crystallographic orientation of the individual magnetosomes with respect to the chain (Komeili, 2012). The roles of relatively few of the magnetosome membrane proteins have been elucidated (Jogler and Schüler, 2009; Murat et al., 2010; Lohsse et al., 2011; Uebe et al., 2011; Komeili, 2012).

All known MTB are phylogenetically affiliated with the *Alpha*-, *Delta*- or *Gammaproteobacteria* classes of the *Proteobacteria* phylum, the *Nitrospirae* phylum or the candidate division OP3 which is part of the *Planctomycetes–Verrucomicrobia–Chlamydiae* (PVC) bacterial superphylum (Lefèvre and Bazylinski, 2013) (Table 1).

Table 1 | Bibliographic listing of magnetotactic bacteria characterized and the composition and morphology of their magnetosome crystals analyzed.

Magnetosome mineral	Strain	Phylogenetic affiliation	Habit	Magnetosome elongation axis	TEM technique of morphology determination*	Average crystal length (nm)	Shape factor (width/length)	References
Magnetite <i>Magnetospirillum magnetotacticum</i> strain MS-1		<i>Alpha-proteobacteria</i>	cubooctahedral	**	Single-projection BF, SAED, HRTEM, EH, BF ET	43	0.9	Devouard et al., 1998; Buseck et al., 2001; Kobayashi et al., 2006
Magnetite <i>Magnetospirillum magneticum</i> strain AMB-1		<i>Alpha-proteobacteria</i>	cubooctahedral	**	Single-projection BF, SAED, HRTEM	45	0.85	Li et al., 2009
Magnetite <i>Magnetospirillum gryphiswaldense</i> strain MSR-1		<i>Alpha-proteobacteria</i>	cubooctahedral	**	Multi-projection BF, SAED, HRTEM, BF ET	33	0.91	Scheffel et al., 2006; Faivre et al., 2008
Magnetite <i>Magnetospira thiophila</i> strain MMS-1 (MV-4)		<i>Alpha-proteobacteria</i>	elongated, octahedral	[111]	Single-projection BF, SAED, HRTEM	22–85	0.85	Meldrum et al., 1993a; Devouard et al., 1998
Magnetite <i>Magnetovibrio blakemorei</i> strain MV-1		<i>Alpha-proteobacteria</i>	elongated, octahedral	[111]	Multi-projection BF, SAED, HRTEM, HAADF ET	60	0.65	Meldrum et al., 1993a; Devouard et al., 1998; Thomas-Kepita et al., 2001; Clemett et al., 2002
Magnetite <i>Magnetovibrio blakemorei</i> strain MV-2		<i>Alpha-proteobacteria</i>	elongated, prismatic	[111]	Single-projection BF, SAED, HRTEM	30–59	0.54	Meldrum et al., 1993a
Magnetite <i>Magnetococcus marinus</i> strain MC-1		<i>Alpha-proteobacteria</i>	octahedral, elongated	[111]	Single-projection BF	30–110	0.93	Meldrum et al., 1993b; Devouard et al., 1998
Magnetite Strain MC-2		<i>Alpha-proteobacteria</i>	octahedral, elongated	ND	Single-projection BF, SAED, HRTEM	30–120	0.85	Devouard et al., 1998
Magnetite <i>Candidatus Magnetococcus yuannducum</i> strain YDC-1		<i>Alpha-proteobacteria</i>	elongated, prismatic	ND	Single-projection BF	108	0.64	Lin and Pan, 2009
Magnetite Strain MO-1		<i>Alpha-proteobacteria</i>	octahedral, elongated	ND	Single-projection BF	64	0.89	Lefèvre et al., 2009
Magnetite QH-2		<i>Alpha-proteobacteria</i>	octahedral, elongated	ND	Single-projection BF	81	0.71	Zhu et al., 2010

(Continued)

Table 1 | Continued

Magnetosome mineral	Strain	Phylogenetic affiliation	Habit	Magnetosome elongation axis	TEM technique of morphology determination*	Average crystal length (nm)	Shape factor (width/length)	References
Magnetite uncultured coccus Itaiju-I	ND	elongated, prismatic	[111]	Multi-projection BF, SAED, HRTEM, EH	210	0.9	Lins et al., 2005	
Magnetite uncultured coccus Itaiju-II	ND	elongated, prismatic	[111]	Multi-projection BF, SAED, HRTEM, EH	130	0.6	Lins et al., 2005	
Magnetite uncultured coccus	ND	elongated, prismatic	[111]	Multi-projection BF, SAED, HRTEM, HAADF ET	< 80	0.88	Simpson et al., 2005	
Magnetite uncultured coccus	ND	elongated, prismatic	ND	HAADF ET	ND	ND	Bussek et al., 2001	
Magnetite Strain BW-2	Gamma- <i>proteobacteria</i>	octahedral	ND	Single-projection BF	67	0.94	Lefèvre et al., 2012	
Magnetite Strain SS-5	Gamma- <i>proteobacteria</i>	octahedral, elongated	[111]	Single-projection BF, SAED, HRTEM	86	0.75	Lefèvre et al., 2012	
Magnetite Strain ZZ-1	<i>Delta-proteobacteria</i>	elongated, bullet, dts1	ND	Single-projection BF	84***	0.44***	Lefèvre et al., 2011b	
Magnetite Strain ML1	<i>Delta-proteobacteria</i>	elongated, bullet, dts1	ND	Single-projection BF	ND	ND	Lefèvre et al., 2011b	
Magnetite Strain AV-1	<i>Delta-proteobacteria</i>	elongated, bullet, dts1	[100]	Multi-projection BF, SAED, HRTEM	30–120	0.45	Lefèvre et al., 2011d	
Magnetite <i>Desulfobacter magneticus</i> strain RS-1	<i>Delta-proteobacteria</i>	elongated, bullet	[100]	Multi-projection BF, SAED, HRTEM, BF ET	40	0.5	Sakaguchi et al., 1993; Pósfai et al., 2006	
Magnetite Ca. Desulfamplus magnetomoritis strain BW-1	<i>Delta-proteobacteria</i>	elongated, bullet	ND	Multi-projection BF, SAED, HRTEM	55***	0.6***	Lefèvre et al., 2011c	
Magnetite Uncultured Multicellular	<i>Delta-proteobacteria</i>	elongated, bullet, dts1	[100]	Single-projection BF, SAED, HRTEM	104	0.4	Keim et al., 2007	
Magnetite Ca. Magnetananas tsingtaoensis	<i>Delta-proteobacteria</i>	elongated, bullet	ND	Single-projection BF	102	0.37	Zhou et al., 2012	

(Continued)

Table 1 | Continued

Magnetosome mineral	Strain	Phylogenetic affiliation	Habit	Magnetosome elongation axis	TEM technique of morphology determination*	Average crystal length (nm)	Shape factor (width/length)	References
Magnetite	<i>Ca.</i> Magnetobacterium bavaricum	<i>Nitrospirae</i>	elongated, bullet	ND	Single-projection BF	110–150	ND	Spring et al., 1993
Magnetite	Strain MHB-1	<i>Nitrospirae</i>	elongated, bullet	ND	Single-projection BF	119***	0.35***	Fries et al., 2005
Magnetite	Strain MYR-1	<i>Nitrospirae</i>	elongated, bullet	[100]	Multi-projection BF, SAED, HRTEM	104	0.36	Li et al., 2010
Magnetite	Strain MWB-1	<i>Nitrospirae</i>	elongated, bullet	ND	Single-projection BF	116	0.35	Lin et al., 2012
Magnetite	<i>Ca.</i> Magnetovulum mohavensis strain LO-1	<i>Nitrospirae</i>	elongated, bullet, fts ²	[110]	Multi-projection BF, SAED, HRTEM	70–200	0.36	Lefèvre et al., 2011a,d
Magnetite	<i>Ca.</i> Thermomagnetovibrio palutensis strain HSMV-1	<i>Nitrospirae</i>	elongated, bullet, fts ²	[110]	Multi-projection BF, SAED, HRTEM	30–220	0.45	Lefèvre et al., 2010, 2011d
Magnetite	Strain SKK-01	Candidate division OP3	elongated, bullet	ND	Single-projection BF	110	0.34	Kolinko et al., 2012
Greigite	Uncultured MMP	<i>Delta</i> -proteobacteria	equidimensional, irregular; elongated, irregular	** and [100]	Multi-projection BF, SAED, HRTEM	60–90	0.86***	Pósfai et al., 1998a,b
Greigite	<i>Ca.</i> Desulfamplus magnetomortis strain BW-1	<i>Delta</i> -proteobacteria	equidimensional, irregular	ND	Multi-projection BF, SAED, HRTEM	33***	0.96***	Lefèvre et al., 2011c
Greigite	Uncultured rods	ND	equidimensional, irregular	** and [100]	HAADF ET	60	0.9	Kasama et al., 2006
Greigite	<i>Ca.</i> Magnetomorium litorale	<i>Delta</i> -proteobacteria	elongated, bullet	ND	Single-projection BF	91	0.44	Wenter et al., 2009

*BF, bright-field; SAED, selected-area electron diffraction; HRTEM, high-resolution transmission electron microscopy; HAADF, high-angle annular dark-field, ND, not determined. **These crystals are equidimensional, therefore there is no elongation. ***Estimated from published TEM micrographs in appropriate references. ¹sts, double triangle shape; ²fts, flat top shape.

While magnetite-producing MTB occur in all five taxa, greigite-producing bacteria are restricted to a particular clade of sulfate-reducing bacteria in the *Deltaproteobacteria* (Lefèvre et al., 2011c; Lefèvre and Bazylinski, 2013).

A compelling feature of magnetosome magnetite crystals is that they have species-specific, two-dimensional projected shapes when observed in an electron microscope (Figure 1). This implies that, in addition to size, orientation and arrangement, the magnetosome membrane proteins control the morphology of the magnetosome crystals.

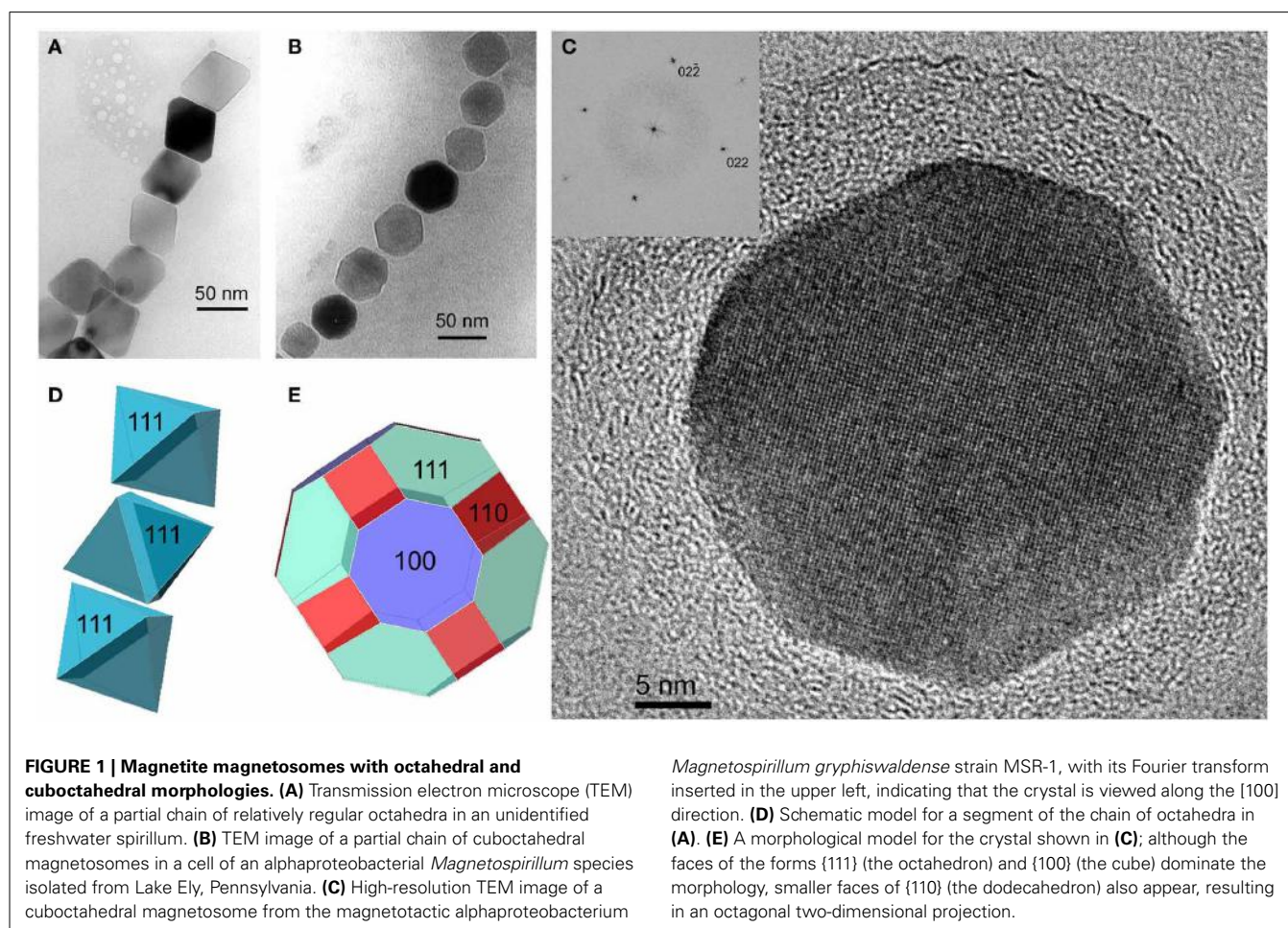
In the past decade, a fortuitous confluence of advances in electron microscopy, increasing success in the axenic cultivation of MTB from diverse environments, and the availability of facilities for rapid sequencing of bacterial genomes, have revealed a relationship between magnetosome crystal composition and morphology and the phylogenetic affiliations of MTB. In this review we describe this relationship and also discuss the implications for the evolutionary history of magnetosome formation and magnetotaxis.

EXPERIMENTAL DETERMINATION OF CRYSTAL MORPHOLOGY

Two-dimensional projections of magnetosomes in bright-field (BF) transmission electron microscopy (TEM) images have been

used for the approximate evaluation of magnetosome morphologies (Matsuda et al., 1983; Mann et al., 1987a,b; Meldrum et al., 1993a,b; Devouard et al., 1998). However, without information about the thickness profile of each crystal, it is difficult to determine 3-dimensional (3D) habits from 2D images. For an unambiguous identification of magnetosome morphologies, it is necessary to tilt the specimen in order to obtain images along several projection directions (Pósfai et al., 2013). By taking into account constraints resulting from the known point group of magnetite, the morphologies of the crystals can be better interpreted and modeled (Lefèvre et al., 2011d). If multi-projection magnetosome outlines are complemented by selected-area electron diffraction (SAED) patterns and high-resolution (HR) TEM images obtained along certain crystallographic directions, the exact relationship between crystal morphology and internal structure can be established (Simpson et al., 2005; Pósfai et al., 2006; Faivre et al., 2008; Li et al., 2010; Lefèvre et al., 2011d).

The ultimate solution for obtaining the precise 3D morphologies of nanocrystals is provided by electron tomography (ET) (Pósfai et al., 2013). The technique is based on large numbers of images acquired as a function of specimen tilt angle, followed by 3D reconstruction and visualization. However, crystalline materials, including the minerals within magnetosomes, can exhibit strong diffraction contrast in BF TEM images. In such cases the



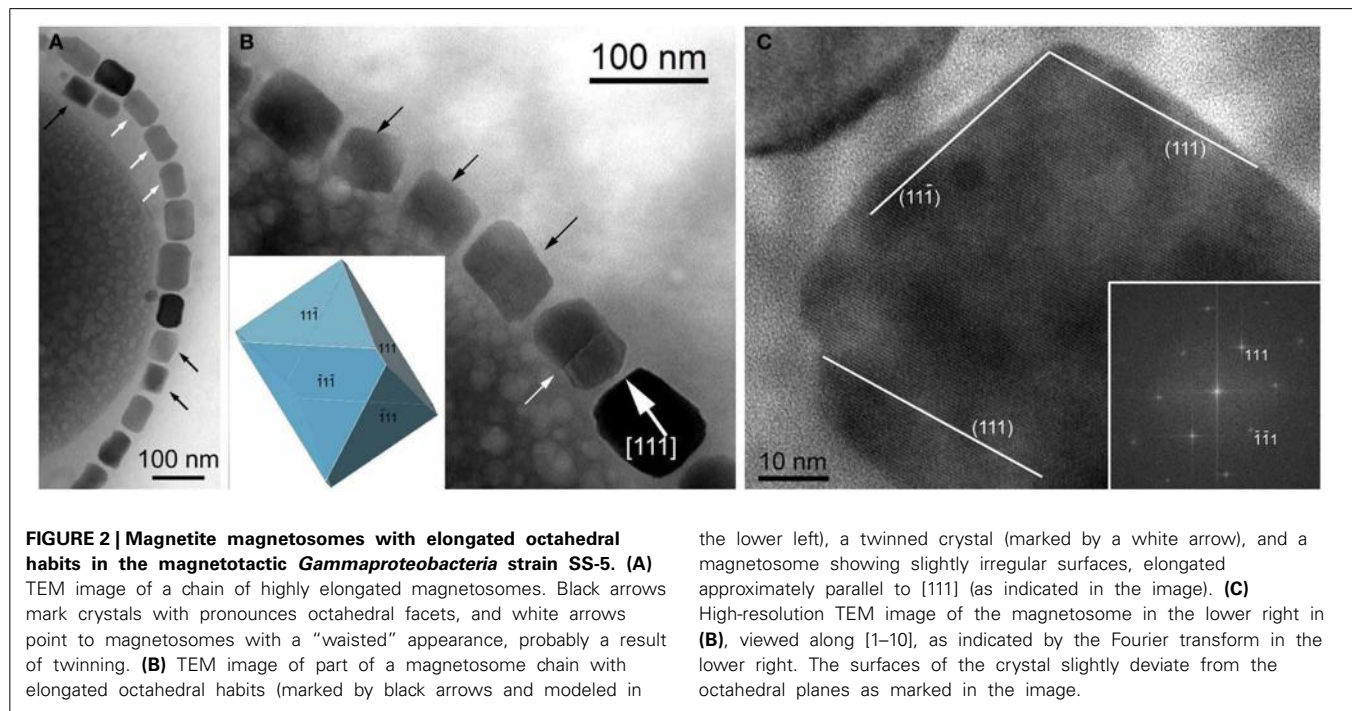
intense diffracted beams are excluded from image formation, resulting in images in which the contrast is no longer dominated by variations in specimen thickness and density. A solution to this problem is provided by the acquisition of tilt series of high-angle annular dark-field (HAADF) images using a scanning transmission electron microscope (Midgley and Weyland, 2011). A HAADF detector collects electrons that are scattered at relatively large angles and are typically unaffected by the crystallography of the sample. Therefore, the contrast in HAADF images is directly related to the thickness of the material that the electron beam passed through, provided that the sample is homogeneous. HAADF ET has been used for the characterization of the morphologies of magnetite crystals from several strains of MTB (Table 1) (Buseck et al., 2001; Thomas-Keppta et al., 2001; Clemett et al., 2002; Kasama et al., 2006). A rarely used but possible alternative to ET is to obtain thickness information using electron holography for the reconstruction of 3D magnetosome morphologies (Lins et al., 2005).

MAGNETITE MAGNETOSOME CRYSTALS

The minerals magnetite and greigite are isostructural, with face-centered cubic, inverse-spinel crystal structures ($Fd\bar{3}m$ space group) (Palache et al., 1944). Three idealized habits based on the low-index forms {100}, {110}, and {111} have been described for magnetite crystals in magnetosomes. These include equidimensional [octahedra and cuboctahedra, a morphology with faces of the {100} (cube) and {111} (octahedron)]; elongated-prismatic; and elongated-anisotropic (Lefèvre et al., 2011d) (Table 1). The cuboctahedral crystal morphology, with six equivalent faces of the form {100} and eight equivalent faces of the form {111}, preserves the symmetry of the cubic crystal system and is considered close to the equilibrium growth form of magnetite (Mann and Frankel,

1989; Devouard et al., 1998) (Figure 1). Elongated octahedral habits also occur in some strains (Figure 2). The elongated-prismatic crystals are cuboctahedra with enhanced growth parallel to one of the $\langle 111 \rangle$ axes. This causes the differential growth of some symmetry-related crystal faces and introduces faces of the form {110} (Figure 3). The growth of the elongated-anisotropic crystals appears to be more complex because this habit lacks a center of symmetry that represents a greater departure from equilibrium (Mann and Frankel, 1989; Li et al., 2010; Lefèvre et al., 2011d). The elongated-anisotropic crystals typically have high-index faces in addition to those of the three low-index forms described above, and can be further grouped into several subcategories depending on their elongation directions (Figures 4, 5).

Magnetotactic *Alpha-* and *Gammaproteobacteria* mineralize magnetite magnetosome crystals with cuboctahedral, elongated octahedral or elongated prismatic habits (Figures 1–3) (Mann et al., 1984a; Lefèvre et al., 2012). For instance, it was shown that MTB of the genus *Magnetospirillum* in the *Alphaproteobacteria* mineralize magnetosomes with cuboctahedral habits comprising {100} and {111} faces (Mann et al., 1984a,b). In other magnetotactic *Alphaproteobacteria*, including magnetotactic cocci and vibrios, the cuboctahedra are elongated parallel to the [111] crystal axis that is oriented parallel to the chain axis. Crystal elongation parallel to [111] results in a non-equidimensional crystal habit with two groups of six {110} faces and two larger and six smaller {111} faces. The six {100} faces remain equidimensional. The result is a prism-like arrangement with a hexagonal cross-section perpendicular to [111] through the center of the crystal (Figure 3) (Towe and Moench, 1981; Meldrum et al., 1993a,b). The remaining faces form corner facets at the intersections between the body {110} and end-cap {111} faces (Figure 3E). The sizes of the crystals, the width/length ratios, and the relative sizes of the corner



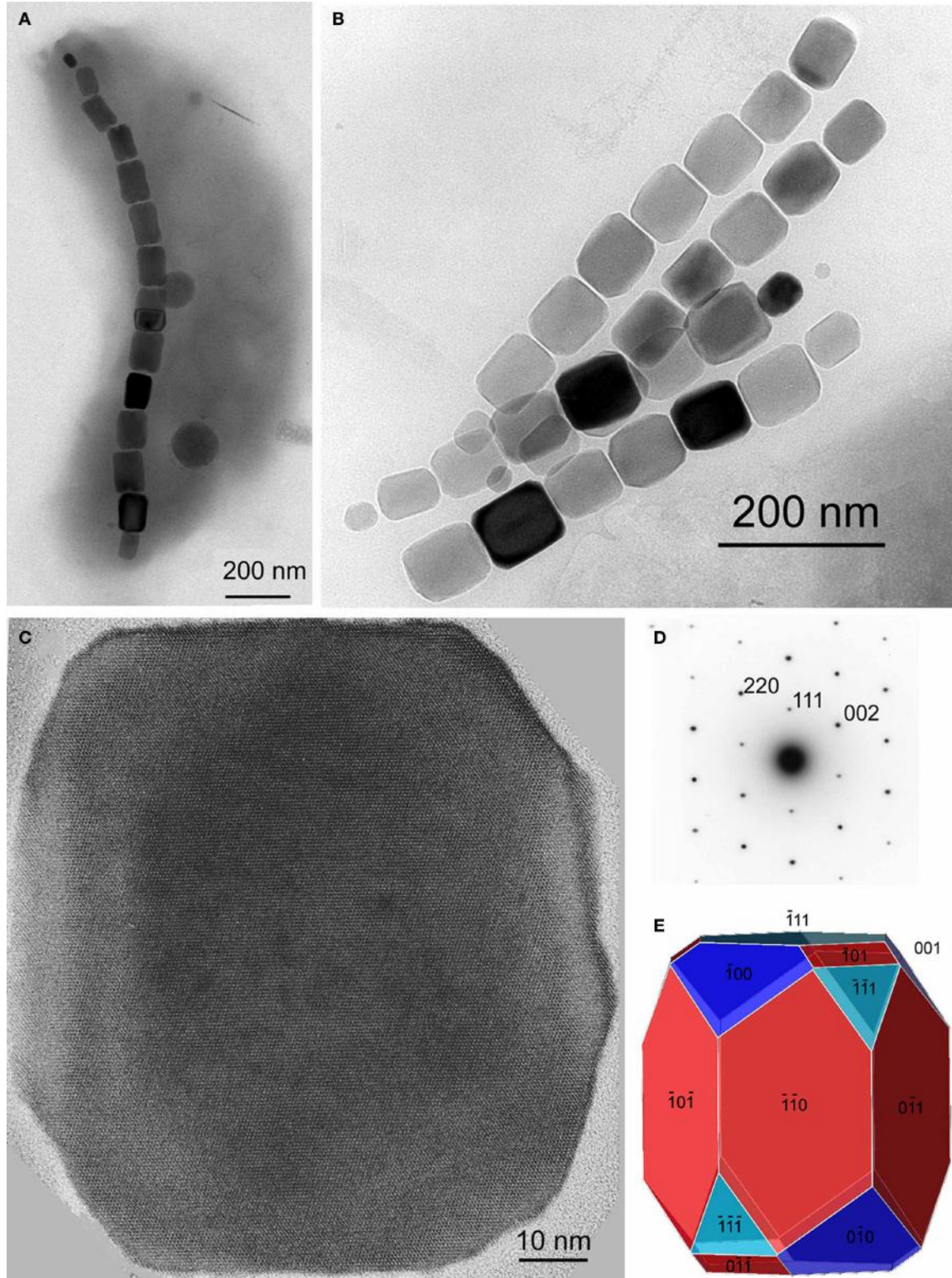


FIGURE 3 | Magnetite magnetosomes with elongated prismatic habits from magnetotactic *Alphaproteobacteria*. (A) TEM image of a cell of a vibrioid MTB from Lake Mead, Nevada, containing a chain of elongated magnetosomes. (B) TEM image of two double chains of elongated magnetosomes from a freshwater coccus. (C) High-resolution

TEM image of a magnetosome from a freshwater coccus with (D) its selected-area electron diffraction pattern (in [1-10] orientation) and (E) a morphological model that consists of six large and six small dodecahedral faces, and smaller faces of the cube and octahedron. The elongation direction is [111].

faces differ between species, resulting in the distinctive projected shapes.

Magnetosomes with elongated-anisotropic habits have been found in three phylogenetic groups of MTB: the *Deltaproteobacteria*, the *Nitrospirae* phylum and the candidate division OP3. The most common 2D projected image of elongated-anisotropic crystals is the bullet or flat-top shape (fts), with one flat end and one narrower, rounded, end (Blakemore et al., 1980; Mann et al., 1987a,b; Thornhill et al., 1994; Isambert et al., 2007) (**Figures 4A,B**). Sometimes the magnetosome crystals with fts projections are bent in one direction along their length (Hanzlik et al., 2002) (**Figure 4B**). Some elongated-anisotropic magnetosomes have distinctive projected images with a double-triangle shape (dts), two isosceles triangles sharing a common base (**Figure 4C**). These dts magnetosomes occur in some MTB phylogenetically affiliated with the *Nitrospirae* and with the *Deltaproteobacteria* (Vali and Kirschvink, 1991; Pósfai et al., 2006; Lins et al., 2007; Li et al., 2010; Lefèvre et al., 2011d). Both projected triangles have the same width, but in mature crystals one triangle is longer than the other.

In MTB of the *Alphaproteobacteria*, magnetosomes arranged in a chain are invariably oriented with a $<111>$ crystal axis parallel to the magnetosome chain axis (Mann et al., 1984a,b). In those strains with elongated-prismatic habits, the axis of elongation is the $<111>$ axis of orientation (Meldrum et al., 1993a,b) (**Table 1**). This is not the case for the elongated-anisotropic magnetosomes in MTB affiliated with either the *Nitrospirae* or the *Deltaproteobacteria* (Lefèvre et al., 2011d). While elongated-anisotropic magnetosomes are usually oriented with their long axes parallel to the chain axis, the axis of elongation can vary among the $<100>$, $<110>$, or $<111>$ axes (**Figures 4, 5**). Since the easy magnetization axis in magnetite is parallel to $<111>$, elongation along this direction maximizes the magnetic moment of the crystal because the directions of shape and magnetocrystalline anisotropies coincide. Therefore, the $<111>$ -elongations of magnetosomes could be interpreted as selected by evolution. However, no trivial explanation exists for the presence of $<100>$ and $<110>$ -type elongations which are highly unusual (or maybe even unknown) in inorganic magnetite crystals, and offer no functional advantage for magnetotaxis.

The elongated-anisotropic magnetosomes in the alkaliophilic dissimilatory sulfate-reducing *Deltaproteobacteria*, strain AV-1, and the freshwater *Nitrospirae* strain LO-1 have the following features: (i) the majority of magnetosome crystals have dts projected images and are single crystals without defects or twinning; a minority are strongly curved and comprise several crystallites that are not all in the same orientation; (ii) the habits of the dts magnetosomes can be modeled on the basis of a regular, or slightly elongated, half-octahedron (four-sided pyramid) as a base, and an elongated, pointed section that consists mostly of high-index faces. The curved outlines suggest that the surface of the elongated section cannot be completely described using Miller-indices; (iii) the axis of elongation of the dts magnetosomes is parallel to [100] (Lefèvre et al., 2011d) (**Figure 5B**).

The bent, elongated-anisotropic, fts magnetite magnetosomes in the moderately thermophilic *Nitrospirae* strain HSMV-1 have the following features: (i) the magnetosomes are highly elongated

and many of them are bent in one direction (hook shaped); (ii) from the analysis of high resolution images and their Fourier transforms the principal elongation axis is [110]; (iii) idealized morphological models have elongated “prismatic” side faces that are parallel to [110] and may include certain faces of the {100}, {111}, {110}, and {112} forms (**Figure 5A**). The narrow, rounded ends of the models consist of faces of the same forms (Lefèvre et al., 2011d). However, it should be noted that these crystals do not appear to be bound by well-developed, smooth, faces and instead, outlines of the crystals are irregular. Thus, any model of these crystals is just an approximation.

GREIGITE MAGNETOSOME CRYSTALS

The first reports on greigite-producing MTB were from samples collected in marine, estuarine, and salt marsh environments (Heywood et al., 1990; Mann et al., 1990). It is only recently that freshwater greigite-producing MTB were described (Lefèvre et al., 2011c; Wang et al., 2013). Only one MTB that synthesizes greigite magnetosomes, *Candidatus Desulfamplus magnetomortis*, is available in pure culture (Lefèvre et al., 2011c). Recognized greigite-producing MTB include the magnetotactic multicellular prokaryotes (MMP) (Farina et al., 1990; Mann et al., 1990) and a variety of relatively large, rod-shaped bacteria (Heywood et al., 1990; Lefèvre et al., 2011c). Like magnetite crystals in magnetosomes, the morphologies of the greigite crystals also appear to be species-and/or strain-specific (Heywood et al., 1991).

While greigite is common in all MTB containing iron sulfide magnetosomes, mackinawite (tetragonal FeS), and tentatively, sphalerite-type cubic FeS were also identified in some (Pósfai et al., 1998a,b). Mackinawite is known to convert to greigite over time under reducing sulfidic conditions (Pósfai et al., 1998b). Orientation relationships between the two minerals indicate that the cubic close-packed S substructure remains unchanged during the transformation; only the Fe atoms rearrange. Planar defects typically occur along the close-packed layers of greigite crystals; such defects indicate that all greigite crystals formed by solid-state transformation from mackinawite or cubic FeS.

In most cases neither the orientations, nor the morphologies of greigite crystals are as strictly controlled as those of magnetite magnetosomes, resulting in fairly disordered chains of irregularly-shaped crystals (Kasama et al., 2006). The habits of greigite magnetosomes are either equidimensional, with irregularly-shaped surfaces that lack clear facets, or slightly elongated parallel to [100]. Since the easy magnetization axis in greigite is thought to be [100] (Hoffmann, 1992), this elongation maximizes the magnetic moment of the crystal. Since all known greigite-producing organisms are affiliated with *Deltaproteobacteria* class, and little information is available on greigite morphologies, further analysis of possible relationships between magnetosome morphologies and the systematics of greigite-producing bacteria appears to be premature.

BIOLOGICAL CONTROL OF MAGNETOSOME MINERALIZATION

The production of magnetite and greigite crystals is under strict genetic control by MTB. The genes encoding the Mam proteins responsible for magnetosome formation are reasonably

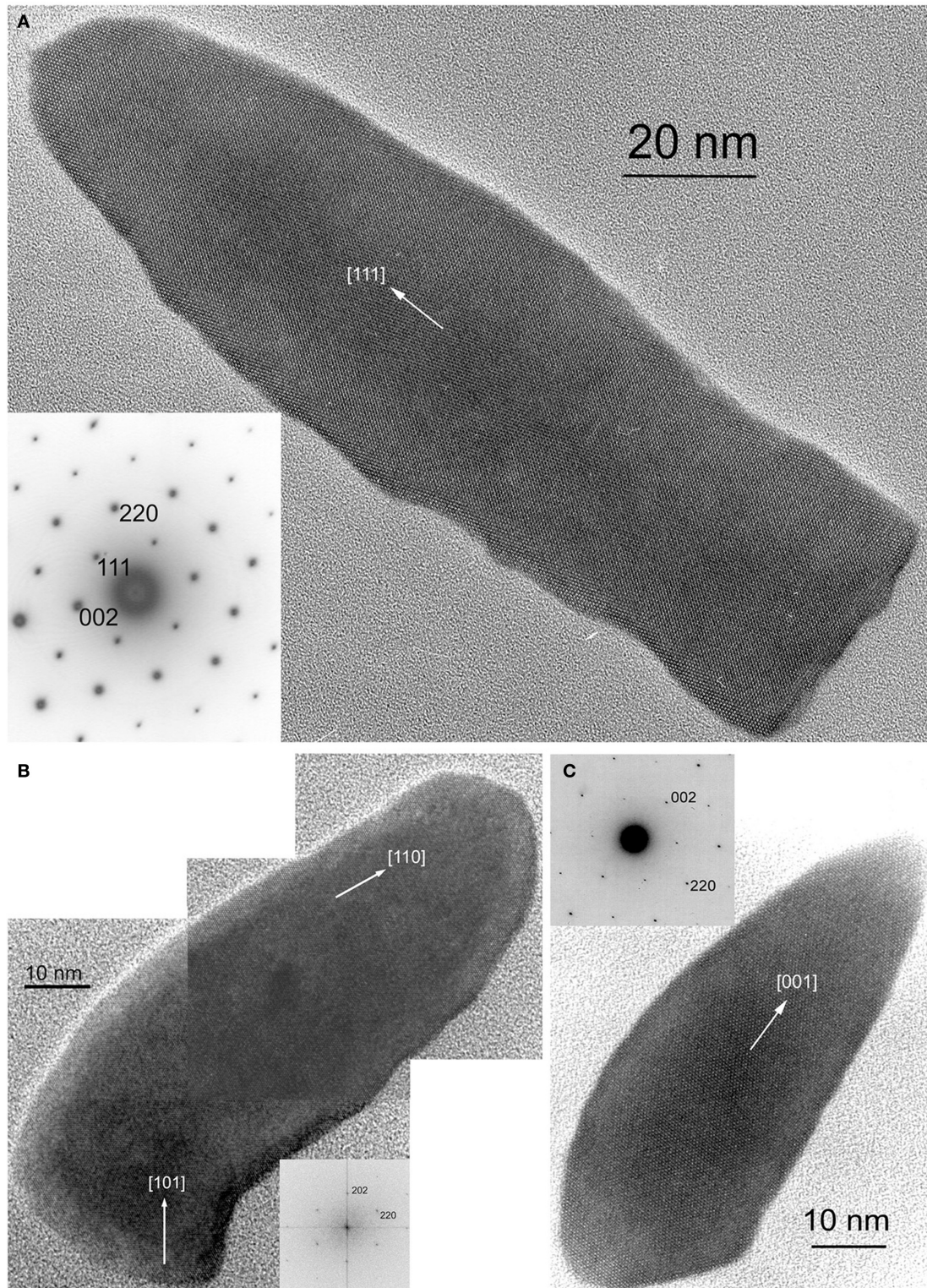
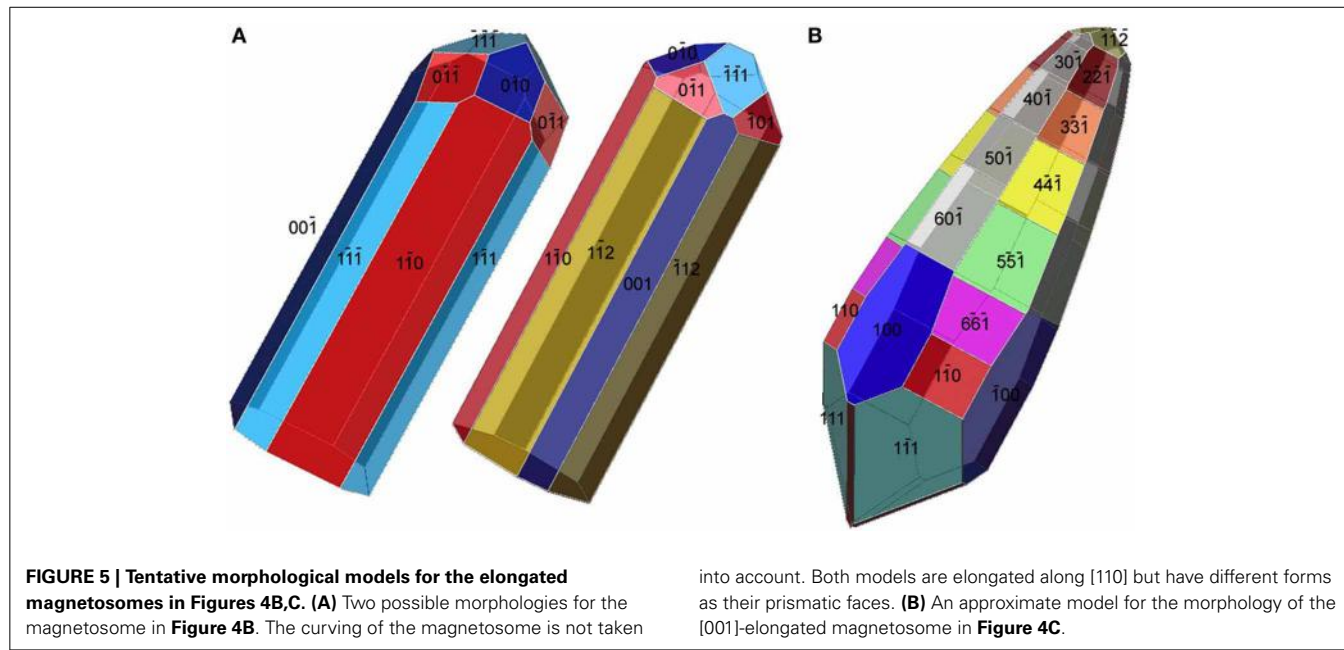


FIGURE 4 | HRTEM images of magnetite magnetosomes with highly anisotropic, elongated, pointed habits but different elongation directions. **(A)** A magnetosome from an unidentified freshwater rod, elongated parallel to [111], with the corresponding selected area electron diffraction (SAED) pattern in the lower left. **(B)** A composite image of a curved, fts magnetosome from the magnetotactic

Nitrospirae strain HSMV-1, elongated parallel to [110], with the corresponding Fourier transform in the lower right. **(C)** A dts magnetosome form the magnetotactic *Delta proteobacteria* strain AV-1, elongated parallel to [001], with the corresponding SAED pattern in the upper left. All three images were obtained with the electron beam parallel to [1-10].



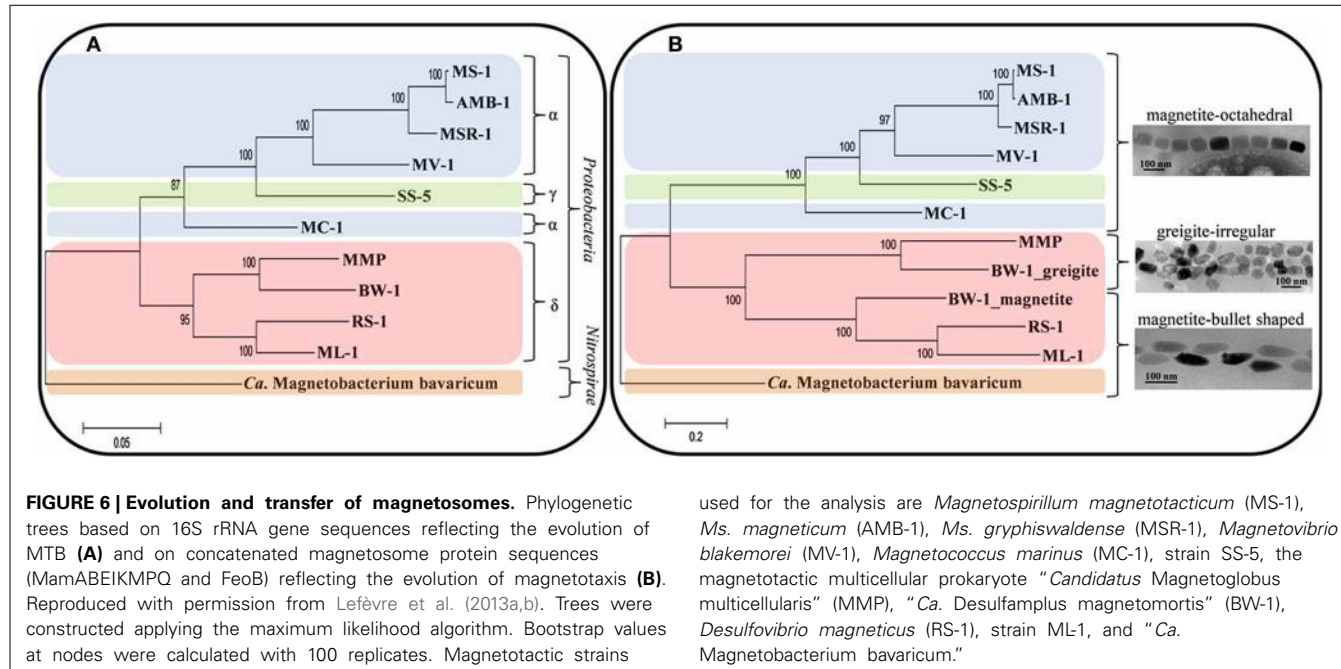
conserved, with some exceptions, and are located as clusters in close proximity within the genomes of all MTB that have been sequenced (Grünberg et al., 2001; Matsunaga et al., 2005; Jogler and Schüler, 2009; Jogler et al., 2009, 2011; Nakazawa et al., 2009; Schübbe et al., 2009; Abreu et al., 2011; Komeili, 2012; Ji et al., 2013; Lefèvre et al., 2013b). In the genomes of some MTB, the clusters are flanked, and occasionally interrupted, by genomic elements characteristic of a “genomic island” (e.g. transposases, insertion sequences, t-RNA genes); hence the name “magnetosome gene island (MAI)” (Schübbe et al., 2003; Ullrich et al., 2005). The similar organization of the MAI in the genomes of different MTB is the basis for the suggestion that the MAI might have been acquired by different bacterial species via horizontal gene transfer, thereby explaining the great diversity of the group and the apparent polyphyletic trait of magnetotaxis (DeLong et al., 1993). However, recent genomic and phylogenetic studies suggest a monophyletic model in which *mam* genes were acquired by vertical descent from a common ancestor of all MTB (discussed in more detail below) (Lefèvre et al., 2013a).

The minimum set of *mam* genes necessary for magnetosome formation, initially recognized in the *Alphaproteobacteria* (Murat et al., 2010, 2012; Lohsse et al., 2011), is also present in the MTB from other phylogenetic affiliations (Lefèvre et al., 2013b). Ten genes (*mamABEIKLMOPQ*) are conserved in all magnetite-producing MTB while only nine of them, excluding *mamL*, appear to be conserved in the two greigite-producing MTB with their genomes sequenced (Abreu et al., 2011; Lefèvre et al., 2013b). In addition to this core of *mam* genes, other genes are present in the vicinity of the chromosomal region containing magnetosome genes. The *mms* genes and the *mamXY* and *mamGFDC* clusters are specific to the magnetotactic *Alphaproteobacteria*, whereas the *mad* genes are specific to and conserved within the *Deltaproteobacteria* class and the *Nitrospirae* phylum (Lefèvre et al., 2013b). Thus, despite the nine *mam* genes

that seem to be absolutely necessary for the formation of magnetite and greigite magnetosomes (vesicle formation, iron uptake, nucleation of the crystal and alignment of magnetosomes) other genes are also MTB-specific but only present in certain groups. These genes are likely involved in control of the crystal size, morphology and organization of the magnetosomes or potential functions related to magnetotaxis (e.g. aerotaxis) (Scheffel et al., 2008; Murat et al., 2010; Lohsse et al., 2011; Lefèvre et al., 2013b).

PHYLOGENETIC SIGNIFICANCE

If the magnetotactic trait was transferred between the different phylogenetic groups that contain MTB through horizontal gene transfer, we would expect to find all magnetosome crystal morphologies in the different groups of MTB. Indeed, the genetic information responsible for mineral type and morphology, although originating from a similar core of Mam proteins, is sufficiently variable to retrace the evolutionary history of the different morphological types. Recently, it was shown that phylogenetic trees based on Mam proteins, reflecting the evolution of magnetosomes, and the tree based on the 16S rRNA gene sequences, reflecting the evolution of MTB, are congruent (Lefèvre et al., 2013a) (Figure 6). This indicates that all MTB evolved from a common ancestor with magnetosome genes. Since the magnetosome genes appear to have been mainly transferred by descent with the accrual of variations over time, it is logical to expect a similar pattern of evolution between the 16S rRNA genes, the Mam proteins and the type of magnetosomes in the different species or strains of MTB (Figure 6). This new model of transfer of magnetosome formation by descent from a common ancestor to all MTB suggests that in the past all bacteria, magnetotactic or not, sharing a common ancestor with MTB (i.e., all the *Proteobacteria* and likely all the *Nitrospirae* and OP3 division) were capable of magnetosome formation, but many lost this capacity over time. Indeed, during evolution, *Proteobacteria* and



Nitrospirae diverged greatly in their ecophysiology. Thus, magnetosome formation likely became obsolete in most microorganisms of these phyla and the magnetotactic trait was lost through the loss of the magnetosome genes (Lefèvre and Wu, 2013).

As previously noted, magnetotactic *Alpha-* and *Gammaproteobacteria*, the later diverging classes of the *Proteobacteria*, biomimic magnetite that include cuboctahedral and elongated prisms (Devouard et al., 1998; Lefèvre et al., 2012) (Figures 1–3). All the elongations are parallel to <111>. In contrast, in the magnetotactic *Deltaproteobacteria*, the most deeply diverging group of the *Proteobacteria* that biomimic magnetite or greigite or both, the magnetite crystals are always bullet-shaped (Figure 4C). Greigite-producing MTB form a monophyletic clade in the *Deltaproteobacteria* class (Lefèvre et al., 2013a). The magnetotactic *Nitrospirae* and strain SKK-01 of the candidate division OP3, the most deeply branching phylogenetic groups that contain MTB (Jogler et al., 2011; Kolinko et al., 2012), are known to biomimic magnetite crystals whose morphologies are very similar, if not identical, to those found in the *Deltaproteobacteria* (Figure 4B) (Lefèvre et al., 2011d). Thus, there is a strong and important correlation between the morphology and the composition of the magnetosomes produced by MTB and their phylogenetic affiliation (Abreu et al., 2011; Jogler et al., 2011; Kolinko et al., 2012; Lefèvre et al., 2012, 2013a). Because MTB in the most deeply branching phylogenetic groups all have magnetite magnetosomes with similar, elongated-anisotropic habits, it has been suggested that the earliest magnetosome mineral phase in MTB was elongated-anisotropic magnetite (Lefèvre et al., 2013a).

The recent sequencing of the genomes of two greigite-bearing bacteria, *Ca. Magnetoglobus multicellularis* (Abreu et al., 2011) and *Ca. Desulfamplus magnetomortis* (Lefèvre et al., 2011c), gave genomic and phylogenetic evidence that the gene cluster responsible for greigite production emerged from duplication

and successive rearrangement of the gene cluster responsible for magnetite formation (Lefèvre et al., 2013b). This duplication likely led to the adaptation of MTB to highly reduced environments. Indeed, greigite producers are generally found in reduced environments with high concentrations of hydrogen sulfide in the sediments (Bazylinski et al., 1995; Lefèvre et al., 2011c). *Ca. Desulfamplus magnetomortis*, the only greigite producer in axenic culture that also produces magnetite, has two clusters of *mam* genes in its genome; one presumably involved in magnetite formation and the other in greigite formation. There is evidence that depending on environmental conditions, this bacterium preferentially mineralizes magnetite (high redox potential) or greigite (reduced conditions) (Lefèvre et al., 2011c, 2013b). In environmental studies of chemically-stratified coastal ponds, it was found that magnetite producers are mostly found at the oxic-anoxic interface (OAI) while greigite producers are found below the OAI, in a more reduced biotope (Bazylinski et al., 1995; Simmons et al., 2004). Thus, even if there is genetic control over the type of crystal mineralized in the magnetosome membrane, environmental parameters also play a role in the regulation of the chemical composition of the crystal. Since octahedral and anisotropic magnetite particles can be formed in microaerobic as well as in anaerobic conditions, it is not known if specific environmental conditions are required for their morphological differentiation.

MAGNETOSOMES IN EUKARYOTES?

A number of eukaryotes also appear to use magnetic fields for orientation, navigation, and homing, a process known as magnetoreception (Kirschvink et al., 2001). In some cases, magnetoreception appears to be due to the presence of magnetosomes or magnetosome-like structures that contain single magnetic domain crystals of magnetite as do most known MTB. These organisms include single-celled eukaryotes such as algae

and protists (Torres de Araujo et al., 1986; Bazylinski et al., 2000, 2012) and higher organisms such as the sockeye salmon, *Oncorhynchus nerka* (Mann et al., 1988) or the honey bee, *Apis mellifera* (Kuterbach et al., 1982). A key question regarding these organisms is how they obtained and built these structures.

The alga, discovered in brackish mud and water samples collected from a coastal mangrove swamp near Fortaleza, Brazil, was tentatively identified as *Anisonema platysomum* and exhibited magnetotaxis (Torres de Araujo et al., 1986). Cells contain numerous, well-organized chains of bullet-shaped magnetite crystals. Other magnetotactic protists have since been shown to contain magnetite crystals (Bazylinski et al., 2000). Thus, the origin of these putative “magnetosomes” in magnetotactic protists is an important question (Bazylinski et al., 2012). There appear to be two possibilities: the protists biomimic the magnetite crystals themselves or they ingest MTB and/or bacterial magnetosomes from lysed MTB cells and incorporate them either temporarily or permanently in the cell. Both scenarios seem to occur in nature. The arrangement of magnetosomes appears to be so precisely structured in the euglenoid alga described by Torres de Araujo et al. (1986), it seems likely that this organism biomimicizes and arranges endogenous magnetite crystals in a highly controlled fashion within the cell, where intracellular structural filaments play a significant role in the synthesis of the magnetosome chain, as has been shown for MTB (Komeili et al., 2006; Scheffel et al., 2006). For this arrangement to occur by ingesting MTB, significant numbers of MTB would have to be consumed and because the magnetite crystals are all bullet-shaped, the MTB would all have to be from specific phylogenetic groups (e.g. *Delta proteobacteria*), which seems implausible. Other magnetotactic protists, including dinoflagellates, biflagellates, and ciliates, contain magnetosomes that are not well-organized in the cell and thus probably ingest MTB and contain the bacterial magnetosomes for an undetermined amount of time (Bazylinski et al., 2000, 2012). The specific crystal habits of these latter protists have not been examined.

Cells of the ethmoid tissue of *Oncorhynchus nerka* contain chains of well-ordered crystals of cuboctahedral crystals of magnetite with {111} faces of adjacent crystals lying perpendicular to the chain axis (Mann et al., 1988). The consistent structural features of these particles suggest that they are biomimicized by the organism as in the magnetotactic alga. If we assume that the magnetite crystals in both the alga and *O. nerka* are biomimicized by the organism and address similar questions that we discuss about biomimicry of magnetosomes in MTB, an obvious question, amongst many others, is how these eukaryotic organisms control the size and morphology of their magnetite crystals? Do these organisms contain similar genes to the magnetosome (e.g. *mam*) genes of MTB? If so, will the genes of the alga be more similar to those of the phylogenetic groups of MTB that biomimicize bullet-shaped magnetosome magnetite crystals and those of *O. nerka* more similar to those of MTB that also produce cuboctahedral magnetosome magnetite particles? How do these findings relate to the evolution of the magnetosome? One intriguing idea discussed a number of years ago was the possibility that an MTB was the ancestral eukaryotic host cell (Vali and Kirschvink, 1991; Kirschvink and Hagadorn, 2000). However, no genes orthologous to Mam, Mms or Mad genes were found in the available genomes

of eukaryotes able to produce intracellular magnetosome-like structures (unpublished data). It is possible that the genes responsible for magnetosome formation in prokaryotes and eukaryotes may have diverged too greatly to be recognized as orthologous. It is also possible that magnetosome formation in prokaryotes and eukaryotes has had separate origins, i.e., magnetosome formation in these two domains is polyphyletic. It is clear that magnetosome formation in eukaryotes is much less understood than in prokaryotes.

CONCLUSIONS AND PERSPECTIVES

We have shown in this review that the morphological properties of magnetosome minerals correlate strongly with specific phylogenetic groups of MTB thus reflecting the evolutionary path of magnetotaxis. While a number of genes are clearly important in the biomimicry process, those genes responsible for magnetosome crystal morphology are not yet known. Nonetheless, phylogenetic analyses of magnetosome proteins indicate that the first magnetosomes contained bullet-shaped crystals of magnetite (Lefèvre et al., 2013a).

In addition, it is known that a number of environmental parameters influence the morphology and composition of the magnetosome crystals, although they have been little studied. Despite the fact that reducing, sulfidic environments appear to favor the formation of greigite (Bazylinski et al., 1995; Simmons et al., 2004; Lefèvre et al., 2011c), and that rates of iron uptake by MTB appear to change the morphology of magnetite crystals (Faivre et al., 2008), we do not know what chemical or physical parameters regulate magnetosome formation and control their morphology. Nevertheless, the environmental factors appear to have only slight control over magnetosome morphologies, and the basic crystal habits (cuboctahedral, elongated-prismatic, and elongated-anisotropic) are clearly determined by genetics.

It is also important to note that magnetite and greigite formation continue to occur under anaerobic conditions (where MTB respire with nitrate, nitrous oxide or sulfate as terminal electron acceptors), where chemical or redox gradients are absent and chemical conditions are homogeneous. Here magnetotaxis does not provide an apparent advantage. This suggests that magnetosomes may have additional functions in the absence of oxygen.

Progress in these domains will require the development of new genetic systems in all taxa in which MTB occur, additional genomic studies of new MTB and highly controlled growth studies in which the effects of specific environmental parameters can be precisely determined. Understanding how eukaryotes biomimic magnetosome-like structures will require initiation of molecular and genomic studies.

ACKNOWLEDGMENTS

Mihály Pósfai received support from the EU FP7 program (grant Bio2MaN4MRI). Dennis A. Bazylinski is supported by US National Science Foundation (NSF) Grant EAR-0920718 and by subcontract SC-12-384 from US Department of Energy contract DE-AC02-07CH11358 to the Ames Laboratory at Iowa State University. Christopher T. Lefèvre is funded by the French national research agency ANR (ANR-12-NANO-0013 entitled MEFISTO).

REFERENCES

- Abreu, F., Cantão, M. E., Nicolás, M. F., Barcellos, F. G., Morillo, V., Almeida, L. G., et al. (2011). Common ancestry of iron oxide- and iron-sulfide-based biomineralization in magnetotactic bacteria. *ISME J.* 5, 1634–1640. doi: 10.1038/ismej.2011.35
- Bazylinski, D. A., and Frankel, R. B. (2003). “Biologically controlled mineralization in prokaryotes,” in *Biomimetication*, eds P. M. Dove, J. J. DeYoreo, and S. Weiner (Washington, DC: Mineralogical Soc America), 217–247.
- Bazylinski, D. A., and Frankel, R. B. (2004). Magnetosome formation in prokaryotes. *Nat. Rev. Microbiol.* 2, 217–230. doi: 10.1038/nrmicro842
- Bazylinski, D. A., Frankel, R. B., Heywood, B. R., Ahmadi, S., King, J. W., Donaghay, P. L., et al. (1995). Controlled biomineralization of magnetite (Fe_3O_4) and greigite (Fe_3S_4). *Appl. Environ. Microbiol.* 61, 3232–3239.
- Bazylinski, D. A., Heywood, B. R., Mann, S., and Frankel, R. B. (1993). Fe_3O_4 and Fe_3S_4 in a bacterium. *Nature* 366, 218–218. doi: 10.1038/366218a0
- Bazylinski, D. A., Lefevre, C. T., and Frankel, R. B. (2012). “Magnetotactic prokaryotes at the oxic-anoxic transition zones of coastal aquatic environments,” in *Anoxia: Evidence for Eukaryote Survival and Paleontological Strategies*, eds A. V. Altenbach, J. M. Bernhard, and J. Seckbach (Dordrecht: Springer), 133–143.
- Bazylinski, D. A., Schlezinger, D. R., Howes, B. H., Frankel, R. B., and Epstein, S. S. (2000). Occurrence and distribution of diverse populations of magnetic prokaryotes in a chemically stratified coastal salt pond. *Chem. Geol.* 169, 319–328. doi: 10.1016/S0009-2541(00)00211-4
- Blakemore, R. P., Frankel, R. B., and Kalmijn, A. J. (1980). South-seeking magnetotactic bacteria in the southern-hemisphere. *Nature* 286, 384–385. doi: 10.1038/286384a0
- Buseck, P. R., Dunin-Borkowski, R. E., Devouard, B., Frankel, R. B., McCartney, M. R., Midgley, P. A., et al. (2001). Magnetite morphology and life on Mars. *Proc. Natl. Acad. Sci. U.S.A.* 98, 13490–13495. doi: 10.1073/pnas.241387898
- Butler, R., and Banerjee, S. (1975). Theoretical single-domain grain-size range in magnetite and titanomagnetite. *J. Geophys. Res.* 80, 4049–4058. doi: 10.1029/JB080i029p04049
- Clemett, S. J., Thomas-Kepra, K. L., Shimmin, J., Morphew, M., McIntosh, J. R., Bazylinski, D. A., et al. (2002). Crystal morphology of MV-1 magnetite. *Am. Miner.* 87, 1727–1730.
- Cox, B. L., Popa, R., Bazylinski, D. A., Lanoil, B., Douglas, S., Belz, A., et al. (2002). Organization and elemental analysis of P-, S-, and Fe-rich inclusions in a population of freshwater magnetococci. *Geomicrobiol. J.* 19, 387–406. doi: 10.1080/01490450290098504
- DeLong, E. F., Frankel, R. B., and Bazylinski, D. A. (1993). Multiple evolutionary origins of magnetotaxis in bacteria. *Science* 259, 803–806. doi: 10.1126/science.259.5096.803
- Devouard, B., Pósfai, M., Hua, X., Bazylinski, D. A., Frankel, R. B., and Buseck, P. R. (1998). Magnetite from magnetotactic bacteria: size distributions and twinning. *Am. Miner.* 83, 1387–1398.
- Dunin-Borkowski, R. E., McCartney, M. R., Frankel, R. B., Bazylinski, D. A., Pósfai, M., and Buseck, P. R. (1998). Magnetic microstructure of magnetotactic bacteria by electron holography. *Science* 282, 1868–1870. doi: 10.1126/science.282.5395.1868
- Faivre, D., Menguy, N., Pósfai, M., and Schüler, D. (2008). Environmental parameters affect the physical properties of fast-growing magnetosomes. *Am. Miner.* 93, 463–469. doi: 10.2138/am.2008.2678
- Farina, M., Esquivel, D., and Lins de Barros, H. G. P. (1990). Magnetic iron-sulfur crystals from a magnetotactic microorganism. *Nature* 343, 256–258. doi: 10.1038/343256a0
- Flies, C. B., Peplies, J., and Schüler, D. (2005). Combined approach for characterization of uncultivated magnetotactic bacteria from various aquatic environments. *Appl. Environ. Microbiol.* 71, 2723–2731. doi: 10.1128/AEM.71.5.2723–2731.2005
- Frankel, R. B. (1984). Magnetic guidance of organisms. *Annu. Rev. Biophys. Bioeng.* 13, 85–103. doi: 10.1146/annurev.bb.13.060184.000505
- Frankel, R. B., and Blakemore, R. P. (1980). Navigational compass in magnetic bacteria. *J. Magn. Magn. Mater.* 15–8, 1562–1564. doi: 10.1016/0304-8853(80)90409-6
- Frankel, R. B., Blakemore, R. P., and Wolfe, R. S. (1979). Magnetite in freshwater magnetotactic bacteria. *Science* 203, 1355–1356. doi: 10.1126/science.203.4387.1355
- Gorby, Y. A., Beveridge, T. J., and Blakemore, R. P. (1988). Characterization of the bacterial magnetosome membrane. *J. Bacteriol.* 170, 834–841.
- Grünberg, K., Wawer, C., Tebo, B. M., and Schüler, D. (2001). A large gene cluster encoding several magnetosome proteins is conserved in different species of magnetotactic bacteria. *Appl. Environ. Microbiol.* 67, 4573–4582. doi: 10.1128/AEM.67.10.4573–4582.2001
- Hanzlik, M., Winklhofer, M., and Petersen, N. (2002). Pulsed-field-remanence measurements on individual magnetotactic bacteria. *J. Magn. Magn. Mater.* 248, 258–267. doi: 10.1016/S0304-8853(02)00353-0
- Heywood, B. R., Bazylinski, D. A., Garratt-Reed, A., Mann, S., and Frankel, R. B. (1990). Controlled biosynthesis of greigite (Fe_3S_4) in magnetotactic bacteria. *Naturwissenschaften* 77, 536–538. doi: 10.1007/BF01139266
- Heywood, B. R., Mann, S., and Frankel, R. B. (1991). “Structure, morphology and growth of biogenic greigite,” in *Materials Synthesis Based on Biological Processes*, eds M. Alpert, P. Calvert, R. B. Frankel, P. Rieke, and D. Tirrell (Pittsburgh, PA: Materials Research Society), 93–108.
- Hoffmann, V. (1992). Greigite (Fe_3S_4): magnetic properties and first domain observations. *Phys. Earth. Planet. Inter.* 70, 288–301. doi: 10.1016/0031-9201(92)90195-2
- Isambert, A., Menguy, N., Larquet, E., Guyot, F., and Valet, J.-P. (2007). Transmission electron microscopy study of magnetites in a freshwater population of magnetotactic bacteria. *Am. Miner.* 92, 621–630. doi: 10.2138/am.2007.2278
- Ji, B., Zhang, S.-D., Arnoux, P., Rouy, Z., Alberto, F., Philippe, N., et al. (2013). Comparative genomic analysis provides insights into the evolution and niche adaptation of marine *Magnetospira* sp. QH-2 strain. *Environ. Microbiol.* doi: 10.1111/1462-2920.12180. [Epub ahead of print].
- Jogler, C., Kube, M., Schübbe, S., Ullrich, S., Teeling, H., Bazylinski, D. A., et al. (2009). Comparative analysis of magnetosome gene clusters in magnetotactic bacteria provides further evidence for horizontal gene transfer. *Environ. Microbiol.* 11, 1267–1277. doi: 10.1111/j.1462-2920.2009.01854.x
- Jogler, C., and Schüler, D. (2009). Genomics, genetics, and cell biology of magnetosome formation. *Annu. Rev. Microbiol.* 63, 501–521. doi: 10.1146/annurev.micro.62.081307.162908
- Jogler, C., Wanner, G., Kolinko, S., Niebler, M., Amann, R., Petersen, N., et al. (2011). Conservation of proteobacterial magnetosome genes and structures in an uncultivated member of the deep-branching *Nitrospira* phylum. *Proc. Natl. Acad. Sci. U.S.A.* 108, 1134–1139. doi: 10.1073/pnas.1012694108
- Kasama, T., Pósfai, M., Chong, R. K. K., Finlayson, A. P., Buseck, P. R., Frankel, R. B., et al. (2006). Magnetic properties, microstructure, composition, and morphology of greigite nanocrystals in magnetotactic bacteria from electron holography and tomography. *Am. Miner.* 91, 1216–1229. doi: 10.2138/am.2006.2227
- Keim, C. N., Martins, J. L., Lins de Barros, H. G. P., and Farina, M. (2007). “Structure, behavior, ecology and diversity of multicellular magnetotactic prokaryotes,” in *Magnetoreception and Magnetosomes in Bacteria Microbiology Monographs*, ed D. Schüler (Berlin: Springer), 103–132. doi: 10.1007/7171_040
- Kirschvink, J. L., and Hagadorn, J. W. (2000). “A grand unified theory of biomineralization,” in *The Biomimetication of Nano- and Micro-Structures*, ed E. Bäuerlein (Weinheim: Wiley), 139–150.
- Kirschvink, J. L., Walker, M. M., and Diebel, C. E. (2001). Magnetite-based magnetoreception. *Curr. Opin. Neurobiol.* 11, 462–467. doi: 10.1016/S0959-4388(00)00235-X
- Kobayashi, A., Kirschvink, J. L., Nash, C. Z., Kopp, R. E., Sauer, D. A., Bertani, L. E., et al. (2006). Experimental observation of magnetosome chain collapse in magnetotactic bacteria: sedimentological, paleomagnetic, and evolutionary implications. *Earth Planet. Sci. Lett.* 245, 538–550. doi: 10.1016/j.epsl.2006.03.041
- Kolinko, S., Jogler, C., Katzmüller, E., Wanner, G., Peplies, J., and Schüler, D. (2012). Single-cell analysis reveals a novel uncultivated magnetotactic bacterium within the candidate division OP3. *Environ. Microbiol.* 14, 1709–1721. doi: 10.1111/j.1462-2920.2011.02609.x
- Komeili, A. (2012). Molecular mechanisms of compartmentalization and biomineralization in magnetotactic bacteria. *FEMS Microbiol. Rev.* 36, 232–255. doi: 10.1111/j.1574-6976.2011.00315.x
- Komeili, A., Li, Z., Newman, D. K., and Jensen, G. J. (2006). Magnetosomes are cell membrane invaginations organized by the actin-like protein MamK. *Science* 311, 242–245. doi: 10.1126/science.1123231
- Komeili, A., Vali, H., Beveridge, T. J., and Newman, D. K. (2004). Magnetosome vesicles are present before magnetite formation, and MamA is required

- for their activation. *Proc. Natl. Acad. Sci. U.S.A.* 101, 3839–3844. doi: 10.1073/pnas.0400391101
- Kuterbach, D. A., Walcott, B., Reeder, R. J., and Frankel, R. B. (1982). Iron-containing cells in the honey bee (*Apis mellifera*). *Science* 218, 695–697. doi: 10.1126/science.218.4573.695
- Lefèvre, C. T., Abreu, F., Schmidt, M. L., Lins, U., Frankel, R. B., Hedlund, B. P., et al. (2010). Moderately thermophilic magnetotactic bacteria from hot springs in Nevada. *Appl. Environ. Microbiol.* 76, 3740–3743. doi: 10.1128/AEM.03018-09
- Lefèvre, C. T., and Bazylinski, D. A. (2013). Ecology, diversity, and evolution of magnetotactic bacteria. *Microbiol. Mol. Biol. Rev.* 77, 497–526. doi: 10.1128/MMBR.00021-13
- Lefèvre, C. T., Bernadac, A., Yu-Zhang, K., Pradel, N., and Wu, L.-F. (2009). Isolation and characterization of a magnetotactic bacterial culture from the Mediterranean Sea. *Environ. Microbiol.* 11, 1646–1657. doi: 10.1111/j.1462-2920.2009.01887.x
- Lefèvre, C. T., Frankel, R. B., Abreu, F., Lins, U., and Bazylinski, D. A. (2011a). Culture-independent characterization of a novel, uncultivated magnetotactic member of the *Nitrospirae* phylum. *Environ. Microbiol.* 13, 538–549. doi: 10.1111/j.1462-2920.2010.02361.x
- Lefèvre, C. T., Frankel, R. B., Pósfai, M., Prozorov, T., and Bazylinski, D. A. (2011b). Isolation of obligately alkaliphilic magnetotactic bacteria from extremely alkaline environments. *Environ. Microbiol.* 13, 2342–2350. doi: 10.1111/j.1462-2920.2011.02505.x
- Lefèvre, C. T., Menguy, N., Abreu, F., Lins, U., Pósfai, M., Prozorov, T., et al. (2011c). A cultured greigite-producing magnetotactic bacterium in a novel group of sulfate-reducing bacteria. *Science* 334, 1720–1723. doi: 10.1126/science.1212596
- Lefèvre, C. T., Pósfai, M., Abreu, F., Lins, U., Frankel, R. B., and Bazylinski, D. A. (2011d). Morphological features of elongated-anisotropic magnetosome crystals in magnetotactic bacteria of the *Nitrospirae* phylum and the *Deltaproteobacteria* class. *Earth Planet. Sci. Lett.* 312, 194–200. doi: 10.1016/j.epsl.2011.10.003
- Lefèvre, C. T., Trubitsyn, D., Abreu, F., Kolinko, S., de Almeida, L. G. P., de Vasconcelos, A. T. R., et al. (2013a). Monophyletic origin of magnetotaxis and the first magnetosomes. *Environ. Microbiol.* 15, 2267–2274. doi: 10.1111/1462-2920.12097
- Lefèvre, C. T., Trubitsyn, D., Abreu, F., Kolinko, S., Jogler, C., de Almeida, L. G. P., et al. (2013b). Comparative genomic analysis of magnetotactic bacteria from the *Deltaproteobacteria* provides new insights into magnetite and greigite magnetosome genes required for magnetotaxis. *Environ. Microbiol.* 15, 2712–2735. doi: 10.1111/1462-2920.12128
- Lefèvre, C. T., Viloria, N., Schmidt, M. L., Pósfai, M., Frankel, R. B., and Bazylinski, D. A. (2012). Novel magnetite-producing magnetotactic bacteria belonging to the *Gamma proteobacteria*. *ISME J.* 6, 440–450. doi: 10.1038/ismej.2011.97
- Lefèvre, C. T., and Wu, L. F. (2013). Evolution of the bacterial organelle responsible for magnetotaxis. *Trends Microbiol.* 21, 534–543. doi: 10.1016/j.tim.2013.07.005
- Le Sage, D., Arai, K., Glenn, D. R., DeVience, S. J., Pham, L. M., Rahn-Lee, L., et al. (2013). Optical magnetic imaging of living cells. *Nature* 496, 486–489. doi: 10.1038/nature12072
- Li, J., Pan, Y., Chen, G., Liu, Q., Tian, L., and Lin, W. (2009). Magnetite magnetosome and fragmental chain formation of *Magnetospirillum magneticum* AMB-1: transmission electron microscopy and magnetic observations. *Geophys. J. Int.* 177, 33–42. doi: 10.1111/j.1365-246X.2009.04043.x
- Li, J., Pan, Y., Liu, Q., Yu-Zhang, K., Menguy, N., Che, R., et al. (2010). Biomineralization, crystallography and magnetic properties of bullet-shaped magnetite magnetosomes in giant rod magnetotactic bacteria. *Earth Planet. Sci. Lett.* 293, 368–376. doi: 10.1016/j.epsl.2010.03.007
- Lin, W., Li, J., and Pan, Y. (2012). Newly isolated but uncultivated magnetotactic bacterium of the phylum *Nitrospirae* from Beijing, China. *Appl. Environ. Microbiol.* 78, 668–675. doi: 10.1128/AEM.06764-11
- Lin, W., and Pan, Y. (2009). Uncultivated magnetotactic cocci from Yuandadu Park in Beijing, China. *Appl. Environ. Microbiol.* 75, 4046–4052. doi: 10.1128/AEM.00247-09
- Lins, U., Keim, C. N., Evans, F. F., Farina, M., and Buseck, P. R. (2007). Magnetite (Fe_3O_4) and greigite (Fe_3S_4) crystals in multicellular magnetotactic prokaryotes. *Geomicrobiol. J.* 24, 43–50. doi: 10.1080/01490450601134317
- Lins, U., McCartney, M. R., Farina, M., Frankel, R. B., and Buseck, P. R. (2005). Habits of magnetosome crystals in coccoid magnetotactic bacteria. *Appl. Environ. Microbiol.* 71, 4902–4905. doi: 10.1128/AEM.71.8.4902-4905.2005
- Lohsse, A., Ullrich, S., Katzenmann, E., Borg, S., Wanner, G., Richter, M., et al. (2011). Functional analysis of the magnetosome island in *Magnetospirillum gryphiswaldense*: the *mamAB* operon is sufficient for magnetite biomineralization. *PLoS ONE* 6:e25561. doi: 10.1371/journal.pone.0025561
- Mann, S., and Frankel, R. B. (1989). “Magnetite biomineralization in unicellular organisms,” in *Biomineralization: Chemical and Biochemical Perspectives*, S. Mann, J. Webb, and R. J. P. Williams (New York, NY: VCH), 389–426.
- Mann, S., Frankel, R. B., and Blakemore, R. P. (1984a). Structure, morphology and crystal-growth of bacterial magnetite. *Nature* 310, 405–407. doi: 10.1038/310405a0
- Mann, S., Moench, T. T., and Williams, R. J. P. (1984b). A high resolution electron microscopic investigation of bacterial magnetite. Implications for crystal growth. *Proc. R. Soc. Lond. B Biol. Sci.* 221, 385–393. doi: 10.1098/rspb.1984.0040
- Mann, S., Sparks, N. H. C., and Blakemore, R. P. (1987a). Structure, morphology and crystal-growth of anisotropic magnetite crystals in magnetotactic bacteria. *Proc. R. Soc. Lond. B Biol. Sci.* 231, 477–487. doi: 10.1098/rspb.1987.0056
- Mann, S., Sparks, N. H. C., and Blakemore, R. P. (1987b). Ultrastructure and characterization of anisotropic magnetic inclusions. *Proc. R. Soc. Lond. B Biol. Sci.* 231, 469–476. doi: 10.1098/rspb.1987.0055
- Mann, S., Sparks, N. H. C., Frankel, R. B., Bazylinski, D. A., and Jannasch, H. W. (1990). Biominerization of ferrimagnetic greigite (Fe_3S_4) and iron pyrite (FeS_2) in a magnetotactic bacterium. *Nature* 343, 258–261. doi: 10.1038/343258a0
- Mann, S., Sparks, N. H., Walker, M. M., and Kirschvink, J. L. (1988). Ultrastructure, morphology and organization of biogenic magnetite from sockeye salmon, *Oncorhynchus nerka*: Implications for magnetoreception. *J. Exp. Biol.* 140, 35–49.
- Matsuda, T., Endo, J., Osakabe, N., Tonomura, A., and Arii, T. (1983). Morphology and structure of biogenic magnetite particles. *Nature* 302, 411–412. doi: 10.1038/302411a0
- Matsunaga, T., Okamura, Y., Fukuda, Y., Wahyudi, A. T., Murase, Y., and Takeyama, H. (2005). Complete genome sequence of the facultative anaerobic magnetotactic bacterium *Magnetospirillum* sp. strain AMB-1. *DNA Res.* 12, 157–166. doi: 10.1093/dnares/ds002
- Meldrum, F. C., Mann, S., Heywood, B. R., Frankel, R. B., and Bazylinski, D. A. (1993a). Electron-microscopy study of magnetosomes in 2 cultured vibrioid magnetotactic bacteria. *Proc. R. Soc. Lond. B Biol. Sci.* 251, 237–242.
- Meldrum, F. C., Mann, S., Heywood, B. R., Frankel, R. B., and Bazylinski, D. A. (1993b). Electron-microscopy study of magnetosomes in a cultured coccoid magnetotactic bacterium. *Proc. R. Soc. Lond. B Biol. Sci.* 251, 231–236. doi: 10.1098/rspb.1993.0034
- Midgley, P. A., and Weyland, M. (2011). “STEM tomography,” in *Scanning Transmission Electron Microscopy: Imaging and Analysis*, eds S. J. Pennycook and P. D. Nellist (Berlin: Springer), 353–392. doi: 10.1007/978-1-4419-7200-2_8
- Moskowitz, B. M., Frankel, R. B., Flanders, P. J., Blakemore, R. P., and Schwartz, B. B. (1988). Magnetic-properties of magnetotactic bacteria. *J. Magn. Magn. Mater.* 73, 273–288. doi: 10.1016/0304-8853(88)90093-5
- Murat, D., Falahati, V., Bertinetti, L., Csencsits, R., Körnig, A., Downing, K., et al. (2012). The magnetosome membrane protein, MmsF, is a major regulator of magnetite biomineralization in *Magnetospirillum magneticum* AMB-1. *Mol. Microbiol.* 85, 684–699. doi: 10.1111/j.1365-2958.2012.08132.x
- Murat, D., Quinlan, A., Vali, H., and Komeili, A. (2010). Comprehensive genetic dissection of the magnetosome gene island reveals the step-wise assembly of a prokaryotic organelle. *Proc. Natl. Acad. Sci. U.S.A.* 107, 5593–5598. doi: 10.1073/pnas.0914439107
- Nakazawa, H., Arakaki, A., Narita-Yamada, S., Yashiro, I., Jinno, K., Aoki, N., et al. (2009). Whole genome sequence of *Desulfovibrio magneticus* strain RS-1 revealed common gene clusters in magnetotactic bacteria. *Genome Res.* 19, 1801–1808. doi: 10.1101/gr.088906.108
- Palache, C., Berman, H., and Frondel, C. (1944). *Dana's System of Mineralogy*. New York, NY: Wiley.
- Penninga, I., Deward, H., Moskowitz, B. M., Bazylinski, D. A., and Frankel, R. B. (1995). Remanence measurements on individual magnetotactic bacteria using a pulsed magnetic-field. *J. Magn. Magn. Mater.* 149, 279–286. doi: 10.1016/0304-8853(95)00078-X
- Pósfai, M., Buseck, P. R., Bazylinski, D. A., and Frankel, R. B. (1998a). Iron sulfides from magnetotactic bacteria: Structure, composition, and phase transitions. *Am. Miner.* 83, 1469–1481.

- Pósfai, M., Buseck, P. R., Bazylinski, D. A., and Frankel, R. B. (1998b). Reaction sequence of iron sulfide minerals in bacteria and their use as biomarkers. *Science* 280, 880–883. doi: 10.1126/science.280.5365.880
- Pósfai, M., Kasama, T., and Dunin-Borkowski, R. E. (2013). “Biominerals at the nanoscale: transmission electron microscopy methods for studying the special properties of biominerals,” in *Minerals at the Nanoscale, EMU Notes in Mineralogy*, eds F. Nieto and K. J. T. Livi (London: European Mineralogical Union and Mineralogical Society of Great Britain and Ireland), 377–435.
- Pósfai, M., Moskowitz, B. M., Arató, B., Schüler, D., Flies, C., Bazylinski, D. A., et al. (2006). Properties of intracellular magnetite crystals produced by *Desulfovibrio magneticus* strain RS-1. *Earth Planet. Sci. Lett.* 249, 444–455. doi: 10.1016/j.epsl.2006.06.036
- Sakaguchi, T., Burgess, J. G., and Matsunaga, T. (1993). Magnetite formation by a sulfate-reducing bacterium. *Nature* 365, 47–49. doi: 10.1038/365047a0
- Scheffel, A., Gärdes, A., Grünberg, K., Wanner, G., and Schüler, D. (2008). The major magnetosome proteins MamGFDC are not essential for magnetite biomineralization in *Magnetospirillum gryphiswaldense* but regulate the size of magnetosome crystals. *J. Bacteriol.* 190, 377–386. doi: 10.1128/JB.01371-07
- Scheffel, A., Gruska, M., Faivre, D., Linaroudis, A., Plitzko, J. M., and Schüler, D. (2006). An acidic protein aligns magnetosomes along a filamentous structure in magnetotactic bacteria. *Nature* 440, 110–114. doi: 10.1038/nature04382
- Schübbe, S., Kube, M., Scheffel, A., Wawer, C., Heyen, U., Meyerdericks, A., et al. (2003). Characterization of a spontaneous nonmagnetic mutant of *Magnetospirillum gryphiswaldense* reveals a large deletion comprising a putative magnetosome island. *J. Bacteriol.* 185, 5779–5790. doi: 10.1128/JB.185.19.5779-5790.2003
- Schübbe, S., Williams, T. J., Xie, G., Kiss, H. E., Brettin, T. S., Martinez, D., et al. (2009). Complete genome sequence of the chemolithoautotrophic marine magnetotactic coccus strain MC-1. *Appl. Environ. Microbiol.* 75, 4835–4852. doi: 10.1128/AEM.02874-08
- Simmons, S. L., Sievert, S. M., Frankel, R. B., Bazylinski, D. A., and Edwards, K. J. (2004). Spatiotemporal distribution of marine magnetotactic bacteria in a seasonally stratified coastal salt pond. *Appl. Environ. Microbiol.* 70, 6230–6239. doi: 10.1128/AEM.70.10.6230-6239.2004
- Simpson, E. T., Kasama, T., Pósfai, M., Buseck, P. R., Harrison, R. J., and Dunin-Borkowski, R. E. (2005). Magnetic induction mapping of magnetite chains in magnetotactic bacteria at room temperature and close to the Verwey transition using electron holography. *J. Phys. Conf. Ser.* 17, 108–121. doi: 10.1088/1742-6596/17/1/017
- Spring, S., Amann, R., Ludwig, W., Schleifer, K. H., Vangemerden, H., and Petersen, N. (1993). Dominating role of an unusual magnetotactic bacterium in the microaerobic zone of a fresh-water sediment. *Appl. Environ. Microbiol.* 59, 2397–2403.
- Thomas-Kepra, K. L., Clemett, S. J., Bazylinski, D. A., Kirschvink, J. L., McKay, D. S., Wentworth, S. J., et al. (2001). Truncated hexa-octahedral magnetite crystals in ALH84001: presumptive biosignatures. *Proc. Natl. Acad. Sci. U.S.A.* 98, 2164–2169. doi: 10.1073/pnas.051500898
- Thornhill, R. H., Burgess, J. H., Sakaguchi, T., and Matsunaga, T. (1994). A morphological classification of bacteria containing bullet-shaped magnetic particles. *FEMS Microbiol. Lett.* 115, 169–176. doi: 10.1111/j.1574-6968.1994.tb06633.x
- Torres de Araujo, F. F., Pires, M. A., Frankel, R. B., and Bicudo, C. E. M. (1986). Magnetite and magnetotaxis in algae. *Biophys. J.* 50, 375–378. doi: 10.1016/S0006-3495(86)83471-3
- Towe, K. M., and Moench, T. T. (1981). Electron-optical characterization of bacterial magnetite. *Earth Planet. Sci. Lett.* 52, 213–220. doi: 10.1016/0012-821X(81)90222-3
- Uebe, R., Junge, K., Henn, V., Poxleitner, G., Katzmull, E., Plitzko, J. M., et al. (2011). The cation diffusion facilitator proteins MamB and MamM of *Magnetospirillum gryphiswaldense* have distinct and complex functions, and are involved in magnetite biomineralization and magnetosome membrane assembly. *Mol. Microbiol.* 82, 818–835. doi: 10.1111/j.1365-2958.2011.07863.x
- Ullrich, S., Kube, M., Schübbe, S., Reinhardt, R., and Schüler, D. (2005). A hyper-variable 130-kilobase genomic region of *Magnetospirillum gryphiswaldense* comprises a magnetosome island which undergoes frequent rearrangements during stationary growth. *J. Bacteriol.* 187, 7176–7184. doi: 10.1128/JB.187.21.7176-7184.2005
- Vali, H., and Kirschvink, J. L. (1991). “Observations of magnetosome organization, surface structure, and iron biominerization of undescribed magnetic bacteria: evolutionary speculations,” in *Iron Biominerals Plenum*, eds R. B. Frankel and R. P. Blakemore (New York, NY: Plenum Press), 97–115.
- Wang, Y., Lin, W., Li, J., and Pan, Y. (2013). High diversity of magnetotactic delta-proteobacteria in a freshwater niche. *Appl. Environ. Microbiol.* 79, 2813–2817. doi: 10.1128/AEM.03635-12
- Wenter, R., Wanner, G., Schüler, D., and Overmann, J. (2009). Ultrastructure, tactic behaviour and potential for sulfate reduction of a novel multicellular magnetotactic prokaryote from North Sea sediments. *Environ. Microbiol.* 11, 1493–1505. doi: 10.1111/j.1462-2920.2009.01877.x
- Zhang, W.-Y., Zhou, K., Pan, H.-M., Yue, H.-D., Jiang, M., Xiao, T., et al. (2012). Two genera of magnetococci with bean-like morphology from intertidal sediments of the Yellow Sea, China. *Appl. Environ. Microbiol.* 78, 5606–5611. doi: 10.1128/AEM.00081-12
- Zhou, K., Zhang, W.-Y., Yu-Zhang, K., Pan, H.-M., Zhang, S.-D., Zhang, W.-J., et al. (2012). A novel genus of multicellular magnetotactic prokaryotes from the Yellow Sea. *Environ. Microbiol.* 14, 405–413. doi: 10.1111/j.1462-2920.2011.02590.x
- Zhu, K., Pan, H., Li, J., Yu-Zhang, K., Zhang, S.-D., Zhang, W.-Y., et al. (2010). Isolation and characterization of a marine magnetotactic spirillum axenic culture QH-2 from an intertidal zone of the China Sea. *Res. Microbiol.* 161, 276–283. doi: 10.1016/j.resmic.2010.02.003

Conflict of Interest Statement: The authors declare that the research was conducted in the absence of any commercial or financial relationships that could be construed as a potential conflict of interest.

Received: 02 September 2013; accepted: 30 October 2013; published online: 26 November 2013.

Citation: Pósfai M, Lefèvre CT, Trubitsyn D, Bazylinski DA and Frankel RB (2013) Phylogenetic significance of composition and crystal morphology of magnetosome minerals. Front. Microbiol. 4:344. doi: 10.3389/fmicb.2013.00344

This article was submitted to Aquatic Microbiology, a section of the journal Frontiers in Microbiology.

Copyright © 2013 Pósfai, Lefèvre, Trubitsyn, Bazylinski and Frankel. This is an open-access article distributed under the terms of the Creative Commons Attribution License (CC BY). The use, distribution or reproduction in other forums is permitted, provided the original author(s) or licensor are credited and that the original publication in this journal is cited, in accordance with accepted academic practice. No use, distribution or reproduction is permitted which does not comply with these terms.



Isolation, cultivation and genomic analysis of magnetosome biomineralization genes of a new genus of South-seeking magnetotactic cocci within the *Alphaproteobacteria*

Viviana Morillo¹, Fernanda Abreu¹, Ana C. Araujo¹, Luiz G. P. de Almeida², Alex Enrich-Prast³, Marcos Farina⁴, Ana T. R. de Vasconcelos², Dennis A. Bazylinski⁵ and Ulysses Lins^{1*}

¹ Instituto de Microbiologia Paulo de Góes, Universidade Federal do Rio de Janeiro, Rio de Janeiro, Brazil

² Laboratório Nacional de Computação Científica, Departamento de Matemática Aplicada e Computacional, Petrópolis, Brazil

³ Instituto de Biologia, Universidade Federal do Rio de Janeiro, Rio de Janeiro, Brazil

⁴ Instituto de Ciências Biomédicas, Universidade Federal do Rio de Janeiro, Rio de Janeiro, Brazil

⁵ School of Life Sciences, University of Nevada at Las Vegas, Las Vegas, NV, USA

Edited by:

Damien Faivre, Max Planck Society, Germany

Reviewed by:

Concepcion Jimenez-Lopez, University of Granada, Spain

Dirk Schüler,

Ludwig-Maximilians-Universität München, Germany

***Correspondence:**

Ulysses Lins, Instituto de Microbiologia Paulo de Góes, Universidade Federal do Rio de Janeiro, Avenida Carlos Chagas Filho, 373, 21941-902 Rio de Janeiro, Brazil
e-mail: ulins@micro.ufrj.br

Although magnetotactic bacteria (MTB) are ubiquitous in aquatic habitats, they are still considered fastidious microorganisms with regard to growth and cultivation with only a relatively low number of axenic cultures available to date. Here, we report the first axenic culture of an MTB isolated in the Southern Hemisphere (Itaipu Lagoon in Rio de Janeiro, Brazil). Cells of this new isolate are coccoid to ovoid in morphology and grow microaerophilically in semi-solid medium containing an oxygen concentration ($[O_2]$) gradient either under chemoorganoheterotrophic or chemolithoautotrophic conditions. Each cell contains a single chain of approximately 10 elongated cuboctahedral magnetite (Fe_3O_4) magnetosomes. Phylogenetic analysis based on the 16S rRNA gene sequence shows that the coccoid MTB isolated in this study represents a new genus in the *Alphaproteobacteria*; the name *Magnetofaba australis* strain IT-1 is proposed. Preliminary genomic data obtained by pyrosequencing shows that *M. australis* strain IT-1 contains a genomic region with genes involved in biomimicry similar to those found in the most closely related magnetotactic cocci *Magnetococcus marinus* strain MC-1. However, organization of the magnetosome genes differs from *M. marinus*.

Keywords: *Magnetofaba australis* strain IT-1, magnetite, magnetosome, South-seeking magnetotactic bacteria, biomimicry genes

INTRODUCTION

Magnetotactic bacteria (MTB) are a morphologically, metabolically, and phylogenetically diverse group of prokaryotes that share the ability to synthesize intracellular, nano-sized magnetic particles called magnetosomes. Each magnetosome consists of a magnetite (Fe_3O_4) or greigite (Fe_3S_4) crystal enveloped by a lipid-bilayer membrane derived from the cytoplasmic membrane (Bazylinski and Frankel, 2004). Magnetosomes are generally organized in linear chains and orient the cell body along geomagnetic field lines while flagella actively propel the cells, resulting in so-called magnetotaxis (Bazylinski and Frankel, 2004; Schüler, 2008). MTB from the Southern Hemisphere swim antiparallel to the vertical component of the geomagnetic field toward the South and are termed South-seeking MTB (SS-MTB). In contrast, MTB from the Northern Hemisphere swim parallel to the vertical component of the geomagnetic field lines and are predominantly North-seeking (NS-MTB) (Blakemore et al., 1980). The inclination of the geomagnetic field lines is believed to direct cells downwards away from toxic concentrations of oxygen in surface waters, thereby helping them locate and maintain an optimal position in vertical gradients which is usually at or

near the oxic-anoxic interface (OAI) (Blakemore, 1982; Frankel and Bazylinski, 1994; Bazylinski and Frankel, 2004). However, there are reports of SS-MTB and NS-MTB in both hemispheres (Simmons et al., 2006).

MTB are considered fastidious microorganisms (Schüler, 2008), although there has recently been a considerable increase in available cultures, including the first cultivation of a greigite producer (Lefevre et al., 2011). The recent availability of MTB cultures has contributed to a better characterization of the physiology and biochemistry of these microorganisms. It has also contributed to an improved understanding of the evolution of MTB and of the biomimicry processes involved since differences in the sequences of magnetosome biomimicry genes in different MTB, particularly the *mam* genes, revealed a strong correlation between these magnetotaxis-related genes and phylogeny based on the 16S rRNA gene (Lefèvre et al., 2013a). Studies of magnetosome biomimicry genes in uncultivated MTB require unique approaches (Abreu et al., 2011; Jogler et al., 2011) that do not usually reveal the complete organization of biomimicry genes or genes involved in magnetotaxis behavior unless the entire genome is sequenced. Moreover,

because not all the magnetosome-related genes may be recognized, a direct correlation with phylogeny based on 16S rRNA gene sequences cannot be made with total accuracy.

The most characterized cultivated MTB strains are phylogenetically affiliated with the *Alphaproteobacteria* and include *Magnetococcus marinus* strain MC-1 (Bazylinski et al., 2013a), *Magnetovibrio blakemorei* strain MV-1 (Bazylinski et al., 2013b), the magneto-ovoid bacterium strain MO-1 (Lefèvre et al., 2009), *Magnetospirillum magneticum* strain AMB-1, *Magnetospirillum gryphiswaldense* strain MSR-1, *Magnetospirillum magnetotacticum* strain MS-1, *Magnetospira thiophilla* strain MMS-1 (Williams et al., 2012) and *Magnetospira* sp. QH-2 strain 1 (Ji et al., 2014). Cultivated strains belonging to *Deltaproteobacteria* include the sulfate-reducer *Desulfovibrio magneticus* strain RS-1, (Sakaguchi et al., 2002), *Candidatus Desulfamplus magnetomortis* strain BW-1 (Lefèvre et al., 2011) and enrichment cultures of the magnetotactic multicellular prokaryotes *Candidatus Magnetoglobus multicellularis* (Abreu et al., 2013). Two cultivated strains, BW-2 and SS-5, both belonging to *Gammaproteobacteria*, have also been reported (Lefèvre et al., 2012).

The biomimicry of magnetosomes is controlled by a set of highly conserved genes in magnetite-producing MTB (Richter et al., 2007; Jogler and Schüler, 2009; Jogler et al., 2009) and, as demonstrated more recently, in greigite-producing MTB as well (Abreu et al., 2011, 2013; Lefèvre et al., 2011, 2013b). In some species, the magnetosome biomimicry genes are clustered on a genomic magnetosome island (MAI), which partially supports the hypothesis of horizontal gene transfer (HGT) between various MTB presumably leading to the wide distribution of these genes among members of different phylogenetic groups (Jogler and Schüler, 2009; Jogler et al., 2009; Abreu et al., 2011). However, certain components of typical genomic islands (transposases, t-RNA sequences, integrases), such as those observed in *M. magneticum* strain AMB-1, *M. gryphiswaldense* strain MSR-1 and *D. magneticus* RS-1, are not universally shared within the MAI of all MTB (e.g., *M. marinus*; Schübbe et al., 2009). Moreover, phylogenetic analysis based on the amino acid sequences of magnetosome proteins from MTB are congruent with the phylogenetic tree based on the 16S rRNA gene sequences of the same microorganisms (Lefèvre et al., 2013a). Therefore, the evolution and divergence of magnetosome proteins and the 16S rRNA gene occurred similarly, suggesting that magnetotaxis originated monophyletically in the *Proteobacteria* phylum (Lefèvre et al., 2013a). Additional genome sequences and culture of MTB species are necessary to understand the evolution of biomimicry in *Bacteria*. Moreover, the availability of new cultures of MTB allows a better characterization of the physiology and biochemistry of these microorganisms, enabling the correlation of these features to magnetosome formation.

Despite being the most prevalent and diverse morphotype of MTB in the environment (Spring et al., 1998; Schübbe et al., 2009), there are currently only two cultivated strains of magnetotactic cocci: *M. marinus* strain MC-1 (Bazylinski et al., 2013a) and the magneto-ovoid bacterium strain MO-1 (Lefèvre et al., 2009). The complete genome sequence of the NS-MTB *M. marinus* has been reported (Schübbe et al., 2009), but further study is required

to better understand the full diversity of the magnetotactic cocci as well as the ecological function and evolution of magnetosome biomimicry in the *Alphaproteobacteria*. Here, we describe both the isolation in axenic culture and the characterization of a new magnetotactic coccus, provisionally named *Magnetofaba australis* strain IT-1 that represents a new genus. We also conducted whole genome sequencing and functional annotation of genes related to magnetosome formation to gain insight into the phylogeny, physiology and biochemistry of this SS-MTB. This strain is the first cultivated SS-MTB, and the genomic data presented here are the first report of biomimicry genes in magnetotactic cocci capable of synthesizing elongated cuboctahedral magnetosomes.

MATERIALS AND METHODS

ISOLATION AND CULTIVATION OF *Magnetofaba australis* STRAIN IT-1.

Samples of water and sediment were collected from the Itaipu Lagoon ($22^{\circ}57'51.90''$ S $43^{\circ}0'45.41''$ W), a brackish to marine coastal lagoon near Rio de Janeiro, Brazil, and stored under dim light at room temperature. MTB were magnetically concentrated using a magnetic isolation apparatus described by Lins et al. (2003). After 20 min, cells were collected in a polypropylene tube. Concentrated South-seeking MTB were magnetically purified repeatedly using the racetrack technique (Wolfe et al., 1987) and inoculated at the OAI of culture tubes. Approximately 4/5 of the tubes were filled with an autotrophic semisolid oxygen concentration gradient ($[O_2]$ -gradient) medium. The medium was used to isolate *M. marinus* (Frankel et al., 1997) and contained bicarbonate as the major carbon source. The medium contained 5 mL of modified Wolfe's minerals elixir, 3.75 mM NH₄Cl, 0.2 mL of 0.2% resazurin and 2 g of Bacto-Agar diluted in 1 L of artificial seawater (ASW). The medium was autoclaved, followed by the addition of 1.5 mL of 0.5 M KHPO₄, pH 7.1, neutral fresh L-cysteine (final concentration of 0.2 g/L) and 2.68 mL of 0.8 M NaHCO₃, 0.5 mL of vitamin solution and 2 mL of 0.01 M ferric quinate (final concentration of 20 μ M). The pH was adjusted to 7.2. Cultures were incubated at 28°C until a microaerophilic band of cells was observed at the OAI and, subsequently, the bands were inoculated into a solid heterotrophic $[O_2]$ -gradient medium applying the dilution-to-extinction technique and shake-tubes (Seeley et al., 1991). Briefly, a band of cells were inoculated into the solid medium before it solidified (approximately at 45°C), followed by 7 serial 10-fold dilution steps. After inoculation and agitation by inversion, each tube was put on ice to solidify the medium quickly without killing a significant number of cells. Colonies grown on shake tubes were individually transferred to semi-solid heterotrophic medium. Each colony in culture was re-inoculated in fresh medium over 10 times to ensure that a pure culture was obtained. Purity of the culture was evaluated by light and electron microscopy and sequencing of the 16S rRNA gene.

The medium chosen for growth and maintenance of *M. australis* strain IT-1 was designed for heterotrophic growth, because cells grew faster and the number of magnetosome per cell was higher than in the autotrophic medium. The heterotrophic medium contained 5 mL of modified Wolfe's minerals (Frankel et al., 1997), 3.75 mM NH₄Cl, 0.2 ml of 0.2% resazurin, 12 mM

HEPES, 12 mM sodium acetate, 3.7 mM sodium succinate and 2 g of Bacto-Agar in 1 L of ASW. The medium was autoclaved, followed by the addition of 1.5 mL of 0.5 M KHPO₄, pH 7.1, neutral fresh L-cysteine (final concentration of 0.2 g/L), 2.68 mL of 0.8 mM NaHCO₃ and 4.8 mM Na₂O₃S₂•5H₂O. The pH was adjusted to 7.2, and 0.5 mL of a vitamin solution (Frankel et al., 1997) and 2.5 mL of 0.01 M ferric quinate were added. Cells were inoculated at the OAI, and the cultures were incubated at 28°C for at least 15 days.

Oxygen concentrations were measured using a Unisense OX 100 oxygen microsensor, with a detection limit of 0.3 μM, coupled to a micromanipulator MM33 (Unisense, Aarhus, Denmark). Measurements were carried in duplicate tubes at 24 h intervals for 8 days in semi-solid heterotrophic medium. Calibration was done by submerging the sensor in a 0.1 M of ascorbate and 0.1 M of NaOH solution (0% O₂ saturation) and oxygenated water (100% O₂ saturation). The oxygen concentration profile was determined to a depth of 11 mm from the culture medium surface in 200 μm steps taking 5 s for each measurement. The O₂ microsensor was stabilized for 2–3 h before any measurement. Data were recorded in the software SensorTrace Pro v3.0.2 (Unisense)

LIGHT AND ELECTRON MICROSCOPY

For light microscopy imaging, drops of ASW containing magnetically-enriched MTB were placed onto coverslips and imaged with Zeiss Axioplan 2 or Zeiss Axioimager microscopes (Carl Zeiss, Göttingen, Germany), both equipped with differential interference optics. A bar magnet was used to direct MTB to the edge of the drop where they accumulated. Transmission electron microscope (TEM) imaging of cells and elemental analysis of both magnetosomes and cell inclusions were performed in unfixed and unstained samples with a Jeol 1200 EX transmission (Jeol, Peabody, MA, USA) electron microscope equipped with a Noran accessory for energy-dispersive X-ray analysis (EDS) (Thermo Scientific, Palm Beach, FL, USA). Cells were placed onto formvar-coated electron microscopy 300 mesh copper grids, rinsed with distilled water and air-dried. Observations were performed at 100 kV, and spectra were acquired using a spot size of approximately 80 nm in diameter. For magnetosome measurements, the grids were observed with a Morgagni TEM (FEI Company, Hillsboro, OR, USA) operating at 80 kV, and images were analyzed using ImageJ software (rsb.info.nih.gov/ij/). Crystal size and shape factor were calculated as (length + width)/2 and width/length, respectively. Analyses of variance were performed using Graphpad InStat version 3.0.

For energy-filtering transmission electron microscopy (EFTEM), unstained ultra-thin sections were imaged with a Zeiss EM902 (Carl Zeiss, Göttingen, Germany) TEM equipped with a mirror-prism. Iron and oxygen maps were calculated using the three-window method with iTEM-EFTEM software (Olympus Soft Imaging Solutions GmbH, Münster, Germany). For high-resolution TEM (HRTEM), ultra-thin sections obtained as described in Abreu et al. (2013) were placed on formvar-coated copper grids and imaged in a FEG-Titan 80-300 (FEI Company, Hillsboro, OR, USA) TEM operated at 300 kV. All images were digitized with a 2kx2k Gatan UltraScan 1000 CCD camera (Gatan, Pleasanton, CA, USA) using the Digital Micrograph

software (Mitchell, 2008). FFT from magnification-calibrated images was obtained using the same software.

16S rRNA PHYLOGENETIC ANALYSIS, GENOME SEQUENCING AND COMPARATIVE ANALYSIS OF GENES RELATED TO MAGNETOSOME FORMATION

The 16S rRNA gene was amplified from *M. australis* strain IT-1 using bacterial specific primers 8bF (5'-GRGTTTGATCCTGGC TCAG-3') and 1512uR (5'-ACGGHTACCTTGTACGACTT-3'). PCR products were cloned into pGEM-T Easy vector (Promega Corporation, Madison, WI) and sequenced using Macrogen sequence service (Macrogen, Korea). The alignment of 16S rRNA gene was performed using CLUSTAL W with BioEdit sequence alignment editor (Hall, 1999). A phylogenetic tree was constructed using MEGA version 5.2 (Tamura et al., 2011). We used the maximum likelihood statistical method based on Kimura 2 parameters (Kimura, 1980) with Gamma distribution and invariant sites (K2 + G + I) for analyses. The bootstrap value was calculated with 1000 replicates.

For DNA preparation for pyrosequencing, *M. australis* strain IT-1 was grown in semisolid medium. After 15 days of growth, bands from different tubes were removed, concentrated by centrifugation and washed several times with sterile distilled water. DNA samples were prepared according to Chen and Kuo (1993). *M. australis* strain IT-1 DNA was sequenced on a 454 GS FLX System sequencer (Roche Diagnostics GmbH/454 Life Sciences Corporation, Branford, CT, USA). The DNA sequences were analyzed with the SABIA (System for Automated Bacterial Integrated Annotation) platform (Almeida et al., 2004). Amino acid sequences of the MAI proteins from *M. magneticum* strain AMB-1 (AP007255) (Matsunaga et al., 2005), *M. gryphiswaldense* strain MRS-1 (AM085146) (Lohße et al., 2011), *M. magnetotacticum* strain MS-1 (NZ_AAAP01003731) (Bertani et al., 2001), *M. marinus* strain MC-1 (NC_008576) (Schübbe et al., 2009), *M. blakemorei* strain MV-1 (FP102531) (Jogler et al., 2009), Gammaproteobacteria strain SS-5 (AFX88983—AFX88992) and *M. australis* strain IT-1 were used for identity, positives and E-value analysis through Blastp. Other sequences used in this work include *Ca. M. multicellularis* (HQ336745 and HQ336746) (Abreu et al., 2011), *D. magneticus* strain RS-1 (AP010904) (Nakazawa et al., 2009), *Ca. D. magnetomortis* strain BW-1 (HF547348) and strains ML-1 (JX869936—JX869937) and FH-1 (KC196864—KC196902) (Lefèvre et al., 2013b). A phylogenetic tree of concatenated MamABEIKMPQ amino acid sequences was constructed using the maximum likelihood statistical method based on WAG (Whelan and Goldman, 2001) with frequencies and gamma distribution (WAG+G+F) for analyses. Bootstrap value was calculated with 1000 replicates. The sequence of the MAI region has been submitted to GenBank/NCBI under the accession number KF933436.

RESULTS

ISOLATION, GROWTH AND PHYLOGENETIC ANALYSES OF STRAIN IT-1

Magnetotactic cocci were the dominant MTB morphotype in the environmental samples. Occasionally, we detected magnetotactic multicellular prokaryotes, as previously described (Lins et al., 2007). After separation using the magnetic “racetrack” (Wolfe et al., 1987), magnetically-enriched cocci were inoculated

at the OAI of the semisolid autotrophic medium. Four weeks later, microaerophilic bands of coccoid MTB were observed and were then inoculated in semisolid heterotrophic [O_2] gradient medium in which the culture was maintained. Cells formed individual colonies in shake tubes of heterotrophic medium (see experimental procedures for details). Single colonies were reinoculated in fresh semisolid medium and resulted in pure cultures of a magnetotactic coccus with an average size of $1.4 \pm 0.3 \times 1.1 \pm 0.3 \mu\text{m}$ ($n = 130$) as observed by light microscopy (**Figure 1A**) and confirmed by TEM (**Figure 1B**). The morphology of cells observed by TEM resembles a “faba” bean, showing well-defined convex and concave surfaces (**Figure 1B**). Cells contain intracellular granules (**Figure 1B**) filled with phosphorus as detected by EDS (**Figure 1E**).

The 16S rRNA gene of the culture was amplified, cloned, and sequenced for phylogenetic analyses. Approximately 50 clones were sequenced. These sequences were 99% similar,

confirming the culture was pure. A consensus sequence was generated (accession number: JX534168) and phylogenetic analysis showed that strain IT-1 is phylogenetically affiliated with the *Alphaproteobacteria* (**Figure 2**). The 16S rRNA gene sequence of strain IT-1 is 93% similar to the sequence of an uncultured magnetotactic coccus collected from intertidal sediments of the Yellow Sea in China (Zhang et al., 2012; accession number JF421219) and 92% similar to sequences of the cultured species *M. marinus* strain MC-1 and MO-1 (accession numbers CP000471 and EF6435202, respectively). Thus, strain IT-1 represents a new genus of the magnetotactic cocci (and MTB in general). The name *Magnetofaba australis* gen. nov., sp. nov., is proposed for strain IT-1 (Ma. gne. to. faba Gr. n. magnēs -étos, a magnet; N.L. pref. magneto-, pertaining to a magnet; N.L. fem. N. faba, a faba bean; aus.trā'lis. L. masc. australis of Southern or of the south, which refers to the polar south-seeking magnetotaxis behavior and because the bacterium was isolated from South hemisphere).

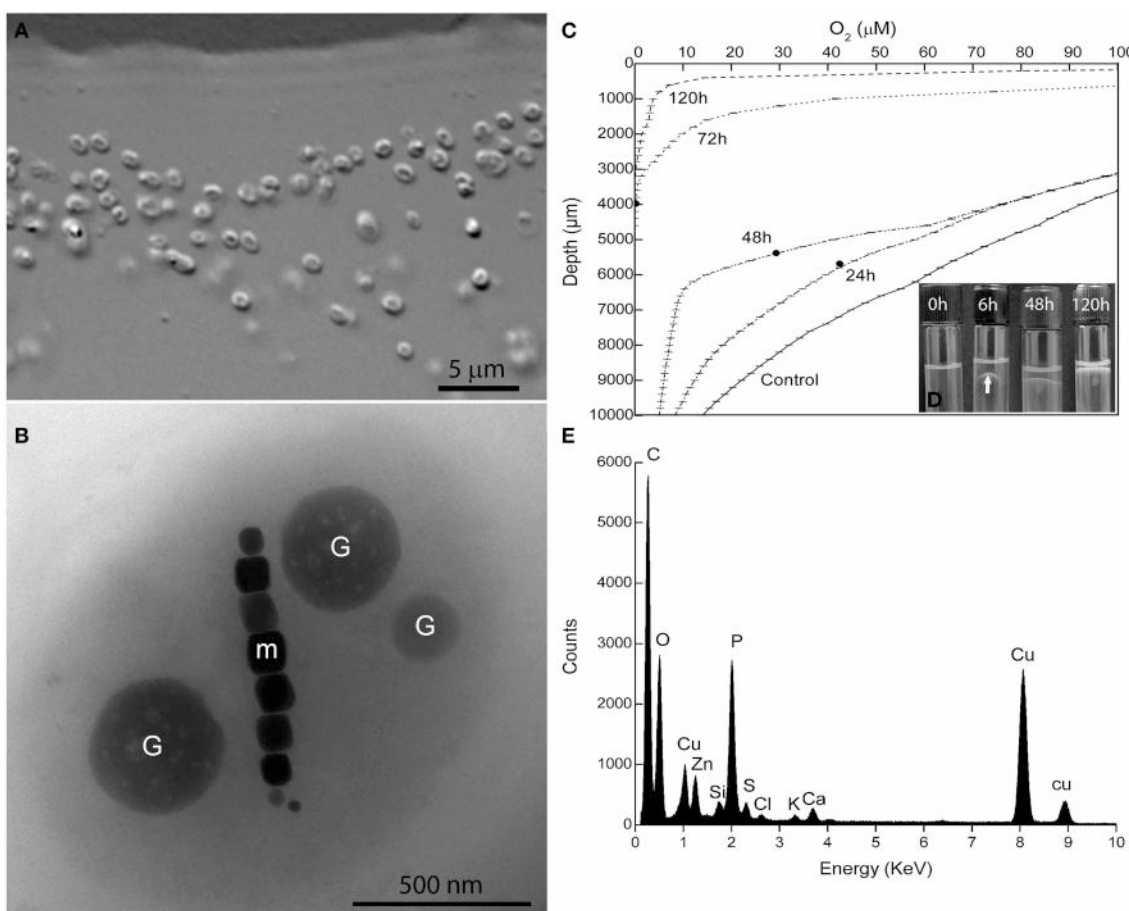


FIGURE 1 | Characterization of *Magnetofaba australis* strain IT-1. (A) Differential interference contrast microscopy of a pure culture showing coccoid to ovoid cells. **(B)** Whole-mount transmission electron microscopy image of strain IT-1 showing a chain of elongated octahedral magnetosomes (m) and three conspicuous granules containing phosphorus (G). **(C)** Oxygen concentration over time (0–120 h) and band formation (D) during strain IT-1 growth in semisolid heterotrophic medium. The

points in the lines represent the position of the band in the culture medium at a given time. Control is represented by a non inoculated tube. Note the band with magnetotactic cells (arrow) after 6 h of inoculation. **(E)** Energy dispersive X-ray microanalysis spectrum of the phosphorus-rich granules. Ca, Zn, and K are cations associated with the granules. Cu peaks come from the supporting grid. The silicon peak is an artifact of the Si (Li) solid state detector used to collect X-rays.

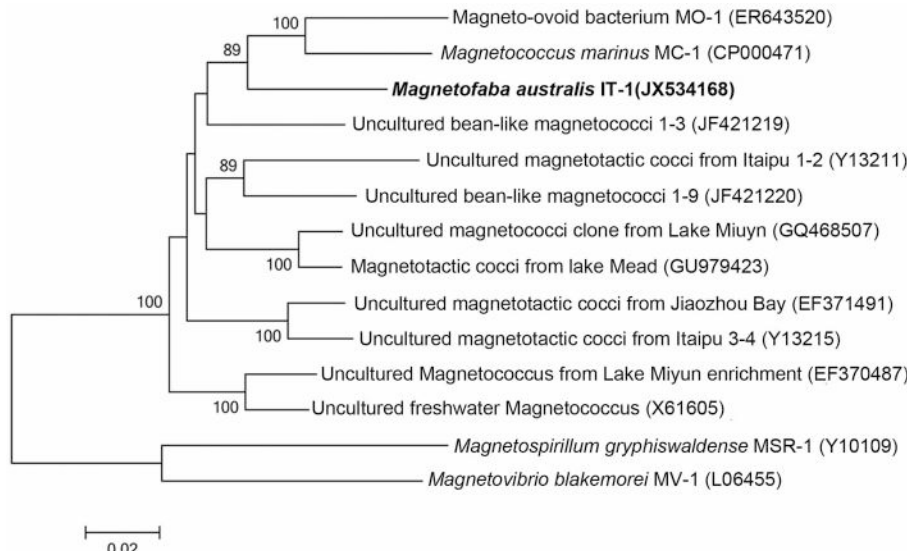


FIGURE 2 | Phylogenetic analysis based on the 16S rRNA gene of strain IT-1 that forms a new genus in the Alphaproteobacteria. Bootstrap values at nodes are percentages of 1000 replicates; values higher than 70 are shown

at the nodes. GenBank accession numbers are given in parentheses. The phylogenetic tree was constructed using the maximum likelihood method algorithm. The scale bar indicates 0.02 substitutions per nucleotide position.

Magnetofaba australis strain IT-1 grows as a microaerophilic band of cells in semisolid medium (Figure 1D). It grows slowly chemolithoautotrophically, using thiosulfate as electron donor and sodium bicarbonate as the major carbon source, forming a fine band of cells at the OAI at least 4 weeks after incubation. Under these conditions, cells biominerize 6 ± 4 magnetosomes/cell ($n = 100$). Heterotrophic growth was also observed using sodium acetate and sodium succinate as the carbon source; cells grown under these conditions produced 9 ± 4 and 7 ± 3 magnetosomes per cell, respectively ($n = 100$ for both). When cells were grown in heterotrophic medium containing both sodium acetate and succinate, a band of magnetotactic cells, which contained 10 ± 3 magnetosomes/cell ($n = 100$), was observed at the OAI after 24 h. This band gradually moved toward the surface of the culture medium after 8 days of incubation (Figure 1D).

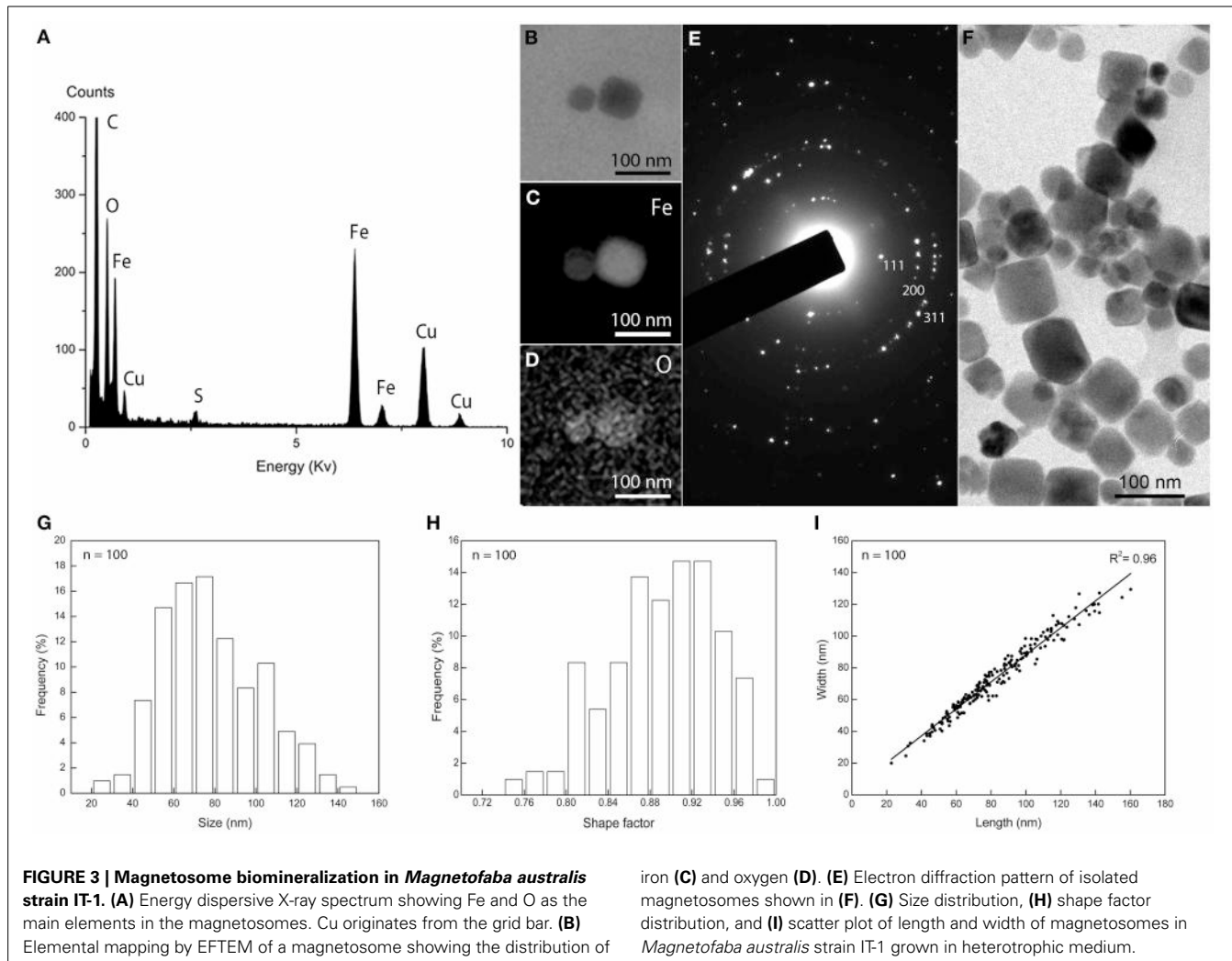
The oxygen concentration in the band was measured over 8 days (Figure 1C) in the heterotrophic medium; cells were initially inoculated at the OAI, in which $[O_2]$ was less than $3 \mu M$. During the first 6 h after inoculation, cells moved up approximately 3 mm, forming a “bell-shaped” band (Figure 1D) in the medium ($[O_2] = 50 \pm 5 \mu M$). After 24 h, the band was positioned between 24.6 ± 0.7 and $43 \pm 1 \mu M O_2$, with a less bent bell-shape. 48 h later, the band was located in $29.2 \pm 2.7 \mu M$ of $[O_2]$. After 72 h, the bell-shaped band became a flat band positioned at $[O_2]$ between $9.4 \pm 1.5 \mu M$. Until this time, the band did not reach the meniscus of the culture medium. As the cells grew (up to 168 h), O_2 was consumed, and the dense population of cells reached the meniscus, presumably to use oxygen present in the headspace of the tube (Figure 1D). At 72 h of incubation the cells of *M. australis* have consumed near 90% of oxygen ($[O_2] < 9.4 \pm 1.5 \mu M$), and the band appears thicker than in

24 and 48 h. With 72 h, it is likely that the magnetite production also increased, given the higher number of cells and that the population remained responding to the magnetic field at the end of the experiment. Therefore, *M. australis* strain IT-1 can grow and synthesize magnetite with $[O_2]$ below $10 \mu M$, similar to the *Magnetospirillum* species, which requires microaerobic conditions ($2-7 \mu M O_2$) to grow and synthesize magnetite (Schüler and Baeuerlein, 1998).

In hanging drop assays under oxic conditions, *M. australis* strain IT-1 exhibited South-seeking polar magnetotaxis swimming under the magnetic field of a bar magnet with a fast back and forth swimming pattern near the edge of the drop. *M. australis* swims at average speeds of $186 \mu m.s^{-1} \pm 63$ ($n = 50$) and can reach $300 \mu m.s^{-1}$. Cells are propelled by two bundles of lophotrichous flagella, each at one extremity of the cell. A helical trajectory was observed when movement was recorded with a CCD camera using dark-field microscopy.

MAGNETOSOMES

Cells of *M. australis* strain IT-1 each produce a single chain of magnetosomes (see Figure 1B). Each chain consists of 10 ± 3 magnetosomes ($n = 100$) in cells grown heterotrophically in semi-solid $[O_2]$ gradient medium. Energy-dispersive X-ray analysis (Figure 3A) and elemental mapping by EFTEM (Figure 3B) confirmed that the magnetosomes contain iron (Figure 3C) and oxygen (Figure 3D). Electron diffraction (Figure 3E) of isolated magnetosome crystals (Figure 3F) were indexed based on standard cubic system for magnetite. Distances and angles between spots were consistent with magnetite (Fe_3O_4). Approximately 4% defective twins and multiple twin magnetosomes are observed in *M. australis* strain IT-1. The crystals are octahedral particles

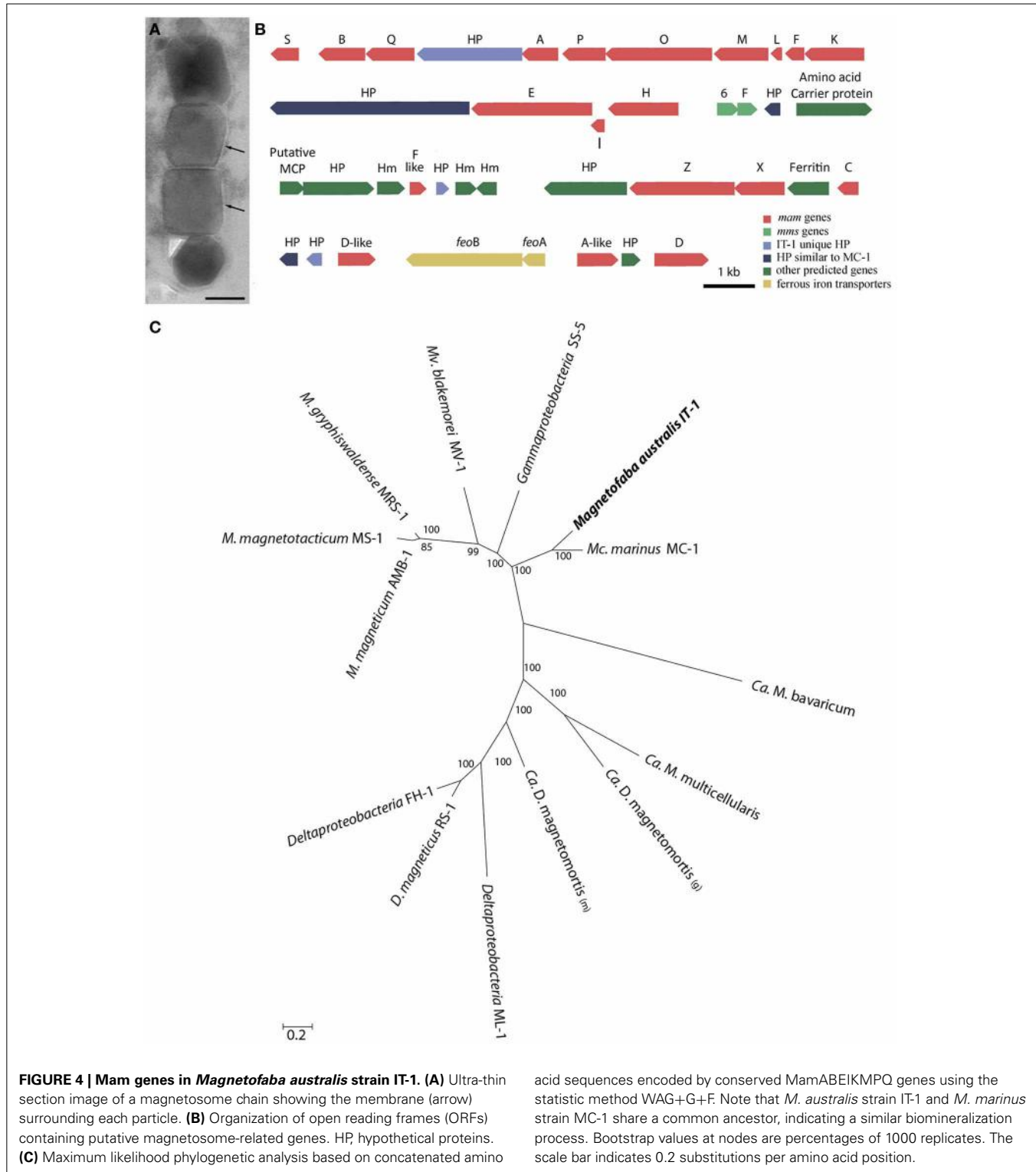


elongated along the $<111>$ axis. **Figure 3G** shows the size distribution of magnetosomes ($n = 100$), estimated by calculating the best fit of an ellipse (major axis = length; minor axis = width). The average size [(length + width)/2] was 78 ± 24 nm (average length = 83 ± 26 nm; average width 74 ± 23 nm). **Figure 3H** shows the shape factor distribution (average of width/length = 0.89 ± 0.05), and **Figure 3I** shows the scatter plot of length and width (adjustment $r^2 = 0.962$). Magnetosomes in *M. australis* strain IT-1 are each enveloped by a membrane, as shown in TEM images of ultra-thin sections (**Figure 4A**).

MAGNETOSOME GENES

Comparative genome analysis of *M. australis* strain IT-1 with other magnetotactic *Alphaproteobacteria* based on genes related to magnetotaxis and magnetosome synthesis revealed a genomic region of 40.399 Kb that contained both genes associated with magnetosome biominerization as well as those that encode some hypothetical proteins present in the putative MAI of *M. marinus*. This region contains 39 genes, 22 of which show a high degree of similarity with the biominerization-related genes of

magnetotactic *Alphaproteobacteria* (*mam* genes and *mms* genes; **Table 1**). This region also contains eight hypothetical proteins, four with high similarity values to hypothetical proteins in the putative MAI of *M. marinus* and four that are not found in any known MTB. A *feoAB* gene cluster was also identified in this region, similar to that found in *Magnetospira* sp QH-2, *Ca. Mg. multicellularis* and *Ca. D. magnetomortis*. **Figure 4B** shows the organization of the genes in *M. australis* strain IT-1. The *mamAB*-like gene cluster has the same gene organization found in *M. marinus* (*mamK*, *mamF*, *mamL*, *mamM*, *mamO*, *mamP*, *mama*, *HP*, *mamQ*, *mamB* and *mamS*) (Schübbe et al., 2009), except that *mamT* is absent. The *mamC* gene is located in the *mamCXZ* gene cluster, similar to *M. blakemorei* (Jogler et al., 2009), and not in the *mamHIEC* gene cluster as in *M. marinus*. The *mms6* gene cluster and the 10 genes encoding MamF-like protein, chemotaxis protein, signal transduction proteins and three hypothetical proteins are located between the *mamAB* and *mamCXZ* gene clusters. At the end of the *mamCXZ* gene cluster, genes encoding MamD-like, FeoB, FeoA, MamA-like and MamD proteins are present. All predicted proteins related to biominerization and magnetotaxis genes described here for *M. australis* strain IT-1 share the highest



similarity to those of *M. marinus*, including MamA-like, MamD-like, MamF-like, FeoB and FeoA proteins. A notable exception is MamC, which is more related to that from *M. magneticum* strain AMB-1 (coverage 86%, identity 63%, *E*-value 5e-038).

The coverage, identity and *E*-value of the Blastp analysis of predicted Mam proteins from magnetotactic *Alphaproteobacteria* and the *Gammaproteobacteria* strain SS-5 were analyzed (Table 1). *M. australis* MamA-like, MamD-like and MamF-like proteins

Table 1 | Comparative analysis of biomineralization genes found in *Magnetofava australis* strain IT-1 and other cultivated magnetotactic bacteria with their genomes sequenced.

IT-1	MC-1	MV-1	AMB-1	MS-1	MSF-1	SS-5							
Protein (locus number)	E-value (%)	Coverage (%)	Identity (%)	E-value (%)	Coverage (%)	Identity (%)	E-value (%)	Coverage (%)	Identity (%)	E-value (%)	Coverage (%)	Identity (%)	
MamS (2777) 1E-061	90	58	1E-035	65	44	1E-023	64	40	5E-024	64	40	2E-023	
MamB (5564) 6E-169	98	73	2E-112	98	52	5E-100	97	46	2E-063	92	38	3E-101	
MamQ (2780) 6E-128	96	62	2E-053	91	34	7E-048	84	34	2E-043	67	37	2E-050	
MamaA (2782) 6E-089	98	58	2E-048	98	35	2E-054	95	39	6E-060	97	38	1E-054	
MampP (5510) 3E-123	98	64	4E-062	67	52	6E-047	67	43	1E-047	67	42	9E-048	
MamO (5499) 0.0	99	57	1E-033	42	27	6E-121	97	35	4E-121	97	35	2E-115	
MamM (5508) HP Similar to 5E-031	95	69	2E-110	96	47	2E-101	89	48	1E-090	83	47	2E-102	
Maml (2787) 7E-016	93	74	7E-016	96	40	6E-007	95	28	1E-006	95	28	7E-006	
MamF (2788) 6E-045	80	70	—	—	3E-029	96	46	9E-028	74	52	5E-029	83	
MamK (2789) 0.0	100	82	5E-113	97	46	7E-132	99	51	1E-122	92	51	6E-129	
MamE (2791) 0.0	100	48	4E-092	98	32	1E-095	98	35	6E-096	98	35	1E-066	
Maml (2792) 9E-029	66	81	2E-025	78	62	4E-014	82	51	4E-014	82	51	2E-014	
MamH (5506) 0.0	100	70	4E-160	97	53	3E-157	95	55	1E-129	81	54	1E-155	
HP similar to 9E-011	28	61	4E-004	26	40	1E-006	36	56	8E-007	36	56	0.12	
MmsF (2798) 7E-056	83	76	5E-039	81	52	1E-036	79	52	8E-035	79	53	2E-035	
MamFlkE (2808)	6E-032	77	47	3E-026	96	39	2E-025	91	45	7E-026	91	44	1E-022
MamZ (2814) 0.0	95	61	1E-171	94	42	0.0	93	51	0.0	93	51	MnsF	
MamX (2815) 6E-104	100	48	3E-026	54	45	2E-056	99	35	2E-010	31	29	1E-057	
MamC (2817) 4E-028	93	62	1E-015	82	62	5E-032	86	63	6E-032	82	63	4E-034	
MamD-like (2822) 1E-018	97	42	—	—	—	—	—	—	—	—	—	—	
FeoB (2827) 81-144	99	59	6E-112	97	50	5E-087	98	45	3E-090	97	45	1E-087	
FeoA (2828) 3E-030	55	61	7E-015	61	40	4E-018	58	40	1E-012	52	39	2E-012	
MamA-like (2830) 9E-041	65	47	1E-013	57	30	1E-020	66	31	1E-020	66	31	MamA	
MamD (2833) 4E-038	92	38	3E-014	96	39	6E-029	63	35	3E-029	63	35	1E-028	

Bold values are related to most similar proteins between *M. australis* strain IT-1 and other MTB according to blastp.

were compared to MamA-like, MamD-like and MamF-like of *M. marinus*, and MamA, MamD and MamF proteins of other MTB. The *M. australis* MamA-like predicted protein is closely related to the *M. marinus* protein sequence (coverage 65%, identity 47%, *E*-value 9e-041), while MamD-like is only related to the MamD-like from *M. marinus* (coverage 97%, identity 42%, *E*-value 1e-018). For some MTB, *M. australis* MamF-like sequences were more similar to MmsF or MmsF-like proteins (e.g., from *M. gryphiswaldense* and *M. blakemorei*). MamF and MmsF of *M. gryphiswaldense* MSR-1 have already been reported to share 65% identity (Murat et al., 2012). *M. australis* strain IT-1 MamA-like predicted proteins with MamA proteins share 30% identity (coverage 57%, *E*-value 7E-018), while MamD-like predicted proteins share 73% identity with MamD (coverage 23%, *E*-value 7E-05), and MamF-like predicted proteins share 33% identity (coverage 89%, *E*-value 2E-016) and 39% identity (coverage 90%, *E*-value 1E-021) with MamF and MmsF, respectively.

Phylogenetic analysis based on concatenated conserved Mam proteins (MamABEIKMPQ) of other MTB showed that *M. australis* strain IT-1 clusters with other *Alphaproteobacteria* that produce magnetite and is most related to *M. marinus* strain MC-1. The *Gammaproteobacteria* strain SS-5, which synthesizes cuboctahedral magnetite magnetosomes, groups with the *Alphaproteobacteria*. Interestingly, after *M. marinus*, MamB, MamQ and MamM of *M. australis* strain IT-1 have the most similarity with MamB of strain SS-5 (coverage 98%, *E*-value 2E-128, identity 59%), MamQ (coverage 67%, *E*-value 6E-053, identity 44%) and MamM (coverage 86%, *E*-value 4E-127, identity 59%). The phylogenetic tree (**Figure 4C**) with concatenated conserved *mam* genes does not show a clear evolutionary event that divides magnetotactic strains producing cuboctahedral and prismatic hexagonal crystals because bacteria such as *M. blakemorei* and *M. marinus* do not form a separate branch. The evolutionary relationship between *M. australis* and *M. marinus* suggests a recent divergence between the cellular magnetosome biomimetic machinery in these species.

DISCUSSION

The number of MTB isolated in culture has recently increased (from 1978 to 2009, 11 MTB were available in axenic cultures; in 2012 this number was 25; Lefèvre and Long-Fei, 2013). However, all cultured MTB were isolated in the Northern Hemisphere and originally showed NS magnetotaxis. This work presents the first isolation of a SS-MTB from the Southern Hemisphere. The new isolate is phylogenetically affiliated with the *Alphaproteobacteria* class of the *Proteobacteria* phylum, a division that contains almost all known Fe₃O₄-producing MTB (DeLong et al., 1993; Spring et al., 1998), and clearly represents a new genus based on 16S rRNA gene sequence similarities. This new coccus represents a third phylogenetic group of MTB occurring in the Itaipu Lagoon (Spring et al., 1998). *M. australis* strain IT-1 is distinct from all the other cultivated magnetotactic cocci examined to date because of its South-seeking polar magnetotactic behavior, it has “faba bean” cell morphology and elongated cuboctahedral magnetite magnetosomes. Based on its 16S rRNA gene sequence, *M. australis* is more related to an uncultured magnetotactic coccus found in the intertidal sediments of the Yellow Sea in China (93% similarity;

Zhang et al., 2012). This uncultured bacterium also shows a bean-like morphology and produces magnetite magnetosomes (Zhang et al., 2012). However, magnetosome crystal morphology, size, shape factor, magnetosome number and swimming speed in *M. australis* are different from the coccus described by Zhang et al. (2012). The close phylogenetic relationships may not be significantly associated to the biomimetic genes, which may result in variations in the regulation of crystal morphology between these MTB. Hopefully, physiological studies and genomic analysis of these MTB will result in information that advances the understanding of biomimetic in bean-like magnetotactic cocci.

Magnetofaba australis strain IT-1 has a swimming speed similar to that observed in strain MO-1 (Lefèvre et al., 2009), higher than speeds found in other magnetotactic cocci (Zhang et al., 2012). Possibly, a highly coordinated flagella rotation is necessary to allow this high swimming speed. The high swimming speed would be advantageous for the survival of *M. australis* strain IT-1 because it would enable the cell to escape quickly from unfavorable environment conditions. Most cells of *M. australis* strain IT-1 (over 80%) has a South-seeking behavior when observed in hanging drop assays under oxic conditions, but we have also found North-seeking cells in the culture flasks. Further studies are necessary to compare the swimming behavior and orientation of magnetotactic cocci, along with their flagellar apparatus at the genetic and structural levels. We believe that such studies can now be performed because of the available SS-MTB cultures.

The role of biomimetic and magnetotaxis genes in MTB is not only key in the determination of how magnetosomes are formed in MTB but also important in understanding the evolution of magnetotaxis (Lefèvre and Bazylinski, 2013). Although several recent reports have addressed this issue (Lefèvre et al., 2013a,b), only a relatively small number of MTB species have been considered thus far. However, advances in the culturing of new strains promises to improve the low number of species available for evolutionary studies. *M. australis* strain IT-1 is the first MTB isolated in axenic culture that produces cuboctahedral magnetite magnetosomes whose magnetosome biomimetic genes have been sequenced. New data on the magnetosome biomimetic genes of coccoid or ovoid MTB increases our understanding of the biomimetic processes in MTB in general. For example, *M. marinus* and *M. australis* share several hypothetical proteins, not found in other MTB that may have key functions in biomimetic or magnetotaxis like the hypothetical protein between MamE and MamK (locus 02790), the hypothetical protein between MmsF and the Amino acid carrier protein (locus 02801), the Amino acid carrier protein (locus 02803), a hemerythrin-like (locus 02811), and a ferritin-like (locus 02816).

The analysis of the putative functions of *mam* genes is also important in the interpretation of the evolution of magnetotaxis. Variations in both the order and sequence of *mam* genes between *M. australis* and the closely related *M. marinus* could explain differences between magnetosome crystal morphology in the two species. The MamC predicted protein sequence of *M. australis* is more similar to that of *M. magneticum* strain AMB-1, which is particularly interesting because cultivated *Magnetospirillum* species described thus far produce cuboctahedral magnetite

crystals that are not elongated (Amann et al., 2007). Scheffel et al. (2008) showed that the protein MamC and other proteins in the same operon (*mamGFDC*) are not essential for magnetosome formation but are involved in controlling crystal size and morphology in *M. gryphiswaldense*. In *M. australis*, *mamC* is organized in a *mamCXZ* operon, similar to *M. blakemorei*. The other proteins involved in the size and shape of magnetosomes (MamD, MamF, Mms6, and MmsF) are more closely related to those found in *M. marinus*. Therefore, the fact that *M. australis* MamC is related to cuboctahedral magnetite-producing bacteria suggests that this protein might be responsible for crystal morphology in this case. Additionally, based on the similarity of *mamXZC* gene organization between *M. australis* and *M. blakemorei*, we speculate that gene organization and/or preferential expression of *mamCXZ* could be involved in crystal elongation. MmsF has been shown to be involved in the geometry of magnetosome maturation, as the deletion of *mmsF* resulted in elongated magnetosomes in *M. magneticum* strain AMB-1 (Murat et al., 2012). However, we did not identify a close similarity between MmsF from *M. australis* strain IT-1 and other MTB that synthesize elongated octahedral crystals. The expression level of MmsF may influence crystal morphology, which could explain how closely related *mam* genes from different species (i.e., *M. australis* and *M. marinus*) produce magnetosomes with different characteristics. Variation in the expression level of the *mamGFDC* operon in *M. gryphiswaldense* resulted in crystals exceeding the size of those of the wild-type (Scheffel et al., 2008). The absence of *mamT* in *M. australis* strain IT-1 reveals a new group of 19 genes common to cultivated magnetotactic *Alphaproteobacteria*: *mamA, B, C, D, E, F, H, I, K, L, M, N, O, P, Q, R, S, X* and *Z*, in addition to the *mms6* and *mmsF* genes. Although *mamT* is present in the *Alpha-* and *Deltaproteobacteria*, it is not essential for biomimetic mineralization. Proteins with similar function (MamP or MamE) are likely sufficient to control the balance between Fe²⁺ and Fe³⁺ in the magnetosome. In *M. magneticum* (Murat et al., 2010) and *M. gryphiswaldense* (Lohße et al., 2011) *mamT* is not essential for magnetosome synthesis.

Considering that both *M. australis* strain IT-1 and *M. marinus* strain MC-1 have a common magnetotactic ancestor and that biomimetic mineralization proteins apparently evolved together in both strains, it is reasonable to assume that a common ancestor exists among all freshwater and marine MTB from the *Magnetococcales* order. No non-MTB belonging to the *Magnetococcales* order has ever been reported, but this fact does not preclude HGT among *Alphaproteobacteria* because strains phylogenetically closer to *Magnetospirillum* do not have the magnetotactic phenotype (Jogler and Schüller, 2009). Thus, magnetosome biomimetic mineralization genes common to all MTB (*mamABEIKMPQ*) might have been acquired from an ancestor common to all MTB (Abreu et al., 2011; Lefèvre et al., 2013a). However, genes such as *mamCDF*, *mamL*, *mamXZ*, *mms6*, and *mmsF* could have been acquired by descent of magnetotactic *Alphaproteobacteria* and magnetotactic cocci, which appear to emerge as the most basal lineage of the *Alpha-* and *Gammaproteobacteria* (Singer et al., 2011; Lefèvre and Bazylinski, 2013). *mamG*, *mamR*, *mamV*, *mamU*, and *mamY* genes were likely acquired recently by *Magnetospirillum* species, given that the magnetotactic cocci

studied so far, *M. marinus* strain MC-1 and *M. australis* strain IT-1, do not contain these genes. Differences observed in the biomimetic mineralization genes between *M. australis* strain IT-1, *M. marinus* strain MC-1 and the other *Alphaproteobacteria* are possibly a result of gene rearrangements, deletions or insertions of new genes through the evolution or a post-acquisition of the biomimetic mineralization genotype among MTB. Culture and sequencing of new species of magnetotactic cocci from freshwater or marine water are needed to improve the understanding the evolutionary events that occurred in the *Alphaproteobacteria* and magnetotactic cocci and will more precisely define the *Magnetococcaceae* family in the *Magnetococcales* order as either the earliest diverging order in the *Alphaproteobacteria* class or as a new class of *Proteobacteria*, as proposed by Singer et al. (2011). *M. australis* strain IT-1 is now the third cultivated magnetotactic coccus that represents a second new genus in the *Magnetococcaceae* family and is the first cultivated SS-MTB.

AUTHOR CONTRIBUTIONS

All authors contributed to the analysis of data and composition of the paper; Viviana Morillo, Fernanda Abreu and Ana C. Araujo: experimental data acquisition and cultivation; Luiz G. P. de Almeida and Ana T. R. de Vasconcelos: pyrosequencing and bioinformatics; Alex Enrich-Prast: microelectrode measurements and interpretation; MF: high-resolution transmission electron microscopy, Viviana Morillo, Fernanda Abreu, Dennis A. Bazylinski and Ulysses Lins: analyzed data and wrote the paper.

ACKNOWLEDGMENTS

We acknowledge Dr. Andrea P. C. Campos and the DIMAT-INMETRO and LABNANO-CBPF for use of high-resolution transmission electron microscopy facilities. Financial support from the Brazilian agencies CAPES, CNPq and FAPERJ is acknowledged. Dennis A. Bazylinski is supported by US National Science Foundation (NSF) Grant EAR-0920718 and by subcontract SC-12-384 from US Department of Energy contract DE-AC02-07CH11358 issued to the Ames Laboratory at Iowa State University.

REFERENCES

- Abreu, F., Cantão, M. E., Nicolas, M. F., Barcello, F. G., Morillo, V., Almeida, L. G., et al. (2011). Common ancestry of iron oxide-iron-sulfide-based biomimetic mineralization in magnetotactic bacteria. *ISME J.* 5, 1634–1640. doi: 10.1038/ismej.2011.35
- Abreu, F., Morillo, V., Nascimento, F. F., Werneck, C., Cantão, M. E., Ciapina, L. P., et al. (2013). Deciphering unusual uncultured magnetotactic multicellular prokaryotes through genomics. *ISME J.* doi: 10.1038/ismej.2013.203. [Epub ahead of print].
- Almeida, L. G., Paixão, R., Souza, R. C., Costa, G. C., Barrientos, F. J., Santos, M. T., et al. (2004). A system for automated bacterial (genome) integrated annotation - SABIA. *Bioinformatics* 20, 2832–2833. doi: 10.1093/bioinformatics/bth273
- Amann, R., Peplies, J., and Schüller, D. (2007). “Diversity and taxonomy of magnetotactic bacteria,” in *Magnetoreception and Magnetosomes in Bacteria*, ed. D. Schüller (Berlin; Heidelberg: Springer-Verlag), 25–36. doi: 10.1007/7171_037
- Bazylinski, D. A., and Frankel, R. B. (2004). Magnetosome formation in prokaryotes. *Nat. Rev. Microbiol.* 2, 217–230. doi: 10.1038/nrmicro842
- Bazylinski, D. A., Williams, T. J., Lefèvre, C. T., Berg, R. J., Zhang, C. L., Bowser, S. S., et al. (2013a). *Magnetococcus marinus* gen. nov., sp. nov., a marine, magnetotactic bacterium that represents a novel lineage (*Magnetococcaceae* fam. nov.; *Magnetococcales* ord. nov.) at the base of the *Alphaproteobacteria*. *Int. J. Syst. Evol. Microbiol.* 63, 801–808. doi: 10.1099/ijss.0.038927-0

- Bazylinski, D. A., Williams, T. J., Lefèvre, C. T., Trubitsyn, D., Fang, J., Beveridge, T. J., et al. (2013b). *Magnetovibrio blakemorei* gen. nov. sp. nov., a magnetotactic bacterium (Alphaproteobacteria: Rhodospirillaceae) isolated from a salt marsh. *Int. J. Syst. Evol. Microbiol.* 63, 1824–1833. doi: 10.1099/ijsm.0.044453-0
- Bertani, L. E., Weko, J., Phillips, K. V., Gray, R. F., and Kirschvink, J. L. (2001). Physical and genetic characterization of the genome of *Magnetospirillum magnetotacticum*, strain MS-1. *Gene* 264, 257–263. doi: 10.1016/S0378-1119(01)00331-6
- Blakemore, R. P. (1982). Magnetotactic bacteria. *Ann. Rev. Microbiol.* 36, 217–238. doi: 10.1146/annurev.mi.36.100182.0001245
- Blakemore, R. P., Frankel, R. B., and Kalmijn, A. J. (1980). South-seeking magnetotactic bacteria in the Southern Hemisphere. *Nature* 286, 384–385. doi: 10.1038/286384a0
- Chen, W., and Kuo, T. (1993). A simple and rapid method for the preparation of Gram-negative genomic DNA. *Nucleic Acids Res.* 21, 2260. doi: 10.1093/nar/21.9.2260
- DeLong, E. F., Frankel, R. B., and Bazylinski, D. A. (1993). Multiple evolutionary origins of magnetotaxis in bacteria. *Science* 259, 803–806. doi: 10.1126/science.259.5096.803
- Frankel, R. B., and Bazylinski, D. A. (1994). Magnetotaxis and magnetic particles in bacteria. *Hyperfine Interac.* 90, 135–142. doi: 10.1007/BF02069123
- Frankel, R. B., Bazylinski, D. A., Johnson, M. S., and Taylor, B. L. (1997). Magneto-aerotaxis in marine coccoid bacteria. *Biophys. J.* 73, 994–1000. doi: 10.1016/S0006-3495(97)78132-3
- Hall, T. A. (1999). BioEdit: a user-friendly biological sequence alignment editor and analysis program for windows 95/98/NT. *Nucleic Acids Symp. Ser.* 41, 95–98.
- Ji, B., Zhang, S., Arnoux, P., Rouy, Z., Alberto, F., Philippe, F., et al. (2014). Comparative genomic analysis provides insights into the evolution and niche adaptation of marine *Magnetospira* sp. QH-2 strain 1. *Environ. Microbiol.* 16, 525–544. doi: 10.1111/1462-2920.12180
- Jogler, C., Kube, M., Schübbe, S., Ullrich, S., Teeling, H., Bazylinski, D., et al. (2009). Comparative analysis of magnetosome gene clusters in magnetotactic bacteria provides further evidence for horizontal gene transfer. *Environ. Microbiol.* 11, 1267–1277. doi: 10.1111/j.1462-2920.2009.01854.x
- Jogler, C., and Schüller, D. (2009). Genomics, genetics, and cell biology of magnetosome formation. *Ann. Rev. Microbiol.* 63, 501–521. doi: 10.1146/annurev.micro.62.081307.162908
- Jogler, C., Wanner, G., Kolinko, S., Niebler, M., Amann, R., Petersen, N., et al. (2011). Conservation of proteobacterial magnetosome genes and structures in an uncultivated member of the deep-branching Nitrospira phylum. *Proc. Natl. Acad. Sci. U.S.A.* 108, 1134–1139. doi: 10.1073/pnas.1012694108
- Kimura, M. (1980). A simple method for estimating evolutionary rate of base substitutions through comparative studies of nucleotide sequences. *J. Mol. Evol.* 16, 111–120. doi: 10.1007/BF01731581
- Lefèvre, C. T., and Bazylinski, D. A. (2013). Ecology, diversity, and evolution of magnetotactic bacteria. *Microbiol. Mol. Biol. Rev.* 77, 497–526. doi: 10.1128/MMBR.00021-13
- Lefèvre, C. T., Bernadac, A., Yu-Zhang, K., Pradel, N., and Long-Fei, W. (2009). Isolation and characterization of a magnetotactic bacterial culture from the Mediterranean Sea. *Environ. Microbiol.* 11, 1646–1657. doi: 10.1111/j.1462-2920.2009.01887.x
- Lefèvre, C. T., and Long-Fei, W. (2013). Evolution of the bacterial organelle responsible for magnetotaxis. *Trends Microbiol.* 21, 534–543. doi: 10.1016/j.tim.2013.07.005
- Lefèvre, C. T., Menguy, N., Abreu, F., Lins, U., Pósfai, M., Prozorov, T., et al. (2011). A cultured greigite-producing magnetotactic bacterium in a novel group of sulfate reducing bacteria. *Science* 334, 1720–1723. doi: 10.1126/science.1212596
- Lefèvre, C. T., Trubitsyn, D., Abreu, F., Kolinko, S., Almeida, L. G. P., Vasconcelos, A. T., et al. (2013a). Monophyletic origin of magnetotaxis and the first magnetosomes. *Environ. Microbiol.* 15, 2267–2274. doi: 10.1111/1462-2920.12097
- Lefèvre, C. T., Trubitsyn, D., Abreu, F., Kolinko, S., Jogler, C., Gonzaga, L., et al. (2013b). Comparative genome analysis of magnetotactic bacteria from the *Deltaproteobacteria* provides new insights into magnetite and greigite magnetosome genes required for magnetotaxis. *Environ. Microbiol.* 15, 2712–2735. doi: 10.1111/1462-2920.12128
- Lefèvre, C. T., Viloria N., Schmidt, M. L., Pósfai, M., Frankel, R. B., and Bazylinski, D. A. (2012). Novel magnetite-producing magnetotactic bacteria belonging to the Gammaproteobacteria. *ISME J.* 6, 440–450. doi: 10.1038/ismej.2011.97
- Lins, U., Freitas, F., Neumann, C. K., Barros, H. L., Esquivel, D. M., and Farina, M. (2003). Simple homemade apparatus for harvesting uncultured magnetotactic microorganisms. *Braz. J. Microbiol.* 34, 111–116. doi: 10.1590/S1517-83822003000200004
- Lins, U., Keim, C., Evans, F., Farina, M., and Buseck, P. (2007). Magnetite (Fe_3O_4) and Greigite (Fe_3S_4) crystals in multicellular magnetotactic prokaryotes. *Geomicrobiol. J.* 24, 43–50. doi: 10.1080/01490450601134317
- Lohße, A., Ullrich, S., Katzenmann, E., Borg, S., Wanner, G., Richter, M., et al. (2011). Functional analysis of the magnetosome island in *Magnetospirillum gryphiswaldense*: the *mamAB* operon is sufficient for magnetite biomineralization. *PLoS ONE* 6:e25561. doi: 10.1371/journal.pone.0025561
- Matsunaga, T., Okamura, Y., Fukuda, Y., Wahyudi, A. T., Murase, Y., and Takemaya, H. (2005). Complete genome sequence of the facultative anaerobic magnetotactic bacterium *Magnetospirillum* sp. strain AMB-1. *DNA Res.* 12, 157–166. doi: 10.1093/dnarese/dsi002
- Mitchell, D. R. G. (2008). DiffTools: software tools for electron diffraction in digital micrograph. *Microsc. Res. Tech.* 71, 588–593. doi: 10.1002/jemt.20591
- Murat, D., Falahati, V., Bertineti, L., Csencsits, R., Kornig, A., Downing, K., et al. (2012). The magnetosome membrane protein, MmsF, is a major regulator of magnetite biomineralization in *Magnetospirillum magneticum* AMB-1. *Mol. Microbiol.* 85, 684–699. doi: 10.1111/j.1365-2958.2012.08132.x
- Murat, D., Quilan, A., Vali, H., and Komeili, A. (2010). Comprehensive genetic dissection of the magnetosome gene island reveals the step-wise assembly of a prokaryotic organelle. *Proc. Natl. Acad. Sci. U.S.A.* 107, 5593–5598. doi: 10.1073/pnas.0914439107
- Nakazawa, H., Arakaki, A., Narita-Yamada, S., Yashiro, I., Jinno, K., Aoki, N., et al. (2009). Whole genome sequence of *Desulfovibrio magneticus* strain RS-1 revealed common gene clusters in magnetotactic bacteria. *Gen. Res.* 19, 1801–1808. doi: 10.1101/gr.088906.108
- Richter, M., Kube, M., Bazylinski, D., Lombardot, T., Reinhardt, R., and Schüller, D. (2007). Comparative genome analysis of four magnetotactic bacteria reveals a complex set of group-specific genes implicated in magnetosome biomineralization and function. *J. Bacteriol.* 189, 4899–4910. doi: 10.1128/JB.00119-07
- Sakaguchi, T., Arakaki, A., and Matsunaga, T. (2002). *Desulfovibrio magneticus* sp. nov., a novel sulfate-reducing bacterium that produces intracellular single-domain-sized magnetite particles. *Int. J. Syst. Evol. Microbiol.* 52, 215–221.
- Scheffel, A., Gärdes, A., Grünberg, K., Wanner, G., and Schüller, D. (2008). The major magnetosome proteins MamGFDC are not essential for magnetite biomineralization in *Magnetospirillum gryphiswaldense* but regulate the size of magnetosome crystals. *J. Bacteriol.* 190, 377–386. doi: 10.1128/JB.01371-07
- Schübbe, S., Williams, T. J., Xie, G., Kiss, H. E., Brettin, T. S., Martinez, D., et al. (2009). Complete genome sequence of the chemolithoautotrophic marine magnetotactic coccus strain MC-1. *Appl. Environ. Microbiol.* 75, 4835–4852. doi: 10.1128/AEM.02874-08
- Schüller, D. (2008). Genetics and cell biology of magnetosome formation in magnetotactic bacteria. *FEMS Microbiol. Rev.* 32, 654–672. doi: 10.1111/j.1574-6976.2008.00116.x
- Schüller, D., and Baerlein, E. (1998). Dynamics of iron uptake and Fe_3O_4 biomineralization during aerobic and microaerobic growth of *Magnetospirillum gryphiswaldense*. *J. Bacteriol.* 180, 159–162.
- Seeley, H. W., Vandemar, P. J., and Lee, J. J. (1991). *Microbes in Action: a Laboratory Manual of Microbiology*, 4th Edn. New York, NY: W. H. Freeman and Co.
- Simmons, S. L., Bazylinski, D. A., and Edwards, K. J. (2006). South-seeking magnetotactic bacteria in the northern hemisphere. *Science* 311, 371–374. doi: 10.1126/science.1122843
- Singer, E., Emerson, D., Webb, E. A., Barco, R. A., Kuenen, J. G., Nelson, W. C., et al. (2011). *Mariprofundus ferrooxydans* PV-1 the first genome of a marine Fe(II) oxidizing Zetaproteobacterium. *PLoS ONE* 6:e25386. doi: 10.1371/journal.pone.0025386
- Spring, S., Lins, U., Amann, R., Schleifer, K. H., Ferreira, L. C., Esquivel, D. M., et al. (1998). Phylogenetic affiliation and ultrastructure of uncultured magnetic bacteria with unusually large magnetosomes. *Arch. Microbiol.* 169, 136–147. doi: 10.1007/s002030050553

- Tamura, K., Peterson, D., Peterson, N., Stecher, G., Nei, M., and Kumar, S. (2011). MEGA5: Molecular evolutionary genetics analysis using maximum likelihood, evolutionary distance, and maximum parsimony methods. *Mol. Biol. Evol.* 28, 2731–2739. doi: 10.1093/molbev/msr121
- Whelan, S., and Goldman, N. (2001). A general empirical model of protein evolution derived from multiple protein families using a maximum-likelihood approach. *Mol. Biol. Evol.* 18, 691–699. doi: 10.1093/oxfordjournals.molbev.a003851
- Williams, T. J., Lefèvre, C. T., Zhao, W., Beveridge, T. J., and Bazylinski, D. A. (2012). *Magnetospira thiophila*, gen. nov. sp. nov., a new marine magnetotactic bacterium that represents a novel lineage within the *Rhodospirillaceae* (*Alphaproteobacteria*). *Int. J. Sys. Evol. Microbiol.* 62, 2443–2450. doi: 10.1099/ijss.0.037697-0
- Wolfe, R. S., Thauer, R. K., and Pfennig, N. (1987). A capillary racetrack method for isolation of magnetotactic bacteria. *FEMS Microbiol. Ecol.* 45, 31–35. doi: 10.1111/j.1574-6968.1987.tb02335.x
- Zhang, W.-Y., Zhou, K., Pan, H.-M., Yue, H.-D., Jiang, M., Xiao, T., et al. (2012). Two genera of magnetococci with bean-like morphology from intertidal sediments of the Yellow Sea, China. *App. Environ. Microbiol.* 78, 5606–5611. doi: 10.1128/AEM.00081-12

Conflict of Interest Statement: The authors declare that the research was conducted in the absence of any commercial or financial relationships that could be construed as a potential conflict of interest.

Received: 30 November 2013; accepted: 10 February 2014; published online: 25 February 2014.

Citation: Morillo V, Abreu F, Araujo AC, de Almeida LGP, Enrich-Prast A, Farina M, de Vasconcelos ATR, Bazylinski DA and Lins U (2014) Isolation, cultivation and genomic analysis of magnetosome biomineralization genes of a new genus of South-seeking magnetotactic cocci within the *Alphaproteobacteria*. *Front. Microbiol.* 5:72. doi: 10.3389/fmicb.2014.00072

This article was submitted to Aquatic Microbiology, a section of the journal *Frontiers in Microbiology*.

Copyright © 2014 Morillo, Abreu, Araujo, de Almeida, Enrich-Prast, Farina, de Vasconcelos, Bazylinski and Lins. This is an open-access article distributed under the terms of the Creative Commons Attribution License (CC BY). The use, distribution or reproduction in other forums is permitted, provided the original author(s) or licensor are credited and that the original publication in this journal is cited, in accordance with accepted academic practice. No use, distribution or reproduction is permitted which does not comply with these terms.



Magnetotactic bacteria from Pavilion Lake, British Columbia

Zachery Oestreicher¹, Steven K. Lower², Eric Rees³, Dennis A. Bazylinski⁴ and Brian H. Lower^{2*}

¹ College of Science and Engineering, Kanazawa University, Kanazawa, Japan

² School of Earth Sciences, School of Environment & Natural Resources, The Ohio State University, Columbus, OH, USA

³ Research and Testing Laboratory, Lubbock, TX, USA

⁴ School of Life Sciences, University of Nevada at Las Vegas, NV, USA

Edited by:

Wei Lin, Chinese Academy of Sciences, China

Reviewed by:

Liang Shi, Pacific Northwest National Laboratory, USA

John Senko, The University of Akron, USA

***Correspondence:**

Brian H. Lower, School of Earth Sciences, School of Environment & Natural Resources, The Ohio State University, 210 Kottman Hall, 2021 Coffey Road, Columbus, OH 43210, USA

e-mail: lower.30@osu.edu

Pavilion Lake is a slightly alkaline, freshwater lake located in British Columbia, Canada ($50^{\circ}51'N$, $121^{\circ}44'W$). It is known for unusual organosedimentary structures, called microbialites that are found along the lake basin. These deposits are complex associations of fossilized microbial communities and detrital- or chemical-sedimentary rocks. During the summer, a sediment sample was collected from near the lake's shore, approximately 25–50 cm below the water surface. Magnetotactic bacteria (MTB) were isolated from this sample using a simple magnetic enrichment protocol. The MTB isolated from Pavilion Lake belonged to the *Alphaproteobacteria* class as determined by nucleotide sequences of 16S rRNA genes. Transmission electron microscopy (TEM) revealed that the bacteria were spirillum-shaped and contained a single chain of cubooctahedral-shaped magnetite (Fe_3O_4) crystals that were approximately 40 nm in diameter. This discovery of MTB in Pavilion Lake offers an opportunity to better understand the diversity of MTB habitats, the geobiological function of MTB in unique freshwater ecosystems, and search for magnetofossils contained within the lake's microbialites.

Keywords: magnetotactic bacteria, microbialites, transmission electron microscope, magnetite nanoparticles, magnetite, magnetosomes

INTRODUCTION

Magnetotactic bacteria (MTB) have been found in a variety of aquatic sediments such as marine environments, freshwater lakes and rivers, hot springs, and brackish waters all over the world (Blakemore, 1975; Moench and Konetzka, 1978; Spring et al., 1994; Bazylinski et al., 1995, 2000; Amann et al., 2007; Lin et al., 2009; Lefèvre et al., 2010, 2011). In these settings, MTB tend to reside in chemically stratified water or sediment at the oxic-anoxic interface. The common feature that is unique to all MTB is their ability to synthesize intracellular membrane-bound crystals of single domain magnetite (Fe_3O_4) and/or greigite (Fe_3S_4) (Bazylinski et al., 1993, 1995; Lower and Bazylinski, 2013). The magnetosomes provide a torque on the cells that passively aligns them with the Earth's geomagnetic field. This in turn reduces their navigational route from three dimensions to one dimension; shortening the time it takes for cells to navigate to their preferred habitat, the oxic-anoxic interface at the bottom of water bodies (Bazylinski et al., 1995; Frankel et al., 2007; Lower and Bazylinski, 2013).

Magnetite from MTB occurs as a very specific size with well-defined crystal morphology that is chemically pure (Devouard et al., 1998; Faivre et al., 2008). Such minerals are preserved in the rock record as "magnetofossils," which have been found in Mesozoic rocks, and may extend back as far as the pre-Cambrian (Kirschvink and Chang, 1984; Chang and Kirschvink, 1989; Kopp et al., 2007; Kopp and Kirschvink, 2008). The distinct size, purity and crystallinity of magnetite made by MTB

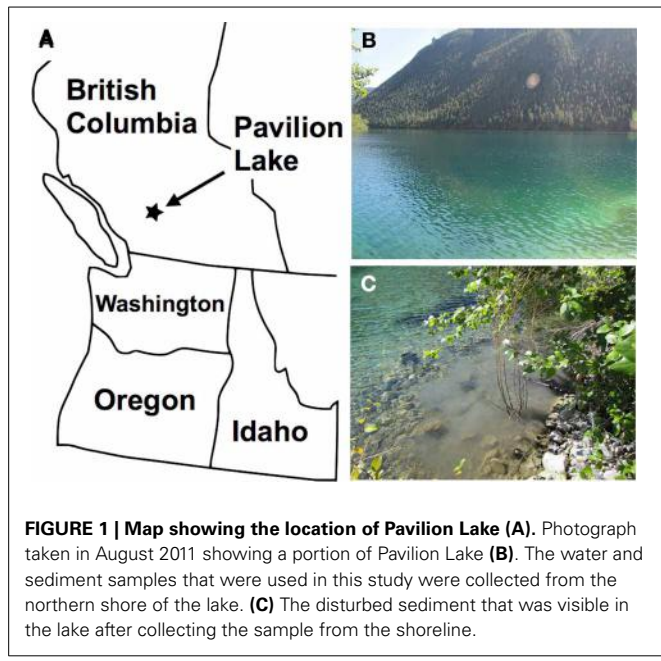
help differentiate it from abiogenic magnetite in the fossil record (Petersen et al., 1986; Chang and Kirschvink, 1989; Devouard et al., 1998; Kobayashi et al., 2006; Kopp and Kirschvink, 2008; Benzerara and Menguy, 2009; Benzerara et al., 2011).

This study investigates uncultured MTB from Pavilion Lake, a deep, slightly alkaline, freshwater lake in British Columbia. This site was selected because it contains large organosedimentary structures called microbialites (Laval et al., 2000). Such structures abound in the fossil record back to nearly 3.5 billion years (Lim et al., 2009) and microbialites, in the form of thrombolites, have been dated as far back as the Proterozoic (Kennard and James, 1986). The MTB that we isolated from Pavilion Lake belonged to the *Alphaproteobacteria* class. Transmission electron microscopy was used to determine the morphology of the cells, and the size and shape of magnetosomes. Scanning transmission electron microscopy was used to determine the chemical composition of the magnetosomes. This is the first time MTB have been described from a microbialite-forming environment. This discovery could be of great value to others interested in potential life forms on other planets or the earliest forms of life on Earth as Pavilion Lake contains microbial fossils in the freshwater microbialites.

MATERIALS AND METHODS

MAGNETOTACTIC BACTERIA COLLECTION

Sediment samples were collected from along the shore of Pavilion Lake (Figure 1) in August 2011. Shallow samples of sediment



were obtained by scraping the sediment approximately 20–45 cm below the surface of the water with a 1-liter container. The containers contained one-half to three-quarters sediment and the remainder was filled with freshwater from the site. The bottles were sealed and brought back to the laboratory for analysis. In the laboratory, the bottle caps were loosened and stored in a dark at room temperature for up to several weeks.

MAGNETOTACTIC BACTERIA ENRICHMENT

Magnetotactic bacteria were isolated from the sediment following a procedure described previously (Oestreicher et al., 2012). Briefly, the south end of a magnet was placed on the outside of the 1-liter sample container just above the sediment-water interface. The north end of a magnet was placed on the opposite side of the container. After 1 h, the water around the south end of the magnet was extracted with a pipette and placed in a racetrack with a cotton plug at the sealed end (Wolfe et al., 1987). This was repeated 12 times for each sample. The south end of a magnet was placed at the racetrack's sealed end, and the magnetotactic cells were allowed to swim through the cotton barrier for approximately 30 min. The racetrack was taken away from the magnet, the tip snapped off, and the bacteria removed with a syringe. A total of 500–1000 μL were collected from each sample. The presence of MTB was confirmed by light microscopy on samples prepared by the hanging drop method (Oestreicher et al., 2012).

TRANSMISSION ELECTRON MICROSCOPY

An aliquot of the enriched cells were placed on a 200 mesh copper grid coated with carbon and formvar (Ted Pella) and analyzed in an FEI Tecnai G² Spirit transmission electron microscope or an FEI Tecnai F20 scanning transmission electron microscope. The accelerating voltage of the G² Spirit was 80 keV with a spot size 2 using the number 2 objective aperture. Images were collected using a Gatan camera and AMT Image Capture software. For the

Tecnai F20, an accelerating voltage of 200 keV was used in the high angle annular dark field (HAADF) mode. Crystals inside the cells were analyzed with the energy-dispersive X-ray (EDX) spectrometer on the Tecnai F20 using only a 100 μm condenser aperture. The specimen was tilted 5° toward the EDAX detector that had an ultrathin Moxtek AP3.3 window with an elevation angle of 20°. The size of the cells and the magnetite crystals were analyzed using FIJI software.

PHYLOGENETIC ANALYSIS

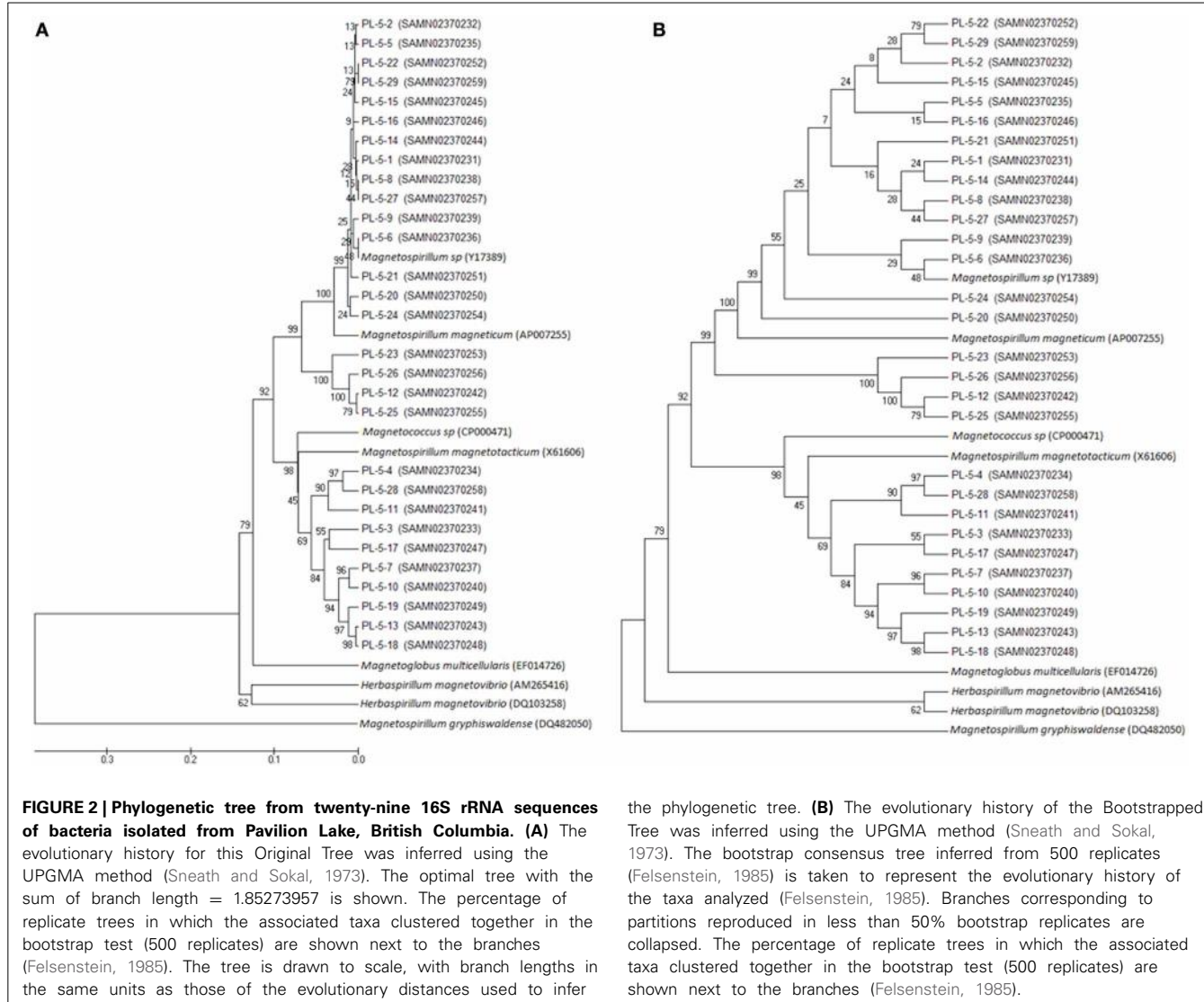
Approximately 500 μL of sample collected from the racetrack was used to obtain DNA for phylogenetic analysis. DNA was obtained from the MTB by homogenizing the cells and resuspending them in RLT buffer (Qiagen) with β -mercaptoethanol. A Qiagen DNA kit was used to isolate the DNA. The 16S rRNA genes were amplified by PCR using 28F and 519R primer pairs (TTTGATCNTGGCTCAG and GWNTTACNGCGGCKGCTG, respectively) and a Qiagen hotstart taq mastermix. The DNA was denatured at 95°C for 5 min, followed by 35 cycles at 94°C for 30 s, 54°C for 45 s, 72°C for 60 s. Finally, an extension reaction was performed at 72°C for 10 min.

The amplified DNA was sequenced and analyzed by the Research and Testing Laboratory in Lubbock, Texas. The DNA sequences were aligned using the default settings in MUSCLE (Edgar, 2004a,b). The sequences were compared with reference sequences from NCBI. A phylogenetic tree was generated using these sequences with the sum of branch length = 1.85273957 shown. The tree shown herein is drawn to scale, with branch lengths in the same units as those of the evolutionary distances used to infer the phylogenetic tree (Sneath and Sokal, 1973). The evolutionary distances were computed using the Maximum Composite Likelihood method (Tamura et al., 2004), and are in the units of the number of base substitutions per site. The analysis involved 37 nucleotide sequences. Codon positions included were 1st + 2nd + 3rd + Noncoding. All ambiguous positions were removed for each sequence pair. There were a total of 1711 positions in the final dataset. A total of 16 operational taxonomic units (OTUs) were generated at a clustering identity of 97% (Table S1). Evolutionary analyses were conducted in MEGA5 (Tamura et al., 2011). All sequence data has been deposited in GenBank as SAMN02370231 to SAMN02370259.

RESULTS

In August 2011, water-sediment samples were collected from Pavilion Lake, British Columbia, Canada (Figure 1). The temperature and pH of the freshwater lake were 20°C and pH 8.3, respectively. This lake is very clear (Figure 1B) with a maximum-recorded depth of 65 m (Laval et al., 2000; Lim et al., 2009). The collected samples were returned to the lab for enrichment of MTB and subsequent analysis of 16S rDNA and examination of the microorganisms by electron microscopy.

An aliquot containing enriched MTB from Pavilion Lake was analyzed by 16S sequencing from all the bacteria contained within the enriched sample. The sample contained 29 different 16S rRNA gene sequences named PL-5-1 through PL-5-29. These sequences were compared with sequences in the NCBI nucleotide database in order to construct a phylogenetic tree (Figure 2). An



Alphaproteobacterium (Genbank accession number DQ482050) was used to root the tree. All 29 of the MTB species isolated from Pavilion Lake were found to group with the *Alphaproteobacteria* (Figure 2).

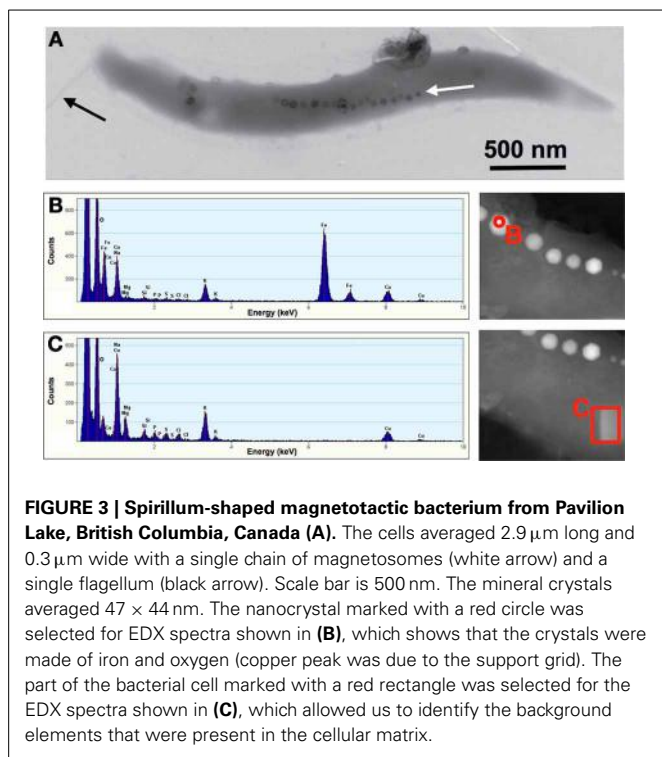
TEM was used to visualize individual bacterial cells that had been isolated from Pavilion Lake. These MTB were found to be spirillum-shaped, $2.9 (\pm 0.6) \mu\text{m}$ long, $0.34 (\pm 0.02) \mu\text{m}$ wide ($n = 7$), containing a single flagellum (Figure 3A). The magnetosomes contained crystals of iron and oxygen indicating Fe_3O_4 (Figure 3B). Background spectra collected from the cellular matrix contained additional elements such as Mg, Na, Si, P, S, Cl, and K (Figure 3C). The Cu peaks that are seen in Figures 3B,C originated from the grid support used to mount the samples for TEM. The other elements (e.g., Na, Mg, P, K, S, Cl) observed in the EDX spectrum are from the cellular matrix (e.g., proteins, cytoplasm) and the dried fluid from the collection process (e.g., Al, Na, Si, Cl).

The Fe_3O_4 crystals in the cells averaged $47 (\pm 4) \text{ nm}$ long and $44 (\pm 5) \text{ nm}$ wide. The size range was $37\text{--}62$ and $33\text{--}56 \text{ nm}$,

respectively, for length and width ($n = 155$, Figure 4) with an average number of 19 crystals per cell ($n = 7$). The magnetite crystals were nearly the same size in length and width (Figure 4C) and most had a shape factor around $0.9 (\pm 0.05)$ (Figure 4A) indicating that the magnetite crystals are single domain magnetite crystals (Figure 4D).

DISCUSSION

This study expands the range of habitats for MTB to include a freshwater ecosystem that contains microbialites. The MTB isolated from Pavilion Lake were spirillum-shaped bacteria from the *Alphaproteobacteria* that are closely related to *Magnetospirillum* (Figure 2). The bacteria were $2.9 \mu\text{m}$ long and $0.3 \mu\text{m}$ wide and contained a single chain of magnetosomes with an average of 19 cuboidal-shaped crystals per cell. The EDX data (Figures 3B,C) clearly demonstrated that the nanometer-sized minerals were composed of iron and oxygen, as expected for Fe_3O_4 . The magnetite nanominerals were approximately 45 nm in diameter (Figure 4).



These measurements for MTB isolated from Pavilion Lake (**Figure 3A**) are similar to other freshwater *Magnetospirillum* bacteria, which have single chains of 15 or more magnetosomes with cuboctahedral shaped magnetite ranging from 40 to 50 nm (Isambert et al., 2007; Faivre and Schüler, 2008; Baumgartner and Faivre, 2011). In addition, the MTB that we isolated from Pavilion Lake had a polar flagellum, similar shape, and similar size as other freshwater *Magnetospirillum* (**Figure 3A**).

Magnetospirillum are ubiquitous in freshwater habitats and are one of the most common magnetotactic forms of *Alphaproteobacteria* (Spring and Bazylinski, 2006; Amann et al., 2007). Environmental parameters have been shown to affect the morphology of magnetosome crystals in culture (Spring and Schleifer, 1995; Faivre et al., 2008; Li and Pan, 2012) as well as the mineral composition both in the environment and in culture (Bazylinski et al., 1995; Simmons and Edwards, 2007; Lefèvre et al., 2011). The chemical composition and crystal morphology of magnetite crystals in our specimens were comparable to other *Magnetospirillum* described in the literature. Therefore, it appears that the unique freshwater environment of Pavilion Lake does not affect the “typical” magnetite crystals in magnetosomes of MTB. Perhaps a more detailed chemical and redox profiling of the microbialites as well as the water and sediment might reveal what environmental parameters are important in this regard.

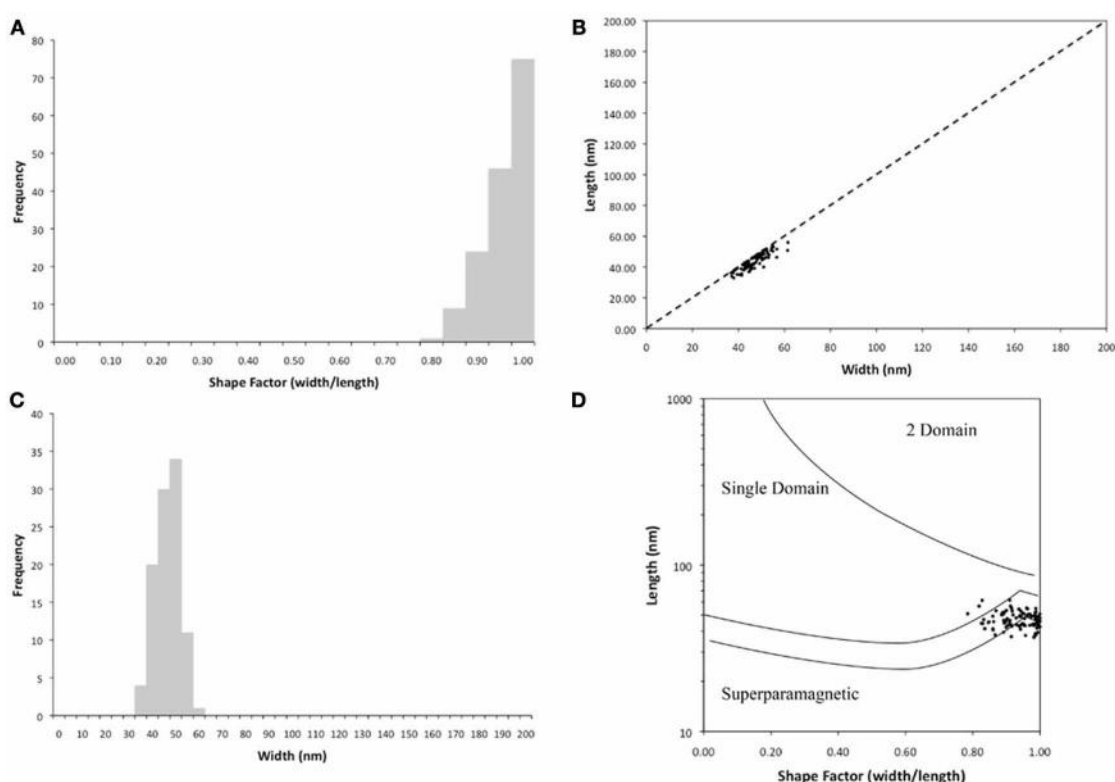


FIGURE 4 | Characterization of the magnetosomes contained within the magnetotactic bacteria that were isolated from Pavilion Lake. (A) Frequency of the shape factor demonstrating that the crystals are nearly equal in width and length. **(B)** Width measurements of the magnetosomes

demonstrate narrow size distribution of the crystals of magnetite. **(C)** Length and width of the magnetite crystals. **(D)** The sizes of the magnetic nanocrystals in our specimens fall within the single domain size range based on (Butler and Banerjee, 1975).

Based on morphological and phylogenetic analysis of the bacteria from Pavilion Lake we were able to isolate one type of MTB (*Alphaproteobacteria*, **Figure 2**). None were found that belonged to the *Deltaproteobacteria* class or *Gammaproteobacteria* class or the *Nitrospirae* phylum. While it is possible that the collection and enrichment protocol used here selected for specific MTB species (Lin et al., 2008), this seems doubtful given the numerous studies where these types of techniques have been used to successfully retrieve MTB from the *Nitrospirae* phylum as well as the *Proteobacteria* (Lefèvre et al., 2011). In addition, MTB of the *Nitrospirae* and the *Deltaproteobacteria* are only known to biomimicry bullet-shaped magnetite magnetosomes (Lefèvre et al., 2013) and we did not observe these using electron microscopy. Thus, it seems more likely that *Nitrospirae* MTB were not present. Of course, one should be mindful of the fact that bacteria were not enriched from our lake samples until several weeks after collection. Some work has shown that this could have selected for one dominant type of MTB during the incubation period in our laboratory (Vali et al., 1987; Flies et al., 2005).

The samples analyzed in this paper confirm that MTB are present in the shallow water along the shoreline of Pavilion Lake. The next logical step is to use Scuba to access deeper parts of Pavilion Lake to determine whether MTB are also present in the microbialites. The presence of MTB in the microbialites in Pavilion Lake would have important implications for finding microfossils in these structures, especially when one considers that magnetite is known to serve as a robust biomarker in magnetofossils (Kirschvink and Chang, 1984; Chang and Kirschvink, 1989; Kobayashi et al., 2006; Kopp et al., 2006; Kopp and Kirschvink, 2008; Jimenez-Lopez et al., 2010; Pósfai et al., 2013). By determining whether magnetofossils and what magnetosome magnetite crystal morphologies are present in the microbialites, much important geologic, paleogeologic and geochemical information might be obtained. For example, it might be ascertained whether MTB played a significant role in the geochemical formation of the microbialites. By knowing what types of magnetofossil magnetite crystals are present, we may also be able to determine which phylogenetic and metabolic types of MTB (Lefèvre et al., 2013; Pósfai et al., 2013) are currently present as well as those associated with the microbialites in the past and when these associations existed. Finally, the presence of magnetofossils in the microbialites, together with geochemical studies, one might be able to determine specific chemical/redox conditions under which magnetite magnetofossils are chemically stable and persist in such environments.

ACKNOWLEDGMENTS

This work was supported by the U.S. National Science Foundation (NSF) grants EAR-0920299, EAR-0920718, EAR-0745808. A portion of this research was also supported by funds from the NSF East Asia and Pacific Summer Institutes Program and The Geological Society of America. Dennis A. Bazylinski is also supported by subcontract SC-12-384 from U.S. Department of Energy contract DE-AC02-07CH11358 to the Ames Laboratory at Iowa State University. We thank S. Cole and R. Montione from OSU-CMIF and H. Colijn from OSU-CEO for their assistance with the microscopy.

SUPPLEMENTARY MATERIAL

The Supplementary Material for this article can be found online at: <http://www.frontiersin.org/journal/10.3389/fmich.2013.00406/abstract>

REFERENCES

- Amann, R., Peplies, J., and Schüler, D. (2007). "Diversity and taxonomy of magnetotactic bacteria," in *Magnetoreception and Magnetosomes in Bacteria*, ed D. Schüler (New York, NY; Berlin; Heidelberg: Springer-Verlag), 25–36. doi: 10.1007/7171_037
- Baumgartner, J., and Faivre, D. (2011). "Magnetite biomimicry in bacteria," in *Molecular Biomimicry*, ed W. E. G. Müller (New York, NY; Berlin; Heidelberg: Springer-Verlag), 3–27.
- Bazylinski, D. A., Frankel, R. B., Heywood, B. R., Mann, S., King, J. W., Donaghay, P. L., et al. (1995). Controlled biomimicry of magnetite (Fe₃O₄) and greigite (Fe₃S₄) in a magnetotactic bacterium. *Appl. Environ. Microbiol.* 61, 3232–3239.
- Bazylinski, D. A., Heywood, B. R., Mann, S., and Frankel, R. B. (1993). Fe₃O₄ and Fe₃S₄ in a bacterium. *Nature* 366, 218–218. doi: 10.1038/366218a0
- Bazylinski, D. A., Schleizinger, D. R., Howes, B. H., Frankel, R. B., and Epstein, S. S. (2000). Occurrence and distribution of diverse populations of magnetic prokaryotes in a chemically stratified coastal salt pond. *Chem. Geol.* 169, 319–328. doi: 10.1016/S0009-2541(00)00211-4
- Benzerara, K., and Menguy, N. (2009). Looking for traces of life in minerals. *Comptes Rendus Palevol* 8, 617–628. doi: 10.1016/j.crpv.2009.03.006
- Benzerara, K., Miot, J., Morin, G., Ona-Nguema, G., Skouri-Panet, F., and Férrard, C. (2011). Significance, mechanisms and environmental implications of microbial biomimicry. *Comptes Rendus Geoscience* 343, 160–167. doi: 10.1016/j.crte.2010.09.002
- Blakemore, R. (1975). Magnetotactic bacteria. *Science* 190, 377–379. doi: 10.1126/science.170679
- Butler, R. F., and Banerjee, S. K. (1975). Theoretical single-domain grain size range in magnetite and titanomagnetite. *J. Geophys. Res.* 80, 4049–4058. doi: 10.1029/JB080i029p04049
- Chang, S. B. R., and Kirschvink, J. L. (1989). Magnetofossils, the magnetization of sediments, and the evolution of magnetite biomimicry. *Annu. Rev. Earth Planet. Sci.* 17, 169–195. doi: 10.1146/annurev.ea.17.050189.001125
- Devouard, B., Posfai, M., Hua, X., Bazylinski, D. A., Frankel, R. B., and Buseck, P. R. (1998). Magnetite from magnetotactic bacteria; size distributions and twinning. *Am. Mineral.* 83, 1387–1398.
- Edgar, R. (2004a). MUSCLE: a multiple sequence alignment method with reduced time and space complexity. *BMC Bioinformatics* 5:113. doi: 10.1186/1471-2105-5-113
- Edgar, R. C. (2004b). MUSCLE: multiple sequence alignment with high accuracy and high throughput. *Nucleic Acids Res.* 32, 1792–1797. doi: 10.1093/nar/gkh340
- Faivre, D., Menguy, N., Posfai, M., and Schüler, D. (2008). Environmental parameters affect the physical properties of fast-growing magnetosomes. *Am. Mineral.* 93, 463–469. doi: 10.2138/am.2008.2678
- Faivre, D., and Schüler, D. (2008). Magnetotactic bacteria and magnetosomes. *Chem. Rev.* 108, 4875–4898. doi: 10.1021/cr078258w
- Felsenstein, J. (1985). Confidence limits on phylogenies: an approach using the bootstrap. *Evolution* 39, 783–791. doi: 10.2307/2408678
- Flies, C. B., Jonkers, H. M., Beer, D., Bosselmann, K., Bottcher, M. E., and Schüler, D. (2005). Diversity and vertical distribution of magnetotactic bacteria along chemical gradients in freshwater microcosms. *FEMS Microbiol. Ecol.* 52, 185–195. doi: 10.1016/j.femsec.2004.11.006
- Frankel, R. B., Williams, T. J., and Bazylinski, D. A. (2007). "Magneto-aerotaxis," in *Magnetoreception and Magnetosomes in Bacteria*, eds D. Schüler (New York, NY; Berlin; Heidelberg: Springer-Verlag), 1–24. doi: 10.1007/7171_2006_036
- Isambert, A., Menguy, N., Larquet, E., Guyot, F., and Valet, J. P. (2007). Transmission electron microscopy study of magnetites in a freshwater population of magnetotactic bacteria. *Am. Mineral.* 92, 621–630. doi: 10.2138/am.2007.2278
- Jimenez-Lopez, C., Romanek, C. S., and Bazylinski, D. A. (2010). Magnetite as a prokaryotic biomarker: a review. *J. Geophys. Res. Biogeosci.* 115, G00G03. doi: 10.1029/2009JG001152
- Kennard, J. M., and James, N. P. (1986). Thrombolites and stromatolites: two distinct types of microbial structures. *Palaios* 1, 492–503. doi: 10.2307/3514631

- Kirschvink, J. L., and Chang, S. B. R. (1984). Ultrafine-grained magnetite in deep-sea sediments: Possible bacterial magnetofossils. *Geology* 12, 559–562. doi: 10.1130/0091-7613(1984)12<559:UMIDSP>2.0.CO;2
- Kobayashi, A., Kirschvink, J. L., Nash, C. Z., Kopp, R. E., Sauer, D. A., Bertani, L. E., et al. (2006). Experimental observation of magnetosome chain collapse in magnetotactic bacteria: sedimentological, paleomagnetic, and evolutionary implications. *Earth Planet. Sci. Lett.* 245, 538–550. doi: 10.1016/j.epsl.2006.03.041
- Kopp, R. E., and Kirschvink, J. L. (2008). The identification and biogeochemical interpretation of fossil magnetotactic bacteria. *Earth Sci. Rev.* 86, 42–61. doi: 10.1016/j.earscirev.2007.08.001
- Kopp, R. E., Raub, T. D., Schumann, D., Vali, H., Smirnov, A. V., and Kirschvink, J. L. (2007). Magnetofossil spike during the paleocene-eocene thermal maximum: ferromagnetic resonance, rock magnetic, and electron microscopy evidence from Ancora, New Jersey, United States. *Paleoceanography* 22, PA4103. doi: 10.1029/2007PA001473
- Kopp, R., Weiss, B., Maloof, A., Vali, H., Nash, C., and Kirschvink, J. (2006). Chains, clumps, and strings: magnetofossil taphonomy with ferromagnetic resonance spectroscopy. *Earth Planet. Sci. Lett.* 247, 10–25. doi: 10.1016/j.epsl.2006.05.001
- Laval, B., Cady, S. L., Pollack, J. C., McKay, C. P., Bird, J. S., Grotzinger, J. P., et al. (2000). Modern freshwater microbialite analogues for ancient dendritic reef structures. *Nature* 407, 626–629. doi: 10.1038/35036579
- Lefèvre, C., Abreu, F., Schmidt, M. L., Lins, U., Frankel, R. B., Hedlund, B. P. et al. (2010). Moderately thermophilic magnetotactic bacteria from hot springs in nevada. *Appl. Environ. Microbiol.* 76, 3740–3743. doi: 10.1128/AEM.03018-09
- Lefèvre, C., Menguy, N., Abreu, F., Lins, U., Posfai, M., Prozorov, T. et al. (2011). A cultured greigite-producing magnetotactic bacterium in a novel group of sulfate-reducing bacteria. *Science* 334, 1720–1723. doi: 10.1126/science.1212596
- Lefèvre, C. T., Frankel, R. B., Abreu, F., Lins, U., and Bazylinski, D. A. (2011). Culture-independent characterization of a novel, uncultivated magnetotactic member of the Nitrospirae phylum. *Environ. Microbiol.* 13, 538–549. doi: 10.1111/j.1462-2920.2010.02361.x
- Lefèvre, C. T., Trubitsyn, D., Abreu, F., Kolinko, S., De Almeida, L. G. P., De Vasconcelos, A. T. R., et al. (2013). Monophyletic origin of magnetotaxis and the first magnetosomes. *Environ. Microbiol.* 15, 2267–2274. doi: 10.1111/j.1462-2920.12097
- Li, J., and Pan, Y. (2012). Environmental factors affect magnetite magnetosome synthesis in magnetospirillum magneticumAMB-1: implications for biologically controlled mineralization. *Geomicrobiol. J.* 29, 362–373. doi: 10.1080/01490451.2011.565401
- Lim, D. S. S., Laval, B. E., Slater, G., Antoniades, D., Forrest, A. L., Pike, W., et al. (2009). Limnology of Pavilion lake, BC, Canada characterization of a microbialite forming environment. *Fund. Appl. Limnol.* 173, 329–351. doi: 10.1127/1863-9135/2009/0173-0329
- Lin, W., Li, J., Schüler, D., Jogler, C., and Pan, Y. (2009). Diversity analysis of magnetotactic bacteria in Lake Miyun, northern China, by restriction fragment length polymorphism. *Syst. Appl. Microbiol.* 32, 342–350. doi: 10.1016/j.syapm.2008.10.005
- Lin, W., Tian, L., Li, J., and Pan, Y. (2008). Does capillary racetrack-based enrichment reflect the diversity of uncultivated magnetotactic cocci in environmental samples? *FEMS Microbiol. Lett.* 279, 202–206. doi: 10.1111/j.1574-6968.2007.01029.x
- Lower, B. H., and Bazylinski, D. A. (2013). The bacterial magnetosome: a unique prokaryotic organelle. *J. Mol. Microbiol. Biotechnol.* 23, 63–80. doi: 10.1159/000346543
- Moench, T. T., and Konetzka, W. (1978). A novel method for the isolation and study of a magnetotactic bacterium. *Arch. Microbiol.* 119, 203–212. doi: 10.1007/BF00964274
- Oestreicher, Z., Lower, S. K., Lin, W., and Lower, B. H. (2012). Collection, isolation and enrichment of naturally occurring magnetotactic bacteria from the environment. *J. Vis. Exp.* 69, e50123. doi: 10.3791/50123
- Petersen, N., Von Dobeneck, T., and Vali, H. (1986). Fossil bacterial magnetite in deep-sea sediments from the South Atlantic Ocean. *Nature* 320, 611–615. doi: 10.1038/320611a0
- Pósfai, M., Lefèvre, C. T., Trubitsyn, D., and Bazylinski, D. A. and Frankel, R. B. (2013). Phylogenetic significance of composition and crystal morphology of magnetosome minerals. *Front. Microbiol.* 4:344. doi: 10.3389/fmicb.2013.00344
- Simmons, S., and Edwards, K. (2007). “Geobiology of magnetotactic bacteria,” in Magnetoreception and magnetosomes in bacteria, ed D. Schüler (New York, NY; Berlin; Heidelberg: Springer-Verlag), 77–102. doi: 10.1007/7171_039
- Sneath, P. H. A., and Sokal, R. R. (1973). *Numerical Taxonomy. The Principles and Practice Of Numerical Classification*. San Francisco, CA: W. H. Freeman & Company.
- Spring, S., Amann, R., Ludwig, W., Schleifer, K.-H., Schüler, D., Poralla, K., et al. (1994). Phylogenetic analysis of uncultured magnetotactic bacteria from the alpha-subclass of proteobacteria. *Syst. Appl. Microbiol.* 17, 501–508. doi: 10.1016/S0723-2020(11)80068-8
- Spring, S., and Bazylinski, D. A. (2006). Magnetotactic bacteria. *Prokaryotes* 2, 842–862. doi: 10.1007/0-387-30742-7_26
- Spring, S., and Schleifer, K.-H. (1995). Diversity of magnetotactic bacteria. *Syst. Appl. Microbiol.* 18, 147–153. doi: 10.1016/S0723-2020(11)80386-3
- Tamura, K., Nei, M., and Kumar, S. (2004). Prospects for inferring very large phylogenies by using the neighbor-joining method. *Proc. Natl. Acad. Sci. U.S.A.* 101, 11030–11035. doi: 10.1073/pnas.0404206101
- Tamura, K., Peterson, D., Peterson, N., Stecher, G., Nei, M., and Kumar, S. (2011). MEGA5: molecular evolutionary genetics analysis using maximum likelihood, evolutionary distance, and maximum parsimony methods. *Mol. Biol. Evol.* 28, 2731–2739. doi: 10.1093/molbev/msr121
- Vali, H., Förster, O., Amarantidis, G., and Petersen, N. (1987). Magnetotactic bacteria and their magnetofossils in sediments. *Earth Planet. Sci. Lett.* 86, 389–400. doi: 10.1016/0012-821X(87)90235-4
- Wolfe, R., Thauer, R., and Pfennig, N. (1987). A “capillary racetrack” method for isolation of magnetotactic bacteria. *FEMS Microbiol. Ecol.* 45, 31–35. doi: 10.1111/j.1574-6968.1987.tb02335.x

Conflict of Interest Statement: The authors declare that the research was conducted in the absence of any commercial or financial relationships that could be construed as a potential conflict of interest.

Received: 30 August 2013; accepted: 07 December 2013; published online: 20 December 2013.

Citation: Oestreicher Z, Lower SK, Rees E, Bazylinski DA and Lower BH (2013) Magnetotactic bacteria from Pavilion Lake, British Columbia. Front. Microbiol. 4:406. doi: 10.3389/fmicb.2013.00406

This article was submitted to Aquatic Microbiology, a section of the journal Frontiers in Microbiology.

Copyright © 2013 Oestreicher, Lower, Rees, Bazylinski and Lower. This is an open-access article distributed under the terms of the Creative Commons Attribution License (CC BY). The use, distribution or reproduction in other forums is permitted, provided the original author(s) or licensor are credited and that the original publication in this journal is cited, in accordance with accepted academic practice. No use, distribution or reproduction is permitted which does not comply with these terms.



Swimming motion of rod-shaped magnetotactic bacteria: the effects of shape and growing magnetic moment

Dali Kong¹, Wei Lin², Yongxin Pan² and Keke Zhang^{1*}

¹ Department of Mathematical Sciences, University of Exeter, Exeter, UK

² Biogeomagnetism Group, Paleomagnetism and Geochronology Laboratory, Key Laboratory of the Earth's Deep Interior, Institute of Geology and Institute of Geophysics, Chinese Academy of Sciences, Beijing, China

Edited by:

Karim Benzerara, Centre National de la Recherche Scientifique, France

Reviewed by:

Michael Chan, The University of Hong Kong, Hong Kong

Andrejs Cebers, University of Latvia, Latvia

Michael Winklhofer, Ludwig-Maximilians-University Munich, Germany

***Correspondence:**

Keke Zhang, Department of Mathematical Sciences, University of Exeter, Harrison Building, North Park Road, EX4 4QF, UK
e-mail: kzhang@ex.ac.uk

We investigate the swimming motion of rod-shaped magnetotactic bacteria affiliated with the *Nitrospirae* phylum in a viscous liquid under the influence of an externally imposed, time-dependent magnetic field. By assuming that fluid motion driven by the translation and rotation of a swimming bacterium is of the Stokes type and that inertial effects of the motion are negligible, we derive a new system of the twelve coupled equations that govern both the motion and orientation of a swimming rod-shaped magnetotactic bacterium with a growing magnetic moment in the laboratory frame of reference. It is revealed that the initial pattern of swimming motion can be strongly affected by the rate of the growing magnetic moment. It is also revealed, through comparing mathematical solutions of the twelve coupled equations to the swimming motion observed in our laboratory experiments with rod-shaped magnetotactic bacteria, that the laboratory trajectories of the swimming motion can be approximately reproduced using an appropriate set of the parameters in our theoretical model.

Keywords: magnetotactic bacteria, rod-shape, stokes flow

1. INTRODUCTION

By converting the mechanical energy of convection-driven fluid motion into the ohmic dissipation taking place in the Earth's outer core, the geodynamo generates and sustains the geomagnetic field (Moffatt, 1978; Zhang and Schubert, 2000) that protects or affects a wide range of life, from human being to micro-scale organisms, on our planet Earth. The whole evolution has taken place in the presence of the Earth's magnetic field and therefore has brought about phenomena such as magnetotaxis and magnetoreception (Winklhofer, 2010). A particular class of living microorganisms is magnetotactic bacteria, first discovered nearly four decades ago by Blakemore (1975), which contain the magnetic crystal of a narrow size carrying permanent magnetization (Bazylinski and Frankel, 2004; Faivre and Schüler, 2008; Lei et al., 2012; Prozorov et al., 2013) that allow them to swim along the lines of the Earth's magnetic field. In other words, the majority of them are north-seeking in the northern hemisphere while south-seeking in the southern hemisphere (Blakemore et al., 1980; Kirschvink, 1980; Frankel, 1984).

It is now well known that, driven by rapid rotation of its helical flagellar filaments which generates torque, a magnetotactic bacterium swims in the form of helical fashion against the viscous drag and torque under the influence of an external magnetic field (Berg and Anderson, 1973; Jones and Aizawa, 1991). From a dynamical point of view, the swimming style and speed of magnetotactic bacteria would sensitively depend on its shape and the strength of its magnetization. The simplest model of swimming magnetotactic bacteria can be constructed upon making the following two assumptions: (1) the bacteria have perfect spherical geometry (Nogueira and Lins de Barros, 1995; Pan et al., 2009) and (2) their movement is extremely slow such that the

Stokes approximation can be made (Batchelor, 1967; Koiller et al., 1996). A huge mathematical advantage of spherical geometry is that the Stokes solution is not only very simple but also available (Batchelor, 1967). The drag force \mathbf{D}_μ on a translating spherical body is given by

$$\mathbf{D}_\mu = -6\pi\mu r_0 \mathbf{v}, \quad (1)$$

where r_0 is the radius of the sphere, μ is the dynamical viscosity of the fluid and \mathbf{v} is the translating velocity, while the viscous torque \mathbf{T}_μ on a rotating spherical body is

$$\mathbf{T}_\mu = -8\pi\mu r_0^3 \boldsymbol{\Omega}, \quad (2)$$

where $\boldsymbol{\Omega}$ represents the angular velocity of its rotation. On the basis of these simple expressions for the viscous drag and torque of a spherical body, Nogueira and Lins de Barros (1995) derived a system of six simple ordinary differential equations that govern the motion of a swimming spherical magnetotactic bacterium. An important characteristic of the spherical model is, as clearly indicated by Equations (1, 2), that the size of its drag force \mathbf{D}_μ and its viscous torque \mathbf{T}_μ does not depend on the direction of its translation or rotation. Erglis et al. (2007) studied the swimming motion of the motile magnetotactic bacterium in a rotating magnetic field by assuming that the velocity of a bacterium is in the direction of its long axis.

While spherical geometry or the swimming direction in the direction of a symmetry axis would dramatically simplify the relevant mathematical analysis, it does not capture the key dynamics of swimming magnetotactic bacteria that are typically non-spherical and may swim in an arbitrary direction. By keeping inertial effects of the swimming motion and using a prolate

spheroid with moderate eccentricity, Cui et al. (2012) derived a system of twelve coupled non-linear ordinary differential equations that govern both the motion and orientation of swimming non-spherical magnetotactic bacteria. It is noteworthy that, as a consequence of the strong stiffness associated with inertial effects, the twelve ordinary differential equations derived by Cui et al. (2012) are highly complicated and numerical integration of the system is quite slow.

Rod-shaped magnetotactic bacteria displayed in **Figure 1A** are found in Lake Miyun near Beijing, China. This type of magnetotactic bacteria, belonging to the *Nitrospirae* phylum, can synthesize hundreds of bullet-shaped magnetosomes in a single cell (Lin et al., 2011). It is recognized that the shape of this particular class of magnetotactic bacteria can be reasonably modeled by a strongly elongated prolate spheroid defined as

$$\frac{x^2}{a^2(1-\mathcal{E}^2)} + \frac{y^2}{a^2(1-\mathcal{E}^2)} + \frac{z^2}{a^2} = 1 \quad (3)$$

with its eccentricity \mathcal{E} satisfying $0 < (1 - \mathcal{E}) \ll 1$, where a is the semi-major axis with $2a$ representing the length of a rod-shaped bacterium. As depicted in **Figure 1B**, the shape of the rod-shaped bacterium in **Figure 1A** can be approximately described by Equation (3) with $\mathcal{E} = 0.96$.

The primary objective of this paper is to study, via both theoretical and experimental methods, the swimming motion of rod-shaped magnetotactic bacteria found in Lake Miyun (Lin et al., 2011). In comparison to the two previous studies—the spherical model by Nogueira and Lins de Barros (1995) and the inertial model by Cui et al. (2012)—there are three new elements in the present study. First, our non-spherical model accounts for, to leading-order approximation, the rod-shaped effect of swimming magnetotactic bacteria by taking the large eccentricity limit $0 < (1 - \mathcal{E}) \ll 1$ in Equation (3). As a consequence of rod-shaped geometry, the size of viscous torque, as we will show, is strongly dependent on the direction of rotation vector Ω . Second, by taking the time-dependent magnetic moment of magnetotactic bacteria, we attempt to model the dynamics of magnetotactic bacteria at the earlier stage of their growing

phase when their magnetite formation is associated with a slow, diffusion-like process (Schüler and Baeuerlein, 1996). Third, we derive, by completely neglecting inertial effects, a new system of the twelve coupled equations that govern both the motion and orientation of rod-shaped magnetotactic bacteria in the laboratory frame of reference and that are much simpler than those of the inertial model derived by Cui et al. (2012).

It should be noticed that the analytical mathematical solutions for the motion of a viscous fluid due to a strongly prolate spheroid translating or rotating in an *arbitrary direction* are required to describe the swimming motion of rod-shaped magnetotactic bacteria. This is closely associated with a classical fluid dynamical problem which was first discussed by Jeffery (1922) and, then, comprehensively reviewed by Happel and Brenner (1965) in a research monograph. While the flow due to a strongly prolate spheroid translating or rotating in the direction *parallel to its symmetry axis* is relatively simply and has been used in various models (see, for example, Han et al., 2009), there exists no mathematical solutions that can be practically employed to study the dynamics of swimming motion of rod-shaped magnetotactic bacteria. This is because the existing solutions (Jeffery, 1922; Happel and Brenner, 1965) are based on the incomplete elliptic-type integrals that have to be evaluated numerically. We therefore need a set of the new analytical solutions that describe the fluid motion of a prolate spheroid translating or rotating in an arbitrary direction and that can be practically useful in modeling the swimming motion of rod-shaped magnetotactic bacteria.

In what follows we shall begin in section 2 by discussing the Stokes flow and the related viscous drag/torque for rod-shaped magnetotactic bacteria. This is followed by presenting our theoretical model and by deriving the twelve governing equations in section 3. Discussion of the results will be presented in section 4 and the paper closes in section 5 with a summary and some remarks.

2. STOKES FLOW, DRAG, AND TORQUE

2.1. STOKES FLOW FOR SWIMMING ROD-SHAPED BACTERIA

Stokes flow is referred to a class of fluid motion in that the speed of flow is extremely slow and the effect of viscosity is very strong

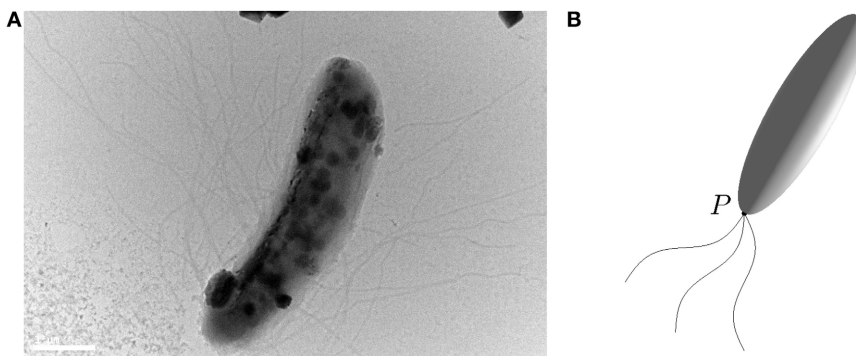


FIGURE 1 | (A) A microscope image (Bar = 1 μ m) of a rod-shaped magnetotactic bacterium found in Lake Miyun near Beijing, China. **(B)** An elongated prolate spheroid with eccentricity $\mathcal{E} = 0.96$ that provides an

approximation of the rod-shaped bacterium for which its swimming motion is powered by the rapid rotation of helical flagellar filaments at a fixed point P .

such that inertial forces are much smaller comparing to viscous forces (Batchelor, 1967). In the language of fluid dynamics, the problem of swimming microorganisms is marked by a very small Reynolds number Re (Purcell, 1977), a dimensionless number defined as

$$Re = \frac{Ua\rho}{\mu},$$

where U is the typical velocity of the fluid motion, ρ is the liquid density, a denotes the typical length scale and μ is the dynamic viscosity of the liquid. Since the swimming speed U is very low and its characteristic dimension a is extremely small, the Stokes approximation, which neglects the inertial term in the Navier-Stokes equation by taking the limit $Re \rightarrow 0$, is usually adopted for describing the motion of microorganisms (Koiller et al., 1996). It follows that the fluid motion generated by swimming rod-shaped magnetotactic bacteria is governed by the Stokes equation and the equation of continuity,

$$\begin{cases} \mu \nabla^2 \mathbf{u} = \nabla p, \\ \nabla \cdot \mathbf{u} = 0, \end{cases} \quad (4)$$

where \mathbf{u} is the velocity of the flow and p is its pressure. For understanding the dynamics of swimming magnetotactic bacteria, it is necessary to have mathematical solutions of the Stokes flow created by both the translation and rotation of a rod-shaped body in an infinite expanse of viscous and incompressible fluid. In other words, we require the analytical solution to (Equation 4) subject to the condition that the fluid velocity \mathbf{u} coincides with the bounding surface of a swimming magnetotactic bacterium at each of its points and $\mathbf{u} \rightarrow 0$ far away from the swimming bacterium.

It is important to notice that, while the mathematical problem of the spherical Stokes flow is classical, simple, two-dimensional and well-known (Batchelor, 1967), the Stokes flow associated with a rod-shaped swimming body is complicated, fully three-dimensional and not widely known. Various authors have considered the Stokes flow in non-spherical geometry. For example, Payne and Pell (1960) considered the Stokes problem in which the configuration of various obstacles has an axis of symmetry and the uniform flow at distant points is parallel to the symmetry axis. Kong et al. (2012) derived the first exact solution of Stokes flow for an arbitrarily rotating or translating oblate spheroid of arbitrary eccentricity using the Papkovich-Neuber formulation. In the following, we shall present the modified solution that is in a suitable form for our mathematical analysis of swimming rod-shaped bacteria in a viscous fluid.

2.2. DRAG ON TRANSLATING ROD-SHAPED BACTERIA AT ARBITRARY ANGLES

In order to describe the swimming motion of a rod-shaped bacterium, we require the mathematical solution of a three-dimensional Stokes flow driven by translating an elongated prolate spheroid with its eccentricity $0 < (1 - \mathcal{E}) \ll 1$ at an arbitrary angle of attack γ , the angle between the direction of the translating velocity \mathbf{v} and the symmetry axis z of a rod-shaped bacterium, which is sketched in Figure 2. Note that cartesian coordinates (x, y, z) are attached to the bacterium's body. Our swimming

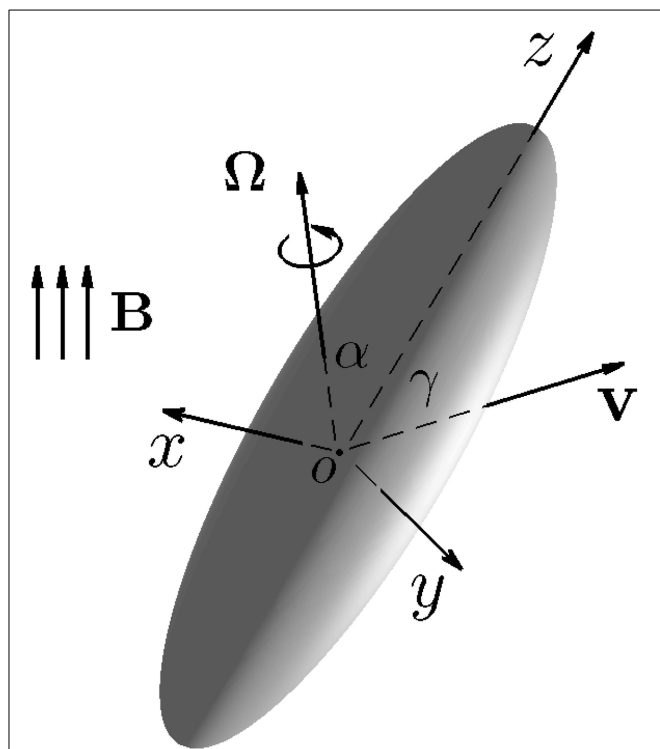


FIGURE 2 | Translation of a rod-shaped bacterium at an arbitrary angle of attack γ with the velocity \mathbf{v} , where cartesian coordinates (x, y, z) are attached to the bacterium's body. Rotation of a rod-shaped a rod-shaped bacterium with an arbitrary angle α and the angular velocity Ω under the influence of an externally imposed, time-dependent magnetic field \mathbf{B} .

model needs an analytical formula that expresses the viscous drag force \mathbf{D}_B on the translating rod-shaped bacterium as a function of \mathcal{E} and γ .

Upon adopting the Papkovich-Neuber formulation (Papkovich, 1932; Neuber, 1934), the flow velocity \mathbf{u} satisfying (Equation 4) can be written in the form

$$\begin{cases} \mathbf{u} = \nabla(\mathbf{r} \cdot \Psi + \chi) - 2\Psi, \\ p = 2\mu(\nabla \cdot \Psi), \end{cases} \quad (5)$$

where \mathbf{r} is the position vector, Ψ , a vector harmonic function, satisfies $\nabla^2 \Psi = 0$ and χ , a scalar harmonic function, is a solution to $\nabla^2 \chi = 0$. Both Ψ and χ can be obtained by using the expansion of prolate spheroidal harmonics (Kong et al., 2012). The main mathematical complication and difficulty in applying the Papkovich-Neuber formulation to the present problem stem from both non-spherical geometry/coordinates and three-dimensionality that make the analysis lengthy and cumbersome.

We first introduce oblate spheroidal coordinates defined by three sets of orthogonal level surfaces: the radial coordinate $\xi \in [\xi_0, \infty)$ characterizes oblate spheroidal surfaces

$$\frac{z^2}{c^2 \xi^2} + \frac{x^2 + y^2}{c^2 (\xi^2 - 1)} = 1,$$

the angular coordinate $\eta \in [-1, 1]$ determines hyperboloids

$$\frac{z^2}{c^2\eta^2} - \frac{x^2 + y^2}{c^2(1 - \eta^2)} = 1,$$

and, finally, the third coordinate is azimuthal angle ϕ which is the same as that in spherical polar coordinates. Here c is the common focal length for all the spheroids and hyperboloids, the bounding surface of an oblate spheroidal body (or a rod-shaped bacterium) is described by

$$\xi = \xi_0 = 1/\mathcal{E}.$$

The domain of Stokes flow in the exterior of the prolate spheroid (or the rod-shaped bacterium) is then defined by $\{\xi_0 \leq \xi < \infty, -1 \leq \eta \leq 1, 0 \leq \varphi \leq 2\pi\}$ while the transformation between prolate spheroidal coordinates (ξ, η, φ) and the corresponding cartesian coordinates (x, y, z) is given by

$$\begin{cases} x = c\sqrt{(\xi^2 - 1)(1 - \eta^2)} \cos \varphi, \\ y = c\sqrt{(\xi^2 - 1)(1 - \eta^2)} \sin \varphi, \\ z = c\xi\eta. \end{cases} \quad (6)$$

In this paper, we shall use $(\hat{\xi}, \hat{\eta}, \hat{\phi})$ to denote unit vectors in oblate spheroidal coordinates and $(\hat{x}, \hat{y}, \hat{z})$ as unit vectors in cartesian coordinates (x, y, z) depicted in **Figure 2**.

Suppose that a rod-shaped bacterium moves with the velocity \mathbf{v} at the speed $|\mathbf{v}|$ written in the form

$$\mathbf{v} = |\mathbf{v}| \left[(\sin \gamma \cos \tilde{\phi}) \hat{x} + (\sin \gamma \sin \tilde{\phi}) \hat{y} + (\cos \gamma) \hat{z} \right],$$

where the angles γ and $\tilde{\phi}$ specify the direction of \mathbf{v} . It can be shown, after some length mathematical analysis, that the three-dimensional solution \mathbf{u}^t and the corresponding pressure p^t describing a Stokes flow driven by translating the bacterium with its velocity \mathbf{v} at arbitrary angles γ and $\tilde{\phi}$ are

$$\begin{aligned} \frac{\hat{\xi} \cdot \mathbf{u}^t}{|\mathbf{v}|} &= \sqrt{\frac{\xi^2 - 1}{\xi^2 - \eta^2}} \eta \cos \gamma \\ &\times \left[\frac{\hat{\xi} + \frac{2\xi}{\xi^2 - 1}}{(\xi_0^2 + 1)\hat{\xi}_0 - 2\xi_0} + \frac{\hat{\xi} - \frac{2\xi}{\xi^2 - 1}}{\frac{\xi_0^2 + 1}{\xi_0^2}\hat{\xi}_0 - \frac{2}{\xi_0}} \right] \\ &+ \frac{\sqrt{1 - \eta^2}}{\sqrt{\xi^2 - \eta^2}} \left[\frac{-\frac{\xi}{2}\hat{\xi} - 1}{\frac{\xi_0^2 - 3}{4}\hat{\xi}_0 - \frac{\xi_0}{2}} + \frac{\frac{\xi}{2}\hat{\xi} - \frac{\xi^2 - 2}{\xi^2 - 1}}{\frac{\xi_0^2 - 3}{2(\xi_0^2 - 1)}\hat{\xi}_0 - \frac{\xi_0}{\xi_0^2 - 1}} \right] \\ &\times \cos(\varphi - \tilde{\phi}) \sin \gamma, \end{aligned} \quad (7)$$

$$\begin{aligned} \frac{\hat{\eta} \cdot \mathbf{u}^t}{|\mathbf{v}|} &= \frac{\sqrt{1 - \eta^2}}{\sqrt{\xi^2 - \eta^2}} \cos \gamma \\ &\times \left[\frac{\frac{\xi}{2}\hat{\xi}}{\frac{\xi_0^2 + 1}{2}\hat{\xi}_0 - \xi_0} + \frac{\frac{\xi}{2}\hat{\xi} - 1}{\frac{\xi_0^2 + 1}{2\xi_0^2}\hat{\xi}_0 - \frac{1}{\xi_0}} \right] \end{aligned}$$

$$+ \frac{1}{\sqrt{\xi^2 - \eta^2}} \left[\frac{\frac{\sqrt{\xi^2 - 1}}{2}\hat{\xi}}{\frac{\xi_0^2 - 3}{4}\hat{\xi}_0 - \frac{\xi_0}{2}} - \frac{\frac{\sqrt{\xi^2 - 1}}{2}\hat{\xi} - \frac{\xi}{\sqrt{\xi^2 - 1}}}{\frac{\xi_0^2 - 3}{2(\xi_0^2 - 1)}\hat{\xi}_0 - \frac{\xi_0}{\xi_0^2 - 1}} \right] \\ \times \eta \cos(\varphi - \tilde{\phi}) \sin \gamma, \quad (8)$$

$$\begin{aligned} \frac{\hat{\phi} \cdot \mathbf{u}^t}{|\mathbf{v}|} &= \left[\frac{\frac{1}{2}\hat{\xi}}{\frac{\xi_0^2 - 3}{4}\hat{\xi}_0 - \frac{\xi_0}{2}} - \frac{\frac{1}{2}\hat{\xi} - \frac{\xi}{\xi^2 - 1}}{\frac{\xi_0^2 - 3}{2(\xi_0^2 - 1)}\hat{\xi}_0 - \frac{\xi_0}{\xi_0^2 - 1}} \right] \\ &\times \sin(\varphi - \tilde{\phi}) \sin \gamma, \end{aligned} \quad (9)$$

$$\begin{aligned} \frac{p^t}{\mu|\mathbf{v}|} &= -\frac{2}{c} \left[\frac{\xi}{\xi^2 - \eta^2} \sqrt{\frac{1 - \eta^2}{\xi^2 - 1}} \sin \gamma \cos(\varphi - \tilde{\phi}) \right. \\ &\left. + \frac{\eta}{\xi^2 - \eta^2} \frac{\cos \gamma}{-\frac{\xi_0^2 + 1}{2}\hat{\xi}_0 + \xi_0} \right], \end{aligned} \quad (10)$$

where

$$\hat{\xi}_0 = \ln \left[\frac{(\xi_0 + 1)}{(\xi_0 - 1)} \right]; \quad \hat{\xi} = \ln \left[\frac{(\xi + 1)}{(\xi - 1)} \right].$$

Here prolate spheroidal coordinates (ξ, η, φ) are employed for the convenience of computing the drag force that involves surface integration over the bounding surface of the bacterium. Analytical expressions (Equations 7–10) represent a solution satisfying both (Equation 4) and the non-slip boundary condition. It is evident that, apart from the special case with the attack angle $\gamma = 0$, this Stokes flow is fully three-dimensional.

With the availability of the three-dimensional solution (Equations 7–10), we are able to derive the drag force \mathbf{D}_B on a swimming rod-shaped bacterium using cartesian coordinates (x, y, z) attached to the bacterium's body as sketched in **Figure 2**. The drag force \mathbf{D}_B on a translating bacterium with the angle of attack γ can be expressed as

$$\mathbf{D}_B = \int_S \mathbf{f}^t dS,$$

where \int_S denotes the surface integration over the bounding surface S of the bacterium, \mathbf{f}^t in tensor notation is

$$f_i^t = (-p^t \delta_{ij} + 2\mu \sigma_{ij}^t) n_j, \quad (11)$$

with δ_{ij} being the Dirac delta function, n_j being unit normal at the bounding surface S and

$$\sigma_{ij}^t = \frac{1}{2} \left(\frac{\partial u_i^t}{\partial x_j} + \frac{\partial u_j^t}{\partial x_i} \right).$$

The tensor σ_{ij}^t can be readily obtained from the expressions (7–9) by performing derivatives in prolate spheroidal coordinates. Evaluating p^t and σ_{ij}^t at the bounding surface $\xi = \xi_0$ of the bacterium, integrating over its bounding surface S , we obtain an analytical formula for the drag force \mathbf{D}_B

on a translating bacterium:

$$\frac{\mathbf{D}_B}{2\pi\mu c} = - \left[\frac{8 + 4(\xi_0^2 - 1)(-2 + \xi_0 \hat{\xi}_0)}{2\xi_0 - (\xi_0^2 - 3)\hat{\xi}_0} \right. \\ + \frac{8\xi_0^2 - 4\xi_0(\xi_0^2 - 1)\hat{\xi}_0}{2\xi_0 - (\xi_0^2 - 3)\hat{\xi}_0} \left. \right] [(\hat{\mathbf{x}} \cdot \mathbf{v})\hat{\mathbf{x}} + (\hat{\mathbf{y}} \cdot \mathbf{v})\hat{\mathbf{y}}] \\ - \left[\frac{4\xi_0^2(\xi_0^2 - 1)(2 - \frac{\xi_0^2 - 1}{\xi_0}\hat{\xi}_0)}{2\xi_0 - 2\xi_0^3 + (\xi_0^4 - 1)\hat{\xi}_0} \right. \\ + \left. \frac{4(\xi_0^2 - 1)(2 - \xi_0 \hat{\xi}_0)}{\xi_0 - (\xi_0^2 + 1)\hat{\xi}_0} \right] (\hat{\mathbf{z}} \cdot \mathbf{v})\hat{\mathbf{z}}, \quad (12)$$

which is valid for an arbitrary angle γ . Expression (12) will be used for constructing a set of the equations describing swimming rod-shaped bacteria. The dependence of the scaled drag force is tabulated in **Table 1** as a function of γ for $\mathcal{E} = 0.96$ (or $\xi_0 = 1.0416667$). Note that we have $|\mathbf{D}_B|/(6\pi\mu a|\mathbf{v}|) \rightarrow 1$ in the spherical limit $\mathcal{E} \rightarrow 0$ and that the size of the drag force is, as expected, significantly reduced as a result of the rod shaped body. **Figure 3** shows how the drag force varies dramatically with the size of eccentricity \mathcal{E} for $\gamma = 45^\circ$, indicating that the dynamics of swimming rod-shaped bacteria would be quite different from that of spherical-shaped bacteria.

2.3. TORQUE ON A ROTATING ROD-SHAPED BACTERIA AT ARBITRARY ANGLES

We also need the mathematical solution of a three-dimensional Stokes flow driven by rotating bacterium with the angular velocity Ω at an arbitrary angle α as sketched in **Figure 2**. Suppose that a bacterium is rotating with the angular velocity Ω in the form

$$\Omega = |\Omega| [(\sin \alpha \cos \beta) \hat{\mathbf{x}} + (\sin \alpha \sin \beta) \hat{\mathbf{y}} + (\cos \alpha) \hat{\mathbf{z}}],$$

Table 1 | The scaled drag force and the scaled viscous torque as a function of γ and α for $\mathcal{E} = 0.96$.

γ or α	$ \mathbf{D}_B /(6\pi\mu a \mathbf{v})$	$ \mathbf{T}_B /(8\pi\mu a^3 \Omega)$
0°	0.424447	0.057270
10°	0.428270	0.063091
20°	0.439094	0.077447
30°	0.455178	0.095336
40°	0.474163	0.113493
50°	0.493565	0.130060
60°	0.511126	0.143900
70°	0.525008	0.154267
80°	0.533874	0.160673
90°	0.536918	0.162839

In the spherical limit $\mathcal{E} \rightarrow 0$ we obtain that $|\mathbf{D}_B|/(6\pi\mu a|\mathbf{v}|) \rightarrow 1$ and $|\mathbf{T}_B|/(8\pi\mu a^3|\Omega|) \rightarrow 1$.

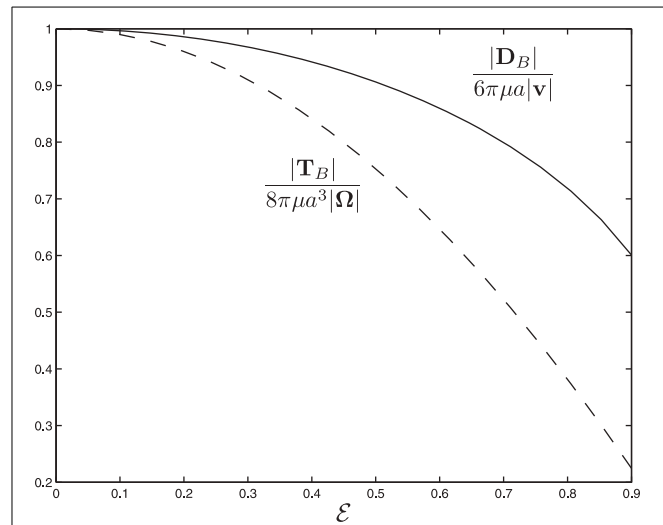


FIGURE 3 | The scaled drag force and the scaled viscous torque as a function of eccentricity \mathcal{E} for $\alpha = 45^\circ$ and $\gamma = 45^\circ$.

where the angles α and β specify the direction of Ω in the cartesian coordinates (x, y, z). A three-dimensional velocity \mathbf{u}^r and the corresponding pressure p^r describing the Stokes flow driven by a rotating rod-shaped bacterium with the angular velocity Ω at arbitrary rotating angles α and β are

$$\frac{\hat{\xi} \cdot \mathbf{u}^r}{c|\Omega|} = -\eta \sqrt{\frac{1 - \eta^2}{\xi^2 - \eta^2}} \left[\frac{\xi_0^2 \hat{\xi}}{(\xi_0^2 + 1) \hat{\xi}_0 - 2\xi_0} \right. \\ \left. - \frac{\frac{2\xi}{\xi^2 - 1} + \hat{\xi}}{\frac{(\xi_0^2 + 1) \hat{\xi}_0}{\xi_0^2 - 1} - \frac{2\xi_0}{\xi_0^2 - 1}} \right] \sin \alpha \sin (\varphi - \beta), \quad (13)$$

$$\frac{\hat{\eta} \cdot \mathbf{u}^r}{c|\Omega|} = \frac{\sqrt{\xi^2 - 1}}{\sqrt{\xi^2 - \eta^2}} \left[\frac{2\xi \hat{\xi} - 4}{\frac{(\xi_0^2 + 1) \hat{\xi}_0}{\xi_0^2} - \frac{2}{\xi_0}} \right. \\ \left. - \frac{\frac{\xi \hat{\xi}}{\xi^2 - 1} - \frac{2\xi^2}{\xi^2 - 1}}{\frac{(\xi_0^2 + 1) \hat{\xi}_0}{\xi_0^2 - 1} - \frac{2\xi_0}{\xi_0^2 - 1}} \right] \sin \alpha \sin (\varphi - \beta), \quad (14)$$

$$\frac{\hat{\phi} \cdot \mathbf{u}^r}{c|\Omega|} = \eta \left[\frac{\frac{\xi \hat{\xi}}{\xi^2 - 1} - \frac{2\xi^2}{\xi^2 - 1}}{\frac{(\xi_0^2 + 1) \hat{\xi}_0}{\xi_0^2} - \frac{2\xi_0}{\xi_0^2 - 1}} - \frac{2\xi \hat{\xi} - 4}{\frac{(\xi_0^2 + 1) \hat{\xi}_0}{\xi_0^2} - \frac{2}{\xi_0}} \right] \\ \times \sin \alpha \cos (\varphi - \beta) \\ + \frac{\hat{\xi} - \frac{2\xi}{\xi^2 - 1}}{\hat{\xi}_0 - \frac{2\xi_0}{\xi_0^2 - 1}} \sqrt{(\xi^2 - 1)(1 - \eta^2)} \cos \alpha, \quad (15)$$

$$\frac{p^r}{\mu|\Omega|} = \frac{-8\eta}{\xi^2 - \eta^2} \sqrt{\frac{1 - \eta^2}{\xi^2 - 1}} \left[\frac{\sin \alpha \sin (\varphi - \beta)}{(\xi_0^2 + 1) \hat{\xi}_0 - 2\xi_0} \right]. \quad (16)$$

Evidently, apart from the special case with $\alpha = 0$, the Stokes flow described by Equations (13–16) is fully three-dimensional.

The viscous torque \mathbf{T}_B acting on the rotating bacterium can be expressible as

$$\mathbf{T}_B = \int_S \mathbf{r}_S \times \mathbf{f}^r dS,$$

where \mathbf{r}_S denotes the position vector for the bounding surface S of the bacterium and the viscous force \mathbf{f}^r on the surface S is given by

$$f_i^r = \left[-p^r \delta_{ij} + \mu \left(\frac{\partial u_i^r}{\partial x_j} + \frac{\partial u_j^r}{\partial x_i} \right) \right] n_j, \quad (17)$$

with the velocity u_i^r and p^r given by Equations (13–16) evaluated at the outer surface $\xi = \xi_0$ of the bacterium. After a lengthy analysis analogous to that for the drag \mathbf{D}_B , the torque \mathbf{T}_B in cartesian coordinates (x, y, z) is found to be

$$\begin{aligned} \frac{\mathbf{T}_B}{8\pi\mu c^3} = & \frac{-1}{-2\xi_0 + (\xi_0^2 + 1)\hat{\xi}_0} [(\hat{\mathbf{x}} \cdot \boldsymbol{\Omega})\hat{\mathbf{x}} + (\hat{\mathbf{y}} \cdot \boldsymbol{\Omega})\hat{\mathbf{y}}] \\ & \times \left[2\xi_0 (\xi_0^2 - 1) \tanh^{-1} \frac{1}{\xi_0} \right. \\ & \left. + \frac{-4 + 8\xi_0^2 - 3\xi_0 (\xi_0^2 - 1)\hat{\xi}_0}{3} \right] \\ & + \frac{4}{3} \left[\frac{(\xi_0^2 - 1)}{-2\xi_0 + (\xi_0^2 - 1)\hat{\xi}_0} \right] (\hat{\mathbf{z}} \cdot \boldsymbol{\Omega})\hat{\mathbf{z}}, \end{aligned} \quad (18)$$

which is valid for arbitrary rotating vector $\boldsymbol{\Omega}$. Here, for example,

$$\hat{\mathbf{x}} \cdot \boldsymbol{\Omega} = |\boldsymbol{\Omega}| (\sin \alpha \cos \beta).$$

The dependence of the scaled torque is tabulated in **Table 1** as a function of α for $\mathcal{E} = 0.96$. It can be seen that we have $|\mathbf{T}_B|/(8\pi\mu a^3 |\boldsymbol{\Omega}|) \rightarrow 1$ in the spherical limit $\mathcal{E} \rightarrow 0$ and that the size of the scaled torque is sensitively dependent on the rotating angle α , ranging from 0.057 at $\alpha = 0$ to 0.163 at $\alpha = 90^\circ$. **Figure 3** shows how the the viscous torque varies dramatically with the size of eccentricity \mathcal{E} for $\alpha = 45^\circ$, indicating again that the dynamics of swimming rod-shaped bacteria would be quite different from that of spherical-shaped bacteria.

3. MODEL AND GOVERNING EQUATIONS

For deriving the equations governing the swimming motion of rod-shaped magnetotactic bacteria, we shall make the following six assumptions: (1) the geometry of a rod-shaped magnetotactic bacterium can be described by an elongated prolate spheroid (Equation 3) with $0 < (1 - \mathcal{E}) \ll 1$; (2) the body of rod-shaped magnetotactic bacteria is non-deformable and, hence, the equation of rigid-body dynamics becomes applicable; (3) interaction between different magnetotactic bacteria during their swimming motion (Ishikawa et al., 2007), as clearly suggested by our laboratory experiments, is weak and, hence, can be negligible; (4) the translation and rotation of magnetotactic bacteria are powered by the rapid rotation of helical flagellar filaments at a fixed point P , as

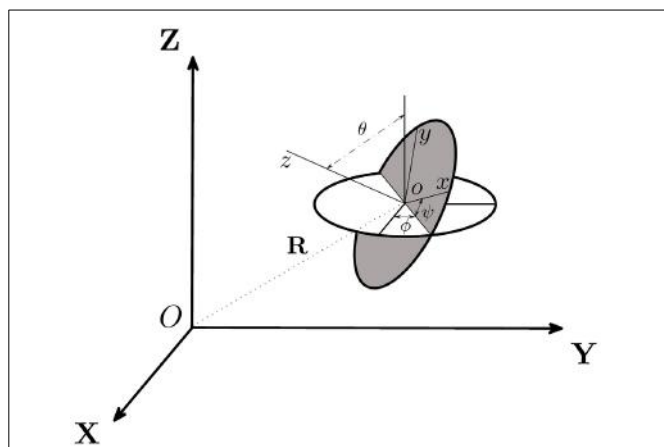


FIGURE 4 | Two cartesian coordinates, (X, Y, Z) and (x, y, z) , used in our theoretical analysis, are related by the three Euler angles (θ, ψ, ϕ) and the position vector R . Cartesian coordinates (X, Y, Z) represent a reference of frame fixed in the laboratory while (x, y, z) denote a reference of frame fixed in the body of the bacterium.

sketched in **Figure 1B**, which, as used and explained by Nogueira and Lins de Barros (1995), may be modeled a driving force \mathbf{F}_B in the body frame:

$$\mathbf{F}_B = F_{12} [\cos(\omega_0 t)\hat{\mathbf{x}} + \sin(\omega_0 t)\hat{\mathbf{y}}] + F_3\hat{\mathbf{z}}, \quad (19)$$

where ω_0 is the frequency of flagellum rotation while F_{12} , F_3 , and ω_0 may be regarded as parameters of the problem; (5) the inertial effects of swimming rod-shaped magnetotactic bacteria are small and, thus, negligible; and finally, (6) the initial phase of growing magnetic moment in a magnetotactic bacterium can be described by the equation

$$\mathbf{m}(t) = \mathbf{m}_0 \left[1 - e^{-(t-t_0)/\tau_0} \right], \quad (20)$$

where \mathbf{m} is parallel to the symmetry axis of the magnetotactic bacterium, \mathbf{m}_0 denotes the magnetic moment in the limit $t \rightarrow \infty$ and τ_0 represents a parameter controlling the grow rate of the magnetic moment.

On the basis of the above six assumptions, we are able to derive the twelve coupled equations that govern the swimming motion of a rod-shaped magnetotactic bacterium with a time-dependent magnetic moment \mathbf{m} in a viscous fluid. Two cartesian coordinates (x, y, z) and (X, Y, Z) , which are sketched in **Figure 4**, are needed to describe the swimming motion. Cartesian coordinates (x, y, z) represent a reference of frame fixed in the bacterium's body with z at its symmetry axis (**Figure 2**); this reference will be referred to as the body frame. The position of the bacterium's center o in **Figure 4** is described by the position vector

$$\mathbf{R} = X\hat{\mathbf{X}} + Y\hat{\mathbf{Y}} + Z\hat{\mathbf{Z}}$$

in cartesian coordinates (X, Y, Z) with the corresponding unit vectors $(\hat{\mathbf{X}}, \hat{\mathbf{Y}}, \hat{\mathbf{Z}})$ fixed in a laboratory; this reference will be referred to as the laboratory frame.

A rod-shaped magnetotactic bacterium swims under the combined action of a propulsive force \mathbf{F}_B , a viscous drag \mathbf{D}_B , a viscous torque \mathbf{T}_B and an externally imposed rotating magnetic field \mathbf{B} . In this paper, subscript B denotes the quantity measured in the body frame of reference (x, y, z) while subscript L for the quantity described in the laboratory frame (X, Y, Z). The relative position between two cartesian coordinates, (x, y, z) and (X, Y, Z), is determined by six variables: the position vector $\mathbf{R} = (X, Y, Z)$ together with three Euler angles (θ, ϕ, ψ) illustrated in **Figure 4**. Additionally, we also introduce the three vectors: a translation vector \mathbf{v}_L of a magnetotactic bacterium in the laboratory frame, a translation vector \mathbf{v} of a magnetotactic bacterium in the body frame and a rotation vector $\boldsymbol{\Omega}$ in the body frame. There exist 12 degrees of freedom that determine the swimming motion of a rod-shaped magnetotactic bacterium: (1) the three position coordinates $\mathbf{R} = (X, Y, Z)$ in the laboratory frame; (2) the three components of its velocity vector $\mathbf{v}_L = (\mathbf{v}_L \cdot \hat{\mathbf{X}}, \mathbf{v}_L \cdot \hat{\mathbf{Y}}, \mathbf{v}_L \cdot \hat{\mathbf{Z}})$ in the laboratory frame; (3) the three components of the angular velocity $\boldsymbol{\Omega} = (\hat{\mathbf{x}} \cdot \boldsymbol{\Omega}, \hat{\mathbf{y}} \cdot \boldsymbol{\Omega}, \hat{\mathbf{z}} \cdot \boldsymbol{\Omega})$ in the body frame and, finally, (iv) the three Euler angles (θ, ϕ, ψ).

The first set of the governing equations is derived from Newton's second law stating that the rate of change of the momentum must be equal to the sum of all external forces acting on it,

$$M \frac{d\mathbf{v}_L}{dt} = \mathbf{F}_L + \mathbf{D}_L,$$

where \mathbf{F}_L and \mathbf{D}_L are the propulsive and viscous forces in the laboratory frame. Upon neglecting inertial effects because the mass M of a rod-shaped magnetotactic bacterium (which is about 9.5×10^{-16} Kg) is extremely small, we may rewrite the above equation as

$$0 = \mathbf{F}_B + \mathbf{D}_B. \quad (21)$$

Note that, by neglecting inertial effects, the forces in the body frame ($\mathbf{F}_B, \mathbf{D}_B$) are the same as those in the laboratory frame ($\mathbf{F}_L, \mathbf{D}_L$). Equation (21) can be solved exactly, after making use of Equations (12, 19), to give the three velocity components in the body frame of reference

$$\mathbf{v} \cdot \hat{\mathbf{x}} = \frac{F_{12} \cos \omega_0 t}{2\pi\mu c} \left[\frac{8 + 4(\xi_0^2 - 1)(-2 + \xi_0 \hat{\xi}_0)}{2\xi_0 - (\xi_0^2 - 3)\hat{\xi}_0} \right]^{-1} + \frac{8\xi_0^2 - 4\xi_0(\xi_0^2 - 1)\hat{\xi}_0}{2\xi_0 - (\xi_0^2 - 3)\hat{\xi}_0}, \quad (22)$$

$$\mathbf{v} \cdot \hat{\mathbf{y}} = \frac{F_{12} \sin \omega_0 t}{2\pi\mu c} \left[\frac{8 + 4(\xi_0^2 - 1)(-2 + \xi_0 \hat{\xi}_0)}{2\xi_0 - (\xi_0^2 - 3)\hat{\xi}_0} \right]^{-1} + \frac{8\xi_0^2 - 4\xi_0(\xi_0^2 - 1)\hat{\xi}_0}{2\xi_0 - (\xi_0^2 - 3)\hat{\xi}_0}, \quad (23)$$

$$\mathbf{v} \cdot \hat{\mathbf{z}} = \frac{F_3 \sin \omega_0 t}{2\pi\mu c} \left[\frac{4\xi_0^2(\xi_0^2 - 1)(2\xi_0 - (\xi_0^2 - 1)\hat{\xi}_0)}{2\xi_0^2(1 - \xi_0^2) + \xi_0(\xi_0^4 - 1)\hat{\xi}_0} \right]$$

$$+ \frac{4(\xi_0^2 - 1)(2 - \xi_0 \hat{\xi}_0)}{\xi_0 - (\xi_0^2 + 1)\hat{\xi}_0} \right]^{-1}. \quad (24)$$

The velocity \mathbf{v} in the body frame needs to be transformed to the laboratory frame of reference, denoted as \mathbf{v}_L by using the three Euler angles, which is expressible as

$$\begin{aligned} \mathbf{v}_L \cdot \hat{\mathbf{X}} &= \mathbf{v} \cdot \hat{\mathbf{x}} (\cos \phi \cos \psi - \sin \phi \cos \theta \sin \psi) \\ &- \mathbf{v} \cdot \hat{\mathbf{y}} (\cos \phi \sin \psi + \sin \phi \cos \theta \cos \psi) \\ &+ \mathbf{v} \cdot \hat{\mathbf{z}} (\sin \phi \sin \theta), \end{aligned} \quad (25)$$

$$\begin{aligned} \mathbf{v}_L \cdot \hat{\mathbf{Y}} &= \mathbf{v} \cdot \hat{\mathbf{x}} (\sin \phi \cos \psi + \cos \phi \cos \theta \sin \psi) \\ &- \mathbf{v} \cdot \hat{\mathbf{y}} (\sin \phi \sin \psi - \cos \phi \cos \theta \cos \psi) \\ &- \mathbf{v} \cdot \hat{\mathbf{z}} (\cos \phi \sin \theta), \end{aligned} \quad (26)$$

$$\begin{aligned} \mathbf{v}_L \cdot \hat{\mathbf{Z}} &= \mathbf{v} \cdot \hat{\mathbf{x}} (\sin \theta \sin \psi) + \mathbf{v} \cdot \hat{\mathbf{y}} (\sin \theta \cos \psi) \\ &+ \mathbf{v} \cdot \hat{\mathbf{z}} \cos \theta. \end{aligned} \quad (27)$$

Note that the three Euler angles are a function of time: $\theta = \theta(t)$, $\psi = \psi(t)$, and $\phi = \phi(t)$. The second set of three equations is derived by relating the position of the bacterium \mathbf{R} in the laboratory frame to its translation velocity \mathbf{v}_L ,

$$\left(\hat{\mathbf{X}} \frac{dX}{dt} + \hat{\mathbf{Y}} \frac{dY}{dt} + \hat{\mathbf{Z}} \frac{dZ}{dt} \right) = \mathbf{v}_L.$$

After making use of Equations (22–24) and (25–27), we can derive the following three equations for determining the position vector $\mathbf{R} = (X, Y, Z)$ in the laboratory frame of reference:

$$\begin{aligned} \frac{dX}{dt} &= \frac{F_{12}}{2\pi\mu c} \left[\frac{8 + 4(\xi_0^2 - 1)(-2 + \xi_0 \hat{\xi}_0)}{2\xi_0 - (\xi_0^2 - 3)\hat{\xi}_0} \right. \\ &\left. + \frac{8\xi_0^2 - 4\xi_0(\xi_0^2 - 1)\hat{\xi}_0}{2\xi_0 - (\xi_0^2 - 3)\hat{\xi}_0} \right]^{-1} \\ &\times [\cos \phi \cos(\omega_0 t + \psi) - \sin \phi \cos \theta \sin(\omega_0 t + \psi)] \\ &+ \frac{F_3}{2\pi\mu c} \left[\frac{4\xi_0^2(\xi_0^2 - 1)(2\xi_0 - (\xi_0^2 - 1)\hat{\xi}_0)}{2\xi_0^2(1 - \xi_0^2) + \xi_0(\xi_0^4 - 1)\hat{\xi}_0} \right. \\ &\left. + \frac{4(\xi_0^2 - 1)(2 - \xi_0 \hat{\xi}_0)}{\xi_0 - (\xi_0^2 + 1)\hat{\xi}_0} \right]^{-1} \sin \phi \sin \theta, \end{aligned} \quad (28)$$

$$\begin{aligned} \frac{dY}{dt} &= \frac{F_{12}}{2\pi\mu c} \left[\frac{8 + 4(\xi_0^2 - 1)(-2 + \xi_0 \hat{\xi}_0)}{2\xi_0 - (\xi_0^2 - 3)\hat{\xi}_0} \right. \\ &\left. + \frac{8\xi_0^2 - 4\xi_0(\xi_0^2 - 1)\hat{\xi}_0}{2\xi_0 - (\xi_0^2 - 3)\hat{\xi}_0} \right]^{-1} \\ &+ \frac{8\xi_0^2 - 4\xi_0(\xi_0^2 - 1)\hat{\xi}_0}{2\xi_0 - (\xi_0^2 - 3)\hat{\xi}_0} \end{aligned}$$

$$\begin{aligned} & \times [\sin \phi \cos(\omega_0 t + \psi) + \cos \phi \cos \theta \sin(\omega_0 t + \psi)] \\ & - \frac{F_3}{2\pi\mu c} \left[\frac{4\xi_0^2 (\xi_0^2 - 1) (2\xi_0 - (\xi_0^2 - 1) \hat{\xi}_0)}{2\xi_0^2 (1 - \xi_0^2) + \xi_0 (\xi_0^4 - 1) \hat{\xi}_0} \right. \\ & \left. + \frac{4(\xi_0^2 - 1) (2 - \xi_0 \hat{\xi}_0)}{\xi_0 - (\xi_0^2 + 1) \hat{\xi}_0} \right]^{-1} \cos \phi \sin \theta, \end{aligned} \quad (29)$$

$$\begin{aligned} \frac{dZ}{dt} = & \frac{F_{12}}{2\pi\mu c} \left[\frac{8 + 4(\xi_0^2 - 1) (-2 + \xi_0 \hat{\xi}_0)}{2\xi_0 - (\xi_0^2 - 3) \hat{\xi}_0} \right. \\ & \left. + \frac{8\xi_0^2 - 4\xi_0 (\xi_0^2 - 1) \hat{\xi}_0}{2\xi_0 - (\xi_0^2 - 3) \hat{\xi}_0} \right]^{-1} \times \sin \theta \sin(\omega_0 t + \psi) \\ & - \frac{F_3}{2\pi\mu c} \left[\frac{4\xi_0^2 (\xi_0^2 - 1) (2\xi_0 - (\xi_0^2 - 1) \hat{\xi}_0)}{2\xi_0^2 (1 - \xi_0^2) + \xi_0 (\xi_0^4 - 1) \hat{\xi}_0} \right. \\ & \left. + \frac{4(\xi_0^2 - 1) (2 - \xi_0 \hat{\xi}_0)}{\xi_0 - (\xi_0^2 + 1) \hat{\xi}_0} \right]^{-1} \cos \theta. \end{aligned} \quad (30)$$

The third set of the equations is derived from the rotational dynamics of the angular momentum \mathbf{L} which is

$$\mathbf{L} = I_x \Omega_x \hat{\mathbf{x}} + I_y \Omega_y \hat{\mathbf{y}} + I_z \Omega_z \hat{\mathbf{z}},$$

where (I_x, I_y, I_z) denote the three principle moments of inertia of a rod-shaped bacterium. It is known that the rate of change of \mathbf{L} must be equal to the sum of all torques acting on the rod-shaped bacterium:

$$\left(I_x \hat{\mathbf{x}} \frac{d\Omega_x}{dt} + I_y \hat{\mathbf{y}} \frac{d\Omega_y}{dt} + I_z \hat{\mathbf{z}} \frac{d\Omega_z}{dt} \right) + \boldsymbol{\Omega} \times \mathbf{L} = \mathbf{T}_F + \mathbf{T}_c + \mathbf{T}_B + \mathbf{T}_M,$$

where \mathbf{T}_F represents the torque imposed by the driving force \mathbf{F}_B ,

$$\mathbf{T}_F = -a\hat{\mathbf{z}} \times \mathbf{F}_B = aF_{12} (\hat{\mathbf{x}} \sin \omega_0 t - \hat{\mathbf{y}} \cos \omega_0 t),$$

$\mathbf{T}_c = -N_c \hat{\mathbf{z}}$ is related to the reaction couple of the flagellar rotation (Nogueira and Lins de Barros, 1995), the viscous torque \mathbf{T}_B in the body frame is given by Equation (18) and the time-dependent magnetic torque in the laboratory frame is

$$\begin{aligned} (\mathbf{T}_M)_{\text{lab}} = \mathbf{m}(t) \times \mathbf{B} = & (m_0 B_0) \left[1 - e^{-(t-t_0)/\tau} \right] \\ & \hat{\mathbf{z}} \times (\hat{\mathbf{X}} \cos \Omega_0 t + \hat{\mathbf{Y}} \cos \Omega_0 t), \end{aligned}$$

where B_0 is the amplitude of the externally imposed, rotating magnetic field \mathbf{B} and Ω_0 denotes the frequency of the magnetic field \mathbf{B} . Since all the torques must be expressed in the same frame of reference, we need to transform $(\mathbf{T}_M)_{\text{lab}}$ in the laboratory

frame to that in the body frame of reference using the three Euler angles. In the body frame, the magnetic torque \mathbf{T}_M is

$$\begin{aligned} \mathbf{T}_M = (m_0 B_0) & \left[1 - e^{-(t-t_0)/\tau} \right] \\ & \left\{ \begin{array}{l} [(\sin \psi \cos \phi + \sin \phi \cos \theta \cos \psi) \cos \Omega_0 t \\ + (\sin \psi \sin \phi - \cos \phi \cos \theta \cos \psi) \sin \Omega_0 t] \hat{\mathbf{x}} \\ + [(\cos \psi \cos \phi - \sin \phi \cos \theta \sin \psi) \cos \Omega_0 t \\ + (\cos \psi \sin \phi + \cos \phi \cos \theta \sin \psi) \sin \Omega_0 t] \hat{\mathbf{y}} \end{array} \right\}. \end{aligned} \quad (31)$$

Furthermore, because of the extremely small moments of inertia (I_x, I_y, I_z) in association with the small mass of the bacterium, we shall neglect inertial effects by writing the angular momentum equation as

$$0 = \mathbf{T}_F + \mathbf{T}_c + \mathbf{T}_M + \mathbf{T}_B. \quad (32)$$

This approximation dramatically simplifies the analysis and allows us to solve the vector equation (32) for the three components of $\boldsymbol{\Omega}$ in the body frame of reference, which are

$$\begin{aligned} \hat{\mathbf{x}} \cdot \boldsymbol{\Omega} = & \frac{-2\xi_0 + (\xi_0^2 + 1) \hat{\xi}_0}{8\pi\mu c^3} \\ & \left\{ aF_{12} \sin \omega_0 t + m_0 B_0 \left(1 - e^{-(t-t_0)/\tau} \right) \right. \\ & \left. + [(\sin \psi \cos \phi + \sin \phi \cos \theta \cos \psi) \cos \Omega_0 t \right. \\ & \left. + (\sin \psi \sin \phi - \cos \phi \cos \theta \cos \psi) \sin \Omega_0 t] \right\} \\ & \times \left[2\xi_0 (\xi_0^2 - 1) \tanh^{-1} \frac{1}{\xi_0} \right. \\ & \left. + \frac{1}{3} (-4 + 8\xi_0^2 - 3\xi_0 (\xi_0^2 - 1) \hat{\xi}_0) \right]^{-1}, \end{aligned} \quad (33)$$

$$\begin{aligned} \hat{\mathbf{y}} \cdot \boldsymbol{\Omega} = & \frac{-2\xi_0 + (\xi_0^2 + 1) \hat{\xi}_0}{8\pi\mu c^3} \\ & \left\{ -aF_{12} \cos \omega_0 t + m_0 B_0 \left(1 - e^{-(t-t_0)/\tau} \right) \right. \\ & \left. + [(\cos \psi \cos \phi - \sin \phi \cos \theta \sin \psi) \cos \Omega_0 t \right. \\ & \left. + (\cos \psi \sin \phi + \cos \phi \cos \theta \sin \psi) \sin \Omega_0 t] \right\} \\ & \times \left[2\xi_0 (\xi_0^2 - 1) \tanh^{-1} \frac{1}{\xi_0} \right. \\ & \left. + \frac{1}{3} (-4 + 8\xi_0^2 - 3\xi_0 (\xi_0^2 - 1) \hat{\xi}_0) \right]^{-1}, \end{aligned} \quad (34)$$

$$\hat{\mathbf{z}} \cdot \boldsymbol{\Omega} = \frac{3N_c [-2\xi_0 + (\xi_0^2 - 1) \hat{\xi}_0]}{32\pi\mu c^3 (\xi_0^2 - 1)}. \quad (35)$$

While (X, Y, Z) in connection with (Equations 28–30) leads to the position of the center o of a rod-shaped bacterium in the laboratory frame, its orientation, which is related to the angular

velocity Ω , is described by the three Euler angles governed by the following three equations

$$\frac{d\theta}{dt} = \hat{\mathbf{x}} \cdot \Omega \cos(\psi) - \hat{\mathbf{y}} \cdot \Omega \sin(\psi), \quad (36)$$

$$\frac{d\phi}{dt} = \hat{\mathbf{x}} \cdot \Omega \csc(\theta) \sin(\psi) + \hat{\mathbf{y}} \cdot \Omega \csc(\theta) \cos(\psi), \quad (37)$$

$$\begin{aligned} \frac{d\psi}{dt} &= -\hat{\mathbf{x}} \cdot \Omega \cot(\theta) \sin(\psi) \\ &\quad - \hat{\mathbf{y}} \cdot \Omega \cot(\theta) \cos(\psi) + \hat{\mathbf{z}} \cdot \Omega, \end{aligned} \quad (38)$$

where $\hat{\mathbf{x}} \cdot \Omega$, $\hat{\mathbf{y}} \cdot \Omega$, and $\hat{\mathbf{z}} \cdot \Omega$ are given by Equations (33–35).

The swimming motion of a rod-shaped magnetotactic bacterium at any instant t , starting from an initial condition at $t = t_0$, can be modeled by mathematical solutions to the twelve coupled equations: (25–27) provide the three components of its velocity v_L in the laboratory frame; (Equations 28–30) lead to its position in the laboratory frame; (Equations 33–35) give its rotation vector Ω ; and (Equations 36–38) describe its orientation in the laboratory frame. Although the twelve coupled equations are non-linear and coupled, they represent a mathematically tractable system enabling us to understand the motion of a swimming rod-shaped magnetotactic bacterium under the influence of an imposed magnetic field in laboratory experiments. In this study, we have solved the twelve coupled equations using Runge–Kutta–Fehlberg 4(5) method with an adaptive time step in which the accuracy is of the order h^4 while an error estimator is of the order h^5 .

4. RESULTS

The swimming motion of rod-shaped magnetotactic bacteria is investigated through both theoretical and experimental methods. Theoretically, for given a set of the model and physical parameters together with an appropriate initial condition, the twelve governing equations are numerically solved to determine the trajectories of swimming motion in the laboratory frame. Experimentally, we record the swimming motion of rod-shaped magnetotactic bacteria found in Lake Miyun, which is illustrated in **Figure 1A**, using charge-coupled device camera under an imposed, time-dependent magnetic field \mathbf{B} in the laboratory frame (see **Figure 2**) given by

$$\mathbf{B} = B_0 \left[\cos(\Omega_0 t) \hat{\mathbf{X}} + \sin(\Omega_0 t) \hat{\mathbf{Y}} \right], \quad (39)$$

where B_0 and Ω_0 are changeable in our laboratory experiments.

A set of the model parameters, geometric or physical, must be specified in order to solve the twelve coupled equations. Several parameters may be regarded as being well known but some are poorly determined. For example, the typical length $2a$ of rod-shaped magnetotactic bacteria and its magnetic moment m_0 can be approximately measured or deduced in a reasonably accurate way. Other parameters such as the amplitude F_{12} , F_3 , and the frequency ω_0 have to be treated as the model parameters of a theoretical problem. The set of parameters used in calculating the swimming motion of rod-shaped magnetotactic bacteria found in Lake Miyun is listed in **Table 2**.

An important quantity is the angle Φ_B ($0 \leq \Phi_B \leq 180^\circ$) between the symmetry axis z (or the direction of the magnetic moment \mathbf{m} which is aligned with the symmetry axis z ,

Table 2 | The values of physical/model parameters for the rod-shaped magnetotactic bacteria used in our calculation.

Parameter	Value
The length of the bacterium	$2a = 5 \times 10^{-6}$ m
The mass of the bacterium	$M = 9.5 \times 10^{-16}$ Kg
Eccentricity	$\mathcal{E} = 0.96$
Focal length	$c = a\mathcal{E} = 2.4 \times 10^{-6}$
Outer surface coordinate	$\xi_0 = 1/\mathcal{E} = 1.0417$
Dynamical viscosity for water	$\mu = 10^{-3}$ Pa S
Magnetic moment	$m_0 = 10^{-14}$ A/m ²
Frequency in Equation (19)	$\omega_0 = 51/s$
Force amplitude in Equation (19)	$F_{12} = 1.1386 \times 10^{-12}$ N
Force amplitude in Equation (19)	$F_3 = 8.8849 \times 10^{-12}$ N
Reaction couple	$N_c = 2.249 \times 10^{-19}$ N m

see **Figure 2**) and the direction of the imposed magnetic field \mathbf{B} during the swimming motion of a rod-shape magnetotactic bacterium. The size of the angle Φ_B cannot be estimated in our laboratory experiments but can be readily computed in theoretical experiments. In particular, we are interested in how the angle Φ_B varies during the growing phase of the bacterium's magnetic moment. Two different phases can be identified in our theoretical model. During the initial growing phase, marked by $(t - t_0)/\tau_0 < O(1)$ in Equation (20), when the magnetic moment $|\mathbf{m}|$ is weak, the angle Φ_B is hardly affected by the existence of the magnetic moment and, hence, the angle Φ_B would change widely and strongly depend on the initial angle used as the initial condition. After its growing phase when the magnetic moment $|\mathbf{m}|$ becomes saturated as $(t - t_0)/\tau_0 > O(1)$ in Equation (20), the angle Φ_B would approach a finite, non-zero average value. Evidently, the angle Φ_B would be small [i.e., the magnetic field \mathbf{B} would be nearly aligned with the symmetry axis z , as clearly indicated by the torque equation (32)], if the magnetic moment $|\mathbf{m}|$ is sufficiently large. It should be noted that, while we have chosen a magnetic moment growth in our model, the resulting dynamics would be the same as that of an increasing strength of the magnetic field which is realizable in experimental studies.

Starting with the angle $\Phi_B = 90^\circ$ and using the set of the parameters listed in **Table 2** together with $B_0 = 14.00 \times 10^{-4}$ T and $\Omega_0 = 2.5133/s$ in Equation (39), we perform two computations of solving the twelve coupled equations as an initial-value problem. The first one takes a fast growth rate with $\tau_0 = 1$ s, the result of which is depicted in **Figure 5A**. It can be seen that, after changing rapidly and widely during the initial growing phase, the angle Φ_B approaches the values that are oscillating around 20° . In the second calculation with a slow growth rate with $\tau_0 = 5$ s, which is shown in **Figure 5B**, it takes a longer time for the angle Φ_B to approach an equilibrium value. In general, the external magnetic field \mathbf{B} is usually not aligned with the magnetic moment \mathbf{m} and the average equilibrium of the angle Φ_B is primarily determined by the torque equation (32).

In contrast to the angle Φ_B , direct comparison can be readily made between the laboratory trajectories of the swimming motion and the corresponding theoretical trajectories. In laboratory experiments, we record the trajectories of a swimming

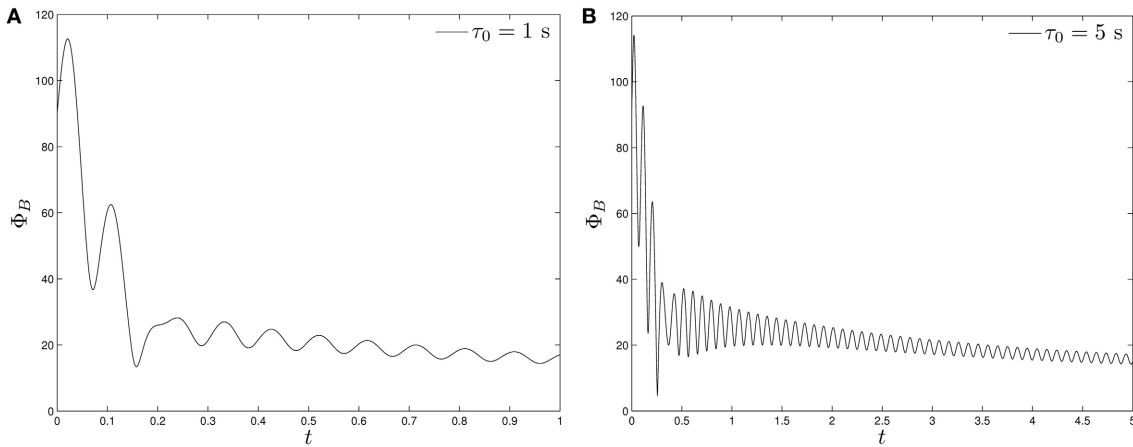


FIGURE 5 | The angle Φ_B of a swimming rod-shaped magnetotactic bacterium as a function of time starting from $\Phi_B = 90^\circ$ under the influence of a rotating magnetic field (Equation 39) with $B_0 = 14.00 \times 10^{-4}$ T and $\Omega_0 = 2.5133/\text{s}$: (A) for $\tau_0 = 1\text{ s}$ and (B) for $\tau_0 = 5\text{ s}$.

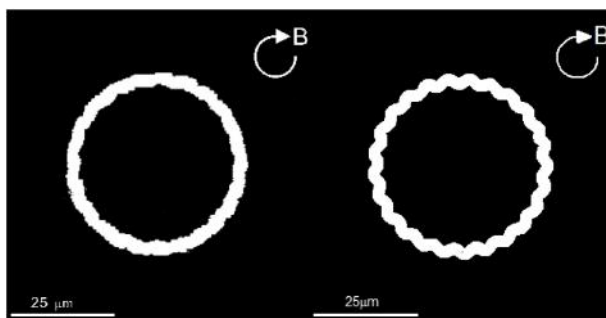


FIGURE 6 | The swimming trajectories of a rod-shaped magnetotactic bacterium under the influence of an externally imposed rotating magnetic field (Equation 39) with $B_0 = 14.00 \times 10^{-4}$ T and $\Omega_0 = 2.5133/\text{s}$. The left panel is recorded in our laboratory experiment with a charge-coupled device camera while the right panel shows a numerical solution of the twelve coupled equations using the parameters listed in Table 2.

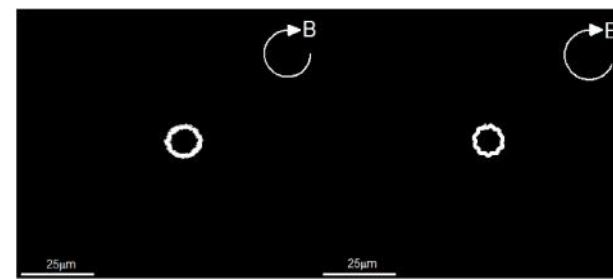


FIGURE 7 | The swimming trajectories of a rod-shaped magnetotactic bacterium under the influence of a rotating magnetic field (Equation 39) with $B_0 = 4.00 \times 10^{-4}$ T and $\Omega_0 = 6.28/\text{s}$. The left panel is recorded in our laboratory experiment with a charge-coupled device camera while the right panel shows a numerical solution of the twelve coupled equations using the parameters listed in Table 2.

rod-shaped magnetotactic bacterium found in Lake Miyun by using a charge-coupled device camera. Two laboratory experiments and their corresponding theoretical experiments are carried out. In the first laboratory experiment, we impose a rotating magnetic field given by Equation (39) with $B_0 = 14.0 \times 10^{-4}$ T with $\Omega_0 = 2.5133/\text{s}$ whose trajectories of swimming motion are depicted on the left panel of Figure 6. It is estimated that the average radius of the trajectories of circular path is about 20.0×10^{-6} m. Theoretically, we employ the set of the parameters listed in Table 2, together with $B_0 = 14.00 \times 10^{-4}$ T and $\Omega_0 = 2.5133/\text{s}$, to solve the twelve coupled equations as a function of time with a moderate value of τ_0 . The right panel of Figure 6 shows the theoretical trajectories of swimming motion for a rod-shaped magnetotactic bacterium after $(t - t_0)/\tau_0 \gg 1$, which give rise to the average radius of the circular path about 20.5×10^{-6} m. It is demonstrated that, for rod-shaped magnetotactic bacteria, the laboratory observations can be largely reproduced by

the solutions of our theoretical model using a set of appropriate parameters.

Since powers of the flagellar motor for a rod-shaped magnetotactic bacterium is fixed, we anticipate that the average radius of circular path would decrease when the rotating frequency Ω_0 of the externally imposed magnetic field increases. In the second experiment, we also impose a rotating magnetic field given by Equation (39) but with $B_0 = 4.00 \times 10^{-4}$ T and an increased frequency $\Omega_0 = 6.28/\text{s}$. The resulting trajectories of swimming motion recorded in our laboratory experiment are depicted on the left panel of Figure 7. It is estimated, from the laboratory observations, that the average radius of circular path decreases to about 5.2×10^{-6} m. The expected decrease is successfully reproduced by the theoretical trajectories of swimming motion, which is depicted on the right panel of Figure 7. Employing the same set of the parameters listed in Table 2 together with $B_0 = 4.00 \times 10^{-4}$ T and $\Omega_0 = 6.28/\text{s}$, the theoretical estimate of the average radius from our computation is about 5.1×10^{-6} m.

5. SUMMARY AND REMARKS

Through both theoretical and experimental methods, we have investigated the swimming motion of rod-shaped magnetotactic bacteria in a viscous liquid under the influence of an externally imposed, rotating magnetic field. It is shown that a fully three-dimensional Stokes flow, driven by the translation and rotation of a swimming rod-shaped bacterium, exerts the complicated viscous drag and torque on the swimming motion. Under the major assumptions that (1) the body of the bacterium is non-deformable, (2) inertial effects are negligible, and (3) interactions between different bacteria are weak and negligible, we have derived a new system of the twelve coupled equations governing both the motion and orientation of a swimming rod-shape magnetotactic bacterium. Of the twelve coupled equations, (25–27) provide the velocity v_L in the laboratory frame, (Equations 28–30) are for the position of the bacterium in the laboratory frame, (Equations 33–35) give its rotation vector Ω and (Equations 36–38) describe the orientation of the bacterium in the laboratory frame.

Using rod-shaped magnetotactic bacteria collected from Lake Miyun near Beijing, China, we have demonstrated that the theoretical swimming patterns described by solutions of the twelve coupled equations are largely similar to those observed in our laboratory experiments under the influence of externally imposed rotating magnetic fields. Despite a good agreement achieved between the theory and the experiments, the weakest component in our theoretical model is perhaps the assumption of non-deformable character of the rod-shaped bacteria under strong viscous and magnetic torques. However, modeling the swimming motion of deformable rod-shaped magnetotactic bacteria without fully understanding how/why rod-shaped magnetotactic bacteria are deformable is, both mathematically and biologically, highly challenging.

ACKNOWLEDGMENTS

This work is supported by the CAS grant KZCX2-YW-T10. Dali Kong and Keke Zhang are supported by UK NERC and STFC grants. We thank Dr. G. A. Paterson for helpful discussions.

REFERENCES

- Blakemore, R. (1975). Magnetotactic bacteria. *Science* 190, 377–379. doi: 10.1126/science.170679
- Blakemore, R. P., Frankel, R. B., and Kalmijn, A. J. (1980). South-seeking magnetotactic bacteria in the southern-hemisphere. *Nature* 286, 384–385. doi: 10.1038/286384a0
- Bazylinski, D. A., and Frankel, R. B. (2004). Magnetosome formation in prokaryotes. *Nat. Rev. Microbiol.* 2, 217–230. doi: 10.1038/nrmicro842
- Batchelor, G. K. (1967). *An Introduction to Fluid Dynamics*. Cambridge: Cambridge University Press.
- Berg, H. C., and Anderson, R. A. (1973). Bacteria swim by rotating their flagellar filaments. *Nature* 245, 380–382. doi: 10.1038/245380a0
- Cui, Z., Kong, D., Pan, Y., and Zhang, K. (2012). On the swimming motion of spheroidal magnetotactic bacteria. *Fluid Dynam. Res.* 44, 055508. doi: 10.1088/0169-5983/44/5/055508
- Erglis, K., Wen, Q., Ose, V., Zeltins, A., Sharipo, A., Janmey, P. A., et al. (2007). Dynamics of magnetotactic bacteria in a rotating magnetic field. *Biophys. J.* 93, 1402–1412. doi: 10.1529/biophysj.107.107474
- Faivre, D., and Schüler, D. (2008). Magnetotactic bacteria and magnetosomes. *Chem. Rev.* 108, 4875–4898. doi: 10.1021/cr078258w
- Frankel, R. B. (1984). Magnetic guidance of organisms. *Annu. Rev. Biophys. Bioeng.* 13, 85–103. doi: 10.1146/annurev.bb.13.060184.000505
- Han, Y., Alsayed, A., Nobili, M., and Yodh, A. G. (2009). Quasi-two-dimensional diffusion of single ellipsoids: aspect ratio and confinement effects. *Phys. Rev. E* 80, 011403. doi: 10.1103/PhysRevE.80.011403
- Happel, J., and Brenner, H. (1965). *Low Reynolds Number Hydrodynamics*. Englewood Cliffs, NJ: Prentice-Hall, INC.
- Ishikawa, T., Sekiya, G., Imai, Y., and Yamaguchi, T. (2007). Hydrodynamic interactions between two swimming bacteria. *Biophys. J.* 93, 2217–2225. doi: 10.1529/biophysj.107.110254
- Jeffery, G. B. (1922). The motion of ellipsoidal particles immersed in a viscous fluid. *Proc. R. Soc. Lond. Ser. A* 102, 161–179. doi: 10.1098/rspa.1922.0078
- Jones, C. J., and Aizawa, S. I. (1991). The bacterial flagellum and flagellar motor: structure, assembly and function. *Adv. Microb. Physiol.* 32, 109–172. doi: 10.1016/S0065-2911(08)60007-7
- Kirschvink, J. L. (1980). South-seeking magnetic bacteria. *J. Exp. Biol.* 86, 345–347.
- Koiller, J., Ehlers, K., and Montgomery, R. (1996). Problems and progress in microswimming. *J. Nonlin. Sci.* 6, 507–541. doi: 10.1007/BF02434055
- Kong, D., Cui, Z., Pan, Y., and Zhang, K. (2012). On the Papkovich-Neuber formulation for Stokes flows driven by a translating/rotating prolate spheroid at arbitrary angles. *Int. J. Pure Appl. Math.* 75, 455–483.
- Lin, W., Jogler, C., Schuler, D., and Pan, Y. (2011). Metagenomic analysis reveals unexpected subgenomic diversity of magnetotactic bacteria within the phylum *nitrospirae*. *Appl. Environ. Microbiol.* 77, 323–326. doi: 10.1128/AEM.01476-10
- Moffatt, H. K. (1978). *Magnetic Field Generation in Electrically Conducting Fluids*. Cambridge, England: Cambridge University Press.
- Neuber, H. (1934). Ein neuer Absatz zur Lösung räumlicher Probleme der Elastizitätstheorie. *Z. Angew. Math. Mech.* 14, 203–212. doi: 10.1002/zamm.19340140404
- Nogueira, F. S., and Lins de Barros, H. G. P. (1995). Study of the motion of magnetotactic bacteria. *Eur. Biophys. J.* 24, 13–21. doi: 10.1007/BF00216826
- Pan, Y., Lin, W., Li, J., Wu, W., Tian, L., Deng, C., et al. (2009). Efficiency of magnetotaxis in magnetotactic coccoid bacteria. *Biophys. J.* 97, 986–991. doi: 10.1016/j.bpj.2009.06.012
- Papkovich, P. F. (1932). The representation of the general integral of the fundamental equations of elasticity theory in terms of harmonic functions (in Russian). *Izv. Akad. Nauk. SSSR Ser. Mat.* 10, 1425–1435.
- Payne, L. E., and Pell, W. H. (1960). The Stokes flow problem for a class of axially symmetric bodies. *J. Fluid Mech.* 7, 529–549. doi: 10.1017/S002211206000027X
- Prozorov, T., Bazylinski, D. A., Mallapragada, S. K., and Prozorov, R. (2013). Novel magnetic nanomaterials inspired by magnetotactic bacteria. *Mater. Sci. Eng. R* 74, 133–172. doi: 10.1016/j.mser.2013.04.002
- Purel, E. M. (1977). Life at low Reynolds number. *AM. J. Phys.* 45, 3–11. doi: 10.1119/1.10903
- Schüler, D., and Baeuerlein, E. (1996). Iron-limited growth and kinetics of iron uptake in *Magnetospirillum gryphiswaldense*. *Arch. Microbiol.* 166, 301–307. doi: 10.1007/s002030050387
- Winklhofer, M. (2010). Magnetoreception. *J. R. Soc. Interface* 7, S131–S134. doi: 10.1098/rsif.2010.0010.focus
- Yan, L., Zhang, S., Chen, P., Liu, H., Yin, H., and Li, H. (2012). Magnetotactic bacteria, magnetosomes and their application. *Microbiol. Res.* 167, 507–519. doi: 10.1016/j.micres.2012.04.002
- Zhang, K., and Schubert, G. (2000). Magnetohydrodynamics in rapidly rotating spherical systems. *Ann. Rev. Fluid Mech.* 32, 411–445. doi: 10.1146/annurev.fluid.32.1.409

Conflict of Interest Statement: The authors declare that the research was conducted in the absence of any commercial or financial relationships that could be construed as a potential conflict of interest.

Received: 26 July 2013; **accepted:** 08 January 2014; **published online:** 30 January 2014. **Citation:** Kong D, Lin W, Pan Y and Zhang K (2014) Swimming motion of rod-shaped magnetotactic bacteria: the effects of shape and growing magnetic moment. *Front. Microbiol.* 5:8. doi: 10.3389/fmicb.2014.00008

This article was submitted to Aquatic Microbiology, a section of the journal Frontiers in Microbiology.

Copyright © 2014 Kong, Lin, Pan and Zhang. This is an open-access article distributed under the terms of the Creative Commons Attribution License (CC BY). The use, distribution or reproduction in other forums is permitted, provided the original author(s) or licensor are credited and that the original publication in this journal is cited, in accordance with accepted academic practice. No use, distribution or reproduction is permitted which does not comply with these terms.



The magnetosome model: insights into the mechanisms of bacterial biominerization

Lilah Rahn-Lee and Arash Komeili*

Plant and Microbial Biology, University of California Berkeley, Berkeley, CA, USA

Edited by:

Damien Faivre, Max Planck Society, Germany

Reviewed by:

Christopher T. Lefèvre, CEA Cadarache, France

Teresa Perez Gonzalez, Max Planck Institute of Colloids and Interfaces, Germany

René Uebe, Ludwig Maximilian University Munich, Germany

***Correspondence:**

Arash Komeili, Plant and Microbial Biology, University of California Berkeley, 101 Koshland Hall #3102, Berkeley, CA 94720, USA
e-mail: komeili@berkeley.edu

Though the most ready example of biominerization is the calcium phosphate of vertebrate bones and teeth, many bacteria are capable of creating biominerals inside their cells. Because of the diversity of these organisms and the minerals they produce, their study may reveal aspects of the fundamental mechanisms of biominerization in more complex organisms. The best-studied case of intracellular biominerization in bacteria is the magnetosome, an organelle produced by a diverse group of aquatic bacteria that contains single-domain crystals of the iron oxide magnetite (Fe_3O_4) or the iron sulfide greigite (Fe_3S_4). Here, recent advances in our understanding of the mechanisms of bacterial magnetite biominerization are discussed and used as a framework for understanding less-well studied examples, including the bacterial intracellular biominerization of cadmium, selenium, silver, nickel, uranium, and calcium carbonate. Understanding the molecular mechanisms underlying the biological formation of these minerals will have important implications for technologies such as the fabrication of nanomaterials and the bioremediation of toxic compounds.

Keywords: intracellular biominerization, magnetotactic bacteria, bioremediation, magnetite, selenium nanospheres, cadmium sulfide, calcium carbonate, nanoparticles

INTRODUCTION

The molecules of life, sugars, lipids, and proteins, are in large measure made of only a few of the elements abundant on earth: carbon, hydrogen, nitrogen, and oxygen. Life has developed a universal economy, including the ribosome, nucleic acid polymerases, and proteases, for using and recycling these elements into new sugars, lipids and proteins. Organisms that build materials out of the remainder of the periodic table to harness the hardness, density, and unique chemistry of these diverse elements must develop whole new mechanisms for obtaining, manipulating, and incorporating them. This is called biominerization.

The most ready examples of biominerization are macroscopic structures built by multicellular organisms, such as the calcium phosphate bones of vertebrates or the magnetite teeth of chitons. However, biominerization is a widespread trait found in many single cell organisms, such as bacteria. The ease of studying bacteria, their deep branching position in the tree of life, and the variety of elements they can mineralize, including toxic pollutants, make bacterial biominerizers an exciting area of study for those seeking to better understand mechanisms of biominerization or looking for better chemistries to construct nanomaterials.

Unfortunately, although bacteria create a wide variety of biominerals, very little is understood mechanistically about any one case. The best studied of these by far is magnetotactic bacteria (MTB), which biomineralize crystals of the iron oxide magnetite (Fe_3O_4) or the iron sulfide greigite (Fe_3S_4) inside membrane-bound organelles called magnetosomes. These minerals have inherent magnetic properties, and it is thought that MTB exploit these magnetic properties for navigation by using the

earth's geomagnetic field to guide their search for their preferred low-oxygen environment (Frankel and Bazylinski, 2009).

There is huge diversity in the size and shape of magnetite or greigite nanocrystals produced by different species of MTB (Lins et al., 2000; Faivre and Schüler, 2008; Schüler, 2008, **Figure 1**). Due to their genetic tractability and ease of growth in the laboratory, two closely related alpha-proteobacteria, *Magnetospirillum magneticum* AMB-1 (AMB-1) and *M. gryphiswaldense* MSR-1 (MSR-1), have been the model systems for the mechanistic understanding of biominerization. These organisms both produce cubo-octohedral magnetite crystals. The current picture of the mechanisms employed by these bacteria to biomineralize magnetite are covered in these reviews (Jogler and Schüler, 2009; Komeili, 2012) and summarized in **Figure 3**.

Bacteria undergo intracellular biominerization under a variety of conditions and for different purposes. In some cases, organisms are fed metals to see if they can mineralize them. For example, *Escherichia coli* and *Rhodopseudomonas palustris* have both been shown to biomineralize cadmium when it is provided to them under experimental conditions (Sweeney et al., 2004; Bai et al., 2009), and AMB-1 can mineralize tellurium nanorods separately from its magnetite crystals, creating a biomagnetic method of recovering this rare element from the environment (Tanaka et al., 2010). Other organisms are able to use biominerization to detoxify pollutants such as nickel, uranium, or silver encountered in the environment by transforming them into less bio-accessible states (Klaus et al., 1999; Zhan et al., 2012; Sousa et al., 2013). Still others manage their own waste products with biominerization, including photosynthesizing cyanobacteria (Couradeau et al., 2012), and selenite-respiring bacteria

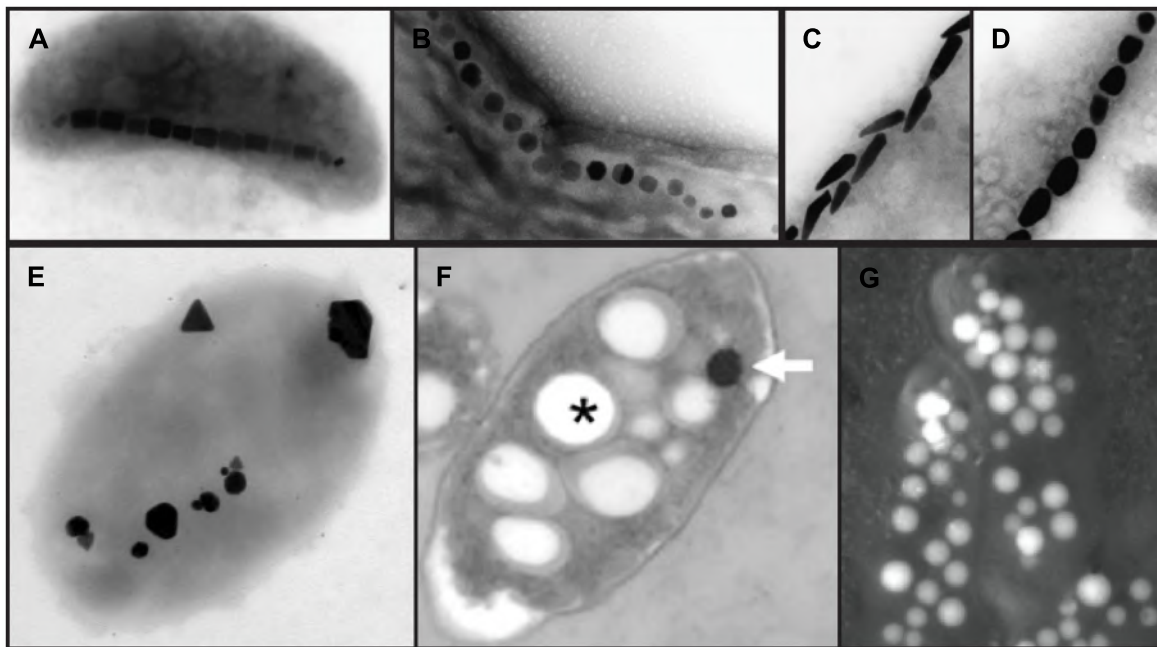


FIGURE 1 | Electron micrographs of intracellular bacterial biominerals. (A–D), magnetite crystals in different species of magnetotactic bacteria, copyright 2008 Federation of European Microbiological Societies (Schüler, 2008). (E), silver minerals in *P. stutzeri*, copyright 1999, National Academy of Sciences, USA (Klaus et al., 1999). (F), *T. selenatis*, copyright 2011 the authors

(Debieux et al., 2011). Asterisk, Poly(3-hydroxybutyrate) granule; arrow, selenium nanosphere. (G), carbonate deposits in a cyanobacterium, copyright 2012 American Association for the Advancement of Science (Couradeau et al., 2012). In this backscatter scanning electron micrograph, electron dense carbonate deposits appear white. Images are not to scale.

(Debieux et al., 2011). Finally, MTB specifically import iron from the environment in order to build an organelle that is useful to the cell.

Although they have exciting implications for nanotechnology, bioremediation, and bacterial cell biology, little is understood about the biomineralization processes described above. MTB biomineralization can serve as a model for these exotic and less well-studied cases. Here, we discuss recent advances in the study of MTB magnetite formation, and speculate about their implications for understanding the diverse array of cases of bacterial intracellular biomineralization.

SOURCE OF THE MINERAL

Before biomineralization can take place, the raw materials must be obtained. For many bacteria, biomineralization is a way to cope with an environmental toxin or a waste product, so the main elements that form the final mineral do not need to be sourced. For example, *Pseudomonas alcaliphila* has been shown to mineralize toxic Ni(II) to Ni(0) (Zhan et al., 2012), and *Thauera selenatis* manages selenite, a waste product of its respiration on selenate, by mineralizing Se(0) nanospheres (Debieux et al., 2011). In both of these cases, the resultant mineral is elemental nickel or selenium, so no further material is needed.

Like *T. selenatis*, cyanobacteria handle carbonate, the waste product of photosynthesis, by precipitating it, in this case with cations such as calcium. Recently, a cyanobacterium from the Gloeobacterales order has been shown to perform this precipitation intracellularly, using calcium as well as the cations

magnesium, strontium, and barium (Couradeau et al., 2012). Remarkably, these other cations were enriched relative to calcium in the mineral, in the case of barium over one thousand fold (Couradeau et al., 2012), suggesting an unknown mechanism for recruiting and incorporating barium into the mineral.

In some cases there are good guesses, if no hard evidence, of the source of co-precipitating elements. For example, *P. stutzeri* survives in toxic concentrations of silver by producing large, periplasmic silver crystals, some in the form of the silver sulfide acanthite (Klaus et al., 1999). The authors of this study hypothesize that the sulfur may be coming from hydrogen sulfide gas, which *P. stutzeri* is known to produce (Slawson et al., 1994; Klaus et al., 1999). A sulfur source is similarly needed for *E. coli* and *R. palustris* to produce cadmium sulfide (CdS) when grown at high cadmium concentrations. Cysteine has been shown to act as a sulfur source during extracellular CdS precipitation (Wang et al., 2000), and indeed the activity of cysteine desulfhydrases, enzymes that remove sulfide from the amino acid cysteine, were found enriched in the cellular fraction of *R. palustris* where biomineralization occurs, and the levels of these enzymes were found to rise later in the cell cycle, during maximum CdS production (Bai et al., 2009).

MTB are different from other biominerizers in that they need to import iron to make magnetite. However, an understanding of MTB iron transport could elucidate the import strategies of co-precipitating elements for other bacteria. Early evidence suggested that MTB could produce siderophores, raising the possibility that they could import insoluble ferric iron (Paoletti and Blakemore,

1986). Partial support for this model comes from the examination of a non-magnetic AMB-1 mutant that appears to have defects in siderophore-mediated iron uptake under simulated iron starvation conditions (Calugay et al., 2004). However, careful analysis of siderophore production by AMB-1 has found that these molecules are made as a result of iron depletion following magnetite production, making it unlikely that they are a central element of biominerization in MTB (Calugay et al., 2003).

Recent studies in MSR-1 suggest that at least some of the iron transport for magnetite synthesis occurs through two copies of the ferrous iron transporter FeoB. The *feo* iron transport genes are common to most bacteria, including all MTB investigated so far, many of which contain additional, magnetosome-specific copies of *feoB* (Lefèvre et al., 2013). Deletions of *feoB1* (Rong et al., 2008) and *feoB2* (Rong et al., 2012) reduce the magnetite content of MSR-1, as does a deletion of *fur*, which encodes an iron response regulator that effects the transcription of both *feoB* genes (Uebe et al., 2010; Qi et al., 2012).

Early transposon mutagenesis of AMB-1 (Matsunaga et al., 1992) yielded a disruption in a gene named *magA* that appeared to be transcriptionally regulated by iron and caused the accumulation of iron when heterologously expressed in *E. coli*-derived membrane vesicles (Nakamura et al., 1995). Indeed, when expressed in mammalian cell culture, *magA* appears to increase cellular iron content (Goldhawk et al., 2009) and cause the formation of small iron deposits (Zurkiya et al., 2008). Recently, however, in-frame deletions have been made of *magA* in both AMB-1 and MSR-1, and no biominerization phenotype was observed (Uebe et al., 2012), leaving the FeoB proteins as the only factors that have been clearly demonstrated to be involved in iron uptake for magnetite formation.

Much is still unknown about MTB iron transport. A double *feoB* deletion is still able to biomineralize some magnetite (Rong et al., 2012), suggesting that other transport systems exist. The magnetosome proteins MamM and MamB, which are members of the cation diffusion facilitator family of metal transporters (Murat et al., 2010; Uebe et al., 2011), and MamZ and MamH, which are members of the major facilitator superfamily of transporters (Raschdorf et al., 2013), have been proposed as additional iron transporters for magnetite biominerization. Although loss of these genes results in a defect in magnetic particle formation, it has not yet been shown whether or not they are transporting iron for biomineralization.

Magnetite crystals are built inside a membrane-bound compartment, and it remains to be elucidated if iron is transported through the cytoplasm, or directly from the periplasm to the compartment, as suggested by Faivre et al. (2007). Transport systems including FeoB could act at any of these steps (**Figure 3**). Whatever the mechanism of iron import, MTB must also source the oxygen for magnetite. O₂ from air is a tempting guess, and early speculation focused on whether there was a competition for oxygen between biominerization and respiration (Blakemore et al., 1985). However, isotope analysis demonstrates that the oxygen in MTB-biomineraled magnetite comes from water (Mandernack et al., 1999). This is a good reminder that the obvious source of the raw materials for biominerization may not be the source that the bacteria actually use.

CHEMISTRY

Once soluble minerals are obtained, they must be manipulated chemically to become insoluble precipitates or crystal deposits. This can happen simply by rearranging chemical bonds, for example soluble uranium VI is precipitated as the insoluble U(VI)-containing uranium phosphate meta-autunite during bioremediation in *Rhodanobacter* A2-61 (Sousa et al., 2013). More often, however, the redox state of the mineral is altered. In many of the cases discussed here, glutathione and other thiols, central players in cellular redox homeostasis, are thought to play key roles in the mineralization process (Sweeney et al., 2004; Debieux et al., 2011).

One of the major redox pathways in microaerophilic or anaerobic bacteria such as MTB is the denitrification pathway, which reduces nitrate to nitrogen gas for respiration. Recently, MSR-1 has been shown to possess a complete denitrification pathway and the first step, the *nap* genes whose products catalyze the reduction of nitrate (NO₃) to nitrite (NO₂), was shown to be essential for growth without oxygen (Li et al., 2012). Intriguingly, deletions of both *nap* genes and *nir* genes, whose products catalyze the reduction of nitrite to nitric oxide (NO), have biominerization defects (Li et al., 2012, 2013). Deletions of these genes also disrupt respiration and growth, presumably with pleotropic effects, making interpretation difficult. However, it is tempting to imagine that they are regulating the redox state of the cell, or perhaps even oxidizing ferrous iron directly in order to allow for magnetite biominerization (Li et al., 2012, 2013). Indeed, a nitrite reductase from *M. magnetotacticum* MS-1 has been shown to oxidize Fe(II) *in vitro* (Yamazaki et al., 1995). Since denitrification genes are common among bacteria, they could also play a role in other biominerization mechanisms.

MTB also contain a dedicated set of redox active proteins. Bioinformatic analysis identified the genes *mamE*, *mamP*, and *mamT* as common to MTB, with their products sharing a unique configuration of two closely spaced CXXCH heme-binding motifs, termed the magnetochrome domain (Siponen et al., 2012). Purified MamP and MamE have spectral and redox characteristics consistent with c-type cytochromes (Siponen et al., 2012). Deletions of these genes (Murat et al., 2010; Quinlan et al., 2011) or of *mamX*, another magnetochrome gene (Raschdorf et al., 2013; Yang et al., 2013), result in biominerization defects, as do point mutations in the putative heme-binding CXXCH motif (Quinlan et al., 2011; Raschdorf et al., 2013). Since some of these genes also contain protein-interaction PDZ motifs, it has been suggested that they form a protein complex that serves as an electron transport chain to regulate electron flow for biomineralization (Siponen et al., 2012).

The recent crystal structure of the magnetochrome protein MamP from strain MO-1 provides our first mechanistic insight into this new class of cytochromes (Siponen et al., 2013). This structure suggests that the functional unit of MamP is a dimer, with four heme groups surrounding a central acidic pocket. Incubating the MamP crystal with Fe(II) before imaging resulted in a new density in the acidic pocket, potentially two atoms of iron (**Figure 2**). To demonstrate that the acidic pocket is important for function, a *mamP* deletion strain of AMB-1 was complemented either with wild type *mamP* or a mutant gene with the acidic residues changed to alanine. The allele lacking the acidic residues

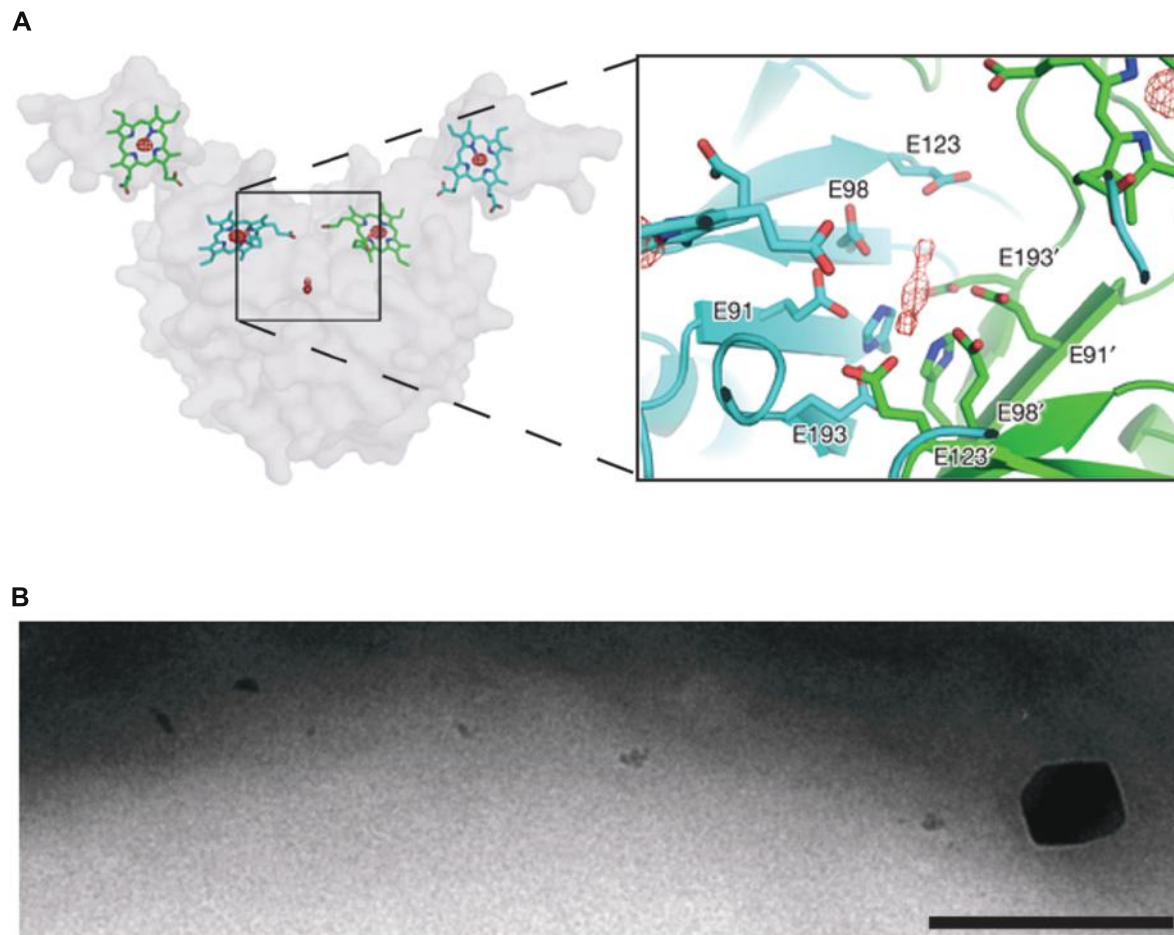


FIGURE 2 | MamP oxidizes iron and regulates magnetite crystal size. (A), the crystal structure of MO-1 MamP with two atoms of iron bound in the acidic pocket, adapted by permission from Macmillan Publishers Ltd: Nature Siponen et al., 2013, copyright 2013. **(B)**, a *mamP* mutant in AMB-1 with many small magnetite crystals and rare large ones. Scale bar 200 nm.

failed to complement even though it was expressed, suggesting the chemical nature of this pocket is important for MamP function. When MO-1 MamP was incubated with Fe(II) *in vitro* first ferrihydrite, which contains Fe(III), and then magnetite, which contains both Fe(II) and Fe(III), were formed, suggesting that MamP bound and then oxidized the iron. As shown in **Figure 2**, in AMB-1 a *mamP* mutant has many small crystals with rare crystals that are larger than normal (Murat et al., 2010). Perhaps inability to regulate the redox state of iron can cause unchecked mineral growth.

Many bacterial biominerizers need to control the redox state of their minerals. It will be interesting to see if the others, like MTB, have dedicated electron transport chains or redox-active proteins for this purpose. *T. selenatis*, which respires selenate and biominerizes selenium, uses its selenate reductases in this process (Debieux et al., 2011), but as its product of respiration is incorporated into the biomineral itself, it is a unique case. MTB also employ general respiration reductases for magnetosome formation. Perhaps this is a common feature of bacterial biominerization.

REGULATION OF MINERAL STATE

In some cases of intracellular bacterial biominerization the type of mineral or crystal phase produced is not strictly controlled. For example, the cyanobacterial carbonate deposits, while similar to the mineral benstonite, have an unusual stoichiometry and are amorphous (Couradeau et al., 2012). *P. stutzeri* and *Rhodanobacter* A2-61 each build three different kinds of crystalline silver or uranium phosphate minerals, respectively (Klaus et al., 1999; Sousa et al., 2013). Other bacteria, however, produce uniform crystalline minerals, suggesting tight regulation over the mineralization process. The CdS crystals produced by *R. palustris* or *E. coli*, for example, are uniform cubic or hexagonal CdS, respectively (Sweeney et al., 2004; Bai et al., 2009). The elemental selenium deposits produced by *T. selenatis* are also uniform (Debieux et al., 2011). No mechanisms are known that regulate the mineral forms in these cases.

For guidance, we can turn to MTB. Some MTB crystallize magnetite, and others greigite. Which mineral is produced is species-specific, suggesting there is genetic control of mineral state. Indeed, a bacterium, *Candidatus Desulfamplus magnatomortis*

BW-1, was recently isolated that can mineralize both. Genomic analysis suggests that this strain possesses two sets of genes for biominerization, one that is more closely related to those of magnetite-producers, and the other to greigite-producers (Lefèvre et al., 2011). BW-1 produces either magnetite or greigite crystals depending on the chemical environment (Lefèvre et al., 2011), though whether this phenomenon is chemical in nature or whether the cell is responding to the environment either genetically or biochemically remains unknown.

Some MTB genes have been shown to affect the mineral state. Although magnetite or greigite are invariably produced in wild-type MTB, recent studies in MSR-1 have uncovered mutant backgrounds in which some of the mineral produced is hematite, an Fe(III)-containing iron oxide (Fe_2O_3). These include the deletion of *mamX*, the PDZ-containing magnetochrome gene described above, or of *mamZ*, a gene with homology to iron reductases and transporters (Raschdorf et al., 2013). In addition, a point mutation in the metal-binding site of MamM, a putative iron transporter, resulted in hematite crystals in MSR-1 (Uebe et al., 2011). Taken together, these results suggest that the abilities of cells to correctly regulate the flow of iron and its redox state are crucial to their ability to direct the biominerization of iron toward magnetite.

These results are consistent with recent studies of the early stages of magnetite formation in AMB-1 (Baumgartner et al., 2013) and MSR-1 (Fdez-Gubieda et al., 2013), which show that iron transforms from a phosphate-rich ferric hydroxide, potentially the previously observed ferritin (Faivre et al., 2007), through a ferrihydrite intermediate, into magnetite (Baumgartner et al., 2013; Fdez-Gubieda et al., 2013). Rarely, small hematite crystals were observed, consistent with previous findings that young magnetite crystals are surrounded by a layer of hematite (Staniland et al., 2007). Ferrihydrite is an iron oxide (Fe_2O_3) coordinated with water. Ferrihydrite and small crystals of hematite both contain Fe(III) and are thought to be unstable enough to transform into the mixed-valence magnetite (Baumgartner et al., 2013), making them attractive intermediates in this process. Perhaps, in mutants where iron redox metabolism is disturbed, some of the transitional hematite cannot be transformed into magnetite, and is able to grow to a stable size. These studies highlight the importance of redox control to the ability of MTB and other bacteria to regulate the type of minerals they produce.

REGULATION OF MINERAL SIZE AND SHAPE

Some cases of bacterial biominerization produce crystals of relatively uniform size and shape, while others are not so well controlled. For example, the CdS nanoparticles produced by *R. palustris* are spherical and have an average diameter of 8 nm, with very few crystals outside the 6–9 nm range (Bai et al., 2009). It is unclear if there is any active mechanism to regulate their size. However, similar crystals produced in the genetically distinct *E. coli* are also small and uniform in size, from 2 to 5 nm (Sweeney et al., 2004), suggesting that under the conditions present inside these bacterial cells CdS crystals cannot get very large. In contrast, the silver crystals produced by *P. stutzeri* vary remarkably in size and shape (Klaus et al., 1999). Some of these crystals are round or small, while others are polygonal or triangular, and some take up

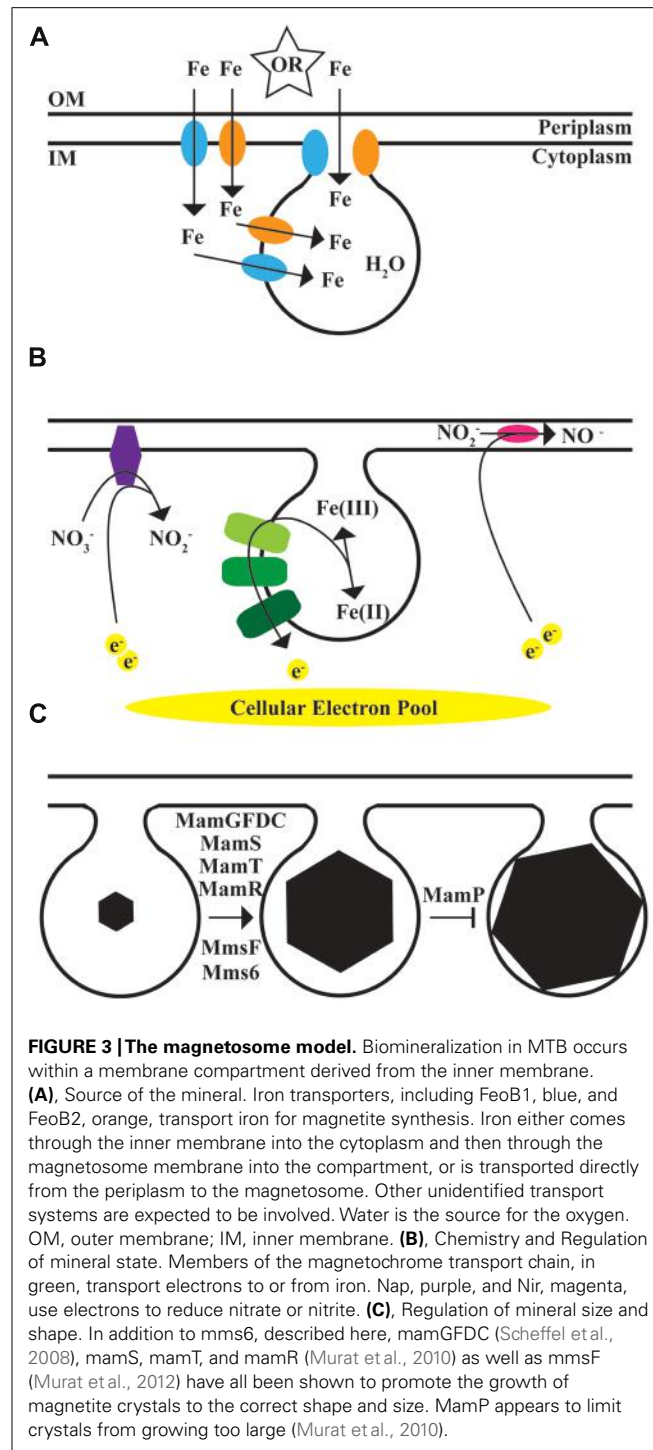
a large portion of the cellular space (Figure 1). Clearly the conditions keeping CdS crystals small and uniform in *R. palustris* and *E. coli* are not acting on the silver crystals in *P. stutzeri*.

MTB build magnetite crystals to sense and respond to magnetic fields (Frankel and Bazylinski, 2009), and crystal size and shape can greatly affect their ability to perform this task. Diverse MTB produce magnetite crystals of different sizes and shapes (Figure 1), presumably fine-tuned for the performance needs of each individual organism. We have some clues as to the genetic factors that control the size and shape of AMB-1 and MSR-1 magnetite crystals (Scheffel et al., 2008; Ding et al., 2010; Murat et al., 2010; Lohss et al., 2011; Quinlan et al., 2011; Uebe et al., 2011; Murat et al., 2012), which are reviewed in Figure 3.

One of these factors that specifically regulate the mineralization of iron is Mms6, a small acidic protein that was identified because it is closely associated with magnetite crystals isolated from AMB-1 (Arakaki et al., 2003). *In vitro* magnetite synthesis reactions produce a wide range of crystal sizes and shapes, but the addition of Mms6 results in a uniform range of crystal sizes and shapes that look similar to crystals made by bacteria *in vivo* (Arakaki et al., 2003, 2010; Amemiya et al., 2007; Prozorov et al., 2007; Galloway et al., 2011). Though short, the Mms6 sequence has a number of interesting features, including an amphipathic character, with a hydrophobic N-terminal domain and hydrophilic C-terminal domain. Recent work suggests that these features allow Mms6 monomers to assemble into micelles with the iron-binding C-termini of the monomers facing outward (Wang et al., 2012; Feng et al., 2013). Upon binding of iron, the Mms6 monomers in the micelle undergo a structural change, which may be important to their function in regulating the mineralization of magnetite (Feng et al., 2013).

Similar conceptually, though not biochemically, to Mms6, a protein named SefA has been isolated from *T. selenatis* that can regulate the precipitation of selenium *in vitro* (Debieux et al., 2011). SefA, which is conserved among a few bacteria known to respire selenate, was identified via its association with the selenium nanospheres that are secreted from *T. selenatis* during respiration on selenite. The strongest evidence that SefA may fulfill a role similar to Mms6 is data from *ex vivo* and *in vitro* experiments. *E. coli* that are grown in the presence of selenite are able to produce small 50 nm selenium deposits inside their cells. However, when SefA is expressed, 300 nm selenium deposits are produced, and the *E. coli* cells are tolerant to growth in higher selenite concentrations (Debieux et al., 2011). Selenite can be reduced *in vitro* to selenium. In the absence of SefA, an amorphous precipitate is created, but if purified SefA protein is included in the reaction, 300 nm selenium nanospheres are produced (Debieux et al., 2011).

Little is known about how the shape or size of biominerals are regulated in other bacterial systems, even for MTB outside of the AMB-1/MSR-1 group of alpha proteobacteria. Potential clues may come from recent genomic work that has identified a group of 29 genes, termed *mad* genes, for magnetosome associated delta proteobacteria, that are conserved among the delta proteobacterial MTB (Lefèvre et al., 2013). Unlike the alpha proteobacteria, these MTBs build elongated, bullet-shaped crystals and do not have the shape-determining factor Mms6. For one of these organisms, *Desulfovibrio magneticus* RS-1, proteomics



work has identified crystal-associated proteins (Matsunaga et al., 2009). Some of these are coded for by the recently identified *mad* genes *mad25* (*DMR_40870*), *mad23* (*DMR_40890*), *mad10* (*DMR_40950*), *mad11* (*DMR_40960*), and *DMR_41300*, which has homology to *mad12*, although it was not identified by Lefevre et al. (2013). It will be exciting to see if any of these candidates prove to be a shape-determining factor for bullet shaped crystals.

The examples of Mms6 and SefA suggest that at least in some cases bacteria that have evolved biominerization systems can regulate the size and shape of their minerals with proteins that have intrinsic properties to bind the mineral and are able to perform at least some of their regulatory functions *in vitro*, away from the rest of the biominerization machinery. Those seeking the regulators of mineral size and shape in other bacterial systems might consider looking for proteins that remain closely associated with the mineral after isolation from the bacteria and testing those proteins for *in vitro* function.

CONCLUSION

The reasons for and conditions under which bacteria produce intracellular biominerals are broad and varied. Intracellular, as opposed to extracellular, biominerization has diverse effects on the cell, including changing cellular pH (Couradeau et al., 2012), buoyancy (Bai et al., 2009; Couradeau et al., 2012), and susceptibility to reactive oxygen species (Guo et al., 2012). Nanomaterials produced in this way have the advantage that their make-up and shape are controlled genetically and they are often surrounded by an organic layer that can aid in dispersal or be modified to carry payloads such as antibodies (Bai et al., 2009; Pollithy et al., 2011). As we discover more of these cases, the magnetosome model can serve as our guide to understanding mechanisms behind the formation of bacterial intracellular biominerals.

ACKNOWLEDGMENTS

Arash Komeili is supported by grants from the Office of Naval Research (N000141310421) and the National Institutes of Health (R01GM084122). We thank members of the Komeili lab for critical reading of the text.

REFERENCES

- Amemiya, Y., Arakaki, A., Staniland, S. S., Tanaka, T., and Matsunaga, T. (2007). Controlled formation of magnetite crystal by partial oxidation of ferrous hydroxide in the presence of recombinant magnetotactic bacterial protein Mms6. *Biomaterials* 28, 5381–5389. doi: 10.1016/j.biomaterials.2007.07.051
- Arakaki, A., Masuda, F., Amemiya, Y., Tanaka, T., and Matsunaga, T. (2010). Control of the morphology and size of magnetite particles with peptides mimicking the Mms6 protein from magnetotactic bacteria. *J. Colloid Interface Sci.* 343, 65–70. doi: 10.1016/j.jcis.2009.11.043
- Arakaki, A., Webb, J., and Matsunaga, T. (2003). A novel protein tightly bound to bacterial magnetic particles in *Magnetospirillum magneticum* strain AMB-1. *J. Biol. Chem.* 278, 8745–8750. doi: 10.1074/jbc.M211729200
- Bai, H. J., Zhang, Z. M., Guo, Y., and Yang, G. E. (2009). Biosynthesis of cadmium sulfide nanoparticles by photosynthetic bacteria *Rhodopseudomonas palustris*. *Colloids Surf. B. Biointerfaces* 70, 142–146. doi: 10.1016/j.colsurfb.2008.12.025
- Baumgartner, J., Morin, G., Menguy, N., Perez Gonzalez, T., Widdrat, M., Cosmidis, J., et al. (2013). Magnetotactic bacteria form magnetite from a phosphate-rich ferric hydroxide via nanometric ferric (oxyhydr)oxide intermediates. *Proc. Natl. Acad. Sci. USA* 110, 14883–14888. doi: 10.1073/pnas.1307119110
- Blakemore, R. P., Short, K. A., Bazylinski, D. A., Rosenblatt, C., and Frankel, R. B. (1985). Microaerobic conditions are required for magnetite formation within *Aquaspirillum magnetotacticum*. *Geomicrobiol. J.* 4, 53–71. doi: 10.1080/0149045809385920
- Calugay, R. J., Miyashita, H., Okamura, Y., and Matsunaga, T. (2003). Siderophore production by the magnetic bacterium *Magnetospirillum magneticum* AMB-1. *FEMS Microbiol. Lett.* 218, 371–375. doi: 10.1016/S0378-1097(02)01188-6
- Calugay, R. J., Okamura, Y., Wahyudi, A. T., Takeyama, H., and Matsunaga, T. (2004). Siderophore production of a periplasmic transport binding protein kinase gene defective mutant of *Magnetospirillum magneticum* AMB-1. *Biochem. Biophys. Res. Commun.* 323, 852–857. doi: 10.1016/j.bbrc.2004.08.179

- Couradeau, E., Benzerara, K., Gérard, E., Moreira, D., Bernard, S., Brown, G. E. Jr., et al. (2012). An early-branching microbialite cyanobacterium forms intracellular carbonates. *Science* 336, 459–462. doi: 10.1126/science.1216171
- Debieux, C. M., Dridge, E. J., Mueller, C. M., Splatt, P., Paszkiewicz, K., Knight, I., et al. (2011). A bacterial process for selenium nanosphere assembly. *Proc. Natl. Acad. Sci. USA* 108, 13480–13485. doi: 10.1073/pnas.1105959108
- Ding, Y., Li, J., Liu, J., Yang, J., Jiang, W., Tian, J., et al. (2010). Deletion of the ftsZ-like gene results in the production of superparamagnetic magnetite magnetosomes in *Magnetospirillum gryphiswaldense*. *J. Bacteriol.* 192, 1097–1105. doi: 10.1128/JB.01292-09
- Faivre, D., Böttger, L. H., Matzanke, B. F., and Schüler, D. (2007). Intracellular magnetite biomineralization in bacteria proceeds by a distinct pathway involving membrane-bound ferritin and an iron(II) species. *Angew. Chem. Int. Ed. Engl.* 46, 8495–8499. doi: 10.1002/anie.200700927
- Faivre, D., and Schüler, D. (2008). Magnetotactic bacteria and magnetosomes. *Chem. Rev.* 108, 4875–4898. doi: 10.1021/cr078258w
- Fdez-Gubieda, M. L., Muela, A., Alonso, J., García-Prieto, A., Olivi, L., Fernández-Pacheco, R., et al. (2013). Magnetite biomineralization in *Magnetospirillum gryphiswaldense*: time-resolved magnetic and structural studies. *ACS Nano.* 7, 3297–3305. doi: 10.1021/nn3059983
- Feng, S., Wang, L., Palo, P., Liu, X., Mallapragada, S. K., and Nilsen-Hamilton, M. (2013). Integrated self-assembly of the mms6 magnetosome protein to form an iron-responsive structure. *Int. J. Mol. Sci.* 14, 14594–14606. doi: 10.3390/ijms140714594
- Frankel, R. B., and Bazylinski, D. A. (2009). Magnetosomes and magneto-aerotaxis. *Contrib. Microbiol.* 16, 182–193. doi: 10.1159/000219380
- Galloway, J. M., Bramble, J. P., Rawlings, A. E., Burnell, G., Evans, S. D., and Staniland, S. S. (2011). Biota templated magnetic nanoparticle arrays. *Small* 8, 204–208. doi: 10.1002/smll.201101627
- Goldhawk, D. E., Lemaire, C., McCreary, C. R., McGirr, R., Dhanvantari, S., Thompson, R. T., et al. (2009). Magnetic resonance imaging of cells overexpressing MagA, an endogenous contrast agent for live cell imaging. *Mol. Imaging* 8, 129–139.
- Guo, F. F., Yang, W., Jiang, W., Geng, S., Peng, T., and Li, J. L. (2012). Magnetosomes eliminate intracellular reactive oxygen species in *Magnetospirillum gryphiswaldense* MSR-1. *Environ. Microbiol.* 14, 1722–1729. doi: 10.1111/j.1462-2920.2012.02707.x
- Jogler, C., and Schüler, D. (2009). Genomics, genetics, and cell biology of magnetosome formation. *Annu. Rev. Microbiol.* 63, 501–521. doi: 10.1146/annurev.micro.62.081307.162908
- Klaus, T., Joerger, R., Olsson, E., and Granqvist, C.G. (1999). Silver-based crystalline nanoparticles, microbially fabricated. *Proc. Natl. Acad. Sci. USA* 96, 13611–13614. doi: 10.1073/pnas.96.24.13611
- Komeili, A. (2012). Molecular mechanisms of compartmentalization and biomimetic mineralization in magnetotactic bacteria. *FEMS Microbiol. Rev.* 36, 232–255. doi: 10.1111/j.1574-6976.2011.00315.x
- Lefèvre, C. T., Menguy, N., Abreu, F., Lins, U., Pósfai, M., Prozorov, T., et al. (2011). A cultured greigite-producing magnetotactic bacterium in a novel group of sulfate-reducing bacteria. *Science* 334, 1720–1723. doi: 10.1126/science.1212596
- Lefèvre, C. T., Trubitsyn, D., Abreu, F., Kolinko, S., Jogler, C., de Almeida, L. G., et al. (2013). Comparative genomic analysis of magnetotactic bacteria from the Deltaproteobacteria provides new insights into magnetite and greigite magnetosome genes required for magnetotaxis. *Environ. Microbiol.* 15, 2712–2735. doi: 10.1111/1462-2920.12128
- Li, Y., Bali, S., Borg, S., Katzmman, E., Ferguson, S. J., and Schüler, D. (2013). Cytochrome c11 nitrite reductase NirS is involved in anaerobic magnetite biomimetic mineralization in *Magnetospirillum gryphiswaldense* and requires NirN for proper d1 heme assembly. *J. Bacteriol.* 195, 4297–4309. doi: 10.1128/JB.00903-12
- Li, Y., Katzmann, E., Borg, S., and Schüler, D. (2012). The periplasmic nitrate reductase nap is required for anaerobic growth and involved in redox control of magnetite biomimetic mineralization in *Magnetospirillum gryphiswaldense*. *J. Bacteriol.* 194, 4847–4856. doi: 10.1128/JB.00903-12
- Lins, U., Freitas, F., Keim, C. N., and Farina, M. (2000). Electron spectroscopic imaging of magnetotactic bacteria: magnetosome morphology and diversity. *Microsc. Microanal.* 6, 463–470.
- Lohsse, A., Ullrich, S., Katzmann, E., Borg, S., Wanner, G., Richter, M., et al. (2011). Functional analysis of the magnetosome island in *Magnetospirillum gryphiswaldense*: the mamAB operon is sufficient for magnetite biomimetic mineralization. *PLoS ONE* 6:e25561. doi: 10.1371/journal.pone.0025561
- Mandernack, K. W., Bazylinski, D. A., Shanks, W. C. III, and Bullen, T. D. (1999). Oxygen and iron isotope studies of magnetite produced by magnetotactic bacteria. *Science* 285, 1892–1896. doi: 10.1126/science.285.5435.1892
- Matsunaga, T., Nakamura, C., Burgess, J. G., and Sode, K. (1992). Gene transfer in magnetic bacteria: transposon mutagenesis and cloning of genomic DNA fragments required for magnetosome synthesis. *J. Bacteriol.* 174, 2748–2753.
- Matsunaga, T., Nemoto, M., Arakaki, A., and Tanaka, M. (2009). Proteomic analysis of irregular, bullet-shaped magnetosomes in the sulphate-reducing magnetotactic bacterium *Desulfovibrio magneticus* RS-1. *Proteomics* 9, 3341–3352. doi: 10.1002/pmic.200800881
- Murat, D., Falahati, V., Bertinetto, L., Csencsits, R., Körnig, A., Downing, K., et al. (2012). The magnetosome membrane protein, MmsF, is a major regulator of magnetite biomimetic mineralization in *Magnetospirillum magneticum* AMB-1. *Mol. Microbiol.* 85, 684–699. doi: 10.1111/j.1365-2958.2012.08132.x
- Murat, D., Quinlan, A., Vali, H., and Komeili, A. (2010). Comprehensive genetic dissection of the magnetosome gene island reveals the step-wise assembly of a prokaryotic organelle. *Proc. Natl. Acad. Sci. USA* 107, 5593–5598. doi: 10.1073/pnas.0914439107
- Nakamura, C., Burgess, J. G., Sode, K., and Matsunaga, T. (1995). An iron-regulated gene, magA, encoding an iron transport protein of *Magnetospirillum* sp. strain AMB-1. *J. Biol. Chem.* 270, 28392–28396. doi: 10.1074/jbc.270.47.28392
- Paoletti, L. C., and Blakemore, R. P. (1986). Hydroxamate production by *Aquaspirillum magnetotacticum*. *J. Bacteriol.* 167, 73–76.
- Pollithy, A., Romer, T., Lang, C., Müller, F. D., Helma, J., Leonhardt, H., et al. (2011). Magnetosome expression of functional camelid antibody fragments (nanobodies) in *Magnetospirillum gryphiswaldense*. *Appl. Environ. Microbiol.* 77, 6165–6171. doi: 10.1128/AEM.05282-11
- Prozorov, T., Mallapragada, S. K., Narasimhan, B., Wang, L., Palo, P., Nilsen-Hamilton, M., et al. (2007). Protein-mediated synthesis of uniform superparamagnetic magnetite nanocrystals. *Adv. Funct. Mater.* 17, 951–957. doi: 10.1002/adfm.200600448
- Qi, L., Li, J., Zhang, W., Liu, J., Rong, C., Li, Y., et al. (2012). Fur in *Magnetospirillum gryphiswaldense* influences magnetosome formation and directly regulates the genes involved in iron and oxygen metabolism. *PLoS ONE* 7:e29572. doi: 10.1371/journal.pone.0029572
- Quinlan, A., Murat, D., Vali, H., and Komeili, A. (2011). The HtrA/DegP family protease MamE is a bifunctional protein with roles in magnetosome protein localization and magnetite biomimetic mineralization. *Mol. Microbiol.* 80, 1075–1087. doi: 10.1111/j.1365-2958.2011.07631.x
- Raschdorf, O., Müller, F. D., Pósfai, M., Plitzko, J. M., and Schüler, D. (2013). The magnetosome proteins MamX, MamZ and MamH are involved in redox control of magnetite biomimetic mineralization in *Magnetospirillum gryphiswaldense*. *Mol. Microbiol.* 89(5), 872–886. doi: 10.1111/mmi.12317
- Rong, C., Huang, Y., Zhang, W., Jiang, W., Li, Y., and Li, J. (2008). Ferrous iron transport protein B gene (feoB1) plays an accessory role in magnetosome formation in *Magnetospirillum gryphiswaldense* strain MSR-1. *Res. Microbiol.* 159, 530–536. doi: 10.1016/j.resmic.2008.06.005
- Rong, C., Zhang, C., Zhang, Y., Qi, L., Yang, J., Guan, G., et al. (2012). FeoB2 Functions in magnetosome formation and oxidative stress protection in *Magnetospirillum gryphiswaldense* strain MSR-1. *J. Bacteriol.* 194, 3972–3976. doi: 10.1128/JB.00382-12
- Scheffel, A., Gärdes, A., Grünberg, K., Wanner, G., and Schüler, D. (2008). The major magnetosome proteins MamGFDC are not essential for magnetite biomimetic mineralization in *Magnetospirillum gryphiswaldense* but regulate the size of magnetosome crystals. *J. Bacteriol.* 190, 377–386. doi: 10.1128/JB.01371-07
- Schüler, D. (2008). Genetics and cell biology of magnetosome formation in magnetotactic bacteria. *FEMS Microbiol. Rev.* 32, 654–672. doi: 10.1111/j.1574-6976.2008.00116.x
- Siponen, M. I., Adryanczyk, G., Ginet, N., Arnoux, P., and Pignol, D. (2012). Magnetochrome: a c-type cytochrome domain specific to magnetotactic bacteria. *Biochem. Soc. Trans.* 40, 1319–1323. doi: 10.1042/BST20120104
- Siponen, M. I., Legrand, P., Widdrat, M., Jones, S. R., Zhang, W. J., Chang, M. C., et al. (2013). Structural insight into magnetochrome-mediated magnetite biomimetic mineralization. *Nature* 502, 681–684. doi: 10.1038/nature12573
- Slawson, R. M., Lohmeier-Vogel, E. M., Lee, H., and Trevors, J. T. (1994). Silver resistance in *Pseudomonas stutzeri*. *Biometals* 7, 30–40. doi: 10.1007/BF00205191

- Sousa, T., Chung, A. P., Pereira, A., Piedade, A. P., and Morais, P. V. (2013). Aerobic uranium immobilization by Rhodanobacter A2-61 through formation of intracellular uranium-phosphate complexes. *Metallooms* 5, 390–397. doi: 10.1039/c3mt00052d
- Staniland, S., Ward, B., Harrison, A., van der Laan, G., and Telling, N. (2007). Rapid magnetosome formation shown by real-time x-ray magnetic circular dichroism. *Proc. Natl. Acad. Sci. USA* 104, 19524–19528. doi: 10.1073/pnas.0704879104
- Sweeney, R. Y., Mao, C., Gao, X., Burt, J. L., Belcher, A. M., Georgiou, G., et al. (2004). Bacterial biosynthesis of cadmium sulfide nanocrystals. *Chem. Biol.* 11, 1553–1559. doi: 10.1016/j.chembiol.2004.08.022
- Tanaka, M., Arakaki, A., Staniland, S. S., and Matsunaga, T. (2010). Simultaneously discrete biominerization of magnetite and tellurium nanocrystals in magnetotactic bacteria. *Appl. Environ. Microbiol.* 76, 5526–5532. doi: 10.1128/AEM.00589–510.
- Uebe, R., Henn, V., and Schüler, D. (2012). The MagA protein of *Magnetospirillum* is not involved in bacterial magnetite biominerization. *J. Bacteriol.* 194, 1018–1023. doi: 10.1128/JB.06356-11
- Uebe, R., Junge, K., Henn, V., Poxleitner, G., Katzmann, E., Plitzko, J. M., et al. (2011). The cation diffusion facilitator proteins MamB and MamM of *Magnetospirillum gryphiswaldense* have distinct and complex functions, and are involved in magnetic biominerization and magnetosome membrane assembly. *Mol. Microbiol.* 82, 818–835. doi: 10.1111/j.1365-2958.2011.07863.x
- Uebe, R., Voigt, B., Schweder, T., Albrecht, D., Katzmann, E., Lang, C., et al. (2010). Deletion of a fur-like gene affects iron homeostasis and magnetosome formation in *Magnetospirillum gryphiswaldense*. *J. Bacteriol.* 192, 4192–4204. doi: 10.1128/JB.00319-10
- Wang, C. L., Maratukulam, P. D., Lum, A. M., Clark, D. S., and Keasling, J. D. (2000). Metabolic engineering of an aerobic sulfate reduction pathway and its application to precipitation of cadmium on the cell surface. *Appl. Environ. Microbiol.* 66, 4497–4502. doi: 10.1128/AEM.66.10.4497-4502.2000
- Wang, L., Prozorov, T., Palo, P. E., Liu, X., Vaknin, D., Prozorov, R., et al. (2012). Self-assembly and biphasic iron-binding characteristics of Mms6, a bacterial protein that promotes the formation of superparamagnetic magnetite nanoparticles of uniform size and shape. *Biomacromolecules* 13, 98–105. doi: 10.1021/bm201278u
- Yamazaki, T., Oyanagi, H., Fujiwara, T., and Fukumori, Y. (1995). Nitrite reductase from the magnetotactic bacterium *Magnetospirillum magnetotacticum*, a novel cytochrome cd1 with Fe(II): nitrite oxidoreductase activity. *Eur. J. Biochem.* 233, 665–671. doi: 10.1111/j.1432-1033.1995.665_2.x
- Yang, J., Li, S., Huang, X., Li, J., Li, L., Pan, Y., et al. (2013). MamX encoded by the mamXY operon is involved in control of magnetosome maturation in *Magnetospirillum gryphiswaldense* MSR-1. *BMC Microbiol.* 13:203. doi: 10.1186/1471-2180-13-203
- Zhan, G., Li, D., and Zhang, L. (2012). Aerobic bioreduction of nickel(II) to elemental nickel with concomitant biominerization. *Appl. Microbiol. Biotechnol.* 96, 273–281. doi: 10.1007/s00253-011-3827-9
- Zurkiya, O., Chan, A.W., and Hu, X. (2008). MagA is sufficient for producing magnetic nanoparticles in mammalian cells, making it an MRI reporter. *Magn. Reson. Med.* 59, 1225–1231. doi: 10.1002/mrm.21606
- Conflict of Interest Statement:** The authors declare that the research was conducted in the absence of any commercial or financial relationships that could be construed as a potential conflict of interest.
- Received: 30 August 2013; paper pending published: 25 September 2013; accepted: 05 November 2013; published online: 26 November 2013.*
- Citation: Rahn-Lee L and Komeili A (2013) The magnetosome model: insights into the mechanisms of bacterial biominerization. *Front. Microbiol.* 4:352. doi: 10.3389/fmicb.2013.00352*
- This article was submitted to Aquatic Microbiology, a section of the journal Frontiers in Microbiology.*
- Copyright © 2013 Rahn-Lee and Komeili. This is an open-access article distributed under the terms of the Creative Commons Attribution License (CC BY). The use, distribution or reproduction in other forums is permitted, provided the original author(s) or licensor are credited and that the original publication in this journal is cited, in accordance with accepted academic practice. No use, distribution or reproduction is permitted which does not comply with these terms.*



Structure and evolution of the magnetochrome domains: no longer alone

Pascal Arnoux^{1,2,3*}, Marina I. Siponen^{1,2,3}, Christopher T. Lefèvre^{1,2,3}, Nicolas Ginet^{1,2,3} and David Pignol^{1,2,3*}

¹ Commissariat à l'énergie Atomique, DSV, IBEB, Lab Bioenerget Cellulaire, Saint-Paul-lez-Durance, France

² Centre National de la Recherche Scientifique, UMR Biol Veget and Microbiol Environ, Saint-Paul-lez-Durance, France

³ Aix-Marseille Université, Saint-Paul-lez-Durance, France

Edited by:

Karim Benzerara, Centre National de la Recherche Scientifique, France

Reviewed by:

Michael R. Twiss, Clarkson University, USA

Raz Zarivach, Ben Gurion University of the Negev, Israel

*Correspondence:

Pascal Arnoux and David Pignol,
Commissariat à l'énergie Atomique,
DSV, IBEB, Lab Bioénergétique
Cellulaire, Saint-Paul-lez-Durance
F-13108, France
e-mail: pascal.arnoux@cea.fr;
david.pignol@cea.fr

Magnetotactic bacteria (MTB) can swim along Earth's magnetic field lines, thanks to the alignment of dedicated cytoplasmic organelles. These organelles, termed magnetosomes, are proteolipidic vesicles filled by a 35–120 nm crystal of either magnetite or greigite. The formation and alignment of magnetosomes are mediated by a group of specific genes, the *mam* genes, encoding the magnetosome-associated proteins. The whole process of magnetosome biogenesis can be divided into four sequential steps; (i) cytoplasmic membrane invagination, (ii) magnetosomes alignment, (iii) iron crystal nucleation and (iv) species-dependent mineral size and shape control. Since both magnetite and greigite are a mix of iron (III) and iron (II), iron redox state management within the magnetosome vesicle is a key issue. Recently, studies have started pointing out the importance of a MTB-specific c-type cytochrome domain found in several magnetosome-associated proteins (MamE, P, T, and X). This magnetochrome (MCR) domain is almost always found in tandem, and this tandem is either found alone (MamT), in combination with a PDZ domain (MamP), a domain of unknown function (MamX) or with a trypsin combined to one or two PDZ domains (MamE). By taking advantage of new genomic data available on MTB and a recent structural study of MamP, which helped define the MCR domain boundaries, we attempt to retrace the evolutionary history within and between the different MCR-containing proteins. We propose that the observed tandem repeat of MCR is the result of a convergent evolution and attempt to explain why this domain is rarely found alone.

Keywords: magnetotactic bacteria, magnetosome, cytochrome, magnetochrome, evolution, iron

INTRODUCTION

Some bacteria found in aquatic environments display the singular ability to align passively along Earth's or artificial magnetic field lines while they swim. The genetically controlled biomineratization of magnetic nanocrystals makes this magnetotaxis possible. Made of iron oxide (magnetite, $\text{Fe}^{2+}\text{Fe}^{3+}\text{O}_4$) and/or iron sulfide (greigite, $\text{Fe}^{2+}\text{Fe}^{3+}\text{S}_4$), these nanomagnets are each embedded in a proteolipidic membrane, forming magnetosomes. These magnetosomes are aligned within the cytoplasm of magnetotactic bacteria (MTB), acting as a compass needle for orientation. A tentative selective advantage would be an efficient localization of the cells in vicinity of the oxic-anoxic transition zone in the water column at their preferred position in the oxygen (and perhaps redox potential) gradient. Since their first scientific description by RP Blakemore in 1975 (Blakemore, 1975), major breakthroughs in MTB isolation and cultivation, combined with advances in genome sequencing technologies have led to ever increasing amounts of information on their ecology, physiology, phylogeny, and evolution (Bazylinski et al., 2013).

Both cultured and uncultured MTB studied thus far are found within the domain Bacteria and affiliated with three phyla: (i) the *Proteobacteria* phylum with MTB belonging to

the *Alpha*-, *Gamma*-, and *Deltaproteobacteria* classes, (ii) the *Nitrospirae* phylum, including several uncultured strains and, (iii) the *Planctomycetes-Verrucomicrobia-Chlamydiae* (PVC) (Lefèvre and Bazylinski, 2013). Regardless the phylogenetic affiliation, the magnetosomes biomineralized by a given species display a very narrow size range (from about 35 to 120 nm) and a given shape (e.g., cubooctahedric, elongated prismatic, bullet shaped). For any given strain, magnetosomes are aligned in chains of constant length and number along the long axis of the cell. When both greigite and magnetite are synthesized, magnetosomes loaded with either mineral are found within the same chain (Lefèvre et al., 2011). Taken together these observations suggest a tight genetic control of the molecular mechanisms governing magnetosome biogenesis. This was confirmed by every comparative genomic analyses published to date with the identification of a series of genes involved in magnetosome biomineralization, specific to and present in MTB, called *mam* (magnetosome membrane) genes. The *mam* genes are organized in clusters in the genome of MTB, in some cases defining a *bona fide* magnetosome genomic island (MAI) (Komeili, 2012). Currently, 13 of these genomic regions have been sequenced, covering all but the PVC phylum of the MTB phylogenetic tree (Grünberg et al.,

2001; Matsunaga et al., 2005; Jogler et al., 2009, 2011; Nakazawa et al., 2009; Schübbe et al., 2009; Lefèvre et al., 2013a,b; Ji et al., 2013). A core gene set composed of *mamA*, *B*, *I*, *E*, *K*, *M*, *O*, *P* and *Q* is conserved among all MTB regardless the chemical composition of the nanocrystal, with an additional gene, *mamL*, in magnetite-producers. These genes are regrouped in *mamAB* or *mamAB-like* operons, referring to the genetic organization described in the paradigm strains *Magnetospirillum magneticum* AMB-1 and *Magnetospirillum gryphiswaldense* MSR-1 (Lefèvre et al., 2013a). These *in silico* analyses are nicely confirmed by genetic and biochemical approaches in these 2 strains where the *mamAB* operon alone is sufficient for magnetite biomineratization and magnetosomes organization (Murat et al., 2010; Ullrich and Schüler, 2010; Lohsse et al., 2011). Other than bioinformatics predictions, a very limited number of molecular mechanisms have been experimentally evidenced so far. One can cite MamK, a bacterial actin-like protein forming *in vitro* and *in vivo* filaments involved in the magnetosome chain assembly (Rioux et al., 2010; Draper et al., 2011; Sonkaria et al., 2012; Ozyamak et al., 2013), MamJ that link the magnetosome to the MamK filament (Scheffel et al., 2006; Scheffel and Schüler, 2007) and MamA that coats the outside of the magnetosome and presumably helps the localization of other magnetosome associated proteins (Zeytuni et al., 2011).

Amongst the Mam proteins, a series of predicted redox proteins exhibit a *c*-type cytochromes motif endemic in MTB and potentially play a role in the iron biocrystallization process that takes place inside the magnetosome (Siponen et al., 2012). The magnetochrome (MCR) domain contains a CXXCH motif that forms a *c*-type heme-binding site, which is only found in four proteins associated with the magnetosome (MamP, E, T, X, see Table 1 for a list of MCR containing proteins). It is usually present as a tandem repeat, rarely alone or in more repeats, and in all cases the MCR-containing proteins are predicted to be associated to the magnetosome membrane through a single membrane spanning α -helix. This original wrapping of *c*-type cytochromes inevitably suggests their participation in an electron transfer chain. Whether it concerns bioenergetics to drive iron import, manage the redox balance of the iron pool or any other molecular mechanisms requiring electron transport is still an open question. Nevertheless, recent studies on MamE, MamX, and MamP were published, hinting at potential functions for MCR domains during magnetosome biogenesis.

In a recent study focused on the biochemistry of MamP and its structural characterization, it was found that MamP displays ferroxidase activity (Siponen et al., 2013). Because of the presence of ferric reductases in MTB (Zhang et al., 2013), as well as the presence of ferrous diffusion facilitators encoded in the MAI (Uebe et al., 2011), Fe(II) is likely the most readily available form of iron for crystal growth. Since both magnetite and greigite are a mix of iron(III) and iron(II), this implies the presence of Fe(II) oxidation occurring in the magnetosome. MCR-containing proteins such as MamP would be involved in the control of the Fe(II) and Fe(III) ratio required for magnetite biomineratization (Siponen et al., 2013). This function is supported by *in vitro* mineralization experiments. Thus, MamP is able to induce magnetite mineralization in the sole presence of Fe(II), whereas chemical synthesis

Table 1 | list of MCR containing proteins.

Bacteria	MamE	MamP	MamT	MamX	Other
AMB-1	3 ^(*)	1	1	1	
MSR-1	1	1	1	1	
MS-1	2	1	1	1	
MC-1	1	1	1	1	
MV-1	1	1	1	1	
QH-2	1	1	1	1	
SS-5	2 ^(\\$)	1	1	-	
RS-1^{\\$}	1 ^(†)	-	-	-	MamP*(‡)
BW-1	1 ^(†)	-	-	-	MamP*(‡)
M. bavaricum	1 ^(§)	1	(#)	(#)	

*Three MamE paralogs with small variations: The "classical" MamE (*amb0963*) with two MCR domains, MamE-Like (*amb0410*) and LimE or Like-MamE (*amb1002*) with four MCR domains.

[†]Different from the classical MamE with the PDZ domain replaced by a TauE domain (Trypsin-MCR1-MCR2-TauE).

[‡]MamP* is different from MamP or MamT but contains two putative MCR domains with the following architecture: MCR1-MCR2-PDZ-NitroFeMoCo.

[#]Homolog absent but the entire genome has not been sequenced yet.

[§]Two paralogs of MamE with one (MamE) containing four MCR domains (MCRA1-MCRA2-Trypsin-MCR1-MCR2-PDZ) and the other (MamE') containing only one MCR domain between the Trypsin and the PDZ domains (Trypsin-MCR0-PDZ).

^{*}Contains only one MCR domain (Trypsin-MCR0-PDZ).

requires mixing iron(II) and iron(III) in appropriate proportion (Baumgartner et al., 2013a). MamP ferroxidase activity is then sufficient to produce the iron(III) required for magnetite growth. Siponen et al. observed that the initial formation of the mineral phase is ferrihydrite (an iron(III) oxide), magnetite appearing later in the assay. This suggests that MamP could be involved in ferrihydrite production, an intermediate of magnetite detected *in vivo* (Baumgartner et al., 2013b; Fdez-Gubieda et al., 2013). Further work using different species is required to firmly establish the role of MamP *in vivo*, and to determine its electron transfer partner(s).

The redundancy of MCR domains across different proteins of the magnetosome membrane can make their functional characterization somewhat difficult. This is particularly true for the laboratory strain *Magnetospirillum magneticum* AMB-1, where multiple paralogs of Mam proteins exist. As a consequence, deletion of the MCR domains in one protein might be compensated by the presence of another MCR-containing paralog. This is well illustrated in the study by Quinlan et al. recently published on MamE in this strain (Quinlan et al., 2011). This protein is predicted as a protease belonging to the HtrA/DegP proteases family and is found in every genome of magnetite-producing MTB known to date. Canonical HtrA/DegP proteases possess a trypsin domain followed by two PDZ domains. A variation of this domain organization is found in MamE with the insertion of tandem MCR domains between trypsin and PDZ domains. In *M. magneticum* AMB-1, the deletion of *limE*, a paralog of *mamE*, has no phenotype, but when *mamE* is also deleted, there is a complete loss of magnetite biomineratization, although empty

magnetosomes still form chains within the cytoplasm. Trans-complementation of this double mutant with a full *mamE* restores the wild-type phenotype whereas *mamE* mutants impaired in the fixation of the two *c*-type hemes only partially complemented the mutant (Quinlan et al., 2011). Complementation with a *mamE* variant impaired in its protease activity did not restore the wild-type phenotype. These observations suggest that the MCR tandem in MamE possesses a limited role in magnetite formation and that the protease function of MamE has a dominant function in crystal nucleation initiation. A search for MCR in this strain however reveals that, beside the MamP, T, X, and MamE, two paralogs of MamE are located elsewhere, one in the magnetosome island (Amb1002; named LimE for Like-MamE Quinlan et al., 2011; 63% identity with MamE), and another one present in a genomic islet that contains homologous *mam* genes distinct from the magnetosome island (Amb0410, named MamE-like Rioux et al., 2010; 53% identity with MamE). It is therefore possible that the functions of the MCR domains of MamE are maintained by the other MamE-like proteins, especially if one considers that one of these proteins (Amb0410) is an out-group in the MCR-containing family of proteins, as it possesses four MCR domains instead of the classical tandem usually found (see below). Further work is needed to clarify the functional roles of the MCR domains of MamE.

The situation is somehow clearer in *M. gryphiswaldense* strain MSR-1 in which only MamE, P, T, and X are predicted to possess two MCR domains, with no paralogs inside or outside the magnetosome island. Recently, the role of MamX was investigated in this species (Raschdorf et al., 2013). MamX is associated to the magnetosome membrane and contains a pair of MCR domains. The authors observed the presence of rare wild-type like magnetite crystals flanked by poorly crystalline particles in a Δ *mamX* strain. These “flake-like” particles were identified as hematite (Raschdorf et al., 2013). Both magnetite and hematite particles evolved concomitantly, suggesting that hematite is not an intermediate in magnetite formation and rather that the fate of these individual particles was determined at an early stage. Trans-complementation of the Δ *mamX* strain yielded a WT phenotype whereas complementation with a variant of MamX devoid of the MCR domains did not restore the WT phenotype. Together with *mamY* and *mamZ*, *mamX* belongs to the *mamXY* operon, which is a signature of magnetotactic *Alphaproteobacteria*. Its neighbor MamZ contains a predicted ferric reductase domain fused to a transporter belonging to the major facilitator superfamily (MFS). The phenotypes of the *mamX*, *mamZ* and *mamH* mutants led the authors to propose a functional MamXZH interaction that would form an iron oxidoreductase and transport complex through the magnetosome membrane. The understanding of this system and the role of the MCR-containing protein MamX need further study. For example, electron transfer partners and directionality of electron flow remain unknown for MamX.

Altogether the bioinformatics and experimental data available on MCR-containing Mam proteins suggest their involvement in iron redox chemistry to ensure the proper mineralization of magnetosomes. By taking advantage of new genomic data available and recent structural data on MCR domain, we attempt to retrace the evolutionary history of this domain within and between the

different MCR-containing proteins. We also hypothesize on the reasons why this domain is rarely found alone but rather in tandem repeats.

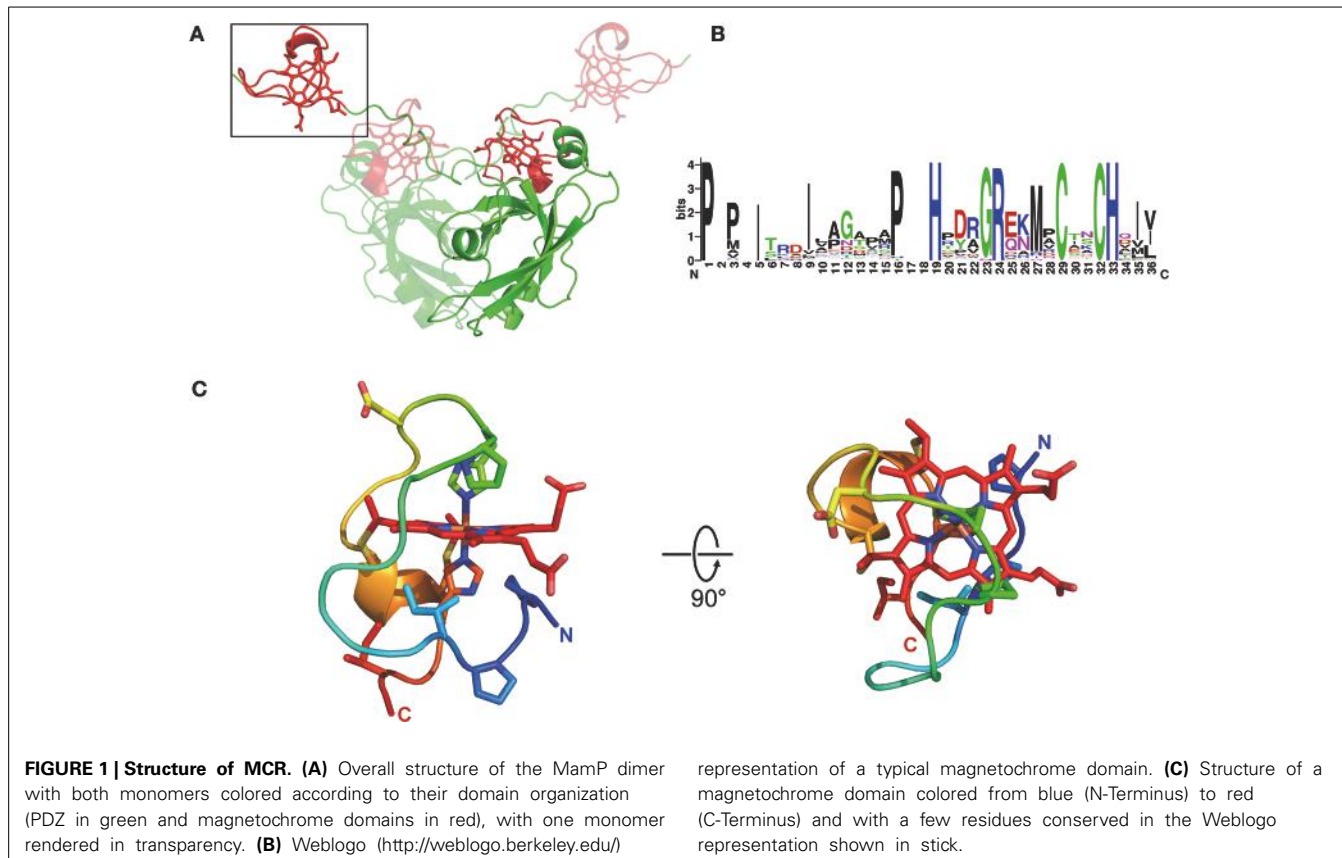
RESULTS

STRUCTURE OF MCR

Newly available information on the structure of the MamP protein from the ovoid magnetotactic bacterium MO-1 has laid the groundwork for understanding the structural basis of MCR function (Siponen et al., 2013). Prior to this X-ray structure determination work, the *c*-type cytochrome domains of MamP were already proposed to define a novel domain that is only found in MTB (Siponen et al., 2012). The primary structure suggested that in MamP, a PDZ was followed by two CX₂CH heme attachment motifs, defining two magnetochrome domains (MCR1 and MCR2). The overall fold of MamP in the crystal revealed a dimer with both monomers mainly stabilized by numerous contacts between their PDZ domains. The first magnetochrome domain (MCR1) is in contact with its own PDZ domain, while the second (MCR2) is projected above the PDZ domain of the other monomer. This structural study allowed the first fold description of a MCR domain, substantiating its uniqueness at the structural level. Indeed, a structural homology search with DaliLite v.3 returns no significant hits, demonstrating the specificity and the uniqueness of these domains (Holm and Park, 2000). Examining the MCR domains in the structure reveals that each MCR clearly defines a single domain, confirming that the MCR is a mono heme *c*-type cytochrome domain and not a diheme as it may have been inferred from its seemingly repeated structure (**Figure 1A**).

Based on bioinformatic analysis the minimal unit defining the MCR domain can be described as [P/T/H]HX_{5–9}CX₂CH. A more in-depth structural analysis suggests that the entire MCR domain is composed of 20 amino acids in MamP (see Materials and Methods section). A detailed examination of the structure identified two hydrophobic residues, which delineate the N-terminal and C-terminal regions of the MCR domain. In the fold, these two residues interact hydrophobically to close off the domain. Based on these observations, we proposed a more accurate delineation of a typical MCR domain: ψ 1X_{5–9}PHX_{5–9}CX₂CH ψ 2 (**Figure 1B**). The MCR domain starts with a hydrophobic residue (ψ 1) directly contacting the heme moiety. This is followed by a PH motif providing the 6th heme ligand and located five residues upstream (in MamP) of the CX₂CH motif anchoring the heme to the polypeptide. Finally, the terminal hydrophobic residue (ψ 2) closes the MCR fold by interacting with the ψ 1 residue. Being composed of 19–28 residues, it represents the smallest mono-heme cytochrome known to date (the mono-heme cytochrome *c*-553 from *Bacillus pasteurii* contains 71 residues surrounding the heme moiety). Overall, this results in a highly solvent-exposed heme moiety, with all four solvent edges exposed (**Figure 1C**).

As previously mentioned, with the exception of MamT, MCR domains are often found in conjunction with other types of domains. In MamP, the MCR domains are C-terminal to a PDZ protein-protein interaction domain. The fold observed in the crystal for the entire protein is dimeric showing that the MCRs provide a redox gateway above the crucible formed by the interaction of both PDZ domains (**Figure 1A**). While structural



information is still unavailable for the MCR domains of MamX, MamE, and MamT, the fold of the MCR in itself is likely to be very similar. However, it is noteworthy to mention that in the case of MamE, the two MCR domains may adopt a different spatial orientation as that in MamP since there is often a consequent amino acid insertion between both MCRs (30–60 amino acids depending on species). Furthermore, in the case of MamE, the MCR domains are flanked N-terminally by a protease domain and C-terminally by two PDZ domains making it difficult to predict any structural information based on the MamP structure. The MCR domains of MamX could hypothetically form a redox gateway above its domain of unknown function, as seen in MamP, but no substantial evidences exist to support this scenario. Only new structural data on these proteins will allow understanding of the overall organization of MCR within their corresponding proteins.

EVOLUTION OF MCR DOMAINS

Among the questions about MCR evolution, we are concerned about their occurrence. For example why MCR domains are almost always found in tandem and so rarely alone or repeated more than twice (Table 1)? And for each tandem, are the two repeated MCR domains similar or not? Did they evolve from a single ancestral tandem of MCR domains or rather evolved from independent duplication events? Such intriguing questions can be approached through the evolutionary history of these MCR domains. Because the MCR domain is “endemic” in MTB, tracing back their evolutionary history should be simplified and, as it is

found in the core genes set common to all MTB, we are expecting a reasonable diversity in our sample population. The structural studies on MamP described above allow a clear delineation of the domain’s boundaries, which should also simplify the constitution of our sample population.

The evolution of a duplicated domain can be considered in two simple evolutionary models where internal duplication of the original domain takes place either before (Figure 2, Model #1) or after (Figure 2, Model #2) functional and sequence divergence of the entire protein. In the first case, MCR1 and MCR2 domains would appear as two separate branches in a phylogenetic tree whatever the protein considered (MamE, P, T, X), whereas in the second case the separation would initially occur between the proteins containing the MCR domains forming separate branches for (MamE, P, T, X). At first sight, the first model seems the simplest to explain the functional diversity observed in MCR-containing proteins. Indeed, an initial (and presumably rare) event of internal domain duplication would have taken place, followed by a functional divergence of the proteins. The second model is probably less intuitive as it depicts a single MCR divergence before the duplication events; however this model does not explain why the domain is rarely found alone but almost always in duplicate, unless we think about convergent evolution. An alternative model explaining why the MCR1 and MCR2 domains share more sequence identity within a family would be that there is a evolutionary constraint on the MCR1 and MCR2 that must be kept similar to each other for the dimer to be functional.

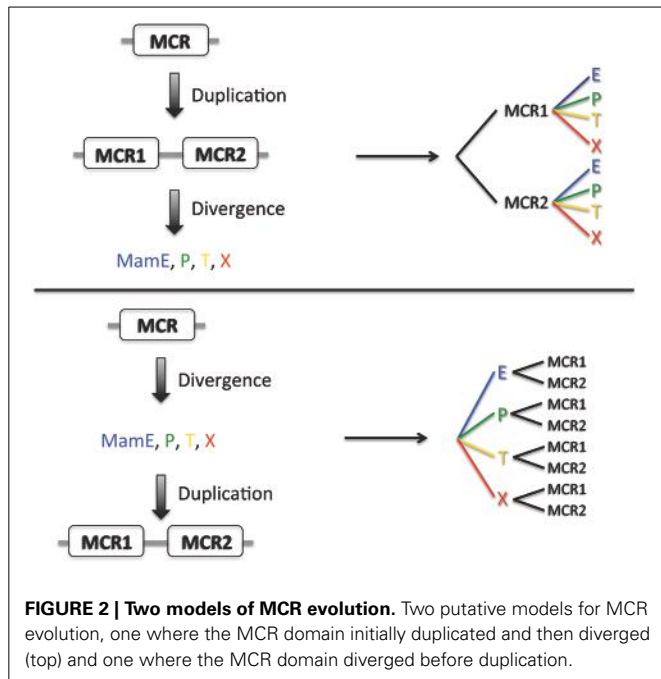


FIGURE 2 | Two models of MCR evolution. Two putative models for MCR evolution, one where the MCR domain initially duplicated and then diverged (top) and one where the MCR domain diverged before duplication.

To generate our dataset, we gathered sequences of MCR containing proteins MamE, P, T, and X from 10 species (see Materials and Methods) and separated them into MCR1 and MCR2 as described above. A protein sequences alignment was computed with all the individual MCR using the Muscle algorithm (Edgar, 2004) and a phylogenetic trees built with MEGA5 software (Tamura et al., 2011); the MCR alignment as well as the individual protein sequence alignment are provided as **Supplementary Figure 1**. The resulting tree presented in **Figure 3** displays several branches with clear boundaries, which is already surprising considering the short size of the MCR domains (19 amino acids) and the low bootstrap values when generated (data not shown). Much to our surprise, we found that the MCR domains do not clusterize according to their position in the amino acid sequence (MCR1 or MCR2) as expected for model #1 but rather form a cluster with the Mam protein they belong to, as predicted in model #2. For instance in the case of MamE and MamT, the MCR domains, regardless of their numbering, form distinct leaves for each protein. Then within each leaf we observe distinct branches leading to the MCR1 and MCR2. This topology is clearly reminiscent to model #2 where divergence of the original MCR domain occurred before the internal duplication.

DISCUSSION

A rather simple evolutionary scheme can be proposed for the MCR-containing Mam proteins where the basic scheme is provided by model #2: an initial sequence divergence event followed by domain duplication. It is interesting to note that even based on short MCR domain sequences, one can relatively easily infer the nature of the protein to which it belongs (MamE, P, T or X).

Whether it is an ancient or more recent evolution, whether or not it is part of the minimal gene set required for magnetosome biosynthesis, the major trend for the magnetochrome domain

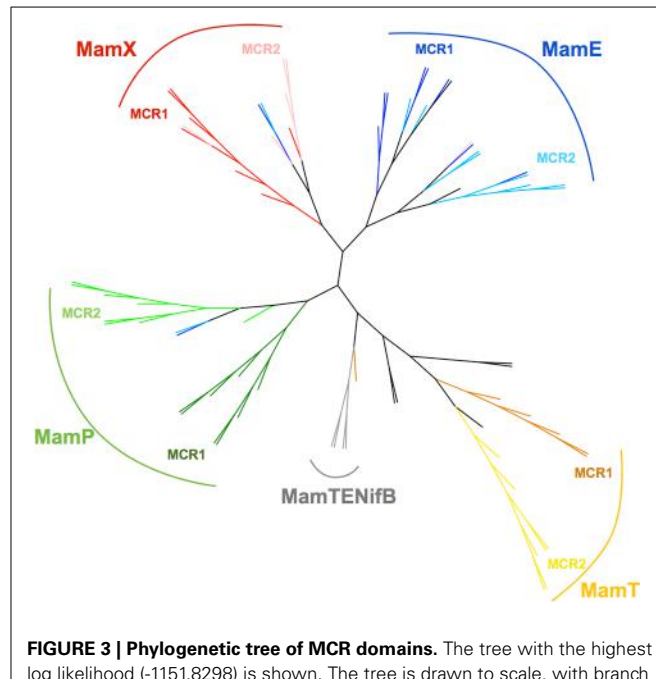


FIGURE 3 | Phylogenetic tree of MCR domains. The tree with the highest log likelihood (-1151.8298) is shown. The tree is drawn to scale, with branch lengths measured in the number of substitutions per site. The analysis involved 88 amino acid sequences. All positions containing gaps and missing data were eliminated. There were a total of 19 positions in the final dataset. Evolutionary analyses were conducted in MEGA5 (Tamura et al., 2011). Tree was edited and drawn with the interactive tree editor iTOL (Letunic and Bork, 2011). Color of the branches is according to the MCR domain position and the Mam protein it belongs to. For MCR 1 and MCR2 of MamE branches are respectively blue and light blue, MamP green and light green; MamT, orange and yellow; MamX, red and salmon; MamTENifB, gray. Out-groups are left black.

evolution is a tandem duplication after a sequence divergence. It seems that when a new protein with a tandem MCR domain is selected by evolution, it always evolves from a lone MCR domain and not from an existing tandem repeat. For example, it is known that MamX is only present in MTB from the *Alphaproteobacteria*, suggesting that it evolved relatively recently. However, its evolutionary history based on the MCR domain only suggests that it did not emerge from the tandem of another MCR-containing protein like previously existing MamP or MamE. What we may be witnessing here is an example of convergent evolution where the tandem repeat is linked to the functional role of the protein. Indeed, this domain is almost always found in tandem and there are only rare examples where it is found either, alone (MamE of *Candidatus Magnetobacterium bavaricum* and MamE' of SS-5) or in triplicate (MamE of strain MC-1). It is tempting to link this pattern to iron and magnetite (or greigite) chemistry. Both magnetite and greigite are a mix of one iron(II) and two iron(III) equivalents. The possibility to abstract or give two electrons by a pair of magnetochrome domains suggests its involvement directly in magnetite or greigite crystal production, not just the iron chemistry that requires a single electron. Such use of two monoheme cytochromes was also suggested to evolve in order to adapt to the storage of the two electron generated from sulfite oxidation (Robin et al., 2013). Although this hypothesis of two

MCR domains adaptation to a two-electron transfer reaction is tempting, it will be difficult to test and further work is definitely needed in order to better understand the complex connections between MTB and MCR.

A hypothesis concerning the evolution of magnetotactic bacteria suggests they all evolved from a common ancestor 2.5–3.0 billion years ago when levels of atmospheric oxygen were low and anaerobic to microaerobic environments dominated. At this time, magnetite/greigite crystals likely did not serve a role in magnetotaxis but rather in scavenging reactive oxygen species and later, when atmospheric oxygen levels increased, served to aid MTB in navigation (Lefèvre et al., 2013a). This ancestor probably had only the *mamAB* operon (including *mamE* and *mamP*) and the magnetite/greigite crystals have diversified since then. Because magnetochrome-containing proteins are the only redox proteins associated to the magnetosome this raises interesting possibilities possibly linking magnetite/greigite crystal shape to the evolution of these magnetochrome-containing proteins.

The three dimensional structure of MamP showed that the first magnetochrome domain contributed to the formation of a crucible in which iron could be stabilized (Siponen et al., 2013). This structural study enabled a better analysis of the evolutionary history of MCR domains by defining the boundaries of this domain. The structure of other MCR-containing proteins such as MamE or MamX will allow to better define the role of the magnetochrome domain in the context of magnetotaxis. Furthermore, these studies will also allow more robust structure-based sequence alignments. Finally, interesting questions that need to be answered in the future relate to the interaction between these MCR containing proteins and the identification of their electron-transfer partners.

METHODS

The complete genomes or contigs discussed in this paper include: *Magnetospirillum magneticum* AMB-1 (GenBank: NC_007626.1), *Magnetospirillum gryphiswaldense* MSR-1 (GenBank: CU459003.1), *Magnetospirillum magneto-tacticum* MS-1 (JGI project 402922), *Magnetococcus* sp. MC-1 (GenBank: CP000471), *Magnetovibrio blakemorei* MV-1 (GenBank: FP102531), *Magnetospira* sp. QH-2 (EMBL: FO538765), strain SS-5 (MamP: JX628772, MamE: JX628767), *Candidatus Magnetobacterium bavaricum* (Jogler et al., 2011), *Desulfovibrio magneticus* RS-1 (NC_012795–NC_012797), *Candidatus Desulfamplus magnetomortis* BW-1 (GenBank: JN830627–JN830646 and JN845570–JN845575).

From a structure based sequence alignment we devised a protein pattern that harvests almost all the magnetochrome domains without many false positive. This pattern is the following:

$$\begin{aligned} & [P] - x(0, 6) - [IVMLQA] - x(6) - [PTH] - X(0, 2) - [H] \\ & -x(1, 3) - [GN] - x(1, 5) - C - x - x - C - H - x - [IVMLFY] \end{aligned}$$

and much of the false positive belong to a single protein subunit, NrfB from a formate dependent Cytochrome c nitrite reductase.

Initial multiple alignment were generated using the MUSCLE program (Edgar, 2004), applying the default settings. Alignment were visualizes using Jalview package. Evolutionary trees were

obtained using the MEGA5 package (Tamura et al., 2011) and by using the Maximum Likelihood method based on the JTT matrix-based model (Jones et al., 1992). Initial tree(s) for the heuristic search were obtained automatically by applying Neighbor-Join and BioNJ algorithms to a matrix of pairwise distances estimated using a JTT model, and then selecting the topology with superior log likelihood value.

SUPPLEMENTARY MATERIAL

The Supplementary Material for this article can be found online at: <http://www.frontiersin.org/journal/10.3389/fmicb.2014.00117/abstract>

Supplementary Figure 1 | Sequence alignment of MCR domains used in this analysis. Sequence alignment is colored as defined by clustalx in Jalview 2 (Waterhouse et al., 2009).

REFERENCES

- Baumgartner, J., Dey, A., Bomans, P. H. H., Le Coadou, C., Fratzl, P., Sommerdijk, N. A., et al. (2013a). Nucleation and growth of magnetite from solution. *Nat. Mater.* 12, 310–314. doi: 10.1038/nmat3558
- Baumgartner, J., Morin, G., Menguy, N., Gonzalez, T. P., Widdrat, M., Cosmidis, J., et al. (2013b). Magnetotactic bacteria form magnetite from a phosphate-rich ferric hydroxide via nanometric ferric (oxyhydr)oxide intermediates. *Proc. Natl. Acad. Sci. U.S.A.* 110, 14883–14888. doi: 10.1073/pnas.1307119110
- Bazylinski, P. D. A., Lefèvre, C. T., and Schüler, D. (2013). “Magnetotactic bacteria,” in *The Prokaryotes*, eds E. Rosenberg, E. F. DeLong, S. Lory, E. Stackebrandt, and F. Thompson (Berlin; Heidelberg: Springer), 453–494. Available online at: <http://link.springer.com/referenceworkentry/10.1007/978-3-642-30141-474> (Accessed October 18, 2013).
- Blakemore, R. (1975). Magnetotactic bacteria. *Science* 190, 377–379. doi: 10.1126/science.170679
- Draper, O., Byrne, M. E., Li, Z., Keyhani, S., Barrozo, J. C., Jensen, G., et al. (2011). MamK, a bacterial actin, forms dynamic filaments in vivo that are regulated by the acidic proteins MamJ and LimJ. *Mol. Microbiol.* 82, 342–354. doi: 10.1111/j.1365-2958.2011.07815.x
- Edgar, R. C. (2004). MUSCLE: multiple sequence alignment with high accuracy and high throughput. *Nucleic Acids Res.* 32, 1792–1797. doi: 10.1093/nar/gkh340
- Fdez-Gubieda, M. L., Muela, A., Alonso, J., García-Prieto, A., Olivi, L., Fernández-Pacheco, R., et al. (2013). Magnetite biomineralization in *Magnetospirillum gryphiswaldense*: time-resolved magnetic and structural studies. *ACS Nano* 7, 3297–3305. doi: 10.1021/nn3059983
- Grünberg, K., Wawer, C., Tebo, B. M., and Schüler, D. (2001). A large gene cluster encoding several magnetosome proteins is conserved in different species of magnetotactic bacteria. *Appl. Environ. Microbiol.* 67, 4573–4582. doi: 10.1128/AEM.67.10.4573–4582.2001
- Holm, L., and Park, J. (2000). DALIWorkbench for protein structure comparison. *Bioinformatics* 16, 566–567. doi: 10.1093/bioinformatics/16.6.566
- Ji, B., Zhang, S.-D., Arnoux, P., Rouy, Z., Alberto, F., Philippe, N., et al. (2013). Comparative genomic analysis provides insights into the evolution and niche adaptation of marine *Magnetospira* sp. QH-2 strain. *Environ. Microbiol.* 16, 525–544. doi: 10.1111/1462-2920.12180
- Jogler, C., Kube, M., Schübbe, S., Ullrich, S., Teeling, H., Bazylinski, D. A., et al. (2009). Comparative analysis of magnetosome gene clusters in magnetotactic bacteria provides further evidence for horizontal gene transfer. *Environ. Microbiol.* 11, 1267–1277. doi: 10.1111/j.1462-2920.2009.01854.x
- Jogler, C., Wanner, G., Kolinko, S., Niebler, M., Amann, R., Petersen, N., et al. (2011). Conservation of proteobacterial magnetosome genes and structures in an uncultivated member of the deep-branching Nitrospira phylum. *Proc. Natl. Acad. Sci. U.S.A.* 108, 1134–1139. doi: 10.1073/pnas.1012694108
- Jones, D. T., Taylor, W. R., and Thornton, J. M. (1992). The rapid generation of mutation data matrices from protein sequences. *Comput. Appl. Biosci.* 8, 275–282.
- Komeili, A. (2012). Molecular mechanisms of compartmentalization and biomineralization in magnetotactic bacteria. *FEMS Microbiol. Rev.* 36, 232–255. doi: 10.1111/j.1574-6976.2011.00315.x

- Lefèvre, C. T., and Bazylinski, D. A. (2013). Ecology, diversity, and evolution of magnetotactic bacteria. *Microbiol. Mol. Biol. Rev.* 77, 497–526. doi: 10.1128/MMBR.00021-13
- Lefèvre, C. T., Menguy, N., Abreu, F., Lins, U., Pósfai, M., Prozorov, T., et al. (2011). A cultured greigite-producing magnetotactic bacterium in a novel group of sulfate-reducing bacteria. *Science* 334, 1720–1723. doi: 10.1126/science.1212596
- Lefèvre, C. T., Trubitsyn, D., Abreu, F., Kolinko, S., De Almeida, L. G. P., De Vasconcelos, A. T., et al. (2013a). Monophyletic origin of magnetotaxis and the first magnetosomes. *Environ. Microbiol.* 15, 2267–2274. doi: 10.1111/1462-2920.12097
- Lefèvre, C. T., Trubitsyn, D., Abreu, F., Kolinko, S., Jogler, C., De Almeida, L. G., et al. (2013b). Comparative genomic analysis of magnetotactic bacteria from the Deltaproteobacteria provides new insights into magnetite and greigite magnetosome genes required for magnetotaxis. *Environ. Microbiol.* 15, 2712–2735. doi: 10.1111/1462-2920.12128
- Letunic, I., and Bork, P. (2011). Interactive Tree Of Life v2: online annotation and display of phylogenetic trees made easy. *Nucleic Acids Res.* 39, W475–W478. doi: 10.1093/nar/grk201
- Lohsse, A., Ullrich, S., Katzmüller, E., Borg, S., Wanner, G., Richter, M., et al. (2011). Functional analysis of the magnetosome island in *Magnetospirillum gryphiswaldense*: the mamAB operon is sufficient for magnetite biomimetic mineralization. *PLoS ONE* 6:e25561. doi: 10.1371/journal.pone.0025561
- Matsunaga, T., Okamura, Y., Fukuda, Y., Wahyudi, A. T., Murase, Y., and Takeyama, H. (2005). Complete genome sequence of the facultative anaerobic magnetotactic bacterium *Magnetospirillum* sp. strain AMB-1. *DNA Res.* 12, 157–166. doi: 10.1093/dnarecs/dsi002
- Murat, D., Quinlan, A., Vali, H., and Komeili, A. (2010). Comprehensive genetic dissection of the magnetosome gene island reveals the step-wise assembly of a prokaryotic organelle. *Proc. Natl. Acad. Sci. U.S.A.* 107, 5593–5598. doi: 10.1073/pnas.0914439107
- Nakazawa, H., Arakaki, A., Narita-Yamada, S., Yashiro, I., Jinno, K., Aoki, N., et al. (2009). Whole genome sequence of *Desulfovibrio magneticus* strain RS-1 revealed common gene clusters in magnetotactic bacteria. *Genome Res.* 19, 1801–1808. doi: 10.1101/gr.088906.108
- Ozyamak, E., Kollman, J., Agard, D. A., and Komeili, A. (2013). The bacterial actin MamK: *in vitro* assembly behavior and filament architecture. *J. Biol. Chem.* 288, 4265–4277. doi: 10.1074/jbc.M112.417030
- Quinlan, A., Murat, D., Vali, H., and Komeili, A. (2011). The HtrA/DegP family protease MamE is a bifunctional protein with roles in magnetosome protein localization and magnetite biomimetic mineralization. *Mol. Microbiol.* 80, 1075–1087. doi: 10.1111/j.1365-2958.2011.07631.x
- Raschdorf, O., Müller, F. D., Pósfai, M., Plitzko, J. M., and Schüller, D. (2013). The magnetosome proteins MamX, MamZ and MamH are involved in redox control of magnetite biomimetic mineralization in *Magnetospirillum gryphiswaldense*. *Mol. Microbiol.* 89, 872–886. doi: 10.1111/mmi.12317
- Rioux, J.-B., Philippe, N., Pereira, S., Pignol, D., Wu, L.-F., and Giné, N. (2010). A second actin-like MamK protein in *Magnetospirillum magneticum* AMB-1 encoded outside the genomic magnetosome island. *PLoS ONE* 5:e9151. doi: 10.1371/journal.pone.0009151
- Robin, S., Arese, M., Forte, E., Sarti, P., Kolaj-Robin, O., Giuffrè, A., et al. (2013). Functional Dissection of the Multi-Domain Di-Heme Cytochrome c550 from *Thermus thermophilus*. *PLoS ONE* 8:e55129. doi: 10.1371/journal.pone.0055129
- Scheffel, A., Gruska, M., Faivre, D., Linaroudis, A., Plitzko, J. M., and Schüller, D. (2006). An acidic protein aligns magnetosomes along a filamentous structure in magnetotactic bacteria. *Nature* 440, 110–114. doi: 10.1038/nature04382
- Scheffel, A., and Schüller, D. (2007). The acidic repetitive domain of the *Magnetospirillum gryphiswaldense* MamJ protein displays hypervariability but is not required for magnetosome chain assembly. *J. Bacteriol.* 189, 6437–6446. doi: 10.1128/JB.00421-07
- Schübbe, S., Williams, T. J., Xie, G., Kiss, H. E., Brettin, T. S., Martinez, D., et al. (2009). Complete genome sequence of the chemolithoautotrophic marine magnetotactic coccus strain MC-1. *Appl. Environ. Microbiol.* 75, 4835–4852. doi: 10.1128/AEM.02874-08
- Siponen, M. I., Adryanczyk, G., Giné, N., Arnoux, P., and Pignol, D. (2012). Magnetochrome: a c-type cytochrome domain specific to magnetotactic bacteria. *Biochem. Soc. Trans.* 40, 1319–1323. doi: 10.1042/BST20120104
- Siponen, M. I., Legrand, P., Widdrat, M., Jones, S. R., Zhang, W.-J., Chang, M. C. Y., et al. (2013). Structural insight into magnetochrome-mediated magnetite biomimetic mineralization. *Nature* 502, 681–684. doi: 10.1038/nature12573
- Sonkaria, S., Fuentes, G., Verma, C., Narang, R., Khare, V., Fischer, A., et al. (2012). Insight into the assembly properties and functional organisation of the magnetotactic bacterial actin-like homolog, MamK. *PLoS ONE* 7:e34189. doi: 10.1371/journal.pone.0034189
- Tamura, K., Peterson, D., Peterson, N., Stecher, G., Nei, M., and Kumar, S. (2011). MEGA5: molecular evolutionary genetics analysis using maximum likelihood, evolutionary distance, and maximum parsimony methods. *Mol. Biol. Evol.* 28, 2731–2739. doi: 10.1093/molbev/msr121
- Uebel, R., Junge, K., Henn, V., Poxleitner, G., Katzmüller, E., Plitzko, J. M., et al. (2011). The cation diffusion facilitator proteins MamB and MamM of *Magnetospirillum gryphiswaldense* have distinct and complex functions, and are involved in magnetite biomimetic mineralization and magnetosome membrane assembly. *Mol. Microbiol.* 82, 818–835. doi: 10.1111/j.1365-2958.2011.07863.x
- Ullrich, S., and Schüller, D. (2010). Cre-lox-based method for generation of large deletions within the genomic magnetosome island of *Magnetospirillum gryphiswaldense*. *Appl. Environ. Microbiol.* 76, 2439–2444. doi: 10.1128/AEM.02805-09
- Waterhouse, A. M., Procter, J. B., Martin, D. M. A., Clamp, M., and Barton, G. J. (2009). Jalview version 2 - a multiple sequence alignment editor and analysis workbench. *Bioinformatics* 25, 1189–1191. doi: 10.1093/bioinformatics/btp033
- Zeytuni, N., Ozyamak, E., Ben-Harush, K., Davidov, G., Levin, M., Gat, Y., et al. (2011). Self-recognition mechanism of MamA, a magnetosome-associated TPR-containing protein, promotes complex assembly. *Proc. Natl. Acad. Sci. U.S.A.* 108, E480–487. doi: 10.1073/pnas.1103367108
- Zhang, C., Meng, X., Li, N., Wang, W., Sun, Y., Jiang, W., et al. (2013). Two bifunctional enzymes with ferric reduction ability play complementary roles during magnetosome synthesis in *Magnetospirillum gryphiswaldense* MSR-1. *J. Bacteriol.* 195, 876–885. doi: 10.1128/JB.01750-12

Conflict of Interest Statement: The authors declare that the research was conducted in the absence of any commercial or financial relationships that could be construed as a potential conflict of interest.

Received: 03 December 2013; accepted: 08 March 2014; published online: 25 March 2014.

Citation: Arnoux P, Siponen MI, Lefèvre CT, Giné N and Pignol D (2014) Structure and evolution of the magnetochrome domains: no longer alone. *Front. Microbiol.* 5:117. doi: 10.3389/fmicb.2014.00117

This article was submitted to Aquatic Microbiology, a section of the journal Frontiers in Microbiology.

Copyright © 2014 Arnoux, Siponen, Lefèvre, Giné and Pignol. This is an open-access article distributed under the terms of the Creative Commons Attribution License (CC BY). The use, distribution or reproduction in other forums is permitted, provided the original author(s) or licensor are credited and that the original publication in this journal is cited, in accordance with accepted academic practice. No use, distribution or reproduction is permitted which does not comply with these terms.



Structure prediction of magnetosome-associated proteins

Hila Nudelman^{1,2} and Raz Zarivach^{1,2*}

¹ Department of Life Sciences, Ben-Gurion University of the Negev, Beer Sheva, Israel

² National Institute for Biotechnology in the Negev, Ben-Gurion University of the Negev, Beer Sheva, Israel

Edited by:

Damien Faivre, Max Planck Society, Germany

Reviewed by:

David Pignol, Commissariat à l'Énergie Atomique, France

Dorothée Murat, Centre National de la Recherche Scientifique, France

***Correspondence:**

Raz Zarivach, Department of Life Sciences and National Institute for Biotechnology in the Negev, Ben-Gurion University of the Negev, P.O. Box 653, Beer-Sheva 84105, Israel
e-mail: zarivach@bgu.ac.il

Magnetotactic bacteria (MTB) are Gram-negative bacteria that can navigate along geomagnetic fields. This ability is a result of a unique intracellular organelle, the magnetosome. These organelles are composed of membrane-enclosed magnetite (Fe_3O_4) or greigite (Fe_3S_4) crystals ordered into chains along the cell. Magnetosome formation, assembly, and magnetic nano-crystal biominerization are controlled by magnetosome-associated proteins (MAPs). Most MAP-encoding genes are located in a conserved genomic region – the magnetosome island (MAI). The MAI appears to be conserved in all MTB that were analyzed so far, although the MAI size and organization differs between species. It was shown that MAI deletion leads to a non-magnetic phenotype, further highlighting its important role in magnetosome formation. Today, about 28 proteins are known to be involved in magnetosome formation, but the structures and functions of most MAPs are unknown. To reveal the structure–function relationship of MAPs we used bioinformatics tools in order to build homology models as a way to understand their possible role in magnetosome formation. Here we present a predicted 3D structural models' overview for all known *Magnetospirillum gryphiswaldense* strain MSR-1 MAPs.

Keywords: magnetosome, structure prediction, Protein structure-function, magnetotactic bacteria, membrane invagination

INTRODUCTION

Magnetotactic bacteria (MTB) are a group of Gram-negative aquatic prokaryotes that can synthesize a unique prokaryotic organelle, called a magnetosome (Bazylinski et al., 2004). The magnetosome contains magnetic crystals enclosed within membrane vesicles, which are aligned as intracellular chains along the cell (Balkwill et al., 1980; Komeili et al., 2006). The magnetosome membrane creates an isolated environment in the cell which is important for mineral crystal nucleation and growth (Komeili et al., 2004). The magnetosome chain forces the bacteria to align passively to the geomagnetic field and the bacteria then swim accordingly with the use of their flagella, a behavior called magnetotaxis (Balkwill et al., 1980; Lower and Bazylinski, 2013). Magnetotaxis is believed to aid MTB to reach regions of optimal oxygen concentrations without long, random movements (Gorby et al., 1988).

The magnetic crystals consist of magnetite (Fe_3O_4) or greigite (Fe_3S_4). Their size typically ranges between 35 and 120 nm and are in the size range of a single-magnetic-domain (SD; Frankel et al., 1979; Mann et al., 1990; Kirschvink, 1992). Each bacteria has a defined species-dependent crystal size and shape and contains one or more magnetosome chains (Balkwill et al., 1980; Bazylinski and Frankel, 2004). The consistent morphology in different species or strains of the magnetic crystals indicates that mineral formation is a highly controlled process (Frankel and Bazylinski, 2009).

It was found that magnetosome formation is under strict control of specific gene expression (Schübbe et al., 2003). Most of these genes are located on a genetically conserved region, known as the magnetosome island (MAI; Schübbe et al., 2003). The MAI is found to be highly conserved in almost all MTB species and

includes a highly conserved and essential operon (*mamAB*), as well as three less conserved operons (*mamGFCD*, *mms6*, and *mamXY*; Fukuda et al., 2006). It was shown that MAI or *mamAB* operon deletion causes the loss of magnetosome formation (Murat et al., 2010; Lohsse et al., 2011).

MamAB operon in *M. gryphiswaldense* MSR-1 includes 17 open reading frames which correspond to ~16.4 kb of DNA (Schübbe et al., 2006). This operon contains genes that are essential for magnetosome formation and have important functions such as membrane invagination, iron transport, and magnetite biominerization (Lohsse et al., 2011). The *mamAB* cluster encodes proteins that are essential for membrane invagination and magnetosome biogenesis (*mamB*, *E*, *I*, *L*, and *Q*), magnetosomal iron transport (*mamB* and *M*), magnetite biominerization (*mamE*, *O*, *T*, *P*, and *S*), and magnetosome chain assembly (*mamK* and *mamJ*; Murat et al., 2010; Yang et al., 2010; Quinlan et al., 2011; Uebe et al., 2011).

In *M. gryphiswaldense* MSR-1, the *mamXY* operon is a ~4.9 kb segment which is located ~28 kb downstream of the *mamAB* operon and consists of *mamY*, *mamX*, *mamZ* (*mamH*-like), and *ftsZ*-like genes (Ding et al., 2010). *mamXY* is conserved among all *Magnetospirillum* bacteria. It was shown in both *M. gryphiswaldense* MSR-1 and *M. magneticum* AMB-1 that *mamXY*-encoding proteins are associated with the magnetosome membrane (Lohsse et al., 2011). Deletion of *M. gryphiswaldense* MSR-1 *mamXY* causes short magnetosome chains with regular shape but smaller particles (Lohsse et al., 2011).

The *mamCD* (2.1 kb) and *mms6* (3.6 kb) operons are not essential for biominerization but they encode genes which control the size and shape of magnetite particles (Scheffel et al., 2008; Murat

et al., 2010; Lohsse et al., 2011; Tanaka et al., 2011; Murat et al., 2012). Deletion of the *mamCD* operon – which contains four genes (*mamC*, *mamD*, *mamF*, and *mamG*) – results in crystals with approximately 75% of the wild type size (Scheffel et al., 2008). The *mms6* operon is located upstream of the *mamCD* operon and contains five genes (*mms6*, *mmsf*, *mgr4070*, *mgr4071*, and *mgr4074*; Faivre and Schüler, 2008). Co-deletion of both operons results in further reduction in the shape regularity and alignment of magnetite crystals (Lohsse et al., 2011).

Based on current scientific data it is suggested that magnetosome formation occurs via several steps that can act simultaneously. These include, (i) protein sorting and inner membrane invagination, (ii) alignment of the magnetosome into chains, (iii) iron uptake and crystal nucleation, and (iv) crystal maturation (Murat et al., 2010). Today, a general model for magnetosome formation and protein involvement is based on genetic approaches but most of the protein functions have yet to be determined (Murat et al., 2010).

One of the most studied strains is the magnetotactic α -proteobacterium *Magnetospirillum gryphiswaldense* MSR-1, which contains all four magnetosome operons (Lohsse et al., 2011). *M. gryphiswaldense* MSR-1 creates more than 60 cubo-octahedral magnetite-containing magnetosomes (Schleifer et al., 1991). In *M. gryphiswaldense* MSR-1 there are over 28 different proteins that are involved in magnetosome formation and most of the corresponding genes are located on the MAI (Schübbe et al., 2006; Richter et al., 2007). Some of these proteins are homologous to known protein families, such as: tetratricopeptide repeat (TPR) proteins, CDF transporters, PDZ proteins, proteases, and more (Okuda et al., 1996).

In order to understand the function of each protein during magnetosome formation it is essential to find their structure–function relationships. Nowadays there are only a few known MTB protein structures that promote understanding of the protein roles during magnetosome formation. MamA and MamP are the only proteins from the *mamAB* operon whose 3D structures have been determined (Zeytuni et al., 2011, 2012; Siponen et al., 2013). In this work we predicted and analyzed the 3D models of magnetosome proteins from *M. gryphiswaldense* MSR-1 strain as a way of elucidating their functions during the

processes of magnetosome formation and present them based on their main predicted function or their association with protein families.

PROTEIN SORTING AND MAGNETOSOME MEMBRANE INVAGINATION

MamI

MamI is a small, 77 residue protein with two predicted integral membrane α -helices (Komeili, 2012). MamI deletion results in the loss of the magnetosome membrane, which might be indicative of MamI involvement in magnetosome membrane invagination (Komeili, 2012). MamI-GFP was shown to be localized to the magnetosome and indicates the presence and position of the magnetosome in the cell (Murat et al., 2010). MamI has no homologous domains or proteins except for its homologues in other MTB species. MamI secondary structure prediction yields a short loop of three amino acids (Thr35, Glu36, and Leu37) between the transmembrane helices (Figure 1; Slabinski et al., 2007). This loop is not predicted to interact with the magnetic particle, which may indicate that MamI has the ability to bend the magnetosome membrane.

MamQ

MamQ deletion in AMB-1 cells results in the complete loss of magnetosome formation (Murat et al., 2010). MamQ is predicted to be an integral membrane protein with 273 amino acids and is homologous to the LemA protein family (Greene and Komeili, 2012). LemA proteins are predicted to have a membrane-spanning domain on their N-terminal in which the non-membrane C-terminal domain (CTD) will be extracellular (pointing towards the magnetosome lumen); yet, its role is still unknown (Lenz et al., 1996).

MamQ secondary structure prediction using XtalPred and PsiPred servers show that MamQ contains a cytosolic unstructured N-terminal followed by an integral membrane helix and a CTD with a helix-turn-helix fold (Figure 1; Slabinski et al., 2007). The model structure of MamQ was based on the LemA template (PDB ID: 2ETD; Arnold et al., 2006). The model presents only the cytosolic-terminal domain (Asn70 to Thr223; Figure 1). Multiple sequence alignment shows high similarities between

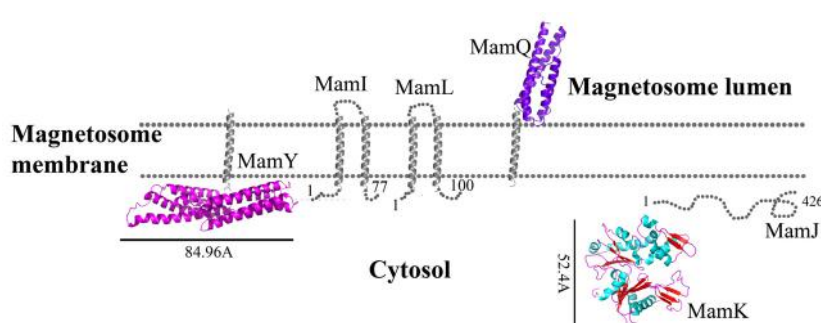


FIGURE 1 | Protein structure predictions that are involved in protein sorting, magnetosome membrane invagination, and magnetosome chain assembly. Structures are in ribbon representation. Predictions of

anchoring transmembrane helices are in gray. Black bars define the protein size in angstroms. *M. gryphiswaldense* MSR-1 MamA structure was determined by X-ray crystallography.

MamQ proteins from other MTB species and good conservation to important residues in *Listeria monocytogenes* LemA (Li, 2003). The MamQ model presents a magnetosomal domain with a negatively charged surface similar to the LemA structure, whose function is still unknown (**Figure 2**).

MamL

The *mamL* gene is located within the *mamAB* operon and its deletion results in the loss of the magnetosome membrane in *M. magneticum* AMB-1 (Murat et al., 2010). MamL is a small, 123 amino acid protein containing two predicted integral membrane α -helices and is very similar to MamI (**Figure 1**; Komeili, 2012). MamL is found only in MTB species and there are no homologous proteins or domains in other organisms (Komeili, 2012).

MamA

MamA is one of the most conserved MAPs and exists in all MTB MAI (Zeytuni et al., 2011). MamA deletion does not have an effect on membrane invagination or iron oxide biominerilization (Komeili et al., 2004; Zeytuni et al., 2011). It was shown that MamA localization is dynamic during cell growth and is not dependent on active magnetite formation (Komeili et al., 2004). It was also shown that MamA-GFP expressed in *M. magneticum* AMB-1 cells were localized to the magnetosome chain and surrounded the magnetosome vesicles (Yamamoto et al., 2010; Zeytuni et al., 2011).

MamA contains several TPR domains and self-assembles into stable homo-oligomeric complexes (Okuda et al., 1996; Zeytuni et al., 2011). TPR motifs are known to be involved in protein-protein interactions and are present in a number of proteins that are functionally unrelated (Blatch and Lässle, 1999). TPR is a 34 amino acid structure arranged as repeats of antiparallel α -helices (Das et al., 1998).

It was shown that purified MamA forms round-shaped complexes with a central pore cavity (Zeytuni et al., 2011). Mutation in the first helix of the MamA TPR motif causes disassembly of MamA complexes, which indicates its involvement in complex formation (Zeytuni et al., 2011). The conserved salt bridge

between Arg50-Asp79 in *M. magneticum* AMB-1 is responsible for stabilization of the N-terminal domain, which is important to MamA complex formation and localization to the magnetosome chain (Zeytuni et al., 2011). The structures of the MamA deletion mutant from *M. magneticum* AMB-1, *M. gryphiswaldense* MSR-1, and *Magnetobacterium bavaricum* are composed of 10 antiparallel α -helices that are folded as five TPR motifs and form a hook-shaped structure (PDB ID: 3AS4, 3AS8, and 2MUC; **Figure 1**; Zeytuni et al., 2011). It was suggested that MamA has three binding sites, two which are needed to create the round homo-oligomeric complexes and one to interact with the magnetosome chain (Zeytuni et al., 2011). Based on many TPR-ligand structures it was shown that the TPR protein family can bind unstructured peptides, helices, or entire TPR motifs (Zeytuni et al., 2011). Compared to other TPR proteins, which have a positive or negative binding pocket in their concave surface, MamA from *M. magneticum* AMB-1 displays a highly positive binding site in the concave surface similar to other MTB species (**Figure 2**; Zeytuni et al., 2011, 2012). The convex surface charge in *Magnetospirillum* species is negative, unlike in *M. bavaricum* strain that presents both positive and negative patches (Zeytuni et al., 2012). It was predicted that the MamA convex side may act as a binding site with other magnetosome-associated proteins (MAPs; Zeytuni et al., 2011). MamA was found to interact with four different proteins or protein fragments *in vivo* (of 26.8, 31.6, 54, and 63.5 kDa) which supports the suggested model in which the MamA convex surface faces the magnetosome membrane and acts as a multi-protein assembly site (Yamamoto et al., 2010; Zeytuni et al., 2011).

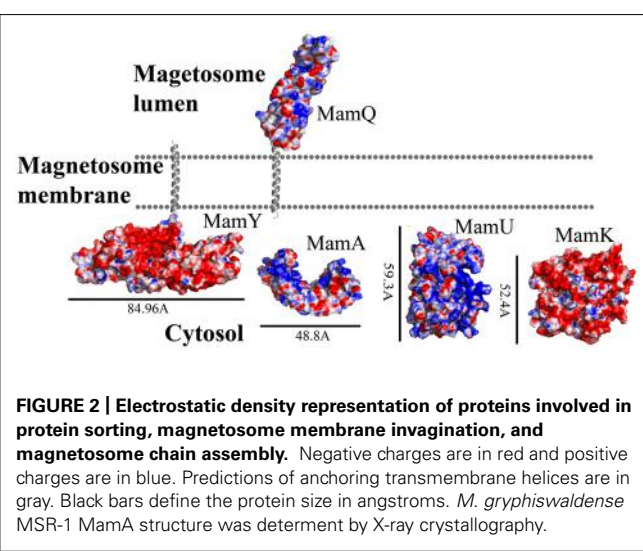
MamU

MamU is a 297 amino acid protein predicted to fold as a mixed α -helices- β -sheets structure (Slabinski et al., 2007). $\Delta mamU$ mutants did not yield any changes in their magnetic response (Murat et al., 2010). One MamU homologous protein family are the diacylglycerol kinases (DGKs), which phosphorylate the second-messenger diacylglycerol (DAG) to phosphatidic acid (PA; Van Blitterswijk and Houssa, 2000). The DGK pathway is known to be a major player in the regulation of cell response (Mérida et al., 2008). Nowadays there are nine known members of the DGK family which contain the conserved catalytic domains and two cysteine rich domains on the protein N-terminal (Van Blitterswijk and Houssa, 2000). The catalytic domain is known to have six conserved aspartate residues which play a major role in the enzyme's activity (Van Blitterswijk and Houssa, 2000).

The MamU model structure is based on a DGK structure (ID: 3T5P chain L; **Figure 1**; Guex and Peitsch, 1997). Sequence alignment between MamU and DGK shows that the conserved aspartates do not appear in the MamU sequence and there is only one cysteine residue on the MamU N-terminal domain. Changes in the electrostatic density map between MamU and DGK indicate that MamU has a different substrate and activity, or that the fold of MamU is different from the DGK protein family.

MamY

MamY is a 371 amino acid protein predicted to have two integral membrane helices at its N-terminal and a large cytosolic



domain at the C-terminal (Slabinski et al., 2007). MamY has a weak homology to BAR domain proteins, which are known to be involved in cellular membrane dynamics (Peter et al., 2004; Tanaka et al., 2010). Deletion of the *mamY* gene yielded an enlarged magnetosome vesicle phenotype with small magnetite crystals (Tanaka et al., 2010). In *M. magneticum* AMB-1 MamY-GFP were localized near to the magnetosome vesicles with small magnetite crystals that are still attached to the inner membrane (Tanaka et al., 2010). It was suggested that MamY's role is to constrict the magnetosome membrane during its invagination, followed by magnetite crystal growth (Tanaka et al., 2010).

While searching for MamY structural models, several proteins were suggested as templates (Arnold et al., 2006; Kelley and Sternberg, 2009). One of these templates was the cytoplasmic domain of a bacterial chemoreceptor from *Thermotoga maritima*, which has a structure of two antiparallel helices that dimerize into a four-helix bundle with another methyl-accepting chemotaxis protein (MCP) subunit (Park et al., 2006). MCP is a transmembrane kinase which is involved in the signaling network that controls bacterial chemotaxis (Park et al., 2006). In addition, MamY structural analysis using Phyre2 shows low conservation to the domain from talin protein (PDB ID: 1SJ8; Kelley and Sternberg, 2009). Talin is a cytoskeletal protein that is known as a linker between actin and the membrane via integrin proteins, which are involved in cell adhesions (Niggli et al., 1994). The talin domain is composed of an N-terminal five-helix bundle and a C-terminal four-helix bundle, which are connected by a short loop (Niggli et al., 1994). MamY model structure shows the cytosolic domain, which is composed of four α -helices on its N-terminal followed by five α -helices (Figure 1). The electrostatic density map of the MamY model presents a highly negatively charged surface, similar to talin's surface charge distribution (Figure 2; Papagrigoriou et al., 2004). Sequence alignment between MamY and talin presents low identity, whilst the MamY model structure has high confidence (95.36%) with the talin structure (Kelley and Sternberg, 2009). From these results we can suggest that MamY may function similarly to the talin protein and plays a role in membrane invagination and magnetosome separation from the inner membrane (Tanaka et al., 2010).

MAGNETOSOME ARRAGMENT INTO CHAIN STRUCTURE

MamJ

MamJ is essential for the magnetosome chain structure and its deletion leads to a new magnetosome arrangement as 3D clusters instead of a linear chain (Scheffel and Schüller, 2007). MamJ is known as an acidic protein which contains 426 amino acids with a repetitive domain structure. It has a central acidic repetitive domain (CAR domain) which is composed of an 88 amino acid motif followed by tandemly arranged copies of a highly acidic, 20 amino acid motif, consisting primarily of Pro and Glu residues arranged in Glu-Pro (Scheffel et al., 2006; Scheffel and Schüller, 2007). The CAR domain is not required for magnetosome restoration in Δ *mamJ* cells, unlike regions at the N- or C-terminal in MamJ (Scheffel and Schüller, 2007).

It is known that MamJ is associated with MamK filaments and magnetosome vesicles, thus creating a linear chain (Scheffel et al., 2006). The interactions between MamJ and MamK apparently

are mediated by two protein–protein interaction domains, one located on the C-terminal and the other located in the MamJ N-terminal region (Scheffel and Schüller, 2007). Recently it was shown, by using FLIM-FRET technique, that co-expression of MamK_mCherry and eGFP_MamJ in *Escherichia coli* create a stable interaction between them which is important for magnetosome alignment (Carillo et al., 2013).

Prediction of MamJ structure using IUPRED and XtalPred servers shows that most of the protein is unstructured (Figure 1; Dosztányi et al., 2005; Slabinski et al., 2007). Additional analysis of the MamJ sequence using the ProDom server has found two conserved domains which exist in TonB protein (Bru et al., 2005). TonB is a highly proline-rich protein that includes a segment consisting of multiple X-Pro dipeptide repeats with an anchor to the cytoplasmic membrane via a single N-terminal transmembrane helix (Hannavy et al., 1990). TonB also functions as a mechanical linkage between the inner and outer membranes through protein–protein interactions (Ollis and Postle, 2012). These predictions support the previous evidence that MamJ can interact with MamK via protein–protein interactions and is involved in magnetosome chain assembly.

MamK

The *mamK* gene encodes a filamentous structure which is similar to prokaryotic MreB and ParM (Sonkaria et al., 2012). MreB-like proteins polymerized into helical filamentous structures that run along the cell length (Carballido-López, 2006). The 3D structure of MreB shows high similarity to eukaryotic actin. The actin-like proteins, similar to actin, function in prokaryotic cells and are required for targeting and positioning proteins or molecular complexes (Carballido-López, 2006).

In *M. magneticum* AMB-1 strain, *mamK* deletion abolishes the filamentous structure near the magnetosome (Komeili et al., 2006), whereas Δ *mamK* in *M. gryphiswaldense* MSR-1 results in shorter, fragmented, and off-center chains and was suggested to be involved in proper magnetosome chain positioning and segregation (Katzmann et al., 2010, 2011). The function of MamK is to organize the magnetosome chain along the cell axis and associate with MamJ, which may act as an anchor between MamK and the magnetosome membrane (Sonkaria et al., 2012). Previously, it was shown that the localization of MamK filaments in the cell does not depend on the presence of MamJ (Scheffel and Schüller, 2007).

Biochemical studies indicate that MamK polymerization is the result of ATP binding whilst filament disassembly happens during ATP hydrolysis (Ozyamak et al., 2013). It seems that ATP stabilizes MamK filaments and prevents their aggregation (Ozyamak et al., 2013). *M. magneticum* AMB-1 MamK form dynamic filaments *in vivo* which depend on the ATPase active site and two proteins (MamJ and LimJ) which are required for promoting MamK filament formation (Draper et al., 2011). Furthermore, MamK filament structure has an architecture of two parallel strands, unlike MreB filaments which are linked in an antiparallel arrangement (Ozyamak et al., 2013). The MamK homology model is based on MreB's structure (PDB ID: 1JFA; Guex and Peitsch, 1997; Sonkaria et al., 2012). The MamK model structure has four domains that are similar to the conserved secondary structure of

the actin-like protein family (**Figure 1**; Carballido-López, 2006; Sonkaria et al., 2012). The electrostatic potential density map of MamK and MreB also shows high similarities, especially in the ATP binding site, suggesting that MamK has a similar activity (**Figure 2**).

IRON TRANSPORT AND NUCLEATION

MamO

MamO is a large, 65.3 kDa protein whose deletion leads to an empty magnetosome phenotype suggesting that MamO might be involved in biominerization, iron transport, and/or magnetite nucleation, or allows for a suitable environment for magnetite synthesis in the magnetosome (Murat et al., 2010). MamO is an integral membrane protein with eight predicted transmembrane α -helices. Based on ProDom prediction, MamO contains two domains: one is similar to the trypsin-like peptidase and the second is similar to integral membrane proteins. The latter are involved in the transport of anions across the cytoplasmic membrane during taurine metabolism as an exporter of sulfoacetate (Yang et al., 2010). Although it seems that MamO has a predicted trypsin-like peptidase domain, expression of MamO in *E. coli* does not show any protease activity. In addition, several single point mutations (T225A, H116A, and D149A) in the predicted active site of the MamO trypsin domain did not affect magnetite crystal formation (Yang et al., 2010; Quinlan et al., 2011).

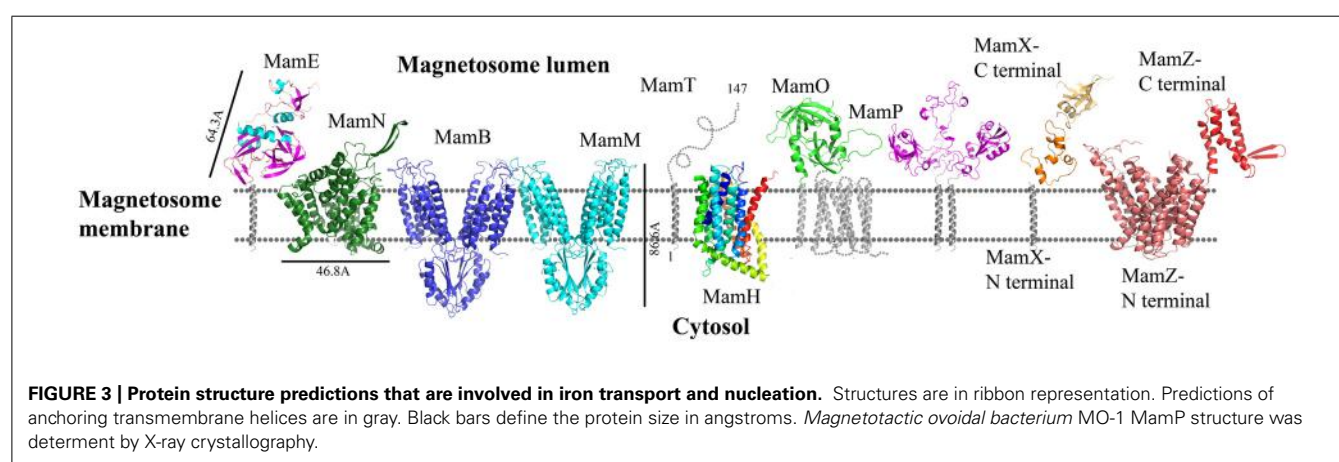
Today there is no direct evidence that any part of MamO has trypsin or protease activity. To explore whether MamO can act as an active protease, we decided to build a homology model using the Swiss-Model server which can aid with understanding MamO function from a structural aspect (Arnold et al., 2006). First, we performed multiple sequence alignment between all known MamO sequences that were found in other MTB species by using the ClustalW server and ESPript 2.2¹ (Li, 2003). This alignment indicates that all MamO variants are highly conserved and contain similar amino acids in the suspected catalytic triad. To further study the MamO fold we analyzed its 3D structure prediction from which we could determine that MSR-1 MamO shares

high similarity to the trypsin-like conserved fold (**Figure 3**). The MamO modeled structure is based on the structure of two different proteins from the HtrA serine protease family (PDB ID: 1LCY, 2Z9I). The first is the mitochondrial serine protease HtrA2 from mammals and the second is HtrA2 from *Mycobacterium tuberculosis*. These proteases contain a protease catalytic triad of His, Ser, and Asp and a PDZ domain on their C-terminal. Both domains are highly conserved in the HtrA family and the PDZ domain is involved in protein–protein interactions (Pallen and Wren, 1997). The structure model of MamO does not contain the PDZ domain which is essential for the HtrA protease activity (Iwanczyk et al., 2007). In contrast to several proteases from the HtrA family, we observe that two residues – Ser and Asp – of the conserved catalytic triad do not appear in the same position in *M. gryphiswaldense* MSR-1 MamO (**Figure 3**). This, together with the lack of the PDZ domain, indicates that MamO is most likely missing the protease activity.

MamE

MSR-1 MamE is a large, 655 amino acid protein which is important for protein localization to the magnetosome membrane and is predicted to fold as a putative serine protease with two PDZ domains and a predicted membrane anchoring the hydrophobic helix on its N-terminal (Yang et al., 2010; Siponen et al., 2012). Recently it was discovered that MamE contains a putative cytochrome c-like domain with a CXXCH motif that acts as covalent thioether bonds to the heme vinyl groups (magnetochrome; Bowman and Bren, 2008; Siponen et al., 2012). Deletion of MamE *in vivo* leads to empty magnetosome vesicles and to the loss of magnetite synthesis (Murat et al., 2010). As a putative serine protease, MamE has a highly conserved catalytic triad. It was shown that site-directed mutagenesis of these residues in *M. magneticum* AMB-1 MamE (His198, Asp221, Ser297) does not affect magnetite crystal nucleation but results in a phenotype characterized by smaller magnetite crystals and the loss of the magnetic response (Quinlan et al., 2011). The same phenotype is similar to the deletion of the magnetochrome domain (Quinlan et al., 2011). There are few hypotheses regarding the functions of magnetochrome, such as electron donation to oxidized iron, extraction of electrons to maintain the magnetosome redox state or to act as a redox

¹<http://escript.ibcp.fr/ESPript/ESPript/>



buffer to maintain the balance between maghemite and magnetite (Siponen et al., 2012).

To understand MamE function and how it is involved in magnetosome formation, we decided to create a homology model. The MSR-1 MamE model was built using the Swiss-PdbViewer program and is based on a serine protease structure (PDB ID: 2Z9I; Guex and Peitsch, 1997; **Figure 3**). From the 3D structure and the multiple sequence alignment we can locate the highly conserved catalytic triad of serine proteases, yet it was not shown experimentally whether MamE has protease activity (**Figure 4**).

Based on domain prediction by InterProScan server and the available 3D model of MamE, a PDZ domain is predicted. PDZ domains are usually known to be involved in protein–protein interactions and signaling complexes (Lee and Zheng, 2010). In a previous study, it was shown that MamE deletion caused mislocalization of magnetosome proteins which could indicate the importance of the PDZ domain to protein–protein interactions (Murat et al., 2010). Prediction of a MamE PDZ domain shows high conservation to PDZ architecture, which consists of six anti-parallel β -strands and two α -helices (Sheng and Sala, 2001). Furthermore, the PDZ domain was shown to interact with the conserved PDZ binding signature at the C-terminal of MSR-1 MamB (Uebe et al., 2011). The major binding site of the MamE PDZ domain lies between α 1 and β 3 and contains a large number of hydrophobic amino acids, similar to the HtrA2-PDZ domains fold which is known to be a binding site for single peptide ligands or hydrophobic amino acids of other proteins (Zhang et al., 2007; Wang et al., 2010). Prediction of the electrostatic density map displays negative and positive patches on the PDZ surface, which is similar to other HtrA2 PDZ domains. Based on all the previous results, we can assume that MamE acts as a serine protease and that its PDZ domain can interact with other proteins that are involved in magnetosome formation.

MamH

MamH is a 428 amino acid protein and in most MTB it is located in the *mamAB* operon, though its function and how it is involved in magnetosome formation are both unknown (Murat

et al., 2010; Lohsse et al., 2011). In MSR-1, MamH is highly similar to MamZ (Raschdorf et al., 2013). Deletion of MamH results in a decrease in the number and size of magnetosomes (Murat et al., 2010; Raschdorf et al., 2013). It was shown that *mamH* deletion in Δ *mamZ* mutants causes a strong effect on the crystals' size, shape, and magnetic response (Raschdorf et al., 2013). Therefore, it was suggested that MamH may be involved in magnetite biominerization (Raschdorf et al., 2013). By searching for homologous proteins or conserved domains with the BLAST server we found similarities to a conserved domain in the Major Facilitator Superfamily (MFS), members of which are known to function as membrane transporters (Pao et al., 1998; Marchler-Bauer et al., 2011; Raschdorf et al., 2013). MFS proteins are single-polypeptide secondary carriers that use the electrochemical potential of the transported substrates (Pao et al., 1998). Prediction of MamH secondary structure shows an organization of 12 transmembrane helices with short connecting loops and a longer loop connecting H6–H7 (Raschdorf et al., 2013; **Figure 3**). This organization is similar to MFS protein structures (Huang et al., 2003). The MamH predicted structural model displays a negative cavity which can bind positive ions or ligands like iron and transfer them through the magnetosomal membrane (PDB ID: 2XUT). The hypothesis that MamH is an integral membrane protein cannot only be based on the sequence prediction but also on the model's electrostatic density map. This contains the positive girdle envelope around the protein exterior, which is usually a characteristic feature of integral membrane proteins (**Figures 3 and 5**). Another structure of MFS proteins indicates a proton-coupled transporter which is essential for phosphate uptake in plants and fungi. The *Piriformospora indica* phosphate transporter (PiPT) is a high affinity phosphate transporter that is involved in improving phosphate nutrition levels in the host plant and is known to be a phosphate/H⁺ symporter from the MFS (Pao et al., 1998; Pedersen et al., 2013). By using Swiss-PdbViewer we created manually another MamH model structure based on PiPT structure which provided a different view for MamH function (PDB ID: 4J05; Guex and Peitsch, 1997). In the MamH PiPT-based electrostatic map we can detect a positive pocket in the magnetosomal side and a negative patch in the cytosolic side. These distinctions are similar to PiPT structure and may result in a new perspective

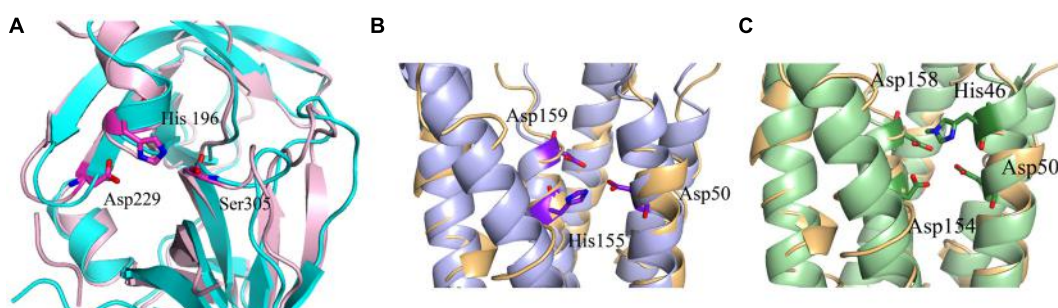
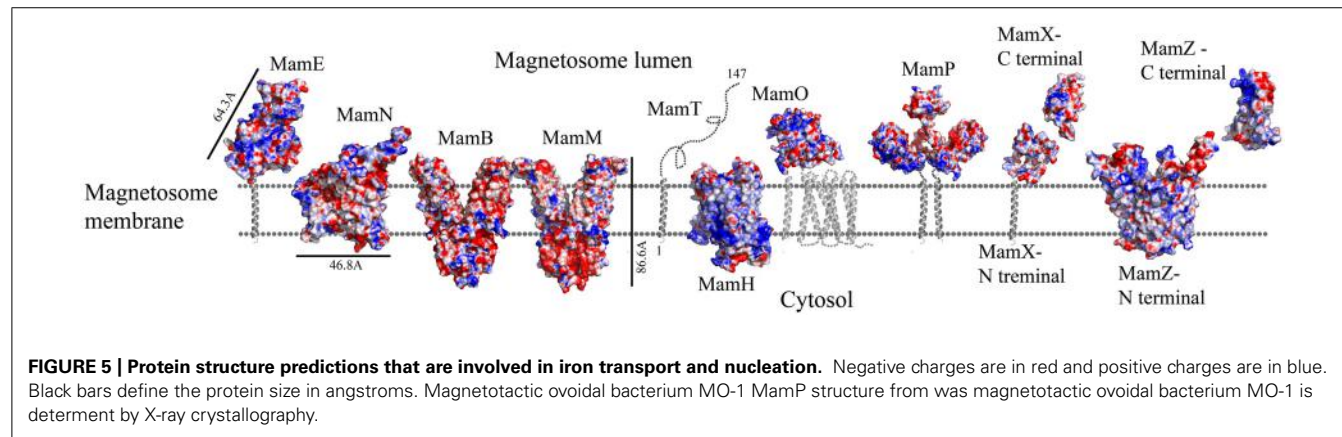


FIGURE 4 | Predicted catalytic/ binding sites of MamE, MamM, and MamB. **(A)** MamE predicted structure (light pink) overlapping with serine protease structure (cyan); the catalytic triad is shown as sticks. **(B)** Overlap of the MamM predicted structure (light blue) with zinc transporter FieF (light orange); the three residues that are predicted to create the negative pocket are presented as sticks. **(C)** Overlap of the MamB predicted structure (light green) with zinc transporter FieF (light orange), the three residues that are predicted to create negative pocket are presented as sticks.

orange); the three residues that are predicted to create the negative pocket are presented as sticks. **(C)** Overlap of the MamB predicted structure (light green) with zinc transporter FieF (light orange), the three residues that are predicted to create negative pocket are presented as sticks.



on MamH function. Recently, it was shown in *M. gryphiswaldense* MSR-1 that there are two iron phases during the biomineralization process: ferrihydrite with high phosphorus content – similar to the bacterial ferritin core – and magnetite (Fdez-Gubieda et al., 2013). It has also been suggested by Baumgartner et al. (2013) that magnetite formation starts from a phosphate-rich ferric hydroxide phase, through a short-lived ferrihydrite phase followed by a final phase of magnetite. These results support our MamH model, which can function as a phosphate transporter clearing phosphate from the magnetosome while biomineralizing magnetite (Fdez-Gubieda et al., 2013).

MamN

MamN is a 437 amino acid protein and its deletion leads to an empty magnetosome chain phenotype (Murat et al., 2010). The inability to synthesize magnetite within the magnetosomes can indicate MamN involvement in biomineralization, iron transport, magnetite nucleation, or chemical environment determination needed for magnetite synthesis in the magnetosome (Murat et al., 2010). However, its deletion does not affect the localization of other magnetosome proteins (Murat et al., 2010).

MamN has homology to a Na^+/H^+ antiporter; this activity can influence the pH within the magnetosome core (Komeili, 2012). It is known that magnetite synthesis requires a basic environment which raises the speculation that a H^+ extruder is needed (Komeili, 2012).

Prediction of the MamN secondary structure, using XtalPred server, presents 11 integral membrane helices (Slabinski et al., 2007). The MamN 3D model structure is based on a sodium-dependent dicarboxylate transporter (NaDC) template (Figure 3; PDB ID: 4F35; Arnold et al., 2006). NaDC is a plasma membrane protein which transports tricarboxylates or dicarboxylates and is known to bind a specific substrate (Mancusso et al., 2012). NaDC contains 11 transmembrane helices and forms a dimer to create a large interface area (Mancusso et al., 2012). MamN model structure shows membrane protein characteristics such as the uncharged girdle and the charged core (Figure 5). The MamN model fits only to the monomeric NaDC but not to the dimeric NaDC structure. Further attempts to create a 3D structure of MamN based on its Na^+/H^+ antiporter homologous protein did not result in a convincing structure.

MamM and MamB

MamM and MamB are large proteins – 34.4 and 31.9 kDa, respectively – and are magnetosome membrane proteins which may be involved in iron transport due to their similarity to the cation diffusion facilitator (CDF) protein family (Uebe et al., 2011). CDF proteins are found in all kingdoms of life and are involved in the transport of divalent metal cations (Paulsen and Saier, 1997). Most members of the CDF family contain six highly conserved transmembrane helices, organized as a transmembrane domain, with cytoplasmic N- and C-terminals (Cragg et al., 2002). It was shown that CDFs create a homodimeric structure and use a proton antiport mechanism to drive substrate translocation across the lipid membrane (Haney et al., 2005; Lu et al., 2009). MamM deletion causes the loss of magnetite crystal formation and results in empty magnetosomes (Uebe et al., 2011). Except for its suggested role in iron transport, MamM is also involved in crystallization initiation and proper localization of other magnetosome proteins (Uebe et al., 2011). In contrast to MamM, MamB deletion causes a lack of magnetosome vesicles (Murat et al., 2010; Uebe et al., 2011). Further experiments indicated that MamM and MamB can interact, and that MamM is required for MamB stabilization (Uebe et al., 2011). It has also been shown that the cytoplasmic CTD in MamM and MamB are involved in MamB stabilization (Uebe et al., 2011).

Replacement of the conserved cysteine residues (Cys9/138) with serine or alanine did not affect MamM function but similar mutations in MamB abolished its function (Uebe et al., 2011). Mutation of Cys138 in MamB blocked its oligomerization and magnetosome formation (Uebe et al., 2011). In MSR-1 the MamB C-terminal has a TPR recognition signature and was shown to interact with MamE's PDZ domain (Quinlan et al., 2011; Uebe et al., 2011). In addition, point mutations in the MamM membranal putative metal binding site (Y46H, Y46D, D50A, H155A, and D159A) lead to changes in crystal size and morphology, which may be the result of a reduction in iron transport rates into the magnetosome vesicles or of the nucleation of magnetite crystals (Uebe et al., 2011). It seems that magnetite can only be stable in a pH range from ~7 to 14 (Bell et al., 1987). Therefore, if MamM is using a H^+/cation antiport mechanism similar to other CDF proteins, it may explain why dysfunction of MamM causes defects in crystal formation (Uebe et al., 2011).

MamM and MamB secondary structure prediction indicates a transmembrane domain with six α -helices followed by a C-terminal cytosolic domain (Uebe et al., 2011). MamM and MamB 3D structures prediction is based on the FieF structure and built manually in SPDB viewer (PDB ID: 3H90; **Figure 3**; Guex and Peitsch, 1997; Uebe et al., 2011). FieF is an *E. coli*, homodimeric, zinc transporter (Lu et al., 2009). Its CTD has a metallochaperone-like fold which is found in cytoplasmic metal carrier proteins (O'Halloran and Culotta, 2000). The FieF active sites which participate in zinc transport are located toward the center of each transmembrane domain and continue to the CTD–CTD interface (Lu et al., 2009). In FieF structure there are four amino acids that bind a zinc ion in a negative pocket located between helix 2 and helix 5 (Asp45, Asp49, His153, and Asp157; Lu et al., 2009). By overlapping the MamM model with FieF's structure we can observe similar amino acids at the zinc binding positions (**Figure 4B**). These amino acids were mutated in MamM leading to protein dysfunction *in vivo*. Similar zinc binding site positions can be found when we overlap MamB onto FieF. There are four residues in MamB that may act as an ion-binding site: His46, Asp50, Asp154, and Asp158 (**Figure 4C**). From multiple sequence alignment using the ClustalW server, we can detect that there are no amino acid conservations between MamM, MamB and FieF CTDs sequences [5]. In MamM CTD we found that the amino acids that are involved in zinc binding in FieF are different and create a negative pocket that may be involved in ion binding. We cannot find such a negative pocket in the MSR-1 MamB 3D model structure that may indicate different activity for MamB (**Figure 5**).

MamP

MamP is a 270 amino acid protein that is predicted to have one transmembrane helix on its N-terminal and two cytochrome c-like motifs (CXXCH) on its C-terminal, similar to MamE and MamT proteins (Siponen et al., 2012). MamP also contains a PDZ domain signature and a putative signal sequence that suggests it is targeted to the inner membrane (Siponen et al., 2012). Mutation in MamP from *M. magneticum* AMB-1 strain causes deficiencies in crystal maturation and the loss of the magnetic response (Siponen et al., 2012). It was suggested that in *M. magneticum* AMB-1 strain MamP could play a role in controlling crystal number and size (Murat et al., 2010). Furthermore, MamP can be involved in the electron transfer chain which is important for magnetosome assembly and magnetite formation (Siponen et al., 2012).

Recently, MamP structure (residues 26–260) from *Magnetotactic ovoidal bacterium* MO-1 strain was determined (Siponen et al., 2013). MamP 3D structure presents a PDZ fold followed by two magnetochrome domains with a 17 residues linker between them (PDB ID: 4JJ0). It was shown that MamP PDZ domain has different properties from other known PDZ domains which are known to interact with peptides from other proteins and may be involved in the protein dimerization state (Iwanczyk et al., 2007). MamP PDZ domains are highly conserved in other species which indicate conservation of the protein dimeric state (Siponen et al., 2013). In *M. gryphiswaldense* MSR-1 MamP structure 3D model, which is based on the determined MamP structure,

show similar characterization (**Figure 3**). It was shown that MamP structure has a highly negative pocket between the two monomers that includes conserved acidic residues (Glu91, His93, Glu98, Glu123, and Glu193) that were suggested to act as an iron-binding site (**Figure 5**). Mutation in these acidic residues to alanine *in vivo* led to magnetic response and crystal size defects (Siponen et al., 2013).

MamT

In *M. gryphiswaldense* MSR-1, MamT contains 174 amino acids and is predicted to have a double cytochrome c CXXCH motif and a membrane-anchoring hydrophobic helix on its N-terminal (Slabinski et al., 2007). MamT secondary structure prediction shows that the CTD is located on the magnetosome lumen and include α -helices and β -sheets (**Figure 3**; Slabinski et al., 2007). A Δ mamT mutant shows defects in crystal maturation and the loss of magnetic response (Murat et al., 2010; Siponen et al., 2012).

MamZ

MamZ is a 661 amino acid protein and is known to have similarities to the ferric reductase-like transmembrane component (YedZ-like domain) on its C-terminal side, whilst its N-terminal has homology to the MFS (Richter et al., 2007; Raschdorf et al., 2013). Recently it was shown that MamZ interacts with the magnetosome membrane and was suggested to create an iron oxidoreductase and transport complex with MamX and MamH (Raschdorf et al., 2013). MamZ deletion shows a slightly reduced magnetic response with two types of crystals that are still aligned into a chain (Raschdorf et al., 2013). Deletion of MamZ C-terminal, which shares homology with YedZ-like domain, reveals the same phenotype as the full MamZ deletion, suggesting that this domain has a critical role in the biominerization process (Raschdorf et al., 2013).

Prediction of MamZ 3D structure is based on two different templates. The N-terminal is predicted based on the glycerol-3-phosphate transporter (GlpT) from *E. coli*, which belongs to the MFS transporter family (PDB ID: 1PW4; Kelley and Sternberg, 2009). GlpT is known to transport glycerol-3-phosphate into the cytoplasm and inorganic phosphate to the periplasm and is composed of 12 transmembrane helices (Huang et al., 2003). MamZ N-terminal model structure presents 12 transmembrane helices with a negative pore facing the magnetosomal side, similar to GlpT (**Figure 5**). The electrostatic density map of MamZ cytosolic side is different from GlpT which is highly positively charged and may indicate a different function (**Figure 5**; Huang et al., 2003). MamZ C-terminal is predicted to have a domain structure from cytochrome bc₁ complex, which is known as ubiquinol-cytochrome c reductase (PDB ID: 3CX5; **Figure 3**; Kelley and Sternberg, 2009). Cytochrome c's function is to transfer electrons from the cytochrome bc₁ complex to cytochrome c oxidase (Solmaz and Hunte, 2008). MamZ C-terminal model structure includes three α -helices and two short β -sheets. The electrostatic density map of MamZ presents two highly charged patches – positive and negative – that are predicted to face the magnetosome lumen (**Figures 3 and 5**).

MamX

The *mamX* gene is conserved in most magnetite-producing α -proteobacteria (Abreu et al., 2011). It has a weak similarity to both the magnetosome serine-like protease MamE and to MamS (Richter et al., 2007; Lohsse et al., 2011). Structure prediction of MamX presents a transmembrane helix on its N-terminal side, two cytochrome c-like domains and a DNA-binding domain on its C-terminal (Söding, 2005; Slabinski et al., 2007). As mentioned above, cytochrome c functions as an electron carrier between different redox partners and can also be found in MamP, MamE, and MamT (Siponen et al., 2012). Deletion of these three proteins shows defects in crystal maturation (Siponen et al., 2012). It was shown that deletion of the cytochrome c domain in MamX abolishes its function (Raschdorf et al., 2013). The two cytochrome c-like domains are predicted to be located between Tyr42 and Val111 and their structures were predicted based on four different templates of cytochrome c domains (PDB ID: 1OGY_B, 1JN1_A, 3ML1_B, and 1QO8_A; **Figure 3**; Söding, 2005). In all these templates the cytochrome c domain creates a ring-like shape around the heme groups, except for the MamX cytochrome c-like domain prediction. By using HHpred server the C-terminal is predicted to be shaped like an OB fold motif (PDB ID: 2CQA_A, 3KDF_D, 3KF6_A; **Figure 3**; Söding, 2005). This motif is observed as a binding domain for oligonucleotides or oligosaccharides (Murzin, 1993). The OB-fold has a five β -sheet coiled fold that forms a closed β -barrel with an α -helix located between the third and fourth strands (Murzin, 1993). The MamX C-terminal predicted structure contains three β -strands followed by an α -helix, similar to the OB fold (Söding, 2005).

CRYSTAL SHAPE AND SIZE

MamR

MamR was shown to be important for crystal number and size control but is not involved in the control of their morphology (Murat et al., 2010; Quinlan et al., 2011). MamR is a small, ~72 amino acid protein with a predicted DNA-binding domain similar to the HTH-17 superfamily (Marchler-Bauer et al., 2011). MamR is also predicted to have a DNA-binding domain similar to the excisionase (Xis) family (Marchler-Bauer et al., 2011).

Phage-encoded excisionase (Xis) proteins are involved in DNA architectural structure and are needed for recruiting integrase to a specific binding site for its excision (Sam et al., 2002). MamR secondary structure prediction shows a fold of four α -helices and two short β -strands (Slabinski et al., 2007).

MamR model structure is based on the DNA-binding protein Rv2175c, from *M. tuberculosis* (PDB ID: 2KFS; Cohen-Gonsaud et al., 2009). Rv2175c is activated by phosphorylation of its N-terminal domain (Cohen-Gonsaud et al., 2009). The MamR model presents a C-terminal with two α -helices followed by two β -sheets and a negative patch on the protein surfaces (**Figures 6 and 7**; Kelley and Sternberg, 2009).

MamS

MamS is a ~19 kDa protein and its deletion leads to a weak magnetic response due to defects in magnetite crystal size and morphology (Murat et al., 2010). In *M. magneticum* AMB-1 strain several small magnetic particles were clustered together in one magnetosome membrane, suggesting MamS involvement in the magnetite post-nucleation event (Murat et al., 2010; Komeili, 2012). According to BLAST server there is no conserved domain in the MamS sequence (Marchler-Bauer et al., 2011). Prediction of its secondary structure indicates a fold containing a transmembrane helix on the N-terminal followed by β -strands on the cytoplasmic side (**Figure 6**; Slabinski et al., 2007). Prediction of the MamS 3D structure is based on the structure of the hypothetical protein YgiW from *E. coli* with unknown function (PDB ID: 1NNX; Kelley and Sternberg, 2009). The MamS structure model displays six β -sheets with two short α -helices, similar to the OB fold which is known to create a β -barrel structure that can bind oligonucleotides or oligosaccharides (Murzin, 1993).

FtsZ-LIKE

The *ftsZ*-like gene was found to be a second copy of the gene encoding the tubulin-like FtsZ protein in *Magnetospirillum* species, but missing the 200 amino acid C-terminal tail (Ding et al., 2010). Deletion of *ftsZ*-like does not affect cell division but results in smaller magnetite crystals (Ding et al., 2010). It was shown that FtsZ-like displays both ATPase and GTPase activities and also has GTP-dependent polymerization into filaments *in vitro* (Ding et al., 2010). FtsZ proteins are known to be involved in cell division and

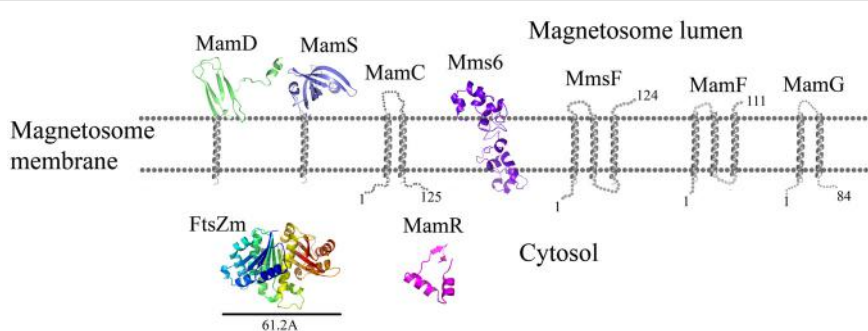
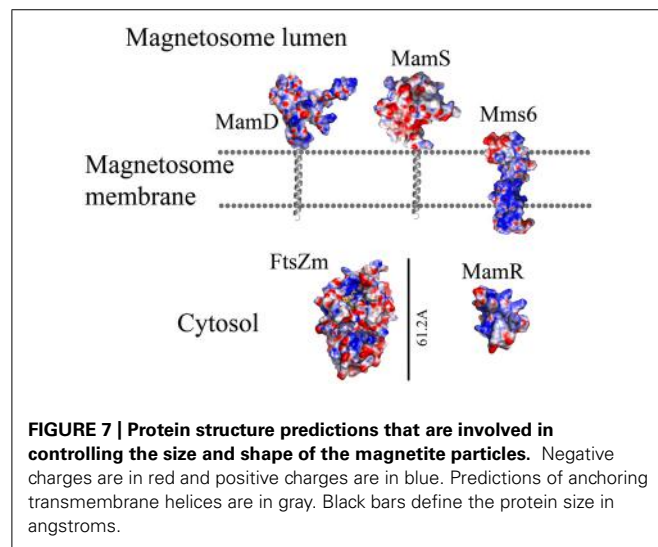


FIGURE 6 | Protein structure predictions that are involved in controlling the size and shape of the magnetite particles. Structures are in ribbon representation. Predictions of anchoring transmembrane helices are in gray. Black bars define the protein size in angstroms.



create the septum which allows the cell to divide into two daughter cells (Scheffers and Driessens, 2001). FtsZ is known to have GTPase activity and to create a filamentous structure within the cell (Mukherjee and Lutkenhaus, 1998). The FtsZ 3D structure contains two domains, one of which is the N-terminal domain, which has a Rossman fold containing the GTP binding site and the other is the CTD, which is required for proper polymerization of FtsZ and interaction with other proteins (Din et al., 1998; Löwe and Amos, 1998).

Prediction of the FtsZ-like 3D structure shows high similarity to other FtsZ proteins (Figure 6; PDB ID: 2RHL; Arnold et al., 2006). The FtsZ-like structure model presents the two known FtsZ protein domains. The electrostatic density map fits the GTP binding pocket characteristics (Figure 7). It can be assumed from the structure and the high homology between the FtsZ proteins that FtsZ-like may be involved in cell division processes (Altschul et al., 1990).

MamC

MamC (also known as Mms13) is a small, 12.4 kDa protein and is strongly conserved in most magnetotactic α -proteobacteria (Abreu et al., 2011). Deletion of MamC does not present any defects in crystal size or shape and is tightly associated with the magnetosome membrane in *M. gryphiswaldense* MSR-1 strain (Wawer et al., 2001; Scheffel et al., 2008). $\Delta mamE$ cells show mislocalization of MamC-GFP to the magnetosome chain (Quinlan et al., 2011). Prediction of MamC secondary structure with XtalPred (Slabinski et al., 2007) displays two transmembrane helices with a connecting loop that is predicted to interact with the magnetite crystal (Figure 6). Based on the secondary structure prediction, the MamC connecting loop is predicted to adopt an α -helix structure with several charged residues.

MamG

MamG is a small, 8 kDa protein specifically expressed in the magnetosome membrane (Lang and Schüler, 2008). MamG has no homologous proteins and contains a similar Leu-Gly dipeptide

motif to MamD and Mms6 (Scheffel et al., 2008). Prediction of its secondary structure in the XtalPred server displays two transmembrane helices and an unstructured C-terminal that faces the bacteria cytosol (Figure 6). Sequence analyses indicate that most of the protein's amino acids are hydrophobic except for the last residues, which are negatively (Asp68, Glu78, and Glu82) and positively charged (Lys71, Arg73, and Lys74).

MamD

MamD is a 30.2 kDa protein which contains a transmembrane helix on its C-terminal and a Leu-Gly repeat domain on its N-terminal, which is located in the magnetosome lumen (Richter et al., 2007; Arakaki et al., 2008). MamD is one of the magnetosome membrane-associated proteins which controls magnetite crystal size (Scheffel et al., 2008). Its secondary structure prediction shows that the N-terminal is located within the magnetosome lumen with β -sheets and α -helices. Prediction of the MamD 3D structure shows only a small part of the magnetosomal side (Gly116 to ALA 158) and displays a β -sheets fold which is based on the CTD of FlgD protein from *Xanthomonas campestris* (PDB ID: 3C12; Figure 6; Kelley and Sternberg, 2009). FlgD is a scaffold protein and is required for flagellar hook assembly (Ohnishi et al., 1994). Sequence alignment between MamD and FlgD presents low sequence identity, which does not suggest a function for MamD. Most of the residues in the MamD structure are hydrophobic with a few polar or negatively charged residues (Kelley and Sternberg, 2009).

MamF

MamF is a small, 12.3 kDa protein which shares 61% identity with MmsF (Lohsse et al., 2011). MamF was shown to be protected against proteolytic degradation due to its integral membrane localization and its highly hydrophobic nature with three predicted transmembrane helices (Gru et al., 2004). *In vivo* localization of MamF-GFP was identified as linear spots along the cell axis in accordance with the magnetosome chain localization (Lang and Schüler, 2008). MamF secondary structure prediction shows three transmembrane helices with short connecting loops (Figure 6; Kelley and Sternberg, 2009). The first loop which predicted to be located in the magnetosomal side and includes highly charged residues (Arg39, Asp40, Asp41, and Glu42) which may indicate a possible interaction with the magnetite particles (McGuffin et al., 2000; Kelley and Sternberg, 2009).

Mms6

In *M. gryphiswaldense* MSR-1 strain, Mms6 is a small, 136 amino acid protein that was suggested to undergo proteolytic cleavage from its proprotein (Gru et al., 2004). In *M. magneticum* AMB-1 strain, $\Delta mms6$ strains showed smaller magnetite crystals with different shapes (Tanaka et al., 2011; Murat et al., 2012). The Mms6 C-terminal is highly acidic and the region between the middle and the C-terminal contains basic amino acids (Arakaki et al., 2003). It was shown that Mms6 possesses iron-binding activity and it was suggested that the C-terminal region can initiate crystal nucleation during magnetite formation and direct the shape of magnetite crystals *in vitro* (Arakaki et al., 2003). Mms6, MamD and MamG have a common Leu and Gly repetitive sequence

(Arakaki et al., 2008). Mms6 can self-assemble into micelles *in vitro* by interactions between the cleaved Mms6 N- and CTDs and, due to iron binding, a conformational change is induced (Feng et al., 2013).

Prediction of the Mms6 secondary structure shows an N-terminal domain that is predicted to be unstructured followed by one transmembrane helix and a C-terminal, which may form an α -helix structure (Figure 6). Mms6 model structure was predicted in 3Dpro server which use structural characterization and statistical terms in the energy function (Cheng et al., 2005). The electrostatic density map of Mms6 3D structure model results in a negative patch on its CTD that can act as an iron binding site (Figure 7). Analysis of the Mms6 model structure and protein sequence indicates that the predicted transmembrane helix (G91 to Y115) contains only hydrophobic residues, which may support the existence of such a helix.

MmsF

MmsF is a 124 amino acid protein and is predicted to have three transmembrane helices but does not show any conserved domain (Slabinski et al., 2007; Murat et al., 2012). In the absence of *mmsF* in *M. magneticum* AMB-1 strains, magnetite synthesis initiation is not affected but the crystal growth is stalled (Murat et al., 2012). It was found that the MmsF sequence is highly homologous between *M. gryphiswaldense* MSR-1 and *M. magneticum* AMB-1 (Murat et al., 2012). MmsF is shown to control crystal size and shape in *M. magneticum* AMB-1 cells (Murat et al., 2012). MmsF was also shown to be associated with the magnetosome membrane by fusing a GFP tag to its N-terminal (Murat et al., 2012). The MmsF N-terminal is located in the cytoplasmic side whilst the C-terminal faces the magnetite crystals (Figure 6; Murat et al., 2012).

CONCLUSION

In this paper we looked at the MAPs, which are encoded in the *M. gryphiswaldense* MSR-1 MAI region. We analyzed each protein sequence and created structural models that will enable better understanding of their function in magnetosome formation (Table 1). By analyzing the size of these proteins some key questions regarding the magnetosome membrane invagination can be answered. One of the questions that still exist in the magnetosome field regards how the magnetosome membrane invaginates. In the literature, the invagination process is described as a curving of the inner membrane that creates a pocket shape. Yet, neither the driving force nor the player were determined in MTB (Komeili et al., 2006). One possible option is that the inner membrane starts to fold into a vesicle – by a yet unknown mechanism – followed by the localization of magnetosome proteins to the vesicles. However, the diameter of the invagination membranous neck is only about 40 Å or less (Komeili et al., 2006) with a highly curved concave turn followed by a convex membrane structure (Figure 8). This geometry is very limited in size and shape, especially with the concave turn. Based on our models, many proteins have domains that are larger in size than the magnetosome invagination diameter. For example, MamB, which is essential to the magnetosome invagination, has a cytoplasmic domain with a size of ~52 Å and a magnetosomal domain in the size of ~37 Å (Figure 3). Other examples are MamO and

MamE, both with large, CTD (~36 Å in size; Figure 3). Even by looking at these few examples we can determine that such proteins cannot pass through this magnetosome invagination neck due to their size, especially if this part is held by other proteins, as suggested by Tanaka et al. (2010). A more probable mechanism that fits our structural data is that the magnetosome proteins are sorted prior to the magnetosome invagination and accumulate on the inner membrane as protein–protein–lipid complexes that might be mimicking lipid rafts (Figure 8). The formation of such a complex, together with the natural curvature of the integral magnetosome membrane helices, may lead to a natural invagination without a special protein support; a process that will gain more force as more proteins are targeted into the membrane complex. Based on the genomic data, deletion of several MAPs (MamB, MamQ, MamI, and MamL) leads to the abolishment of magnetosome invagination (Murat et al., 2010) and we can suggest these as hubs for the protein–protein interaction, or as proteins with correct curvatures needed for the magnetosome invagination.

From the prediction of structures it can also be shown that some of the proteins have protein–protein interaction domains (such as PDZ and TPR domains). Such domains can be indicative of the creation of possible protein networks that are involved in magnetosome formation. It has already been shown that such interactions exist between MAPs; for example, between the MamE PDZ domain and the CTD of MamB (Uebe et al., 2011), between MamK and MamJ, and even between MamA and other proteins (Yamamoto et al., 2010). Except for the protein–protein interaction domains there are other redundant predicted domains that appear in magnetosome proteins such as: proteases (MamO and MamE), cytochrome c domains (MamE, MamT, MamX, and MamZ), CDF (MamM and MamB), and transporters (MamO, MamN, MamH, and MamZ). This redundancy can be found in the function of all four genes in the *mamCD* and *mms6* operons which control the size and shape of magnetite crystals (Scheffel et al., 2008). These repetitive functions and domains indicate the ability of the bacteria to ensure magnetosome formation and its activity.

Another question that is raised from protein structure predictions and protein orientations in the magnetosome membrane is why we do not see a gap between the magnetosome membranes and the mineral crystal in electron microscopy (EM) images. In EM experiments of magnetosome vesicles the magnetosome membrane is attached directly to the magnetic particle without a ~3 nm gap that will fit our predicted protein domain (Murat et al., 2010; Abreu et al., 2013). The distance between the magnetosome membrane and the particle is not enough to contain the proteins that are directed to the magnetosome lumen (MamQ, MamE, MamO, MamP, MamX, MamD, and MamZ; Figures 1, 3 and 6). One explanation is that this may be the result of a similar density between the membrane and proteins together with a large contrast between the mineral and the membrane that hinders the detection protein gaps, as seen in EM. Another hypothesis is that protein degradation by magnetosome proteases is taking place during mineral maturation that reduces the proteins' outer membrane domains. Yet, more experiments will need to be conducted in order to resolve this issue.

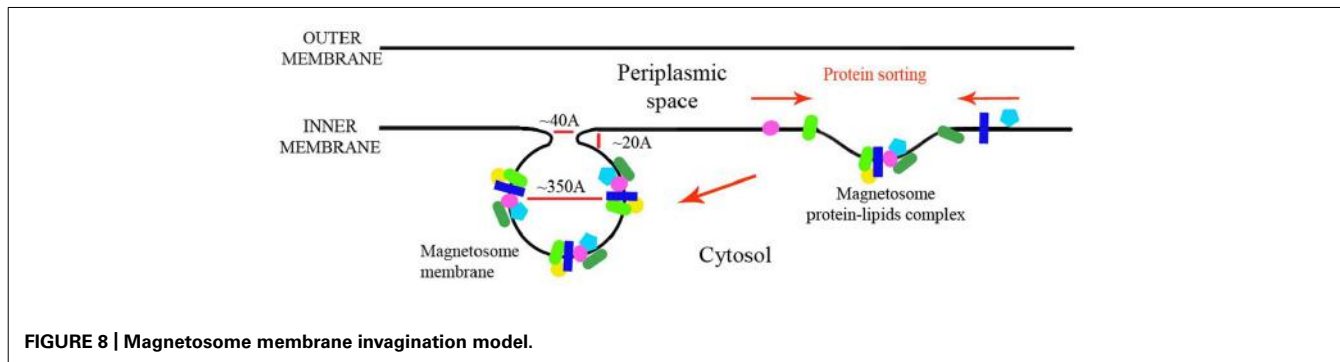
Table 1 | Summary and characteristic of all magnetosome-associated proteins that are encoded in *Magnetospirillum gryphiswaldense* MSR-1 strain.

Protein	Number of amino acid	Transmembrane helices	Domain	Predicted structure template	% Structure confidence or sequence identity (E value)	Major function in
MamE	591	1 (27–48)	Magnetochrome, trypsin and PDZ	2Z9I	100%	Biomineralization
MamT	174	1 (10–28)	Magnetochrome	Secondary structure only	—	Biomineralization
Mamo	632	8 (1-N-terminal, 7-C-terminal)	Trypsin and anion transport	1LCY	17%	Biomineralization, iron transport
MamH	428	12	MFS, similar to MamZ	2XUJ, 4JOD (PiPT)	100%	Biomineralization
Maml	77	2	No conserved domain	Secondary structure only	—	Membrane invagination
MamP	270	1 (N-terminal)	PDZ, magnetochrome	4JJ3 (MamP; MO-1)	—	Biomineralization
MamN	437	11	Na ⁺ /H ⁺ antiporter	4F35 (monomer)	100%	Biomineralization, iron transport and nucleation
MamD	314	1 (C-terminal)	No conserved domain	3C12 (FigD) – only N-terminal	77.10%	Crystal shape
MamM	318	3	CDF, metal carrier	3H90 (FieF)	100%	Iron transport
MamB	297	3	CDF, metal carrier	3H90 (FieF)	100%	Iron transport
MamQ	273	1 (N-terminal)	LemA protein	2ETD (Lema)	100%	MM formation
MamR	72	—	DNA-binding	2KFS (RV2175c)	95.50%	Crystal shape
MamS	180	1 (N-terminal)	OB fold	1NNX (YgiW)	91.80%	Post-nucleation
MamZ	661	18	YedZ-like domain (C-terminal), MFS (N-TER)	1PV4 (GlpT), 3CX5 (cytochrome C)	N-terminal (100%), C-terminal (32.86%)	Biomineralization (C-terminal)
MamJ	426	—	CAR domain mostly unstructured, TonB	Unstructured protein	—	Magnetosome arragment into chain structure
MamK	360		Filaments structure (MreB, ParM)-actin-like, ATP binding site	1JCF (MreB)	100%	Magnetosome arragment into chain structure
MamL	123	2	Similar to MamI	Secondary structure only	—	Membrane invagination

(Continued)

Table 1 | Continued

Protein	Number of amino acid	Transmembrane helices	Domain	Predicted structure template	% Structure confidence or sequence identity (E value)	Major function in
MamA	217	–	TPR	3AS4 (MamA, AMB-1), 3AS8 (MamA, MSR-1, 2MUC (<i>M. bavaricum</i>))	Structure was determinant	Surrounded the magnetosome vesicles
MamU	297	–	DGKs	3T5P	2.00E-15	Membrane invagination
MamX	269	1 (N-terminal)	Similar to MamE and MamS, cytochrome, DNA-binding domain	1OGY, 1JN1, 3ML1, 1QO8 (cytochrome C) 2CQA, 3KDF, 3KF6 (OB fold)	90% (N-terminal)	Crystal maturation
MamY	371	2 (N-terminal)	BAR domain	1S,8 (talin)	69% (C-terminal)	
FtsZ like	323	–	GTPase actin domain	2RHL	95.40 %	Membrane invagination
MamC	125	2	No conserved domain	Secondary structure only	1.00E-92	Crystal size and cell division
MamG	84	2	Similar to MamD and Mms6	Secondary structure only	–	Crystal size and shape
MamF	124	3	Similar to MmsF	Secondary structure only	–	Crystal size and shape
Mms6	136	1	C-terminal highly acidic involved in nucleation	Base on energy calculations of the sequence	–	Crystal size and shape



METHODS

All MTB protein sequences were extracted from the NCBI website², followed by homologous protein and conserved domain searching with the BLAST server³. To analyze the protein sequences and to predict their structures we used several different servers: XtalPred⁴ and PsiPred⁵ were used to identify protein secondary structure (McGuffin et al., 2000; Slabinski et al., 2007). Swiss-Model⁶, HHpred⁷, Phyre⁸, and PsiPred servers were used to predict the protein structures and to identify their possible functions (Guex and Peitsch, 1997; McGuffin et al., 2000; Söding, 2005; Kelley and Sternberg, 2009). Each model structure was energetically minimized in the Swiss PDB Viewer program for a few energy minimization cycles (Guex and Peitsch, 1997). Electrostatic calculations were performed via the APBS tool and images were prepared using PyMOL (Baker et al., 2001; DeLano, 2002). All the obtained model structure files are available at <http://lifeserv.bgu.ac.il/wb/zarivach/pages/research/predicted-structures.php>.

ACKNOWLEDGMENTS

We thank Mr. Samuel Cronin for his help with the manuscript. This study was supported by the Israel Ministry of Science, Technology and Space under the EMBO YIP programme.

REFERENCES

- Abreu, F., Cantão, M. E., Nicolás, M. F., Barcellos, F. G., Morillo, V., Almeida, L. G., et al. (2011). Common ancestry of iron oxide- and iron-sulfide-based biominerization in magnetotactic bacteria. *ISME J.* 5, 1634–1640. doi: 10.1038/ismej.2011.35
- Abreu, F., Sousa, A. A., Aronova, M. A., Kim, Y., Cox, D., Leapman, R. D., et al. (2013). Cryo-electron tomography of the magnetotactic vibrio *Magnetovibrio blakemorei*: insights into the biominerization of prismatic magnetosomes. *J. Struct. Biol.* 181, 162–168. doi: 10.1016/j.jsb.2012.12.002
- Altschul, S. F., Gish, W., Miller, W., Myers, E. W., and Lipman, D. J. (1990). Basic local alignment search tool. *J. Mol. Biol.* 215, 403–410.
- Arakaki, A., Nakazawa, H., Nemoto, M., Mori, T., and Matsunaga, T. (2008). Formation of magnetite by bacteria and its application. *J. R. Soc. Interface* 5, 977–999. doi: 10.1098/rsif.2008.0170
- ²<http://www.ncbi.nlm.nih.gov/>
- ³<http://blast.ncbi.nlm.nih.gov/>
- ⁴<http://ffas.burnham.org/XtalPred-cgi/xtal.pl>
- ⁵<http://bioinf.cs.ucl.ac.uk/psipred/>
- ⁶<http://swissmodel.expasy.org/>
- ⁷<http://toolkit.tuebingen.mpg.de/hhpred>
- ⁸<http://www.sbg.bio.ic.ac.uk/~phyre/>
- Arakaki, A., Webb, J., and Matsunaga, T. (2003). A novel protein tightly bound to bacterial magnetic particles in *Magnetospirillum magneticum* strain AMB-1. *J. Biol. Chem.* 278, 8745–8750. doi: 10.1074/jbc.M211729200
- Arnold, K., Bordoli, L., Kopp, J., and Schwede, T. (2006). The SWISS-MODEL workspace: a web-based environment for protein structure homology modelling. *Bioinformatics* 22, 195–201. doi: 10.1093/bioinformatics/bti770
- Baker, N. A., Sept, D., Joseph, S., Holst, M. J., and McCammon, J. A. (2001). Electrostatics of nanosystems: Application to microtubules and the ribosome. *Proc. Natl. Acad. Sci. U.S.A.* 98, 10037–10041. doi: 10.1073/pnas.181342398
- Balkwill, D. L., Maratea, D., and Blakemore, R. P. (1980). Ultrastructure of a magnetotactic spirillum. *J. Bacteriol.* 141, 1399–408.
- Baumgartner, J., Morin, G., Menguy, N., Perez Gonzalez, T., Widdrat, M., Cosmidis, J., et al. (2013). Magnetotactic bacteria form magnetite from a phosphate-rich ferric hydroxide via nanometric ferric (oxyhydr)oxide intermediates. *Proc. Natl. Acad. Sci. U.S.A.* 110, 14883–14888. doi: 10.1073/pnas.1307119110
- Bazylinski, D. A., Dean, A. J., Williams, T. J., Long, L. K., Middleton, S. L., and Dubbelz, B. L. (2004). Chemolithoautotrophy in the marine, magnetotactic bacterial strains MV-1 and MV-2. *Arch. Microbiol.* 182, 373–387. doi: 10.1007/s00203-004-0716-y
- Bazylinski, D. A., and Frankel, R. B. (2004). Magnetosome formation in prokaryotes. *Nat. Rev. Microbiol.* 2, 217–230. doi: 10.1038/nrmicro842
- Bell, P. E., Mills, A. L., and Herman, J. S. (1987). Biogeochemical conditions favoring magnetite formation during anaerobic iron reduction biogeochemical conditions favoring magnetite formation during anaerobic iron reduction. *Appl. Environ. Microbiol.* 53, 2610–2616.
- Blatch, G. L., and Lässle, M. (1999). The tetratricopeptide repeat: a structural motif mediating protein-protein interactions. *BioEssays news Rev. Mol. Cell. Dev. Biol.* 21, 932–939.
- Bowman, S. E. J., and Bren, K. L. (2008). The chemistry and biochemistry of heme c: functional bases for covalent attachment. *Nat. Prod. Rep.* 25, 1118–1130. doi: 10.1039/b717196j
- Bru, C., Courcelle, E., Carrère, S., Beausse, Y., Dalmar, S., and Kahn, D. (2005). The ProDom database of protein domain families: more emphasis on 3D. *Nucleic Acids Res.* 33, D212–D215. doi: 10.1093/nar/gki034
- Carballido-López, R. (2006). The bacterial actin-like cytoskeleton. *Microbiol. Mol. Biol. Rev.* 70, 888–909. doi: 10.1128/MMBR.00014-06
- Carillo, M. A., Bennet, M., and Faivre, D. (2013). Interaction of proteins associated with the magnetosome assembly in magnetotactic bacteria as revealed by two-hybrid two-photon excitation fluorescence lifetime imaging microscopy förster resonance energy transfer. *J. Phys. Chem. B*, 117, 14642–14648. doi: 10.1021/jp4086987
- Cheng, J., Randall, A. Z., Sweredoski, M. J., and Baldi, P. (2005). SCRATCH: a protein structure and structural feature prediction server. *Nucleic Acids Res.* 33, W72–W76. doi: 10.1093/nar/gki396
- Cohen-Gonsaud, M., Barthe, P., Canova, M. J., Stagier-Simon, C., Kremer, L., Roumestand, C., et al. (2009). The *Mycobacterium tuberculosis* Ser/Thr kinase substrate Rv2175c is a DNA-binding protein regulated by phosphorylation. *J. Biol. Chem.* 284, 19290–19300. doi: 10.1074/jbc.M109.019653
- Cragg, R. A., Christie, G. R., Phillips, S. R., Russi, R. M., Küry, S., Mathers, J. C., et al. (2002). A novel zinc-regulated human zinc transporter, hZTL1, is localized to the enterocyte apical membrane. *J. Biol. Chem.* 277, 22789–22797. doi: 10.1074/jbc.M200577200

- Das, A. K., Cohen, P. W., and Barford, D. (1998). The structure of the tetratricopeptide repeats of protein phosphatase 5: implications for TPR-mediated protein-protein interactions. *EMBO J.* 17, 1192–1199. doi: 10.1093/emboj/17.5.1192
- DeLano, W. L. (2002). PyMol: an open-source molecular graphics tool. *Ccp4 Newslett. Protein Crystallogr.* 40, 11.
- Din, N., Quardokus, E. M., Sackett, M. J., and Brun, Y. V. (1998). Dominant C-terminal deletions of FtsZ that affect its ability to localize in Caulobacter and its interaction with FtsA. *Mol. Microbiol.* 27, 1051–1063. doi: 10.1046/j.1365-2958.1998.00752.x
- Ding, Y., Li, J., Liu, J., Yang, J., Jiang, W., Tian, J., et al. (2010). Deletion of the ftsZ-like gene results in the production of superparamagnetic magnetite magnetosomes in *Magnetospirillum gryphiswaldense*. *J. Bacteriol.* 192, 1097–1105. doi: 10.1128/JB.01292-09
- Dosztányi, Z., Csizmok, V., Tompa, P., and Simon, I. (2005). IUPred: web server for the prediction of intrinsically unstructured regions of proteins based on estimated energy content. *Bioinformatics* 21, 3433–3434. doi: 10.1093/bioinformatics/bti541
- Draper, O., Byrne, M. E., Li, Z., Keyhani, S., Barrozo, J. C., Jensen, G., et al. (2011). MamK, a bacterial actin, forms dynamic filaments in vivo that are regulated by the acidic proteins MamJ and LimJ. *Mol. Microbiol.* 82, 342–354. doi: 10.1111/j.1365-2958.2011.07815.x
- Faivre, D., and Schüler, D. (2008). Magnetotactic bacteria and magnetosomes. *Chem. Rev.* 108, 4875–4898. doi: 10.1021/cr078258w
- Fdez-Gubieda, M. L., Alicia Muela, Javier Alonso, Ana García-Prieto, L. O., and Rodrigo Fernandez-Pacheco, and J. M. B. (2013). Magnetite biominerilization in *Magnetospirillum gryphiswaldense*: time-resolved magnetic and structural studies. *ACS Nano* 7, 3297–3305. doi: 10.1021/nn3059983
- Feng, S., Wang, L., Palo, P., Liu, X., Mallapragada, S. K., and Nilsen-Hamilton, M. (2013). Integrated self-assembly of the mms6 magnetosome protein to form an iron-responsive structure. *Int. J. Mol. Sci.* 14, 14594–14606. doi: 10.3390/ijms140714594
- Frankel, R. B., and Bazylinski, D. A. (2009). Magnetosomes and magneto-aerotaxis. *Contrib. Microbiol.* 16, 182–193. doi: 10.1159/000219380
- Frankel, R. B., Blakemore, R. P., and Wolfe, R. S. (1979). Magnetite in freshwater magnetotactic bacteria. *Science* 203, 1355–1356. doi: 10.1126/science.203.4387.1355
- Fukuda, Y., Okamura, Y., Takeyama, H., and Matsunaga, T. (2006). Dynamic analysis of a genomic island in *Magnetospirillum* sp. strain AMB-1 reveals how magnetosome synthesis developed. *FEBS Lett.* 580, 801–812. doi: 10.1016/j.febslet.2006.01.003
- Gorby, Y. A., Beveridge, T. J., and Blakemore, R. P. (1988). Characterization of the bacterial magnetosome membrane. *J. Bacteriol.* 170, 834–841.
- Greene, S. E., and Komeili, A. (2012). Biogenesis and subcellular organization of the magnetosome organelles of magnetotactic bacteria. *Curr. Opin. Cell Biol.* 24, 490–495. doi: 10.1016/j.cel.2012.05.008
- Gru, K., Mu, E., Otto, A., Reszka, R., Linder, D., Kube, M., et al. (2004). Biochemical and proteomic analysis of the magnetosome membrane in *Magnetospirillum gryphiswaldense*. 70, 1040–1050. doi: 10.1128/AEM.70.2.1040-1050.2004
- Guex, N., and Peitsch, M. C. (1997). SWISS-MODEL and the Swiss-PdbViewer: an environment for comparative protein modeling. *Electrophoresis* 18, 2714–2723. doi: 10.1002/elps.1150181505
- Haney, C. J., Grass, G., Franke, S., and Rensing, C. (2005). New developments in the understanding of the cation diffusion facilitator family. *J. Ind. Microbiol. Biotechnol.* 32, 215–226. doi: 10.1007/s10295-005-0224-3
- Hannavy, K., Barr, G. C., Dorman, C. J., Adamson, J., Mazengera, L. R., Gallagher, M. P., et al. (1990). Ton B protein of *Salmonella typhimurium* A model for signal transduction between membranes. *J. Mol. Biol.* 216, 897–910. doi: 10.1016/S0022-2836(99)80009-6
- Huang, Y., Lemieux, M. J., Song, J., Auer, M., and Wang, D.-N. (2003). Structure and mechanism of the glycerol-3-phosphate transporter from *Escherichia coli*. *Science* 301, 616–620. doi: 10.1126/science.1087619
- Iwanczyk, J., Damjanovic, D., Kooistra, J., Leong, V., Jomaa, A., Ghirlando, R., et al. (2007). Role of the PDZ domains in *Escherichia coli* DegP protein. *J. Bacteriol.* 189, 3176–3186. doi: 10.1128/JB.01788-06
- Katzmann, E., Müller, F. D., Lang, C., Messerer, M., Winklhofer, M., Plitzko, J. M., et al. (2011). Magnetosome chains are recruited to cellular division sites and split by asymmetric septation. *Mol. Microbiol.* 82, 1316–1329. doi: 10.1111/j.1365-2958.2011.07874.x
- Katzmann, E., Scheffel, A., Gruska, M., Plitzko, J. M., and Schüler, D. (2010). Loss of the actin-like protein MamK has pleiotropic effects on magnetosome formation and chain assembly in *Magnetospirillum gryphiswaldense*. *Mol. Microbiol.* 77, 208–224. doi: 10.1111/j.1365-2958.2010.07202.x
- Kelley, L. A., and Sternberg, M. J. E. (2009). Protein structure prediction on the Web: a case study using the Phyre server. *Nat. Protoc.* 4, 363–371. doi: 10.1038/nprot.2009.2
- Kirschvink, J. C. D. R. J. L. (1992). Magnetic domain state and coercivity predictions for biogenic greigite (Fe3S4): a comparison of theory with magnetosome observations. *J. Geophys. Res.* 97 17309–17315. doi: 10.1029/92JB01290
- Komeili, A. (2012). Molecular mechanisms of compartmentalization and biominerilization in magnetotactic bacteria. *FEMS Microbiol. Rev.* 36, 232–255. doi: 10.1111/j.1574-6976.2011.00315.x
- Komeili, A., Li, Z., Newman, D. K., and Jensen, G. J. (2006). Magnetosomes are cell membrane invaginations organized by the actin-like protein MamK. *Science* 311, 242–245. doi: 10.1126/science.1123231
- Komeili, A., Vali, H., Beveridge, T. J., and Newman, D. K. (2004). Magnetosome vesicles are present before magnetite formation, and MamA is required for their activation. *Proc. Natl. Acad. Sci. U.S.A.* 101, 3839–3844. doi: 10.1073/pnas.0400391101
- Lang, C., and Schüler, D. (2008). Expression of green fluorescent protein fused to magnetosome proteins in microaerophilic magnetotactic bacteria. *Appl. Environ. Microbiol.* 74, 4944–4953. doi: 10.1128/AEM.00231-08
- Lee, H.-J., and Zheng, J. J. (2010). PDZ domains and their binding partners: structure, specificity, and modification. *Cell Commun. Signal.* 8, 8. doi: 10.1186/1478-811X-8-8
- Lenz, L. L., Dere, B., and Bevan, M. J. (1996). Identification of an H2-M3-restricted *Listeria* epitope: implications for antigen presentation by M3. *Immunity* 5, 63–72. doi: 10.1016/S1074-7613(00)80310-6
- Li, K.-B. (2003). ClustalW-MPI: ClustalW analysis using distributed and parallel computing. *Bioinformatics* 19, 1585–1586. doi: 10.1093/bioinformatics/btg192
- Lohsse, A., Ullrich, S., Katzmann, E., Borg, S., Wanner, G., Richter, M., et al. (2011). Functional analysis of the magnetosome island in *Magnetospirillum gryphiswaldense*: the mamAB operon is sufficient for magnetite biominerilization. *PLoS ONE* 6:e25561. doi: 10.1371/journal.pone.0025561
- Löwe, J., and Amos, L. A. (1998). Crystal structure of the bacterial cell-division protein FtsZ. *Nature* 391, 203–206. doi: 10.1038/34472
- Lower, B. H., and Bazylinski, D. A. (2013). The bacterial magnetosome: a unique prokaryotic organelle. *J. Mol. Microbiol. Biotechnol.* 23, 63–80. doi: 10.1159/000346543
- Lu, M., Chai, J., and Fu, D. (2009). Structural basis for autoregulation of the zinc transporter YipP. *Nat. Struct. Mol. Biol.* 16, 1063–1067. doi: 10.1038/nsmb.1662
- Mancuso, R., Gregorio, G. G., Liu, Q., and Wang, D.-N. (2012). Structure and mechanism of a bacterial sodium-dependent dicarboxylate transporter. *Nature* 491, 622–626. doi: 10.1038/nature11542
- Mann, S., Sparks, N. H. C., Frankel, R. B., Bazylinski, D. A., and Jannasch, H. W. (1990). Biominerilization of ferrimagnetic greigite (Fe3S4) and iron pyrite (FeS2) in a magnetotactic bacterium. *Nature* 343, 258–261. doi: 10.1038/343258a0
- Marchler-Bauer, A., Lu, S., Anderson, J. B., Chitsaz, F., Derbyshire, M. K., DeWeese-Scott, C., et al. (2011). CDD: a Conserved Domain Database for the functional annotation of proteins. *Nucleic Acids Res.* 39, D225–D229. doi: 10.1093/nar/gkq1189
- McGuffin, L. J., Bryson, K., and Jones, D. T. (2000). The PSIPRED protein structure prediction server. *Bioinformatics* 16, 404–405. doi: 10.1093/bioinformatics/16.4.404
- Mérida, I., Avila-Flores, A., and Merino, E. (2008). Diacylglycerol kinases: at the hub of cell signalling. *Biochem. J.* 409, 1–18. doi: 10.1042/BJ20071040
- Mukherjee, A., and Lutkenhaus, J. (1998). Dynamic assembly of FtsZ regulated by GTP hydrolysis. *EMBO J.* 17, 462–469. doi: 10.1093/emboj/17.2.462
- Murat, D., Falahati, V., Bertinetto, L., Csencsits, R., Körnig, A., Downing, K., et al. (2012). The magnetosome membrane protein, MmsF, is a major regulator of magnetite biominerilization in *Magnetospirillum magneticum* AMB-1. *Mol. Microbiol.* 85, 684–699. doi: 10.1111/j.1365-2958.2012.08132.x
- Murat, D., Quinlan, A., Vali, H., and Komeili, A. (2010). Comprehensive genetic dissection of the magnetosome gene island reveals the step-wise assembly of a prokaryotic organelle. *Proc. Natl. Acad. Sci. U.S.A.* 107, 5593–5598. doi: 10.1073/pnas.0914439107

- Murzin, A. G. (1993). OB(oligonucleotide/oligosaccharide binding)-fold:common structural and functional solution for non-homologous sequences. *EMBO J.* 12, 861–867.
- Niggli, V., Kaufmann, S., Goldmann, W. H., Weber, T., and Isenberg, G. (1994). Identification of functional domains in the cytoskeletal protein talin. *Eur. J. Biochem.* 224, 951–957. doi: 10.1111/j.1432-1033.1994.00951.x
- O'Halloran, T. V., and Culotta, V. C. (2000). Metallochaperones, an intracellular shuttle service for metal ions. *J. Biol. Chem.* 275, 25057–25060. doi: 10.1074/jbc.R000006200
- Ohnishi, K., Ohta, Y., Aizawa, S., Macnab, R. M., and Iino, T. (1994). FlgD is a scaffolding protein needed for flagellar hook assembly in *Salmonella typhimurium*. *J. Bacteriol.* 176, 2272–2281.
- Okuda, Y., Denda, K., and Fukumori, Y. (1996). Cloning and sequencing of a gene encoding a new member of the tetratricopeptide protein family from magnetosomes of *Magnetospirillum magnetotacticum*. *Gene* 171, 99–102. doi: 10.1016/0378-1119(95)00008-9
- Ollis, A. A., and Postle, K. (2012). Identification of functionally important TonB-ExbD periplasmic domain interactions in vivo. *J. Bacteriol.* 194, 3078–3087. doi: 10.1128/JB.00018-12
- Ozyamak, E., Kollman, J., Agard, D. A., and Komeili, A. (2013). The bacterial actin MamK: in vitro assembly behavior and filament architecture. *J. Biol. Chem.* 288, 4265–4277. doi: 10.1074/jbc.M112.417030
- Pallen, M. J., and Wren, B. W. (1997). MicroReview The HtrA family of serine proteases. *Mol. Microbiol.* 26, 209–221. doi: 10.1046/j.1365-2958.1997.5601928.x
- Pao, S., Paulsen, I., and Saier, M. (1998). Major facilitator superfamily. *Microbiol. Mol. Biol Rev.* 62, 1–34.
- Papagrigoriou, E., Gingras, A. R., Barsukov, I. L., Bate, N., Fillingham, I. J., Patel, B., et al. (2004). Activation of a vinculin-binding site in the talin rod involves rearrangement of a five-helix bundle. *EMBO J.* 23, 2942–2951. doi: 10.1038/sj.emboj.7600285
- Park, S.-Y., Borbat, P. P., Gonzalez-Bonet, G., Bhatnagar, J., Pollard, A. M., Freed, J. H., et al. (2006). Reconstruction of the chemotaxis receptor-kinase assembly. *Nat. Struct. Mol. Biol.* 13, 400–407. doi: 10.1038/nsmb1085
- Paulsen, I. T., and Saier, M. H. (1997). A novel family of ubiquitous heavy metal ion transport proteins. *J. Membr. Biol.* 156, 99–103. doi: 10.1007/s00239900192
- Pedersen, B. P., Kumar, H., Waight, A. B., Risnenay, A. J., Roe-Zurz, Z., Chau, B. H., et al. (2013). Crystal structure of a eukaryotic phosphate transporter. *Nature* 496, 533–536. doi: 10.1038/nature12042
- Peter, B. J., Kent, H. M., Mills, I. G., Vallis, Y., Butler, P. J. G., Evans, P. R., et al. (2004). BAR domains as sensors of membrane curvature: the amphiphysin BAR structure. *Science* 303, 495–499. doi: 10.1126/science.1092586
- Quinlan, A., Murat, D., Vali, H., and Komeili, A. (2011). The HtrA/DegP family protease MamE is a bifunctional protein with roles in magnetosome protein localization and magnetite biomimetication. *Mol. Microbiol.* 80, 1075–1087. doi: 10.1111/j.1365-2958.2011.07631.x
- Raschdorf, O., Müller, F. D., Pósfai, M., Plitzko, J. M., and Schüller, D. (2013). The magnetosome proteins MamX, MamZ, and MamH are involved in redox control of magnetite biomimetication in *Magnetospirillum gryphiswaldense*. *Mol. Microbiol.* 86, 872–886. doi: 10.1111/mmi.12317
- Richter, M., Kube, M., Bazylinski, D. A., Lombardot, T., Glöckner, F. O., Reinhardt, R., et al. (2007). Comparative genome analysis of four magnetotactic bacteria reveals a complex set of group-specific genes implicated in magnetosome biomimetication and function. *J. Bacteriol.* 189, 4899–4910. doi: 10.1128/JB.00119-07
- Sam, M. D., Papagiannis, C. V., Connolly, K. M., Corselli, L., Iwahara, J., Lee, J., et al. (2002). Regulation of directionality in bacteriophage λ site-specific recombination: structure of the Xis protein. *J. Mol. Biol.* 324, 791–805. doi: 10.1016/S0022-2836(02)01150-6
- Scheffel, A., Gärdes, A., Grünberg, K., Wanner, G., and Schüller, D. (2008). The major magnetosome proteins MamGFDC are not essential for magnetite biomimetication in *Magnetospirillum gryphiswaldense* but regulate the size of magnetosome crystals. *J. Bacteriol.* 190, 377–386. doi: 10.1128/JB.01371-07
- Scheffel, A., Gruska, M., Faivre, D., Linaroudis, A., Plitzko, J. M., and Schüller, D. (2006). An acidic protein aligns magnetosomes along a filamentous structure in magnetotactic bacteria. *Nature* 440, 110–114. doi: 10.1038/nature04382
- Scheffel, A., and Schüller, D. (2007). The acidic repetitive domain of the *Magnetospirillum gryphiswaldense* MamJ protein displays hypervariability but is not required for magnetosome chain assembly. *J. Bacteriol.* 189, 6437–6446. doi: 10.1128/JB.00421-07
- Scheffers, D., and Driessens, A. J. (2001). The polymerization mechanism of the bacterial cell division protein FtsZ. *FEBS Lett.* 506, 6–10. doi: 10.1016/S0014-5793(01)02855-1
- Schleifer, K.-H., Schüller, D., Spring, S., Weizenegger, M., Amann, R., Ludwig, W., et al. (1991). The genus *Magnetospirillum* gen. nov. description of *Magnetospirillum gryphiswaldense* sp. nov. and transfer of *Aquaspirillum magnetotacticum* to *Magnetospirillum magnetotacticum* comb. nov. *Syst. Appl. Microbiol.* 14, 379–385. doi: 10.1016/S0723-2020(11)80313-9
- Schübbe, S., Kube, M., and Scheffel, A. (2003). Characterization of a spontaneous nonmagnetic mutant of *Magnetospirillum gryphiswaldense* reveals a large deletion comprising a putative magnetosome island. *J. Bacteriol.* 185, 5779–5790. doi: 10.1128/JB.185.19.5779-5790.2003
- Schübbe, S., Würdemann, C., Peplies, J., Heyen, U., Wawer, C., Glöckner, F. O., et al. (2006). Transcriptional organization and regulation of magnetosome operons in *Magnetospirillum gryphiswaldense*. *Appl. Environ. Microbiol.* 72, 5757–5765. doi: 10.1128/AEM.00201-06
- Sheng, M., and Sala, C. (2001). PDZ domains and the organization of supramolecular complexes. *Annu. Rev. Neurosci.* 24, 1–29. doi: 10.1146/annurev.neuro.24.1.1
- Siponen, M. I., Adryanczyk, G., Ginet, N., Arnoux, P., and Pignol, D. (2012). Magnetochrome: a c-type cytochrome domain specific to magnetotactic bacteria. *Biochem. Soc. Trans.* 40, 1319–1323. doi: 10.1042/BST20120104
- Siponen, M. I., Legrand, P., Widdrat, M., Jones, S. R., Zhang, W.-J., Chang, M. C. Y., et al. (2013). Structural insight into magnetochrome-mediated magnetite biomimetication. *Nature* 502, 681–684. doi: 10.1038/nature12573
- Slabinski, L., Jaroszewski, L., Rytlewski, L., Wilson, I. A., Lesley, S. A., and Godzik, A. (2007). XtalPred: a web server for prediction of protein crystallizability. *Bioinformatics* 23, 3403–3405. doi: 10.1093/bioinformatics/btm477
- Söding, J. (2005). Protein homology detection by HMM-HMM comparison. *Bioinformatics* 21, 951–960. doi: 10.1093/bioinformatics/bti125
- Solmarz, S. R. N., and Hunte, C. (2008). Structure of complex III with bound cytochrome c in reduced state and definition of a minimal core interface for electron transfer. *J. Biol. Chem.* 283, 17542–17549. doi: 10.1074/jbc.M710126200
- Sonkaria, S., Fuentes, G., Verma, C., Narang, R., Khare, V., Fischer, A., et al. (2012). Insight into the assembly properties and functional organisation of the magnetotactic bacterial actin-like homolog, MamK. *PLoS ONE* 7:e34189. doi: 10.1371/journal.pone.0034189
- Tanaka, M., Arakaki, A., and Matsunaga, T. (2010). Identification and functional characterization of liposome tubulation protein from magnetotactic bacteria. *Mol. Microbiol.* 76, 480–488. doi: 10.1111/j.1365-2958.2010.07117.x
- Tanaka, M., Mazuyama, E., Arakaki, A., and Matsunaga, T. (2011). MMS6 protein regulates crystal morphology during nano-sized magnetite biomimetication in vivo. *J. Biol. Chem.* 286, 6386–6392. doi: 10.1074/jbc.M110.183434
- Uebe, R., Junge, K., Henn, V., Poxleitner, G., Katzmüller, E., Plitzko, J. M., et al. (2011). The cation diffusion facilitator proteins MamB and MamM of *Magnetospirillum gryphiswaldense* have distinct and complex functions, and are involved in magnetite biomimetication and magnetosome membrane assembly. *Mol. Microbiol.* 82, 818–835. doi: 10.1111/j.1365-2958.2011.07863.x
- Van Blitterswijk, W. J., and Houssa, B. (2000). Properties and functions of diacylglycerol kinases. *Cell. Signal.* 12, 595–605. doi: 10.1016/S0898-6568(00)00113-3
- Wang, C. K., Pan, L., Chen, J., and Zhang, M. (2010). Extensions of PDZ domains as important structural and functional elements. *Protein Cell* 1, 737–751. doi: 10.1007/s13238-010-0099-6
- Wawer, C., Tebo, B. M., Gru, K., and Schu, D. (2001). A large gene cluster encoding several magnetosome proteins is conserved in different species of magnetotactic bacteria. *Appl. Environ. Microbiol.* 67, 4573–4582. doi: 10.1128/AEM.67.10.4573-4582.2001
- Yamamoto, D., Taoka, A., Uchihashi, T., Sasaki, H., Watanabe, H., Ando, T., et al. (2010). Visualization and structural analysis of the bacterial magnetic organelle

- magnetosome using atomic force microscopy. *Proc. Natl. Acad. Sci. U.S.A.* 107, 9382–9387. doi: 10.1073/pnas.1001870107
- Yang, W., Li, R., Peng, T., Zhang, Y., Jiang, W., Li, Y., et al. (2010). mamO and mamE genes are essential for magnetosome crystal biominerization in *Magnetospirillum gryphiswaldense* MSR-1. *Res. Microbiol.* 161, 701–705. doi: 10.1016/j.resmic.2010.07.002
- Zeytuni, N., Baran, D., Davidov, G., and Zarivach, R. (2012). Inter-phylum structural conservation of the magnetosome-associated TPR-containing protein, MamA. *J. Struct. Biol.* 180, 479–487. doi: 10.1016/j.jsb.2012.08.001
- Zeytuni, N., Ozyamak, E., Ben-Harush, K., Davidov, G., Levin, M., Gat, Y., and Moyal, T. (2011). Self-recognition mechanism of MamA, a magnetosome-associated TPR-containing protein, promotes complex assembly. *Proc. Natl. Acad. Sci. U.S.A.* 108, E480–E487. doi: 10.1073/pnas.1103367108
- Zhang, Y., Appleton, B. A., Wu, P., Wiesmann, C., and Sidhu, S. S. (2007). Structural and functional analysis of the ligand specificity of the HtrA2/Omi PDZ domain. 16, 1738–1750.

Conflict of Interest Statement: The authors declare that the research was conducted in the absence of any commercial or financial relationships that could be construed as a potential conflict of interest.

Received: 11 September 2013; accepted: 08 January 2014; published online: 29 January 2014.

Citation: Nudelman H and Zarivach R (2014) Structure prediction of magnetosome-associated proteins. *Front. Microbiol.* 5:9. doi: 10.3389/fmicb.2014.00009

This article was submitted to Aquatic Microbiology, a section of the journal *Frontiers in Microbiology*.

Copyright © 2014 Nudelman and Zarivach. This is an open-access article distributed under the terms of the Creative Commons Attribution License (CC BY). The use, distribution or reproduction in other forums is permitted, provided the original author(s) or licensor are credited and that the original publication in this journal is cited, in accordance with accepted academic practice. No use, distribution or reproduction is permitted which does not comply with these terms.



The effect and role of environmental conditions on magnetosome synthesis

Cristina Moisescu^{1*}, Ioan I. Ardelean¹ and Liane G. Benning²

¹ Department of Microbiology, Institute of Biology Bucharest, Bucharest, Romania

² School of Earth and Environment, University of Leeds, Leeds, UK

Edited by:

Damien Faivre, Max Planck Society, Germany

Reviewed by:

Zongze Shao, State Oceanic Administration, China

Mihály Pósfai, University of Pannonia, Hungary

***Correspondence:**

Cristina Moisescu, Department of Microbiology, Institute of Biology Bucharest, 296 Splaiul Independentei, Bucharest 060031, Romania

e-mail: cristina.moisescu@ibiol.ro

Magnetotactic bacteria (MTB) are considered the model species for the controlled biominerization of magnetic Fe oxide (magnetite, Fe_3O_4) or Fe sulfide (greigite, Fe_3S_4) nanocrystals in living organisms. In MTB, magnetic minerals form as membrane-bound, single-magnetic domain crystals known as magnetosomes and the synthesis of magnetosomes by MTB is a highly controlled process at the genetic level. Magnetosome crystals reveal highest purity and highest quality magnetic properties and are therefore increasingly sought after as novel nanoparticulate biomaterials for industrial and medical applications. In addition, "magnetofossils," have been used as both past terrestrial and potential Martian life biosignature. However, until recently, the general belief was that the morphology of mature magnetite crystals formed by MTB was largely unaffected by environmental conditions. Here we review a series of studies that showed how changes in environmental factors such as temperature, pH, external Fe concentration, external magnetic fields, static or dynamic fluid conditions, and nutrient availability or concentrations can all affect the biominerization of magnetite magnetosomes in MTB. The resulting variations in magnetic nanocrystals characteristics can have consequence both for their commercial value but also for their use as indicators for ancient life. In this paper we will review the recent findings regarding the influence of variable chemical and physical environmental control factors on the synthesis of magnetosome by MTB, and address the role of MTB in the global biogeochemical cycling of iron.

Keywords: magnetotactic bacteria, biominerization, environmental conditions, magnetite characteristics, biogeochemistry

INTRODUCTION

Biominerization represents the process by which living organisms produce minerals (Walcott et al., 1979). Biominerization is a widespread phenomenon, and all six taxonomic domains include members capable of inducing the synthesis of biominerals (Clark and Evans, 1997; Kirschvink et al., 2001). Minerals formed through biological means can be extracellular or intracellular. They are diverse and they often have specific functions. For example, Fe_3O_4 biominerals act as magnetic sensors (Hesse, 1994; Lohmann et al., 2001), CaCO_3 protects against predation (Gower, 2008), CaCO_3 , CaSO_4 , or BaSO_4 are important as gravitational sensors (Halstead, 1994) while Fe_2O_3 biominerals passivate surfaces and help reduce corrosion (Rothman and Wieland, 1996).

Prokaryotes play a major role in the deposition and weathering of minerals in the Earth's crust (Frankel and Bazylinski, 2003; Lefèvre and Bazylinski, 2013). Yet, inorganic, metal-rich intracellular minerals are not so commonly found in the prokaryotic genera (Fortin and Langley, 2005). The synthesis of minerals by prokaryotes can be classified into biologically induced mineralization (BIM) and biologically controlled mineralization (BCM) (Lowenstam, 1981; Lowenstam and Weiner, 1989). Minerals that form by BIM processes generally nucleate and grow extracellularly, as an unintended and uncontrolled consequence of metabolic activities. These minerals (also often called

biominerals) are however most often characterized by poor crystallinity, broad particle-size distributions, and a lack of specific crystal morphologies. Therefore, BIM is equivalent to inorganic mineral formation under equivalent environmental conditions. Furthermore, the minerals produced by BIM are in general indistinguishable from the minerals produced by purely inorganic chemical reactions (Frankel and Bazylinski, 2003). In contrast, in BCM, minerals are usually deposited on or within the cell, the organism exerting a significant degree of control over the nucleation and growth of the minerals and thus over the composition, size, habit, and intracellular location of the minerals (Bazylinski and Frankel, 2000). The BCM process is therefore a highly controlled process at the metabolic and genetic level. These are true biominerals. As the topic of this paper is the intracellular biominerization in bacteria, the BIM process will not be further discussed and all our focus will be on BCM biomineralization with specific emphasis on iron biominerals.

One of the most interesting and most studied examples of BCM, with respect to the synthesis of Fe minerals, is the formation of bacterial magnetosomes (Lower and Bazylinski, 2013). Microbial magnetosomes represent a special category of intracellular organelles that are synthesized by magnetotactic bacteria (MTB), which use the magnetosomes for geomagnetic navigation in their aquatic habitat. The unique characteristics and properties of magnetosomes that will be discussed below have in the last few

decades attracted huge interest, because their properties can be exploited for a variety of applications. These span many diverse disciplines from microbiology, cellular biology, geobiology, and bio(nano)technology (Bazylinski and Frankel, 2000; Lang et al., 2007; Schuler, 2008). Furthermore, magnetosome biominer-alization and their assembly in chains is of great interest for the production of biologically inspired magnetic materials, and they have also been suggested as potential biomarker for detection of extant life signatures on other planets (McKay et al., 1996).

The formation of magnetosomes represents a fascinating example of how apparently simple organisms can translate genetic information into extremely complex inorganic cellular structures (Jogler and Schüller, 2009). A plethora of fundamental biominer-alization mechanisms are crucial during magnetosome synthesis and thus MTB can serve as a relatively simple and accessible model for the study of biominer-alization processes in general. From the pioneering paper of Blakemore (1975), the subject of magnetosome biominer-alization has evolved to a unique and interdisciplinary area of research. It is not the scope of this paper to review the whole literature about the role of MTB and magnetosomes but we will focus our review on the effect of different chemical and physical environmental factors on the synthesis of magnetosome by MTB, and address the role of MTB in the global biogeochemical cycling of iron.

MAGNETOSOME SYNTHESIS

Presently, three minerals with magnetic properties, magnetite (Fe_3O_4), maghemite (Fe_2O_3), and greigite (Fe_3S_4) have been identified in different organisms, from prokaryotes to complex organisms (including humans) (Kirschvink and Hagadorn, 2000). Despite the fact that several studies have addressed the localization and characterization of cellular ultrastructures of ferromagnetic inclusions in various organisms, most of the presently available information comes from the studies of MTB. The intra-cellular magnetic particles produced by MTB reflect best the optimization processes of natural selection.

MAGNETOSOME CRYSTALS SYNTHESIZED BY MTB

The term “magnetotactic bacteria” represents a morphological, metabolical, and phylogenetical diverse group of prokaryotes capable of passively aligning and actively swimming parallel to the geomagnetic field lines (Bazylinski and Frankel, 2004). MTB were first described in 1891 in the work of Massart (1891) and in the studies of Bellini (1963a,b) as a group of bacteria in which the direction of movement is apparently influenced by the magnetic field. Only their accidental rediscovery in 1974 by Blakemore (1975) re-initiated and stimulated new research activities over the last few decades. MTB represent a collection of diverse bacteria that possess the most unambiguous magnetoreceptive behavior called magnetotaxis (Blakemore, 1982). It was proposed that in natural environments magnetotaxis may enable the cells to locate and maintain an optimal position in the water column or in sediments, and that this aligns with their main metabolic needs (Ardelean et al., 2008). In addition, in contrary to a true taxis, the magnetic assisted taxis could help MTB in their navigation toward optimum growth conditions, when a magnetic field is present, therefore reducing a tri-dimensional search

to a more advantageous single-dimensional one (Bazylinski and Frankel, 2004). The great diversity of MTB is expressed in different cell morphologies, a cosmopolitan distribution, and different phylogenetic traits (Fassbinder et al., 1990; Bazylinski and Frankel, 2004; Bazylinski and Lefevre, 2013). Despite their diversity, all MTB are Gram-negative, motile by means of monotrichous, bipolar or lophotrichous flagella, and all possess a microaerophilic (Schleifer et al., 1991; Spring et al., 1993) or anaerobic, sulfate-reducing respiratory metabolism (Bazylinski et al., 1988; Sakaguchi et al., 1993). Furthermore, in MTB cell division occurs at a central point of the cells and the magnetosome chains are cleaved into two even chains with the resulting number of magnetosomes being directly proportional to the cell length (Staniland et al., 2010). The most important characteristic that sets them apart from other bacteria is their ability to synthesize nanometer-sized crystals of a magnetic mineral that is either magnetite (Fe_3O_4) (Frankel et al., 1979), greigite (Fe_3S_4) (Mann et al., 1990) or both (Bazylinski et al., 1993b, 1995; Lins et al., 2007). The formation of such magnetosomes through a biominer-alization process is highly genetically controlled and this leads to magnetic crystals that are of exceptional high purity, specific sizes and shapes and that assemble in well-ordered chains, that ultimately function as an extremely efficient magnetic sensor (Rodgers et al., 1990; Schuler, 1999). Even though the composition, size and morphology of the magnetic crystals may vary from species to species they are highly conserved within the same bacterial species or genus (Bazylinski et al., 1994). The high chemical purity of MTB magnetosomes, and magnetite’s in particular (Bazylinski, 1995; Bazylinski and Frankel, 2000), is not surprising. As compared to their mineralogical equivalent, the incorporation of trace elements reduces the magnetic moment of the abiotically formed magnetite particles (Kopp and Kirschvink, 2008). Although for many years it was believed that in magnetite, Fe cannot be replaced by other transition metal ions such as Ti, Cr, Co, Cu, Ni, Hg or Pb, recent studies showed that this is not universally applicable. For example, Ti was discovered in magnetite particles of an uncultured magnetotactic coccus (Towe and Moench, 1981), Mn in the magnetite particles of a brackish-to-marine coccus (Keim et al., 2009), and Co in the magnetite magnetosomes from three species of *Magnetospirillum* (Staniland et al., 2008). The effects that these “impurities” have on magnetosome characteristics are discussed in section The Effect of Chemical Impurities. The second most common mineral type forming MTB magnetosomes is greigite. Compared to magnetite, greigite magnetosome crystals are less strictly controlled, both chemically and crystallographically and some greigite-producers can incorporate up to 10 atom% Cu into their crystals (Bazylinski et al., 1993a; Pósfai et al., 1998). Although the reason for these differences is not yet fully understood, the main difference is most likely linked to the mechanisms of formation of magnetite vs. greigite. In abiotic systems, experimental studies have shown that magnetic nanocrystals of greigite form in reducing environments most often via a nanocrystalline, non-stoichiometric Fe^{2+} precursor, mackinawite (Cahill et al., 2000; Hunger and Benning, 2007; Csákberényi-Malasics et al., 2012), while magnetite forms often via reductive dissolution of an Fe^{3+} precursor, ferrihydrite (Lovley, 1991; Hansel et al., 2003).

The physical volume and shape of individual magnetite crystals determine how well grains function as discrete bar magnets. Both mature magnetite and greigite magnetosome crystals vary in size between 30 and 120 nm (Bazylinski et al., 1994; Frankel et al., 1998; Moisescu et al., 2008; Pósfai et al., 2013). This is also the size range that characterizes the single magnetic domain crystals (SD) (Butler and Banerjee, 1975; Moskowitz, 1995). Although the boundary between the single magnetic and multi magnetic domain for greigite may be at much larger sizes (Hoffmann, 1992), in general, for both minerals, the isolates with sizes smaller than 30 nm fall within the superparamagnetic region (SPM) and the ones greater than 120 nm have multiple magnetic domains and are called multi-domain magnetic crystals (MD). The crystals best suited for magnetoreception are SD crystals, and these are usually preferred and propagated during their evolution into magnetosomes inside MTB.

Biominerals formed by MTB consist of highly uniform crystals with narrow crystal size distributions (CSD) and shape factors (SFD) (Devouard et al., 1998; Arato et al., 2005; Jandacka et al., 2013). In the last few decades various studies (Meldrum et al., 1993; Pósfai and Arato, 2000) have shown that crystal size distribution curves of MTB magnetosomes are normal asymmetric and negatively skewed with sharp cut-offs toward larger sizes. In contrast, magnetite crystals produced in abiotic reactions lead to magnetite crystals with low crystallinity and log normal broad size distributions. The strict control of biomineralization exerted by MTB stops the magnetosomes from growing once they reached a certain, strain-specific size. Only few exceptions to this universal rule are known and these are MTB that produce Gaussian size distributions (Devouard et al., 1998; Pósfai et al., 2001; Arato et al., 2005).

The three most common MTB-produced magnetosome magnetite crystal morphologies are equidimensional cubo-octahedra, elongate hexa-octahedral prisms, and irregular and elongate tooth, bullet, arrowhead (Mann et al., 1987; Thornhill et al., 1994), or arrow-head (Bazylinski et al., 1995) shapes. Common magnetosome greigite morphologies include equidimensional cubo-octahedra and pleiomorphic elongate rectangular prisms (Bazylinski et al., 1994; Pósfai et al., 1998). Furthermore, under non-stressed environmental conditions the shapes of specific magnetosome crystals appear to be constant within given species or strains for both magnetite and greigite magnetosomes although minor variations of shape and size can occur primarily in greigite magnetosomes (Pósfai et al., 1998). However, as we will discuss below in section Influence of Environmental Factors on Magnetosome Characteristics, stressed environments can induce dramatic changes in shapes and sizes of magnetite magnetosomes.

Idealized crystal habits for magnetite, derived from high-resolution electron microscopic studies, are most often combinations of {100} (cube), {110} (dodecahedron), and {111} (octahedron) forms. The idealized habits of cuboidal magnetosome crystals are cubo-octahedra, composed of {100} + {111} forms with equal development of the six symmetry-related faces of the {100} form and the eight symmetry-related faces of the {111} form (Mann et al., 1984). In MTB with elongate magnetite particles, the crystals are typically elongated along a [111] axis (the “easy” direction of

magnetization), with some exceptions (Mann et al., 1987; Taylor and Barry, 2004). Greigite crystals are often elongated along the [100] axis (Pósfai et al., 1998), considered by some the greigite magnetocrystalline “easy” axis (Bazylinski and Moskowitz, 1997).

Crystallographic defects are rare in magnetite magnetosomes grown by MTB under optimal conditions (Devouard et al., 1998), the only deviation from an ideal structure being the spinel-law twins, stacking-fault defects or sub-grain boundaries. With the exception of twinning along the [111] easy axis, crystallographic defects usually reduce the magnetic moment of magnetite particles. In contrast, greigite magnetosome crystals commonly exhibit planar defects along (222) planes, uneven contrast or wrinkles, believed to be associated with the conversion of the precursor mackinawite into greigite (Pósfai et al., 1998; Hunger and Benning, 2007). These differences imply once again that greigite formation by MTB is less well regulated compared to magnetite magnetosome formation and the smaller differences between magnetosome greigite crystals and abiotic greigite crystals could hamper identification of greigite magnetofossils.

MAGNETOSOME CRYSTALS SYNTHESIZED BY OTHER ORGANISMS

In the last few decades it was discovered that not only MTB are capable of producing magnetic intracellular inclusions. Other organisms, starting with single cell prokaryotes and even multicellular eukaryotes, may contain various metal or metalloid inclusions with magnetic properties. These are known as non-crystal magnetosomes or magnet-sensitive inclusions (Vainshtein et al., 1997; Kirschvink et al., 2001; Ariskina, 2003; Langley, 2006). These metal-rich magnetic intracellular inclusions seem to have a widespread distribution (in 4 of 6 Kingdoms), similar species specific shapes and sizes, and the producing organisms seem to be apart on the evolutionary scale. However, few details are known about these other organisms that produce such magnetites and additional in depth studies to address their occurrence in prokaryotic genera and in other animals through thorough microbiological, chemical, crystallographic, and high-resolution electron microscopic and spectroscopic analyses are needed. The formation or characteristics of these non-crystal magnetosomes will not be pursued further in the present paper and below we will concentrate only on crystalline magnetosomes found in MTB, disregarding the non-crystal magnetic inclusions found in other species (Ariskina, 2003; Fortin and Langley, 2005; Pósfai and Dunin-Borkowski, 2009).

INFLUENCE OF ENVIRONMENTAL FACTORS ON MAGNETOSOME CHARACTERISTICS

Despite their relatively ubiquitous distribution, MTB were for a long time considered to be mesophilic and neutrophilic microorganisms with regard to their growth temperature and pH. Only recently, due to the discovery of new thermophilic and alkaliphilic species, have MTB been re-classified as extremophilic (Bazylinski and Lefevre, 2013). These newly discovered extremophilic MTB behave similarly to mesophilic MTB, in that their magnetosomes, although synthesized under extreme conditions, are very similar to magnetosomes formed in moderate environments. This new discovery extends significantly the range of environmental parameters at which MTB can survive, grow, and

synthesize magnetosomes. These extremophilic MTB most likely either evolved from other thermophilic or alkaliphilic non-magnetotactic strains, that for some reason, gained the ability to synthesize magnetosomes, or simply from mesophilic MTB that adapted with time to a specific extreme environment, yet without losing the ability to synthesize magnetosomes. However, what happens with MTB when the environmental conditions change rapidly and the bacteria need to adapt fast or do not have time to adapt? How do such abrupt changes affect magnetosome synthesis or bacterial growth? Faivre et al. (2008) suggested that the variation in environmental parameters such as Fe bioavailability, pH and temperature, could have a considerable impact on cell physiology and consecutively on the physical and microstructural characteristics of bacterially formed magnetite crystals. Yet, only few studies have addressed this subject. Below we review all studies that tested the effects and roles of multiple environmental parameter variations on magnetite magnetosome synthesis and discuss how the changes in these parameters can result in changes in the possible commercial value of MTB magnetosome crystal or their potential use as indicators for ancient life.

THE EFFECT OF Fe CONCENTRATION, pH, AND TEMPERATURE

Iron is particularly important in MTB not only for its function as a protein cofactor but mostly for the BCM of the nanometer-sized Fe mineral crystals within their cells. Faivre et al. (2008) showed that the sizes and morphologies of mature magnetosomes synthesized by *M. gryphiswaldense* MSR-1 (DSM 6361) are influenced by the initial Fe availability. Although the mean particle size of the studied magnetosomes was similar to that of the reference magnetosomes, the physical properties such as CSD, aspect ratio, and morphology were significantly different. They showed that an initial Fe starvation period followed by the addition of Fe^{3+} lead to an induced synthesis of magnetosomes with positively skewed broad shape CSDs and irregular morphologies. The majority of the formed crystals revealed a cube-like shape, with small (110) and (111) faces. In these induced cells, a rate of Fe^{3+} uptake of $30 \text{ nmol min}^{-1} (\text{mg dry weight})^{-1}$ was measured. This is 30 times higher compared to $\sim 1 \text{ nmol min}^{-1} (\text{mg dry weight})^{-1}$ measured for permanently iron-supplemented cells. In addition, the change from a generally cubo-octahedral morphology in the reference magnetosomes, to shapes with nearly equal (100) and (111) faces and little to no expression of (110) faces, indicates that the biological control over magnetite biomineralization by this strain of MTB was highly affected by the variation of environmental parameters. This shows that—at least in this case, Fe uptake rates occupied a key role in controlling magnetosome crystal formation. The authors concluded that the cells could not cope with such high Fe uptake rates, and thus they exerted a lesser biochemical control over the mineralization process. They also concluded that a slower uptake rate will result in the formation of crystals with classical crystal shape and sizes. Furthermore, the Faivre et al. (2008) study also showed that variations in iron uptake need to be taken into consideration when defining and evaluating any morphological biomarker signatures because under varying environmental conditions MTB can form magnetosomes with unexpected morphologies (Faivre et al., 2008).

In view of this conclusion, our recent study (Moisescu et al., 2011) aimed to mimic other possible environmental variations, such as pH and temperature and to co-evaluate the Fe uptake rates under these changing conditions. We grew first *M. gryphiswaldense* MSR-1 (DSM 6361) at optimum conditions (i.e., pH 7.0 and 28°C) and our Fe uptake rates, crystal morphologies, and sizes were in good agreement with many other MTB studies at optimal conditions (Schuler and Baeuerlein, 1996; Schubbe et al., 2003; Faivre et al., 2008). From these experiments, we determined an Fe uptake rate of v_{\max} of $0.8 \text{ nmol min}^{-1} (\text{mg dry weight})^{-1}$ which is close to most literature values reported for studies with the same strain also grown at optimum conditions. Not surprisingly, when the temperature and especially the pH were shifted away from the optimum (i.e., we varied temperature between 4 and 35°C and pH between 5.0 and 9.0), the ability of MSR-1 to control the biomineralization process was altered. These variations in environmental growth conditions resulted in the synthesis of magnetites with a dramatically changed range in crystal sizes and crystal morphologies (Figures 1A–C) and culminated in the formation of unique pyramidal morphologies that had never been described before in any other biotic or abiotic systems (Figure 1D).

Our results revealed that at ambient conditions when we changed the pH of the growth medium, we observed at all pH values (except at pH 5.0) still high levels of Fe uptake, but interestingly we also observed changes in the formed magnetosomes. Overall, the determined uptake rates were 4–17 times slower than those measured at the optimum pH 7.0. According to Faivre et al. (2008), a slower Fe uptake rate will determine the synthesis of magnetosomes with better-defined sizes and shapes. Apparently this does not apply in the case of pH variations. The magnetites synthesized at pH 6.0 (Figure 1A) were equivalent

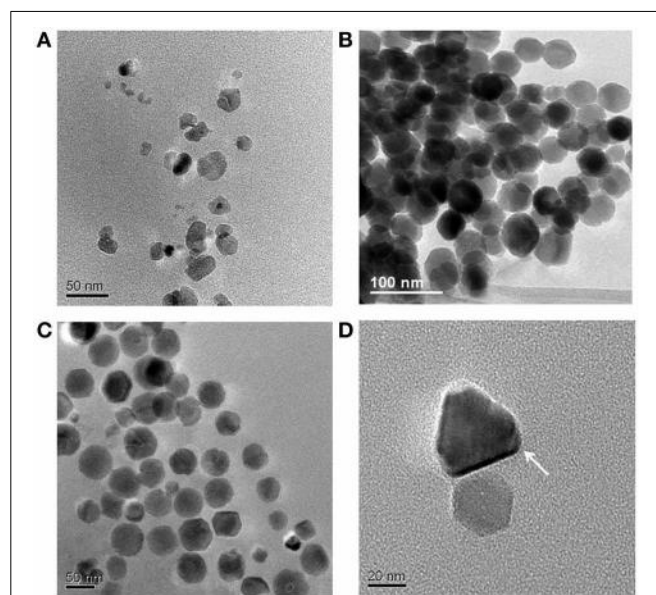


FIGURE 1 | TEM images of magnetite crystals synthesized by *M. gryphiswaldense* cells grown at 28°C and at different pH values: (A) 6.0; (B) 7.0; (C) 8.0; (D) 9.0.

to immature, poorly developed, or extracellular crystals formed through a BIM process (Devouard et al., 1998; Faivre and Zuddas, 2006; Faivre et al., 2008). These crystals were usually very small and characterized by poor crystallinity, no specific morphology, and the majority fell into the SPM. They had broad, asymmetric, and positively skewed normal CSDs, with sharp cut-offs toward smaller sizes and a $SFD < 0.75$, characteristics typical for immature or abiotic magnetites. At pH 8.0 (**Figure 1C**), we found larger SD crystals, with roundish morphologies, and asymmetric negatively skewed CSD and SFD, characteristics more similar to typical intracellular magnetites synthesized by MTB. The main difference observed between crystals formed at pH 6.0 and those formed at pH 9.0 was the well-defined crystal morphology and the appreciably bigger sizes of the pH 9.0 crystals and the fact that they mostly plotted in the SD region. Interestingly, at pH 9.0 an unexpected anisotropic, pyramidal crystal habit was observed (**Figure 1D**), which makes these crystals unique among both biotic and abiotic magnetites and in principle, this morphology could constitute a physical signature of a biological origin.

The second variable we tested was temperature (Moisescu et al., 2011). In contrast to the changes we observed due to variations in pH, our results revealed that temperature variations had a far weaker effect. Changing temperature during magnetosome growth lead either to a total inhibition of magnetosome synthesis (at 4 and 35°C) or showed no modifications in sizes and shapes of the synthesized magnetites (at 10 and 20°C) compared to the optimal temperature conditions (28°C).

These results suggest that it is not only the Fe uptake rate that influenced the size and morphology of magnetite crystals formed by MTB but that other environmental factors, especially pH, also have a great impact on the number, size, and morphology of magnetite crystals synthesized by MTB.

THE EFFECT OF CHEMICAL IMPURITIES

Many studies showed that MTB cells have a high affinity and specificity for Fe and are capable of up-taking Fe even from very limited concentrations (Nakamura et al., 1993; Schuler and Baeuerlein, 1996; Dubbels et al., 2004). Whereas greigite magnetosomes can contain different metal impurities (Bazylinski et al., 1993a; Pósfa et al., 1998), magnetite was considered for a long time to be of exceptionally high chemical purity, a characteristic that has for a long time been used to discriminate magnetosome magnetite crystals from abiotic crystals.

Recently, however Staniland et al. (2008) showed that magnetosomes containing Co could be produced by three strains of *Magnetospirillum*. *In vivo* Co doping of magnetosomes was achieved (reaching 0.2–1.4% Co) and the magnetite magnetosomes synthesized in the Co systems were slightly larger, more uniform in size and with a narrower CSD, and nearly isotropic or of slightly elongated shapes that aligned parallel to the direction of the chain. An increase in the coercive field of these particles by 36–45% was also attributed to the effect of Co doping. The Co was found to be localized more in the surface layer of the crystal than in the core, indicating that in the initial phases of magnetosome formation, Fe was the preferred magnetosome seed material. Although some crystal imperfections appeared in the

Co-doped magnetosomes, so far additional details about these effects are lacking.

Another study followed the Mn accumulation by an uncultured MTB from a coastal lagoon in Rio de Janeiro (Keim et al., 2009). The authors showed that when exposed to a high metal concentration this uncultured strain could incorporate into some of the growing magnetite crystals up to 2.8 atom% Mn with respect to the total metal content (Fe/Mn). In those magnetosomes where high Mn contents were observed, the Mn ions were always colocalized with Fe, and the Mn was homogeneously dispersed throughout the entire magnetite structure and not only on the surface of the crystal as in the case of Co.

These two reports of Co and Mn ions incorporated in magnetite crystals formed by both cultured and uncultured MTB, suggest the possibility that other metal impurities commonly found in inorganic magnetite, such as Ti, Cr, and Zn (Clark and Evans, 1997) could also be incorporated in bacterial magnetite. However, so far, studies done to elucidate the exact mechanisms and effects of such metal impurities are still inconclusive (Towe and Moench, 1981; Keim et al., 2001). This means that the high chemical purity that used to be a prime biosignature of magnetotactic magnetite crystals can no longer be taken as a strict characteristic for the biogenic origin of magnetite crystals.

THE EFFECT OF OXYGEN ON MAGNETITE FORMATION UNDER STATIC OR DYNAMIC FLUID CONDITIONS

The majority of MTB species have a microaerophilic or anaerobic respiratory metabolism. Many studies showed that the concentration of O_2 during MTB growth has a huge influence on magnetite magnetosome synthesis because it can impair the development of magnetosomes (Schuler and Baeuerlein, 1998; Heyen and Schuler, 2003). Therefore, magnetosome development is strictly correlated with a narrow range of (low) O_2 concentrations.

Popa et al. (2009) evaluated the effects of various levels of initial O_2 and of various liquid: gas ratios on cultures of *M. magneticum* (strain AMB-1). They monitored magnetite magnetosome formation at different initial O_2 levels, with or without stirring. Their results revealed that under O_2 -stress but stirred ($\geq 45 \mu M O_2/150 rpm$) 95% of the formed magnetite crystals were dwarf magnetites. These dwarf magnetites consisted of non-euhedral spheroids ($\sim 25 nm$, with some as small as 10 nm) very similar in shape and size to immature crystals that had formed in equivalent cell cultures grown at optimum O_2 concentrations. Some of the formed particles were also elongated yet still non-euhedral in shape. In addition, a slightly elevated number of non-aligned magnetite particles per cell (11 ± 2 vs. $\sim 5 \pm 2\%$ in cells with normal magnetite particles) were observed. All magnetite crystals that formed under O_2 -stress were SD magnetite, and none showed a SP behavior. The magnetic signatures, Fe^{2+}/Fe^{3+} , ratios and XRD patterns were comparable to mature magnetite crystals formed in cultures grown at normal O_2 concentrations ($\leq 18.7 \mu M O_2/150 rpm$) (Popa et al., 2009). In stirred growth experiments carried out at higher levels of O_2 ($50–100 \mu M/150 rpm$), magnetite biominerilization was strongly inhibited. Conversely, in fully anaerobic conditions (i.e., 0% O_2) only normal (euhedral, SD) mature crystals formed. These results suggest that O_2 concentration is in fact important for magnetite

synthesis, whereas stirring alone has no other influence than to enhance the O₂ effect.

These observations are supported by the results of Li and Pan (2012) who showed that under aerobic and anaerobic but using four different stirring growth conditions (anaerobic static, aerobic static, aerobic-80 rpm rotating, and aerobic-120 rpm rotating), the O₂ parameter was the one parameter that truly affected the biomineralization of magnetite magnetosomes in *M. magneticum* strain AMB-1. When stirred (120 rpm) anaerobic and aerobic conditions were compared, the data revealed that in the presence of high O₂ contents the cells produced fewer magnetosomes and these were of decreasing grain sizes. The CSD of the magnetosomes was negatively skewed and relatively wide. For the anaerobic and aerobic static cultures predominantly SD particles were observed, while a near normal and narrow distribution with a mixture of SD and SPM particles were observed in the aerobic-80 and –120 rpm stirred cultures. The SFDs indicated a change in crystal shape from more elongated to cubic-like crystals. The magnetosomes produced under the four different stirred conditions were mostly arranged into a single linear fragmented chain. Among the magnetosomes in each chain the frequency of twinned crystals (occasionally even multiple twins) increased gradually, reaching a maximum in the aerobic-120 rpm stirred cultures. High resolution electron microscopy studies confirmed that the magnetosomes formed by these AMB-1 cells were pure magnetite, with a truncated octahedron crystal habit (Li and Pan, 2012). Although the magnetite produced under anaerobic and aerobic stirred growth conditions had similar CSD and SFD, there was a 2 K decrease in the Verwey transition and a 27% decrease in the magnetic coercivity for the aerobically grown magnetites. These changes clearly demonstrate that O₂ concentration dramatically influences the biomineralization of magnetite magnetosomes confirming the Popa et al. (2009) results. However, the Li and Pan (2012) results also revealed that stirring does not seem to significantly affect magnetosome formation.

THE EFFECT OF EXTERNAL MAGNETIC FIELDS ON MAGNETITE MAGNETOSOME FORMATION

In order to evaluate the role of the geomagnetic field on magnetite magnetosome biomineratization Wang et al. (2008) conducted a set of experiments where a hypomagnetic field (i.e., a weak static magnetic field) less than 500 nT was applied during the culturing of *M. magneticum* strain AMB-1. The results showed that exposure to hypomagnetic field had no significant effects on cell shape but the growth of AMB-1 was restrained during the stationary-phase. Furthermore, exposure to such an external magnetic field during growth increased the percentage of bacteria that contained mature SD magnetosomes in their exponential growth phase. The formed magnetic particles were enlarged although, the amount of Fe depletion from the culture media by cells grown in a 500 nT hypomagnetic field, showed no significant difference from cultures grown in the geomagnetic field. There was also no significant difference in the average particle number per cell between the two groups, but the average size of magnetic particles in cells exposed to hypomagnetic field was larger (>50 nm) and they contained a larger proportion (57%) of SD particles compared to those grown in the geomagnetic field only. These

authors also reported that the CSD of the magnetic particles grown only under geomagnetic field had a log-normal distribution with a cut-off toward larger sizes. Conversely, the CSD for the hypomagnetic field group was close to normal distribution. Finally, no significant differences were observed between the SFDs of both groups, and the majority of magnetic particles formed were cubo-octahedrons.

Wang et al. (2008) also showed that using non-magnetic cells (i.e., cells lacking magnetosomes) leads to similar results like in those from the magnetic pre-cultures: enlarged magnetic particles, same Fe depletion and same average number of magnetic particles per cell.

When external fields higher than the Earth's magnetic field were applied (i.e., 0.2 T; Wang and Liang, 2009) to either magnetic or non-magnetic cells of the *M. magneticum* strain AMB-1, these author's results showed that such a static magnetic field could restrain the cellular growth but increase the percentage of cells containing mature magnetosomes by 29%. Although no significant effect was observed on cell shape, an increased number of magnetic particles per cell were observed. In addition, the Fe depletion ability of cells grown under a static high magnetic field was slightly higher (~5%) compared to only geomagnetic field exposed cells. All magnetic crystals that AMB-1 formed when grown in a normal geomagnetic field were closely aligned in chains, whereas an abnormal arrangement was observed in cells exposed to an enhanced static magnetic field (i.e., changes in chain linearity, arrangement of neighboring magnetosomes, and increased number of magnetosome crystals by ~29%).

These results suggest that exposure to magnetic fields, regardless if solely geomagnetic or to an external field play an important role in the biomineratization of magnetosomes. Variations in field strengths seem clearly to affect the control ability of MTB to biomineralize, with consequences mainly with respect to magnetic particles sizes (Wang et al., 2008; Wang and Liang, 2009).

THE EFFECT OF NUTRIENT CONCENTRATIONS

Basic nutrients for all cell types are carbon (C), hydrogen (H), oxygen (O), and nitrogen (N). Recently, it was suggested that during MTB growth, iron (Fe) also serves as a nutrient rather than just a storage mineral (Naresh et al., 2012). This was concluded from the fact that Fe was more correlated with C and N, compared to the correlation between C and N which are used mainly as an energy source (C), and for biosynthetic processes (N). When C is limited, cell growth is slower and magnetosome synthesis is slower in contrast to when C is not limited, and magnetosomes are synthesized much faster. In addition, as we discussed above, both Fe and O₂ concentrations are two of the fundamental controls on magnetosome production in MTB. As to the Fe and N relationship, during the lag and exponential growth phases there is a substantial demand of N to form proteins for assembly of magnetosome vesicles, and to transport and incorporate Fe for magnetosome synthesis. After the vesicles assemble, proteins promote the nucleation of Fe crystals leading to MTB magnetosomes (Naresh et al., 2012). This was clearly demonstrated recently by Siponen et al. (2013), who showed that the magnetosome associated protein MamP plays the crucial role in magnetite crystal growth inside MTB (Siponen et al., 2013).

Interestingly, iron and carbon cycling via magnetosomes has been suggested by Kirschvink and Chang (1984) as being important also in the fossil record. They were the first to propose that magnetosomes preserved as magnetofossils might serve as paleoenvironmental indicators (i.e., paleoxygen or paleocarbon indicators) (see also below) (Kirschvink and Chang, 1984). Hesse (1994) inferred that O₂ depletion coupled with an increase in organic C flux may have disfavored MTB growth and thus led to the production of elongated crystals at lower O₂ levels compared to equidimensional particles produced at optimal conditions. Hesse (1994) also found that the abundance of SD magnetite and the ratio of equidimensional to elongate magnetofossils decreased during glacial stages. This led him to hypothesize that these morphological changes may reflect differences in growth rather than in preservation. Likewise, Yamazaki and Kawahata (1998) found that the ratio of equidimensional to elongate magnetofossils was higher in areas where the organic C flux was lower and that a clear link existed between organic C and magnetofossil morphology (Yamazaki and Kawahata, 1998). On the contrary, during glacial intervals an increased organic C content leads to an increase in equidimensional magnetofossils coupled with a decrease in total magnetofossils abundance (Lean and McCave, 1998). Finally, in lake sediments Snowball et al. (1999) revealed a direct relationship between magnetosome concentration and the percentage of total organic C and thus also suggested that the production of magnetosomes by MTB is controlled primarily by the supply of organic C (Snowball et al., 1999). Other chemical parameters have also been inferred to play an important role during the synthesis of MTB magnetites. For example, salinity or nitrate are believed to both strongly influence the number and composition of MTB communities (Simmons et al., 2004; Jogler et al., 2010; Lin and Pan, 2010) yet further studies to better quantify these effects are needed.

Many of these studies show that under certain conditions, magnetosome size, synthesis pathways, etc. can all be affected by environmental factors. Although magnetosome biomineralization has been shown to be a highly controlled BCM process, these studies showed that the role of MTB in providing a suitable chemical environment for intracellular magnetite precipitation is limited when unfavorable environmental conditions are present. In order to fully elucidate the variability in magnetosome synthesis more high-resolution records of these environmental variations must be evaluated in order to provide a full picture of MTB magnetosome formation conditions.

Taking into account the proposed main stages of magnetosome formation as described by Murat et al. (2010) and Komeili (2012), we have drawn up a simple schematic diagram (Figure 2) that shows the levels at which environmental factors will most likely affect magnetosome synthesis. It has to be noted however that the vast majority—if not all—of the significant work done on the (bio)chemical reactions leading to magnetosome formation in MTB and any genetic and environmental controls affecting growth, have been derived from studies on pure strains cultivated in the laboratory in organic-rich, well stirred, nutrient-rich media—i.e., most often under optimal conditions. In our opinion, many more laboratory experiments done on pure cultures or microcosms as well as studies of microbiota in

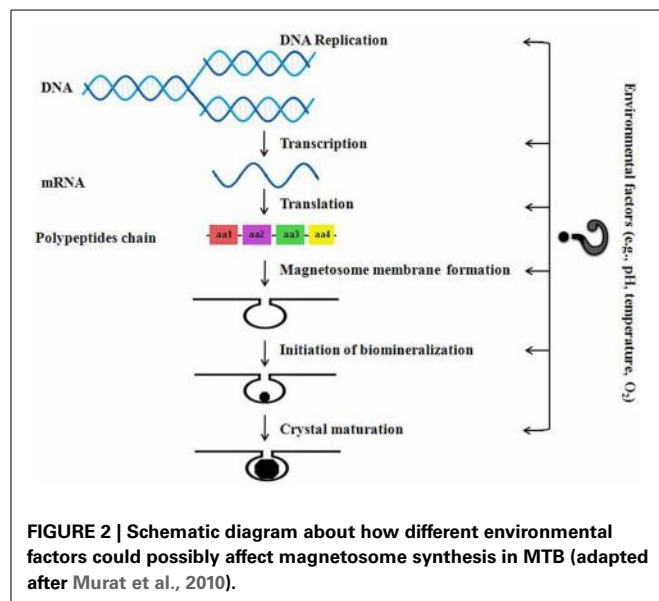


FIGURE 2 | Schematic diagram about how different environmental factors could possibly affect magnetosome synthesis in MTB (adapted after Murat et al., 2010).

natural environments have to be carried out in order to significantly change our understanding of the impact of the plethora of possible environmental factors on the biology of MTB (e.g., magnetosome synthesis, distribution and motility of MTB, competition with other bacteria for resources, etc.). Such studies need to include the quantification of the selective advantages of MTB with magnetosomes (synthesized in different conditions, thus having different shapes, sizes and magnetic properties) over MTB without magnetosomes, and over other heterotrophic microorganisms (belonging to endogenous microbiota). So far, to the best of our knowledge only one such experiment was carried out under laboratory conditions (Smith et al., 2006). These authors tested a pure strain and they took into account only one main parameter: the concentration of oxygen. They argued that, according to their experimental results and the derived theoretical model, the key benefit of magnetotaxis is an enhancement of bacterium's ability to detect oxygen, not an increase in its average speed moving away from high oxygen concentrations (Smith et al., 2006).

BIMARKERS FOR ANCIENT LIFE

As mentioned above, Kirschvink and Chang (1984) proposed that magnetosomes preserved as magnetofossils could serve as biomarkers for paleoenvironmental conditions. In principle, magnetofossils found in the terrestrial geologic record that possess all or some of the above characteristics in terms of SD, size, shapes, relative purity, etc. are presumed to originate from MTB. This is particularly because inorganically magnetites form via different pathways and lead to different magnetite shapes compared to MTB magnetites. Moreover, because other animals produce only minor amounts of magnetic nanocrystals, and animals are less abundant than bacteria, the straightforward conclusion was that magnetofossils come from MTB. Furthermore, it has been suggested that microorganisms similar to Earth's MTB may have led to similar magnetic crystal signatures on other planets in our solar system (Thomas-Keprta et al., 2000). On Earth, the natural

selection of bacterial magnetosomes has left a clear fingerprint on their size, shape, crystallinity, and chemistry, a set of distinctive features that cannot be mimicked yet through any known inorganic processes and this makes magnetofossils relatively easy to identify in the geologic sections.

The development of sensitive techniques to characterize the magnetofossils and infer their origin is the key to a correct identification of MTB in the fossil records. There have been many attempts to establish a coherent set of criteria for the determination of magnetofossils biogenicity (Petersen et al., 1986; Thomas-Kepra et al., 2000, 2001; Clemett et al., 2002; Weiss et al., 2004; Arato et al., 2005; Faivre and Zuddas, 2006; Kopp et al., 2006). In this context, Kopp and Kirschvink (2008) proposed six criteria that can be used when rating possible magnetofossils. These authors also tested these criteria on various geological examples. For their comparison Kopp and Kirschvink (2008) used samples derived from well understood stratigraphic, geochemical, and paleomagnetic contexts, and/or from localities with robust paleomagnetic data (Chang, 1988; Hounslow and Maher, 1996; Montgomery et al., 1998; Maher et al., 1999). Their results showed that such a method and these criteria work very well in distinguishing and maybe even confirming MTB-derived magnetofossils in ancient sediments.

Their evaluations were based on the following criteria:

- (1) context and geological robustness,
- (2) single domain (criterion SD),
- (3) size and shape (score S),
- (4) chain quality/length (score C),
- (5) chemical perfection (criterion ChP),
- (6) crystallographic perfection (criterion CrP).

Among these, the SD, S and C criteria are the most important as they are believed to offer the clearest evidence for a biological origin of magnetite or greigite crystals.

In order to test if these criteria can be validated also with experimental samples, where different environmental parameters have been varied during magnetite magnetosome growth, we have tested their validity by ascertaining whether MTB produced magnetites that had formed at different pH values (Moisescu et al., 2011) would pass the biogenicity tests based on the criteris set out by Kopp and Kirschvink (2008). The first criteris must naturally be ignored, because experimental MTB nanocrystals cannot be placed within a stratigraphic context and thus the paleomagnetic quality index cannot be attributed to the experimental samples, despite the fact that such an attribute is part of the first criterion.

However, when we considered the nanocrystals synthesized at optimal conditions ($\text{pH } 7$, xx mM Fe and $T = 28^\circ\text{C}$) we found that with a S score of 4 and a C score of 3, anyone would judge the magnetite nanocrystals produced in experimental settings (Moisescu et al., 2011) to be magnetofossils. Such an evaluation would be valid regardless of which set of magnetofossil robustness criteria would be selected from **Table 1**.

Conversely, for the magnetosomes that we synthesized at optimal Fe concentrations and ambient temperatures but at a pH value of 6.0 (Moisescu et al., 2011), the TEM images confirmed that an important number of particles meet the requirements

Table 1 | Proposed magnetofossil robustness criteria (Kopp and Kirschvink, 2008).

Context	Criteria
Environment analogous to younger magnetofossil bearing environments; Paleomagnetic data robust	$*S \geq 3$; or $S \geq 2$ and $**C \geq 3$; or $S \geq 2$ and $C \geq 2$ and $***\text{ChP}$
Environment analogous to younger magnetofossil bearing environments; Paleomagnetic data not robust	$S \geq 3$ and ChP ; or $S \geq 3$ and $C \geq 3$; or $S \geq 3$ and $C \geq 2$ and ChP
Environment analogous to younger magnetofossil-bearing environment; Sediments have undergone burial metamorphism or paleomagnetic data remagnetized	$S = 4$ and ChP ; or $S \geq 3$ and $C \geq 3$ and ChP ; or $S \geq 3$ and $C \geq 2$ and ChP and $****\text{CrP}$
Unique environment	$S = 4$ and $C \geq 3$ and ChP and CrP

*S, size and shape score; **C, chain quality/length score; ***ChP, chemical perfection criterion; ****CrP, crystallographic perfection criterion.

for single domain behavior, although the majority fell within the SPM. Thus, these magnetosome samples passed the SD test. Kopp and Kirschvink (2008) found that the size and shape of the magnetosomes was one of the most important criterions in evaluating biogenicity. Based on the narrowness of the size and shape distributions evidenced from the coercivity or ferromagnetic resonance (FMR) spectra, the presence of SD particles with truncated edges (e.g., cubo-octahedral or hexa-octahedral morphologies), elongated SD particles, and statistics for SD populations with narrow size and shape distributions they scored this criterion between 0 and 4 points. In our study (Moisescu et al., 2011) the magnetosomes formed at pH 6.0 revealed very few crystals with a cubo-octahedral like morphology or elongated shapes (the majority of the particles had irregular shapes) and the statistical analysis showed broad CSD and SFD. Thus these magnetites earned only 1 point for the S score. Similarly, score C (quality of chain identification) was graded from 0 to 4, with zero indicating the absence of chains, one is for either SEM or low-temperature thermal demagnetization indication of chains, two is for FMR or TEM indication of short chains of ambiguous origin, three is for FMR or TEM identification of short chains, and four is for TEM identification of long chains in magnetic extracts. TEM images of pH 6.0 magnetic extracts, showed particles in short chains of ambiguous origin, yielding a C score of 2. As no other mineral phase, except magnetite was detected in these samples, the pH 6.0 samples passed the ChP score. As to the crystallographic perfection, the majority of the crystals had many imperfections so they failed the CrP criterion. When tested against any of the sets of robustness criterias presented in **Table 1** (after Kopp and Kirschvink, 2008), our pH 6.0 samples achieved a S score of 1 and a C score of 2. Thus, based on this criteria, these experimentally produced

magnetite magnetosome samples could not be considered robust magnetofossils.

We performed a similar analysis for the magnetite magnetosome samples that we produced at pH 8.0 and 9.0. Interestingly, only the pH 8.0 magnetites (with a S score of 2, and a C score of 2) would be judged as robust magnetofossils according to the first set of criteria (Kopp and Kirschvink, 2008). The pH 9.0 samples could be considered robust if only we give them a generous C score of 2 instead the more realistic score of 1 (although only one or two very short and ambiguous chains could be identified in our TEM images), or a S score of 3 instead of 2 if we give points for the unique anisotropic prismatic crystals observed in these samples (**Table 2**, **Figure 1D**). Thus, such evaluations may not be the most adequate.

Although all the samples from our work were clearly bacterial in origin, only two (i.e., pH 7.0 and 8.0) passed the magnetofossil robustness criteria evaluation, while the other two could easily be considered of abiotic origin. Consequently, not even these excellent criteria are always foolproof when it comes to precisely determine the biotic or abiotic origin of a magnetofossil. For that reason, we consider that a revision of these criteria, which should include more detailed analyses that should embrace other magnetosome qualities, is desperately needed if such criteria are to be used to identify biofossils.

BIOGEOCHEMICAL CYCLING OF Fe

For magnetosome synthesis, MTB require high quantities of Fe, which they usually rapidly convert to magnetite, a metabolic inert form that can no longer be used as an Fe source by other organisms (the “end of the road” for Fe; Martins et al., 2007). These observations suggest that MTB play an important role in the biogeochemical cycling of Fe in aquatic environments (Simmons and Edwards, 2006, 2007). Considering that the potential of MTB in the biogeochemical cycling of Fe could be quantitatively significant (e.g., $38 \pm 28 \mu\text{g Fe cm}^{-2} \text{ year}^{-1}$; Simmons and Edwards, 2007), an estimate of the MTB contribution to the Fe cycle became necessary.

In a previous study (Moisescu et al., 2011), using optimal MTB growth conditions we estimated that the MTB contribution to the biogeochemical Fe cycling was $1.6 \mu\text{mol Fe L}^{-1} \text{ year}^{-1}$. This is equivalent to $\sim 0.078 \text{ mg Fe L}^{-1} \text{ year}^{-1}$ Fe being tied up in an inert mineral form that becomes inaccessible for any further biogeochemical processes (Barbeau et al., 1996). This estimate

could theoretically be used for calculations of the effect of the entire MTB population present in a natural environment that is characterized by a certain concentration of dissolved iron.

Nevertheless, in nature, pH, temperature, nutrients, oxygen levels or iron concentrations will vary due to short-time or seasonal environmental changes and thus any such estimate has to be carefully calibrated. We have therefore estimated in a first instance a potential pH-dependent contribution of MTB to the biogeochemical cycling of Fe and derived minimum and maximum values of 0.98 and $4.2 \mu\text{mol Fe L}^{-1} \text{ year}^{-1}$ respectively. This corresponds to 0.06 – $0.24 \text{ mg Fe L}^{-1} \text{ year}^{-1}$ removed. A similar calculation, if we take only temperature fluctuations into account, leads to an estimate of the MTB contribution of between 0.3 and $4.2 \mu\text{mol Fe L}^{-1} \text{ year}^{-1}$ (respectively 0.02 – $0.24 \text{ mg Fe L}^{-1} \text{ year}^{-1}$). All these estimates were based on values for Fe in aqueous media and thus they offer only a general view over the total annual iron cycling in aquatic environments and do not purport to present global perspective. However, despite being speculative, these estimates show the vast potential of MTB in sequestering Fe and thus in affecting and majorly impacting the global biogeochemical cycling of Fe.

SUMMARY AND OUTLOOK

The first indication that bacteria may be capable of synthesizing intracellular minerals came with the discovery of MTB and was confirmed by the electron microscopy studies of Frankel et al. (1979), who provided the first proof of intracellular magnetite production in bacteria.

Magnetite and greigite magnetosomes from MTB have been optimized by evolution resulting in a perfect fusion of physico-chemical and magnetic properties to support remarkable biological functions such as magnetotaxis. We discussed above how the intracellular metabolism and chemistry of MTB may be highly affected by the environmental conditions in which MTB cells are synthesizing their magnetic mineral particles and how these may end up having characteristics very different from those expected from a highly controlled BCM process. Taking all these aspects into account, the criteria to assess the origin of magnetites in environmental samples, need to be revised in order to derive a more accurate and reliable biogenicity indicator.

We are however, still only at the beginning of our journey to fully describe how these characteristics may vary depending on variations in external, environmental factors during

Table 2 | Magnetofossils scores of MTB magnetites that had formed in our cultures (Moisescu et al., 2011) at different pH values.

Sample	Stratigraphic context	SD	S	C	ChP	CrP	Age	Robustness	Source
pH 7.0	ND	+	4	3	+	+	NA	Robust	Moisescu et al., 2011
pH 6.0	ND	+	1	2	+	–	NA	Not robust	Moisescu et al., 2011
pH 8.0	ND	+	2	2	+	–	NA	Not robust	Moisescu et al., 2011
pH 9.0	ND	+	2	1	+	–	NA	Not robust	Moisescu et al., 2011
Chalk deposits	*PQ 5	+	2	4	ND	ND	Cretaceous	Robust	Kopp and Kirschvink, 2008
Carbonate platform	ND	+	1	2	ND	ND	Paleoproterozoic	Not robust	Kopp and Kirschvink, 2008

For comparison, two examples of robust or not robust magnetofossil samples were included from the analyses of Kopp and Kirschvink (2008).

ND, not determined; NA, not applicable; *paleomagnetic quality index.

magnetosome synthesis. We realize that more in depth studies are needed in order to describe in full details all possible variations and consequences of such variations on MTB related processes. In this way, will we be able to answer the question whether magnetites preserved in meteorites or in Earth's ancient rock record are biotic or abiotic in origin, and this might help us understand the origin of life on Earth or on other planets.

AUTHOR CONTRIBUTIONS

Cristina Moisescu, Ioan I. Ardelean, and Liane G. Benning conceived and carried out the data analysis for a part of the experiments reviewed in this manuscript. Cristina Moisescu, Ioan I. Ardelean, and Liane G. Benning substantially contributed to the conception, drafting and critically revising the manuscript for its important intellectual content. Cristina Moisescu, Ioan I. Ardelean, and Liane G. Benning gave their approval of the final revised version of the manuscript to be submitted.

ACKNOWLEDGMENTS

This work was in part supported by an FP6 Marie Curie MIR-EST "Mineral-Fluid Interface Reactivity" Early Stage Training Network (MEST-CT-2005-021120) and an UK Natural Environment Research Council Standard Grant to LGB (NE/J008745/1). We would like to specially acknowledge Frontiers for granting us a full waiver of the publishing fee.

REFERENCES

- Arato, B., Szanyi, Z., Flies, C., Schuler, D., Frankel, R. B., Buseck, P. R., et al. (2005). Crystal-size and shape distributions of magnetite from uncultured magnetotactic bacteria as a potential biomarker. *Am. Mineral.* 90, 1233–1241. doi: 10.2138/am.2005.1778
- Ardelean, I., Moisescu, C., and Popoviciu, D. R. (2008). "Magnetotactic bacteria and their potential for terraformation," in *From Fossils to Astrobiology*. Series: Cellular origin, life in extreme habitats and astrobiology, eds Joseph Seckbach and Maud M. Walsh (Dordrecht: Springer), 335–350.
- Ariskina, E. V. (2003). Magnetic inclusions in prokaryotic cells. *Microbiology* 72, 251–258. doi: 10.1023/A:1024231512124
- Barbeau, K., Moffett, J. W., Caron, D. A., Croot, P. L., and Erdner, D. L. (1996). Role of protozoan grazing in relieving iron limitation of phytoplankton. *Nature* 380, 61–64. doi: 10.1038/380061a0
- Bazylinski, D. A. (1995). Structure and function of the bacterial magnetosome. *ASM News* 61, 337–343.
- Bazylinski, D. A., and Frankel, R. B. (2000). "Biologically controlled mineralization of magnetic iron minerals by magnetotactic bacteria," in *Environmental Microbe-Mineral Interactions*, ed D. R. Lovley (Washington, DC: American Society for Microbiology), 109–144.
- Bazylinski, D. A., and Frankel, R. B. (2004). Magnetosome formation in prokaryotes. *Nat. Rev. Microbiol.* 2, 217–230. doi: 10.1038/nrmicro842
- Bazylinski, D. A., Frankel, R. B., Heywood, B. R., Mann, S., King, J. W., Donaghay, P. L., et al. (1995). Controlled biomineralization of magnetite (Fe_3O_4) and greigite (Fe_3S_4) in a magnetotactic bacterium. *Appl. Environ. Microbiol.* 61, 3232–3239.
- Bazylinski, D. A., Frankel, R. B., and Jannasch, H. W. (1988). Anaerobic magnetite production by a marine, magnetotactic bacterium. *Nature* 334, 518–519. doi: 10.1038/334518a0
- Bazylinski, D. A., Garratt-Reed, A. J., Abedi, A., and Frankel, R. B. (1993a). Copper associated with iron sulfide magnetosomes in a magnetotactic barium. *Arch. Microbiol.* 160, 35–42.
- Bazylinski, D. A., Heywood, B. R., Mann, S., and Frankel, R. B. (1993b). Fe_3O_4 and Fe_3S_4 in a bacterium. *Nature* 366, 218.
- Bazylinski, D. A., Garratt-Reed, A. J., and Frankel, R. B. (1994). Electron microscopic studies of magnetosomes in magnetotactic bacteria. *Microsc. Res. Tech.* 27, 389–401. doi: 10.1002/jemt.1070270505
- Bazylinski, D. A., and Lefevre, C. T. (2013). Magnetotactic bacteria from extreme environments. *Life* 3, 259–307. doi: 10.3390/life3020295
- Bazylinski, D. A., and Moskowitz, B. M. (1997). Microbial biomimicry of magnetic iron minerals: microbiology, magnetism and environmental significance. *Rev. Mineral.* 35, 181–223.
- Bellini, S. (1963a). *Su di un Particolare Comportamento di Batteri D'acqua Dolce*. Pavia: Microbiology Institute, University of Pavia.
- Bellini, S. (1963b). *Ulteriori Studi Sui "Batteri Magnetosensibili."* Pavia: Institute of Microbiology, University of Pavia.
- Blakemore, R. P. (1975). Magnetotactic bacteria. *Science* 190, 377–379. doi: 10.1126/science.170679
- Blakemore, R. P. (1982). Magnetotactic bacteria. *Annu. Rev. Microbiol.* 36, 217–238. doi: 10.1146/annurev.mi.36.100182.001245
- Butler, R. F., and Banerjee, S. K. (1975). Theoretical single-domain grain size range in magnetite and titanomagnetite. *J. Geophys. Res.* 80, 4049–4058. doi: 10.1029/JB080i029p04049
- Cahill, C. L., Benning, L. G., Barnes, H. L., and Parise, J. B. (2000). *In situ* time-resolved X-ray diffraction of iron sulfides during hydrothermal pyrite growth. *Chem. Geol.* 167, 53–63. doi: 10.1016/S0009-2541(99)00199-0
- Chang, S. B. R. (1988). *Bacterial Magnetite in Sedimentary Deposits and its Geophysical and Paleological Implication*. Ph.D. thesis. (Pasadena, CA).
- Clark, T. M., and Evans, J. (1997). Influence of chemical composition on the crystalline morphologies of magnetite. *IEEE Trans. Magn.* 33, 4257–4259. doi: 10.1109/20.617928
- Clemett, S. J., Thomas-Kepra, K. L., Shimmin, J., Morphew, M., McIntosh, J. R., Bazylinski, D. A., et al. (2002). Crystal morphology of MV-1 magnetite. *Am. Mineral.* 87, 1727–1730.
- Csákberényi-Malasics, D., Rodriguez-Blanco, J. D., Kis, V. K., Rečnik, A., Benning, L. G., and Pósfai, M. (2012). Structural properties and transformations of precipitated FeS. *Chem. Geol.* 294–295, 249–258. doi: 10.1016/j.chemgeo.2011.12.009
- Devouard, B., Posfai, M., Hua, X., Bazylinski, D. A., Frankel, R. B., and Buseck, P. R. (1998). Magnetite from magnetotactic bacteria: size distributions and twinning. *Am. Mineral.* 83, 1387–1398.
- Dubbels, B. L., Dispirito, A. A., Morton, J. D., Semrau, J. D., Neto, J. N. E., and Bazylinski, D. A. (2004). Evidence for a copper-dependent iron transport system in the marine, magnetotactic bacterium strain MV-1. *Microbiology* 150, 2931–2945. doi: 10.1099/mic.0.27233-0
- Faivre, D., Menguy, N., Posfai, M., and Schuler, D. (2008). Environmental parameters affect the physical properties of fast-growing magnetosomes. *Am. Mineral.* 93, 463–469. doi: 10.2138/am.2008.2678
- Faivre, D., and Zuddas, P. (2006). An integrated approach for determining the origin of magnetite nanoparticles. *Earth Planet. Sci. Lett.* 243, 53–60. doi: 10.1016/j.epsl.2006.01.012
- Fassbinder, J. W. E., Stanjek, H., and Vali, H. (1990). Occurrence of magnetic bacteria in soil. *Nature* 343, 161–163. doi: 10.1038/343161a0
- Fortin, D., and Langley, S. (2005). Formation and occurrence of biogenic iron-rich minerals. *Earth Sci. Rev.* 72, 1–19. doi: 10.1016/j.earscirev.2005.03.002
- Frankel, R. B., and Bazylinski, D. A. (2003). Biologically induced mineralization by bacteria. *Rev. Mineral. Geochem.* 54, 95–114. doi: 10.2113/0540095
- Frankel, R. B., Blakemore, R. P., and Wolfe, R. S. (1979). Magnetite in freshwater magnetotactic bacteria. *Science* 203, 1355–1356. doi: 10.1126/science.203.4387.1355
- Frankel, R. B., Zhang, J. P., and Bazylinski, D. A. (1998). Single magnetic domains in magnetotactic bacteria. *J. Geophys. Res. Solid Earth* 103, 30601–30604. doi: 10.1029/97JB03512
- Gower, L. B. (2008). Biomimetic model systems for investigating the amorphous precursor pathway and its role in biomimicry. *Chem. Rev.* 108, 4551–4627. doi: 10.1021/cr800443h
- Halstead, T. W. (1994). Introduction: an overview of gravity sensing, perception, and signal transduction in animals and plants. *Adv. Space Res.* 14, 315–316. doi: 10.1016/0273-1177(94)90417-0
- Hansel, C. M., Benner, S. G., Neiss, J., Dohnalkova, A., Kukkadapu, R. K., and Fendorf, S. (2003). Secondary mineralization pathways induced by dissimilatory iron reduction of ferrihydrite under advective flow. *Geochim. Cosmochim. Acta* 67, 2977–2992. doi: 10.1016/S0016-7037(03)00276-X
- Hesse, P. P. (1994). Evidence for bacterial palaeoecological origin of mineral magnetic cycles in oxic and sub-oxic Tasman Sea sediments. *Mar. Geol.* 117, 1–17. doi: 10.1016/0025-3227(94)90003-5

- Heyen, U., and Schuler, D. (2003). Growth and magnetosome formation by microaerophilic *Magnetospirillum* strains in an oxygen-controlled fermentor. *Appl. Microbiol. Biotechnol.* 61, 536–544. doi: 10.1007/s00253-002-1219-x
- Hoffmann, V. (1992). Greigite (Fe_3S_4): magnetic properties and first domain observations. *Phys. Earth Planet. Inter.* 70, 288–301. doi: 10.1016/0031-9201(92)90195-2
- Hounslow, M. W., and Maher, B. A. (1996). Quantitative extraction and analysis of carriers of magnetization in sediments. *Geophys. J. Int.* 124, 57–74. doi: 10.1111/j.1365-246X.1996.tb06352.x
- Hunger, S., and Benning, L. G. (2007). Greigite: the intermediate phase on the pyrite formation pathway. *Geochem. Trans.* 8, 1–20. doi: 10.1186/1467-4866-8-1
- Jandacka, P., Alexa, P., Pistora, P., Li, J., Vojtкова, H., and Hendrych, A. (2013). Size distributions of nanoparticles from magnetotactic bacteria as signatures of biologically controlled mineralization. *Am. Mineral.* 98, 2105–2114. doi: 10.2138/am.2013.4429
- Jogler, C., Niebler, M., Lin, W., Kube, M., Wanner, G., Kolinko, S., et al. (2010). Cultivation-independent characterization of *Candidatus Magnetobacterium bavaricum* via ultrastructural, geochemical, ecological and metagenomic methods. *Environ. Microbiol.* 12, 2466–2478. doi: 10.1111/j.1462-2920.2010.02220.x
- Jogler, C., and Schüller, D. (2009). Genomics, genetics, and cell biology of magnetosome formation. *Annu. Rev. Microbiol.* 63, 501–521. doi: 10.1146/annurev.micro.62.081307.162908
- Keim, C. M., Lins, U., and Farina, M. (2009). Manganese in biogenic magnetite crystals from magnetotactic bacteria. *FEMS Microbiol. Lett.* 292, 250–253. doi: 10.1111/j.1574-6968.2009.01499.x
- Keim, C. N., Lins, U., and Farina, M. (2001). Elemental analysis of uncultured magnetotactic bacteria exposed to heavy metals. *Can. J. Microbiol.* 47, 1132–1136. doi: 10.1139/w01-119
- Kirschvink, J. L., and Chang, S.-B. R. (1984). Ultrafine-grained magnetite in deep-sea sediments: possible bacterial magnetofossils. *Geology* 12, 559–562. doi: 10.1130/0091-7613(1984)12%3C559:UMIDSP%3E2.0.CO;2
- Kirschvink, J. L., and Hagadorn, J. W. (2000). “A grand unified theory of biomagnetization,” in *The Biomagnetisation of Nano- and Micro-Structures*, ed. E. Baerlein (Weinheim: Wiley-VCH Verlag GmbH), 139–150.
- Kirschvink, J. L., Walker, M. M., and Diebel, C. E. (2001). Magnetite based magnetoreception. *Curr. Opin. Neurobiol.* 11, 462–467. doi: 10.1016/S0959-4388(00)00235-X
- Komeili, A. (2012). Molecular mechanisms of compartmentalization and biomagnetization in magnetotactic bacteria. *FEMS Microbiol. Rev.* 36, 232–255. doi: 10.1111/j.1574-6976.2011.00315.x
- Kopp, R. E., and Kirschvink, J. L. (2008). The identification and biogeochemical interpretation of fossil magnetotactic bacteria. *Earth Sci. Rev.* 86, 42–61. doi: 10.1016/j.earscirev.2007.08.001
- Kopp, R. E., Weiss, B. P., Maloof, A. C., Vali, H., Nash, C. Z., and Kirschvink, J. L. (2006). Chains, clumps, and strings: magnetofossil taphonomy with ferromagnetic resonance spectroscopy. *Earth Planet. Sci. Lett.* 247, 10–25. doi: 10.1016/j.epsl.2006.05.001
- Lang, C., Schuler, D., and Faivre, D. (2007). Synthesis of magnetite nanoparticles for bio- and nanotechnology: genetic engineering and biomimetics of bacterial magnetosomes. *Macromol. Biosci.* 7, 144–151. doi: 10.1002/mabi.200600235
- Langley, S. (2006). “Metal inclusions in bacteria,” in *Inclusions in Prokaryotes*, ed. J. Shively (Berlin; Heidelberg: Springer), 311–319. doi: 10.1007/3-540-33774-1_12
- Lean, C. M. B., and McCave, I. N. (1998). Glacial to interglacial mineral magnetic and palaeoceanographic changes at Chatham Rise, SW Pacific Ocean. *Earth Planet. Sci. Lett.* 163, 247–260. doi: 10.1016/S0012-821X(98)00191-5
- Lefèvre, C. T., and Bazylinski, D. A. (2013). Ecology, diversity, and evolution of magnetotactic bacteria. *Microbiol. Mol. Biol. Rev.* 77, 497–526. doi: 10.1128/MMBR.00021-13
- Li, J., and Pan, Y. (2012). Environmental factors affect magnetite magnetosome synthesis in *Magnetospirillum magneticum* AMB-1: implications for biologically controlled mineralization. *Geomicrobiol. J.* 29, 362–373. doi: 10.1080/01490451.2011.565401
- Lin, W., and Pan, Y. X. (2010). Temporal variation of magnetotactic bacterial communities in two freshwater sediment microcosms. *FEMS Microbiol. Lett.* 302, 85–92. doi: 10.1111/j.1574-6968.2009.01838.x
- Lins, U., Keim, C., Evans, F., Farina, M., and Buseck, P. (2007). Magnetite (Fe_3O_4) and greigite (Fe_3S_4) crystals in multicellular magnetotactic prokaryotes. *Geomicrobiol. J.* 24, 43–50. doi: 10.1080/01490450601134317
- Lohmann, K. J., Cain, S. D., Dodge, S. A., and Lohmann, C. M. F. (2001). Regional magnetic field as navigational markers for sea turtles. *Science* 294, 364–366. doi: 10.1126/science.1064557
- Lovley, D. R. (1991). Dissimilatory Fe(III) and Mn(IV) reduction. *Microbiol. Rev.* 55, 259–287. doi: 10.1101/S0065-2911(04)49005-5
- Lowenstam, H. A. (1981). Minerals formed by organisms. *Science* 211, 1126–1131. doi: 10.1126/science.7008198
- Lowenstam, H. A., and Weiner, S. (1989). *On Biomineralization*. New York, NY: Oxford University Press, Inc.
- Lower, B. H., and Bazylinski, D. A. (2013). The bacterial magnetosome: a unique prokaryotic organelle. *J. Mol. Microbiol. Biotechnol.* 23, 63–80. doi: 10.1159/000346543
- Maher, B. A., Thompson, R., and Hounslow, M. W. (1999). “Introduction,” in *Quaternary Climates, Environments and Magnetism*, eds B. A. Maher and R. Thompson (Cambridge: Cambridge University Press), 1–48. doi: 10.1017/CBO9780511535635.002
- Mann, S., Moench, T. T., and Williams, R. J. P. (1984). A high resolution electron microscopic investigation of bacterial magnetite. Implications for crystal growth. *Proc. R. Soc. Lond. B Biol. Sci.* 221, 385–393. doi: 10.1098/rspb.1984.0040
- Mann, S., Sparks, N. H. C., and Blakemore, R. P. (1987). Ultrastructure and characterization of anisotropic magnetic inclusions in magnetotactic bacteria. *Proc. R. Soc. Lond. B Biol. Sci.* 231, 469–476. doi: 10.1098/rspb.1987.0055
- Mann, S., Sparks, N. H. C., Frankel, R. B., Bazylinski, D. A., and Jannasch, H. W. (1990). Biomineralization of ferrimagnetic greigite (Fe_3S_4) and iron pyrite (Fe_3S_2) in a magnetotactic bacterium. *Nature* 343, 258–261. doi: 10.1038/343258a0
- Martins, J. L., Silveira, T. S., Abreu, F., Silva, K. T., da Silva-Neto, I. D., and Lins, U. (2007). Grazing protozoa and magnetosome dissolution in magnetotactic bacteria. *Environ. Microbiol.* 9, 2775–2781. doi: 10.1111/j.1462-2920.2007.01389.x
- Massart, J. (1891). Recherches sur les organismes inférieurs. *Bull. Acad. R. Sci. Lett.* 22, 148–167.
- McKay, D. S., Gibson, E. K. Jr., Thomas-Keprta, K. L., Vali, H., Komanek, C. S., Clemett, S. J., et al. (1996). Search for past life on Mars: possible relic biogenic activity in Martian meteorite ALH84001. *Science* 273, 924–930. doi: 10.1126/science.273.5277.924
- Meldrum, F. C., Mann, S., Heywood, B. R., Frankel, R. B., and Bazylinski, D. A. (1993). Electron microscopy study of magnetosomes in a cultured coccoid magnetotactic bacterium. *Proc. R. Soc. B Biol. Sci.* 251, 231–236. doi: 10.1098/rspb.1993.0034
- Moisescu, C., Bonneville, S., Staniland, S., Ardelean, I., and Benning, L. G. (2011). Iron uptake kinetics and magnetosome formation by *Magnetospirillum gryphiswaldense* as a function of pH, temperature and dissolved iron availability. *Geomicrobiol. J.* 28, 590–600. doi: 10.1080/01490451.2011.594146
- Moisescu, C., Bonneville, S., Tobler, D., Ardelean, I., and Benning, L. G. (2008). Controlled biomineralization of magnetite (Fe_3O_4) by *Magnetospirillum gryphiswaldense*. *Mineral. Mag.* 72, 333–336. doi: 10.1180/minmag.2008.072.1.333
- Montgomery, P., Hailwood, E. A., Gale, A. S., and Burnett, J. A. (1998). The magnetostriatigraphy of Coniacian late Campanian chalk sequences in southern England. *Earth Planet. Sci. Lett.* 156, 209–224. doi: 10.1016/S0012-821X(98)00008-9
- Moskowitz, B. M. (1995). Biomineralization of magnetic minerals. *Rev. Geophys. Suppl.* 33, 123–128. doi: 10.1029/95RG00443
- Murat, D., Quinlan, A., Vali, H., and Komeili, A. (2010). Comprehensive genetic dissection of the magnetosome gene island reveals the step-wise assembly of a prokaryotic organelle. *Proc. Natl. Acad. Sci. U.S.A.* 107, 5593–5598. doi: 10.1073/pnas.0914439107
- Nakamura, C., Sakaguchi, T., Kudo, S., Burgess, J. G., Sode, K., and Matsunaga, T. (1993). Characterization of iron uptake in the magnetic bacterium *Aquaspirillum* sp. AMB-1. *Appl. Biochem. Biotechnol.* 39–40, 169–176. doi: 10.1007/BF02918987
- Naresh, M., Das, S., Mishra, P., and Mittal, A. (2012). The chemical formula of a magnetotactic bacterium. *Biotechnol. Bioeng.* 109, 1205–1216. doi: 10.1002/bit.24403
- Petersen, N., Von Dobeneck, T., and Vali, H. (1986). Fossil bacterial magnetite in deep-sea sediments from the South Atlantic Ocean. *Nature* 320, 611–615. doi: 10.1038/320611a0

- Popa, R., Fang, W., Nealon, K. H., Souza-Egipsy, V., Berquo, T. S., Banerje, S. K., et al. (2009). Effect of oxidative stress on the growth of magnetic particles in *Magnetospirillum magneticum*. *Int. Microbiol.* 12, 49–57. doi: 10.2436/20.1501.01.81
- Pósfai, M., and Arato, B. (2000). Magnetotactic bacteria and their mineral inclusions from Hungarian freshwater sediments. *Acta Geol. Hung.* 43, 463–476.
- Pósfai, M., Buseck, P. R., Bazylinski, D. A., and Frankel, R. B. (1998). Iron sulfides from magnetotactic bacteria: structure, composition, and phase transitions. *Am. Mineral.* 83, 1469–1481.
- Pósfai, M., Cziner, K., Marton, E., Marton, P., Buseck, P. R., Frankel, R. B., et al. (2001). Crystal-size distributions and possible biogenic origin of Fe sulfides. *Eur. J. Mineral.* 13, 691–703. doi: 10.1127/0935-1221/2001/0013-0691
- Pósfai, M., and Dunin-Borkowski, R. E. (2009). Magnetic nanocrystals in organisms. *Elements* 5, 235–240. doi: 10.2113/gselements.5.4.235
- Pósfai, M., Lefèvre, C. T., Trubitsyn, D., Bazylinski, D. A., and Frankel, R. B. (2013). Phylogenetic significance of composition and crystal morphology of magnetosome minerals. *Front. Microbiol.* 4:344. doi: 10.3389/fmicb.2013.00344
- Rodgers, F. G., Blakemore, R. P., Blakemore, N., Frankel, R. B., Bazylinski, D. A., Maratea, D., et al. (1990). Intercellular structure in a many-celled magnetotactic prokaryote. *Arch. Microbiol.* 154, 18–22. doi: 10.1007/BF00249172
- Rothman, J. E., and Wieland, F. T. (1996). Protein sorting by transport vesicles. *Science* 272, 227–234. doi: 10.1126/science.272.5259.227
- Sakaguchi, T., Burgess, J. G., and Matsunaga, T. (1993). Magnetite formation by a sulphate-reducing bacterium. *Nature* 365, 47–49. doi: 10.1038/365047a0
- Schleifer, K. H., Schuler, D., Spring, S., Weizenegger, M., Amann, R., Ludwig, W., et al. (1991). The genus *Magnetospirillum* gen. nov., description of *Magnetospirillum gryphiswaldense* sp. nov. and transfer of *Aquaspirillum magnetotacticum* to *Magnetospirillum magnetotacticum* comb. nov. *Syst. Appl. Microbiol.* 14, 379–385. doi: 10.1016/S0723-2020(11)80313-9
- Schubbe, S., Kube, M., Scheffel, A., Wawer, C., Heyen, U., Meyerderkirs, A., et al. (2003). Characterization of a spontaneous nonmagnetic mutant of *Magnetospirillum gryphiswaldense* reveals a large deletion comprising a putative magnetosome island. *J. Bacteriol.* 185, 5779–5790. doi: 10.1128/JB.185.19.5779-5790.2003
- Schuler, D. (1999). Formation of magnetosomes in magnetotactic bacteria. *J. Mol. Microbiol. Biotechnol.* 1, 79–86.
- Schuler, D. (2008). Genetics and cell biology of magnetosome formation in magnetotactic bacteria. *FEMS Microbiol. Rev.* 32, 654–672. doi: 10.1111/j.1574-6976.2008.00116.x
- Schuler, D., and Baeuerlein, E. (1996). Iron-limited growth and kinetics of iron uptake in *Magnetospirillum gryphiswaldense*. *Arch. Microbiol.* 166, 301–307. doi: 10.1007/s002030050387
- Schuler, D., and Baeuerlein, E. (1998). Dynamics of iron uptake and Fe_3O_4 biomineralization during aerobic and microaerobic growth of *Magnetospirillum gryphiswaldense*. *J. Bacteriol.* 180, 159–162.
- Simmons, S., and Edwards, K. (2007). “Geobiology of magnetotactic bacteria,” in *Magnetoreception and Magnetosomes in Bacteria*, ed D. Schüler (Berlin; Heidelberg: Springer-Verlag), 77–102. doi: 10.1007/7171_039
- Simmons, S. L., and Edwards, K. J. (2006). The contribution of magnetotactic bacteria to reduced iron flux in stratified marine environments. *Geochim. Cosmochim. Acta* 70, A591–A591. doi: 10.1016/j.gca.2006.06.1096
- Simmons, S. L., Sievert, S. M., Frankel, R. B., Bazylinski, D. A., and Edwards, K. J. (2004). Spatiotemporal distribution of marine magnetotactic bacteria in a seasonally stratified coastal salt pond. *Appl. Environ. Microbiol.* 70, 6230–6239. doi: 10.1128/AEM.70.10.6230-6239.2004
- Siponen, M. I., Legrand, P., Widdrat, M., Jones, S. R., Zhang, W.-J., Chang, M. C. Y., et al. (2013). Structural insight into magnetochrome-mediated magnetite biomineralization. *Nature* 502, 681–684. doi: 10.1038/nature12573
- Smith, M. J., Sheehan, P. E., Perry, L. L., O’Connor, K., Csonka, L. N., Applegate, B. M., et al. (2006). Quantifying the magnetic advantage in magnetotaxis. *Biophys. J.* 91, 1098–1107. doi: 10.1529/biophysj.106.085167
- Snowball, I. F., Sandgren, P., and Petterson, G. (1999). The mineral magnetic properties of an annually laminated Holocene lake sediment sequence in northern Sweden. *Holocene* 9, 353–362. doi: 10.1191/095968399670520633
- Spring, S., Amann, R., Ludwig, W., Schleifer, K. H., van Gemerden, H., and Petersen, N. (1993). Dominating role of an unusual magnetotactic bacterium in the microaerobic zone of a freshwater sediment. *Appl. Environ. Microbiol.* 59, 2397–2403.
- Staniland, S., Moisescu, C., and Benning, L. G. (2010). Cell division in magnetotactic bacteria splits magnetosome chain in half. *J. Basic Microbiol.* 50, 392–396. doi: 10.1002/jobm.20090408
- Staniland, S., Williams, W., Telling, N., Van Der Laan, G., Harrison, A., and Ward, B. (2008). Controlled cobalt doping of magnetosomes *in vivo*. *Nat. Nanotechnol.* 3, 158–162. doi: 10.1038/nnano.2008.35
- Taylor, A. P., and Barry, J. C. (2004). Magnetosomal matrix: ultrafine structure may template biomineralization of magnetosomes. *J. Microsc.* 213, 180–197. doi: 10.1111/j.1365-2818.2004.01287.x
- Thomas-Keprra, K. L., Bazylinski, D. A., Kirschvink, J. L., Clemett, S. J., McKay, D. S., Wentworth, S. J., et al. (2000). Elongated prismatic magnetite crystals in ALH84001 carbonate globules: potential Martian magnetofossils. *Geochim. Cosmochim. Acta* 64, 4049–4081. doi: 10.1016/S0016-7037(00)00481-6
- Thomas-Keprra, K. L., Clemett, S. J., Bazylinski, D. A., Kirschvink, J. L., McKay, D. S., Wentworth, S. J., et al. (2001). Truncated hexa-octahedral magnetite crystals in ALH84001: presumptive biosignatures. *Proc. Natl. Acad. Sci. U.S.A.* 98, 2164–2169. doi: 10.1073/pnas.051500898
- Thornhill, R. H., Grant Burgess, J., Sakaguchi, T., and Matsunaga, T. (1994). A morphological classification of bacteria containing bullet-shaped magnetic particles. *FEMS Microbiol. Lett.* 115, 169–176. doi: 10.1111/j.1574-6968.1994.tb06633.x
- Towe, K. M., and Moench, T. T. (1981). Electron-optical characterization of bacterial magnetite. *Earth Planet. Sci. Lett.* 52, 213–220. doi: 10.1016/0012-821X(81)90222-3
- Vainshtein, M., Suzina, N., and Sorokin, V. (1997). A new type of magnet-sensitive inclusions in cells of photosynthetic bacteria. *Syst. Appl. Microbiol.* 20, 182–186. doi: 10.1016/S0723-2020(97)80064-1
- Walcott, C., Gould, J. L., and Kirschvink, J. L. (1979). Pigeons have magnets. *Science* 184, 180–182. doi: 10.1126/science.184.4133.180
- Wang, X. K., Ma, Q., Jiang, W., Lv, J., Pan, W., Song, T., et al. (2008). Effects of hypomagnetic field on magnetosome formation of *Magnetospirillum magneticum* AMB-1. *Geomicrobiol. J.* 25, 296–303. doi: 10.1080/01490450802258295
- Wang, X., and Liang, L. (2009). Effects of static magnetic field on magnetosome formation and expression of mamA, mms13, mms6 and magain *Magnetospirillum magneticum* AMB-1. *Bioelectromagnetics* 30, 313–321. doi: 10.1002/bem.20469
- Weiss, B. P., Sam Kim, S., Kirschvink, J. L., Kopp, R. E., Sankaran, M., Kobayashi, A., et al. (2004). Ferromagnetic resonance and low-temperature magnetic tests for biogenic magnetite. *Earth Planet. Sci. Lett.* 224, 73–89. doi: 10.1016/j.epsl.2004.04.024
- Yamazaki, T., and Kawahata, H. (1998). Organic carbon flux controls the morphology of magnetofossils in marine sediments. *Geology* 26, 1064–1066. doi: 10.1130/0091-7613(1998)026%3C1064:OCFTM%3E2.3.CO;2
- Conflict of Interest Statement:** The authors declare that the research was conducted in the absence of any commercial or financial relationships that could be construed as a potential conflict of interest.
- Received:** 18 November 2013; **accepted:** 23 January 2014; **published online:** 11 February 2014.
- Citation:** Moisescu C, Ardelean II and Benning LG (2014) The effect and role of environmental conditions on magnetosome synthesis. *Front. Microbiol.* 5:49. doi: 10.3389/fmicb.2014.00049
- This article was submitted to Aquatic Microbiology, a section of the journal *Frontiers in Microbiology*.
- Copyright © 2014 Moisescu, Ardelean and Benning. This is an open-access article distributed under the terms of the Creative Commons Attribution License (CC BY). The use, distribution or reproduction in other forums is permitted, provided the original author(s) or licensor are credited and that the original publication in this journal is cited, in accordance with accepted academic practice. No use, distribution or reproduction is permitted which does not comply with these terms.



Changes of cell growth and magnetosome biomineralization in *Magnetospirillum magneticum* AMB-1 after ultraviolet-B irradiation

Yinzha Wang^{1,2}, Wei Lin^{1,2}, Jinhua Li^{1,2} and Yongxin Pan^{1,2*}

¹ Biogeomagnetism Group, Paleomagnetism and Geochronology Laboratory, Key Laboratory of the Earth's Deep Interior, Institute of Geology and Geophysics, Chinese Academy of Sciences, Beijing, China

² France-China Bio-Mineralization and Nano-Structures Laboratory, Chinese Academy of Sciences, Beijing, China

Edited by:

Damien Faivre, Max Planck Society, Germany

Reviewed by:

Dennis A. Bazylinski, University of Nevada, at Las Vegas, USA
Ulysses Lins, Universidade Federal do Rio de Janeiro, Brazil

***Correspondence:**

Yongxin Pan, Institute of Geology and Geophysics, Chinese Academy of Sciences, 19 BeiTuCheng W Rd., Beijing 100029, China
e-mail: yxpan@mail.igcas.ac.cn

Effects of ultraviolet radiation on microorganisms are of great interest in field of microbiology and planetary sciences. In the present study, we used *Magnetospirillum magneticum* AMB-1 as a model organism to examine the influence of ultraviolet-B (UV-B) radiation on cell growth and magnetite biominerization of magnetotactic bacteria (MTB). Live AMB-1 cells were exposed to UV-B radiation for 60, 300 and 900 s, which correspond to radiation doses of 120 J/m², 600 J/m², and 1800 J/m², respectively. After irradiation, the amounts of cyclobutane pyrimidine dimers (CPD) and reactive oxygen species (ROS) of the cells were increased, and cell growth was stunted up to ~170 h, depending on the UV-B radiation doses. The UV-B irradiated cells also produced on average more magnetite crystals with larger grain sizes and longer chains, which results in changes of their magnetic properties.

Keywords: magnetotactic bacteria, ultraviolet-B radiation, cell growth, microbial biominerization, rock magnetic measurement

INTRODUCTION

Solar ultraviolet radiation (wavelengths 10–400 nm) fluctuation is proposed as one of the most important selective pressures on the evolution of life on Earth (Cockell, 1998; Garcia-Pichel, 1998; Häder et al., 2007; Sinha and Häder, 2008; Weigand and Sundin, 2012). Although the stratospheric ozone protects organisms on Earth from UV radiation exposure (Solomon, 1999), the ozone layer can be stripped away by solar wind when the strength of the Earth's magnetic field is low. For instance, during geomagnetic excursion or polarity reversal, the field is thought to 20% of its typical strength (Reid and Isaksen, 1976; McKenzie et al., 2003; Glassmeier and Vogt, 2010; Stadelmann et al., 2010; Valet and Valladas, 2010). Consequently, the depletion of the ozone layer will lead to increased penetration of harmful radiation to the Earth's surface, which may affect aquatic ecosystems (Hargreaves, 2003; Wulff et al., 2008). UV-C radiation (wavelengths 10–280 nm) can normally be absorbed by the ozone layer, but UV-B (wavelengths 280–320 nm) and UV-A radiation (wavelengths 320–400 nm) can reach the biosphere and influence living organisms (Zepplin et al., 1998; Zenoff et al., 2006; Konhauser et al., 2007; Santos et al., 2013). In addition to enhancing production of intracellular reactive oxygen species (ROS) (similar to the UV-A radiation), UV-B radiation could directly damage DNA in organisms and thus should be more detrimental to organism health (Qiu et al., 2005b; Hernandez et al., 2006; Santos et al., 2013).

Microorganisms are the earliest known species to have appeared on Earth. Various microorganisms could form minerals and thus can leave fossil records that have been used to trace early life on Earth and other planets such as Mars (Li et al., 2013a). However, how UV radiation influences the microbial

biomineralization and the formation of fossil biominerals or mineral-encrusted cells (i.e., microfossils) is still poorly understood (Cockell, 1998; Garcia-Pichel, 1998; Häder et al., 2007; Singh et al., 2010). Recent investigations on aquatic bacterial isolates have revealed that UV-B radiation could lead to DNA lesion and cellular oxidative stress (Agogué et al., 2005; Santos et al., 2011, 2012, 2013; Matallana-Surget et al., 2012; Singh et al., 2012). On the other hand, some microorganisms have evolved strategies to mitigate such irradiation damage (Sinha and Häder, 2008; Schmidt et al., 2009; Weigand and Sundin, 2009; Singh et al., 2010; Weigand et al., 2011). For example, *in vitro* biomineralization of iron-silica biominerals of filamentous cyanobacterium *Calothrix* help the bacteria efficiently coping with UV irradiation. Compared with non-mineralized bacteria, the mineralized bacteria represent remarkable resistance to UV irradiation as revealed by the rates of photosynthesis, chlorophyll-a content, and phycocyanin autofluorescence (Phoenix et al., 2001). Cyanobacterium *Lynbya majuscula* was found to produce chemical compounds that were able to absorb UV radiation and synthesize an incrassate cell sheath under enhanced UV-B irradiation (Mandal et al., 2011).

Magnetotactic bacteria (MTB) are able to synthesis single domain (SD) magnetic particles within intracellular membrane organelles called magnetosome (Bazylinski and Frankel, 2004; Faivre and Schüler, 2008). The magnetosome, usually arranged in chain(s), facilitate MTB to navigate along the Earth's magnetic field and efficiently find the optimal living conditions in aquatic and sedimentary environments, a process known as magnetotaxis (Bazylinski and Frankel, 2004; Pan et al., 2009). After MTB die and are buried, the magnetosome crystals can be preserved as

fossil biominerals (magnetofossils), which are potential geological records for paleoenvironmental and paleomagnetic information, as well as biosignatures for searching early life on Earth and extraterrestrial life (Petersen et al., 1986; Chang and Kirschvink, 1989; McKay et al., 1996; Yamazaki and Kawahata, 1998; Arató et al., 2005; Pan et al., 2005; Kopp and Kirschvink, 2008; Paterson et al., 2013). Previous studies have demonstrated that environmental factors, such as salinity, temperature, the strength of geomagnetic field, oxygen and iron resource, can influence the overall diversity of MTB communities in nature and the compositional, physical, and magnetic features of magnetosomes (e.g., Lins et al., 2007; Faivre et al., 2008; Lin et al., 2011, 2013a,b; Li and Pan, 2012; Wang et al., 2013). However, to our knowledge, the influence of UV radiation on MTB has not been studied yet, although it is of particular interest for better understanding the evolution of magnetotaxis in early history of Earth. During a geomagnetic excursion or polarity reversal, where the dipolar geomagnetic field was weak and the UV radiation was strong, how MTB respond to the environmental changes also remains unknown. In the present study, we have investigated the effects of UV-B radiation on cell growth and magnetite biomineralization of *Magnetospirillum magneticum* AMB-1. Possible relationships between magnetosome formation and UV-B irradiation are discussed.

MATERIALS AND METHODS

PREPARATION OF CELL AND GROWTH CONDITIONS

A facultative anaerobic MTB strain *Magnetospirillum magneticum* AMB-1 (ATCC700264) was used in this study. In all experiments, cells were cultivated in the magnetic spirillum growth medium (MSGM) (Blakemore et al., 1979). This medium (1 L) contains 5 ml of Wolfe's mineral solution, 10 ml of Wolfe's vitamin solution, 0.68 g of potassium phosphate, 0.12 g of sodium nitrate, 0.05 g of sodium acetate, 0.035 g of ascorbic acid, 0.37 g of tartric acid, 0.37 g of succinic acid, and 50 µM of ferric quinate. In order to obtain a uniform genotype strain, originally activated AMB-1 cells were plated onto MSGM agar plate for 7 days, single clone was picked up and enlarged cultivated for the following studies. Non-magnetic AMB-1 cells were obtained by growing cells under 220 rpm rotation at 26°C with free air exchange. The non-magnetic cells were then inoculated equally to twelve UV-B penetrable quartz bottles. Each bottle contained 300 mL of MSGM culture medium and was incubated under the same cultivation condition. When the cell density reached ~1.0 × 10⁷ cells/ml at early exponent phase, the bottle was used for the irradiation experiment.

SOURCE OF UV-B RADIATION AND IRRADIATION EXPERIMENT

The irradiation experiment system is shown in Figure 1. UV-B radiation was obtained from USHIO ultraviolet lamps (USHIO America, USA). The lamps were coated with special blended phosphor to emit radiation peaking at 306 nm. The radiation intensity of light source was measured by a double-channel UV-B radiometer with a detective range between 275 and 330 nm (Beijing Normal University, China). The double-sided UV-B irradiation system with an averaged UV-B radiation intensity of 2.0 W/m² was used to carry out the experiment. The irradiation

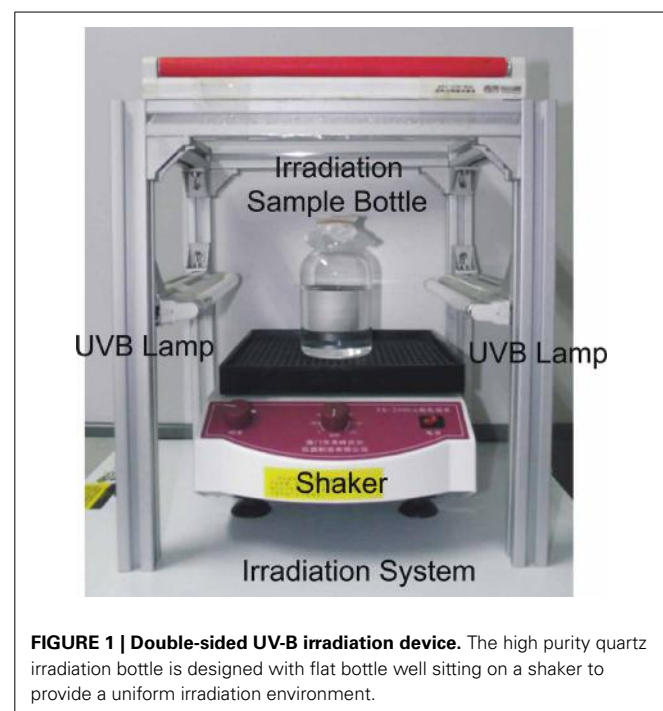


FIGURE 1 | Double-sided UV-B irradiation device. The high purity quartz irradiation bottle is designed with flat bottle well sitting on a shaker to provide a uniform irradiation environment.

bottles containing AMB-1 inoculations were exposed to UV-B radiation for 60, 300, and 900 s, which were equivalent to radiation doses of 120, 600, and 1800 J/m², respectively. To ensure even exposure the bottles were rotated at 50 rpm during irradiation. Non-irradiated cell samples (bottles covered with aluminum foils) were taken as experimental control. All twelve irradiation bottles with AMB-1 cells were divided into the four different experiment groups with tripled repeats of each UV-B radiation condition.

After the irradiation, 10 mL of cells were immediately taken from the bottle for cyclobutane pyrimidine dimers (CPD) and ROS analyses. The rest of the culture was centrifuged at 4°C 6000 rpm for 10 min. Then the cells of each sample were washed by 0.9% NaCl (wt/vol) and inoculated into 500-mL fresh MSGM medium, respectively under anaerobic condition in the dark. The cell growth of each group was examined through the optical density at 600 nm (OD₆₀₀). As the sample reached stationary phase for 40 h, the cells were harvested for cell morphology, magnetosome crystal, and magnetic analyses.

DETERMINATION OF RELATIVE CPD PRODUCTION

The relative CPD production was used to assess the DNA damage in the UV-B irradiated cells. The DNA was extracted using TIANamp Bacteria DNA Kit (TIANGEN, China). The concentrations of DNA were determined by the absorbance at 260 nm and calculated by Lambert-beer law. In order to generate a uniform comparison, each DNA sample was diluted to 1 µg/mL. For enzyme-linked immunosorbent assay, first, 0.04% protamine sulfate was coated to a polyvinylchloride flat-bottomed microtitre plate for 2 h at 37°C. Fifty microliters of the denatured DNA were put into the plate wells and incubated for 1 h at 90°C. The plate was washed 5 times by phosphate-buffered saline with

twain (PBS-T) after drying. Then 200 μ L of 3% BSA were added to each well and incubated at 37°C for 30 min and washed as described above. After blocking, 100 μ L anti-thymine dimer antibody [H3] (abcam, USA) were added and incubated at 37°C for 1 h, then washed again. The plate with 100 μ L/well HRP affinipure goat anti-mouse IgG (EarthOx, USA) was incubated at 37°C for 30 min. Then, the plate was washed 3 times with PBS-T and 2 times with citrate-phosphate buffer of pH 5.0. Finally, 100 μ L of o-phenylene diamine and 0.007% hydrogen peroxide in citrate-phosphate buffer were then added to each well and incubated for 30 min at 37°C. Fifty microliters of 2 mol/L H₂SO₄ were added to stop the reactions. The absorbance was then read at 490 nm using a microplate reader (SynergyTMH4, BioTek, USA) to determine the CPD photoproduct. The relative generations of CPD were normalized by the absorbance of the blank control.

DETECTION OF ROS GENERATION

The generation of ROS was analyzed by using DCFH-DA method based on previous report (He and Häder, 2002). DCFH-DA can be taken by cell and hydrolyzed to DCFH, which can not pass through cell membranes and is trapped within cell. Intracellular ROS can oxidize nonfluorescent DCFH into DCF, a highly fluorescent compound. Here, after irradiation, 2 mM 5 μ L DCFH-DA were immediately added to 200 μ L of the irradiated samples and incubated at 37°C for 30 min in dark. The fluorescence of the samples was measured using a spectrofluorometer (SynergyTMH4, BioTek, USA) with the excitation wavelength of 488 nm and emission wave lengths between 500 and 600 nm. The fluorescence intensity at 525 nm, after subtraction of the fluorescence of blank control then normalizing to the protein content, was used to determine the relative ROS contents. Protein content was obtained by BCA protein assay kit (Thermo Scientific, USA).

CELLS AND MAGNETOSOMES ANALYSES

Morphologies of cells and magnetosome crystals of irradiated AMB-1 were analyzed using a JEOL JEM-1400 transmission electron microscope (TEM) with an accelerating voltage of 80 kV. About 20 μ L of cells were dropped onto a copper TEM grid covered with carbon-coated formvar film for 2 h, then washed twice with sterilized distilled water and dried in air. Magnetosome sizes

were defined as (length + width)/2, and the shape factors as width/length by measuring TEM micrographs.

For rock magnetic measurements, the cells were harvested by centrifugation at 4°C. To prevent possible oxidation, the cell pellets were immediately transferred into a COY anaerobic chamber [$(\text{O}_2) < 300 \text{ ppm}$, COY-7000220A, USA] and loaded into non-magnetic gelatin capsules and dried for overnight. The samples were stored in -20°C with N₂ protection prior to measurements (Li and Pan, 2012). Room temperature magnetic measurements were performed on a Model 3900 vibrating sample magnetometer (Princeton Measurements Corporation, USA, sensitivity $5.0 \times 10^{-10} \text{ Am}^2$). Hysteresis loops were measured between $\pm 300 \text{ mT}$ in 3 mT increments with 500 ms averaging time. The hysteresis parameters saturation magnetization (M_s), saturation remanence (M_{rs}), and coercivity (B_c) were determined after paramagnetic correction. Remanence coercivity (B_{cr}) was determined from a back-field demagnetization of the saturation isothermal remanent magnetization (SIRM) acquiring at 1.5 T field. First-order reversal curves (FORCs) were measured and calculated using the FORCinel version 1.22 software (Roberts et al., 2000; Harrison and Feinberg, 2008; Egli et al., 2010). The median coercivity (B_c , FORC) and half-width interaction field ($B_{b, 1/2}$) were calculated (Muxworthy and Dunlop, 2002; Winklhofer and Zimanyi, 2006; Li et al., 2013b).

Low-temperature magnetic measurements were performed on a Quantum Design Magnetic Property Measurement System (MPMS XP-5). Zero-field cooling (ZFC) and field cooling (FC) curves were acquired by first cooling the samples from 300 to 10 K in a zero field and in a 2.5 T field, respectively, and then measuring the demagnetization of remanence in zero field during warming from 10 to 300 K. The Verwey transition temperature (T_v) were determined as the temperature for the maximum value of the first derivative of the FC curves. The δ -ratio ($\delta_{\text{FC}}/\delta_{\text{ZFC}}$), where $\delta = (M_{80K} - M_{150K})/M_{80K}$, were calculated according to Moskowitz et al. (1993).

RESULTS

THE CELL GROWTH AFTER UV-B IRRADIATION

The effect of UV-B radiation on cell growth indicates a clear dose dependence as revealed by OD₆₀₀ (Figure 2). The initial OD₆₀₀ values of all samples were about 0.025 after re-suspending

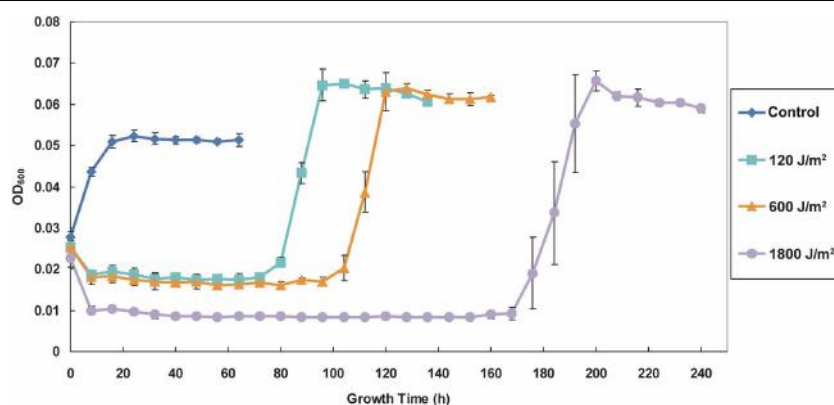


FIGURE 2 | Growth curves of the control (non-irradiated) and the irradiated AMB-1 cells. The diamond, square, triangle and circle shaped lines indicate the growth density (determine as OD₆₀₀) of the control and irradiated cells after 120, 600, and 1800 J/m² irradiation.

the irradiated cells in fresh medium. After the first 8 h following re-suspension, the cell concentrations of the 120, 600, and 1800 J/m² irradiated samples slightly decreased to 0.019, 0.018, and 0.01, respectively, which indicates differing degrees of cell density loss. Subsequently, before they reached exponential growth phases and stationary phases, the irradiated samples remained relatively stable at low levels cell density (static phase or recovery time) for 72, 96, and 168 h for the groups received 120, 600, and 1800 J/m² irradiation, respectively. The non-irradiated control group exhibited rapid growth after re-suspension and reached constant at stationary phase within 24 h. We also note that the 1800 J/m² irradiation group had the longest recovery period and the largest standard deviation during growing at exponent phase, which suggests that the higher dose of irradiation might have caused more damage to cells in this group. Compared with the control group, all irradiated groups had a relatively higher OD₆₀₀ in the stationary phase after recovery.

VARIATIONS OF THE CPD FORMATION AND THE ROS ACCUMULATION

As expected, UV-B radiation caused significant deleterious effects on DNA and cellular levels that correspond to the generation of CPD and the accumulation of ROS, respectively, which also exhibited dose-dependent patterns (Figure 3). CPD, induced by UV-B photons, is a photoproduct known as DNA lesions, which can blocks DNA replication and transcription. ROS is a collection of superoxide radical (O_2^-), hydroxylradial (OH^-), hydrogen peroxide (H_2O_2) and singlet oxygen (1O_2) (He and Häder, 2002). These free radicals can lead to damages of lipids, proteins, and DNA. In our experiments, the strain AMB-1 exhibited distinct detrimental effects under different levels of UV-B irradiation.

Specifically, for the control, 120, 600, and 1800 J/m² groups, the amount of relative CPD generation were 0.118 ± 0.018 , 0.133 ± 0.037 , 0.599 ± 0.023 , and 0.680 ± 0.011 , while the ROS value reached 24.07 ± 1.79 , 36.81 ± 5.58 , 74.33 ± 7.37 , and 98.66 ± 1.22 (determined by normalized relative units), respectively.

CHANGES OF THE CELL SIZE, MAGNETOSOMES AND CHAIN STRUCTURES

The detailed information of the AMB-1 cells and magnetosomes after the bacteria recovered from UV-B irradiation are summarized in Table 1. Figures 4A–D are representative TEM micrographs of the AMB-1 cells of the four experiment groups. Interestingly, all UV-B irradiated cells produced larger grain sizes and longer magnetosome chains compared with the non-irradiated cells. Statistic analyses of each group indicate that the magnetosome grain size of the irradiated cells was nearly 10 nm larger on average than the non-irradiated cells. For the irradiated groups, we noticed decreased number of subchains per cell (N_s), increased number of magnetosomes per cell (N_m) and per subchain (N_{sm}) (Table 2). However, the average cell lengths of the irradiated cells were about 0.4 μm shorter than the control group. Although all irradiated samples had differences in cell size and magnetosome parameters, no clear dose-related change trend was observed.

THE COERCIVITY, FORC DIAGRAMS AND 8-RATIOS

Magnetic properties of the whole cell samples were displayed in Table 2 and Figure 5. Consistent with previous studies on whole-cell MTB samples, all samples were characterized by Stoner-Wohlfarth-type hysteresis loops with M_{rs}/M_s ratio close to 0.5 (Stoner and Wohlfarth, 1948), and central-ridged FORC

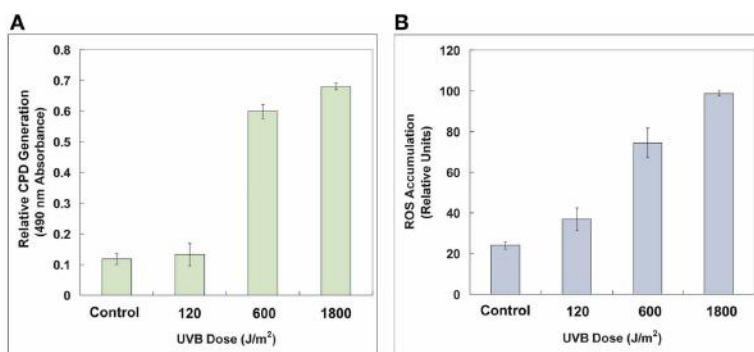


FIGURE 3 | Relative CPD generation (A) and ROS accumulation (B) of the control and the irradiated AMB-1 cells. The CPD formation was determined by 490 nm absorbance. The ROS content was characterized by 525 nm fluorescent intensity normalized protein content. See text for details.

Table 1 | Cell length, magnetosome, and subchain information of the AMB-1 samples at different irradiation levels.

UV-B dose (J/m ²)	Cell length(μm)	Magnetosome			Magnetosome chain	
		Size (nm)	Shape factor	N_m (per cell)	N_s (per cell)	N_{sm} (per subchain)
Control	3.01 ± 0.41	45.44 ± 10.31	0.913 ± 0.077	11 ± 3	3 ± 1	3 ± 2
120	2.64 ± 0.65	54.24 ± 13.84	0.860 ± 0.088	20 ± 6	2 ± 1	10 ± 4
600	2.56 ± 0.38	55.43 ± 14.43	0.857 ± 0.089	19 ± 5	2 ± 1	9 ± 3
1800	2.61 ± 0.43	55.79 ± 13.78	0.859 ± 0.085	21 ± 5	2 ± 1	10 ± 4

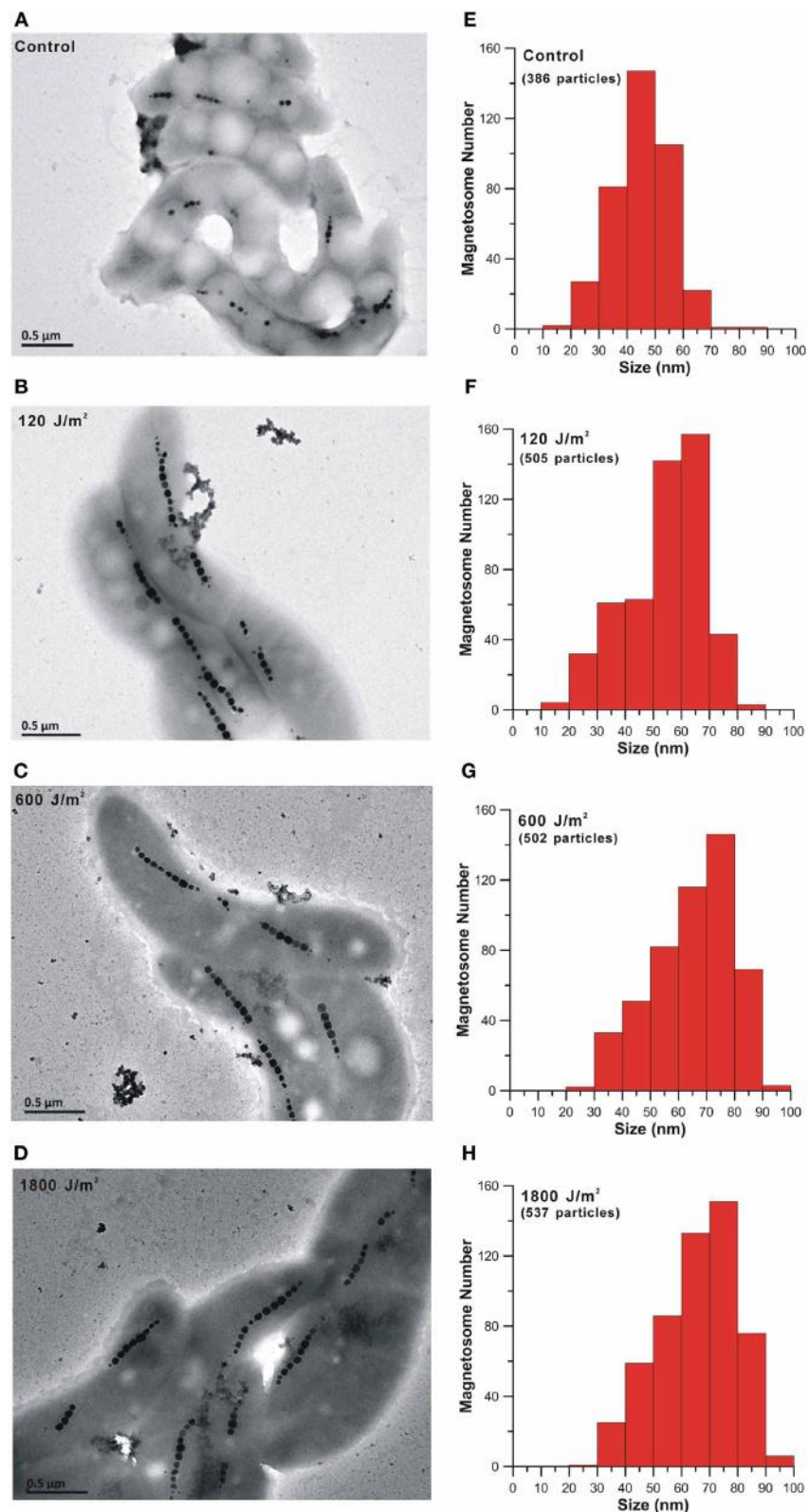
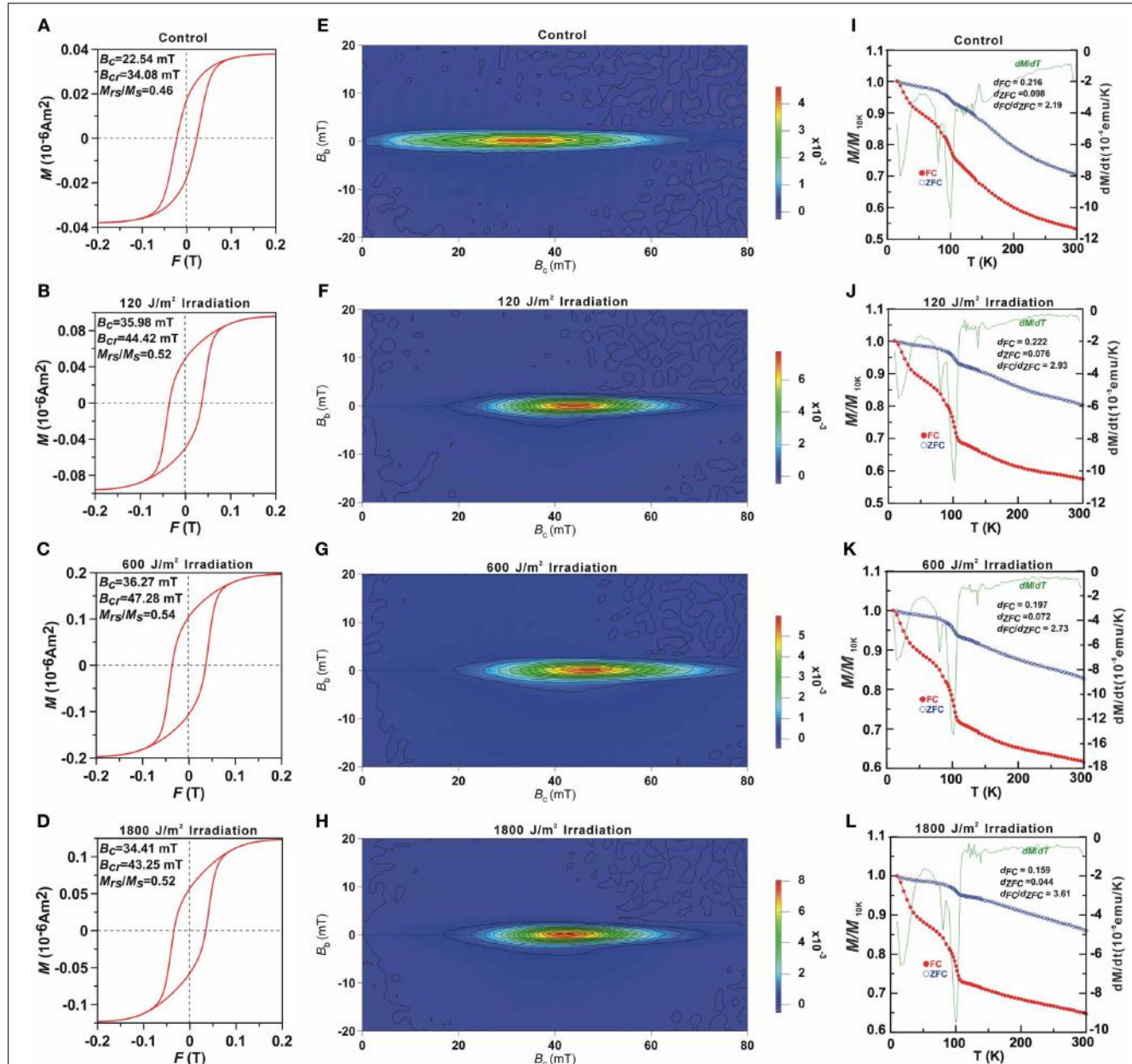


FIGURE 4 | TEM micrographs of cell morphology and magnetosome chains and histograms of magnetosome grain sizes of the control (A and E) and the irradiated AMB-1 cells (B–D and F–H).

Table 2 | Magnetic parameters of the bulk AMB-1 samples at different irradiation levels.

UV-B dose (J/m ²)	B_c (mT)	B_{cr} (mT)	B_{cr}/B_c	M_{rs}/M_s	B_c , FORC(mT)	$B_{b1/2}$ (mT)	T_f (K)	δ_{FC}	δ_{ZFC}	δ_{FC}/δ_{ZFC}
Control	22.54	34.08	1.51	0.46	34.9	1.31	102	0.216	0.098	2.19
120	35.98	44.42	1.23	0.52	43.6	1.41	102	0.222	0.076	2.93
600	36.27	47.28	1.30	0.54	46.0	1.51	102	0.197	0.072	2.73
1800	34.41	43.25	1.26	0.52	43.4	1.41	102	0.159	0.044	3.61

**FIGURE 5 | Room temperature hysteresis loops (A–D), FORC diagrams (E–H) and low temperature magnetization curves (I–L) of the control and the irradiated cell bulk samples. In (I–L) the red, blue and green lines represent the FC, ZFC curves and first derivative of FC curves, respectively.**

diagrams characterized with a narrow distributed along B_c axis (**Figures 5E–H**), indicating non-interacting uniaxial SD assemblages (Egli et al., 2010). In comparison, the room temperature magnetic parameters B_c , B_{cr} and, B_c , FORC of the UV-B radiation-treated samples were nearly identical, but about 10 mT higher than the control group. The decreased B_{cr}/B_c values, increased M_{rs}/M_s values and right-shifted FORCs suggest that the radiation treated samples possess magnetite crystals with larger grain sizes and/or longer chains, which have also been confirmed by the TEM observations (**Figure 4**).

Low-temperature measurements (**Figures 5I–L**) showed that the magnetic remanence of the UV-B radiation treated cells decreased rapidly at both $\sim 15\text{--}30$ and ~ 102 K in FC curves. The T_v of 102 K was similar to previous reports of magnetosome produced by strain AMB-1 (e.g., Li et al., 2009), which indicates no distinct change in the magnetosome composition by irradiation treatment. The δ -ratio of the control, 120, 600, and 1800 J/m² irradiated samples were 2.10, 2.93, 2.73, and 3.61, respectively, which further demonstrates better magnetosome chain structures in the radiation treated groups (Moskowitz et al., 1993).

DISCUSSION

THE BIOLOGICAL DELETERIOUS EFFECTS OF UV-B IRRADIATION ON AMB-1 CELLS

In this study, *M. magneticum* AMB-1 was used as a model organism to probe the UV-B biological effects on the cell growth and biominerization. We found an initial decrease of cell density (OD₆₀₀) and a significant inhibition of growth of the AMB-1 after the bacteria were irradiated under doses of 120, 600, and 1800 J/m² (**Figure 2**). The increased CPD formation and the ROS accumulation (**Figure 3**) indicated clearly UV-B dose-dependent deleterious effects on both DNA and cellular levels after UV-B irradiation. The self-repair after UV-B radiation might cause the observed prolonged static period of irradiated AMB-1 cells (Agogué et al., 2005; Goosen and Moolenaar, 2008). However, after the cells fully recovered (40 h after reaching stationary growth phases), the accumulations of CPD were 0.075 ± 0.007 , 0.086 ± 0.027 , 0.092 ± 0.036 and 0.088 ± 0.033 , and the ROS values were 31.45 ± 5.48 , 25.76 ± 3.56 , 30.04 ± 8.31 , and 30.50 ± 3.64 for the control, 120, 600, and 1800 J/m² irradiated groups, respectively. Those values of the irradiated groups were comparable to the non-irradiated control group, which suggests that AMB-1 cells are able to repair the UV-B radiation damage.

Previous studies on repair strategies of aquatic organisms have demonstrated that after UV-B irradiation bacteria displayed a high efficient DNA light and dark repair to eliminate CPD that would block the replication and transcriptional process and lethiferous (Goosen and Moolenaar, 2008). For ROS that leads to cell membrane damage and cellular injuries, a series of antioxidant enzyme (e.g., superoxide dismutase, catalase, and peroxidase) can be induced to mitigate the negative effects caused by ROS (He and Häder, 2002; Xie et al., 2009; Santos et al., 2012). Transcriptome analysis of UV irradiated bacteria such as *Deinococcus* sp. and cyanobacterium *Synechocystis* also exhibited the up regulation of DNA repair and stress response-related genes. Both base/nucleotide excision repair and recombinational repair pathway participated in UV induced damage repair. Genes that

were involved in scavenging oxygen radicals were also noticed up regulated after UV irradiation (Reid and Isaksen, 1976; Huang et al., 2002; Qiu et al., 2005a,b; Yuan et al., 2012).

Except for high efficiency removal of toxic oxygen species and specialized light and dark repair systems, other abilities (e.g., positive migration and production of UV screening pigments and compounds) can also help bacteria in avoiding harmful UV radiation (Ehling-Schulz and Scherer, 1999; Goosen and Moolenaar, 2008; Singh et al., 2010). Compared with non-magnetotactic bacteria in nature, MTB may migrate efficiently to deeper water layer or into sediments to avoid harmful UV radiation owing to their unique magnetotaxis. In addition, magnetite/greigite crystals may protect MTB from UV radiation.

POSSIBLE EFFECTS ON MAGNETOSOME BIOMINERALIZATION

TEM observations revealed that the irradiated cells, with a prolonged static phase, synthesized more and larger magnetosomes, as well as longer chains, which were further confirmed by various rock magnetic measurements. All irradiated samples had higher B_c , B_{cr} , M_s , M_{rs} and δ -ratio, and the FORC diagrams exhibited right shifts. Increased B_c , B_{cr} and B_c , FORC were largely due to the increased magnetosome chain lengths and grain sizes, while higher M_s and M_{rs} were probably caused by increased magnetosome production, consistent with previous studies on magnetite particles within the SD range (Kobayashi et al., 2006; Kopp and Kirschvink, 2008; Li et al., 2009). When we reinoculated these irradiated but fully recovered cells into the same fresh medium once more, however, no enhancement of magnetosome biominerization was detected in the stationary phases compared with the non-irradiated group. This suggests that the observed enhanced magnetite biominerization maybe the regulation induced by irradiation rather than a genetic imprint or radiation selection under the used experimental condition for AMB-1. Some self-repair processes and related metabolism changes may influence the crystallization of magnetosomes as well. At this stage, we cannot exclude that the prolonged recovery time of irradiated cells might affect the magnetite magnetosome formation.

Magnetite magnetosome biominerization of MTB have been well documented by the molecular biologists and mineralogists (Bazylinski et al., 2007; Faivre and Schüler, 2008; Pósfai and Dunin-Borkowski, 2009). Previous studies have shown that biominerization of chain arranged magnetite magnetosomes undergo several steps: formation of membrane vesicles on filamentary skeleton, iron uptake and magnetite crystallization within magnetosome membrane (Komeili, 2012). It has been found that the synthesis of magnetite magnetosome was closely related to nitrate reduction pathway (Bazylinski and Blakemore, 1983; Ge et al., 2011; Wang et al., 2011; Li et al., 2012). Iron and oxygen metabolism regulation also had significant influences on biominerization of the cultured MSR-1 strain (Qi et al., 2012; Rong et al., 2012). Based on TEM micrographs, in addition to the magnetosome changes, the irradiated groups possess less round granules (possibly PHA which described by Keim et al., 2005; Silva et al., 2008) than the non-irradiated control group (data not shown). This is likely caused by the prolonged cell growth or some potential modification in the metabolism pathways within the irradiated cells. It also implies

that the UV-B radiation may induce metabolism changes in AMB-1, which in turn affects magnetosome biomineralization. This suggestion is also supported by previous reports that UV radiation can strongly affect the metabolism of other microorganisms. For example, up regulated nitrate reduction genes such as *nap* and *nos* genes and genes related to iron-sequestering (*bpc* and *hemH*) and peroxide metabolism (e.g., *oxyR*, *katG*, and *sodB*) were verified through transcriptome analyses of both radio-resistant bacterium *Deinococcus* species and a facultative anaerobic *Gammaproteobacteria Shewanella oneidensis* MR-1 after UV irradiation (Qiu et al., 2005a,b). Nevertheless, further investigations on time-series culture medium composition analyses and transcriptome of the irradiated AMB-1 cells are needed to reveal the mechanisms of these phenomena.

It is reasonable to assume that the enhanced biomineralization of magnetosomes in MTB may have some benefits for resistance of irradiation. The large size, number, and improved chain structures of magnetosomes in the MTB cell may greatly help bacteria to mitigate damage caused by UV-B. For example, the magnetosomes themselves are able to prevent the radiation and eliminate intracellular ROS (Guo et al., 2012). Moreover, the better magnetite magnetosome formation in cells may enhance the sensibility of magnetotaxis navigation to escape from UV exposure when magnetic field is low. A deep-branching group MTB, affiliating within the *Nitrospira* phylum, which contains a few hundred to a thousand bullet-shaped magnetite magnetosomes, are widely found in aquatic environments (Spring et al., 1993; Pan et al., 2005; Li et al., 2010; Jogler et al., 2011; Lin et al., 2012). Our new data support that the synthesis of large amount of magnetosomes within one cell might be significant evolutionary benefit for such MTB that lived on early Earth as the geomagnetic field was probably weak and the UV radiation was strong.

ACKNOWLEDGMENTS

We thank Haitao Chen for help in experiments of cell culture, Zuohan Peng and Jingyi Yang for cell damage analyses, and Greig A. Paterson for improving the language of this manuscript. This work was supported by the CAS/SAFEA International Partnership Program for Creative Research Teams (KZCX2-Yinzhaow Wang-T10), the CAS project, and NSFC grants 41330104 and 41104041.

SUPPLEMENTARY MATERIAL

The Supplementary Material for this article can be found online at: <http://www.frontiersin.org/journal/10.3389/fmicb.2013.00397/abstract>

REFERENCES

- Agogué, H., Joux, F., Obernosterer, I., and Lebaron, P. (2005). Resistance of marine bacterioneuston to solar radiation. *Appl. Environ. Microbiol.* 71, 5282–5289. doi: 10.1128/AEM.71.9.5282-5289.2005
- Arató, B., Szányi, Z., Flies, C., Schüller, D., Frankel, R. B., Buseck, P. R., et al. (2005). Crystal-size and shape distributions of magnetite from uncultured magnetotactic bacteria as a potential biomarker. *Am. Mineral.* 90, 1233–1240. doi: 10.2138/am.2005.1778
- Bazylinski, D. A., and Blakemore, R. (1983). Denitrification and assimilatory nitrate reduction in *Aquaspirillum magnetotacticum*. *Appl. Environ. Microbiol.* 46, 1118–1124.
- Bazylinski, D. A., and Frankel, R. B. (2004). Magnetosome formation in prokaryotes. *Nat. Rev. Microbiol.* 2, 217–230. doi: 10.1038/nrmicro842
- Bazylinski, D. A., Frankel, R. B., and Konhauser, K. O. (2007). Modes of biomineralization of magnetite by microbes. *Geomicrobiol. J.* 24, 465–475. doi: 10.1080/01490450701572259
- Blakemore, R., Maratea, D., and Wolfe, R. (1979). Isolation and pure culture of a freshwater magnetic spirillum in chemically defined medium. *J. Bacteriol.* 140, 720–729.
- Chang, S. B. R., and Kirschvink, J. L. (1989). Magnetofossils, the magnetization of sediments, and the evolution of magnetite biomineralization. *Annu. Rev. Earth Planet. Sci.* 17, 169. doi: 10.1146/annurev.ea.17.050189.001125
- Cockell, C. S. (1998). Biological effects of high ultraviolet radiation on early Earth—a theoretical evaluation. *J. Theor. Biol.* 193, 717–729. doi: 10.1006/jtbi.1998.0738
- Egli, R., Chen, A. P., Winklhofer, M., Kodama, K. P., and Horng, C. S. (2010). Detection of noninteracting single domain particles using first-order reversal curve diagrams. *Geochem. Geophys. Geosyst.* 11, Q01Z11. doi: 10.1029/2009GC002916
- Ehling-Schulz, M., and Scherer, S. (1999). UV protection in cyanobacteria. *Eur. J. Phycol.* 34, 329–338. doi: 10.1080/09670269910001736392
- Faivre, D., Menguy, N., Pósfai, M., and Schüller, D. (2008). Environmental parameters affect the physical properties of fast-growing magnetosomes. *Am. Mineral.* 93, 463–469. doi: 10.2138/am.2008.2678
- Faivre, D., and Schüller, D. (2008). Magnetotactic bacteria and magnetosomes. *Chem. Rev.* 108, 4875. doi: 10.1021/cr078258w
- Garcia-Pichel, F. (1998). Solar ultraviolet and the evolutionary history of cyanobacteria. *Orig. Life Evol. Biosph.* 28, 321–347. doi: 10.1023/A:1006545303412
- Ge, X., Wang, K., Bo, T., Kou, Y., Liu, W., and Chen, G. (2011). *Magnetospirillum magneticum* AMB-1 peroxiredoxins contribute to the aerotolerance and genetic stability of the genomic magnetosome island. *FEMS Microbiol. Lett.* 320, 118–127. doi: 10.1111/j.1574-6968.2011.02298.x
- Glassmeier, K. H., and Vogt, J. (2010). Magnetic polarity transitions and biospheric effects. *Space Sci. Rev.* 155, 387–410. doi: 10.1007/s11214-010-9659-6
- Goosen, N., and Moolenaar, G. F. (2008). Repair of UV damage in bacteria. *DNA Repair* 7, 353–379. doi: 10.1016/j.dnarep.2007.09.002
- Guo, F. F., Yang, W., Jiang, W., Geng, S., Peng, T., and Li, J. L. (2012). Magnetosomes eliminate intracellular reactive oxygen species in *Magnetospirillum gryphiswaldense* MSR-1. *Environ. Microbiol.* 14, 1722–1729. doi: 10.1111/j.1462-2920.2012.02707.x
- Häder, D. P., Kumar, H., Smith, R., and Worrest, R. (2007). Effects of solar UV radiation on aquatic ecosystems and interactions with climate change. *Photochem. Photobiol. Sci.* 6, 267–285. doi: 10.1039/b700020k
- Hargreaves, B. R. (2003). “Water column optics and penetration of UVR,” in *UV Effects in Aquatic Organisms and Ecosystems*, eds E. W. Helbling and H. Zagarese (London: The Royal Society of Chemistry), 59–105. doi: 10.1039/9781847552266-00059
- Harrison, R. J., and Feinberg, J. M. (2008). FORCinel: an improved algorithm for calculating first-order reversal curve distributions using locally weighted regression smoothing. *Geochem. Geophys. Geosyst.* 9, Q05016. doi: 10.1029/2008GC001987
- He, Y. Y., and Häder, D. P. (2002). Involvement of reactive oxygen species in the UV-B damage to the cyanobacterium *Anabaena* sp. *J. Photochem. Photobiol. B* 66, 73–80. doi: 10.1016/S1011-1344(01)00278-0
- Hernandez, E. A., Ferreyra, G. A., and Mac Cormack, W. P. (2006). Response of two Antarctic marine bacteria to different natural UV radiation doses and wavelengths. *Antarct. Sci.* 18, 205–212. doi: 10.1017/S0954102006000241
- Huang, L., McCluskey, M. P., Ni, H., and LaRossa, R. A. (2002). Global gene expression profiles of the cyanobacterium *Synechocystis* sp. strain PCC 6803 in response to irradiation with UV-B and white light. *J. Bacteriol.* 184, 6845–6858. doi: 10.1128/JB.184.24.6845-6858.2002
- Jogler, C., Wanner, G., Kolinko, S., Niebler, M., Amann, R., Petersen, N., et al. (2011). Conservation of proteobacterial magnetosome genes and structures in an uncultivated member of the deep-branching *Nitrospira* phylum. *Proc. Natl. Acad. Sci. U.S.A.* 108, 1134–1139. doi: 10.1073/pnas.1012694108
- Keim, C. N., Solórzano, G., Farina, M., and Lins, U. (2005). Intracellular inclusions of uncultured magnetotactic bacteria. *Int. Microbiol.* 8, 111–117.
- Kobayashi, A., Kirschvink, J. L., Nash, C. Z., Kopp, R. E., Sauer, D. A., Bertani, L. E., et al. (2006). Experimental observation of magnetosome chain collapse in magnetotactic bacteria: sedimentological, paleomagnetic, and evolutionary implications. *Earth Planet. Sci. Lett.* 245, 538–550. doi: 10.1016/j.epsl.2006.03.041

- Komeili, A. (2012). Molecular mechanisms of compartmentalization and biomineralization in magnetotactic bacteria. *FEMS Microbiol. Rev.* 36, 232–255. doi: 10.1111/j.1574-6976.2011.00315.x
- Konhauser, K. O., Amskold, L., Lalonde, S. V., Posth, N. R., Kappler, A., and Anbar, A. (2007). Decoupling photochemical Fe (II) oxidation from shallow-water BIF deposition. *Earth Planet. Sci. Lett.* 258, 87–100. doi: 10.1016/j.epsl.2007.03.026
- Kopp, R. E., and Kirschvink, J. L. (2008). The identification and biogeochemical interpretation of fossil magnetotactic bacteria. *Earth Sci. Rev.* 86, 42–61. doi: 10.1016/j.earscirev.2007.08.001
- Li, J., Benzerara, K., Bernard, S., and Beyssac, O. (2013a). The link between biomineralization and fossilization of bacteria: insights from field and experimental studies. *Chem. Geol.* 359, 49–69. doi: 10.1016/j.chemgeo.2013.09.013
- Li, J., Ge, K., Pan, Y., Williams, W., Liu, Q., and Qin, H. (2013b). A strong angular dependence of magnetic properties of magnetosome chains: implications for rock magnetism and paleomagnetism. *Geochim. Geophys. Geosyst.* 14, 3887–3907. doi: 10.1002/ggge.20228
- Li, J., and Pan, Y. (2012). Environmental factors affect magnetite magnetosome synthesis in *Magnetospirillum magneticum* AMB-1: implications for biologically controlled mineralization. *Geomicrobiol. J.* 29, 362–373. doi: 10.1080/01490451.2011.565401
- Li, J., Pan, Y., Chen, G., Liu, Q., Tian, L., and Lin, W. (2009). Magnetite magnetosome and fragmental chain formation of *Magnetospirillum magneticum* AMB-1: transmission electron microscopy and magnetic observations. *Geophys. J. Int.* 177, 33–42. doi: 10.1111/j.1365-246X.2009.04043.x
- Li, J., Pan, Y., Liu, Q., Yu-Zhang, K., Menguy, N., Che, R., et al. (2010). Biominerization, crystallography and magnetic properties of bullet-shaped magnetite magnetosomes in giant rod magnetotactic bacteria. *Earth Planet. Sci. Lett.* 293, 368–376. doi: 10.1016/j.epsl.2010.03.007
- Li, Y., Katzmann, E., Borg, S., and Schüller, D. (2012). The periplasmic nitrate reductase Nap is required for anaerobic growth and involved in redox control of magnetite biominerization in *Magnetospirillum gryphiswaldense*. *J. Bacteriol.* 194, 4847–4856. doi: 10.1128/JB.00903-12
- Lin, W., Li, J., and Pan, Y. (2012). Newly isolated but uncultivated magnetotactic bacterium of the phylum *Nitrospinae* from Beijing, China. *Appl. Environ. Microbiol.* 78, 668–675. doi: 10.1128/AEM.06764-11
- Lin, W., Wang, Y., Gorby, Y., Nealson, K., and Pan, Y. (2013a). Integrating niche-based process and spatial process in biogeography of magnetotactic bacteria. *Sci. Rep.* 3, 1643. doi: 10.1038/srep01643
- Lin, W., Bazylinski, D. A., Xiao, T., Wu, L. F., and Pan, Y. (2013b). Life with compass: diversity and biogeography of magnetotactic bacteria. *Environ. Microbiol.* doi: 10.1111/1462-2920.12313. [Epub ahead of print].
- Lin, W., Wang, Y., Li, B., and Pan, Y. (2011). A biogeographic distribution of magnetotactic bacteria influenced by salinity. *ISME J.* 6, 475–479. doi: 10.1038/ismej.2011.112
- Lins, U., Keim, C. N., Evans, F. F., Farina, M., and Buseck, P. R. (2007). Magnetite (Fe_3O_4) and greigite (Fe_3S_4) crystals in multicellular magnetotactic prokaryotes. *Geomicrobiol. J.* 24, 43–50. doi: 10.1080/01490450601134317
- Mandal, S., Rath, J., and Adhikary, S. P. (2011). Adaptation strategies of the sheathed cyanobacterium *Lyngbya majuscula* to ultraviolet-B. *J. Photochem. Photobiol. B* 102, 115–122. doi: 10.1016/j.jphotobiol.2010.09.011
- Matallana-Surget, S., Joux, F., Wattiez, R., and Lebaron, P. (2012). Proteome analysis of the UVB-resistant marine bacterium *Photobacterium angustum* S14. *PLoS ONE* 7:e42299. doi: 10.1371/journal.pone.0042299
- McKay, D. S., Gibson, E. K., Thomas-Kepra, K. L., Vali, H., Romanek, C. S., Clemett, S. J., et al. (1996). Search for past life on Mars: possible relic biogenic activity in Martian meteorite ALH84001. *Science* 273, 924–930. doi: 10.1126/science.273.5277.924
- McKenzie, R. L., Björn, L. O., Bais, A., and Ilyasd, M. (2003). Changes in biologically active ultraviolet radiation reaching the Earth's surface. *Photochem. Photobiol. Sci.* 2, 5–15. doi: 10.1039/b21155c
- Moskowitz, B. M., Frankel, R. B., and Bazylinski, D. A. (1993). Rock magnetic criteria for the detection of biogenic magnetite. *Earth Planet. Sci. Lett.* 120, 283–300. doi: 10.1016/0012-821X(93)90245-5
- Muxworthy, A. R., and Dunlop, D. J. (2002). First-order reversal curve (FORC) diagrams for pseudo-single-domain magnetites at high temperature. *Earth Planet. Sci. Lett.* 203, 369–382. doi: 10.1016/S0012-821X(02)00880-4
- Pan, Y., Lin, W., Li, J., Wu, W., Tian, L., Deng, C., et al. (2009). Reduced efficiency of magnetotaxis in magnetotactic coccoid bacteria in higher than geomagnetic fields. *Biophysic. J.* 97, 986–991. doi: 10.1016/j.biophysj.2009.06.012
- Pan, Y., Petersen, N., Davila, A. F., Zhang, L., Winklhofer, M., Liu, Q., et al. (2005). The detection of bacterial magnetite in recent sediments of Lake Chiemsee (southern Germany). *Earth Planet. Sci. Lett.* 232, 109–123. doi: 10.1016/j.epsl.2005.01.006
- Paterson, A. G., Wang, Y., and Pan, Y. (2013). The fidelity of paleomagnetic records carried by magnetosome chains. *Earth Planet. Sci. Lett.* 383, 82–91. doi: 10.1016/j.epsl.2013.09.031
- Petersen, N., von Dobeneck, T., and Vali, H. (1986). Fossil bacterial magnetite in deep-sea sediments from the South Atlantic Ocean. *Nature* 320, 611–615. doi: 10.1038/320611a0
- Phoenix, V., Konhauser, K., Adams, D., and Bottrell, S. (2001). Role of biomimetic mineralization as an ultraviolet shield: implications for Archean life. *Geology* 29, 823–826. doi: 10.1130/0091-7613(2001)029<0823:ROBAAU>2.0.CO;2
- Pósfai, M., and Dunin-Borkowski, R. E. (2009). Magnetic nanocrystals in organisms. *Elements* 5, 235–240. doi: 10.2113/gselements.5.4.235
- Qi, L., Li, J., Zhang, W., Liu, J., Rong, C., Li, Y., et al. (2012). Fur in *Magnetospirillum gryphiswaldense* influences magnetosomes formation and directly regulates the genes involved in iron and oxygen metabolism. *PLoS ONE* 7:e29572. doi: 10.1371/journal.pone.0029572
- Qiu, X., Tiedje, J. M., and Sundin, G. W. (2005a). Genome-wide examination of the natural solar radiation response in *Shewanella oneidensis* MR-1. *Photochem. Photobiol.* 81, 1559–1568. doi: 10.1562/2005-04-15-RA-490
- Qiu, X., Sundin, G. W., Wu, L., Zhou, J., and Tiedje, J. M. (2005b). Comparative analysis of differentially expressed genes in *Shewanella oneidensis* MR-1 following exposure to UVC, UVB, and UVA radiation. *J. Bacteriol.* 187, 3556–3564. doi: 10.1128/JB.187.10.3556-3564.2005
- Reid, G., and Isaksen, I. (1976). Influence of ancient solar-proton events on the evolution of life. *Nature* 259, 177–179. doi: 10.1038/259177a0
- Roberts, A. P., Pike, C. R., and Verosub, K. L. (2000). First-order reversal curve diagrams: a new tool for characterizing the magnetic properties of natural samples. *J. Geophys. Res. Solid Earth* 105, 28461–28476. doi: 10.1029/2000JB900326
- Rong, C., Zhang, C., Zhang, Y., Qi, L., Yang, J., Guan, G., et al. (2012). FeoB2 functions in magnetosome formation and oxidative stress protection in *Magnetospirillum gryphiswaldense* strain MSR-1. *J. Bacteriol.* 194, 3972–3976. doi: 10.1128/JB.00382-12
- Santos, A., Lopes, S., Baptista, I., Henrique, I., Gomes, N., Almeida, A., et al. (2011). Diversity in UV sensitivity and recovery potential among bacterioneuston and bacterioplankton isolates. *Lett. Appl. Microbiol.* 52, 360–366. doi: 10.1111/j.1472-765X.2011.03011.x
- Santos, A. L., Gomes, N., Henrique, I., Almeida, A., Correia, A., and Cunha, Á. (2012). Contribution of reactive oxygen species to UV-B-induced damage in bacteria. *J. Photochem. Photobiol. B* 117, 40–46. doi: 10.1016/j.jphotobiol.2012.08.016
- Santos, A. L., Oliveira, V., Baptista, I., Henrique, I., Gomes, N. C., Almeida, A., et al. (2013). Wavelength dependence of biological damage induced by UV radiation on bacteria. *Arch. Microbiol.* 195, 63–74. doi: 10.1007/s00203-012-0847-5
- Schmidt, É. C., Scariot, L. A., Rover, T., and Bouzon, Z. L. (2009). Changes in ultrastructure and histochemistry of two red macroalgae strains of *Kappaphycus alvarezii* (*Rhodophyta, Gigartinales*), as a consequence of ultraviolet B radiation exposure. *Micron* 40, 860–869. doi: 10.1016/j.micron.2009.06.003
- Silva, K. T., Abreu, F., Keim, C. N., Farina, M., and Lins, U. (2008). Ultrastructure and cytochemistry of lipid granules in the many-celled magnetotactic prokaryote, *Candidatus Magnetoglobus multicellularis*. *Micron* 39, 1387–1392. doi: 10.1016/j.micron.2008.05.009
- Singh, S. P., Häder, D. P., and Sinha, R. P. (2010). Cyanobacteria and ultraviolet radiation (UVR) stress: mitigation strategies. *Ageing Res. Rev.* 9, 79–90. doi: 10.1016/j.arr.2009.05.004
- Singh, V. P., Srivastava, P. K., and Prasad, S. M. (2012). Impact of low and high fluence rates of UV-B radiation on growth and oxidative stress in *Phormidium foveolarum* and *Nostoc muscorum* under copper toxicity: differential display of antioxidants system. *Acta Physiol. Plant.* 34, 2225–2239. doi: 10.1007/s11738-012-1023-x
- Sinha, R. P., and Häder, D. P. (2008). UV-protectants in cyanobacteria. *Plant Sci.* 174, 278–289. doi: 10.1016/j.plantsci.2007.12.004
- Solomon, S. (1999). Stratospheric ozone depletion: a review of concepts and history. *Rev. Geophys.* 37, 275–316. doi: 10.1029/1999RG900008

- Spring, S., Amann, R., Ludwig, W., Schleifer, K. H., van Gemerden, H., and Petersen, N. (1993). Dominating role of an unusual magnetotactic bacterium in the microaerobic zone of a freshwater sediment. *Appl. Environ. Microbiol.* 59, 2397–2403.
- Stadelmann, A., Vogt, J., Glassmeier, K. H., Kallenrode, M. B., and Voigt, G. H. (2010). Cosmic ray and solar energetic particle flux in paleomagnetospheres. *Earth Planets Space* 62, 333. doi: 10.5047/eps.2009.10.002
- Stoner, E. C., and Wohlfarth, E. (1948). A mechanism of magnetic hysteresis in heterogeneous alloys. *Philos. T. R. Soc. A.* 240, 599–642. doi: 10.1098/rsta.1948.0007
- Valet, J. P., and Valladas, H. (2010). The Laschamp-Mono lake geomagnetic events and the extinction of Neanderthal: a causal link or a coincidence? *Quaternary Sci. Rev.* 29, 3887–3893. doi: 10.1016/j.quascirev.2010.09.010
- Wang, K., Ge, X., Bo, T., Chen, Q., Chen, G., and Liu, W. (2011). Interruption of the denitrification pathway influences cell growth and magnetosome formation in *Magnetospirillum magneticum* AMB-1. *Lett. Appl. Microbiol.* 53, 55–62. doi: 10.1111/j.1472-765X.2011.03063.x
- Wang, Y., Lin, W., Li, J., and Pan, Y. (2013). High diversity of magnetotactic *delta*-proteobacteria in a freshwater niche. *Appl. Environ. Microbiol.* 79, 2813–2817. doi: 10.1128/AEM.03635-12
- Weigand, M. R., and Sundin, G. W. (2009). Long-term effects of inducible mutagenic DNA repair on relative fitness and phenotypic diversification in *Pseudomonas cichorii* 302959. *Genetics* 181, 199–208. doi: 10.1534/genetics.108.096131
- Weigand, M. R., and Sundin, G. W. (2012). General and inducible hypermutation facilitate parallel adaptation in *Pseudomonas aeruginosa* despite divergent mutation spectra. *Proc. Natl. Acad. Sci. U.S.A.* 109, 13680–13685. doi: 10.1073/pnas.1205357109
- Weigand, M. R., Tran, V. N., and Sundin, G. W. (2011). Growth parameter components of adaptive specificity during experimental evolution of the uvr-inducible mutator *Pseudomonas cichorii* 302959. *PLoS ONE* 6:e15975. doi: 10.1371/journal.pone.0015975
- Winklhofer, M., and Zimanyi, G. T. (2006). Extracting the intrinsic switching field distribution in perpendicular media: a comparative analysis. *J. Appl. Phys.* 99, 08E710–708E713. doi: 10.1063/1.2176598
- Wulff, A., Roleda, M., Zacher, K., and Wiencke, C. (2008). UV radiation effects on pigments, photosynthetic efficiency and DNA of an Antarctic marine benthic diatom community. *Aquat. Biol.* 3, 167–177. doi: 10.3354/ab00076
- Xie, Z., Wang, Y., Liu, Y., and Liu, Y. (2009). Ultraviolet-B exposure induces photo-oxidative damage and subsequent repair strategies in a desert cyanobacterium *Microcoleus vaginatus*. *Gom. Eur. J. Soil Biol.* 45, 377–382. doi: 10.1016/j.ejsobi.2009.04.003
- Yamazaki, T., and Kawahata, H. (1998). Organic carbon flux controls the morphology of magnetofossils in marine sediments. *Geology* 26, 1064–1066.
- Yuan, M., Chen, M., Zhang, W., Lu, W., Wang, J., Yang, M., et al. (2012). Genome sequence and transcriptome analysis of the radioreistant bacterium *Deinococcus gobiensis*: insights into the extreme environmental adaptations. *PLoS ONE* 7:e34458. doi: 10.1371/journal.pone.0034458
- Zenoff, V. F., Sineriz, F., and Farías, M. (2006). Diverse responses to UV-B radiation and repair mechanisms of bacteria isolated from high-altitude aquatic environments. *Appl. Environ. Microbiol.* 72, 7857–7863. doi: 10.1128/AEM.01333-06
- Zepp, R. G., Callaghan, T., and Erickson, D. (1998). Effects of enhanced solar ultraviolet radiation on biogeochemical cycles. *J. Photochem. Photobiol. B* 46, 69–82. doi: 10.1016/S1011-1344(98)00186-9
- Conflict of Interest Statement:** The authors declare that the research was conducted in the absence of any commercial or financial relationships that could be construed as a potential conflict of interest.
- Received: 21 October 2013; accepted: 04 December 2013; published online: 19 December 2013.*
- Citation: Wang Y, Lin W, Li J and Pan Y (2013) Changes of cell growth and magnetosome biominerilization in *Magnetospirillum magneticum* AMB-1 after ultraviolet-B irradiation. *Front. Microbiol.* 4:397. doi: 10.3389/fmicb.2013.00397*
- This article was submitted to Aquatic Microbiology, a section of the journal Frontiers in Microbiology.*
- Copyright © 2013 Wang, Lin, Li and Pan. This is an open-access article distributed under the terms of the Creative Commons Attribution License (CC BY). The use, distribution or reproduction in other forums is permitted, provided the original author(s) or licensor are credited and that the original publication in this journal is cited, in accordance with accepted academic practice. No use, distribution or reproduction is permitted which does not comply with these terms.*



Paleomagnetic and paleoenvironmental implications of magnetofossil occurrences in late Miocene marine sediments from the Guadalquivir Basin, SW Spain

Juan C. Larrasoña^{1,2 *†}, Qingsong Liu³, Pengxiang Hu³, Andrew P. Roberts⁴, Pilar Mata¹, Jorge Civis¹, Francisco J. Sierro⁵ and José N. Pérez-Asensio⁶

¹ Instituto Geológico y Minero de España, Madrid, Spain

² Institute of Earth Sciences Jaume Almera, CSIC, Barcelona, Spain

³ State Key Laboratory of Lithospheric Evolution, Institute of Geology and Geophysics, Chinese Academy of Sciences, Beijing, China

⁴ Research School of Earth Sciences, The Australian National University, Canberra, Australia

⁵ Departamento de Geología, Universidad de Salamanca, Salamanca, Spain

⁶ Department of Earth Sciences, University of Geneva, Geneva, Switzerland

Edited by:

Damien Faivre, Max Planck Society, Germany

Reviewed by:

Ann Marie Hirt, Swiss Institute of Technology Zürich, Switzerland

Michael Winklhofer, Ludwig-Maximilians-University Munich, Germany

***Correspondence:**

Juan C. Larrasoña, Instituto Geológico y Minero de España, calle Ríos Rosas, 23 28003 Madrid, Spain
e-mail: jc.larra@igme.es

†Present address:

Juan C. Larrasoña, Institute of Earth Sciences Jaume Almera, CSIC, Lluís Solé i Sabaris s/n, 08028 Barcelona, Spain

Although recent studies have revealed more widespread occurrences of magnetofossils in pre-Quaternary sediments than have been previously reported, their significance for paleomagnetic and paleoenvironmental studies is not fully understood. We present a paleo- and rock-magnetic study of late Miocene marine sediments recovered from the Guadalquivir Basin (SW Spain). Well-defined paleomagnetic directions provide a robust magnetostratigraphic chronology for the two studied sediment cores. Rock magnetic results indicate the dominance of intact magnetosome chains throughout the studied sediments. These results provide a link between the highest-quality paleomagnetic directions and higher magnetofossil abundances. We interpret that bacterial magnetite formed in the surface sediment mixed layer and that these magnetic particles gave rise to a paleomagnetic signal in the same way as detrital grains. They, therefore, carry a magnetization that is essentially identical to a post-depositional remanent magnetization, which we term a bio-depositional remanent magnetization. Some studied polarity reversals record paleomagnetic directions with an apparent 60–70 kyr recording delay. Magnetofossils in these cases are interpreted to carry a biogeochemical remanent magnetization that is locked in at greater depth in the sediment column. A sharp decrease in magnetofossil abundance toward the middle of the studied boreholes coincides broadly with a major rise in sediment accumulation rates near the onset of the Messinian salinity crisis (MSC), an event caused by interruption of the connection between the Mediterranean Sea and the Atlantic Ocean. This correlation appears to have resulted from dilution of magnetofossils by enhanced terrigenous inputs that were driven, in turn, by sedimentary changes triggered in the basin at the onset of the MSC. Our results highlight the importance of magnetofossils as carriers of high-quality paleomagnetic and paleoenvironmental signals even in dominantly terrigenous sediments.

Keywords: Guadalquivir Basin, late Miocene, marine sediments, rock magnetism, magnetotactic bacteria, Messinian salinity crisis

INTRODUCTION

Magnetosomes are submicron crystals of magnetite (Fe_3O_4) or greigite (Fe_3S_4) that grow intracellularly, forming chains, within magnetotactic bacteria (MTB) to assist them in navigation within aquatic environments (Blakemore, 1975; Bazylinski and Frankel, 2004; Faivre and Schüler, 2008; Kopp and Kirschvink, 2008). Aside from having important applications in microbiology and biotechnology (see Faivre and Schüler, 2008), magnetosomes (or magnetofossils when found in the sedimentary record) are important in Earth science because they have ideal sizes (single domain, SD) for recording stable paleomagnetic signals. In addition, variations in magnetofossil abundances in sediments and sedimentary rocks have been interpreted to provide information concerning the

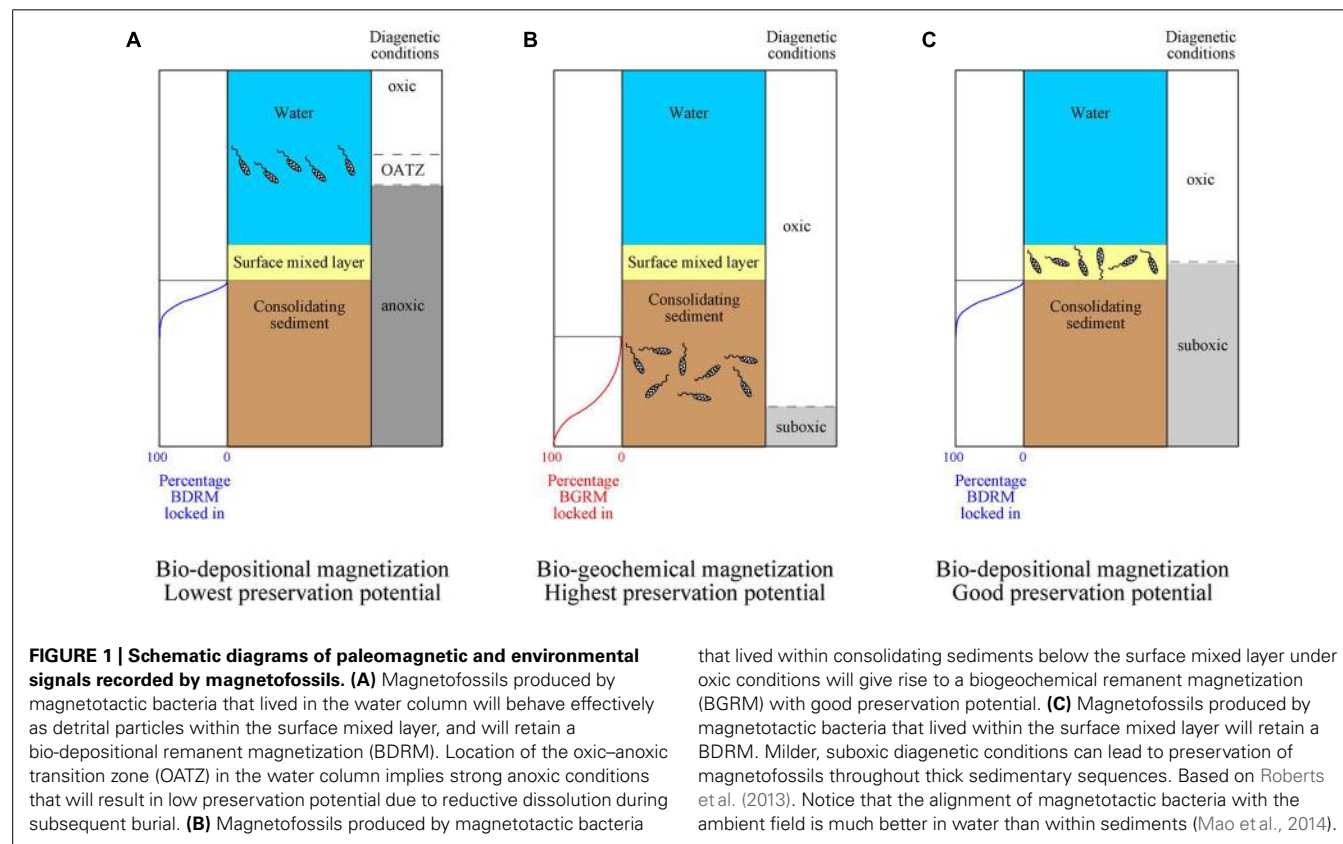
response of MTB communities to changing paleoenvironmental conditions (Tarduno and Wilkison, 1996; Lean and McCave, 1998; Tarduno et al., 1998; Yamazaki and Kawahata, 1998; Dinarès-Turell et al., 2003; Roberts et al., 2011; Larrasoña et al., 2012; Lin et al., 2012; Yamazaki and Ikehara, 2012; Yamazaki et al., 2013).

Magnetite-producing MTB thrive typically around the oxic-anoxic transition zone (OATZ; Faivre and Schüler, 2008; Kopp and Kirschvink, 2008), although they have also been linked with micro-aerobic environments (Blakemore et al., 1985; Schüler and Baeuerlein, 1998) and even oxic conditions (Yamazaki and Shimojo, 2013) decoupled from the occurrence of an OATZ (Roberts et al., 2013). Under reducing diagenetic conditions, the OATZ can occur within the water column or the uppermost centimeters of

the sediment column (e.g., the bioturbated surface sedimentary mixed layer). In this case, magnetosome chains that accumulate after bacterial death will behave in the same way as any other detrital grain subjected to pelitization, bioturbation and other processes within the surface mixed layer (Paterson et al., 2013; Roberts et al., 2013; Mao et al., 2014). Magnetofossil chains are expected to adhere onto sediment particles instead of being freely suspended in pore waters, which explains the overall poor alignment of magnetofossil chains (as compared with water) typically reported in MTB-bearing modern sediments (Mao et al., 2014). With ongoing sedimentation and burial, magnetofossils are likely to acquire a magnetization that is essentially identical to a post-depositional remanent magnetization (PDRM) but that, given its origin and distinctive significance, we refer to as a bio-depositional remanent magnetization (BDRM). Magnetofossils in this case should carry a syn-depositional signal that can be used to study short-period geomagnetic field behavior and will provide reliable magnetostratigraphic data. They will also record a paleoenvironmental signal that is contemporaneous with any other sediment constituent (e.g., detrital particles, foraminiferal tests, etc.). Under anoxic conditions, however, preservation of magnetofossils (and detrital magnetic minerals) is unlikely given that reductive dissolution will occur under such conditions (**Figure 1A**; Bazylinski and Frankel, 2004; Faivre and Schüller, 2008; Kopp and Kirschvink, 2008). Such reductive dissolution is responsible for liberation of Fe^{2+} that, after its upward flux, is used by MTB to synthesize magnetosomes around the OATZ (Faivre

and Schüller, 2008; Kopp and Kirschvink, 2008; Roberts et al., 2011, 2013). Strongly reducing conditions are typical in continental margin sediments, where high organic carbon supply and high accumulation rates favor burial and degradation of organic matter within sediments (Roberts et al., 2013). Magnetofossils might be preserved at discrete intervals due to transient disruption of reducing conditions. This seems to have been the case for magnetofossils that accumulated during the Paleocene-Eocene thermal maximum in the North American Atlantic continental margin (Kopp et al., 2007; Lippert and Zachos, 2007; Dickens, 2008).

When oxic depositional conditions prevail, it is possible that microaerobic conditions persist throughout the sediment column. In this case, upward diffusion of Fe^{2+} liberated by dissolution of the most reactive iron (oxyhydr)oxides [e.g., ferric hydroxide, ferrihydrite and lepidocrocite (Poulton et al., 2004)] at greater depths is used by MTB to biomimic magnetosomes (Roberts et al., 2011, 2013). An extreme case of MTB living in oxic conditions is found in pelagic red clays (Yamazaki and Shimono, 2013). When MTB live within consolidating sediments in these cases, accumulation of magnetosomes after death of the MTB can result in acquisition of a remanent magnetization with an age that will be delayed with respect to that of the host sediment (Tarduno and Wilkison, 1996; Tarduno et al., 1998; Abrajewitch and Kodama, 2009; Roberts et al., 2013; **Figure 1B**). This magnetization is referred to as a biogeochemical remanent magnetization (BGRM; Tarduno and Wilkison, 1996; Tarduno et al., 1998).



A BGRM is likely to occur in deep-sea sediments (pelagic carbonates, clays, and oozes), where low organic carbon fluxes, non-zero oxygen contents, and low accumulation rates favor oxidation of most organic matter before it is buried in the sediment, which favors magnetofossil preservation (Roberts et al., 2013). Depths at which BGRMs lock in within pelagic carbonate environments from the equatorial Pacific Ocean have been reported to range from some tens of cm to 4 m, which corresponds to a delay in remanence acquisition between 40 and 420 kyr (Tarduno and Willkison, 1996). A similar delay of several tens of kyr has been reported by Yamazaki and Shimono (2013) in red clays from the North and South Pacific Ocean. In these cases, magnetofossils are unlikely to provide a depositional signal that can be used to make paleoenvironmental inferences or to study geomagnetic field behavior over short timescales (e.g., secular variation, relative paleointensity, polarity transitions). In contrast, a BGRM is still likely to provide paleomagnetic data that can be used to determine paleomagnetic pole positions and paleolatitude variations, because it will be locked in after initial sediment compaction and will be less affected by inclination shallowing. Magnetostratigraphic data based on BGRMs are likely to be complicated in periods such as the Neogene, when chron duration is often <300 kyr.

When diagenetic conditions are neither strongly reducing, nor strongly oxic, suboxic conditions can be found through thick sedimentary sequences (Roberts et al., 2011). In this case, MTB can live within or below the surface mixed layer, where magnetofossils will give rise to a syn-depositional BDRM or a post-depositional BGRM that is preserved due to subsequent suboxic conditions (**Figure 1C**; Roberts et al., 2013). The fact that most pelagic carbonates and clays provide superb records of geomagnetic polarity changes suggests that such BDRMs are far more common than previously considered in pelagic sediments (Roberts et al., 2013). Suboxic conditions in pelagic settings appear to be linked to fertilization of phytoplankton productivity by eolian dust, which delivers nutrients at concentrations large enough to fuel bacterial metabolism at the seafloor but not in such large amounts to drive reducing diagenetic conditions (Roberts et al., 2011, 2013; Larrasoña et al., 2012; Yamazaki and Ikehara, 2012).

In recent years, technical improvements aimed at discriminating sources of fine-grained magnetic minerals, such as hysteresis measurements, unmixing of isothermal remanent magnetization (IRM) curves, first-order reversal curve (FORC) diagrams, ferromagnetic resonance (FMR) measurements, high- and low-temperature magnetic measurements, and transmission electron microscope (TEM) observations, enable improved identification of magnetofossils in the sedimentary record (Moskowitz et al., 1993; Egli, 2004; Weiss et al., 2004; Kopp et al., 2006; Liu et al., 2012; Chang et al., 2013; Roberts et al., 2013). Of special relevance is the use of FORC diagrams because they enable conclusive identification of the non-interacting SD properties due to magnetofossils even if they are mixed with other magnetic components. Thus, intact magnetosome chains produce a characteristic “central ridge” on FORC diagrams due to these properties (Yamazaki, 2008; Abrajevitch and Kodama, 2009; Yamazaki, 2009; Egli et al., 2010; Roberts et al., 2011; Larrasoña et al., 2012; Roberts et al., 2012;

Yamazaki and Ikehara, 2012; Channell et al., 2013a,b; Heslop et al., 2013; Paterson et al., 2013; Roberts et al., 2013; Yamazaki et al., 2013). Disrupted magnetosome chains can also be identified because chain disruption increases the magnetic interaction between magnetosome particles and nearby chains (Kind et al., 2011; Li et al., 2012; Roberts et al., 2012, 2013). Improved methods for identifying biogenic magnetite in sediments has enabled rapid expansion of the database of pre-Quaternary magnetofossils in sediments, which until recently were considered rare (Kopp and Kirschvink, 2008). This has boosted renewed interest in the implications of magnetofossils as carriers of paleomagnetic and paleoenvironmental signals (e.g., Roberts et al., 2012, 2013).

Here we present a magnetostratigraphic study of marine sediments from the late Miocene sedimentary fill of the Guadalquivir Basin (GB). These sediments were recovered in two boreholes drilled in the western sector of the basin (Huelva-1 and Montemayor-1). Paleomagnetic data from these sediments have been used to constrain age models for the boreholes (Larrasoña et al., 2008; Jiménez-Moreno et al., 2013), but details of their paleomagnetic behavior and remanence carriers have not been published previously. Here we provide a description of these paleomagnetic data, which are combined with new hysteresis, FORC, and high- and low-temperature (low-T) measurements to demonstrate that the magnetic mineral assemblage within the studied sediments is dominated by biogenic magnetite. Biostratigraphic and paleoenvironmental data for the studied sediments enable us to discuss the relevance of magnetofossils as reliable carriers of paleomagnetic and paleoenvironmental signals.

MATERIALS AND METHODS

The GB is an ENE-WSW elongated basin that constitutes the foreland of the Betic Cordillera in SW Spain (Sierra et al., 1996; González-Delgado et al., 2004; **Figure 2A**). The GB is limited to the north by the Paleozoic and Mesozoic rocks of the Iberian Massif, and to the South by the Mesozoic and Cenozoic rocks of the Betic Cordillera. During the late Miocene, the GB developed in response to the stacking of tectonic units in the external Betics and the resulting flexural subsidence of the Iberian Massif (Sierra et al., 1996; García-Castellanos et al., 2002; González-Delgado et al., 2004). During the Tortonian stage, the GB constituted the Atlantic side of the Betic Corridors, which, together with the Rifian Corridors in Morocco, enabled connection between the Mediterranean Sea and the Atlantic Ocean (**Figure 2B**). In the lower GB, warm and salty Mediterranean Outflow Waters (MOW) met the cooler and fresher Atlantic Upwelled Waters (AUW; Pérez-Asensio et al., 2012a). Progressive closure of the Betic Corridors led to the GB becoming a wide embayment open to the Atlantic Ocean (Sierra et al., 1996; Martín et al., 2009) and, eventually, to interruption of the connection between the Atlantic Ocean and the Mediterranean Sea during the Messinian salinity crisis (MSC; Krijgsman et al., 1999; Manzi et al., 2013). The sedimentary fill of the GB is made up of a lower marine sequence (late Tortonian–early Pliocene) and an upper continental sequence (late Pliocene to Recent; Sierra et al., 1996; González-Delgado et al., 2004; Salvany et al., 2011).

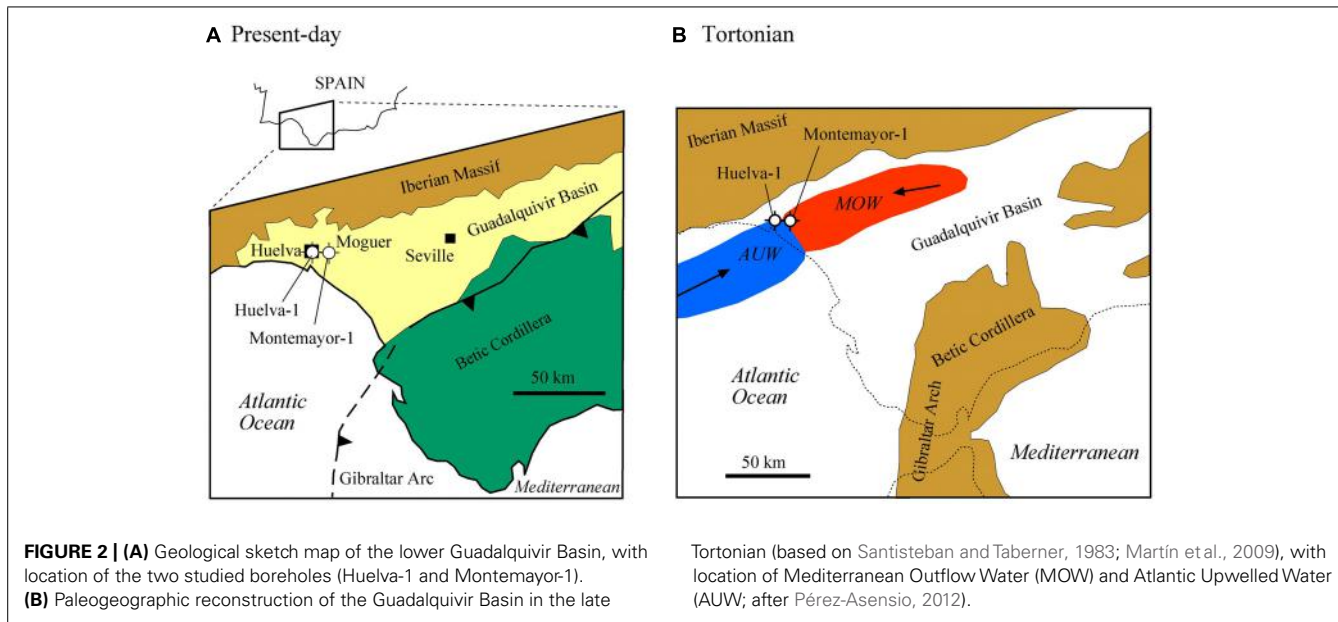


FIGURE 2 | (A) Geological sketch map of the lower Guadalquivir Basin, with location of the two studied boreholes (Huelva-1 and Montemayor-1). **(B)** Paleogeographic reconstruction of the Guadalquivir Basin in the late

The Huelva-1 and Montemayor-1 boreholes were drilled by the IGME (Spanish Geological Survey) in the city of Huelva and near the village of Moguer, respectively, in the western sector of the GB (the so-called lower GB; **Figure 2A**). In this part of the basin, the sedimentary sequence reaches its maximum thickness and is not affected by tectonic uplift, so that sediments retain their original horizontal attitude. In the Huelva-1 and Montemayor-1 boreholes, marine sediments were recovered from the three lowermost lithostratigraphic units that constitute the sedimentary fill of the lower GB (Sierro et al., 1996; González-Delgado et al., 2004; **Figures 3 and 4**). The lowermost unit, the Niebla Formation (late Tortonian), is composed of mixed carbonate-siliciclastic coastal deposits that onlap unconformably the Paleozoic–Mesozoic basement (Pendón et al., 2004). The second unit, the Arcillas de Gibraleón Formation (late Tortonian–Messinian), mainly consists of greenish-bluish clays that accumulated in a deep marine trough at the foothills of the Betic Cordillera, and represents the largest volume of sediments in the lower GB (González-Delgado et al., 2004). The uppermost unit, the Arenas de Huelva Formation (early Pliocene), is constituted by sands and silts that accumulated in a shallow marine environment (González-Delgado et al., 2004), and is overlain by transitional sands of the Arenas de Bonares Formation (Mayoral and Pendón, 1987). Continued sedimentation throughout the late Miocene drove the WSW-directed migration of maximum sediment thicknesses along the longitudinal axis of the basin (Sierro et al., 1996). The Huelva-1 borehole encompasses the Niebla Formation (4 m) and most (172 m) of the Arcillas de Gibraleón Formation. The Montemayor-1 borehole includes the Niebla Formation (0.5 m), the Arcillas de Gibraleón Formation (198 m), the Arenas de Huelva (42 m), and the lowermost 14.5 m of the Arenas de Bonares Formation. Both boreholes reached the basement of the basin and include Quaternary deposits in their uppermost meters.

Paleomagnetic samples were taken from the cores parallel to the bedding plane using an electric drill. Sampling resolution ranges

between 10 and 100 cm and excluded the uppermost 10–20 m of each core, where the unconsolidated nature of the sediments prevented this type of sampling. The natural remanent magnetization (NRM) was measured using two cryogenic magnetometers (GM400 and 2-G Enterprises) and was demagnetized using a TSD-1 thermal demagnetizer at the Paleomagnetic Laboratory of the Institute of Earth Sciences Jaume Almera (CCITUB-CSIC), Barcelona. Biostratigraphic results are based on identification of a series of planktic foraminiferal (PF) events, whose determination is based on quantitative and qualitative changes of *globorotaliid* and *neogloboquadrinid* species (Sierro et al., 1993, 1996; González-Delgado et al., 2004).

In order to characterize the magnetic mineralogy of the studied samples, variations in magnetic susceptibility from room temperature to 700°C (χ -T curves) were measured in an argon atmosphere using a Kappabridge KLY-3 magnetic susceptibility meter equipped with a CS-3 furnace. Magnetic hysteresis and FORC measurements were conducted on selected samples to discriminate magnetic mineralogy, domain state, and magnetic interactions among magnetic particles (Day et al., 1977; Roberts et al., 2000). Hysteresis and FORC measurements were made on ~700–800 mg samples using a Princeton Measurements Corporation vibrating sample magnetometer. FORCs were measured following the protocol of Egli et al. (2010) for optimal identification of magnetofossils. We used averaging times of around 0.3–0.5 s and 1 s depending on the magnetization of the sample. FORC diagrams were produced using the VARIFORC software of Egli (2013), which enables variable smoothing that takes into account variable signal-to-noise ratios in different areas within the diagram. Key parameters for VARIFORC calculations (see Egli, 2013 for details) were: $s_{c,0} = 9$, $s_{c,1} = 9$, $s_{b,0} = 9$, $s_{b,1} = 9$, and $\lambda = 0.03$. Statistical significance levels were calculated for the FORC distributions, and confidence intervals were calculated for profiles through parts of the FORC distributions, following Heslop and Roberts (2012). Low-T measurements of a M_r applied at 20 K

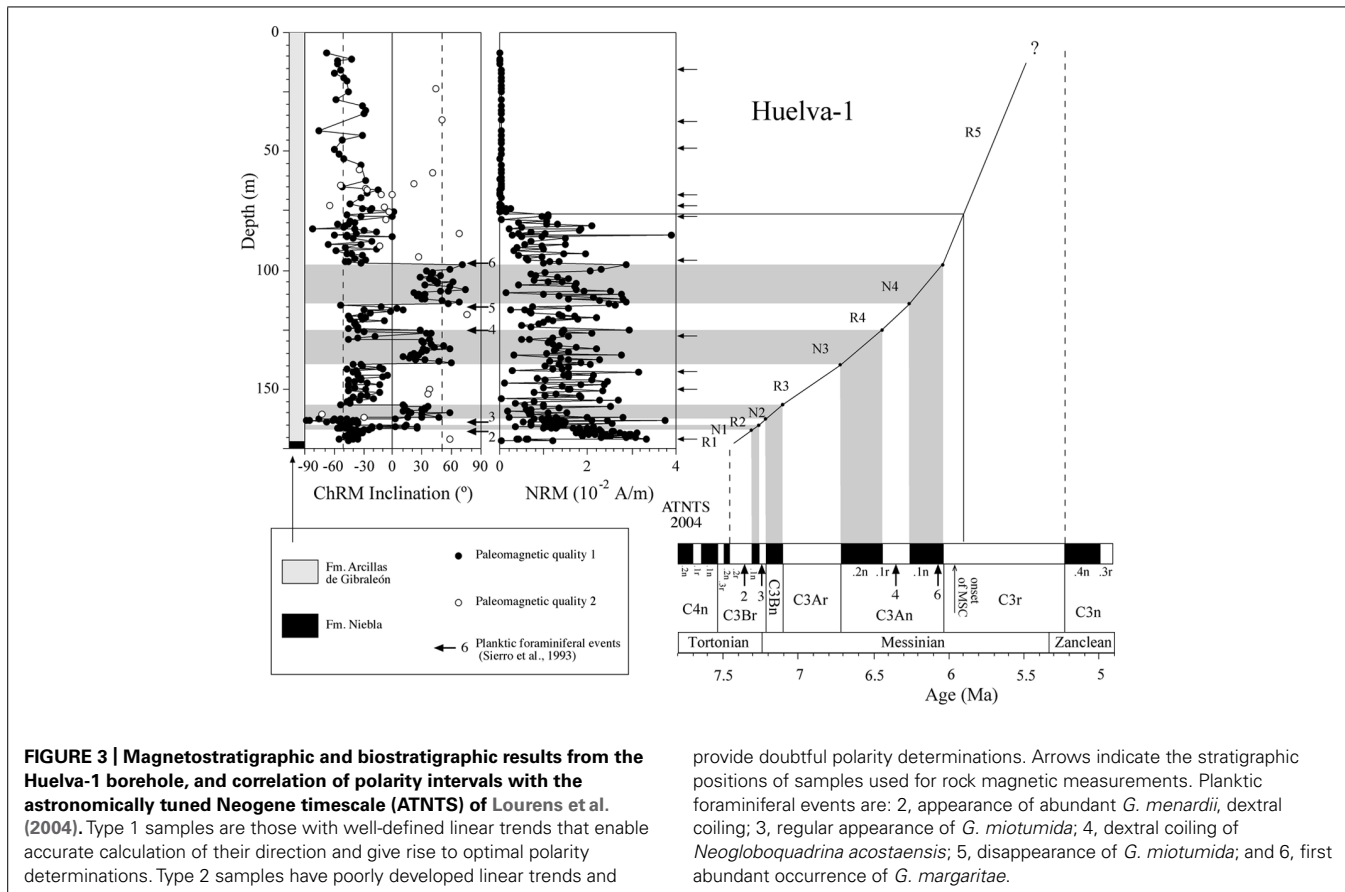


FIGURE 3 | Magnetostatigraphic and biostratigraphic results from the Huelva-1 borehole, and correlation of polarity intervals with the astronomically tuned Neogene timescale (ATNTS) of Lourens et al. (2004). Type 1 samples are those with well-defined linear trends that enable accurate calculation of their direction and give rise to optimal polarity determinations. Type 2 samples have poorly developed linear trends and

provide doubtful polarity determinations. Arrows indicate the stratigraphic positions of samples used for rock magnetic measurements. Planktic foraminiferal events are: 2, appearance of abundant *G. menardii*, dextral coiling; 3, regular appearance of *G. miotumida*; 4, dextral coiling of *Neogloboquadrina acostaensis*; 5, disappearance of *G. miotumida*; and 6, first abundant occurrence of *G. margaritae*.

and warmed to room temperature were made with a Quantum Designs Magnetic Property Measurement System (MPMS). These measurements were made after cooling the samples to 20 K both in the presence field cooled (FC) and absence zero-field cooled (ZFC) of a 2.5 T magnetic field. Differences between FC and ZFC low-T measurements, expressed as the normalized difference between the magnetization above and below the Verwey transition for each curve ($\delta_{\text{FC}}/\delta_{\text{ZFC}}$), were used to identify intact magneto-some chains in the studied samples and their possible surficial oxidation (Moskowitz et al., 1993). All rock magnetic experiments were performed at the Institute of Geology and Geophysics in Beijing, China.

A representative set of carbon-coated sediment chip fragments was studied using a scanning electron microscope (SEM) to determine the relative amount and microtextures of pyrite, and hence to obtain insights into the presence and strength of reducing diagenetic conditions in the Gibraleón Formation marls. This was done using a Jeol JSM6400, operated at 20 kV, at the National Centre for Electron Microscopy in Madrid. Chemical compositions of sediment constituents were determined using energy dispersive spectroscopy (EDS).

RESULTS

MAGNETOBIOSTRATIGRAPHY

Thermal demagnetization results indicate the presence of two paleomagnetic components. A low-T component unblocks

typically below 200°C and has shallow inclinations. This component is interpreted as an unstable component acquired during drilling, and will not be discussed further. A characteristic remanent magnetization (ChRM) directed toward the origin of the orthogonal vector component plot with both positive and negative directions is identified above 200°C and up to 600°C, which suggests that magnetite is the main carrier of the NRM (Figure 5). Stable ChRM directions with unblocking temperatures up to 600°C are typically associated with larger NRM intensities (Figures 5A,B). When the NRM is weaker, the ChRM has maximum unblocking temperatures of <450°C but still with a well-defined linear trend directed to the origin of the demagnetization plots (Figures 5C–E). Regardless, samples with reliable ChRM directions are labeled as Type 1. Type 2 samples have less clearly identified ChRM directions (e.g., Figure 5F), and are not considered further. Type 1 ChRM directions have both positive and negative inclinations regardless of NRM intensity, which suggests that the ChRM provides a reliable record of geomagnetic polarity reversals. The mean of the positive (normal polarity) ChRM directions in the Huelva-1 core is $33.6^\circ \pm 17.5^\circ$, whereas the mean of the negative (reversed polarity) ChRM directions is $-39.4^\circ \pm 14.5^\circ$ (the error given is the standard deviation because the azimuth of the boreholes is unknown and α_{95} cannot be calculated). For the Montemayor-1 core, these mean values are $30.6^\circ \pm 15.8^\circ$ and $-37.9^\circ \pm 12.9^\circ$, respectively. The mean values are significantly shallower than the expected inclination for

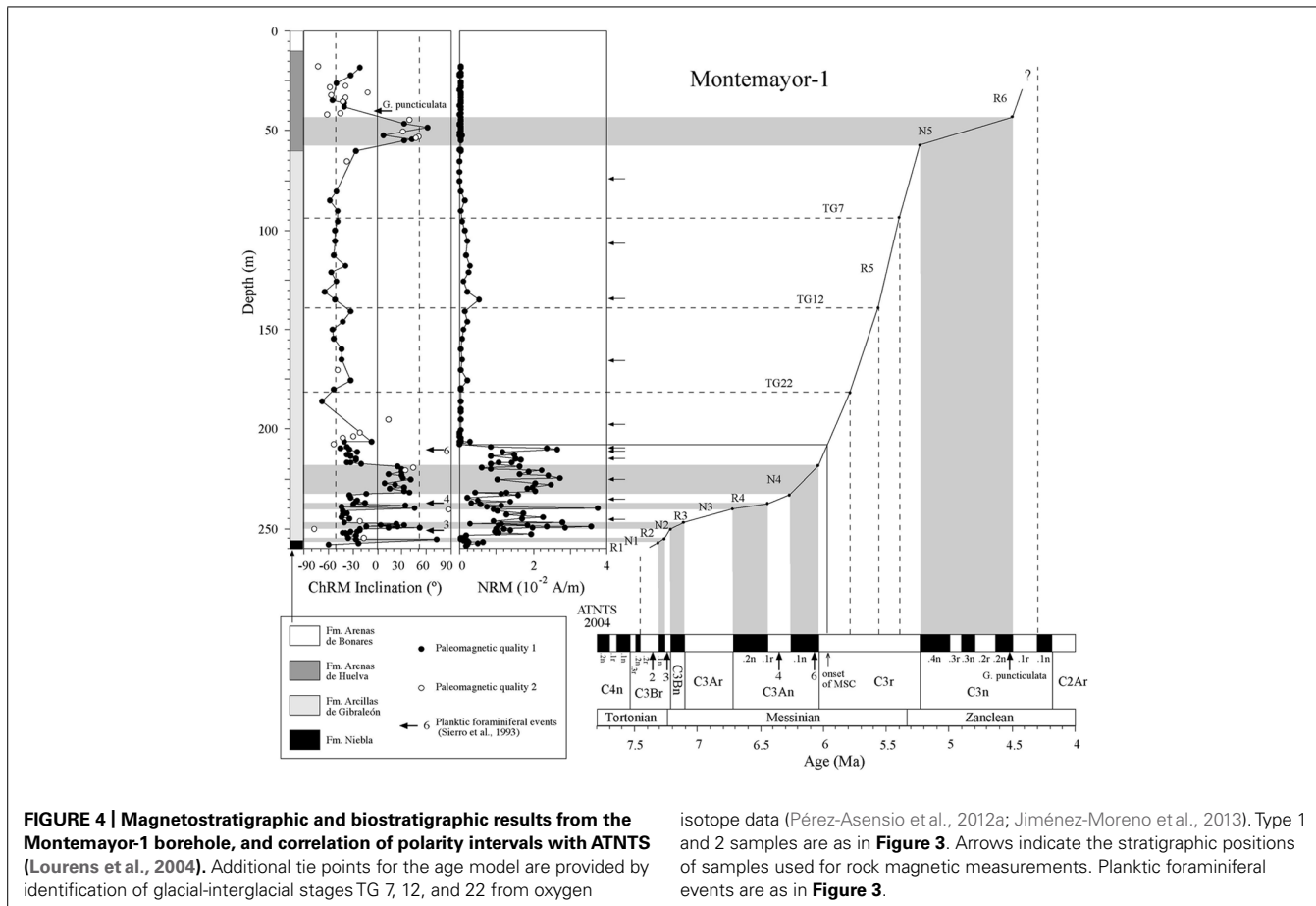


FIGURE 4 | Magnetostratigraphic and biostratigraphic results from the Montemayor-1 borehole, and correlation of polarity intervals with ATNTS (Lourens et al., 2004). Additional tie points for the age model are provided by identification of glacial-interglacial stages TG 7, 12, and 22 from oxygen

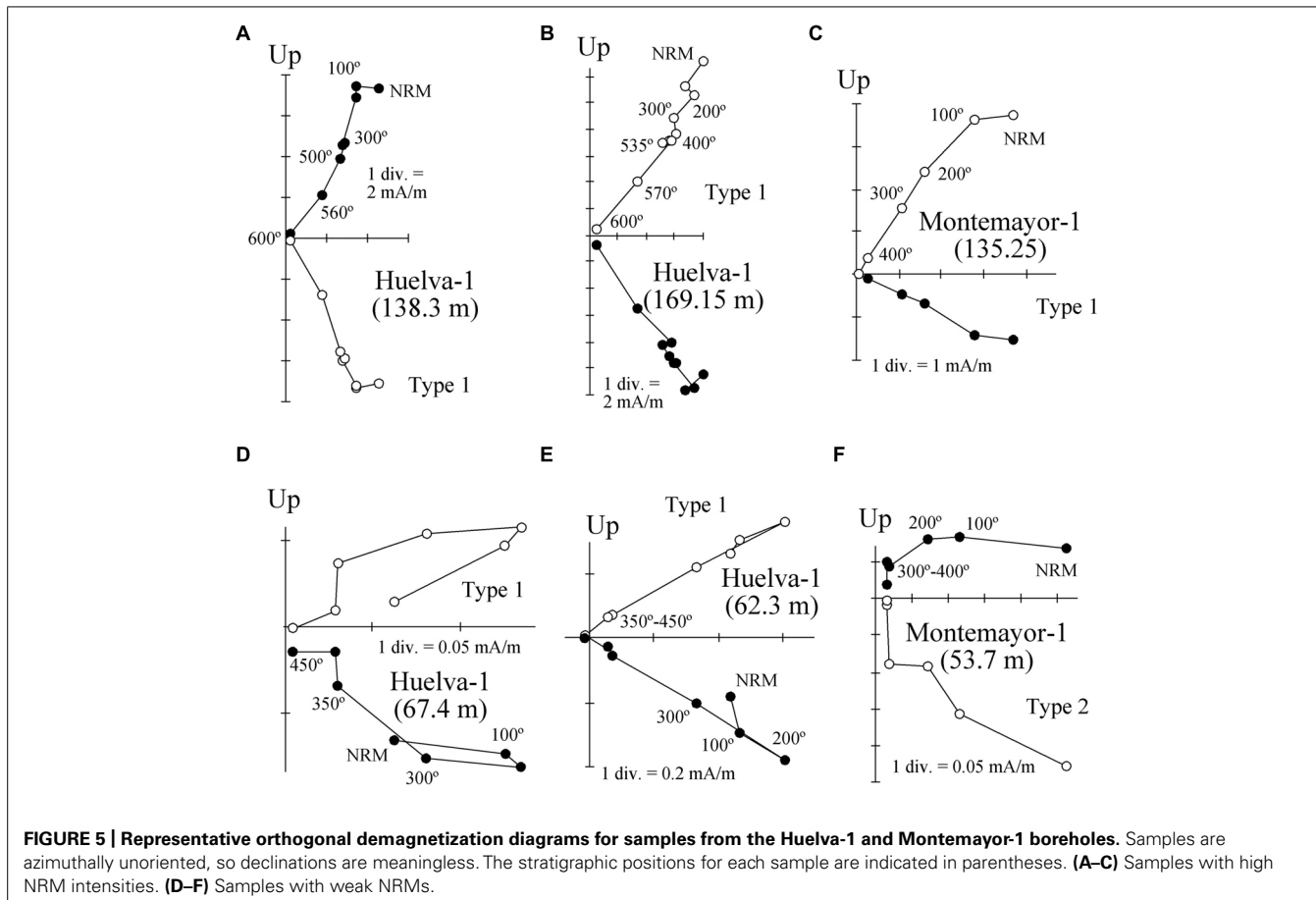
isotope data (Pérez-Asensio et al., 2012a; Jiménez-Moreno et al., 2013). Type 1 and 2 samples are as in **Figure 3**. Arrows indicate the stratigraphic positions of samples used for rock magnetic measurements. Planktic foraminiferal events are as in **Figure 3**.

a geocentric axial dipole field at the studied site latitude during the late Miocene (over 50°). The azimuth of the boreholes is unknown, therefore the magnetic polarity stratigraphy is based on the ChRM inclination. Eleven polarity intervals are documented (labeled N1–N5 and R1–R6 for normal and reversed polarity intervals, respectively). The Huelva-1 core includes magnetozones R1–R5, whereas the Montemayor-1 core includes magnetozones R1–R6. The polarity record has a largely square-wave shape that attests to its quality. The exceptions are magnetozones N3 and R4 in the Huelva-1 borehole (**Figure 3**), where reversed and normal polarity directions are recorded down to 2.7 and 4.6 m below their upper boundaries, respectively. A sharp decrease in NRM intensity occurs at around 208 m and 76 m in the Montemayor-1 and Huelva-1 boreholes, respectively (**Figures 3 and 4**).

Planktic foraminiferal event 2 (appearance of abundant *Globorotalia menardii*, dextral coiling) is identified in the uppermost part of magnetozone R1 in the Huelva-1 borehole (**Figure 3**). PF3 (regular appearance of *G. miotumida*, a marker for the Tortonian/Messinian boundary) and PF4 (dextral coiling of *Neogloborotalia acostaensis*) are identified within magnetozone R2 and at the top of magnetozone N3, respectively, in both boreholes (**Figures 3 and 4**). PF 5 (disappearance of *G. miotumida*) is only identified in the Huelva-1 borehole, in the uppermost part of magnetozone R4. PF6 (first abundant occurrence of

G. margaritae) has been identified in both boreholes near the magnetozone N4/R5 boundary. The appearance of *G. puncticulata* is found in the lower part of magnetozone R6 in the Montemayor-1 core.

The magnetozone pattern and the position of PF events enable straightforward correlation of the studied cores to the astronomically tuned geomagnetic polarity timescale (ATNTS2004) of Lourens et al. (2004; **Figures 3 and 4**). PF2, PF3, and PF4 are located within chron C3Br.2r, C3Br.1r and the lower part of C3An.1r, respectively (Lourens et al., 2004). Thus, magnetozone R1 must correlate with chron C3Br.2r, R2 with C3Br.1r and R4 with C3An.1r. This correlation implies that the long magnetozone R5 correlates with C3r, which is consistent with the long duration of this chron and with the presence of PF6 near the boundary with chron C3An.1n. The appearance of *G. puncticulata* is dated at 4.52 Ma near the top of chron C3n.2n (Lourens et al., 2004). Keeping in mind the litoral facies of the Arenas de Huelva Formation and the possible lack of continuity in such facies, this suggests that magnetozone N5 represents an amalgamation of the lower part of chron C3n due to discontinuous sedimentation (Jiménez-Moreno et al., 2013). In this case, magnetozone R6 probably correlates with chron C3n.1r. The magnetostratigraphic results presented here indicate that the Huelva-1 borehole is continuous and spans from the latest Tortonian (chron C3Br.2r, ca. 7.4 Ma) to the latest Messinian (uppermost part of chron C3r,



ca 5.4 Ma). The Montemayor-1 borehole spans from the latest Tortonian (chron C3Br.2r, ca 7.4 Ma) to the lower Pliocene (Zanclean, chron C3r/C2Ar boundary, ca 4.3–4.2 Ma), which provides a continuous late Miocene record. The only stratigraphic gap appears to be at the base of the Huelva Formation, which marks a sedimentary break that is attributed to a combination of sea level changes (González-Delgado et al., 2004) and tectonic processes (Salvany et al., 2011). Oxygen isotopic data for benthic and planktic foraminifera from the Montemayor-1 borehole enable identification of three distinctive glacial-interglacial stages (TG7, 12 and 22) within chron C3r, which enable refinement of the age model within this long chron (Pérez-Asensio et al., 2012a; Jiménez-Moreno et al., 2013). The age models thereby established for the Huelva-1 and Montemayor-1 boreholes enable calculation of linear sediment accumulation rates (SARs), which have similar trends at both boreholes (Figures 3 and 4). SARs were <5 cm/kyr until around 6.4 Ma with the exception of a transient increase (up to 8–14 cm/kyr) near the Tortonian/Messinian boundary. After 6.4 Ma, SARs progressively increased and underwent a major rise (exceeding 15 cm/kyr) at around 6 Ma, broadly coincident with the onset of the MSC.

ROCK MAGNETISM

Our rock magnetic study focuses on the clays of the Gibraleón Formation because they represent most of the recovered sequences

and, as opposed to the Huelva and Niebla formations, have high NRM intensities and sedimentary facies suitable for hosting biogenic magnetite. The main decay observed in the χ -T heating curves for samples located below 208 m and 76 m in the Montemayor-1 and Huelva-1 boreholes, respectively, which are characterized by high NRMs, is a drop at around 580°C (Figures 6A,B). This drop, which is sometimes preceded by a Hopkinson peak (Figure 6B), indicates the presence of magnetite. Above 580°C, the magnetic susceptibility signal persists and does not disappear completely until about 680°C (Figures 6A,B), which indicates variable contributions from hematite. In many samples, a subtle hump can be observed superimposed on the χ -T curve just below 300°C (Figures 6A,B). This can be interpreted as due to the thermally induced breakdown of minor amounts of maghemite (Liu et al., 2012). Cooling curves typically have higher χ values than heating curves below 580°C, which indicates widespread formation of magnetite during heating (Figures 6A,B). In samples above 208 m and 76 m in the Montemayor-1 and Huelva-1 boreholes, respectively, which are characterized by lower NRMs, thermally induced formation of magnetite above 450°C completely obscures the χ signal (Figure 6C). In these cases, a major increase in χ in the cooling curve below 530°C might suggest that the newly formed magnetite is not stoichiometric.

Hysteresis loops for all of the studied samples saturate below 200 mT, which is consistent with the dominance of magnetite.

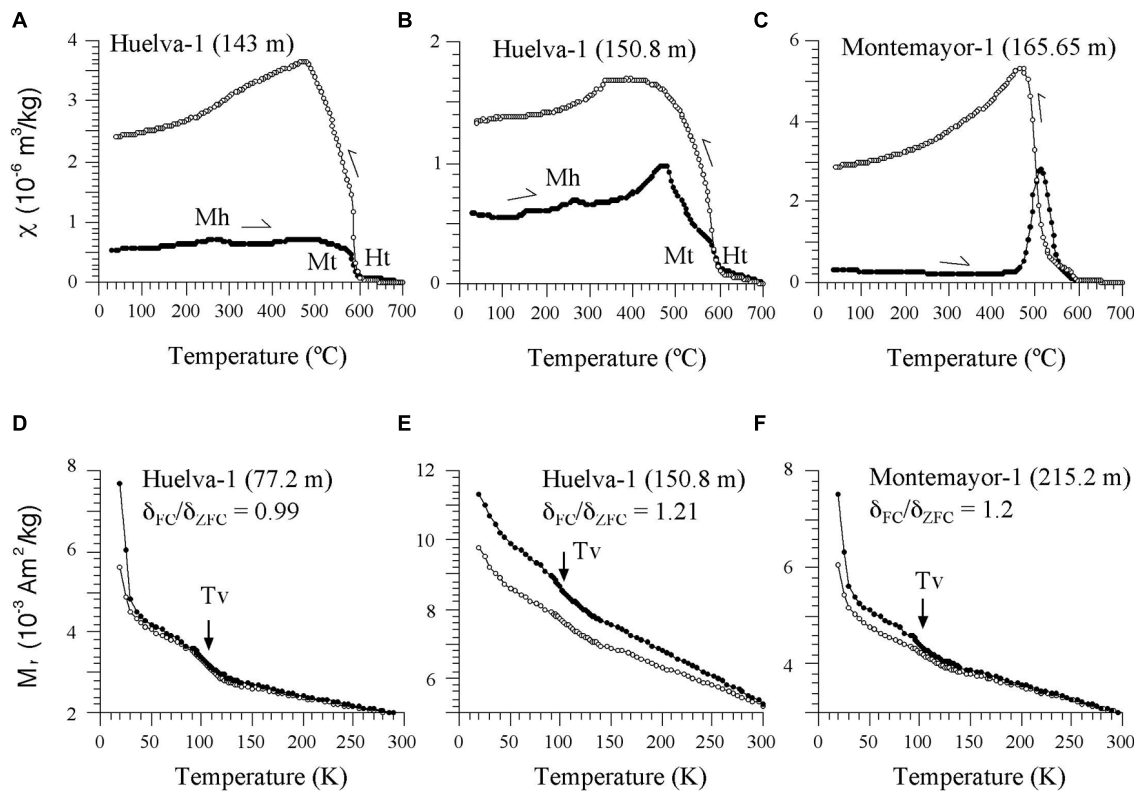


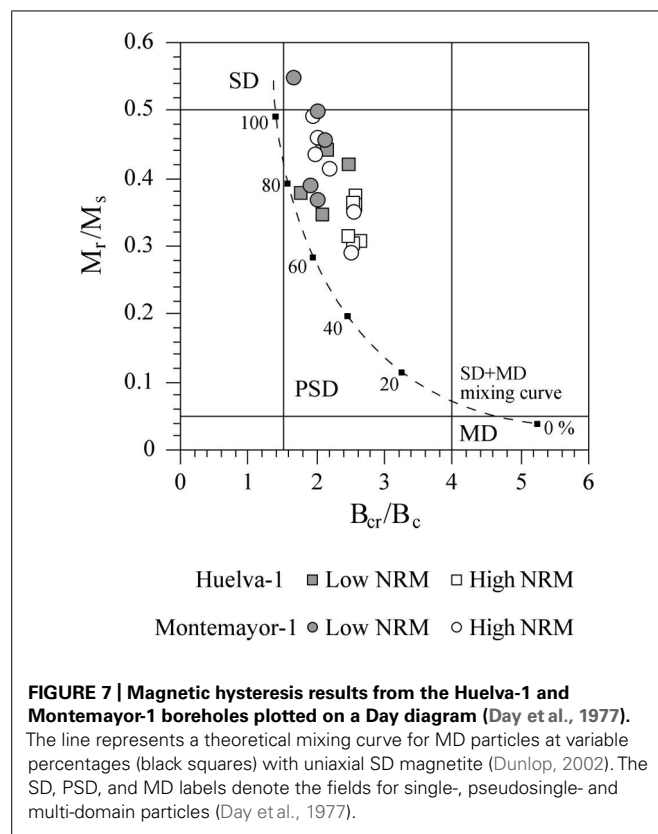
FIGURE 6 | (A-C) Representative χ -T curves for samples from the Huelva-1 and Montemayor-1 boreholes. Mt, magnetite; Ht, hematite; Mh, maghemite. **(D-F)** Representative low-T experiments for samples from the Huelva-1 and

Montemayor-1 boreholes, with indication of the Verwey transition (Tv) and δ_{FC}/δ_{ZFC} ratios of Moskowitz et al. (1993). The stratigraphic positions for each sample are indicated in parentheses.

All samples lie between the SD field and the upper left-hand part of the pseudo-single domain (PSD) region of the Day plot (Day et al., 1977; Figure 7). Samples lie slightly to the right of the theoretical line that represents mixtures of about 60–100% of equidimensional SD magnetite with multi-domain (MD) magnetite (Dunlop, 2002), which suggests an additional contribution from superparamagnetic (SP) material. The mean M_r/M_s value for Huelva-1 and Montemayor-1 samples is 0.37 and 0.43, respectively, which is close to the theoretical value of 0.5 for uniaxial SD magnetite grains and similar to other sediments where biogenic SD magnetite dominates the magnetic mineral assemblage (Kopp et al., 2007; Lippert and Zachos, 2007; Roberts et al., 2011; Larrasoña et al., 2012; Roberts et al., 2012, 2013). Samples from the upper parts of the two boreholes, where NRM intensities are distinctively lower, are characterized by larger M_r/M_s values (Figure 7), which points to a larger relative contribution of SD magnetite in these sediments.

First-order reversal curve distributions of samples from the two studied boreholes are similar in all cases. They are characterized by closed concentric contours about a central peak located between 20 and 30 mT (Figure 8). Vertical profiles through the peak of the coercivity distributions have a narrow distribution (e.g., <5 mT) around the dominant central peak, whereas horizontal profiles along $B_b = 0$ mT have a skewed Gaussian shape with variable spreading. These features, which

are statistically significant at the 0.05 level (see dark contours calculated following Heslop and Roberts (2012) in Figure 8), define the “central ridge” signature that is typical of intact magnetosome chains (Egli et al., 2010; Roberts et al., 2011, 2012, 2013). Variable coercivity peaks likely indicate mixtures of the so-called “biogenic soft” and “biogenic hard” magnetosome components, whose coercivities (of about 20 and 40 mT, respectively) likely reflect different magnetosome morphologies (Egli et al., 2010; Yamazaki and Ikehara, 2012; Roberts et al., 2013). In some cases (Figures 8A,C), the slight spreading of the outer contours around the peak of the FORC distributions points to some magnetostatic interactions due likely to disruption of a portion of the total number of magnetosome chains (Egli et al., 2010; Kind et al., 2011; Li et al., 2012; Roberts et al., 2012, 2013). The background magnetization observed in the vertical profiles below the narrow central peak suggests an additional contribution of coarser-grained magnetite of probable detrital origin. This detrital component appears to also be responsible for the large spreading observed in the horizontal profile in some samples (Figure 8B). The overall weaker magnetization of samples from the upper parts of boreholes Huelva-1 and Montemayor-1 made high-resolution FORC measurements too noisy to enable reliable identification of magnetic components. Nevertheless, hysteresis ratios of weakly magnetic samples are similar to those of samples with a clear central ridge signature in the FORC diagrams,



which suggests that magnetofossils also dominate their magnetic assemblages.

Low-T data indicate the presence of the Verwey transition at around 105 K both in the FC and ZFC curves in all samples (**Figures 6D–F**). The FC and ZFC cooled curves typically diverge below the Verwey transition, which gives further support for the occurrence of magnetofossils in the studied samples. $\delta_{\text{FC}}/\delta_{\text{ZFC}}$ values range between ~ 1 and 1.21, which suggests that the magnetosome surfaces are partially oxidized (Moskowitz et al., 1993). This is consistent with the occurrence of maghemite as evidenced by the χ -T curves (**Figures 6A–C**).

Scanning electron microscope observations indicate that the studied sediments contain minor amounts of pyrite that occur typically within foraminiferal tests or near other organic remains such as coccolithophore shells (**Figure 9**). Most pyrite occurs in framboids that are $< 15 \mu\text{m}$ in diameter and that consist of small ($< 1 \mu\text{m}$) individual crystals. Framboidal pyrite is often accompanied by euhedral pyrite crystals that are typically $< 15 \mu\text{m}$ in size (**Figure 9A**).

DISCUSSION

PALEOMAGNETIC IMPLICATIONS OF MAGNETOFOSIL PRESERVATION

χ -T and low-T experiments, coupled with hysteresis and FORC results, indicate that the magnetic mineral assemblage of the Gibraleón Formation clays is dominated by fossilized intact magnetosome chains that are in some cases partially oxidized. Significant disruption of magnetofossil chains might have been prevented by adhesion of magnetofossil chains onto the surface

of clay particles (e.g., Mao et al., 2014). In the absence of TEM images, an alternative origin for fine-grained magnetite linked to diagenetic oxidation of pyrite might be proposed (e.g., Brothers et al., 1996; Rowan and Roberts, 2006). We discard this possibility because: (1) pyrite in the studied clays is never observed in association with iron oxide overgrowths (**Figure 9**), and (2) this process often occurs during late diagenesis and would result in a prominent paleomagnetic overprint (Brothers et al., 1996; Rowan and Roberts, 2006) rather than in a pristine magnetostatigraphic record (**Figures 3 and 4**). Nevertheless, TEM observations are needed to corroborate the occurrence of magnetofossils in the studied clays and to assist in identifying different magnetosome morphologies. The Gibraleón Formation clays also contain variable amounts of hematite, which is a common constituent of Saharan dust transported into the NE Atlantic Ocean and has been reported in Quaternary sediments off the SW Iberian margin (Channell et al., 2013b). An eolian origin is therefore most likely for the hematite in the studied clays, although its contribution to the NRM is negligible (**Figure 5**). The NRM intensity of the clays is linked to the concentration of magnetofossils, as indicated by the similar NRM and M_s variations in both studied boreholes (**Figure 10**). This indicates that the magnetofossil concentration affects the quality of paleomagnetic data by enhancing the NRM. The mean of both normal and reversed polarity directions for the two studied boreholes is 15° to 20° shallower than expected. Inclination shallowing in fine-grained marine sediments has been typically interpreted as due to rolling of magnetic particles as they are deposited on a substrate for a DRM (e.g., King, 1955) or to sediment compaction that will affect a PDRM carried by detrital magnetic particles (Kent, 1973). Given that the magnetic mineral assemblage in the studied sediments is dominated by intact magnetosome chains, which are typically elongated with a length/width ratio that exceeds five (see Faivre and Schüller, 2008), a likely explanation for the observed paleomagnetic inclination shallowing is depositional flattening of magnetosome chains into the bedding plane. Subsequent sediment compaction might have also contributed to the observed inclination flattening, especially if magnetosome chains are adhered onto clay particles (Mao et al., 2014). More detailed studies are necessary to separate the contribution from these processes, which likely operate in concert in clay-rich lithologies that contain intact magnetofossil chains. Methods that enable discrimination between subfabrics of paramagnetic (e.g., low-T AMS) and ferrimagnetic minerals (e.g., AARM) would be of special relevance. Regardless, magnetofossils from the Gibraleón Formation are interpreted to carry a BDRM, which has recorded all polarity chronos regardless of their short durations, especially near the Tortonian/Messinian boundary (e.g., < 50 kyr; **Figures 3 and 4**). Possible delayed magnetizations have only been found down to 2.7 and 4.6 m below the uppermost boundaries of chrons C3An.1r and 2n, respectively, in the Huelva-1 borehole (**Figure 3**). Keeping in mind SARs of about 4 and 8 cm/kyr for these chrons, respectively (**Figure 10**), a delay of 68 and 58 kyr, respectively, can be estimated for the lock in time of magnetizations carried by magnetofossils at these depths. Higher-resolution studies are necessary to confirm and better characterize any BGRM in the studied boreholes.

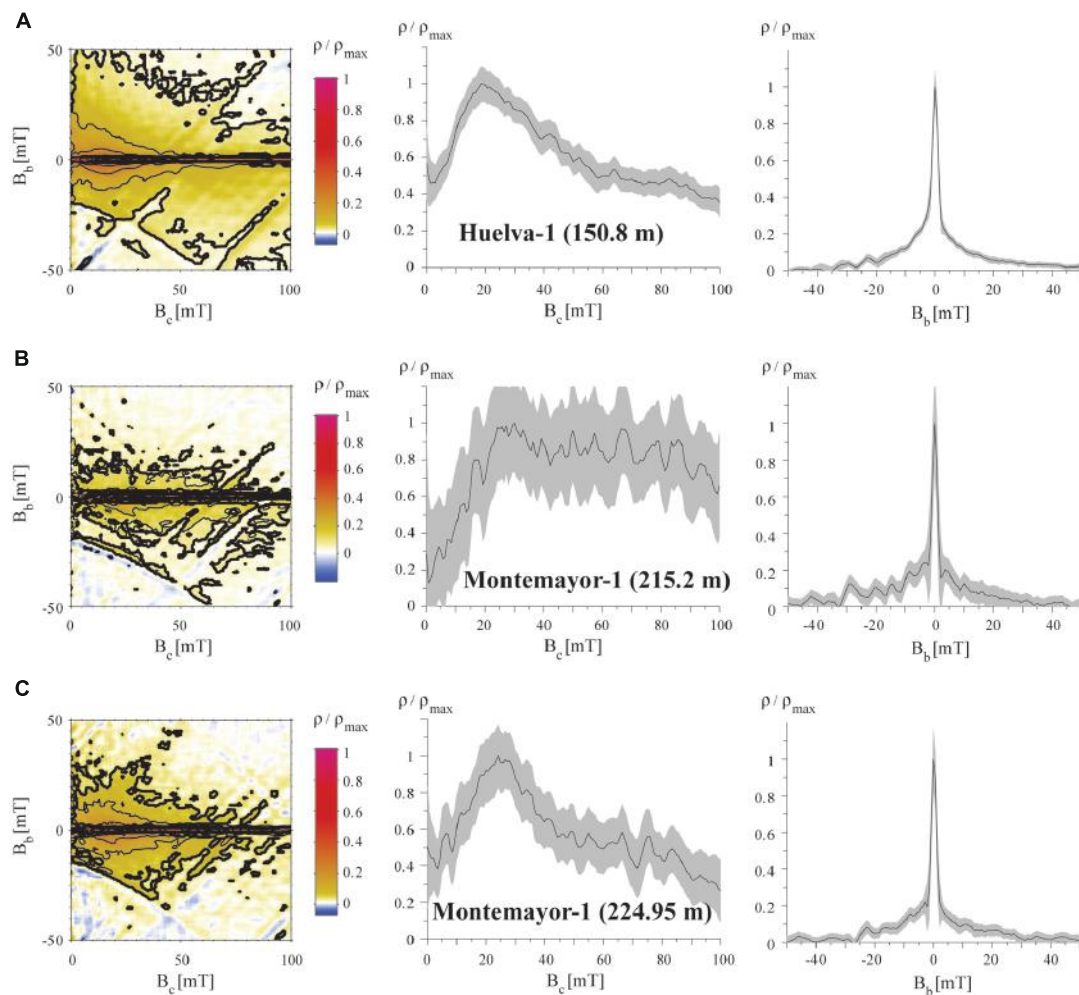


FIGURE 8 | Representative FORC diagrams for samples from the Gibraleón Formation in the Huelva-1 (A) and Montemayor-1 (B,C) boreholes, plotted with horizontal and vertical profiles through the FORC distributions. The stratigraphic position for each sample is shown in parentheses. All samples have a central ridge signature typical of intact magnetosome chains (Egli et al., 2010),

with variable contributions from other detrital magnetic particles and some magnetic interactions that result from partial collapse of magnetosome chains. VARIFORC parameters used to calculate the FORC distributions (Egli, 2013) are listed in Section 2. Confidence intervals on the profiles were calculated following Heslop and Roberts (2012).

PALEOENVIRONMENTAL IMPLICATIONS OF MAGNETOFossil PRESERVATION

Benthic foraminiferal assemblages and sedimentary facies indicate that clays of the Gibraleón Formation accumulated in a slope environment, although its lowermost (until about 7.2 Ma) and uppermost (after about 5.85 Ma) parts (Figure 10) accumulated in outer continental shelf environments (Pérez-Asensio, 2012; Pérez-Asensio et al., 2012b). Benthic foraminiferal assemblages point to oligotrophic and mesotrophic conditions during deposition of most of this formation, with the exception of one short-lived interval before 7.2 Ma (Figure 10; Pérez-Asensio, 2012). Oxygen isotopic data indicate that the lower GB was flushed by both the MOW and the AUW until 6.18 Ma (Pérez-Asensio, 2012; Pérez-Asensio et al., 2012a). After 6.18 Ma, rapid reduction and cessation of flow of the MOW suggests closure of the last marine Betic Corridors (Pérez-Asensio et al., 2012a; Figure 10). Later, at

about 5.97 Ma, the onset of the MSC led to disconnection of the Mediterranean basin from the Atlantic Ocean (Manzi et al., 2013). Our results indicate that magnetofossils dominate the magnetic mineral assemblage throughout the Gibraleón Formation regardless of changes in depositional setting, nutrient conditions, SARs, and important paleoceanographic events such as cessation of flow of the MOW and onset of the MSC (Figure 10). Mild, suboxic diagenetic conditions are required for preservation of magnetofossils through expanded sections of pelagic sediments that record a syn-depositional remanent magnetization (Roberts et al., 2011, 2013). Clays from the Gibraleón Formation are greenish-bluish in colour, which suggests that iron has been reduced and that sulphate reduction might have occurred. It should be noticed, however, that $\chi-T$ and low-T experiments indicate that magnetosomes are partially converted into maghemite by surficial oxidation, and it is unlikely that maghemite would

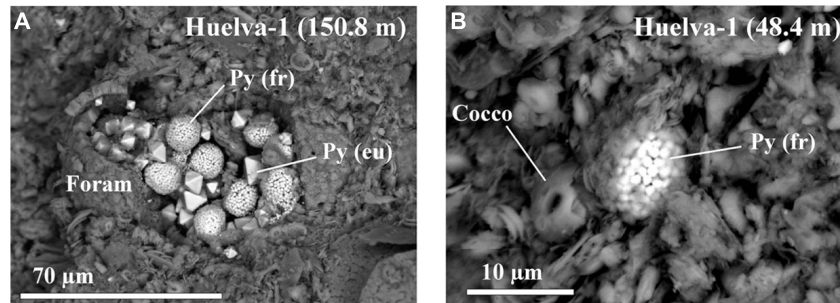


FIGURE 9 | Representative back-scattered scanning electron microscope images of pyrite microtextures in the Gibraleón Formation clays. (A) Framboidal and euhedral pyrite infilling a calcareous foraminifer shell dispersed within a matrix dominated by clays and quartz.

(B) Framboidal pyrite located beside a coccolith embedded within the sediment matrix. The stratigraphic positions for each sample are indicated in parentheses. Py (fr), frambooidal pyrite; Py (eu), euhedral pyrite crystal; Foram, foraminifer shell; Cocco, coccolith.

have survived reductive dissolution (Smirnov and Tarduno, 2000). SEM observations of pyrite microtextures indicate that reducing diagenetic conditions in clays from the Gibraleón Formation were mild and closely linked with organic-rich microenvironments (e.g., within foraminiferal tests). We interpret that flushing of the bottom waters in the lower GB by either the MOW and/or the AUW, coupled with mostly oligotrophic and mesotrophic conditions, led to mild diagenetic conditions suitable for flourishing of MTB and preservation of their magnetofossils throughout the Gibraleón Formation. Our results expand the settings in which magnetite magnetofossils can dominate the magnetic properties of sediments to include continental margin sedimentary sequences.

In view of the mild diagenetic conditions that favored preservation of magnetofossils throughout the Gibraleón Formation, and keeping in mind that they largely appear to carry a BDRM that is affected by inclination shallowing, we interpret that MTB lived within the surface mixed layer and, therefore, carry a reliable syn-depositional paleoenvironmental signal. In this case, the main feature needing explanation is the sharp drop observed in magnetofossil abundance at 5.9 Ma and 5.97 Ma in the Huelva-1 and Montemayor-1 boreholes, respectively (Figure 10). Pollen data from the Montemayor-1 borehole indicate that glacial/interglacial variability reported at orbital timescales was not significantly modified after the onset of the MSC at 5.97 Ma (Jiménez-Moreno et al., 2013), which suggests that climate variability is not the underlying cause for the observed drop in magnetofossil abundances. In both boreholes, the decreased magnetofossil content predates the change from meso- to oligotrophic conditions and from slope to shelf environments at 5.85 Ma, and postdates cessation of flow of the MOW by more than 200 kyr (Figure 10). In the Montemayor-1 borehole, however, the sharp shift in magnetofossil abundance coincides strikingly with the onset of the MSC at 5.97 Ma (Manzi et al., 2013; Figure 10B). It should be noted that the age of the drop was established by assuming a linear SAR between the two nearest tie points, namely the chron C3r/C3An boundary and glacial stage TG22 (Figure 10B). For the Huelva-1 borehole, the relevant tie points are the chron C3r/C3An boundary and the base of the Huelva Formation, which is located about 20 m higher in the borehole and, according to

results from Montemayor-1, is dated near the Miocene/Pliocene boundary (Figure 4). Keeping in mind this coarser age constraint, we interpret that the sharp drop in magnetofossil abundances is synchronous at the two boreholes and coincident with the MSC onset. The estimated SARs are also constrained by the positions of tie points used to construct the age models. We therefore associate the drop in magnetofossil abundance to a major rise in SAR at the chron C3r/C3An boundary (6.033 Ma), which follows a steady increase that started at 6.5 Ma (Figure 10). This link between magnetofossil abundance and SAR is supported by the overall inverse correlation between M_s and SAR (Figure 11), and therefore suggests that magnetofossil concentrations are controlled by terrigenous dilution. High-frequency changes in NRM intensity also suggest changes in magnetofossil abundance over much shorter timescales, but the extent and significance of such changes need to be assessed with more detailed rock-magnetic data. The marked rise in SAR appears to be linked to the onset of the MSC at 5.97 Ma (Manzi et al., 2013). We tentatively attribute this increased SAR to a change in sedimentation pattern in the GB during the MSC. Thus, closure of the Betic Corridors at that time might have conditioned delivery of large amounts of sediment that resulted from denudation of the Betic Cordillera, which was previously deposited in the Mediterranean Sea, into the Atlantic Ocean. This, in turn, would have accelerated westward progradation of sedimentary systems along the axis of the GB and the arrival of enhanced terrigenous inputs to the locations of the studied boreholes. Regardless of this interpretation, our results indicate that magnetofossils from the Gibraleón Formation carry paleoenvironmental signals that will help to better constrain the paleoceanographic and sedimentary evolution of the GB during the MSC.

CONCLUSIONS

Our results indicate that the magnetic mineral assemblage from the late Miocene Gibraleón Formation is dominated by intact magnetofossil chains. We suggest that ventilation of bottom waters in the lower GB, coupled with mostly oligotrophic and mesotrophic conditions, led to sustained suboxic diagenetic conditions suitable for flourishing of MTB and preservation of their magnetofossils throughout the Gibraleón Formation. Our results

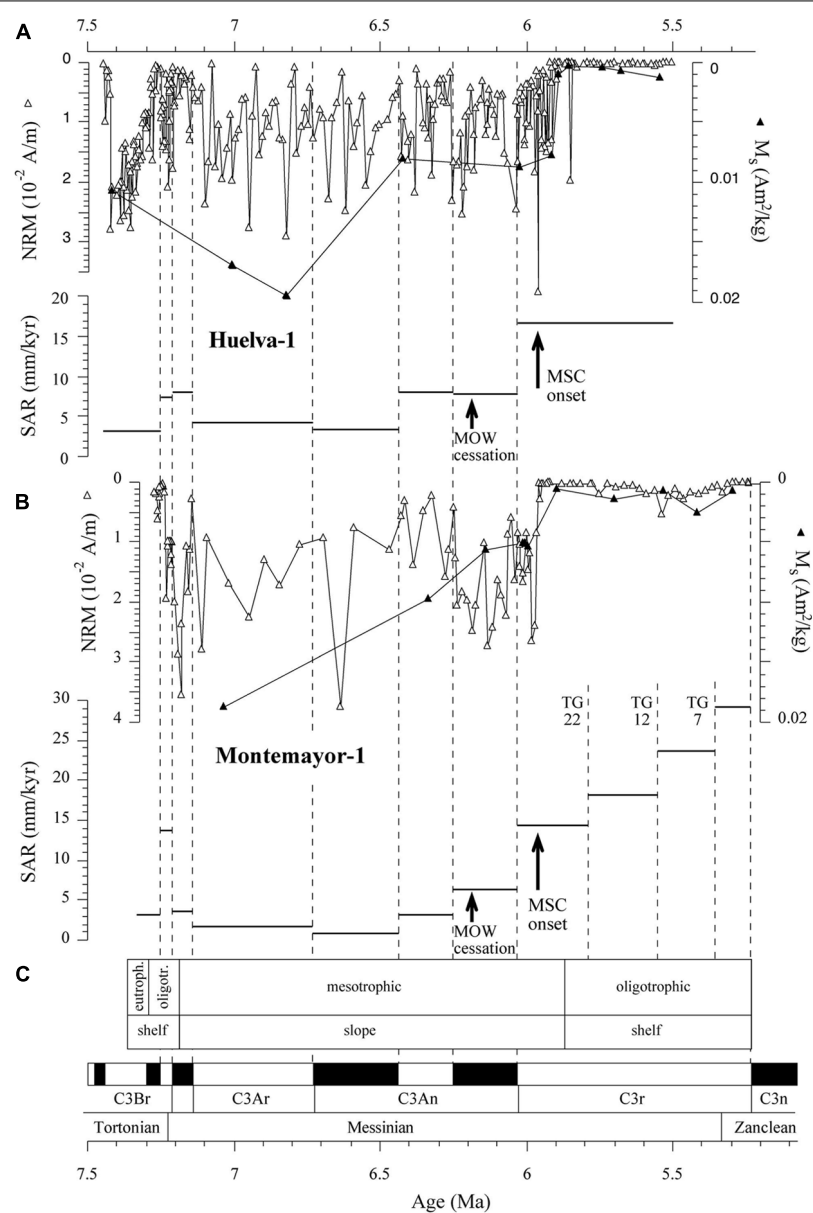


FIGURE 10 | NRM, M_s and sediment accumulation rate (SAR) variations as a function of age for the Huelva-1 (A) and Montemayor-1 (B) boreholes, shown with trophic conditions and depositional context (C) inferred from benthic foraminiferal assemblages in the Montemayor-1 borehole (Pérez-Asensio, 2012;

Pérez-Asensio et al., 2012a). Cessation of flow of the Mediterranean Outflow Water (MOW) along the Betic Corridors (Pérez-Asensio et al., 2012a) and onset of the Messinian salinity crisis (MSC; Manzi et al., 2013) are also shown. Dashed vertical lines mark the tie points used in the age models, including glacial-interglacial (TG) stages.

expand the range of settings in which magnetofossils can dominate the magnetic properties to include expanded continental margin sedimentary sequences, provided that diagenetic conditions remained suboxic and not anoxic. The concentration of magnetofossils also determines the quality of paleomagnetic data, which provides a robust magnetostratigraphic chronology for the studied sedimentary sequence despite recording paleomagnetic inclinations that are 15–20° shallower than expected. This observation is interpreted to indicate that MTB lived within the sedimentary surface mixed layer, so that magnetofossils were affected by

sediment compaction upon burial. Our results might also indicate depositional flattening of magnetosome chains due to their large length/width ratio. Regardless, our results suggest that magnetofossils carry a magnetization that is essentially identical to a post-depositional remanent magnetization, which, given its origin and distinctive significance, we refer to as a BDRM. The only exceptions to this syn-depositional pattern of remanence acquisition occur at the tops of chrons C3An.1r and 2n, where paleomagnetic directions appear to be delayed by ~60–70 kyr. Magnetofossils in these cases are interpreted to carry a BGRM.

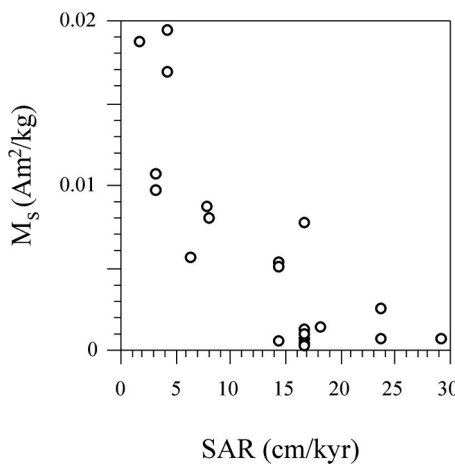


FIGURE 11 | Illustration of the inverse correlation between M_s , which is taken as a proxy for the concentration of magnetofossils, and estimated SAR.

Magnetofossil abundances decrease sharply in the two studied boreholes that coincided, within the limits of the age model, with a major rise in sediment accumulation rate near the onset of the MSC. Sedimentary changes triggered in the GB at the onset of the MSC appear to have caused enhanced terrigenous inputs and dilution of magnetofossil abundances. Our results indicate that magnetofossils can carry high-quality paleomagnetic data and useful paleoenvironmental signals even in dominantly terrigenous sediments.

AUTHOR CONTRIBUTIONS

Juan C. Larrasoña, Pilar Mata and Jorge Civis designed the study. Juan C. Larrasoña, Francisco J. Sierra and Jorge Civis produced magnetobiostratigraphic data. Qingsong Liu, Pengxiang Hu, and Andrew P. Roberts provided and processed rock magnetic data. José N. Pérez-Asensio provided paleoenvironmental data from the Montemayor-1 borehole. Juan C. Larrasoña led the writing of the paper, with input from all co-authors.

ACKNOWLEDGMENTS

This study was funded by the Guadalcyc project (MINECO, CGL2012-30875), ARC grant DP120103952, and NSFC grant 41374073. We are grateful to E. Beamuñ and M. Garcés for technical assistance at the paleomagnetic laboratory of the Institute of Earth Sciences Jaume Almera (CCiTUB-CSIC).

REFERENCES

- Abrajevitch, A., and Kodama, K. (2009). Biochemical vs. detrital mechanism of remanence acquisition in marine carbonates: a lesson from the K-T boundary interval. *Earth Planet. Sci. Lett.* 286, 269–277. doi: 10.1016/j.epsl.2009.06.035
- Bazylinski, D. A., and Frankel, R. B. (2004). Magnetosome formation in prokaryotes. *Nat. Rev. Microbiol.* 2, 217–230. doi: 10.1038/nrmicro842
- Blakemore, R. P. (1975). Magnetotactic bacteria. *Science* 190, 377–379. doi: 10.1126/science.170679
- Blakemore, R. P., Short, K. A., Bazylinski, D. A., Rosenblatt, C., and Frankel, R. B. (1985). Microaerobic conditions are required for magnetite formation within *Aquaspirillum magnetotacticum*. *Geomicrobiol. J.* 4, 53–71. doi: 10.1080/01490458509385920
- Brothers, L. A., Engel, M. H., and Elmore, R. D. (1996). The late diagenetic conversion of pyrite to magnetite by organically complexed ferric iron. *Chem. Geol.* 130, 1–15. doi: 10.1016/0009-2541(96)00007-1
- Chang, L., Winklhofer, M., Roberts, A. P., Heslop, D., Florindo, F., Dekkers, M. J., et al. (2013). Low-temperature magnetic properties of pelagic carbonates: oxidation of biogenic magnetite and identification of magnetosome chains. *J. Geophys. Res.* 118, 1–17. doi: 10.1002/2013JB010381
- Channell, J. E. T., Ohneiser, C., Yamamoto, Y., and Kesler, M. S. (2013a). Oligocene-Miocene magnetic stratigraphy carried by biogenic magnetite at Sites U1334 and U1335 (equatorial Pacific Ocean). *Geochem. Geophys. Geosyst.* 14, 265–282. doi: 10.1029/2012GC004429
- Channell, J. E. T., Hodell, D. A., Margari, V., Skinner, L. C., Tzedakis, P. C., and Kesler, M. S. (2013b). Biogenic magnetite, detrital hematite, and relative paleointensity in quaternary sediments from the Southwest Iberian Margin. *Earth Planet. Sci. Lett.* 376, 99–109. doi: 10.1016/j.epsl.2013.06.026
- Day, R., Fuller, M., and Schmidt, V. A. (1977). Hysteresis properties of titanomagnetites: grain size and composition dependence. *Phys. Earth Planet. Inter.* 13, 260–266. doi: 10.1016/0031-9201(77)90108-X
- Dickens, G. R. (2008). The riddle of the clays. *Nat. Geosci.* 1, 86–88. doi: 10.1038/ngeo118
- Dinarès-Turell, J., Hoogakker, B. A. A., Roberts, A. P., Rohling, E. J., and Sagnotti, L. (2003). Quaternary climatic control of biogenic magnetite production and eolian dust input in cores from the Mediterranean Sea. *Palaeogeogr. Palaeoclimatol. Palaeoecol.* 190, 195–209. doi: 10.1016/S0031-0182(02)00605-3
- Dunlop, D. J. (2002). Theory and application of the Day plot (Mrs/Ms versus Hcr/Hc). 1. Theoretical curves and tests using titanomagnetite data. *J. Geophys. Res.* 107, B2056. doi: 10.1029/2001JB000486
- Egli, R. (2004). Characterization of individual rock magnetic components by analysis of remanence curves. 3. Bacterial magnetite and natural processes in lakes. *Phys. Chem. Earth* 29, 869–884. doi: 10.1016/j.pce.2004.03.010
- Egli, R. (2013). VARIFORC: an optimized protocol for calculating non-regular first-order reversal curve (FORC) diagrams. *Global Planet. Change* 110, 302–320. doi: 10.1016/j.gloplacha.2013.08.003
- Egli, R., Chen, A. P., Winklhofer, M., Kodama, K. P., and Horng, C.-S. (2010). Detection of noninteracting single domain particles using first-order reversal curve diagrams. *Geochem. Geophys. Geosyst.* 11, Q01Z11. doi: 10.1029/2009GC002916
- Faivre, D., and Schüler, D. (2008). Magnetotactic bacteria and magnetosomes. *Chem. Rev.* 108, 4875–4898. doi: 10.1021/cr078258w
- García-Castellanos, D., Fernández, M., and Torné, M. (2002). Modelling the evolution of the Guadalquivir foreland basin (southern Spain). *Tectonics* 21. doi: 10.1029/2001TC001339
- González-Delgado, J. A., Civis, J., Dabrio, C. J., Goy, J. L., Ledesma, S., Pais, J., et al. (2004). “Cuenca del Guadalquivir”, in *Geología de España*, ed. J. A. Vera (Madrid: SGE-IGME), 543–550.
- Heslop, D., and Roberts, A. P. (2012). Estimation of significance levels and confidence intervals for first-order reversal curve distributions. *Geochem. Geophys. Geosyst.* 13, Q12Z40. doi: 10.1029/2012GC004115
- Heslop, D., Roberts, A. P., Chang, L., Davies, M., Abrajevitch, A., and De Deckker, P. (2013). Quantifying magnetite magnetofossil contributions to sedimentary magnetizations. *Earth Planet. Sci. Lett.* 382, 58–65. doi: 10.1016/j.epsl.2013.09.011
- Jiménez-Moreno, G., Pérez-Asensio, N., Larrasoña, J. C., Aguirre, J., Civis, J., Rivas-Carballo, M. R., et al. (2013). Vegetation, sea-level and climate changes during the Messinian salinity crisis. *Geol. Soc. Am. Bull.* 125, 432–444. doi: 10.1130/B30663.1
- Kent, D. V. (1973). Post-depositional remanent magnetisation in deep-sea sediment. *Nature* 246, 32–34. doi: 10.1038/246032a0
- Kind, J., Gehring, A. U., Winklhofer, M., and Hirt, A. M. (2011). Combined use of magnetometry and spectroscopy for identifying magnetofossils in sediments. *Geochem. Geophys. Geosyst.* 12, Q08008. doi: 10.1029/2011GC003633
- King, R. F. (1955). The remanent magnetism of artificially deposited sediments. *Geophys. J. Int.* 7, 115–134. doi: 10.1111/j.1365-246X.1955.tb06558.x
- Kopp, R. E., and Kirschvink, J. L. (2008). The identification and biogeochemical interpretation of fossil magnetotactic bacteria. *Earth Sci. Rev.* 86, 42–61. doi: 10.1016/j.earscirev.2007.08.001
- Kopp, R. E., Raub, T. D., Schumann, D., Vali, H., Smirnov, A. V., and Kirschvink, J. L. (2007). Magnetofossil spike during the Paleocene-Eocene thermal maximum: ferromagnetic resonance, rock magnetic, and electron microscopy evidence from Ancora, New Jersey, United States. *Paleoceanography* 22, PA4103. doi: 10.1029/2007PA001473

- Kopp, R. E., Weiss, B. P., Maloof, A. C., Vali, H., Nash, C. Z., and Kirschvink, J. L. (2006). Chains, clumps, and strings: magnetofossil taphonomy with ferromagnetic resonance spectroscopy. *Earth Planet. Sci. Lett.* 247, 10–25. doi: 10.1016/j.epsl.2006.05.001
- Krijgsman, W., Hilgen, F. J., Raffi, I., Sierro, F. J., and Wilson, D. S. (1999). Chronology, causes and progression of the Messinian salinity crisis. *Nature* 400, 652–655. doi: 10.1038/23231
- Larrasoña, J. C., González-Delgado, J. A., Civis, J., Sierra, F. J., Alonso-Gavilán, G., and Pais, J. (2008). Magnetobiostratigraphic dating and environmental magnetism of Late Neogene marine sediments recovered at the Huelva-1 and Montemayor-1 boreholes (lower Guadalquivir Basin, Spain). *Geotemas* 10, 1175–1178.
- Larrasoña, J. C., Roberts, A. P., Chang, L., Schellenberg, S. A., Fitz Gerald, J. D., Norris, R. D., et al. (2012). Magnetotactic bacterial response to Antarctic dust supply during the Palaeocene-Eocene thermal maximum. *Earth Planet. Sci. Lett.* 333–334, 122–133. doi: 10.1016/j.epsl.2012.04.003
- Lean, C. M. B., and McCave, I. N. (1998). Glacial to interglacial mineral magnetic and palaeoceanographic changes at Chatham Rise, SW Pacific Ocean. *Earth Planet. Sci. Lett.* 163, 247–260. doi: 10.1016/S0012-821X(98)00191-5
- Li, J. H., Wu, W. F., Liu, Q. S., and Pan, Y. X. (2012). Magnetic anisotropy, magnetostatic interactions and identification of magnetofossils. *Geochem. Geophys. Geosyst.* 13, Q10Z51. doi: 10.1029/2012GC004384
- Lin, W., Wang, Y. Z., and Pan, Y. X. (2012). Short-term effects of temperature on the abundance and diversity of magnetotactic cocci. *Microbiologyopen* 1, 53–63. doi: 10.1002/mbo3.7
- Lippert, P. C., and Zachos, J. C. (2007). A biogenic origin for anomalous fine-grained magnetic material at the Paleocene-Eocene boundary at Wilson Lake, New Jersey. *Paleoceanography* 22, PA4104. doi: 10.1029/2007PA001471
- Liu, Q. S., Roberts, A. P., Larrasoña, J. C., Banerjee, S. K., Guyodo, Y., Tauxe, L., et al. (2012). Environmental magnetism: principles and applications. *Rev. Geophys.* 50, RG4002. doi: 10.1029/2012RG000393
- Lourens, L. J., Hilgen, F. J., Shackleton, N. J., Laskar, J., and Wilson, D. S. (2004). “The Neogene period”, in *A Geologic Time Scale 2004*, eds F. M. Gradstein, J. G. Ogg, and A. G. Smith (Cambridge: Cambridge University Press), 409–440.
- Manzi, V., Gennari, R., Hilgen, F., Krijgsman, W., Lugli, S., Roveri, M., et al. (2013). Age refinements of the Messinian salinity crisis onset in the Mediterranean. *Terra Nova* 25, 315–322. doi: 10.1111/ter.12038
- Mao, X., Egli, R., Petersen, N., Hanzlik, M., and Zhao, X. (2014). Magnetotaxis and acquisition of detrital remanent magnetization by magnetotactic bacteria in natural sediment: first experimental results and theory. *Geochem. Geophys. Geosyst.* doi: 10.1002/2013GC005034 [Epub ahead of print].
- Martin, J. M., Braga, J. C., Aguirre, J., and Puga-Bernabéu, A. (2009). History and evolution of the North-Betic Strait (Prebetic Zone, Betic Cordillera): a narrow, early Tortonian, tidal-dominated, Atlantic-Mediterranean marine passage. *Sediment. Geol.* 216, 80–90. doi: 10.1016/j.sedgeo.2009.01.005
- Mayoral, E., and Pendón, J. G. (1987). Icnofacies y sedimentación en zona costera. Plioceno superior (?), litoral de Huelva. *Acta Geol. Hisp.* 21–22, 507–513.
- Moskowitz, B. M., Frankel, R. B., and Bazylinski, D. A. (1993). Rock magnetic criteria for the detection of biogenic magnetite. *Earth Planet. Sci. Lett.* 120, 283–300. doi: 10.1016/0012-821X(93)90245-5
- Paterson, G. A., Wang, Y. Z., and Pan, Y. X. (2013). The fidelity of paleomagnetic records carried by magnetosome chains. *Earth Planet. Sci. Lett.* 383, 82–91. doi: 10.1016/j.epsl.2013.09.031
- Pendón, J. G., Ruiz, F., Abad, M., González-Regalado, M. L., Baceta, J. I., and Tosquella, J. (2004). Transgressive sequences on foreland margins: a case study of the Central Guadalquivir Basin. *Riv. Ital. Paleont. Strat.* 110, 503–515.
- Pérez-Asensio, J. N. (2012). *Paleoecological and Paleoceanographical Study of Messinian Deposits from the Lower Guadalquivir Basin (SW Spain)*. Ph. D. thesis, University of Granada, Spain.
- Pérez-Asensio, J. N., Aguirre, J., Schmiedl, G., and Civis, J. (2012a). Impact of restriction of the Atlantic-Mediterranean gateway on the Mediterranean Outflow Water and eastern Atlantic circulation during the Messinian. *Paleoceanography* 27, PA3222. doi: 10.1029/2012PA002309
- Pérez-Asensio, J. N., Aguirre, J., Schmiedl, G., and Civis, J. (2012b). Messinian paleoenvironmental evolution in the lower Guadalquivir Basin (SW Spain) based on benthic foraminifera. *Palaeogeogr. Palaeoclimatol. Palaeoecol.* 326–328, 135–151. doi: 10.1016/j.palaeo.2012.02.014
- Poulton, S. W., Krom, M. D., and Raiswell, R. (2004). A revised scheme for the reactivity of iron (oxyhydr)oxide minerals towards dissolved sulphide. *Geochim. Cosmochim. Acta* 68, 3703–3715. doi: 10.1016/j.gca.2004.03.012
- Roberts, A. P., Chang, L., Heslop, D., Florindo, F., and Larrasoña, J. C. (2012). Searching for single domain magnetite in the “pseudo-single-domain” sedimentary haystack: implications of biogenic magnetite preservation for sediment magnetism and relative paleointensity determinations. *J. Geophys. Res.* 117, B08104. doi: 10.1029/2012JB009412
- Roberts, A. P., Florindo, F., Chang, L., Heslop, D., Jovane, L., and Larrasoña, J. C. (2013). Magnetic properties of pelagic marine carbonates. *Earth Sci. Rev.* 127, 111–139. doi: 10.1016/j.earscirev.2013.09.009
- Roberts, A. P., Florindo, F., Villa, G., Chang, L., Jovane, L., Bohaty, S. M., et al. (2011). Magnetotactic bacterial abundance in pelagic marine environments is limited by organic carbon flux and availability of dissolved iron. *Earth Planet. Sci. Lett.* 310, 441–452. doi: 10.1016/j.epsl.2011.08.011
- Roberts, A. P., Pike, C. R., and Veresub, K. L. (2000). First-order reversal curve diagrams: a new tool for characterizing the magnetic properties of natural samples. *J. Geophys. Res.* 105, 28461–28475. doi: 10.1029/2000JB900326
- Rowan, C. J., and Roberts, A. P. (2006). Magnetite dissolution, diachronous greigite formation, and secondary magnetizations from pyrite oxidation: Unravelling complex magnetizations in Neogene marine sediments from New Zealand. *Earth Planet. Sci. Lett.* 241, 119–137. doi: 10.1016/j.epsl.2005.10.017
- Salvany, J. M., Larrasoña, J. C., Mediavilla, C., and Rebollo, A. (2011). Chronology and tectono-sedimentary evolution of the upper pliocene to quaternary deposits of the lower Guadalquivir basin, SW Spain. *Sediment. Geol.* 241, 22–39. doi: 10.1016/j.sedgeo.2011.09.009
- Santisteban, C., and Taberner, C. (1983). Shallow marine and continental conglomerates derived from coral reef complexes after desiccation of the deep marine basin: the Tortonian-Messinian deposits of the Fortuna Basin, SE Spain. *J. Geol. Soc. Lond.* 140, 401–411. doi: 10.1144/gsjgs.140.3.0401
- Schüler, D., and Baeuerlein, E. (1998). Dynamics of iron uptake and Fe_3O_4 biominerallization during aerobic and microaerobic growth of magnetospirillum gryphiswaldense. *J. Bacteriol.* 180, 159–162.
- Sierra, F. J., Flores, J. A., Civis, J., González-Delgado, J. A., and Francés, G. (1993). Late Miocene globorotaliid event-stratigraphy and biogeography in the NE-Atlantic and Mediterranean. *Mar. Micropal.* 21, 143–168. doi: 10.1016/0377-8398(93)90013-N
- Sierra, F. J., González-Delgado, A., Dabrio, C. J., Flores, A., and Civis, J. (1996). “Late Neogene depositional sequences in the foreland basin of Guadalquivir (SW Spain)”, in *Tertiary Basins of Spain*, eds P. F. Friend and C. J. Dabrio (Cambridge: Cambridge University Press), 339–345. doi: 10.1017/CBO9780511524851.048
- Smirnov, A., and Tarduno, J. A. (2000). Low-temperature magnetic properties of pelagic sediments (Ocean Drilling Program Site 805C): tracers of maghemitization and magnetic mineral reduction. *J. Geophys. Res.* 105, 16457–16471. doi: 10.1029/2000JB900140
- Tarduno, J. A., and Wilkison, S. (1996). Non-steady state magnetic mineral reduction, chemical lock-in, and delayed remanence acquisition in pelagic sediments. *Earth Planet. Sci. Lett.* 144, 315–326. doi: 10.1016/S0012-821X(96)00174-4
- Tarduno, J. A., Tian, W., and Wilkison, S. (1998). Biogeochemical remanent magnetization in pelagic sediments of the western equatorial Pacific Ocean. *Geophys. Res. Lett.* 25, 3987–3990. doi: 10.1029/1998GL900079
- Weiss, B. P., Kim, S. S., Kirschvink, J. L., Kopp, R. E., Sankaran, M., Kobayashi, A., et al. (2004). Ferromagnetic resonance and low-temperature magnetic test for biogenic magnetite. *Earth Planet. Sci. Lett.* 224, 73–89. doi: 10.1016/j.epsl.2004.04.024
- Yamazaki, T. (2008). Magnetostatic interactions in deep-sea sediments inferred from first-order reversal curve diagrams: implications for relative paleointensity normalization. *Geochem. Geophys. Geosyst.* 9, Q02005. doi: 10.1029/2007GC001797
- Yamazaki, T. (2009). Environmental magnetism of pleistocene sediments in the North Pacific and Ontong-Java Plateau: temporal variations of detrital and biogenic components. *Geochem. Geophys. Geosyst.* 10, Q07Z04. doi: 10.1029/2009GC002413
- Yamazaki, T., and Kawahata, H. (1998). Organic carbon flux controls the morphology of magnetofossils in sediments. *Geology* 26, 1064–1066. doi: 10.1130/0091-7613(1998)026<1064:OCFCTM>2.3.CO;2

- Yamazaki, T., and Ikehara, M. (2012). Origin of magnetic mineral concentration variation in the Southern Ocean. *Paleoceanography* 27, PA2206. doi: 10.1029/2011PA002271
- Yamazaki, T., and Shimono, T. (2013). Abundant bacterial magnetite occurrence in oxic red clay. *Geology* 41, 1191–1194. doi: 10.1130/G34782.1
- Yamazaki, T., Yamamoto, Y., Acton, G., Guidry, E. P., and Richter, C. (2013). Rock magnetic artifacts on long-term relative paleointensity variations in sediments. *Geochem. Geophys. Geosyst.* 14, 29–43. doi: 10.1002/ggge.20064

Conflict of Interest Statement: The authors declare that the research was conducted in the absence of any commercial or financial relationships that could be construed as a potential conflict of interest.

Received: 31 October 2013; accepted: 10 February 2014; published online: 04 March 2014.

Citation: Larrasoña JC, Liu Q, Hu P, Roberts AP, Mata P, Civis J, Sierro FJ and Pérez-Asensio JN (2014) Paleomagnetic and paleoenvironmental implications of magnetofossil occurrences in late Miocene marine sediments from the Guadalquivir Basin, SW Spain. *Front. Microbiol.* 5:71. doi: 10.3389/fmicb.2014.00071

This article was submitted to Aquatic Microbiology, a section of the journal *Frontiers in Microbiology*.

Copyright © 2014 Larrasoña, Liu, Hu, Roberts, Mata, Civis, Sierro and Pérez-Asensio. This is an open-access article distributed under the terms of the Creative Commons Attribution License (CC BY). The use, distribution or reproduction in other forums is permitted, provided the original author(s) or licensor are credited and that the original publication in this journal is cited, in accordance with accepted academic practice. No use, distribution or reproduction is permitted which does not comply with these terms.



Surface expression of protein A on magnetosomes and capture of pathogenic bacteria by magnetosome/antibody complexes

Jun Xu¹, Junying Hu¹, Lingzi Liu¹, Li Li¹, Xu Wang¹, Huiyuan Zhang², Wei Jiang¹, Jiesheng Tian^{1*}, Ying Li¹ and Jilun Li¹

¹ Department of Microbiology, College of Biological Sciences, China Agricultural University, Beijing, China

² Food Safety Testing Centre, Beijing Entry-Exit Inspection and Quarantine Bureau, Beijing, China

Edited by:

Wei Lin, Chinese Academy of Sciences, China

Reviewed by:

Raz Zarivach, Ben Gurion University of the Negev, Israel

Changqian Cao, Chinese Academy of Sciences, China

***Correspondence:**

Jiesheng Tian, Department of Microbiology, College of Biological Sciences, China Agricultural University, Room 3037, Yuan Ming Yuan West Road No. 2, Haidian District, Beijing 100193, China
e-mail: tianhome@cau.edu.cn

Magnetosomes are membrane-enclosed magnetite nanocrystals synthesized by magnetotactic bacteria (MTB). They display chemical purity, narrow size ranges, and species-specific crystal morphologies. Specific transmembrane proteins are sorted to the magnetosome membrane (MM). MamC is the most abundant MM protein of *Magnetospirillum gryphiswaldense* strain MSR-1. MamF is the second most abundant MM protein of MSR-1 and forms stable oligomers. We expressed staphylococcal protein A (SPA), an immunoglobulin-binding protein from the cell wall of *Staphylococcus aureus*, on MSR-1 magnetosomes by fusion with MamC or MamF. The resulting recombinant magnetosomes were capable of self-assembly with the Fc region of mammalian antibodies (Abs) and were therefore useful for functionalization of magnetosomes. Recombinant plasmids pBBR-mamC-spa and pBBR-mamF-spa were constructed by fusing spa (the gene that encodes SPA) with mamC and mamF, respectively. Recombinant magnetosomes with surface expression of SPA were generated by introduction of these fusion genes into wild-type MSR-1 or a mamF mutant strain. Studies with a Zeta Potential Analyzer showed that the recombinant magnetosomes had hydrated radii significantly smaller than those of WT magnetosomes and zeta potentials less than -30 mV, indicating that the magnetosome colloids were relatively stable. Observed conjugation efficiencies were as high as 71.24 µg Ab per mg recombinant magnetosomes, and the conjugated Abs retained most of their activity. Numbers of *Vibrio parahaemolyticus* (a common pathogenic bacterium in seafood) captured by recombinant magnetosome/Ab complexes were measured by real-time fluorescence-based quantitative PCR. One mg of complex was capable of capturing as many as 1.74×10^7 *Vibrio* cells. The surface expression system described here will be useful for design of functionalized magnetosomes from MSR-1 and other MTB.

Keywords: *Magnetospirillum gryphiswaldense*, magnetosome, MamF, surface display, protein A, functionalization, *Vibrio parahaemolyticus*

INTRODUCTION

The bacterium *Vibrio parahaemolyticus* is a major cause of food-borne illnesses resulting from consumption of raw seafood and is involved in gastroenteritis, wound infection, and septicemia (Newton et al., 2012). Conventional methods for the detection of *V. parahaemolyticus* include the use of selective, differential agar media, biochemical testing, and examination of colony morphology (Kaysner and DePaola, 2004). Such methods usually involve time-consuming laboratory procedures and provide limited knowledge regarding pathogenicity.

Techniques based on polymerase chain reaction (PCR) have been used increasingly in recent years to detect pathogenic strains of *V. parahaemolyticus* by targeting the amplification of specific gene sequences with appropriate primers. A thermolabile direct hemolysin (TLH) is specific for *V. parahaemolyticus*. Its gene, *tlh*, is a frequently used target in various detection strategies (Su and

Liu, 2007). However, PCR in this case is inhibited by a variety of substances present in food or in the environment (Rosset et al., 1992; Powell et al., 1994; Waleed and Peter, 2000). Removal of such inhibitory substances is a crucial step in the preparation of template DNA samples for PCR-based detection of food pathogens.

Immunomagnetic separation (IMS) is a powerful technique for the specific isolation and concentration of target bacteria from food samples (Spanová et al., 2003; Ångela et al., 2008; Mercanoglu et al., 2009). Magnetosomes (also termed bacterial magnetic particles, or BMPs; this abbreviation is used hereafter for convenience) are being used increasingly as carriers for IMS assays (Arakaki et al., 2008; Fairve and Schüller, 2008). BMPs are synthesized by MTB and are composed of membrane-enclosed, single-domain ferrimagnetic iron oxide (magnetite, Fe₃O₄), or iron sulfide (greigite, Fe₃S₄) crystals (Schüller, 2002). At least 20

proteins have been identified on the magnetosome membrane (MM) of *Magnetospirillum gryphiswaldense* strain MSR-1 (hereafter termed “MSR-1”). Grünberg et al. (2004) reported that MamC was the most abundant MM-associated protein and that MamF was the second most abundant and the most stable. Expression of foreign functional proteins on the BMP surface can be facilitated by genetic engineering of MM-associated proteins. Many recent studies have attempted to produce various types of functionalized BMPs, for instance by the BMP-specific display of functional moieties, such as enzymes, coupling groups, gold particles, or oligonucleotides (BMP surface display system, Yoshino et al., 2010).

In the present study, staphylococcal protein A (SPA) was expressed on magnetosomes by fusion with MamC or MamF. SPA is an immunoglobulin G-binding protein (antibody-binding protein) encoded by the *spa* gene and can be isolated from the cell wall of *Staphylococcus aureus*. It binds the heavy chain within the fragment crystallizable region (Fc region, or tail region) of most immunoglobulins under a wide variety of conditions (Sidorin and Solov'eva, 2011). The resulting recombinant magnetosomes (BMP-A) were capable of self-assembly with many mammalian antibodies (Abs) without a loss of Ab activity. These recombinant BMPs were characterized and their Ab-binding efficiencies were evaluated. The capture efficiencies of magnetosome complexes (BMP-A-Ab) for *V. parahaemolyticus* were also investigated.

MATERIALS AND METHODS

BACTERIAL STRAINS, PRIMERS, PROBES, CULTURE MEDIA, AND GROWTH CONDITIONS

The bacterial strains, mutants, plasmids, and primers used in this study are listed in **Tables 1, 2**. *Escherichia coli* (*E. coli*) strains were grown at 37°C in Luria-Bertani (LB) medium (Sambrook and Russel, 2001). *M. gryphiswaldense* strains were grown at

30°C in sodium lactate/ ammonium chloride/yeast extract (L AY) medium as described previously (Liu et al., 2008). Heat-killed cells of *V. parahaemolyticus* strain 09vp109 were from the Beijing Entry-Exit Inspection and Quarantine Bureau (Beijing, China).

Bicinchoninic acid (BCA) kits were from Pierce Biotechnology (Rockford, Illinois, USA). Abs were prepared by Kirkegaard and Perry Laboratories (KPL) Biotechnology (Gaithersburg, Maryland, USA). Other chemical reagents were from Beijing Chemical Reagents Co., China.

Primers and probes were designed using ABI 7000 Primer Express software (<http://www.lifetechnologies.com/global/en/home/technical-resources/software-downloads/abi-prism-7000-sequence-detection-system.html>). The probe used for real-time fluorescence quantitative PCR (FQ-PCR) was labeled with 6-carboxyfluorescein reporter dye (FAM) at the 5'-end and 6-carboxy-tetramethylrhodamine quencher dye (TAMRA) at the 3'-end.

CONSTRUCTION OF RECOMBINANT PLASMIDS AND STRAINS

Mutant strain *M. gryphiswaldense* ΔF was constructed by replacing *mamF* with the gentamicin resistance gene (aminoglycoside acetyltransferase gene, *aac*). Plasmid pUC-GM was digested by *Kpn*I to generate an *aac* gene fragment. The upstream and downstream fragments of *mamF* gene were amplified by the corresponding primers (**Table 2**) from genomic DNA of MSR-1, and referred to as U and D, respectively. Fragments U and D were digested by *Xba*I/*Kpn*I and *Kpn*I/*Pst*I and then connected with the *aac* gene fragment by T4 DNA ligase to generate a U-aac-D fragment. The U-aac-D fragment was cloned into a suicide plasmid pUX19. The recombinant plasmid was transformed into *E. coli* S17-1 and then transferred into MSR-1 by biparental conjugation. Mutant bacterial strains were screened as described previously (Liu et al., 2008).

Table 1 | *M. gryphiswaldense* strains and plasmids in this study.

	Strain or plasmid	Genotype	Source
Strains			
<i>M. gryphiswaldense</i> MSR-1	Wild-type (WT)	DSMZ	
<i>M. gryphiswaldense</i> ΔF	MSR-1 <i>mamF</i> mutant	Present study	
<i>M. gryphiswaldense</i> MSR-CA	MSR-1 harboring pBBR-mamC-spa; Nx ^r , Km ^r	Present study	
<i>M. gryphiswaldense</i> MSR-FA	MSR-1 harboring pBBR-mamF-spa; Nx ^r , Km ^r	Present study	
<i>M. gryphiswaldense</i> ΔF-FA	<i>mamF</i> mutant harboring pBBR-mamF-spa; Nx ^r , Km ^r , Gm ^r	Present study	
<i>S. aureus</i> ATCC 6538	WT	CGMCC	
<i>E. coli</i> DH5α	<i>endA1 hsdR17[r-</i> m ⁺]supE44 thi-1 recA1 gyrA[NalR]RelA relA1Δ[lacZYA-argF]U169 deoR[ø80]Δ (M15)]	Stock culture in our laboratory	
<i>E. coli</i> S17-1	<i>Pro thi hsdR recA</i> , chromosomal integration of RP4-2-Tc::Mu-Km::Tn7, Sm ^r Tra ⁺		
<i>V. parahaemolyticus</i> 09vp109	WT		
Plasmids			
pUC-GM	Amp ^r , pUC18 harboring gentamicin resistance gene	Laboratory collection	
pUX19	Suicide vector; Km ^r		
PMD18-T simple	PCR cloning vector; Amp ^r	TaKaRa	
pBBR1MCS-2	Expression vector/LacZ promoter; Km ^r	Kovach et al., 1995	
pBBR-mamC-spa	pBBR1MCS-2 harboring gene fragment of mamC-spa; Km ^r	Present study	
pBBR-mamF-spa	pBBR1MCS-2 harboring gene fragment of mamF-spa; Km ^r	Present study	

DSMZ, German Collection of Microorganisms and Cell Cultures GmbH; CGMCC, China General Microbiological Culture Collection Center.

Table 2 | Primers used for PCR.

Target gene	Primer	Oligonucleotide sequences(s) (5' to 3')
<i>mamC</i>	F-mamC ^e	^a <u>CCGGAATTCCGCCTGACCCCTGAATTAAGGAC</u>
	R-mamC ^f	^b <u>GAAACCGCCGCCACCAGAGCCACCACCGCCGGAGGCCAATTCTCCCTCAGAATG</u>
<i>mamF</i>	F-mamF ^e	^a <u>CCGGAATTCCGCAGGGCAAGCAATGG</u>
	R-mamF ^f	^b <u>GAAACCGCCGCCACCAGAGCCACCACCGCCGGAGATCAGGGCGACTACATGG</u>
<i>spa</i>	F-spa ^e	^c <u>TCTGGTGGCGCGGTTCCGGTGGCGGTGGCAAAAAGAAAACATTATTCAATTCTGAAACTA</u>
	R-spa ^f	^d <u>CGCGGATCCTTATAAGTCGCGACGACGTCC</u>
<i>mamF</i> upstream fragment	mamF-D1	CGGGTACCCCTGATGGAAAGACCGTGCT
	mamF-D2	AACTGCAGAGATAACAACAACCAACGCCC
<i>mamF</i> downstream fragment	mamF-G1	GCTCTAGACGACTTCTTCATCGCTCTG
	mamF-G2	CGGGTACCCATTGCTTGCCTCGCTT
<i>tih</i>	F-tih ^e	TGTCGAGACGCTAACTTCTG
	R-tih ^f	AAACTCTCAGCACCAAGACG

^arecognition site of restriction endonuclease *Bam*HI; ^bLinker sequence; ^ccomplementary linker sequence of sequence b; ^drecognition site of restriction endonuclease *Eco*RI; ^eforward primer; ^freverse primer.

mamC, *mamF*, and *spa* genes were amplified from genomic DNA of MSR-1 or *S. aureus* ATCC 6538 by the corresponding primers (Table 2). The start codon of *spa* and the stop codons of *mamC* and *mamF* were removed during amplification. The three above fragments were recovered to generate *mamC-spa* and *mamF-spa* fragments by fusion PCR (Komeili et al., 2004). These two fragments were respectively cloned into pMD18-T simple cloning vector and transformed into *E. coli* DH5α. After overnight culture of the recombinant strains, two plasmids were extracted and digested with *Eco*RI and *Bam*HI. The recovered fragments were then cloned into the broad host plasmid vector pBBR1MCS-2, resulting in plasmids pBBR-mamC-spa and pBBR-mamF-spa, respectively (Figure 1). These plasmids contained a linker consisting of 15 amino acids between the *spa* and *mam* genes, and recognition sites of restriction endonucleases *Bam*HI and *Eco*RI flanking the sides of the *mam-spa* fusion genes.

Plasmids pBBR-mamC-spa and pBBR-mamF-spa were introduced into *E. coli* S17-1 by transformation (Sambrook and Russel, 2001) and then transferred into MSR-1 or *M. gryphiswaldense* ΔF by conjugation as described previously (Liu et al., 2008).

PREPARATION OF MAGNETOSOME-AB COMPLEXES

Magnetosomes or recombinant magnetosomes (BMP-As) of *M. gryphiswaldense* strains were isolated and purified as described previously (Li et al., 2010). The membrane proteins of BMPs or BMP-As were extracted as described by Grünberg et al. (2004) and identified by Northern blotting. The proteins of each sample (generally from 0.25 mg magnetosomes) were separated by SDS-PAGE, and the bands were transferred onto a nitrocellulose membrane by electroblotting and blocked overnight at 4°C. A dilute solution of primary Ab (mouse mAb, 0.5–5.0 mg/mL) was incubated with the membrane under gentle agitation for 1 h at room temperature. The membrane was rinsed to remove unbound primary Ab and then placed in a solution of secondary Ab (goat anti-mouse IgG) for 1 h. The secondary Ab was linked to alkaline phosphatase, which was then used to catalyze 5-bromo-4-chloro-3-indolyl phosphate (BCIP) and nitro blue tetrazolium

(NBT) into a blue precipitate in proportion to the amount of protein.

The hydrated radii and zeta potentials of magnetosomes were analyzed by a Zeta Potential Analyzer (Brookhaven Instruments Corp., Long Island, State of New York USA). Samples were prepared as described by Takahashi et al. (2010).

Chemical modification of magnetosomes by bis(sulfosuccinimidyl) suberate (BS³) was performed as described previously (Li et al., 2010). The procedure for self-assembly of recombinant magnetosome was as follows. BMP-A or Ab (each 1 mg) was resuspended in 1 mL of 1 mM phosphate-buffered saline (PBS; pH 7.4). The magnetosome and Ab suspensions were mixed, placed in a mild ultrasonic bath (30 W) for 2 min, and incubated on a rotary shaker at 150 × g for 60–90 min. The resulting BMP-A-Ab complexes were isolated by a NdFeB magnet, washed three times with 1 mL of 10 mM PBS (pH 7.4), and resuspended in 500 μL of 1 mg/mL Ab solution. After repeated dispersion, incubation, collection, and washing as above, the complexes were blocked with sterile 0.5% BSA solution overnight at 4°C and stored.

Ab concentrations before and after reaction with magnetosomes were determined using a BCA kit, and linkage rates were calculated by the equation:

$$\text{Linkage rate } (\mu\text{g Ab/mg magnetosomes}) = (C_1 - C_2) \times V/M$$

where C₁ = Ab concentration before reaction with magnetosomes; C₂ = Ab concentration after reaction with magnetosomes; V = volume of Ab solution reacting with magnetosomes; M = weight of magnetosomes conjugated with Ab. C₁ and C₂ were calculated by the equation $\gamma = kx$, where γ = OD₅₆₂ detected by the BCA kit; x = Ab concentration; k = slope.

IMS AND CAPTURE EFFICIENCY DETECTION OF *V. PARAHAEAMOLYTICUS* BY FQ-PCR

Serially 10-fold diluted *Vibrio* suspensions (10^{-3} , 10^{-4} , 10^{-5} , 10^{-6} ; each 1 mL) were mixed with 1 mg BMP-A-Ab complexes. The mixtures were dispersed by sonication for 2 min and incubated on a rotary shaker (150 × g) for 1 h at room temperature. BMP-A-Ab-Vibrio complexes were isolated using a magnet and

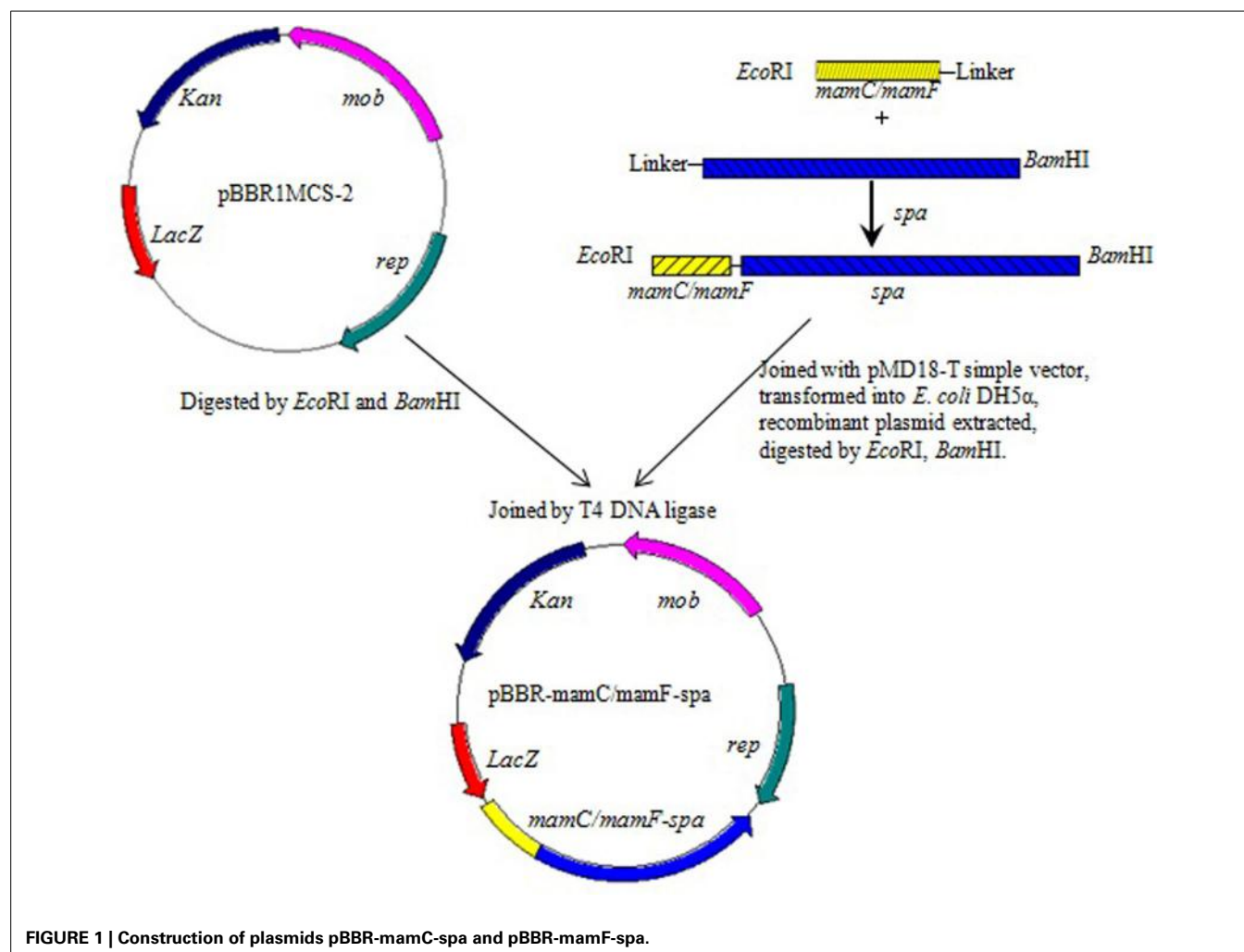


FIGURE 1 | Construction of plasmids pBBR-mamC-spa and pBBR-mamF-spa.

washed three times with 1 mL of 10 mM PBS buffer to remove free bacterial cells. Control mixtures of *Vibrio* and BMP-As (without Ab) were incubated in PBS under the same conditions. The resulting precipitate was resuspended in 100 μ L PBS. The concentrated cell suspension was incubated for 10 min at 98°C and centrifuged at 10,000 \times g for 3 min at room temperature. The supernatants were used as templates. FQ-PCR was performed as described previously (Li et al., 2010).

V. parahaemolyticus strains produce species-specific TLHs, and the *tlh* gene has been used as a probe to confirm the identity of *Vibrio* species (McCarthy et al., 1999). We measured the fluorescence intensity of *tlh* FQ-PCR products to estimate the number of *Vibrio* cells trapped by BMP-A-Ab complexes. Standard curves were constructed using a 10⁻¹–10⁻⁶ serial 10-fold dilution of *Vibrio* genomic DNA, and the threshold cycle (Ct) value was plotted against the log of DNA weight (ng) by linear regression. The average weight of a pair of DNA bases is 1 \times 10⁻²¹ g, and the whole genome of *V. parahaemolyticus* (5165770 bp; Makino et al., 2003) was estimated to weigh 5.2 \times 10⁻¹⁵ g. The number of *Vibrio* was calculated as the amount of DNA divided by the weight of genome.

RESULTS

CONSTRUCTION OF RECOMBINANT PLASMIDS AND STRAINS ENCODING FUSION PROTEINS

SPA is an immunoglobulin G-binding protein. Magnetosome-specific expression of SPA could facilitate efficient localization and appropriate orientation of various Abs on the surface of magnetosomes. In the present study, SPA was expressed on magnetosomes by fusing its gene (*spa*; 1503 bp) with the abundant MM protein genes *mamC* (378 bp) or *mamF* (336 bp) from *M. gryphiswaldense*. The fusion genes *mamC-spa* and *mamF-spa* were generated by fusion PCR from *mamC*, *mamF*, or *spa* PCR products. These genes were cloned into the broad host plasmid vector pBBR1MCS-2 (5144 bp), resulting in plasmids pBBR-mamC-spa and pBBR-mamF-spa, which were then introduced into MSR-1 by conjugation. The recombinant strains harboring plasmid pBBR-mamC-spa and pBBR-mamF-spa were termed MSR-CA and MSR-FA, respectively.

To increase the amount of SPA on the recombinant magnetosomes (BMP-As), a *mamF* mutant strain of *M. gryphiswaldense* was constructed by allelic gene replacement. The native *mamF*

gene in the MSR-1 genome was replaced by a gentamicin resistance gene (aminoglycoside acetyltransferase gene; *aac*), resulting in strain ΔF . The mutant strain harboring plasmid pBBR-mamF-spa was termed ΔF -FA. Recombinant magnetosomes from strains MSR-1, MSR-CA, MSR-FA, and ΔF -FA were termed BMP-WT, BMP-CA, BMP-FA, and ΔF -BMP-FA, respectively.

The expression of SPA on magnetosomes was confirmed by western blotting. The membrane proteins of purified magnetosomes were separated by SDS-PAGE and transferred onto a nitrocellulose membrane by electroblotting. The protein bands were colored by sequential treatment with primary Ab, secondary Ab, and BCIP-NBT. SPA was found in all the recombinant magnetosomes (**Figure 2**).

CHARACTERIZATION OF RECOMBINANT MAGNETOSOMES

Strains as above were collected by centrifugation after 3 days of culture, and their magnetosomes were isolated and purified. Transmission electronic microscopy (**Figure 3**) showed generally similar morphology of WT magnetosomes (diameter range 35–84 nm) and recombinant magnetosomes. The magnetosomes of ΔF -FA were slightly smaller (24–48 nm) than those of the other strains.

The hydrated radii and zeta potentials of magnetosomes were analyzed by a Zeta Potential Analyzer. All zeta potentials were lower than -30 mV, indicating that the aqueous colloids were moderately stable. The expression of foreign proteins can affect the amount of electrical charge on interfaces between magnetosomes and aqueous solutions. The large hydrated radii of BMP-WTs indicated that several BMP-WT gathered into a larger

particle in suspension. The expression of foreign proteins on magnetosomes in the case of BMP-CA and BMP-FA was associated with smaller values of hydrated radii and polydispersity, indicating improved dispersity and uniformity. ΔF -BMP-FA had the smallest hydrated radii and best dispersity because they had the largest amount of foreign proteins.

EFFICIENCY OF MAGNETOSOME LINKAGE TO POLYCLONAL Ab

Polyclonal Abs were linked with SPA on the surface of magnetosomes by self-assembly to form functional magnetic carriers (BMP-Ab) for capturing *Vibrio*. In an attempt to improve linkage rate, various values of pH (6.0, 7.2, 7.9), incubation time (30, 60, 90, 120 min), and ratio of Ab to magnetosomes (250 μ g, 500 μ g, 1.0 mg, and 1.5 mg Ab per mg magnetosomes) were used for the linkage of BMP-CA to Ab (**Figure 4**). The maximal linkage rate was achieved with pH 7.2, incubation time 120 min, and ratio 1:1.

Linkage rates of different magnetosome-Ab linking methods were compared under these optimal conditions (**Figure 5**). BMP-WTs were linked to Ab by nonspecific adsorption or BS³, and BMP-CA and ΔF -BMP-FA were linked to Ab by self-assembly.

The percentage of Ab linked to BMP-WT by nonspecific adsorption was almost 20% and could not be ignored. However, the percentages of Ab coupled to magnetosomes by covalent linkage or self-assembly were significantly higher. The linkage rate of ΔF -BMP-FA magnetosomes to Ab was much higher than that of other magnetosomes, indicating that ΔF -BMP-FA is the best candidate for magnetic carrier carriers for IMS (**Table 3**).

IMMUNOMAGNETIC SEPARATION OF *V. PARAHAEAMOLYTICUS*

Anti-*Vibrio* rabbit polyclonal Ab was linked to recombinant magnetosomes (BMP-CA, BMP-FA, and ΔF -BMP-FA) by self-assembly. WT magnetosomes (BMP-WT) were linked to Ab by BS³. Magnetosome-Ab complexes (BMP-A-Ab) were used to capture *V. parahaemolyticus*. FQ-PCR was performed with the species-specific gene *tth* as template. A standard curve was constructed by plotting the threshold cycle (Ct) value against the log of *Vibrio* DNA weight (ng) by linear regression. The number of *Vibrio* cells was estimated based on the amount of DNA attached to the magnetosomes (**Table 4**).

Each type of magnetosome (1 mg) was mixed with 1 mL of diluted *V. parahaemolyticus* suspension (10^{-4} ; approximately 2×10^8 cfu). WT magnetosomes bound a much lower number of *Vibrio* than did the other magnetosomes, indicating that many Ab

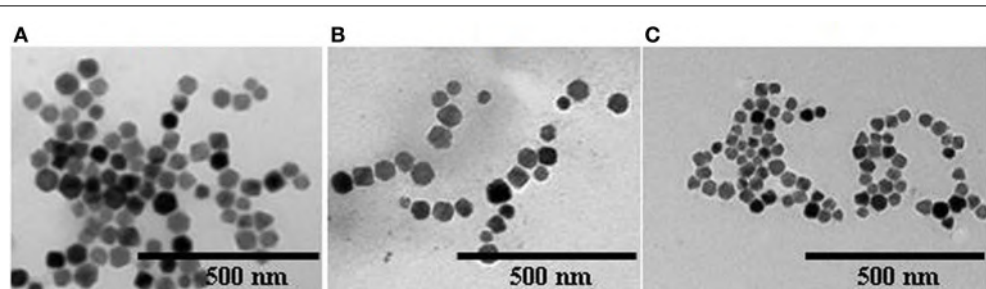
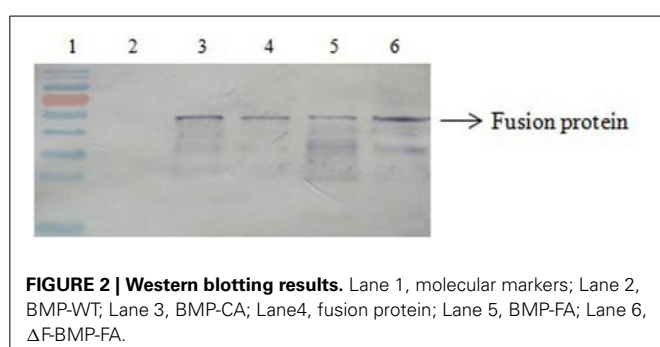


FIGURE 3 | Electron micrographs of magnetosomes from various strains. (A), BMP-WT; **(B)**, BMP-FA; **(C)**, ΔF -BMP-FA.

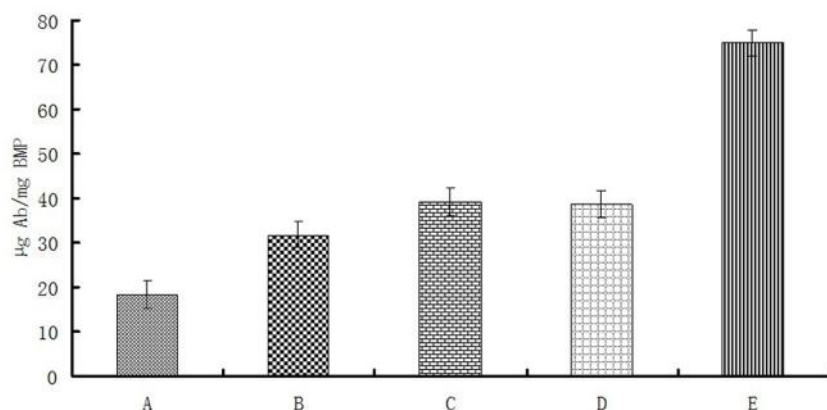
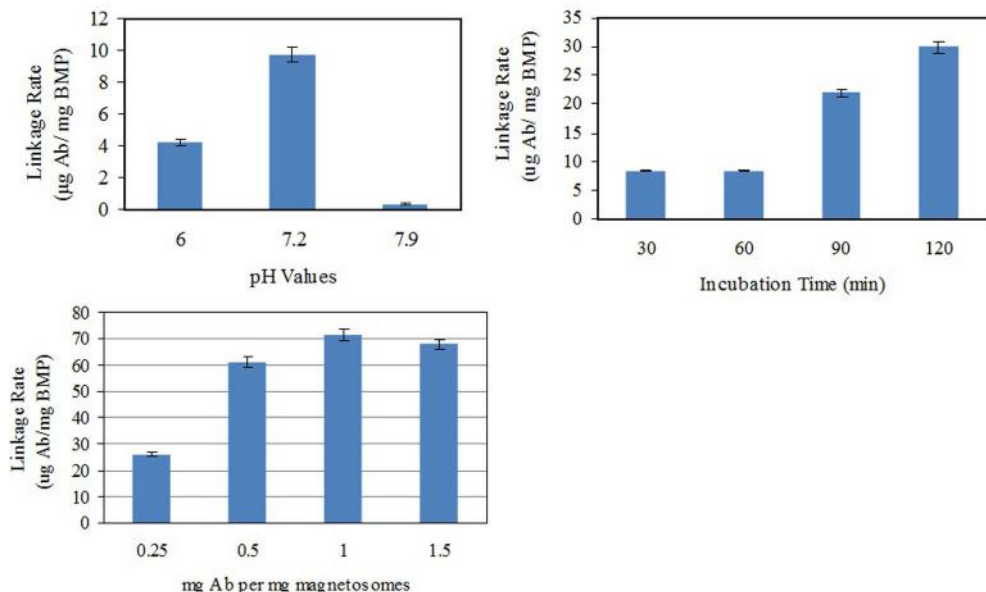


FIGURE 5 | Magnetosome-Ab linkage rates for different linkage methods under optimal conditions as in Figure 4. (A), Nonspecific adsorption of BMP-WT on Ab; (B), BS^3 linkage of BMP-WT to Ab; (C), self-assembly of BMP-CA and Ab; (D), self-assembly of BMP-FA and Ab; (E) self-assembly of ΔF -BMP-FA and Ab.

Table 3 | Particle size and zeta potential of magnetosomes from various strains.

Strain	BMP-WT	BMP-CA	BMP-FA	ΔF -BMP-FA
Hydrated radius (nm)	494.7 ± 18.6	325.2 ± 4.2	334.3 ± 5.1	152.5 ± 0.2
Zeta potential (mV)	-38.27 ± 0.73	-34.09 ± 0.5	-35.12 ± 0.6	-31.09 ± 0.79
Polydispersity	0.354	0.335	0.337	0.230

molecules failed to work. ΔF -BMP-FA captured the highest number of *Vibrio*, indicating that ΔF -BMP-FA is the best candidate for a magnetic carrier of IMS for detection of pathogenic *Vibrio*.

DISCUSSION

Although MTB are ubiquitous and highly abundant in many aquatic habitats, they are very difficult to culture in laboratory

or industrial situations. To date, fewer than 20 MTB strains have been successfully isolated and cultured in laboratories worldwide (Greene and Komeili, 2012). *M. gryphiswaldense* MSR-1, the type strain of the genus *Magnetospirillum*, is the only MTB strain that has been cultured on a relatively larger scale (in a 1.5-ton fermenter) (Zhang et al., 2011). Mass production of magnetosomes facilitates its detailed biotechnological and

Table 4 | Amount of DNA in *Vibrio* captured by magnetosome-Ab complexes.

Magnetosome	BMP-WT	BMP-CA	BMP-FA	ΔF -BMP-FA
Amount of DNA (ng)	6.092	76.202	70.226	95.581
Number of <i>Vibrio</i> ($\times 10^8$)	0.117	1.47	1.35	1.84

nanotechnological studies. These bacterial magnetic nanoparticles are distinguished by unique properties such as ferrimagnetism, nanoscale size, monocrystalline structure, narrow size distribution, uniform morphology, and membrane-bound structure, and thus have been developed and investigated for various potential applications, including immunoassays, magnetofection, therapeutic drug delivery, and enzyme immobilization (Yoshino et al., 2010).

The term “surface display systems” in microbiology refers to a group of powerful techniques that utilize naturally-occurring microbial functional components to express heterologous proteins or peptides. Since the description of the first phage-display system in the mid-1980s, a variety of new systems have been reported for yeast, Gram-positive bacteria, Gram-negative bacteria, bacterial endospores, ribosomes, and mRNAs (Ullman et al., 2011). A recently developed display system based on magnetosomes (BMPs) provides superior performance for immunomagnetic separation, which facilitates high-throughput screening (HTS) (Yoshino et al., 2010). However, only a few studies have investigated or compared the effects of different fusion strategies for MM proteins (Li et al., 2010; Pollithy et al., 2011).

We have recently detected over 200 proteins on magnetosome surfaces (unpubl. data). Some of these proteins are unique to the magnetosome. MamC and MamF, the most abundant proteins on MSR-1 magnetosomes, are small proteins composed respectively of 125 amino acids (12.4 kDa) and 111 amino acids (12.3 kDa). We constructed fusion proteins by fusing *mamC* and *mamF* with the SPA (43 kDa) gene, *spa*. The recombinant magnetosomes were capable of self-assembly with various mammalian Abs without loss of Ab activity. We have evaluated and compared several magnetosome surface display strategies. The highest linkage rate of Abs and recombinant magnetosomes was obtained when the genomic MM genes for constructing fusion proteins were eliminated in recipient strains. It can be explained that there were more functional fusion proteins on the recombinant magnetosomes in the mutant recipient strain than in the wild type MSR-1. The strategy of genetic manipulation developed here would also be applied to the other magnetotactic bacterial pure cultures, such as *M. magneticum* AMB-1 and *Magnetococcus marinus* MC-1. Compared to the chemically produced magnetic beads, it was much more convenient for preparing recombinant magnetosome and antibody complexes because of omitting the coating and linkage procedures. Moreover, the capture efficiency of pathogens and the dispersibility in water were obviously improved comparing with magnetosome—antibody complexes connected with crosslinker (Li et al., 2010). Thus the technique in this study is also suitable for the detection and diagnosis of other pathogens, and makes it simpler, faster, and cheaper.

Our findings are consistent with a previous report that *mamF* deletion in MSR-1 resulted in slightly smaller magnetosome size (Scheffel et al., 2008). Although our fusion proteins contained a fragment corresponding to MamF, the recombinant magnetosomes were smaller than WT magnetosomes. At this stage, we are unclear whether functional MamF is present in the recombinant *M. gryphiswaldense* strain ΔF -FA (which harbors pBBR-mamF-spa), which needs further investigations.

Interestingly, we have detected the proteins MamC and MamF (generally thought to bind to MM) in cytosol and on membranes following fusion with SPA (data not shown). These findings suggest that the binding ability of MM proteins can be affected by fusion with larger soluble proteins, resulting in less SPAs on the surface of recombinant magnetosomes.

Further studies for design of functionalized magnetosomes using the system described here are in progress. Binding abilities of other MM proteins should be investigated in detail. Smaller recombinant proteins containing SPA Ig-binding domains or larger MM binding proteins could also be constructed for more efficient magnetosome display system. The magnetosome surface play technique will include but not limited to improving the separation, detection, and diagnostic analyses, or displaying SPA protein. Other functional moieties, such as enzymes, receptors, peptide hormones, growth factors, autotiotinylation signals, and protein tags for “click chemistry” could be expressed on the magnetosome particles by using our display strategies. These would endow the recombinant magnetosomes with serious functions, or even benefit the formation and reconstruction of magnetic nanostructures, such as magnetic nanotubes and nanowires *in vitro*.

ACKNOWLEDGMENTS

This study was supported by the National Natural Science Foundation of China (Grant No. 31270093). The authors thank Dr. S. Anderson for English editing of the manuscript.

REFERENCES

- Angela, N. M., Fabricio, R. C., Rita, de C. S., Roberta, J. R., Jose, B. C., Odir, A. D., et al. (2008). Detection of *Salmonella typhimurium* in raw meats using in-house prepared monoclonal antibody coated magnetic beads and PCR assay of the *fimA* gene. *J. Immunoassay Immunochem.* 29, 58–69. doi: 10.1080/15321810701735096
- Arakaki, A., Nakazawa, H., Nemoto, M., Mori, T., and Matsunaga, T. (2008). Formation of magnetite by bacteria and its application. *J. R. Soc. Interface* 5, 977–999. doi: 10.1098/rsif.2008.0170
- Faivre, D., and Schüler, D. (2008). Magnetotactic bacteria and magnetosomes. *Chem. Rev.* 108, 4875–4898. doi: 10.1021/cr078258w
- Greene, S. E., and Komeili, A. (2012). Biogenesis and subcellular organization of the magnetosome organelles of magnetotactic bacteria. *Curr. Opin. Cell Biol.* 24, 1–6. doi: 10.1016/j.ceb.2012.05.008
- Grünberg, K., Müller E. C., Otto, A., Reszka, R., Linder, D., Kube, M., et al. (2004). Biochemical and proteomic analysis of the magnetosome membrane in *Magnetospirillum gryphiswaldense*. *Appl. Environ. Microbiol.* 70, 1040–1050. doi: 10.1128/AEM.70.2.1040-1050.2004
- Kaysner, C. A. and DePaola, A. Jr. (2004). *Bacteriological Analytical Manual*, Chapter 9 Vibrio. Available online: <http://www.fda.gov/Food/FoodScienceResearch/LaboratoryMethods/ucm070830.htm>
- Komeili, A., Vali, H., Beveridge, T. J., and Newman, D. K. (2004). Magnetosome vesicles are present before magnetite formation, and MamA is required for their activation. *Proc. Natl. Acad. Sci. U.S.A.* 101, 3839–3844. doi: 10.1073/pnas.0400391101

- Kovach, M. E., Elzer, P. H., Hill, D. S., Robertson, G. T., Farris, M. A., Roop, R. M., et al. (1995). Four new derivatives of the broad-host-range cloning vector pBBR1MCS, carrying different antibiotic-resistance cassettes. *Gene* 166, 175–176. doi: 10.1016/0378-1119(95)00584-1
- Li, A., Zhang, H., Zhang, X., Wang, Q., Tian, J., Li, Y., et al. (2010). Rapid separation and immunoassay for low levels of *Salmonella* in foods using magnetosome-antibody complex and real-time fluorescence quantitative PCR. *J. Sep. Sci.* 33, 3437–3443. doi: 10.1002/jssc.201000441
- Liu, J., Ding, Y., Jiang, W., Tian, J., Li, Y., and Li, J. (2008). A mutation upstream of an ATPase gene significantly increases magnetosome production in *Magnetospirillum gryphiswaldense*. *Appl. Microbiol. Biotechnol.* 81, 551–558. doi: 10.1007/s00253-008-1665-1
- Makino, K., Oshima, K., Kurokawa, K., Yokoyama, K., Uda, T., Tagomori, K., et al. (2003). Genome sequence of *Vibrio parahaemolyticus*: a pathogenic mechanism distinct from that of *V. cholerae*. *Lancet* 361, 743–749. doi: 10.1016/S0140-6736(03)12659-1
- McCarthy, S. A., DePaola, A., Cook, D. W., Kaysner, C. A., and Hill, W. E. (1999). Evaluation of alkaline phosphatase- and digoxigenin-labelled probes for detection of the thermostable hemolysin (*tth*) gene of *Vibrio parahaemolyticus*. *Lett. Appl. Microbiol.* 28, 66–70. doi: 10.1046/j.1365-2672.1999.00467.x
- Mercanoglu, T. B., Ben, U., and Aytac, S. A. (2009). Rapid detection of *Salmonella* in milk by combined immunomagnetic separation-polymerase chain reaction assay. *J. Dairy Sci.* 92, 2382–2388. doi: 10.3168/jds.2008-1537
- Newton, A., Kendall, M., Vugia, D. J., Henao, O. L., and Mahon, B. E. (2012). Increasing rates of vibriosis in the United States, 1996–2010: review of surveillance data from 2 systems. *Clin. Infect. Dis.* 54(Suppl. 5), S391–S395. doi: 10.1093/cid/cis243
- Pollithy, A., Romer, T., Lang, C., Müller, F. D., Helma, J., Leonhardt, H., et al. (2011). Magnetosome expression of functional camelid antibody fragments (nanobodies) in *Magnetospirillum gryphiswaldense*. *Appl. Environ. Microbiol.* 77, 6165–6171. doi: 10.1128/AEM.05282-11
- Powell, H. A., Gooding, C. M., Garrett, S. D., Lund, B. M., and McKee, R. A. (1994). Proteinase inhibition of the detection of *Listeria monocytogenes* in milk using the polymerase chain reaction. *Lett. Appl. Microbiol.* 18, 59–61. doi: 10.1111/j.1472-765X.1994.tb00802.x
- Rossen, L., Nørskov, P., Holmstrøm, K., and Rasmussen, O. F. (1992). Inhibition of PCR by components of food samples, microbial diagnostic assays and DNA-extraction solution. *Int. J. Food Microbiol.* 17, 37–45. doi: 10.1016/0168-1605(92)90017-W
- Sambrook, J., and Russel, D. W. (2001). *Molecular Cloning: a Laboratory Manual*, 3rd Edn. Cold Spring Harbor, NY: Cold Spring Harbor Laboratory Press.
- Scheffel, A., Gärdes, A., Grünberg, K., Wanner, G., and Schüler, D. (2008). The major magnetosome proteins MamGFDC are not essential for magnetite biominerization in *Magnetospirillum gryphiswaldense* but regulate the size of magnetosome crystals. *J. Bacteriol.* 190, 377–386. doi: 10.1128/JB.01371-07
- Schüler, D. (2002). The biominerization of magnetosomes in *Magnetospirillum gryphiswaldense*. *Int. Microbiol.* 5, 209–214. doi: 10.1007/s10123-002-0086-8
- Sidorin, E. V., and Solov'eva, T. F. (2011). IgG-binding proteins of bacteria. *Biochemistry (Mosc.)* 76, 295–308. doi: 10.1134/S0006297911030023
- Spanová, A., Rittich, B., Horák, D., Lenfeld, J., Prodelalová, J., Sucíková, J., et al. (2003). Immunomagnetic separation and detection of *Salmonella* cells using newly designed carriers. *J. Chromatogr. A* 1009, 215–221. doi: 10.1016/S0021-9673(03)00431-X
- Su, Y. C., and Liu, C. (2007). *Vibrio parahaemolyticus*: a concern of seafood safety. *Food Microbiol.* 24, 549–558. doi: 10.1016/j.fm.2007.01.005
- Takahashi, M., Yoshino, T., and Matsunaga, T. (2010). Surface modification of magnetic nanoparticles using asparagines-serine polypeptide designed to control interactions with cell surfaces. *Biomaterials* 31, 4952–4957. doi: 10.1016/j.biomaterials.2010.02.048
- Ullman, C. G., Frigotto, L., and Cooley, R. N. (2011). *In vitro* methods for peptide display and their applications. *Brief. Funct. Genomics* 10, 125–134. doi: 10.1093/bfgp/elr010
- Waleed, A. A., and Peter, R. (2000). Effects of amplification facilitators on diagnostic PCR in the presence of blood, feces, and meat. *J. Clin. Microbiol.* 38, 4463–4470.
- Yoshino, T., Maeda, Y., and Matsunaga, T. (2010). Bioengineering of Bacterial Magnetic Particles and their Applications in Biotechnology. *Recent Pat. Biotechnol.* 4, 214–225. doi: 10.2174/187220810793611455
- Zhang, Y., Zhang, X., Jiang, W., Li, Y., and Li, J. (2011). Semicontinuous culture of *Magnetospirillum gryphiswaldense* MSR-1 cells in an autofermentor by nutrient-balanced and isosmotic feeding strategies. *Appl. Environ. Microbiol.* 77, 5851–5856. doi: 10.1128/AEM.05962-11

Conflict of Interest Statement: The authors declare that the research was conducted in the absence of any commercial or financial relationships that could be construed as a potential conflict of interest.

Received: 24 August 2013; **accepted:** 17 March 2014; **published online:** 03 April 2014. **Citation:** Xu J, Hu J, Liu L, Li L, Wang X, Zhang H, Jiang W, Tian J, Li Y and Li J (2014) Surface expression of protein A on magnetosomes and capture of pathogenic bacteria by magnetosome/antibody complexes. *Front. Microbiol.* 5:136. doi: 10.3389/fmicb.2014.00136

This article was submitted to Aquatic Microbiology, a section of the journal *Frontiers in Microbiology*.

Copyright © 2014 Xu, Hu, Liu, Li, Wang, Zhang, Jiang, Tian, Li and Li. This is an open-access article distributed under the terms of the Creative Commons Attribution License (CC BY). The use, distribution or reproduction in other forums is permitted, provided the original author(s) or licensor are credited and that the original publication in this journal is cited, in accordance with accepted academic practice. No use, distribution or reproduction is permitted which does not comply with these terms.



A key time point for cell growth and magnetosome synthesis of *Magnetospirillum gryphiswaldense* based on real-time analysis of physiological factors

Jing Yang^{1,2}, Shuqi Li^{1,2}, Xiuliang Huang^{1,2}, Tao Tang^{1,2}, Weizhong Jiang³, Tongwei Zhang^{1,4} and Ying Li^{1,2*}

¹ Key Laboratory of Agro-biotechnology and Key Laboratory of Soil Microbiology, Ministry of Agriculture, College of Biological Sciences, China Agricultural University, Beijing, China

² France-China Biominerization and Nano-structure Laboratory, Beijing, China

³ College of Water Resources and Civil Engineering, China Agricultural University, Beijing, China

⁴ Institute of Geology and Geophysics, Chinese Academy of Sciences, Beijing, China

Edited by:

Wei Lin, Chinese Academy of Sciences, China

Reviewed by:

Wei Lin, Chinese Academy of Sciences, China

Jianbo Sun, Columbia University, USA

***Correspondence:**

Ying Li, State Key Laboratory of Agro-biotechnology and College of Biological Sciences, China Agricultural University, No.2, Yuanmingyuan West Road, Beijing, 100193, China
e-mail: yingli528@vip.sina.com

Pure culture of magnetotactic bacteria with high magnetosome yield has been achieved for only a few strains. The major obstacles involve the nutritional requirements and culture conditions of the cells. To increase cell density and magnetosome production, it is necessary to elucidate the physiological characteristics of a particular strain during cell growth and develop an appropriate artificial control strategy. Large-scale culture of *Magnetospirillum gryphiswaldense* strain MSR-1 was successfully performed for 48 h in a 42-L autofermentor, and several key physiological parameters were measured in real time. Maximal values of cell density (OD_{565}) (19.4) and cell yield (dry weight) (4.76 g/L) were attained at 40 h. The key time point for cell growth and magnetosome formation was found to be 18–20 h. At this point, cells entered the log phase of growth, the maximal values of C_{mag} (1.78), iron content (0.47%), and magnetosome number (26 ± 3 per cell) were observed, superoxide dismutase (SOD) activity began to decrease more rapidly, ATP content dropped to an extremely low level (0.17 fmol), and reducing power (NADH/NAD⁺ ratio) began to increase very rapidly. Excessive levels of dissolved oxygen (≥ 20 ppb) and lactic acid in the medium caused notable cytotoxic effects after 20 h. Artificial control measures for fermentation must be based on realistic cell physiological conditions. At the key time point (18–20 h), cell density is high and magnetosomes have matured. The process of magnetosome synthesis involves a high consumption of ATP and reducing power, and the cells require replenishment of nutrients prior to the 18–20 h time point. Culture conditions that effectively minimize dissolved oxygen accumulation, lactic acid content, and reducing power at this point will enhance magnetosome yield without obvious inhibition of cell growth.

Keywords: *Magnetospirillum gryphiswaldense*, submerged culture, physiological features, magnetosome synthesis, key time point

INTRODUCTION

Magnetotactic bacteria (MTB) are a group of aquatic microbes characterized by the ability to orient along magnetic field lines based on the presence of intracellular nano-sized “magnet needles” termed magnetosomes. Magnetosomes are membrane-bound magnetite (Fe_3O_4) or greigite (Fe_3S_4) crystals that form one or multiple chains within the cell (Jogler and Schüler, 2009; Komeili, 2012). Because of their narrow size distribution (30–120 nm) and uniform morphology, magnetosomes have potential applications in magnetic separation techniques, diagnostics, and analytic detection (Matsunaga et al., 2004; Pollithy et al., 2011). All MTB known to date are difficult to culture because of their strict requirements in terms of nutrition, oxygen, and redox potential (Zhang et al., 2010; Zhu et al., 2010). Most known MTB are obligatory anaerobic, facultative anaerobic, or microaerobic. Therefore, only a small proportion of MTBs can be

axenically isolated and cultured, and the obtainable cell densities do not allow the purification of sufficient numbers of magnetosomes for industrial applications (Jogler and Schüler, 2009). Improved methods are needed to increase MTB cell density and magnetosome yield at a reasonable cost.

Magnetospirillum gryphiswaldense MSR-1 is an MTB strain that has been the subject of considerable genetic research and can be cultured at high densities relative to other MTB (Jogler and Schüler, 2009). In a 2008 study, we achieved MSR-1 fermentation cell density (OD_{565}) 7.24, cell yield 2.17 g/L, and magnetosome yield 41.7 mg/L (Sun et al., 2008). In 2010, we achieved cell density 12.0 and magnetosome yield 83.23 mg/L (Liu et al., 2010). In 2011, using an improved strategy for high-density culture of MSR-1 and large-scale magnetosome production through semicontinuous culture and reduction of osmotic factors that tend to inhibit cell growth, we achieved cell yield 9.16 g/L and

magnetosome yield 356.52 mg/L (Zhang et al., 2011). In each of these studies, we focused on optimization of culture medium, adjustment of oxygen level and pH, and addition of nutrients, but did not carefully monitor cell physiological indicators. Increased knowledge of the physiological characteristics of the dynamic cell growth process will be helpful. *i.e.*, better understanding of the physiology and growth principles of MTBs will allow us to reduce the effects of specific physiological inhibitors and further increase magnetosome yield. By analyzing cells cultured under physiological conditions, we can elucidate realistic principles of MSR-1 growth and develop improved stability control strategies.

We report here new comprehensive findings on MSR-1 culture and cell physiological features during submerged culture in a 42-L autofermentor. In preliminary experiments, we evaluated a variety of physiological parameters, including growth curves, magnetism [C_{mag} value, ratio of maximal and minimal scattering intensities (Schüler et al., 1995)], dissolved oxygen (dO_2) and lactic acid (LA) levels in medium, iron content, ATP content, reducing power, and superoxide dismutase (SOD) activity in cells. Striking changes in most of these parameters were observed between hours 18–20 of culture, indicating a key time point for MSR-1 cell growth and magnetosome synthesis. The decreased levels of dO_2 , LA, and reducing power occurring at this key time point can be exploited for the improvement magnetosome yield without obvious inhibition of cell growth. This study is the first to utilize physiological parameters for the evaluation of MSR-1 phenotype during fermentation. Our findings may be applicable to the culture of other MTB and microaerobic bacteria.

MATERIALS AND METHODS

SUBMERGED CULTURE OF CELLS IN A 42-L AUTOFERMENTOR

M. gryphiswaldense strain MSR-1 (DSM6361) was purchased from Deutsche Sammlung von Mikroorganismen und Zellkulturen (Brunswick, Germany). Seed culture was performed as described previously (Liu et al., 2010). The 42-L fermentor was filled with 30 L of medium containing 1.5 g sodium thioglycolate, 6 g magnesium sulfate heptahydrate, 15 g yeast extract, 6 g peptone, and 15 mL Wolfe's mineral solution. Feed medium contained 4.2 g ferric citrate, 129 g sodium lactate, 52.6 g LA, and 54.9 g ammonium chloride in a volume of 700 mL. MSR-1 cells were continuously cultured in the fermentor for 48 h, at which point the OD_{565} value began to decrease following a long-term rise. The temperature and pH were controlled to 30°C and 6.8, respectively, during culture. The pH was adjusted via the feed medium. The dO_2 concentration was recorded using two probes that had different purposes. One probe was used for relative measurement (percent % as unit of data) and had lower accuracy. The other probe was used for absolute measurement (ppb as unit of data) and had higher accuracy. Calibration prior to measurements was required for the former probe but not for the latter. Before inoculation, we maintained an initial stirring rate (120 rpm) and airflow rate (0.94 L/min) for 2 h to ensure that oxygen was at saturation level in the medium. We then calibrated the dO_2 as closely as possible to 100% (there were occasional minor fluctuations). The various

study parameters were recorded after inoculation as functions of time (Table 1).

Samples were taken every few hours for further analysis. After sampling, cell density (OD_{565}) and magnetism (C_{mag}) were measured immediately using the same spectrophotometer at wavelength 565 nm as described by Schüler et al. (1995). A 2-mL culture sample was centrifuged, and the LA concentration of the supernatant was measured immediately using a SBA-40C Biosensor analyzer (Institute of Biology, Shandong Academy of Sciences, China). Cells (in a defined volume) were washed twice with 50 mM Tris buffer (pH 7.0) and centrifuged at 4°C, and the cell pellets were stored at -80°C. Culture samples were suspended in an appropriate volume of sterile distilled water for subsequent measurements.

IRON CONTENT

Another 2-mL culture sample was centrifuged in a 1.5-mL tube, and the pellet was dried at 60°C until it reached a constant weight. Iron content was measured by Inductively Coupled Plasma Optical Emission Spectrometry (ICP-OES; model Optima 5300DV, Perkin Elmer, Waltham MA, USA). The percentage of iron in cells was calculated as the iron content divided by the dry weight.

ATP CONTENT

Another 2-mL culture sample was added with 10% trichloroacetic acid solution (1:1, v/v), incubated on ice for 10 min, and

Table 1 | Adjustment of dissolved oxygen (dO_2) and corresponding values of OD_{565} and C_{mag} during submerged culture of MSR-1 cells.

Time (h)	Stirring rate (rpm)	Airflow rate (L/min)	dO_2		OD_{565}	C_{mag}
			(%)	(ppb)		
0	120	0.94	102.70	2451	0.1	0.74
8	120	0.95	0.00	12	0.3	0.24
10	140	1.45	0.00	4	0.4	0.80
12	160	1.95	0.00	4	0.7	1.39
14	180	1.97	0.00	3	1.1	1.38
16	180	1.95	0.00	2	1.5	1.65
18	200	1.95	0.00	3	1.7	1.52
20	230	2.95	0.00	6	2.1	1.78
22	250	3.98	0.00	4	3.2	1.65
24	270	3.96	0.00	17	4.8	1.71
26	280	3.99	0.00	35	6.3	1.38
28	290	3.98	0.00	9	8.3	1.50
30	300	3.97	0.00	215	10.8	1.54
32	300	1.97	0.00	186	13.7	1.68
34	300	1.95	0.00	204	14.6	1.41
36	300	1.95	12.40	661	16.8	1.43
38	300	1.95	21.60	962	18.1	1.20
40	300	1.95	29.80	1247	19.4	1.12

dO_2 was measured using two probes with differing accuracies (see Materials and Methods). To maintain dO_2 at the level suitable for magnetosome synthesis (0.0%), the stirring rate was changed at 10, 12, 14, 18, 20, 22, 24, 26, 28, and 30 h, and the airflow rate was changed at 10, 12, 20, 22, and 32 h.

centrifuged for 5 min at 4°C. The ATP content of the supernatant was measured using an AF-100 ATP analyzer (DKK-TOA Corp., Tokyo, Japan). The ATP content of the sample was calculated as total ATP content / volume of sample/OD₅₆₅ of sample.

REDUCING POWER

Reducing power was measured by a modification of the method of Perez et al. (2008). For NADH measurement, a 1-mL sample was incubated with 50 µL KOH (0.4 mol/L, pH 12.3) for 10 min at 30°C, centrifuged (12,000 rpm) for 10 min at 4°C, and the supernatant was assayed. For NAD⁺ measurement, a 1-mL sample was incubated with 125 µL HCl (0.4 mol/L, pH 1.3) for 10 min at 5°C, centrifuged (12,000 rpm) for 10 min at 4°C, and the supernatant was assayed. The reducing power was calculated as the ratio of NADH to NAD⁺.

TRANSMISSION ELECTRON MICROSCOPY (TEM)

A culture sample was placed on a copper grid, washed twice with distilled water, dried, and observed with a transmission electron microscope (model JEM1230; JEOL, Tokyo, Japan).

SUPEROXIDE DISMUTASE ACTIVITY

Cells were lysed by ultrasonication (ice bath, 50 W, 200 times, 50% duty cycle). Cell debris was removed by centrifugation at 4°C to yield a supernatant (used as crude enzyme extract), and the protein content (mg) was measured by Coomassie Brilliant Blue assay (Chial et al., 1993). The total SOD activity was measured using a SOD assay kit (Jiancheng Corp., Nanjing, China). The SOD activity of a sample was calculated as the total SOD activity divided by protein content.

RESULTS

PRECISE CONTROL OF DISSOLVED OXYGEN CONCENTRATION ENSURES OPTIMAL CONDITIONS FOR MAGNETOSOME FORMATION

We performed several preliminary experiments to obtain stable results based on our past experience. Although there were slight differences in the data from different batches, the overall trends for cell growth rate and magnetosome yield were consistent (see Figures 1A, S1). The results from a representative experiment are shown in Figure 1 as an example. As showed in Figure 1, cells grew slowly ($OD_{565} \leq 2.0$) until hour 20. Thereafter, cell growth entered the log phase. Maximal values of OD_{565} (19.4) (Figure 1A) and cell yield (dry weight) (4.76 g/L) were observed at hour 40. In MSR-1 culture, high dO₂ levels (>1%) promote cell growth but inhibit magnetosome formation (Heyen and Schüller, 2003; Liu et al., 2010). To balance these conflicting effects, we set the initial (hour 0) stirring rate to 120 rpm, the airflow rate to 0.94 L/min and the saturated dO₂ under these conditions to 100% (showed 102.7% after setting), based on the results of our previous study (Liu et al., 2010). After inoculation, the dO₂ level decreased rapidly to 0.0% at 8 h (Table 1). During this period, cell density (OD_{565}) increased 3-fold (from 0.1 at 0 h to 0.3 at 8 h), indicating a high oxygen requirement during the early stage of cell growth. To maintain a suitable dO₂ (0.0%) for magnetosome formation, we subsequently altered the stirring rate at 2-h intervals between 10 and 30 h and altered the airflow rate at 10, 12, 20, 22, and 32 h

(Table 1). To precisely control dO₂ concentration, we used two probes with differing accuracies as described in Materials and Methods, one for relative dO₂ measurement (percent %), the other for absolute measurement (ppb). This approach allowed us to accurately detect even tiny changes of dO₂, particularly at extremely low concentrations. From 28 to 34 h, the absolute dO₂ level gradually increased nearly 23-fold, from 9 to 204 ppb, while the probe used for relative measurement continuously showed a value below the limit of detection (0.0%), which may have caused a delay in adjusting the stirring rate and airflow rate in the fermentor (Table 1). A high dO₂ concentration affected magnetosome formation. From 8 to 24 h, the absolute dO₂ concentration remained <20 ppb, while the C_{mag} value increased from 0.24 at 8 h to 1.78 at 20 h and remained high until 24 h (Figure 1B). dO₂ increased gradually from 17 ppb at 24 h to 1247 ppb at 40 h, while C_{mag} decreased from 1.71 at 24 h to 1.12 at 40 h. Taken together, these findings indicate that the optimal concentration of absolute dO₂ for magnetosome production is <20 ppb.

LACTIC ACID CONCENTRATION REFLECTS GROWTH STATE

The LA feed medium contained LA, sodium lactate, ferric citrate, and ammonium chloride (see Materials and Methods). The LA in this medium was utilized both as a carbon source and a pH regulator. The supply of feed medium was auto-controlled via a computer to maintain a pH value of 6.8 throughout cell culture. The LA concentration in medium at each time point was recorded using a Biosensor analyzer and used as an indicator of the cell growth state. The LA concentration decreased rapidly from 0.26 g/L at 12 h to 0.01 g/L at 26 h, corresponding to the log phase of growth curve and reflecting the high cellular demand for LA as a source of carbon and energy for growth (Figure 1C). The LA concentration then increased from 0.01 g/L at 26 h to 0.16 g/L at 40 h. Excessive LA was present during this period and was associated with frequent pH fluctuations and rapid cellular metabolism (Figure 1C).

THE PERIOD 18–20 H IS A KEY TIME POINT FOR IRON METABOLISM AND MAGNETOSOME PRODUCTION

C_{mag} can be a useful parameter for estimating the magnetosome content of cells (Schüller et al., 1995), but it is based on an indirect method. A more direct method of measurement is based on TEM and the iron content of cells. The iron content in MTB can be 100-fold (or more) higher than in *E. coli* (Blakemore et al., 1979) and is concentrated primarily in magnetosomes (Kasama et al., 2006). We measured iron content by ICP-OES as described in Materials and Methods. C_{mag} and iron content both increased gradually from 8 to 20 h, reached maximal values (1.78 and 0.47%) at 20 h, and then decreased (to 1.12 and 0.20%, respectively) at 40 h (Figure 1D). TEM showed that the average number of magnetosomes per cell increased from 12 to 24 during the initial phase (0–20 h) and that magnetosome chains were not integrated at 12 h (Figures 2, S2 and Table 2). From 20 to 40 h, the average magnetosome number remained essentially constant (26 ± 3), and the chains were gradually integrated and matured (Figures 2, S2). We concluded that 20 h is an important transitional time point for magnetosome production. In view of the rapid decrease of

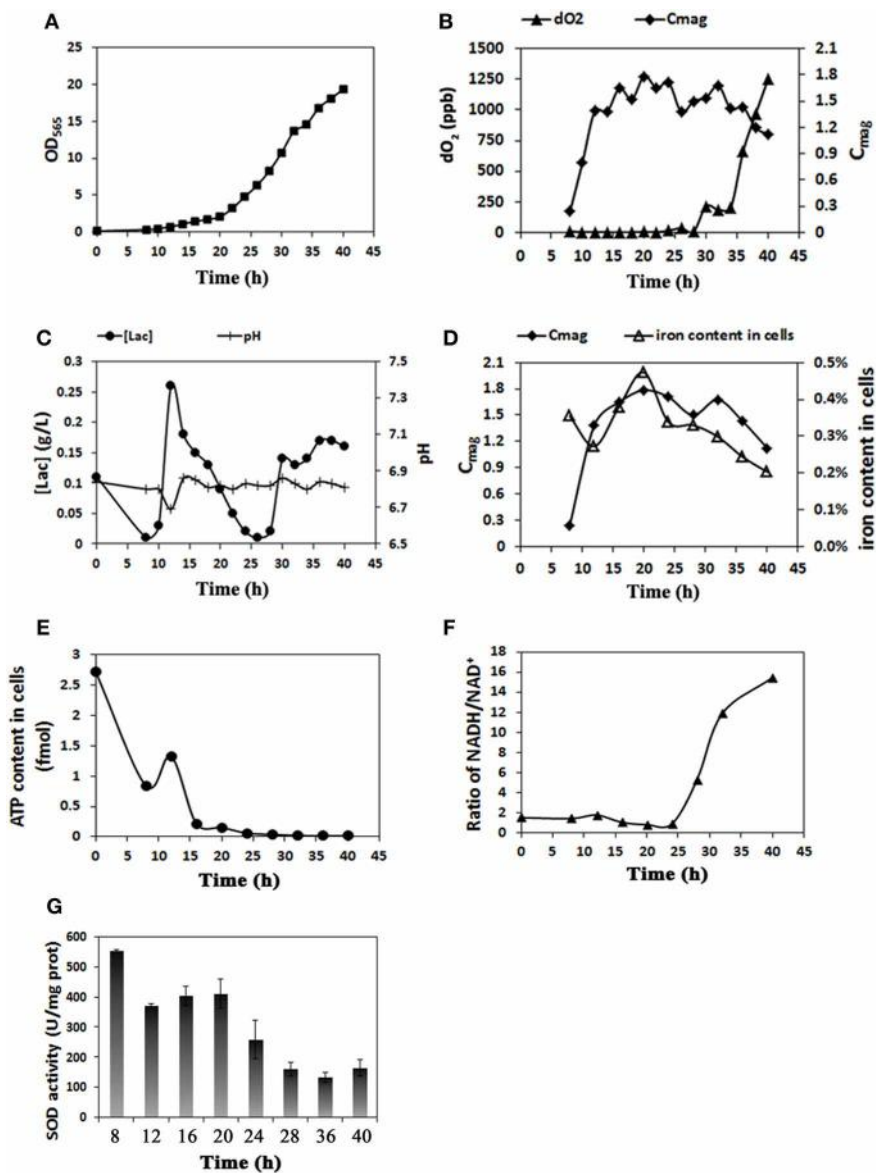


FIGURE 1 | Real-time physiological parameters of MSR-1 cells in submerged culture in a 42 L autofermentor. **(A)** Cell growth curve (OD_{565}). Cells entered the log growth phase at 20 h and reached maximal OD at 40 h. **(B)** Comparison of dissolved oxygen ($d\text{O}_2$) concentration and C_{mag} revealed that the optimal absolute $d\text{O}_2$ concentration for magnetosome production is <20 ppb. **(C)** Lactic acid concentration ($[\text{lac}]$)

and pH value were under coordinated control. **(D)** The level of iron content was closely related to that of C_{mag} . **(E)** Cell ATP content decreased rapidly from 0 to 20 h and much more gradually thereafter. **(F)** The NADH/NAD^+ ratio was low from 0 to 25 h and increased rapidly thereafter. **(G)** SOD activity assays at sampling times from 8 to 40 h. SOD activity was notably reduced after 20 h.

LA content in medium around this time (Figure 1C), it is clearly important to provide sufficient nutritional supplements prior to 20 h to ensure the rapid growth of new cells.

MAGNETOSOME SYNTHESIS CONSUMES A LARGE AMOUNT OF ATP AND ACCUMULATES REDUCING POWER

The formation of magnetosomes in MTB is presumed to consume a large amount of energy. The availability of ATP as an energy source has been shown to be required for iron uptake in MTB (Nakamura et al., 1995; Schüller, 1999). We used an ATP

analyzer to measure the ATP content of cells. From 0 to 20 h, the period of magnetosome synthesis, energy (i.e., ATP content) in cells decreased rapidly from 2.73 to 0.17 fmol. From 20 to 40 h, the ATP content continued to decrease from 0.17 fmol to near zero (0.02 fmol); however, the rate of decrease was lower than that from 0 h to 20 h (Figure 1E).

NADH plays an important role in ATP generation in cells and provides a proton gradient across the inner mitochondrial membrane for ATP production by ATP synthetase (Bonora et al., 2012). We used a modified enzyme reduction

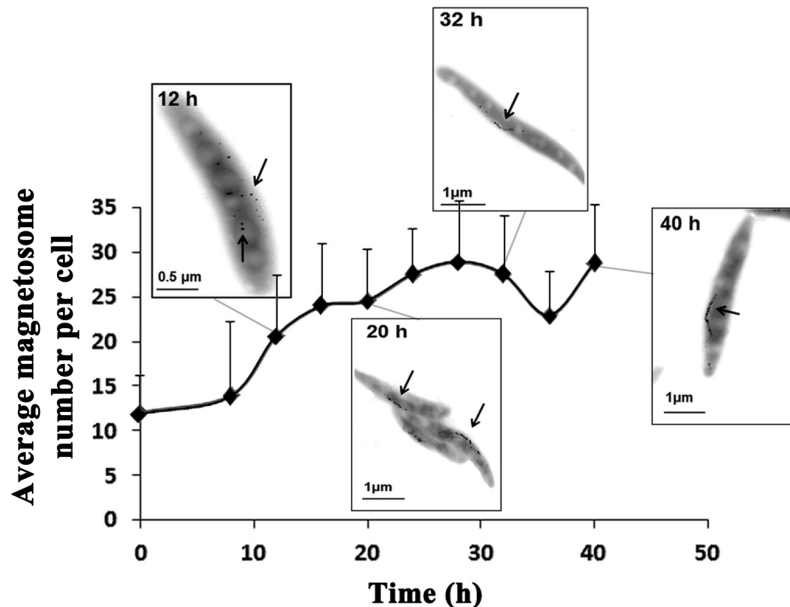


FIGURE 2 | Magnetosome number increased as a function of time. Typical TEM photos taken at 12, 20, 32, and 40 h are shown. At 8 h, magnetosomes were scattered. From 20 to 40 h, magnetosome chains became completed and mature. Magnetosomes are indicated by arrows.

Table 2 | Statistical processing of magnetosome number per cell at different time points.

Groups	Sampling time points									
	0 h	8 h	12 h	16 h	20 h	24 h	28 h	32 h	36 h	40 h
Percentage of magnetosome number per cell (%)										
0–5	5.6	4.8	0.0	0.0	0.0	0.0	0.0	0.0	0.0	0.0
6–10	44.4	42.9	10.0	0.0	3.4	0.0	0.0	0.0	0.0	0.0
11–15	27.8	23.8	10.0	8.7	3.4	0.0	0.0	0.0	4.8	0.0
16–20	16.7	23.8	25.0	26.1	24.1	4.3	10.0	13.0	38.1	12.5
21–25	5.6	4.8	25.0	26.1	27.6	34.8	20.0	26.1	23.8	20.8
26–30	0.0	0.0	25.0	21.7	31.0	30.4	40.0	13.0	19.0	16.7
31–35	0.0	0.0	5.0	13.0	13.8	21.7	20.0	43.5	14.3	37.5
36–40	0.0	0.0	0.0	4.3	0.0	8.7	10.0	4.3	0.0	12.5
AVE*	11.7	14.3	20.9	23.9	24.5	28.1	28.6	28.1	22.7	28.0
SD**	4.3	8.7	7.0	6.4	5.5	5.3	6.9	6.3	5.3	6.7

*Average magnetosome number per cell.

** Standard deviation.

method to measure reducing power (as the ratio NADH/NAD⁺) (Perez et al., 2008). In contrast to the trend for ATP, the NADH/NAD⁺ ratio remained low (≤ 2) and fluctuated slightly during the first 20 h (Figure 1F). Thereafter, as the cells entered the log phase of growth and the magnetosomes matured, the NADH/NAD⁺ ratio increased rapidly to 15 at 40 h. These findings indicate that the process of magnetosome synthesis consumes a large amount of ATP and accumulates reducing power.

SUPEROXIDE DISMUTASE ACTIVITY DECREASES RAPIDLY AFTER 20 h

SOD in microbes helps remove the superoxide anion radical (O_2^-) and hydrogen peroxide (H_2O_2), which have destructive

effects on cell macromolecules (Cabiscol et al., 2000). In MTB, SOD also reduces oxidative stress during magnetosome formation. We used a SOD assay kit to monitor SOD activity in cells. The activity declined gradually from 555 U/mg at 8 h to 410 U/mg at 20 h and then rapidly to 164 U/mg at 40 h (Figure 1G).

DISCUSSION

The development of improved methods for high-yield magnetosome production has been a major goal of MTB research for over a decade. Progress in this area has been achieved primarily through optimization of pH, temperature, redox potential, dO₂ level, and growth medium and feed medium composition (Heyen

and Schüler, 2003; Sun et al., 2008; Liu et al., 2010; Zhang et al., 2011). Our knowledge of the physiological characteristics of MTB during the dynamic process of cell growth remains fragmentary (Ban et al., 2010). Even the reason why the growth of several MTBs is promoted by trace quantities of peptone remains unclear (Heyen and Schüler, 2003; Zhu et al., 2010). We recently observed that sodium chloride acts as a physiological inhibitor of MSR-1 growth (Zhang et al., 2011). Further studies of physiological factors in MTB are needed.

We achieved successful large-scale culture of MSR-1 in a 42-L fermentor during 48 h in the present study. Maximal cell density and cell yield were 19.4 (OD₅₆₅) and 4.76 g/L (dry weight), respectively. Higher values were attained in one of our previous studies (Liu et al., 2010). We measured the dynamic values of 9 key physiological parameters: growth curve, magnetism (C_{mag}), dO₂ and LA content in medium, iron content, magnetosome number, ATP content, reducing power, and SOD activity in cells. The period from 18 to 20 h was identified as a key time point for cell growth and magnetosome formation. During this period, cell growth entered its log phase, maximal cellular values of C_{mag} (1.78), iron content (0.47%), and magnetosome number (26 ± 3) were reached, SOD activity began to decline more rapidly, ATP content dropped to near-zero, and reducing power (NADH/NAD⁺ ratio) increased rapidly. To precisely control dO₂, we performed measurements using two probes with differing accuracies. The optimal dO₂ concentrations for magnetosome production were 0.0% (relative) and <20 ppb (absolute).

LA in feed medium is used as both a carbon source and pH regulator. From 12 to 26 h, the LA concentration decreased rapidly, corresponding to the log phase of growth and reflecting the high cellular demand for LA as a source of carbon and energy for growth. We therefore recommend that pure sodium lactate be added intermittently to the feed medium during this period to meet the requirements of the cells. From 26 to 40 h, the LA concentration increased greatly, resulting in excessive LA levels associated with frequent pH fluctuations and rapid cellular metabolism. Excessive levels of organic acids such as LA have been shown to inhibit cell growth (Pieterse et al., 2005); this effect may explain the gradual reduction of growth rate we observed. As an alternative to the use of LA, we can adjust the pH using other compounds (e.g., carbon dioxide) or by adding feed medium manually at later stages.

ATP is the major energy source in cells and is required for physiological processes such as cell metabolism, signal transduction, and molecular transportation. In MTB, ATP is also involved in iron uptake (Nakamura et al., 1995; Schüler, 1999) and inducing the polymerization of MamK (Mitraki et al., 2012), an actin-like protein involved in the alignment of magnetosome chains (Scheffel et al., 2005). Our findings demonstrate that magnetosome synthesis in MTB consumes large amounts of ATP. NADH plays an important role in generating ATP and provides a proton gradient across the inner mitochondrial membrane for ATP production by ATP synthetase (Bonora et al., 2012). In contrast to the usual trend of ATP change, NADH was accumulated during the fermentation process. We found previously that reducing power is significantly increased during magnetosome synthesis

and that excessive reducing power suppresses magnetosome synthesis and cell growth in later periods (unpubl. data). A high NADH/NAD⁺ ratio indicates that little NADH is being used to supply protons, resulting in a low cellular ATP content. In MTB, excessive reducing power is consumed through polyhydroxybutyrate (PHB) synthesis and hydrogen release (Ban et al., 2010). This process may account in part for the fact that MTB contain many PHB granules (Schultheiss et al., 2005; Komeili, 2006). When PHB synthase gene was knocked out in MSR-1, the amount of magnetosome increased nearly 30% compared with wild-type strain (Liu et al., 2008). So, it seems that an energy competition exists between the PHB and magnetosome synthesis process.

H₂O₂ can form a hydroxyl radical (HO·) when it receives an electron from ferrous iron. HO· is the only reactive oxygen species that can directly damage most biomolecules (Imlay, 2003). In the present study, magnetosomes reached their maximal number at 20 h. At this point, reductions were observed for the intracellular iron content (Figure 1D) and the amount of SOD used to remove reactive oxygen species (Figure 1G). This could be explained as, in the late log phase, when dO₂ and nutrients were enough, magnetosome formation and maturation maybe cannot catch up the cell dividing rate, resulting in diluted magnetosomes in cells, which was indicated by the C_{mag} trend (Figure 1D). Therefore, the reduced SOD activity may be caused similarly from diluted reactive oxygen species. Recent studies have shown that magnetosomes and artificial magnetic nanoparticles are able to scavenge reactive oxygen species (Gao et al., 2007; Guo et al., 2012). This ability may account in part for the observed decrease in SOD activity.

CONCLUSION

Artificial manipulation of fermentation processes for maximizing yield must be based on realistic cell physiological conditions. We found that 18–20 h is a key time point for *M. gryphiswaldense* MSR-1 cell growth and magnetosome synthesis. At this point, cell density is high, magnetosomes have matured, and cells require replenishment of nutrients. Culture conditions that effectively minimize dO₂ accumulation, LA content, and reducing power at this point will promote magnetosome yield without obvious inhibition of cell growth. Artificial culture of MTB requires precise control of dO₂ at low concentrations (≤ 20 ppb) that are suitable for magnetosome synthesis. Future analytical transcriptome studies involving the forced expression of MSR-1 genes that are involved in the metabolism of ATP, NADH, oxygen and iron will help us elucidate the optimal conditions for MTB culture.

ACKNOWLEDGMENTS

This study was supported by the National Natural Science Foundation of China (Grants No. 31270093 and J1103520) and the Undergraduate Innovation Program of China Agricultural University (Grant No. 2010-BKS-16). The authors thank Dr. Wei Jiang for technical help with submerged culture, Dr. Jingwen Lu for help with determination of cell ATP content, and Dr. S. Anderson for English editing of the manuscript.

SUPPLEMENTARY MATERIAL

The Supplementary Material for this article can be found online at: http://www.frontiersin.org/Aquatic_Microbiology/10.3389/fmicb.2013.00210/abstract

FIGURE S1 | A set of representative preliminary fermentation data: growth and C_{mag} curves. Cell growth enters the log phase at 20 h, with a maximum OD₅₆₅ value at 36 h. C_{mag} increased gradually from 8 to 20 h, reached maximal values at 20 h,

REFERENCES

- Ban, J., Jiang, W., Li, Y., Zhang, Y., and Li, J. (2010). Functional analysis of hydrogenases and their effects on cell growth and magnetosome synthesis in *Magnetospirillum gryphiswaldense*. *Chin. Sci. Bull.* 55, 1271–1277. doi: 10.1007/s11434-009-0744-8
- Blakemore, R. P., Maratea, D., and Wolfe, R. S. (1979). Isolation and pure culture of a freshwater magnetic spirillum in chemically defined medium. *J. Bacteriol.* 140, 720–729.
- Bonora, M., Paterniani, S., Rimessi, A., De Marchi, E., Suski, J. M., Bononi, A., et al. (2012). ATP synthesis and storage. *Purinergic Signal.* 8, 343–357. doi: 10.1007/s11302-012-9305-8
- Cabiscol, E., Tamarit, J., and Ros, J. (2000). Oxidative stress in bacteria and protein damage by reactive oxygen species. *Int. Microbiol.* 3, 3–8.
- Chial, H. J., Thompson, H. B., and Splittergerber, A. G. (1993). A spectral study of the charge forms of Coomassie blue G. *Anal. Biochem.* 209, 258–266. doi: 10.1006/abio.1993.1117
- Gao, L., Zhuang, J., Nie, L., Zhang, J., Zhang, Y., Gu, N., et al. (2007). Intrinsic peroxidase-like activity of ferromagnetic nanoparticles. *Nat. Nanotechnol.* 2, 577–583. doi: 10.1038/nnano.2007.260
- Guo, F. F., Yang, W., Jiang, W., Geng, S., Peng, T., and Li, J. L. (2012). Magnetosomes eliminate intracellular reactive oxygen species in *Magnetospirillum gryphiswaldense* MSR-1. *Environ. Microbiol.* 14, 1722–1729. doi: 10.1111/j.1462-2920.2012.02707.x
- Heyen, U., and Schüler, D. (2003). Growth and magnetosome formation by microaerophilic *Magnetospirillum* strains in an oxygen-controlled fermentor. *Appl. Microbiol. Biotechnol.* 61, 536–544.
- Imlay, J. A. (2003). Pathways of oxidative damage. *Annu. Rev. Microbiol.* 57, 395–418. doi: 10.1146/annurev.micro.57.030502.090938
- Jogler, C., and Schüler, D. (2009). Genomics, genetics, and cell biology of magnetosome formation. *Annu. Rev. Microbiol.* 60, 501–521. doi: 10.1146/annurev.micro.62.081307.162908
- Kasama, T., Pósfai, M., Chong, R. K. K., Finlayson, A. P., Buseck, P. R., Frankel, R. B., et al. (2006). Magnetic properties, microstructure, composition, and morphology of greigite nanocrystals in magnetotactic bacteria from electron holography and tomography. *Am. Mineral.* 91, 1216–1229. doi: 10.2138/am.2006.2227
- Komeili, A. (2006). Magnetosomes are cell membrane invaginations organized by the actin-Like protein MamK. *Science* 311, 242–245. doi: 10.1126/science.1123231
- Komeili, A. (2012). Molecular mechanisms of compartmentalization and biominerization in magnetotactic bacteria. *FEMS Microbiol. Rev.* 36, 232–255. doi: 10.1111/j.1574-6976.2011.00315.x
- Liu, J. N., Ding, Y., Jiang, W., Tian, J. S., Li, Y., and Li, L. J. (2008). A mutation upstream of an ATPase gene significantly increases magnetosome production in *Magnetospirillum gryphiswaldense*. *Appl. Microbiol. Biotechnol.* 81, 551–558. doi: 10.1007/s00253-008-1665-1
- Liu, Y., Li, G. R., Guo, F. F., Jiang, W., Li, Y., and Li, L. J. (2010). Large-scale production of magnetosomes by chemostat culture of *Magnetospirillum gryphiswaldense* at high cell density. *Microb. Cell Fact.* 9, 99. doi: 10.1186/1475-2859-9-99
- Matsunaga, T., Okamura, Y., and Tanaka, T. (2004). Biotechnological application of nano-scale engineered bacterial magnetic particles. *J. Mater. Chem.* 14, 2099–2105. doi: 10.1039/b404844j
- Mitraki, A., Sonkaria, S., Fuentes, G., Verma, C., Narang, R., Khare, V., et al. (2012). Insight into the assembly properties and functional organisation of the magnetotactic bacterial actin-like homolog, MamK. *PLoS ONE* 7:e34189. doi: 10.1371/journal.pone.0034189
- Nakamura, C., Kikuchi, T., Burgess, J. G., and Matsunaga, T. (1995). Iron-regulated expression and membrane localization of the magA protein in *Magnetospirillum* sp. strain AMB-1. *J. Biochem.* 118, 23–27.
- Perez, J. M., Arenas, F. A., Pradenas, G. A., Sandoval, J. M., and Vasquez, C. C. (2008). *Escherichia coli* YqhD exhibits aldehyde reductase activity and protects from the harmful effect of lipid peroxidation-derived aldehydes. *J. Biol. Chem.* 283, 7346–7353. doi: 10.1074/jbc.M708846200
- Pieterse, B., Leer, R. J., Schuren, F. H., and van der Werf, M. J. (2005). Unravelling the multiple effects of lactic acid stress on *Lactobacillus plantarum* by transcription profiling. *Microbiology* 151, 3881–3894. doi: 10.1099/mic.0.28304-0
- Pollithy, A., Romer, T., Lang, C., Muller, F. D., Helma, J., Leonhardt, H., et al. (2011). Magnetosome expression of functional camelid antibody fragments (nanobodies) in *Magnetospirillum gryphiswaldense*. *Appl. Environ. Microbiol.* 77, 6165–6171. doi: 10.1128/AEM.05282-11
- Scheffel, A., Gruska, M., Faivre, D., Linaroudis, A., Plitzko, J. M., and Schüler, D. (2005). An acidic protein aligns magnetosomes along a filamentous structure in magnetotactic bacteria. *Nature* 440, 110–114. doi: 10.1038/nature04382
- Schüler, D. (1999). Formation of magnetosomes in magnetotactic bacteria. *J. Mol. Microbiol. Biotechnol.* 1, 79–86.
- Schüler, D., Uhl, R., and Bäuerlein, E. (1995). A simple light scattering method to assay magnetism in *Magnetospirillum gryphiswaldense*. *FEMS Microbiol. Lett.* 132, 139–145. doi: 10.1111/j.1574-6968.1995.tb07823.x
- Schlütheiss, D., Handrick, R., Jendrossek, D., Hanzlik, M., and Schüler, D. (2005). The presumptive magnetosome protein Mms16 Is a poly(3-Hydroxybutyrate) granule-bound protein (Phasin) in *Magnetospirillum gryphiswaldense*. *J. Bacteriol.* 187, 2416–2425. doi: 10.1128/JB.187.7.2416-2425.2005
- Sun, J. B., Zhao, F., Tang, T., Jiang, W., Tian, J. S., Li, Y., et al. (2008). High-yield growth and magnetosome formation by *Magnetospirillum gryphiswaldense* MSR-1 in an oxygen-controlled fermentor supplied solely with air. *Appl. Microbiol. Biotechnol.* 79, 389–397. doi: 10.1007/s00253-008-1453-y
- Zhang, W. J., Chen, C. F., Li, Y., Song, T., and Wu, L. F. (2010). Configuration of redox gradient determines magnetotactic polarity of the marine bacteria MO-1. *Environ. Microbiol. Rep.* 2, 646–650. doi: 10.1111/j.1758-2229.2010.00150.x
- Zhang, Y., Zhang, X., Jiang, W., Li, Y., and Li, J. (2011). Semicontinuous culture of *Magnetospirillum gryphiswaldense* MSR-1 cells in an autofermentor by nutrient-balanced and isosmotic feeding strategies. *Appl. Environ. Microbiol.* 77, 5851–5856. doi: 10.1128/AEM.05962-11
- Zhu, K., Pan, H., Li, J., Zhang, K. Y., Zhang, S. D., Zhang, W. Y., et al. (2010). Isolation and characterization of a marine magnetotactic spirillum axenic culture QH-2 from an intertidal zone of the China Sea. *Res. Microbiol.* 161, 276–283. doi: 10.1016/j.resmic.2010.02.003

Conflict of Interest Statement: The authors declare that the research was conducted in the absence of any commercial or financial relationships that could be construed as a potential conflict of interest.

Received: 20 April 2013; accepted: 07 July 2013; published online: 24 July 2013.

Citation: Yang J, Li S, Huang X, Tang T, Jiang W, Zhang T and Li Y (2013) A key time point for cell growth and magnetosome synthesis of *Magnetospirillum gryphiswaldense* based on real-time analysis of physiological factors. *Front. Microbiol.* 4:210. doi: 10.3389/fmicb.2013.00210

This article was submitted to Frontiers in Aquatic Microbiology, a specialty of Frontiers in Microbiology.

Copyright © 2013 Yang, Li, Huang, Tang, Jiang, Zhang and Li. This is an open-access article distributed under the terms of the Creative Commons Attribution License, which permits use, distribution and reproduction in other forums, provided the original authors and source are credited and subject to any copyright notices concerning any third-party graphics etc.